

FINAL PROJECT REPORT

LOAD MODELING TRANSMISSION RESEARCH

Prepared for CIEE By:

Lawrence Berkeley National Laboratory



Project Manager: Bernard Lesieutre

Authors: Richard Bravo, Robert Yinger, Dave Chassin, Henry Huang, Ning Lu,
Ian Hiskens, Giri Venkataramanan

Date: March, 2010



A CIEE Report

DISCLAIMER

This draft report was prepared as the result of work sponsored by the California Energy Commission. It does not necessarily represent the views of the Energy Commission, its employees or the State of California. The Energy Commission, the State of California, its employees, contractors and subcontractors make no warrant, express or implied, and assume no legal liability for the information in this report; nor does any party represent that the uses of this information will not infringe upon privately owned rights. This report has not been approved or disapproved by the California Energy Commission nor has the California Energy Commission passed upon the accuracy or adequacy of the information in this report.

Acknowledgments

The authors would like to thank Larry Miller, Lloyd Cibulka, Jim Cole, and Merwin Brown of the California Institute for Energy and Environment. The researchers also thank members of the WECC Load Modeling Task Force for their technical assistance and guidance. The authors also thank Dmitry Kosterev and Steve Yang of the Bonneville Power Administration for their contributions to this work through the testing of air conditioning units at BPA facilities, and continued engagement in and support for load modeling activities.

This project comprises many sub tasks. The principal researchers and report authors for these tasks are listed below. Bernard Lesieutre (LBNL) compiled this final report from task reports and white papers. (See appendices.)

The testing of AC units at SCE was led by Richard Bravo and Robert Yinger. The testing of AC units at BPA was conducted by BPA staff with assistance from Bernard Lesieutre (LBNL).

The development of the performance model was led by Henry Huang and Ning Lu (PNNL). The development of the dynamic phasor model was led by Bernard Lesieutre (LBNL).

The research on potential solutions to the delayed voltage recovery problems was led by Richard Bravo and Robert Yinger (SCE).

The research and development for the load composition data tool was conducted by David Chassin (PNNL).

The research for the white paper on load monitoring was conducted by Henry Huang (PNNL).

The research for the white paper on uncertainty analysis was conducted by Ian Hiskens (University of Wisconsin-Madison).

The white paper on solar generation and load models was written by Giri Venkataramanan (University of Wisconsin-Madison).

The white paper on fault-induced delayed voltage recovery was written by Bernard Lesieutre (LBNL)

The research on motor protection was led by Bernard Lesieutre (LBNL).

Disclaimer

This document was prepared as an account of work sponsored by the United States Government. While this document is believed to contain correct information, neither the United States Government nor any agency thereof, nor The Regents of the University of California, nor any of their employees, makes any warranty, express or implied, or assumes any legal responsibility for the accuracy, completeness, or usefulness of any information, apparatus, product, or process disclosed, or represents that its use would not infringe privately owned rights. Reference herein to any specific commercial product, process, or service by its trade name, trademark, manufacturer, or otherwise, does not necessarily constitute or imply its endorsement, recommendation, or favoring by the United States Government or any agency thereof, or The Regents of the University of California. The views and opinions of authors expressed herein do not necessarily state or reflect those of the United States Government or any agency thereof, or The Regents of the University of California.

Ernest Orlando Lawrence Berkeley National Laboratory is an equal opportunity employer.

This work was funded by the California Energy Commission, Public Interest Energy Research Program that supports the Energy Systems Integration Program through California Institute for Energy and Environment under Work for Others Contract No. 500-02-004 and supported by the U.S. Department of Energy under Contract No. DE-AC02-05CH11231.

Preface

The California Energy Commission's Public Interest Energy Research (PIER) Program supports public interest energy research and development that will help improve the quality of life in California by bringing environmentally safe, affordable, and reliable energy services and products to the marketplace.

The PIER Program conducts public interest research, development, and demonstration (RD&D) projects to benefit California.

The PIER Program strives to conduct the most promising public interest energy research by partnering with RD&D entities, including individuals, businesses, utilities, and public or private research institutions.

- PIER funding efforts are focused on the following RD&D program areas:
- Buildings End-Use Energy Efficiency
- Energy Innovations Small Grants
- Energy-Related Environmental Research
- Energy Systems Integration
- Environmentally Preferred Advanced Generation
- Industrial/Agricultural/Water End-Use Energy Efficiency
- Renewable Energy Technologies
- Transportation

Load Modeling Transmission Research is the draft final report for the WECC Load Modeling Transmission Research project (contract number 500-02-004), work authorization number MR-049 conducted by Lawrence Berkeley National Laboratory. The information from this project contributes to PIER's Energy Systems Integration Program.

For more information about the PIER Program, please visit the Energy Commission's website at www.energy.ca.gov/research/ or contact the Energy Commission at 916-654-4878.

Table of Contents

Acknowledgments	iii
Preface	v
Report Organization	xv
Abstract	xvii
Executive Summary	1
1.0 Introduction.....	5
1.1. Background	5
1.2. Overview of Research, Results, and Recommendations.....	9
1.2.1. Air Conditioner Testing and Modeling.....	9
1.2.2. Potential Solutions to Delayed Voltage Recovery	11
1.2.3. Load Composition Data Tool	12
1.2.4. Load Monitoring	12
1.2.5. Uncertainty Analysis	13
1.2.6. Solar Generation and Load Models	14
1.2.7. Fault-Induced Delayed Voltage Recovery	14
1.2.8. Motor Protection.....	14
1.3. Summary.....	15
1.3.1. Benefits to California	16
2.0 Air Conditioner Modeling.....	18
2.1. Introduction.....	18
2.2. Task Approach.....	18
2.2.1. Laboratory Testing	18
2.2.2. Performance Model.....	19
2.2.3. Dynamic Phasor Model	20
2.3. Task Results.....	21
2.3.1. Test Results.....	21
2.3.2. Performance Model.....	29
2.3.3. Dynamic Phasor Model	30
2.4. Conclusions and Recommendations.....	41
2.4.1. Conclusions.....	41

2.4.2.	Recommendations.....	41
2.4.3.	Benefit to California	41
3.0	Potential Solutions to Delayed Voltage Recovery.....	43
3.1.	Introduction.....	43
3.2.	Task Approach.....	43
3.2.1.	Unit Level	43
3.2.2.	System Level	44
3.3.	Task Results.....	44
3.3.1.	Unit Level	44
3.3.2.	System Level	45
3.3.3.	Economic Assessment.....	46
3.4.	Conclusions and Recommendations.....	47
3.4.1.	Conclusions	47
3.4.2.	Recommendations.....	47
3.4.3.	Benefit to California	47
4.0	Load Composition Data Tool.....	49
4.1.	Introduction.....	49
4.2.	Task Approach.....	50
4.3.	Task Results.....	52
4.4.	Conclusions and Recommendations.....	54
4.4.1.	Conclusions	54
4.4.2.	Recommendations.....	54
4.4.3.	Benefits to California	54
5.0	Load Monitoring.....	56
5.1.	Introduction.....	56
5.2.	Task Approach.....	56
5.3.	Task Results.....	57
5.3.1.	Load Monitoring Device Options	57
5.3.2.	EXISTING LOAD MONITORING EXAMPLES	58
5.4.	Conclusions and Recommendations.....	59
5.4.1.	Conclusions	59
5.4.2.	Recommendations.....	62
5.4.3.	Benefits to California	62
6.0	Uncertainty Analysis.....	63

6.1.	Introduction.....	63
6.2.	Task Approach.....	63
6.2.1.	Trajectory Sensitivities.....	64
6.2.2.	Test System.....	66
6.3.	Task Results.....	67
6.3.1.	Uncertainty Analysis	67
6.3.2.	Parameter Ranking.....	68
6.3.3.	System Stress Indicator.....	69
6.3.4.	Parameter Estimation	70
6.4.	Conclusions and Recommendations.....	71
6.4.1.	Recommendations.....	72
6.4.2.	Benefits to California	72
7.0	Solar Generation and Load Models	74
7.1.	Introduction.....	74
7.2.	Task Approach.....	74
7.3.	Task Results.....	75
7.3.1.	PV System Models.....	75
7.3.2.	PV System Modeling Issues.....	76
7.3.3.	Candidate System Model	80
7.4.	Conclusions and Recommendations.....	82
7.4.1.	Conclusions	82
7.4.2.	Recommendations.....	82
7.4.3.	Benefit to California	82
8.0	Fault-Induced Delayed Voltage Recovery	85
8.1.	Introduction.....	85
8.2.	Task Approach.....	86
8.3.	Task Results.....	86
8.3.1.	FIDVR Phenomenon	86
8.3.2.	Solutions	89
8.4.	Conclusions and Recommendations.....	92
8.4.1.	Conclusions	92
8.4.2.	Recommendations.....	92
8.4.3.	Benefits to California	93
9.0	Motor Protection	94

9.1. Introduction.....	94
9.2. Project Approach.....	94
9.3. Project Results.....	95
9.3.1. Test Results.....	95
9.3.2. National Electric Code.....	97
9.4. Conclusions and Recommendations.....	100
9.4.1. Conclusions.....	100
9.4.2. Recommendations.....	100
9.4.3. Benefit to California.....	100
10.0 References.....	102
11.0 Glossary.....	106

Appendices

Appendix A: Air Conditioner Stalling Effects Study Air Conditioner Testing Procedures

Appendix B: Air Conditioner Test Report

Appendix C: Performance Model Evaluation

Appendix D: Recommended Model For Single Phase Compressor

Appendix E: Air Conditioner Stalling Unit Level Solutions Test Report

Appendix F: Air Conditioner Stalling Solutions Summary Report

Appendix G: WECC Load Composition Data Tool Specification

Appendix H: Load Monitoring

Appendix I: Uncertainty in Power System Models

Appendix J: Scoping Study to Assess Solar Generation Characteristics and Its Impacts on Load Modeling

Appendix K: Fault-Induced Delayed Voltage Recovery

List of Figures

Figure 1 Typical Delayed Voltage Recovery	7
Figure 2 Delayed Voltage Recovery	8
Figure 3 WECC Composite Load Model	8
Figure 4 Power/Voltage Curves	18
Figure 5 Stall Current	21
Figure 6 Stall Real and Reactive Power	24
Figure 7 Pressure Relief Valve	25
Figure 8 Thermal Protection Switch Tripping Time	27
Figure 9 Contactor Dropout Voltage	28
Figure 10 Voltage ramp measured at terminal of motor. The voltage initially is 0.98 pu.	31
Figure 11 Measured and simulated active power	32
Figure 12 Measured and simulated reactive power	32
Figure 13 Voltage Oscillation Test. The applied voltage varies between 90% and 110% of nominal at frequencies: 0.1 Hz, 0.25 Hz, 0.7 Hz, 1.5Hz, and 2 Hz.	33
Figure 14 Active Power, simulated and calculated from measurements for the voltage oscillation test.	34
Figure 15 Reactive Power, simulated and calculated from measurements for the voltage oscillation test.	34
Figure 16 Simulation voltage consistent with laboratory voltage. The voltage magnitude increases as frequency decreases because the supply line voltage drop decreases.....	35
Figure 17 Frequency. The frequency drops from 60Hz to 58.5Hz and returns to 60Hz in 0.25Hz increments.	36
Figure 18. Calculated and simulated active power. The response is small and proportional to frequency.....	36
Figure 19 Calculated and simulated reactive powers. The reactive power increases with decrease in frequency.	37
Figure 20 Plot of active power for 3-cycle 52% voltage sag test. The motor stalls.....	39
Figure 21 Plot of reactive power for 3-cycle, 52% voltage sag test. The motor stalls.	39

Figure 22 Plot of active power for 3-cycle, 54% voltage sag test. The motor recovers. (Note that the apparent delay in measured response, approximately 1 cycle, is due to calculation of power from data – using a 1-cycle window.).....	40
Figure 23 Plot of reactive power for 3-cycle, 54% voltage sag test. The motor recovers. (Note that the apparent delay in measured response, approximately 1 cycle, is due to calculation of power from data – using a 1-cycle window.)	41
Figure 24 System-Level Solutions Simulations.....	46
Figure 25. The WECC composite load model structure includes static loads, electronic loads, constant-torque three-phase motors (A), high inertia speed-squared load motors (B), low inertia speed-squared load motors (C), and constant-torque single-phase motors (D).....	50
Figure 26 Curve Decomposition for Top-Down Load Composition Analysis.....	60
Figure 27 IEEE 39 bus system.....	66
Figure 28 Zone 3 protection on line 23-24, 95% confidence interval bounds.	68
Figure 29 Trajectory sensitivities for all load indices.....	69
Figure 30 Trajectory and sensitivity variation for increasing system stress.....	70
Figure 31 Block diagram of typical grid-connected PV system.....	75
Figure 32 A graph of measured direct and diffuse irradiance on (a) a summer day, and (b) a winter day (From Thomson 2007)	77
Figure 33 Response of the PV generator to increase and decrease in grid voltage (From Yun 2004)	79
Figure 34 V Voltage tolerance curves of 9 commercial PV inverters (From Kunte 2008).....	80
Figure 35 Structure of a candidate PV system model to be incorporated within the framework of load modeling.....	81
Figure 36. Torque Speed Curve for Motor.	87
Figure 37 Contactor Model (LMTF 2006).....	95
Figure 38. Thermal Relay Characteristic (LMTF 2006)	96
Figure 39. Thermal relay model (LMTF 2006).....	97

List of Tables

Table 1 Stall Window.....	22
Table 2 Stall Calculation.....	27
Table 3 Stalling Time after Contactor Reclosed.....	29
Table 4 Unit Level Devices Test Results	45
Table 5 Economic Assessment.....	47
Table 6 Prototype Conditions.....	52
Table 7 Prototype Load Composition	53
Table 8 Features of Different Monitoring Options	57

Report Organization

The WECC Load Modeling Transmission Research project was funded by the California Energy Commission's Public Interest Energy Research program through Contract #500-02-004, Work Authorization #MR-049 and subsequently through Contract #500-99-013, Work Authorization BOA-99-208-P. Multiple research tasks were conducted in parallel:

- Air Conditioner Load Modeling
- Potential Solutions to Delayed Voltage Recovery
- Load Composition Data Tool
- Load Monitoring
- Uncertainty Analysis
- Solar Generation and Load Models
- Fault-Induced Delayed Voltage Recovery
- Motor Protection

The background and overview for the entire project is presented in the Introduction, and it may be considered an extended executive summary. Subsequent chapters are organized by task.

Abstract

The research presented in this report primarily focuses on improving power system load models to better represent their impact on system behavior. The previous standard load model fails to capture the delayed voltage recovery events that are observed in the Southwest and elsewhere. These events are attributed to stalled air conditioner units after a fault. To gain a better understanding of their role in these events and to guide modeling efforts, typical air conditioner units were tested in laboratories. Using data obtained from these extensive tests, new load models were developed to match air conditioner behavior. An air conditioner model is incorporated in the new WECC composite load model. These models are used in dynamic studies of the West and can impact power transfer limits for California. Unit-level and system-level solutions are proposed as potential solutions to the delayed voltage recovery problem.

Keywords: Electricity grid, reliability, load models, air conditioners, fault-induced delayed voltage recovery, load composition, single-phase induction motor, compressors, voltage stability.

Executive Summary

Introduction

Grid planning and operating decisions rely on simulations of dynamic behavior of the power system. Both technical and commercial segments of the industry must be confident that the simulation models and database are accurate and up to date. If the transfer limits are set using overly optimistic models, a grid operator may unknowingly operate the system beyond its capability, thereby increasing the risk of widespread outages, such as occurred during summer 1996 outages. If the models are pessimistic, a grid operator may be overly conservative and impose unnecessary restrictions on the transfer paths, thereby unnecessarily raising electricity costs or increasing the risk of power shortages in energy deficient regions. Therefore, having realistic models is very important to ensure reliable and economic power system operation.

SCE and other utilities experience occurrences of delayed voltage recovery following faults on their electrical systems. Under normal conditions voltage recovers to nominal levels less than one second after the fault is cleared, but over the past few years there have been several instances at some SCE substations when voltage recovery was delayed for more than 30 seconds after normal fault clearing. These events primarily occurred during the heavy summer load at substations located in hot climates and serving new housing developments. Stalling air conditioner units are believed to be causing the delayed voltage recoveries.

The WECC load modeling task force has developed a new composite load model to improve the accuracy of grid simulations. Researchers on this project are members of the load modeling task force and the models developed here are incorporated into the new model.

Purpose

The purpose of this research program is to improve the accuracy of load models in general, and air conditioner models in particular. Success relies on coordination with WECC which establishes base case models for dynamic studies for the Western Interconnection. Failure to address this modeling problem either increases the risk to California electricity supply by grid instabilities and outages, or reduces the amount of power that can be imported into, and transported within, California.

Project Objectives

The high priority objectives for this project include

- Testing AC units to understand their behavior and how they can impact the grid.
- Develop improved load models to represent AC load behavior in grid studies.
- Identify potential solutions to mitigate the delayed voltage recovery problem.
- Develop a load composition data tool for the new WECC composite load model.

Additional research was directed towards producing white papers on other load modeling issues. These include:

- Technologies supporting, and applications for load monitoring.
- Uncertainty and sensitivity analyses.
- Solar generation and load models
- Review of nation-wide occurrences and potential solutions for Fault-Induced Delayed Voltage Recovery (FIDVR) – which is becoming the accepted name for the delayed voltage recovery phenomenon.
- Review of motor protection and their application in load modeling.

Project Results

For air conditioner modeling, the primary results include

- Testing of multiple units at SCE and BPA.
- Development of two load models to represent AC load behavior – a static performance model and a dynamic phasor model. Both of these models capture the fundamental features observed in laboratory tests.
- The performance model has been incorporated into the WECC composite load model in the PSLF simulation software; the dynamic phasor model is being programmed in PSLF.
- Research was conducted on identifying potential solutions to mitigate delayed voltage recovery. The solutions include potential unit-level solutions, and system level solutions. In the short term a practical approach may combine both. In the long term, changes in manufacturing standards would provide the most direct solution.
- Specifications for the load composition data tool are complete, and a prototype has been developed.

The white papers conclude

- Load monitoring is valuable for model validation, and may help with estimation of load composition and control performance. The white paper reviews monitoring technologies suitable for these purposes.
- Sensitivity models are needed to understand the models that are used to simulate the grid. This sensitivity model can be used to guide model validation, and to perform uncertainty analysis.
- Solar generators are connected through power electronic controls whose dynamics need be considered in models. Many installations will reside within traditional distribution networks and a representation for this could be added to the WECC composite load model.
- Fault-induced delayed voltage recovery occurs across the nation. Comparing and coordinating research efforts are underway. They have been the subject of two DOE sponsored workshops between the power industry and AC manufacturers.

- Motor protection is deemed necessary for accurate load models. The “delay” in delayed voltage recovery is due to the action of thermal protection. Motor protection on other installations needs attention.

Conclusions

Extensive progress has been made on load modeling since the commencement of this research project. The testing and analysis of air conditioners has led to the development of models to represent their behavior. WECC has introduced a new composite load model that includes the models resulting from this research project. The load composition data tool is designed to fill in the details required for the new load model. Project researchers have been leaders in the national discussion on fault-induced delayed voltage recovery, and the results and models from this research program inform that discussion. In short, the research conducted for this project is already in use by industry.

Recommendations

The primary goals of studying the delayed voltage recovery problem and improving models have been met. The study for best short- and long-term solutions continues.

It is imperative that California investigate further the way to mitigate the A/C stalling to prevent the FIDVR events that can have a negative impact in the grid or in a drastic scenario compromise grid operation.

The white papers conducted under this project have investigated other emerging issues with load models, some of which are already under investigation. Two new priority load modeling research topics include

- Sensitivity modeling for parameter estimation and model validation

New and improved Load Models and Load Composition methods have been developed for use in the Western Electricity Coordinating Council (WECC) region under this project. Continuing research is needed to develop and analyze sensitivity models to assist with model validation. It is also recommended to continue research on load monitoring to support load modeling activities for purposes of system validation and the potential use of top-down load models. Additionally, load-monitoring activities associated with direct load control offer opportunities not only for better load models, but also for loads to assist grid reliability.

- Modeling of controlled power electronic coupled devices, including solar generation.

As distributed PV systems become more widespread there is increasing concern about possible impacts on the electric system, especially within or adjacent to areas of high penetration. In contrast to typical power electronic loads that couple to the grid through a rectifier circuit, PV generators couple through an inverter circuit. The controls for power electronic grid coupling introduces dynamics related to voltage and frequency

that are not present in power electronic loads. New dynamic models for PV systems suitable for grid simulations are needed to examine possible impacts and potential solutions.

Benefits to California

The goal of this project was to develop specific models to improve the accuracy of dynamic simulations. There was a specific emphasis on the delayed voltage recovery problem which has a direct benefit to California:

- California utilities are known to be susceptible to fault-induced delayed voltage recovery. This research improved the fundamental understanding of the phenomenon and the results and models are guiding decisions to help mitigate the problem. A specific benefit of such mitigation is to decrease the likelihood that such events will be contained and not lead to widespread outage.

Additional what papers were directed towards related dynamic load modeling issues. Better dynamic load models offer several benefits to California:

- Improved models aid the decision process for the investment in system solutions to the delayed voltage recovery problem, and other dynamic issues.
- The use of improved model in system studies will increase confidence in the specification of path rating and the deployment of remedial action schemes. This increases confidence in operations.

1.0 Introduction

The research presented in this report focuses on power system loads and their impact on system dynamic behavior. Unusual delayed voltage recovery events in Southern California motivated this work. Correspondingly, much of this program's research addressed the causes, modeling, and solutions to these types of events. These research activities supported and were supported by the WECC Load Modeling Task Force (LMTF). Members of the LMTF served as technical advisors for this work, and supported complementary research projects. The results of this research program directly contributed to activities of the LMTF, and are being incorporated into system planning studies in WECC. The results are also informing potential policy decisions in the industry with regard to air conditioner units.

This chapter reviews the background motivating this program, provides an overview of the research activities, and summarizes the results and recommendations of this work.

1.1. Background

Grid planning and operating decisions rely on simulations of dynamic behavior of the power system. Both technical and commercial segments of the industry must be confident that the simulation models and database are accurate and up to date. If the transfer limits are set using overly optimistic models, a grid operator may unknowingly operate the system beyond its capability, thereby increasing the risk of widespread outages, such as occurred during summer 1996 outages. If the models are pessimistic, a grid operator may be overly conservative and impose unnecessary restrictions on the transfer paths, thereby unnecessarily raising electricity costs or increasing the risk of power shortages in energy deficient regions. Therefore, having realistic models is very important to ensure reliable and economic power system operation.

A power system model consists of generator, transmission and load models. Load representation is the most challenging and the least accurate of these three components. A vast amount of work has been done over the last 30 years including two issues of Institute of Electrical and Electronic Engineers (IEEE) load modeling recommendations and literally hundreds of technical papers worldwide. Yet the sheer magnitude of the modeling of load components, the complexity of the load compositions and the hourly and seasonal change in loads in the real system represent a challenge to load representation in power system studies.

In 2001, an "interim" composite load model containing a static part and a dynamic part (modeled essentially to IEEE load modeling recommendations) was developed and implemented in the WECC. This was a first of its kind region-wide implementation in North America in a North American Electric Reliability Council region. The model was designed primarily to capture the effects of dynamic induction motor loads for highly stressed North to South oscillatory flow conditions during summer peaks in the WECC, which can limit power imports into California, or alternatively, increase the risk of relying on higher levels of imports. At the time of its implementation, the WECC Modeling and Validation Work Group (MVWG)

stated that the “interim” model should be replaced with a full-scale composite load model WECC-wide. The WECC LMTF was assigned this task in 2002.

The interim motor model did not capture significant dynamic phenomena that have been observed in certain locations of the WECC. Of particular concern is the inability of the interim load model to represent a delayed voltage recovery from transmission fault. In one particular event, it took approximately 30 seconds for voltage to recover, while the simulations predicted almost instantaneous voltage recovery. Further improvement to the interim model is required also in the simulation of the power oscillations on the California – Oregon Intertie and other key interties in the WECC. Accurate load models are required to assess the damping of power oscillations. To improve models it useful to examine events to understand their cause.

SCE and other utilities experience occurrences of delayed voltage recovery following faults on their electrical systems as shown in Figure 1. Under normal conditions voltage recovers to nominal levels less than one second after the fault is cleared, but over the past few years there have been several instances at some SCE substations when voltage recovery was delayed for more than 30 seconds after normal fault clearing. These events primarily occurred during the heavy summer load at substations located in hot climates and serving new housing developments. Stalling air conditioner units are believed to be causing the delayed voltage recoveries.

Figure 1 shows a typical delayed voltage recovery profile on a SCE 220 KV circuit. This figure indicates that right after the fault, voltage decreased to 79 percent of nominal voltage (point 1). The radial distribution circuit voltage being much lower, the dip in voltage caused air conditioning units to stall; the stalled air conditioning units kept the voltage from recovering to a nominal level (point 2). When the air conditioner units’ thermal overload protection switches tripped, the voltage recovered, but overshot the nominal voltage (in this case 6 percent above). Because the capacitor banks were still connected to the circuit an over-voltage occurred (point 3). This over-voltage caused another problem, the capacitor banks tripping off (point 4). With the capacitors tripped off and the load (including air conditioners) returning, the voltage went below the nominal voltage (points 5 & 6) making the circuit more vulnerable to other similar chains of events.

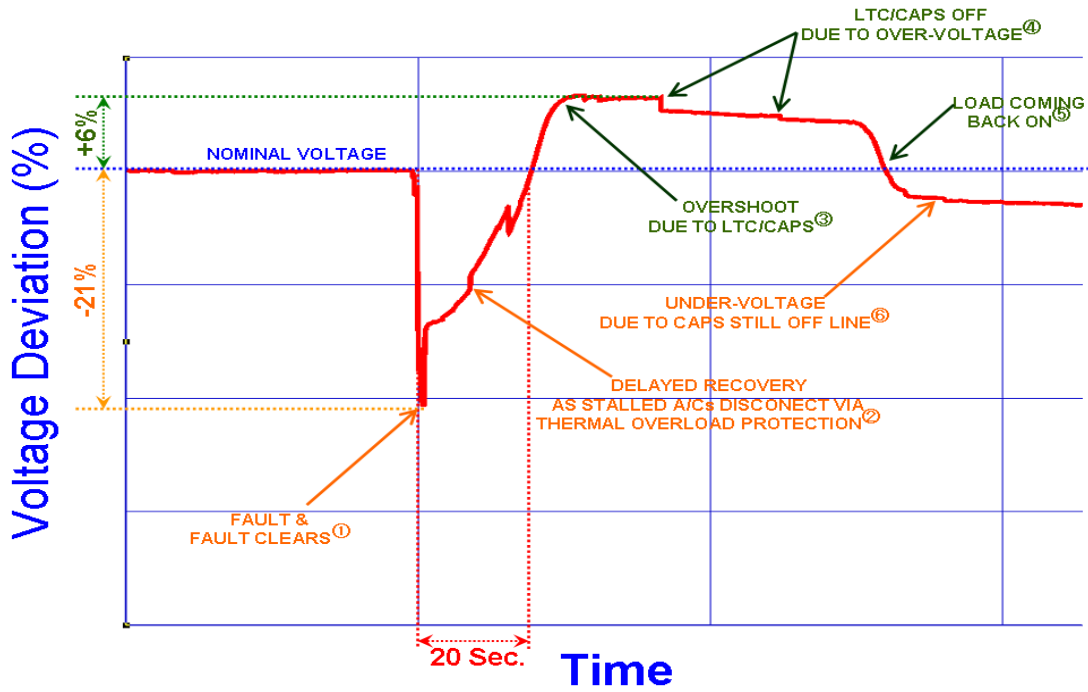


Figure 1 Typical Delayed Voltage Recovery

The WECC interim load model did not replicate the observed system response of the delayed voltage recovery events. Specifically, the WECC motor model does not accurately represent the behavior of small induction motors used in air conditioner compressors. This mismatch of real measurements versus the WECC interim load model is shown in Figure 2.

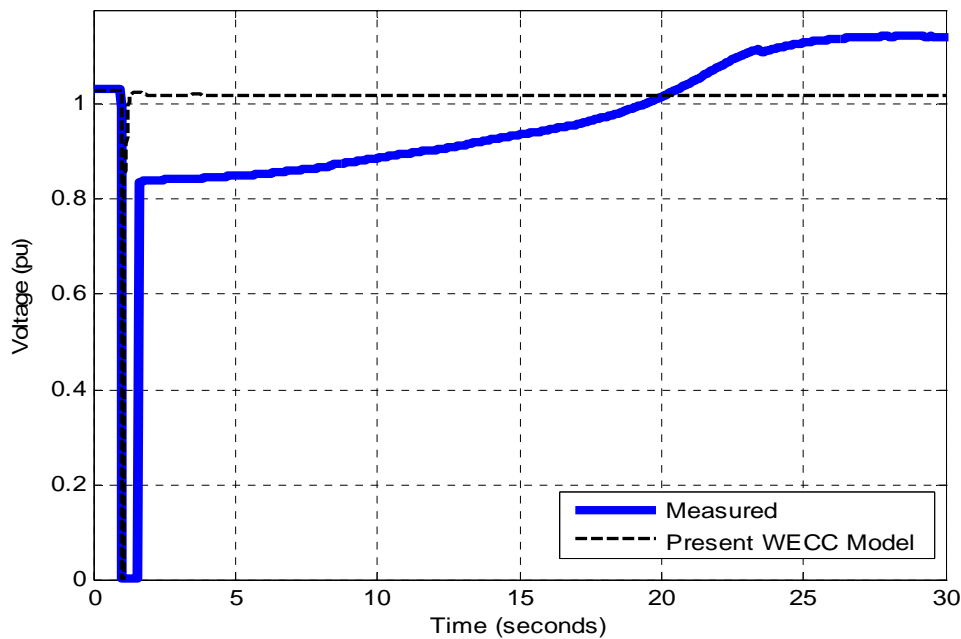


Figure 2 Delayed Voltage Recovery

The purpose of this research program is to improve the accuracy of load models in general, and air conditioner models in particular. In addition to improved modeling, researchers investigated ways to mitigate the negative impact of stalled air conditioners on the grid. Failure to address this modeling problem either increases the risk to California electricity supply by grid instabilities and outages, or reduces the amount of power that can be imported into, and transported within, California.

The new WECC Composite Load Model is shown below in Figure 3. This detailed model enables simulations to replicate observed behavior in measurements. The model includes an electrical representation for a distribution system including a substation transformer, shunt reactances, and a feeder equivalent. This presents the realistic separation of end-use load from the transmission network. The end-use load models include four types of motor models, including representations for three phase air conditioners and single-phase air conditioners. It also includes a separate characteristic for electronic loads – which increases in percentage and importance of load.

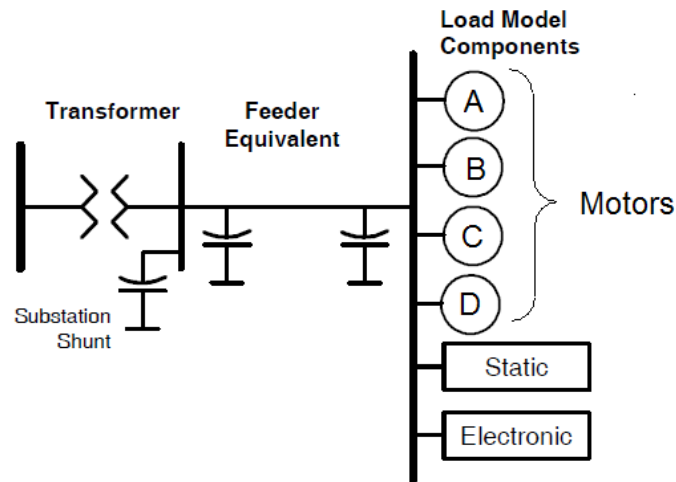


Figure 3 WECC Composite Load Model

Formerly the interim load model was uniformly applied across the entire system. The new composite load model is intended to vary. It is recognized, for instance, that air conditioner load is not uniform across the system, nor heating load, industrial load, etc. With the new model comes a challenge of describing the load characteristics for each location.

The remainder of this chapter contains an introduction to the research projects and a summary of results and recommendations. The subsequent chapters discuss the individual projects in some detail, leaving the complete details to reports attached in the appendices.

1.2. Overview of Research, Results, and Recommendations

The primary research projects conducted under this program were aimed to better load model representation in WECC. There was particular interest in air conditioner loads to characterize the observed delayed voltage recovery phenomenon. On this topic there were three area of research:

1. Air conditioner testing and modeling
2. Potential Solutions to the delayed voltage recovery problem

These topics are the subjects of Chapters 2-3 respectively.

The load model data tool to help vary the composite load model by location is presented in Chapter 4:

3. Load composition data tool

In addition to these main topics listed above and mentioned in Section 1.1, several preliminary studies were conducted to examine research needs in areas relevant to load modeling. These include

4. Load monitoring (Chapter 5)
5. Uncertainty analysis (Chapter 6)
6. Solar generation and load models (Chapter 7)
7. Fault-induced delayed voltage recovery (Chapter 8)
8. Motor protection (Chapter 9)

1.2.1. Air Conditioner Testing and Modeling

Air Conditioner Testing

Air conditioner units were acquired and tested by staff at Southern California Edison and Bonneville Power Administration. SCE acquired 10 units, and BPA acquired 18 units. Tests were conducted to reveal the dynamic behavior of the loads subject to fault conditions and system voltage and frequency oscillations. The conditions contributing to stall were characterized, including temperature, voltage, fault duration and type of unit.

Principal Findings:

- **Air conditioners are prone to stall quickly – even for short duration, normally-cleared faults.**

- Stalled currents, active power, and reactive power levels are multiples of nominal values
- Unit-level under-voltage contacts do not remove stalled air-conditioners from the system. (That is, the observed voltage sags still exceed the level at which they act.)
- Unit-level thermal protection eventually will remove the stalled units from the system.

These characteristics are consistent with the observed delayed voltage recovery phenomenon: units stall quickly – high stall current pulls down the system voltage – voltage recovers as thermal protection removes units from the system after some delay – the recovered voltage exceeds the pre-fault level due to load loss.

Air Conditioner Modeling

Guided by data collected from the tests, project researchers used both a top-down and a bottom-up approach to develop two different types of models for air conditioning units. The static “performance model” (top-down) represents the active and reactive consumptions as a function of temperature and voltage. There are three regimes of operation: running, stalled, and tripped (off-line). For each regime, a polynomial function of voltage is used.

Principal Finding:

- The static performance model gives a good match to static running and stall characteristics of tested units.

Principal Result:

- The performance model has been incorporated into the PSLF model for the WECC composite load model.

WECC members have run and are analyzing simulations of the Interconnect with this model in place.

The second model, the “dynamic phasor model,” (bottom-up) was developed from first principles. The researchers adapted a standard single phase induction motor model - the type of motor driving air-conditioner compressors – to a form suitable for the simulation programs used by WECC. This physically-based model is mathematically represented by nonlinear differential and algebraic equations, and it is similar in form to other motor models used in power system dynamic simulations.

Principal Finding:

- The dynamic phasor model gives a good match to static and dynamic behavior observed in unit tests.

Principal Result:

- WECC has hired a consultant to program the dynamic phasor model in the PSLF simulation software.

These two models are relatively new and are currently under necessary evaluation by WECC members.

Recommendation: WECC members evaluate the performance model and the dynamic phasor model in their studies.

1.2.2. Potential Solutions to Delayed Voltage Recovery

Testing units, understanding the phenomenon, and the use of better models does not solve the problem. To address the problem with potential solutions, project researchers examined unit-level solutions and system-level solutions. Generally unit-level solutions involve removing the stalled units as quickly as possible and the corresponding project tested different technologies for achieving this object. Perhaps the most promising in the short time frame is the use of controllable thermostats. The system level solutions consider fast-acting controlled reactive power sources.

Principal Recommendation:

- **A practical near-term potential solution involves both the use of unit-level control to remove the stalled air-conditioner, and system-level control of reactive power.**

Because the unit test results show that the air conditioners are prone to stall for normally-cleared faults, there is little opportunity in the short term to prevent this stalling. Once stalled the units must be taken off-line as quickly as possible. Fast reactive power controls are needed to maintain proper system voltage when air conditioner load is lost and then returns a short while later.

The ideal long-term solution involves the design of air-conditioner units that have a certain amount of low-voltage ride through, and to automatically and quickly remove stalled units from service. This type of solution requires cooperation with manufacturers. Motivated by research conducted under this program and recognizing that the delayed voltage recovery is a problem across the country, the U.S. Department of Energy has hosted two workshops between power industry and air conditioner manufacturers to discuss this topic. Researchers on this project were key contributors to the workshop.

Principal Result:

- **Two U.S. Department of Energy Workshops on Fault Induced Delayed Voltage Recovery (FIDVR) – April 2008, and September 2009.¹**

NERC has also published a white paper on FIDVR²

¹ 2008 workshop presentations are available at <http://sites.energetics.com/acstallingworkshop/agenda.html>. 2009 workshop presentations have not been posted.

Recommendation:

- **Continue engagement with industry to establish standards to address the delayed voltage recover problem.**

1.2.3. Load Composition Data Tool

The detailed WECC composite load model is intended to model different end-use loads depending on location. The load composition data tool uses a database with information about different locations (weather, typical end-use load by customer type). Then it helps compute the load model parameters for a given location, guided by the percentage of different customer type at that location: residential, commercial, industrial, and agricultural.

Principal Results:

- **Specifications for the load composition data tool.** This is necessary for further vendor development.
- **Prototype load composition data tool.**³

Recommendation:

- **Use prototype tool for WECC studies, and encourage WECC to pursue development.**

1.2.4. Load Monitoring

The goal of load monitoring is to disaggregate load composition by monitoring electrical waveforms on feeders. This white paper focuses on the technologies that may support load monitoring and potential applications.

Principal Finding:

- **Monitoring equipment is available that could assist load monitoring**
- **Applications include providing valuable information for model validation, estimating load composition (potentially in real time), and aiding in load-centered control performance.**

As part of a complementary study supported by BPA, researchers have examined electrical signals from monitored feeders to determine if information may be available for load monitoring. Their initial assessment (unpublished to date) is that there is information in the data. However, it would require a major research project to attempt the disaggregation, and it should be considered high-risk, high payoff research.

Recommendation:

² Available at www.nerc.com/docs/pc/tis/FIDV_R_Tech_Ref_V1-1_PC_Approved.pdf.

³ Available at <http://sourceforge.net/projects/gridlab-d/files/load-composition/>.

- **Consider initiating a project on load monitoring.**

In comparison to other recommendations, this should be considered a lower-priority task.

1.2.5. Uncertainty Analysis

Load models remain the least certain of modeled elements in system simulations. This white paper examines the use of sensitivity-based models for uncertainty analysis. The paper highlights several uses for sensitivity models.

Principal Findings:

- 1. Sensitivity-based models can be used to estimate uncertainty in simulation outcomes.**
- 2. Sensitivity-augmented simulations (trajectory sensitivities) can help identify when a simulation result is near instability.**
- 3. Sensitivity-based models can be used to guide parameter estimation for purposes of model validation.**

Practical application for the first finding is relatively straight-forward: given a simulation result, a sensitivity model expressed in terms of (load model) parameters, and a characterization of the uncertainty in the load model parameters (probability density) – one simply calculates the range of simulation outcomes. Additional research is not required on the mechanics, but estimation of uncertainty in parameter values is needed.

The second finding is explained by noting that an unstable trajectory is highly sensitive to almost all perturbations. Trajectory sensitivities will be high near a point of instability, even if the instability is not directly observed in the result. The tool used to calculate these sensitivity trajectories relies on a particular class of simulation algorithm that, unfortunately, are not used in the most common power system simulation software.

The third finding touches on the important problem of reconciling observed behavior and simulated behavior. This load modeling program was motivated by the inability of the interim load model to represent the delayed voltage recovery problem. The new composite load model has the ability to represent this behavior, but that does not necessarily mean that it will if the model parameters are incorrect. Tuning of model parameters to match observed data, and then validating with more data is important. In a complementary project supported by BPA, researchers have conducted preliminary research on this topic using an approach similar to that outlined in this uncertainty analysis white paper. The results are promising but require a dedicated research project to complete.

Recommendation:

- **Initiate a projected dedicated to WECC model validation**

1.2.6. Solar Generation and Load Models

This white paper takes a first look at solar generation in distribution systems. While this is not strictly load modeling, it has features similar to load models in a power system context. The installations considered here are widely distributed and relatively small compared to large generating stations.

Solar generation interfaces to the grid through power electronic circuits. When placed in distribution grids they might be considered to appear as negative power electronic loads. However, their controls and operation differ from typical power electronic loads that essentially operate near constant power at unity power factor for a wide range of voltage. The solar power generator power electronics use a Maximum Power Point Tracking (MPPT) function in the DC/DC converter module. This dynamics of this module impacts the dynamics as seen from the grid. This and the impact of protection equipment necessitate the testing and development of a model for use in power grid studies.

Recommendation:

- **Conduct and complete comprehensive tests of PV generators and develop a suitable model grid simulations**

This should be considered a high priority research item. The white paper indicates that such tests have been initiated by SCE with the National Renewable Energy Lab.

1.2.7. Fault-Induced Delayed Voltage Recovery

This white paper reviews the literature on delayed voltage recover, and presentations at meetings and workshops. The paper provides an explanation for the phenomenon, lists sample reported occurrences, and discusses the potential solutions to the problem.

The short-term practical solutions combine unit-level and system-level design solutions. These are consistent with the solutions discussed in the potential solutions section. The ideal long-term solution involves participation with industry manufacturers to include modifications to unit design to help mitigate or prevent stalling. As noted above, this topic has received considerable attention: it is the subject of a NERC white paper, and has been the focus of two DOE sponsored workshops.

1.2.8. Motor Protection

In part this topic is addressed in the delayed voltage recovery research. The voltage response directly depends on the protection. The “delay” in delayed voltage recovery is a due to the delayed response of thermal protection. For these devices the response of protection has been studied in the laboratory experiments in this program.

A review of the National Electric Code shows that air conditioner protection is treated in a section on its own, and that other motor protection requirements are dictated in another section. These requirements may form a basis for initial modeling motor protection under the

assumption that most installations are up to code. A more detailed investigation is warranted to further clarify motor protection installations in practice.

Recommendation: Conduct in-depth study of practical motor protection in installations.

Comment: WECC has initiated a study of this type.

1.3. Summary

The primary objectives of this program were directed towards the development of a new load model that would be suitable for study of the delayed voltage recovery phenomenon. Extensive laboratory experiments were conducted, and load models were developed for this purpose. The near-term practical solutions to this problem appear to involve unit-level control (or thermostatic if possible), and system-level reactive power controls. The best long-term solution is sought with cooperation of manufacturers, and two DOE sponsored workshops have been held with this objective. Continued effort is needed to establish policies and standards to ensure manufacture of units with desirable protection when stalled, or with some low-voltage ride through capability.

The new WECC composite load model is a great improvement over the interim model. It is necessary to populate the model with credible parameters and a prototype load composition data tool has been designed for this purpose.

Recommended new priority load modeling research include

- Sensitivity modeling for parameter estimation and model validation

New and improved Load Models and Load Composition methods have been developed for use in the Western Electricity Coordinating Council (WECC) region under this project. Continuing research is needed to develop and analyze sensitivity models to assist with model validation. It is also recommended to continue research on load monitoring to support load modeling activities for purposes of system validation and the potential use of top-down load models. Additionally, load-monitoring activities associated with direct load control offer opportunities not only for better load models, but also for loads to assist grid reliability.

- Modeling of controlled power electronic coupled devices, including solar generation.

As distributed PV systems become more widespread there is increasing concern about possible impacts on the electric system, especially within or adjacent to areas of high penetration. In contrast to typical power electronic loads that couple to the grid through a rectifier circuit, PV generators couple through an inverter circuit. The controls for power electronic grid coupling introduces dynamics related to voltage and frequency that are not present in power electronic loads. New dynamic models for PV systems suitable for grid simulations are needed to examine possible impacts and potential solutions.

1.3.1. Benefits to California

The goal of this project was to develop specific models to improve the accuracy of dynamic simulations. There was a specific emphasis on the delayed voltage recovery problem which has a direct benefit to California:

- California utilities are known to be susceptible to fault-induced delayed voltage recovery. This research improved the fundamental understanding of the phenomenon and the results and models are guiding decisions to help mitigate the problem. A specific benefit of such mitigation is to increase the likelihood that such events will be contained and not lead to widespread outage.

Additional what papers were directed towards related dynamic load modeling issues. Better dynamic load models offer several benefits to California:

- Improved models aid the decision process for the investment in system solutions to the delayed voltage recovery problem, and other dynamic issues.
- The use of improved model in system studies will increase confidence in the specification of path rating and the deployment of remedial action schemes. This increases confidence in operations.

2.0 Air Conditioner Modeling

2.1. Introduction

This chapter summarizes the air conditioner testing procedures and results from studies conducted by Southern California Edison for this project. Similar tests and consistent results were obtained by independent studies conducted by Bonneville Power Administration. These tests and results were presented at various WECC Load Modeling Task Force Meetings and they form the basis for the modeling efforts.

The results of the air conditioner tests help quantify the observed delayed voltage recovery behavior:

- Air conditioners stall during normally cleared fault scenarios.
- Contactors operate between 35% and 55% nominal voltage. Stalled air conditioners are electrically connected to the system during post-fault delayed voltage events until they trip on thermal protection.
- Thermal protection trips air conditioner units after some voltage-dependent time. After the removal of stalled air conditioners from the system, the voltage recovers, and typically exceeds the pre-fault voltage. The delay is due to the delay in thermal protection operations.

The details of the test procedures and the results are presented in Appendices A and B. The summary of results from Appendix B is presented here.

These test results characterize much of the behavior of air conditioner loads during conditions under which the delayed voltage recovery phenomenon is likely to occur. These devices need to be correctly modeled to capture their impact on dynamic stability characteristics. Researchers on this project undertook two different approaches to modeling the tested behaviors. A top-down approach characterized the raw data from tests via a static model whose mathematical form was chosen to match the data. A bottom approach imposed a physically based-model and fit parameters to match the data.

The details of the model development are contained in Appendices C and D, from which the summaries in this chapter are extracted.

2.2. Task Approach

2.2.1. Laboratory Testing

SCE began air conditioner testing in 2005 to determine how the units would respond when exposed to various under-voltage transient conditions. The test results help SCE to properly model the electrical system and determine possible solutions. SCE tested ten (10) air conditioner units, in its Pomona Electric Vehicle Technical Center (EVTC), typically found in the service territory. The diversity of the tested air conditioner units included sizes (tonnage),

compressor technology (reciprocating and scroll), refrigerant technology (R22 and R-410A), vintage (new and old), and efficiencies (10 thru 13 SEER).

The ten (10) air conditioner units were tested under different undervoltage transients including the Long Notch, Delayed Recovery and Circuit Breaker Clearing type of transient. The Long Notch transient (drop in voltage that was held for 30 seconds) was used to establish the threshold voltage where the air conditioner compressor stalled. The Delayed Recovery transient (drop in voltage followed by a 30 seconds recovery to nominal voltage) simulates the typical delayed voltage recovery event observed in SCE system. The Circuit Breaker transient (short duration drop in voltage held for 3, 6, 9, and 12 cycles) simulates the typical transient generated by the tripping and reclosing of circuit breakers commonly used in the SCE system.

In addition, SCE performed additional testing on the air conditioners for the WECC Load Modeling Task Force which included frequency oscillations, voltage oscillations, and different arrangements of undervoltage transients.

2.2.2. Performance Model

The performance model sets out to capture the observed behavior air conditioner models as a function for voltage. This generic power/voltage form shown below in Figure 4 is motivated from test results summarized in the previous chapter. There are three operating characteristics, running stalled, and tripped. The mathematical models relating voltage to real and reactive power in running and stalling regions are given below. In the tripped region the motor is removed from service, and the amount of load removed is determined using thermal protection characteristics.

Running:

$$P_{run} = a_1 + \frac{a_2}{V - a_0} + a_3(V - a_0) + a_4(V - a_0)^4$$

$$Q_{run} = b_1 + \frac{b_2}{V - b_0} + b_3(V - b_0) + b_4(V - b_0)^4$$

Stalling:

$$P_{stall} = K_{p1}V^3 + K_{p2}V^2$$

$$Q_{stall} = K_{q1}V^3 + K_{q2}V^2$$

Temperature dependence for each parameters a and b in the above equations of P_{run} , Q_{run} , P_{stall} and Q_{stall} :

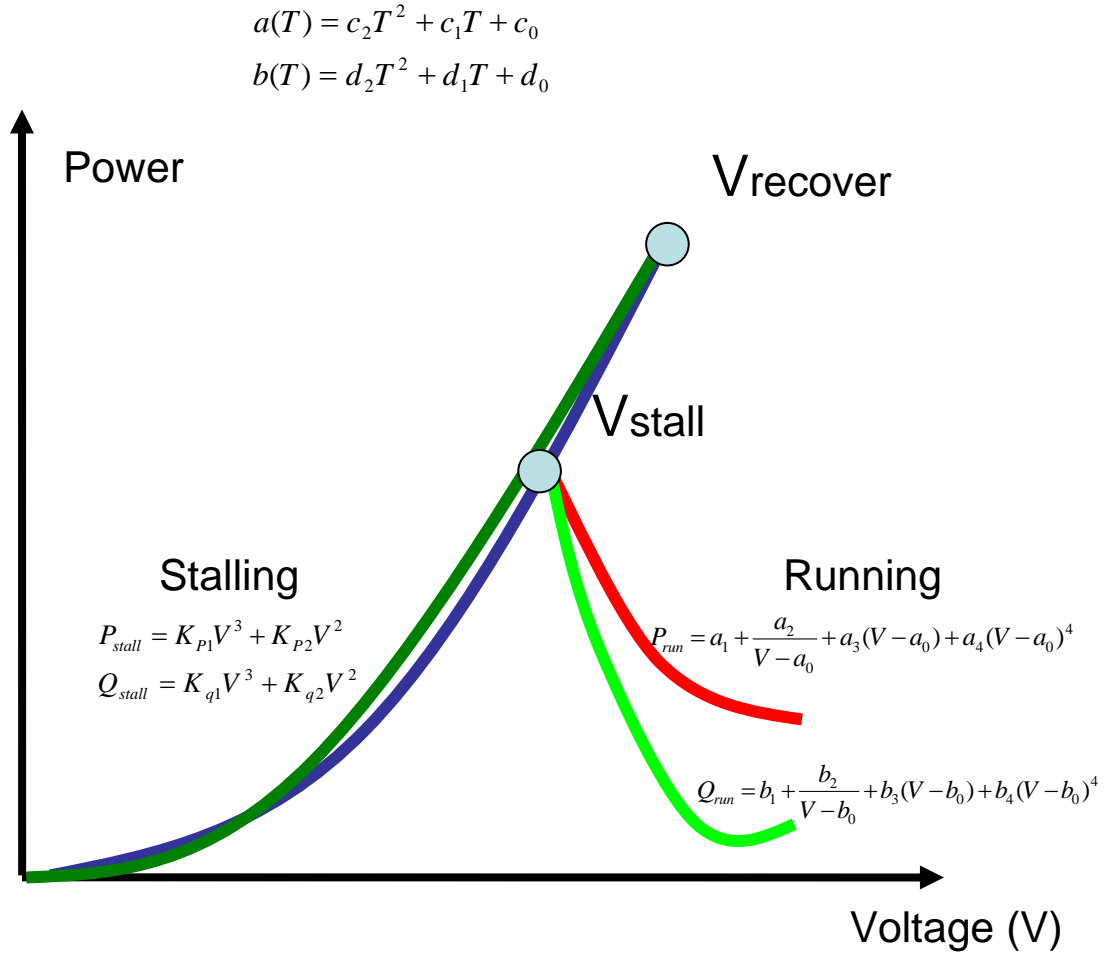


Figure 4 Power/Voltage Curves

2.2.3. Dynamic Phasor Model

The objective is to develop a model that represents the impact of residential air-conditioners on power system dynamic performance. The principal interest is in modeling the air-conditioner impact on dynamic voltage stability and oscillation damping. The model is expected to:

- Accurately capture the sensitivities of motor real and reactive power requirements as a function of its voltage and frequency
- Represent the motor impact on damping of low frequency inter-area oscillations
- Reasonably predict the stalling phenomenon, as well as accurately represent motor current, real and reactive power during the stalled state

The equations below represent a single-phase induction motor driving a compressor load. This model is derived from first principles and verified using data from laboratory tests conducted

by Bonneville Power Administration. The details of the model derivation are presented in Appendix D. The mathematical representation for the model is

$$\begin{aligned}
|V_s| &= \left(r_{ds} + j \frac{\omega_s}{\omega_b} X'_{ds} \right) (I_{ds}^R + jI_{ds}^I) + j \left(\frac{\omega_s}{\omega_b} \right) \frac{X_m}{X_r} (\Psi_{dr}^R + j\Psi_{dr}^I) \\
|V_s| &= \left(r_{qs} + j \frac{\omega_s}{\omega_b} X'_{qs} + j \frac{\omega_b}{\omega_s} X_c \right) (I_{qs}^R + jI_{qs}^I) + j \left(\frac{\omega_s}{\omega_b} \right) \frac{nX_m}{X_r} (\Psi_{qr}^R + j\Psi_{qr}^I) \\
\begin{bmatrix} \Psi_f^R + j\Psi_f^I \\ \Psi_b^R + j\Psi_b^I \end{bmatrix} &= \begin{pmatrix} 1 & -j \\ 2 & 1 \end{pmatrix} \begin{bmatrix} \Psi_{dr}^R + j\Psi_{dr}^I \\ \Psi_{qr}^R + j\Psi_{qr}^I \end{bmatrix} \quad \begin{bmatrix} \Psi_{dr}^R + j\Psi_{dr}^I \\ \Psi_{qr}^R + j\Psi_{qr}^I \end{bmatrix} = \begin{bmatrix} 1 & 1 \\ j & -j \end{bmatrix} \begin{bmatrix} \Psi_f^R + j\Psi_f^I \\ \Psi_b^R + j\Psi_b^I \end{bmatrix} \\
\begin{bmatrix} I_f^R + jI_f^I \\ I_b^R + jI_b^I \end{bmatrix} &= \begin{pmatrix} 1 & -jn \\ 2 & 1 \end{pmatrix} \begin{bmatrix} I_{ds}^R + jI_{ds}^I \\ I_{qs}^R + jI_{qs}^I \end{bmatrix} \quad \begin{bmatrix} I_{ds}^R + jI_{ds}^I \\ I_{qs}^R + jI_{qs}^I \end{bmatrix} = \begin{bmatrix} 1 & 1 \\ j/n & -j/n \end{bmatrix} \begin{bmatrix} I_f^R + jI_f^I \\ I_b^R + jI_b^I \end{bmatrix} \\
T_o' \frac{d}{dt} (\Psi_f^R + j\Psi_f^I) &= X_m (I_f^R + jI_f^I) - (\text{sat}(\Psi_f, \Psi_b) + j(\omega_s - \omega_r)T_o') (\Psi_f^R + j\Psi_f^I) \\
(\Psi_b^R + j\Psi_b^I) &= \frac{X_m (I_b^R + jI_b^I)}{(\text{sat}(\Psi_f, \Psi_b) + j(\omega_s + \omega_r)T_o')} \\
\frac{2H}{\omega_b} \frac{d\omega_r}{dt} &= \frac{X_m}{X_r} 2(I_f^I \Psi_f^R - I_f^R \Psi_f^I - I_b^I \Psi_b^R + I_b^R \Psi_b^I) - T_{mech} \\
I_s &= [(I_{ds}^R + jI_{ds}^I) + (I_{qs}^R + jI_{qs}^I)] e^{j\phi}
\end{aligned}$$

This is a detailed representation that is similar in structure and derivation to many standard motor models. The variables represent physical quantities include voltage, flux, rotor speed, torque, etc. (See Appendix D for complete description). While it may appear complex to a reader unfamiliar with such equipment, it should be understandable to experts. By comparison, it is certainly more complex than the performance model presented in the previously. It however offers to capture dynamic phenomenon not represented by the performance model. The value of this dynamic information is still under investigation.

2.3. Task Results

2.3.1. Test Results

This summary section contains the testing results for the air conditioning units when exposed to the *delayed recovery* type of transients, similar to that observed during the delayed voltage recovery events at SCE.

Stall Voltage

The ten tested air conditioning units had similar stalling voltages within $\pm 5\%$ (voltage level where compressor ceased to turn) at each of the tested temperatures. These voltages varied with the outdoor air temperature that the compressor and condensing coils were subjected to. The stall response time (time it takes the air conditioner compressor to stop turning) on the tested air conditioners was approximately 6 cycles after the under-voltage condition occurred. Test results indicated that the stalling voltage average at 80 °F is 61%, at 100 °F is 65%, and at 115 °F is 69%. Table 1 indicates the stalling windows (voltages between the stall threshold voltage and the contactor dropout voltage) for the ten tested air conditioner units when exposed to the *delayed recovery* type of transients. Air conditioner unit #10 did not stall at 80 °F and it operated down to the voltage where the contactor opened without stalling. Opening of the contactor did not prevent the air conditioner units from stalling; it just delayed stalling until the contactor reclosed.

Table 1 Stall Window

	Stall Window (80°F)		Stall Window (100°F)		Stall Window (115°F)	
	Stall Threshold	Contactor Dropout	Stall Threshold	Contactor Dropout	Stall Threshold	Contactor Dropout
AC #1	64%	50%	66%	50%	68%	50%
AC #2	56%	50%	61%	50%	66%	50%
AC #3	59%	35%	67%	35%	73%	35%
AC #4	62%	50%	67%	50%	75%	50%
AC #5	57%	50%	62%	50%	67%	45%
AC #6	59%	45%	64%	40%	68%	40%
AC #7	57%	50%	61%	50%	67%	50%
AC #8	64%	45%	67%	55%	69%	50%
AC #9	67%	55%	70%	55%	73%	55%
AC #10	none	45%	64%	50%	68%	55%

The major influence on the three stall parameters, current (I_{STALL}) and real power (P_{STALL}) and reactive power (Q_{STALL}), was the supply voltage. The higher the terminal voltage when the stall occurs, the higher the stall parameter values. The values of these parameters were also proportional to the unit size.

Figure 5 below indicates the typical current (I) behavior of an air conditioner unit when exposed to the *delayed recovery* type of transient. The normal running current (I_{FLA}) is approximately 17, 22, and 27 Amps at nominal voltage (100% or 240 V) for the three simulated outdoor temperatures 80, 100, 115 °F respectively. The normal running current was found to be inversely proportional to the supply voltage, the lower the voltage the higher the normal running current. This behavior continues down to where the unit starts stalling (stalling

threshold voltage). The current jumped from as low as 17 Amps (at nominal voltage and 80 °F) to 100 Amps (at 70% applied voltage) when the unit stalled. The stall current (I_{STALL}) was found to be directly proportional to the applied voltage; the higher the voltage applied to the compressor terminals during the stall the higher the stall current (blue, green, and red plot lines). This behavior continues down to where the contactor drops out (contactor drop out voltage).

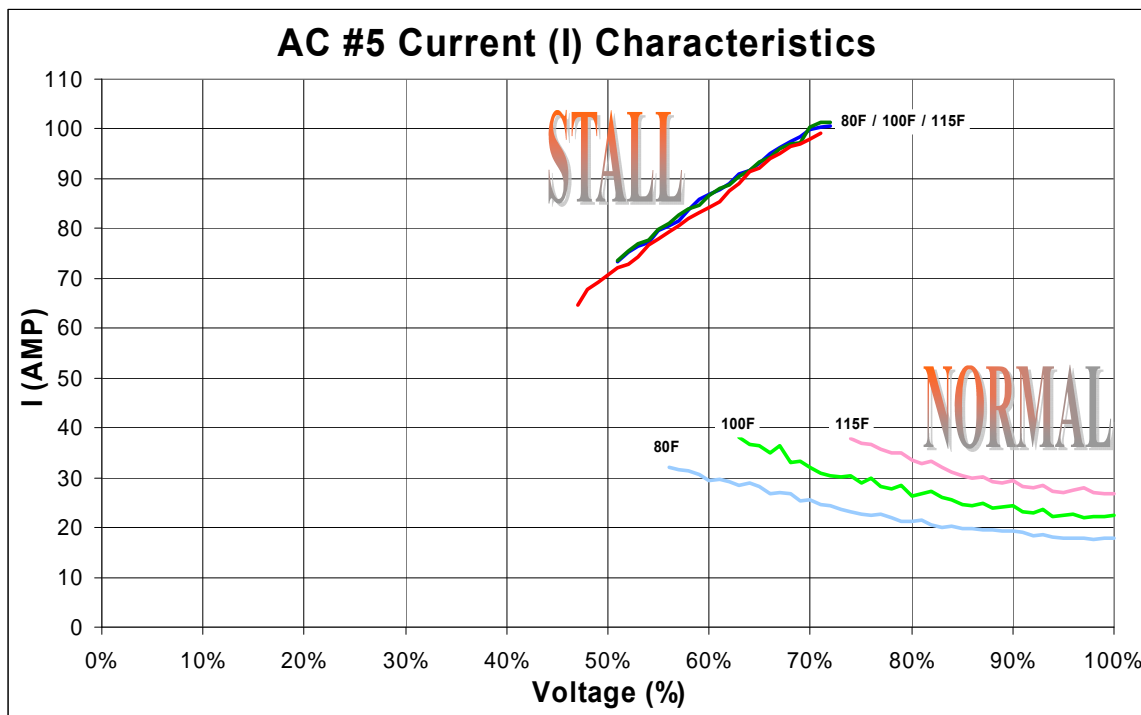


Figure 5 Stall Current

Figure 6 indicates the typical power (real P and reactive Q) behavior of an air conditioner unit when exposed to the *delayed recovery* type of transient. The normal running real power (P) is approximately 4000, 5000, and 6000 Watts and the normal running reactive power (Q) is approximately 900, 1100, and 1300 VARs at nominal voltage (100% or 240 V) for the three simulated outdoor temperatures 80, 100, 115 °F respectively. The normal real power (NORMAL WATTS plot line) did not change significantly when the applied voltage decreased all the way down until the unit stall point. The normal reactive power (NORMAL VARS plot line) was found to be inversely proportional to the applied voltage down to approximately 85% then started being proportional to the applied voltage until the unit stalled (stall threshold voltage).

The real power jumped from 4000 Watts (at nominal voltage and 80 °F) to as high as 12,000 Watts (at 70% applied voltage) when the unit stalled. The reactive power jumped from 900 VARs (at nominal voltage and 80 °F) to as high as 12,000 VARs (at 70% applied voltage) when the unit stalled. When stalled, both the real and reactive powers were found to be directly proportional to the applied voltage, the higher the voltage the higher the Watts and VARs. This behavior continues down to where the contactor drops out (contactor drop out voltage).

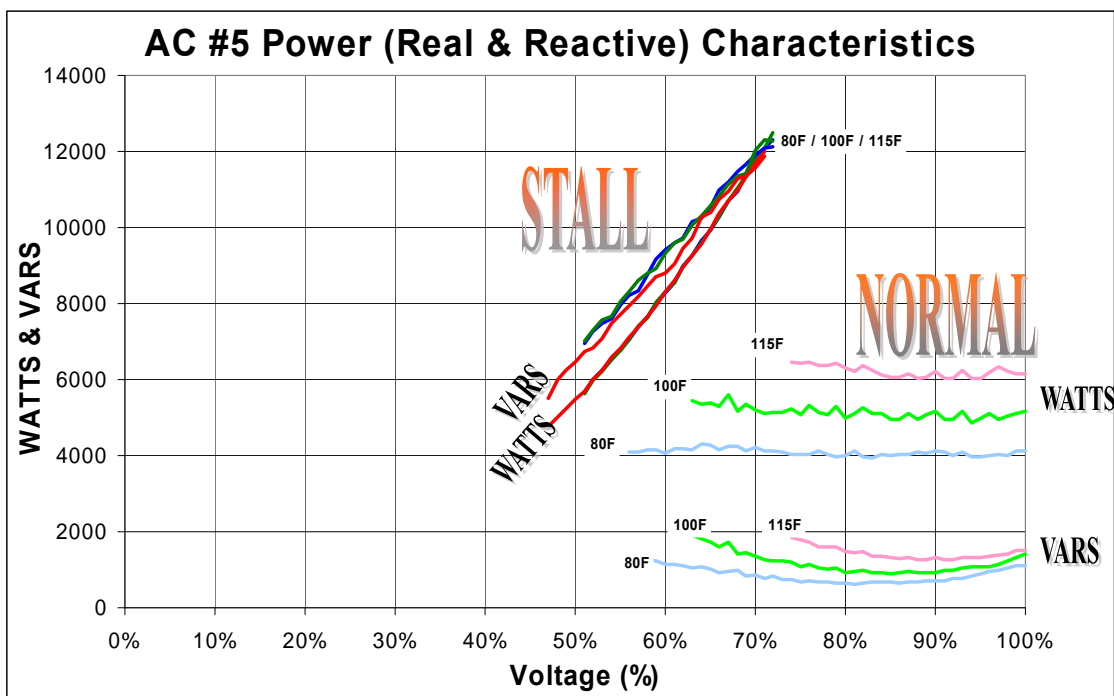


Figure 6 Stall Real and Reactive Power

Metering Devices

Air conditioner systems usually use either thermostatic expansion valves (TXV) or orifice metering devices to control the proper flow of refrigerant in the high-pressure side of the cooling coil (indoor coil). Controlling the proper flow of refrigerant in the high-pressure side is critical because too much flow can cause the cooling coil to freeze and therefore not produce any cooling. The orifice-metering device has a unique advantage that it brings the pressure quickly into equalization after the compressor shuts down. The TXV helps the cooling coil maintain proper flow using a sophisticated feedback system but pressure equalization is achieved at a much slower rate (1 to 2 minutes) than the orifice. The TXV helps the cooling coil have the proper flow when the system is undercharged, maintaining its efficiency. It offers no

improvement when the system is overcharged. Since TXVs are commonly used in new air conditioner installations, most of the air conditioner units tested had TXV valves.

When stalled, the compressor ceases to turn and therefore does not generate pressure. The high-pressure (liquid line) and low-pressure (vapor line) need to equalize in order for the compressors to restart smoothly. Most air conditioners rely on thermostats (which commonly have a 5 minutes delay) to avoid short cycling which allows pressure equalization before a restart is attempted.

Most of the tested air conditioner units with scroll compressors went into IDLE (drawing the same running amps without producing any cooling) or NO-LOAD (drawing about ½ the running amps without producing any cooling) condition after a *circuit breaker clearing* generated type of transient. It seems that some mechanical device prevented them from restarting normally. Researchers opened a scroll compressor and found a pressure relief valve between the high pressure and low-pressure chambers (see Figure 7). This valve is designed to prevent too much pressure from building up in the high-pressure side, releasing it into the low-pressure chamber. This valve may have stuck open when the compressor went into either IDLE or NO-LOAD condition because the unit draws current but no pressure is built up, and no cooling is produced. The air conditioner unit had to be turned off and then back on again to resume normal running condition.



Figure 7 Pressure Relief Valve

Some air conditioner units have high-pressure and low-pressure switches that are in series with the thermostat circuit to protect the compressor from harmful high-pressure conditions. One of

the units (air conditioner unit #5) shut itself down under normal running conditions (at nominal voltage) due to high pressure when the outdoor temperature reached 120°F. This indicated that this particular air conditioner unit, under normal charging conditions, would not work properly at in areas where the temperature reaches 120°F.

Thermal Protection Switch

All of the tested air conditioning units' compressors have a thermal protection switch that opens to protect the motor from overheating due to extended stall currents. Without the thermal protection switch, the motor might overheat and fail when high currents are present for long periods. When exposed to the *delayed recovery* type of transients, most of the tested air conditioner compressors (except A/C #7) stalled for as short as 1.0 second and as long as 20 seconds before the thermal protection switch opened to protect the compressor (as seen in Figure 8). Air conditioner unit #7 stalled for as long as 11.6 seconds without opening the thermal protection switch during the 30 second transient. In this unit, when the voltage rose above 162 V, the compressor resumed normal running condition. Air conditioner unit #9's (used unit) thermal protection switch opened only at the higher test temperatures (100 °F and 115 °F) and only after the compressor stalled for more than 12 seconds. Air conditioner unit #10's thermal protection switch opened only at the highest test temperature (115 °F). All the units restarted normally after the thermal protection switch reclosed except for air conditioner units #6 and #8. These two units needed to be turned off and then on again in order to run normally.

Figure 8 shows the thermal protection switch average tripping time versus the stall voltage for each of the tested air conditioner units except for #7 and #9. Each air conditioner unit had similar linear thermal protection switch tripping time slopes at the three tested temperatures except for unit # 9, which behaved differently for each of the three tested temperatures. The thermal protection tripping time was found to be inversely proportional to the sag voltage, the lower the voltage the longer the thermal protection switch tripping time. The thermal protection tripping time can be as short as 1.0 second and as long as 20 seconds as shown in the figure below. The right end of each plot is where the unit started stalling (stall threshold) and the left end is where the contactor opens (contactor dropout voltage).

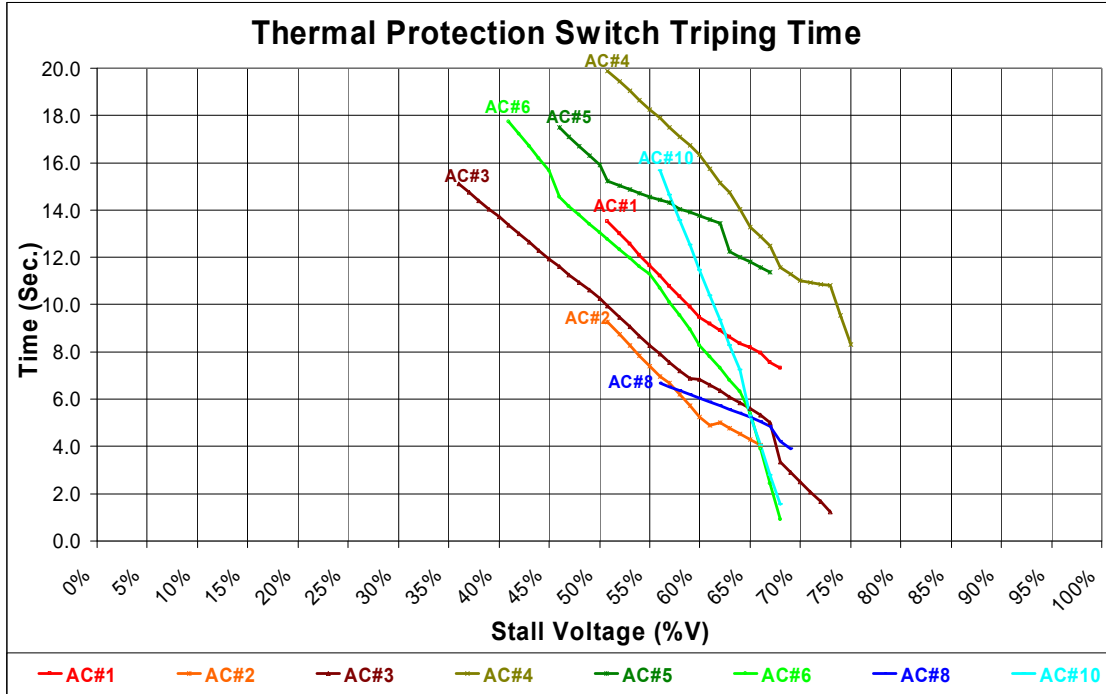


Figure 8 Thermal Protection Switch Tripping Time

Table 2 indicates the stalling window (between the stall threshold voltage and contactor dropout voltage). The thermal protection switch (TPS) tripping time for each of the tested units can be calculated with the t_{TPS} formula shown below in the table.

Table 2 Stall Calculation

$t_{TPS} = (m * V) + \Phi$								
	Stall Window (80°F)		Stall Window (100°F)		Stall Window (115°F)		Slope (m)	Constant (Φ)
	High	Low	High	Low	High	Low		
AC #1	64%	51%	66%	51%	68%	51%	-44.0000	35.8667
AC #2	56%	51%	61%	51%	66%	51%	-31.2333	24.5817
AC #3	59%	36%	67%	36%	73%	36%	-31.6667	25.8500
AC #4	62%	51%	67%	51%	75%	51%	-49.6667	46.1333
AC #5	57%	51%	62%	51%	67%	46%	-27.3333	30.1500
AC #6	59%	46%	64%	41%	68%	41%	-47.8718	36.9962
AC #7	57%	51%	61%	51%	67%	51%	-68.3333	49.0500
AC #8	64%	46%	67%	56%	69%	51%	-22.7500	20.0442
AC #9	67%	56%	70%	56%	73%	56%	-67.0000	44.1500 @ 80°F
							-62.3077	46.3846 @ 100°F
							-26.0000	22.9000 @ 115°F
AC #10	none	46%	64%	51%	68%	56%	-105.5208	74.7625

Contactor Dropout

All the tested air conditioners have a main power contact relay (called the contactor) that has a 24 VAC coil connected in series with the thermostat contact. All of the contactors were found to

have a quick response time (2 cycles to open/close when voltage is applied). These units use standard contactors (off the shelf type) which were not specifically designed for air conditioner use. From the tests, the contactor dropout voltage varied from about 55% down to 35% as seen in the Figure 9. This means that when the supply voltage goes below these values (below brown line on the figure below) the contactor will open tripping off the compressor. While the contactor is open, the compressor is off, but as soon as it recloses, the air conditioner compressor stalls when exposed to the *delayed recovery* type of transient.

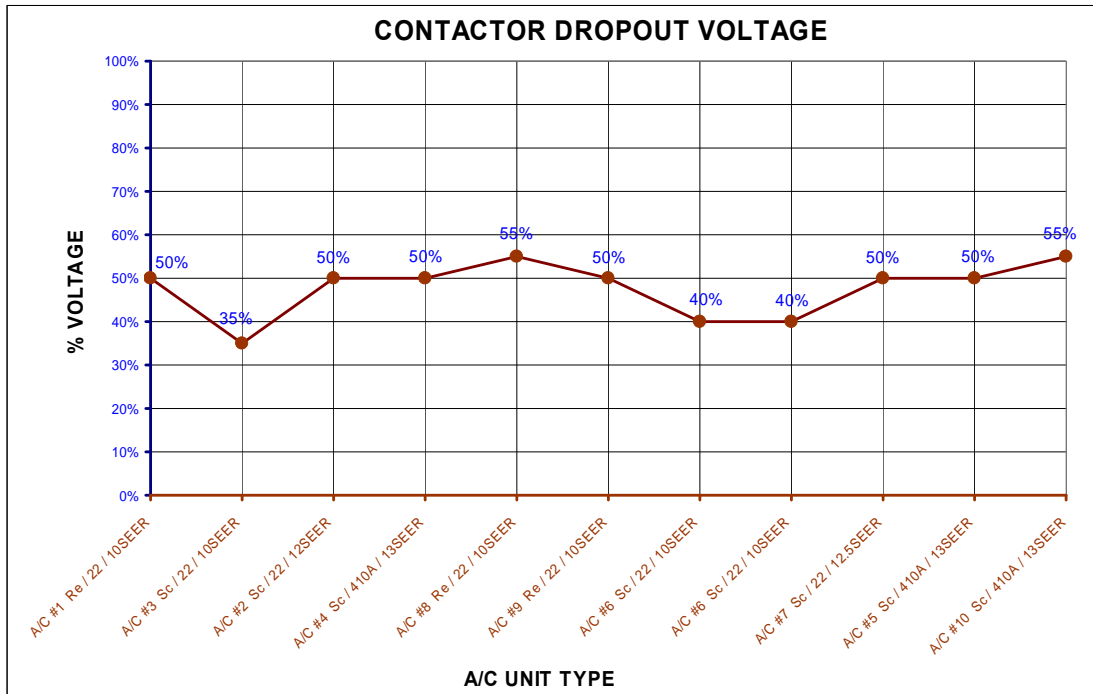


Figure 9 Contactor Dropout Voltage

Opening the contactor did not prevent the air conditioner units from stalling; it just delayed it until the supply voltage reaches the contactor threshold voltage. Table 1 indicates the maximum stalling times after the contactor recloses for all of the tested air conditioner units. This maximum time is when the voltage at the compressor is just above the contactor dropout voltage.

Table 3 Stalling Time after Contactor Reclosed

	Contactor Dropout Voltage (%)	Max. Stall Time After Contactor Reclosed (sec.)
A/C #1 Re / 22 / 10SEER	50%	11.5
A/C #3 Sc / 22 / 10SEER	35%	11.8
A/C #2 Sc / 22 / 12SEER	50%	5.5
A/C #4 Sc / 410A / 13SEER	50%	15.9
A/C #8 Re / 22 / 10SEER	55%	5.6
A/C #9 Re / 22 / 10SEER	50%	11.2
A/C #6 Sc / 22 / 10SEER	40%	11.4
A/C #6-OC Sc / 22 / 10SEER	40%	8.1
A/C #7 Sc / 22 / 12.5SEER	50%	6.4
A/C #5 Sc / 410A / 13SEER	50%	8.1
A/C #10 Sc / 410A / 13SEER	55%	6.6

2.3.2. Performance Model

A report on the evaluation of the performance model is given in Appendix C. In that document the performance model is tested under the following fault conditions:

- Voltage ramp down and ramp up
- Voltage sags
- Voltage oscillations
- Voltage humps (over voltages)
- Frequency oscillations
- Frequency sags
- Frequency ramp down and ramp up

The researchers make the following observations about their evaluation of the performance model:

1. The performance model is numerically robust.
2. The model can reasonably simulate voltage recovery caused by stalling. The voltage recovery process is mainly determined by thermal relay parameters.
3. The model simulates the worst case scenario. The key assumption is that once the voltage is below V_{stall} , all the motors at the feeder will stall. Because of the cascaded effect, the assumption is valid for most cases. That is, once the motors at the end of the

feeder stall, it will draw huge current and bring the voltage down along the feeder. This will cause the other motors along the feeder to stall.

4. There are two potential numerical problems:
 - a. The frequency dependency calculation. The default settings are 1.0 and -3. Unless the frequency calculation is off too much, numerically, the model will function well. However, the model will be more stable if a maximum frequency change allowed is used to cap the maximum P and Q changes.
 - b. The discontinuity in the running and stalling curves. The model did not fail to function properly because of this, but it might be an issue for weak systems where instantaneous real and reactive power increases are limited by their regulating capabilities.

2.3.3. Dynamic Phasor Model

The figures in this section present representative comparative plots of measured test data and simulations using this phasor model. These comparisons include

- Voltage ramp test
- Voltage oscillation test
- Frequency step test
- Voltage sag tests

Voltage Ramp Test

The applied voltage ramp down and ramp up is shown below in Figure 10.

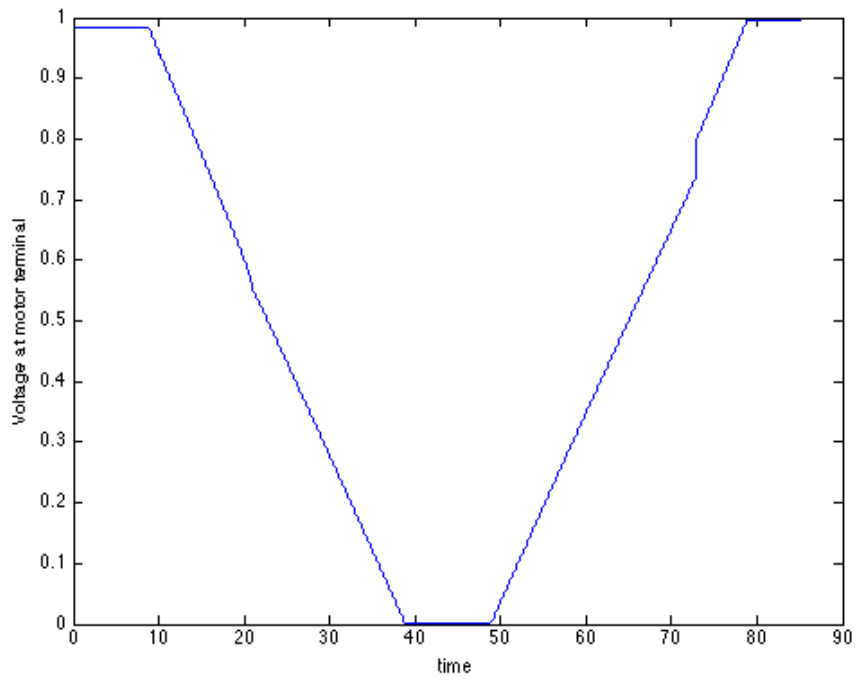


Figure 10 Voltage ramp measured at terminal of motor. The voltage initially is 0.98 pu.

The measured and simulated active and reactive powers are shown below in Figure 11 and Figure 12 respectively. There is excellent agreement. The difference near the end of the data and simulation is the action of the thermal protection shown in the data, and not represented in the model here.

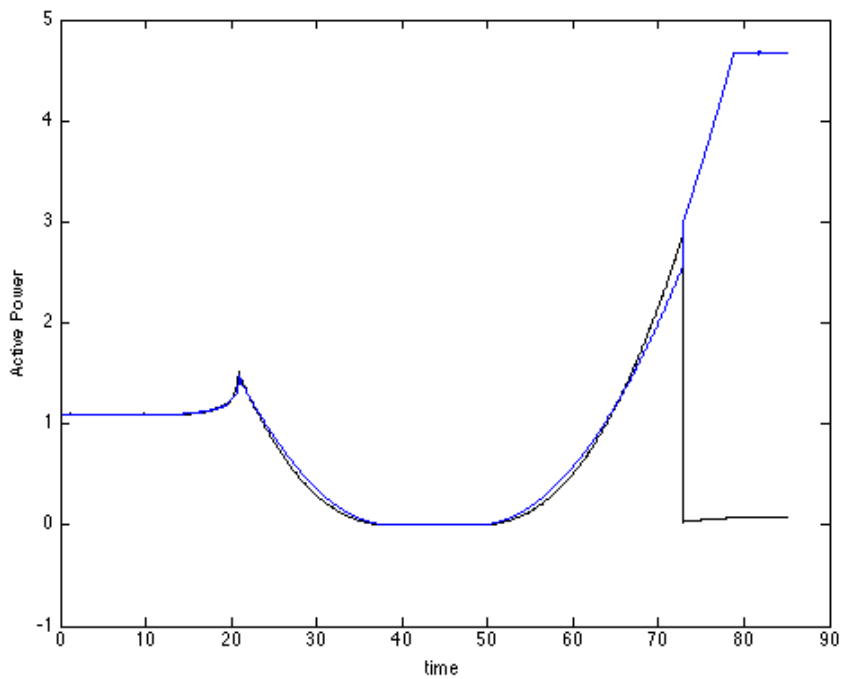


Figure 11 Measured and simulated active power

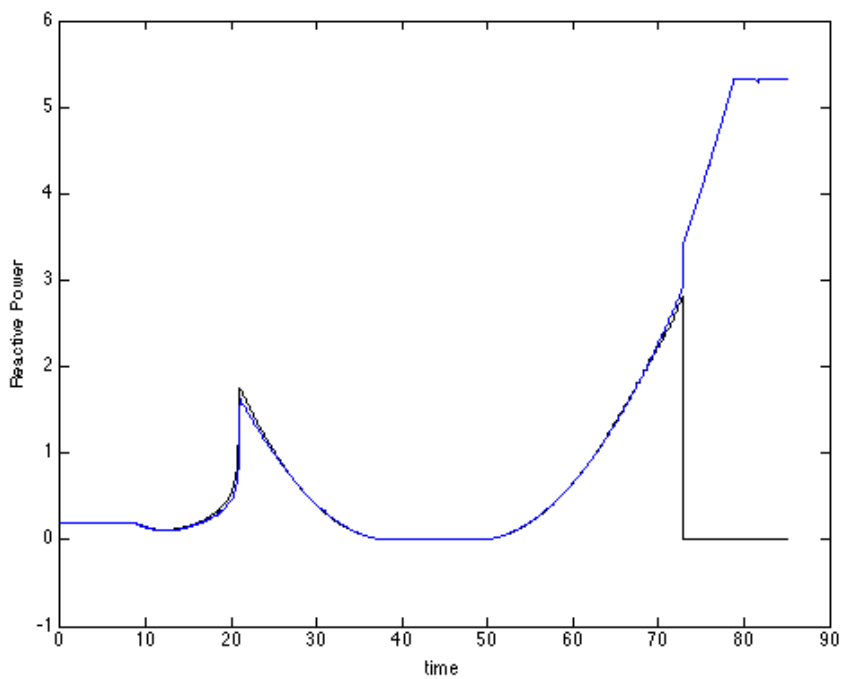


Figure 12 Measured and simulated reactive power

Voltage Oscillation Test

In this test, the magnitude of the applied voltage oscillations between 90% and 110% of the nominal value. The applied oscillations are at frequencies of 0.1Hz, 0.25Hz, 0.7Hz, 1.5Hz, and 2Hz, and is shown in Figure 13.

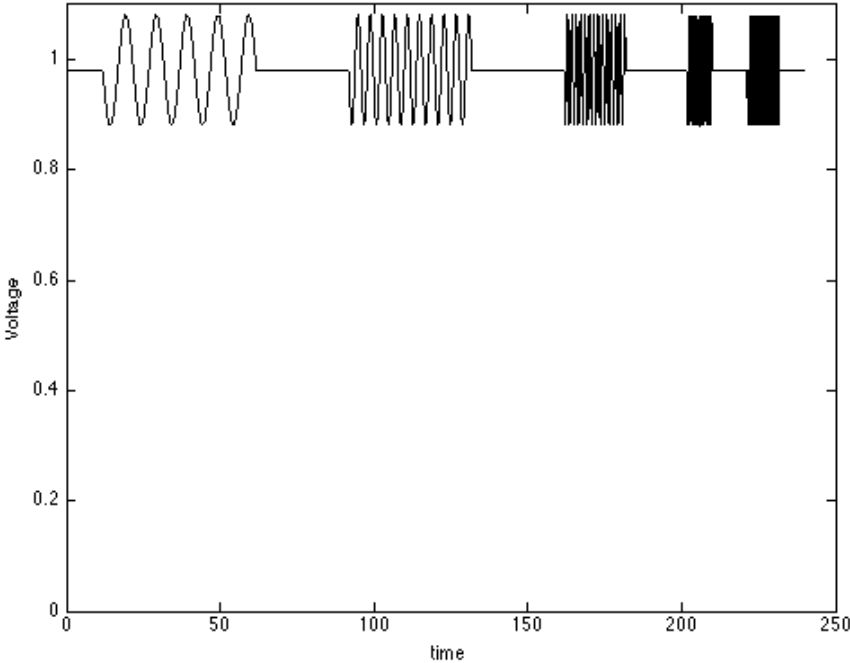


Figure 13 Voltage Oscillation Test. The applied voltage varies between 90% and 110% of nominal at frequencies: 0.1 Hz, 0.25 Hz, 0.7 Hz, 1.5Hz, and 2 Hz.

The resulting active and reactive powers are shown in Figure 14 and Figure 15 below. The match is very good.

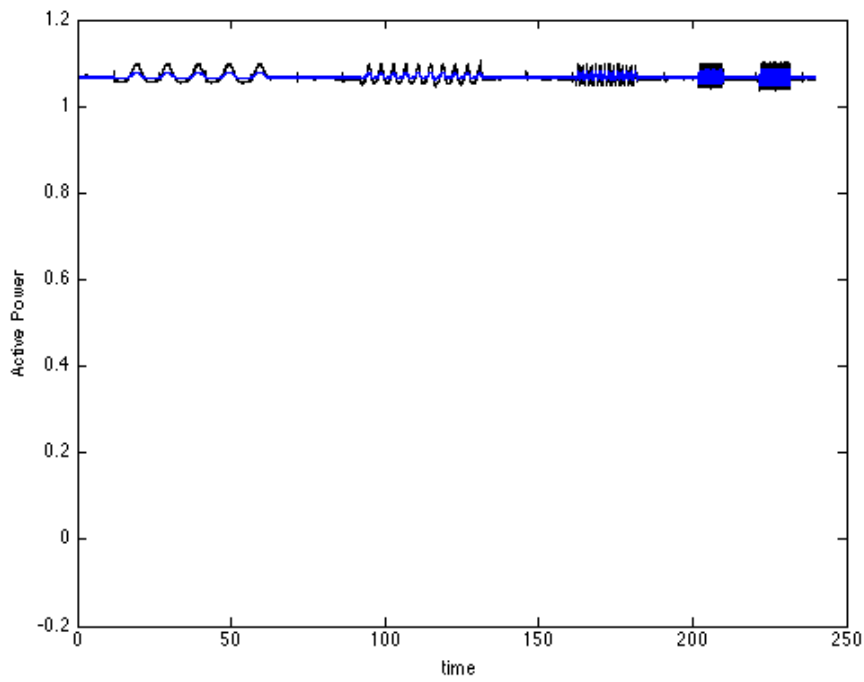


Figure 14 Active Power, simulated and calculated from measurements for the voltage oscillation test.

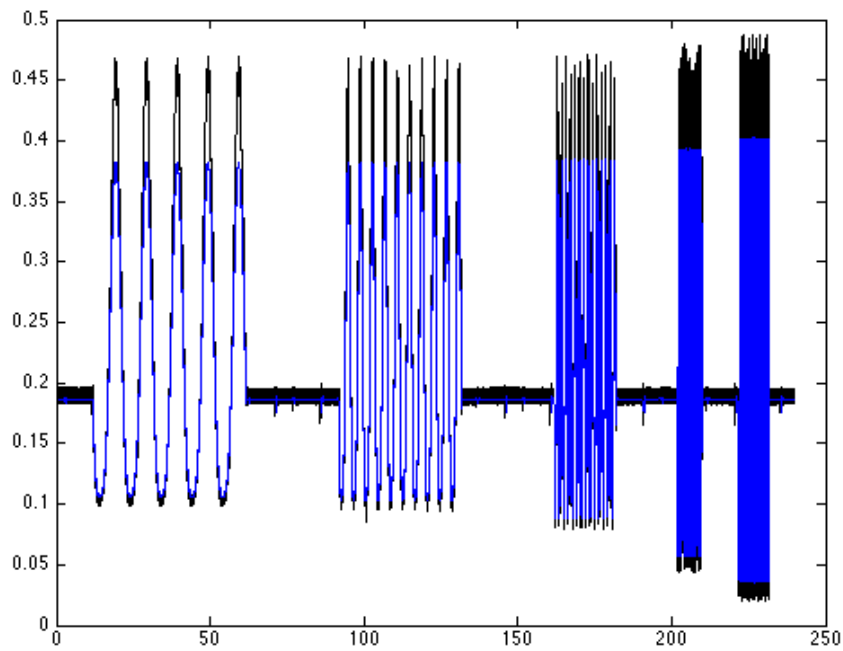


Figure 15 Reactive Power, simulated and calculated from measurements for the voltage oscillation test.

Frequency Tests

In the next test, the supply frequency is decreased from 60Hz to 58.5Hz in 0.25Hz increments, and then increased back again to 60Hz (shown below in Figure 17). Care must be taken to accurately calculate the active and reactive powers of the fundamental frequency components as the frequency changes. Calculating values assuming 60Hz - modulating by 60Hz sinusoids and averaging over integer periods - results in oscillations and *bias*. In this calculation it is convenient to modulate by signals of the correct frequencies, but averaged using a fixed window length. This results in oscillations, but removes the bias. Then a 1sec average is applied to smooth out the oscillations. Also, the applied voltage as seen from the terminal of the single phase motor changes with frequency. The voltage drop from the laboratory supply to motor depends on frequency as seen in Figure 16.

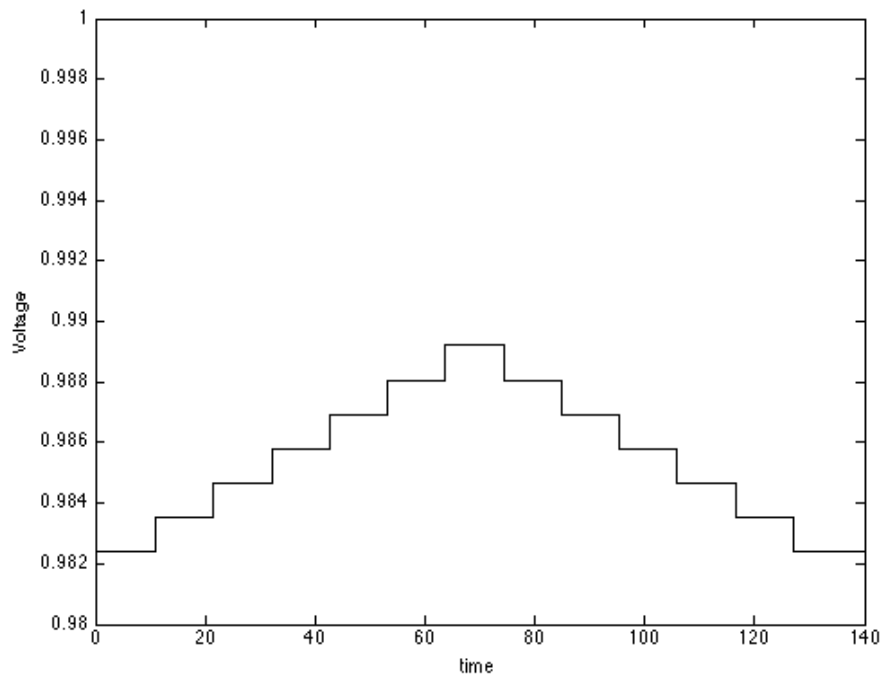


Figure 16 Simulation voltage consistent with laboratory voltage. The voltage magnitude increases as frequency decreases because the supply line voltage drop decreases.

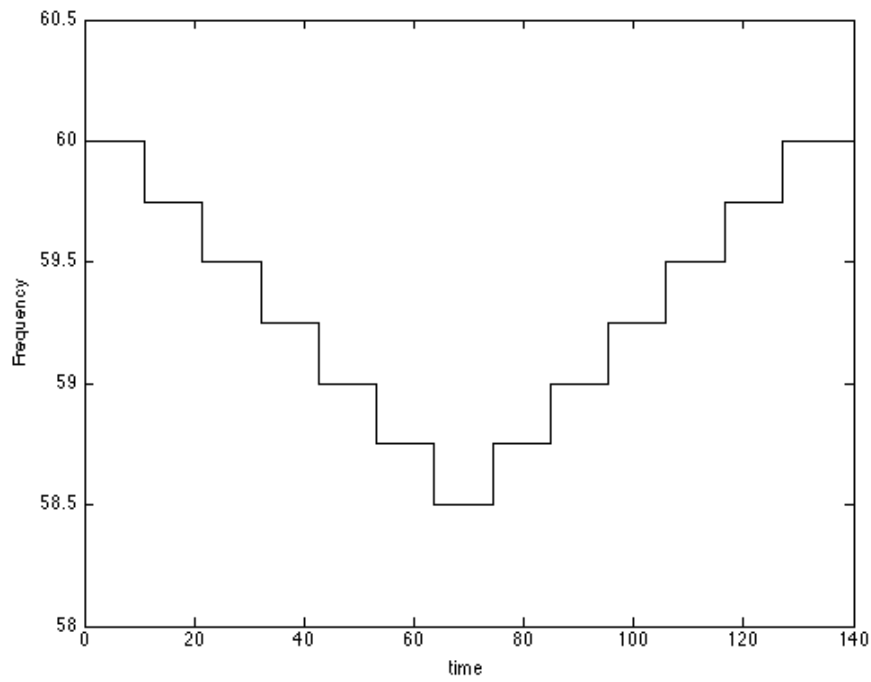


Figure 17 Frequency. The frequency drops from 60Hz to 58.5Hz and returns to 60Hz in 0.25Hz increments.

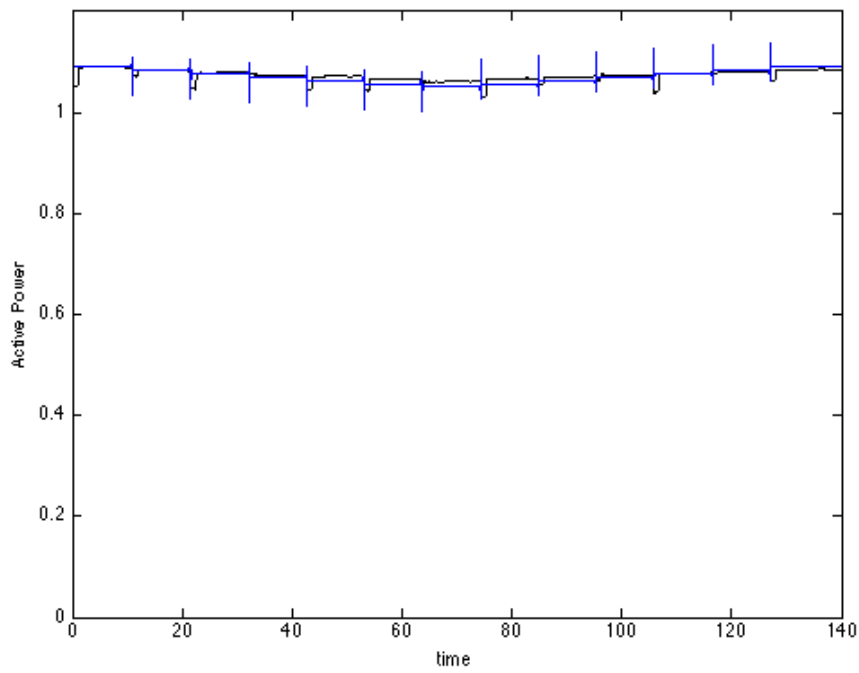


Figure 18. Calculated and simulated active power. The response is small and proportional to frequency.

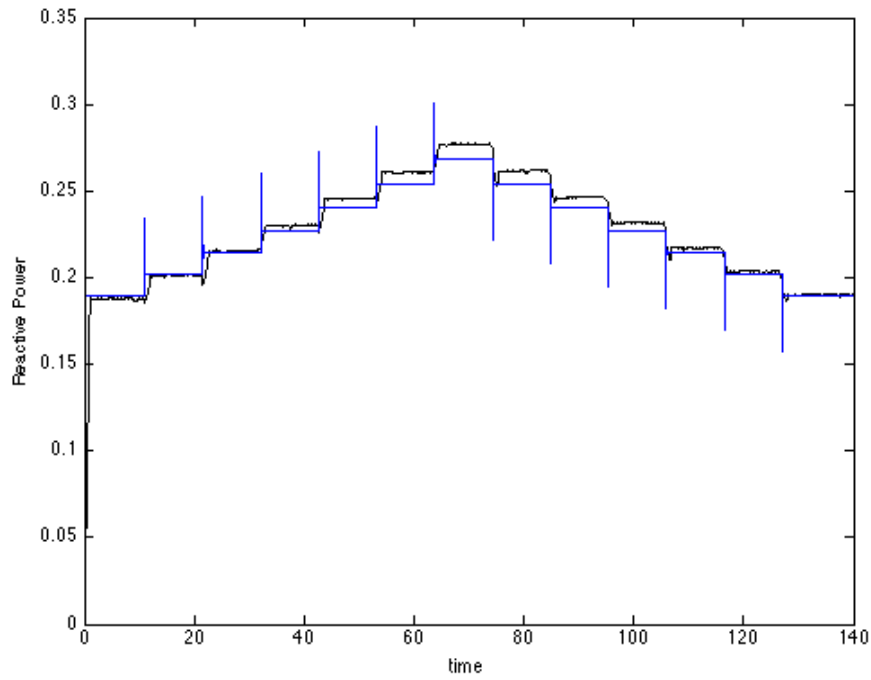


Figure 19 Calculated and simulated reactive powers. The reactive power increases with decrease in frequency.

The simulated responses shown in Figure 18 and Figure 19 are close to the measured responses. The applied frequency variation down to 58.5 Hz is large. The model should accurately represent the load frequency response for even large events.

Voltage Sag Tests

The voltage sag tests characterize the response of the air conditioner to faults in the network. The voltage profile for these tests has three parts, a pre-fault voltage at 100% nominal, a sag level for some specified fault duration, and a post-fault recovery level. The output of a particular test is simply whether or not the motor stalled. The simulation model is used to attempt to repeat the results, and in this case the model's Inertia constant, H , is tuned to best match the data.

An important point about the voltage levels in the test: there is a small voltage drop from the laboratory supply source to the terminal of the motor. While the difference is usually small, it is important to account for these few percent when trying to match the results with simulations. The particular tests examined here are those that distinguish between motor recovery and motor stall. The terminal voltage is noted when discussing these tests.

Six-cycle fault tests

The sag voltage was decreases to 0 pu and raised to various recovery voltages including 100%. The motor remained stalled in all cases.

Three-cycle fault, 100% recover tests

In these tests the recovery voltage was returned to 100% after a 3-cycle voltage sag. Repeated tests determined that the motor remained stalled for a voltage sag of 0.52 per unit, but recovered for a voltage sag of 0.54 pu.

The simulation must account for the voltage drop in the supply line. The terminal voltage at 100% supply is 0.98 pu. The voltage sags of 0.52 and 0.54, correspond to terminal voltages of 0.49 pu and 0.51 pu, respectively. For the case when the motor stalled, the high current kept the terminal voltage around 0.90 pu. In the recovery case, the terminal voltage recovered initially to around 0.90 pu and increased to 0.98 as the motor quickly returned to speed. In the simulation a pre-fault voltage of 0.98 pu, sag voltages of 0.49 pu and 0.51 pu, and a recovery voltage of 0.90 pu were used.

Keeping all other parameters constant, and modeling the mechanical load as constant torque, the inertia constant is found to be $H = 0.0219$ sec. The following four plots compare the active and reactive powers computed from measurements and simulated using the model described here. The model distinguishes between the stall/non stall conditions, and follows the dynamics reasonably well.

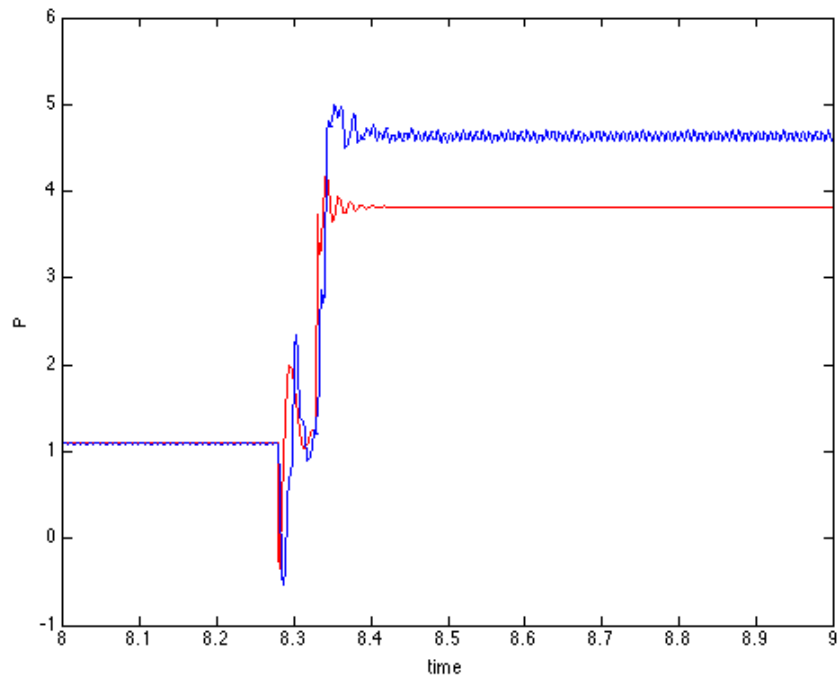


Figure 20 Plot of active power for 3-cycle 52% voltage sag test. The motor stalls.

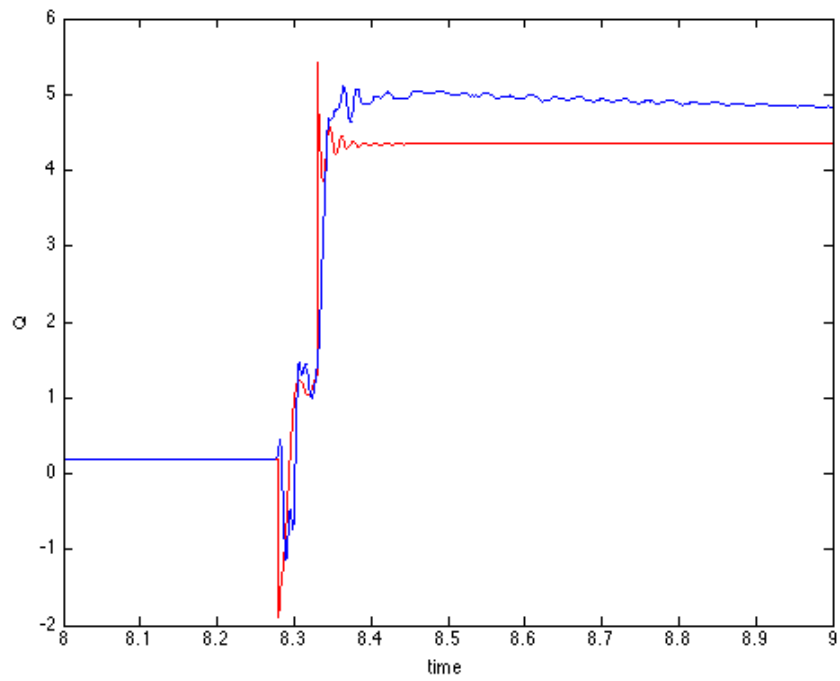


Figure 21 Plot of reactive power for 3-cycle, 52% voltage sag test. The motor stalls.

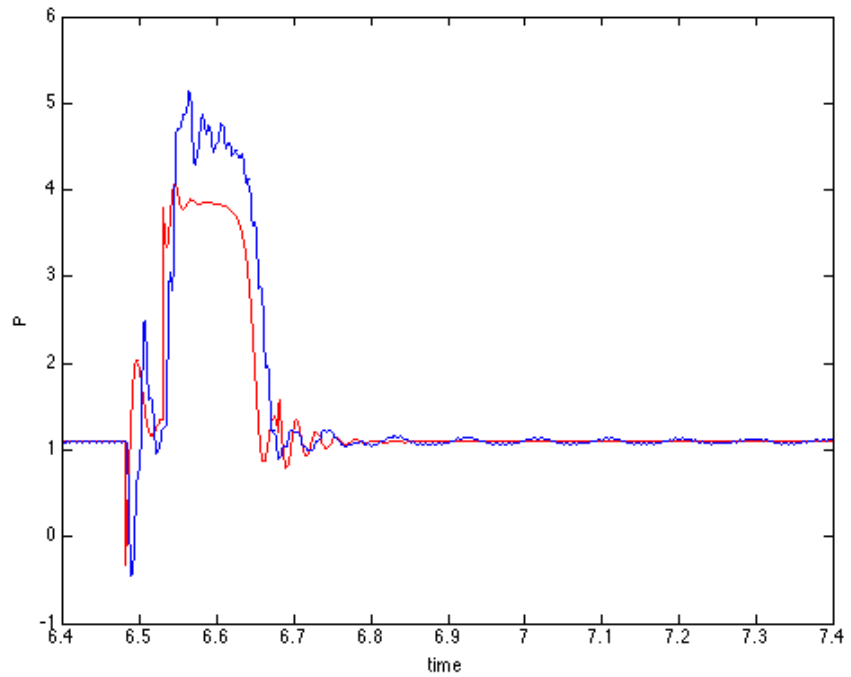


Figure 22 Plot of active power for 3-cycle, 54% voltage sag test. The motor recovers. (Note that the apparent delay in measured response, approximately 1 cycle, is due to calculation of power from data – using a 1-cycle window.)

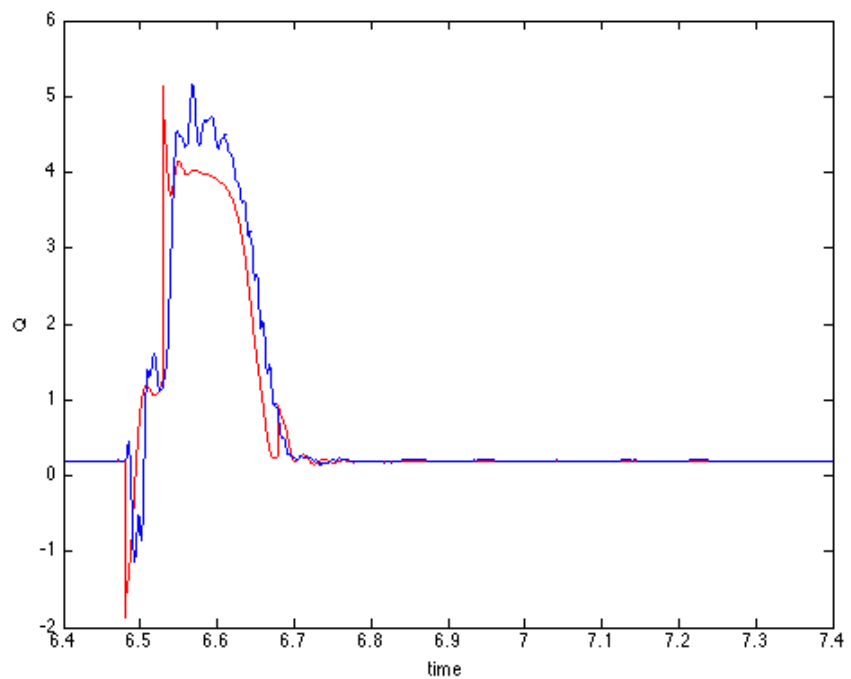


Figure 23 Plot of reactive power for 3-cycle, 54% voltage sag test. The motor recovers. (Note that the apparent delay in measured response, approximately 1 cycle, is due to calculation of power from data – using a 1-cycle window.)

The model presented here is clearly capable of representing the behavior observed in the laboratory tests. The laboratory tests are comprehensive. The voltage ramp tests operating conditions between full and zero voltage – identifying the motor stall voltage along the way. The voltage oscillation tests for the response that may be observed in the system under certain conditions, as does the frequency test. Both, in fact, test for frequencies beyond those typically observed in the system. The voltage sag tests confirm that the model can capture the stall/recover characteristics of these motors.

Continuing work involves the application of the model in system-wide studies. The model is being implemented in the PSLF software to enable these studies.

2.4. Conclusions and Recommendations

2.4.1. Conclusions

Extensive laboratory tests were performed on typical air conditioner units. The results of these tests were consistent with the hypothesis that stalled air conditioners explain the observed delayed voltage recovery phenomenon.

Two approaches to load modeling yielded two models for air conditioner loads. Both match the laboratory test data well. Both are being implemented in the PSLF. The performance model is already implemented and being tested by WECC LMTF members on system-level studies.

2.4.2. Recommendations

The differences, if any, between the two load models will be revealed in comparative system studies. The static characteristics are consistent and any significant difference would only arise due to their treatment of dynamics.

Once WECC determines the most suitable model to use in the WECC composite load model, it will be used in standard simulation runs for the West.

2.4.3. Benefit to California

The extensive test that led to the development of new load models will benefit California and the rest of the WECC region through more accurate dynamic simulations. These simulations are used to establish path transfer ratings and to study the impact of specific events of interest. Improved simulations will increase reliability of the electric grid in California.

3.0 Potential Solutions to Delayed Voltage Recovery

3.1. Introduction

SCE's investigation focused on two approaches for mitigating the air conditioner stalling problem. The first approach was solving the problem at its source, the individual air conditioner units. SCE tested various digital thermostats, under-voltage protection devices, and load control switches to assess their ability to mitigate the air conditioner stalling problem. The second approach attempted to mitigate the problem at the power systems grid. SCE contracted the Electric Power Research Institute (EPRI) to perform simulations to assess the effectiveness of voltage support devices, static VAR compensators (SVC) and synchronous condensers to resolve the air conditioner stalling problem.

The details of unit-level tests at SCE are presented in Appendix E, and a summary report of unit-level and system-level approaches is in Appendix F, and presented here.

3.2. Task Approach

3.2.1. Unit Level

SCE tested selected digital programmable thermostats, under-voltage protection devices, and load control switches to determine their ability to mitigate the air conditioner stalling problem.

Of the three digital programmable thermostats tested for response to under-voltage transients, only one thermostat had under-voltage protection, the Honeywell. This thermostat may help mitigate the air conditioner stalling problem, but its under-voltage protection and response times do not currently meet SCE's proposed stall protection specifications.

The use of digital programmable thermostats with proposed under-voltage protection is one of the easiest retrofitting solutions because it does not require a certified electrician. In California, retrofitting thermostats requires a certified electrician only when branch circuits are rated 100 VA or greater and most residential thermostats circuits are rated below 24 VA. It is important to mention that this solution would not protect older units, those installed prior to the mid-1990s, because they lack the common "C" wire. This wire powers the thermostat electronics used for measuring voltage. The effectiveness of this solution will only become evident as new air conditioner units having the common "C" wire, replace older air conditioners.

Three under-voltage protection devices manufactured by Diversified Electronics (DE) were tested that may have the under-voltage protection to help mitigate the air conditioner stalling problem. These three relays are off-the-shelf devices making them conveniently attainable, but they also come with disadvantages. First, two are plug-in devices, making them suitable only for window air conditioners and possibly some plug-in air handler units. Second, they do not have randomly distributed short cycle-prevention allowing them to restart at different times after voltage are restored to normal conditions. Third, they use normally open (N.O.) contacts that prevent the units from restarting if the under-voltage relay fails. Another disadvantage is

the retrofit cost – installing any of these under-voltage protection relays in California would require a qualified electrician for retrofit.

All other tested under-voltage protection devices provided limited stall protection; while helping to some degree, they will not alleviate the air conditioner stalling problem.

SCE worked with other entities such as Corporate System Engineering (CSE), Pacific Northwest National Laboratory (PNNL), and Cannon Technologies to modify their devices to mitigate the air conditioner stalling problem. The first two entities, CSE and PNNL agreed to modify their devices to meet SCE’s proposed under-voltage protection scheme; both devices were prototypes. Cannon’s off-the-shelf device (load control switch) required software modifications to meet SCE’s proposed under-voltage protection scheme. Because the state of California requires a certified electrician when servicing circuits rated 100 VA or more, implementation of all three of these devices will require an additional labor cost of \$70 to \$100 per installation, making it a less attractive solution.

3.2.2. System Level

EPRI was contracted by SCE to develop a more representative load model for use in dynamic studies as well as the study of mitigation field equipment such as Static VAR Compensators (SVC), and synchronous condensers (Pourbeik 2007).⁴

3.3. Task Results

3.3.1. Unit Level

Table 1 provides the test results for each device and assesses how well they mitigate air conditioner stalling. The *Potential* column is an SCE assessment of how viable these devices are for protecting air conditioners from stalling.

⁴ As the research tasks were conducted in parallel, the new WECC composite load model with air conditioner representation was not yet available.

Table 4 Unit Level Devices Test Results

	Manuf.	Model	UV Threshold (%V)	Response Time (sec.)	Electronics Shutdown (%V)	Re-close Delay (sec.)	Control Contacts	Potential (%)
Thermostats	Honeywell	RTH7400D100	60%	0.760	can't tell	290	N.O.	Medium-High
	Totaline	P374-1800	none	none	can't tell	none	N.O.	none
	Ritetemp	8022C	none	none	can't tell	none	N.O.	none
Under-Voltage Relays	ICM	ICM491	86%	5.100	75%	6	N.O.	Low
	DE	CV-200RS-20 Plug-in	83%	0.300	can't tell	300	N.O.	Medium
	DE	CV-100RS Plug-in	78%	0.232	can't tell	300	N.O.	Medium
	DE	CV-240-AFN Mount-in	83%	0.483	can't tell	300	N.O.	Medium
	Kriwan	INT369	68%	0.294	can't tell	120	N.O.	Medium-Low
	CSE	N/A	78%	0.25	15%	180 ~ 300	N.C.	High
	PNNL	N/A	77%	0.033	40%	180 ~ 300	N.C.	High
LCS	Cannon	N/A	80%	0.264	33%	180 ~ 300	N.C.	High

3.3.2. System Level

EPRI modeling indicated that SVCs and synchronous condensers at the system level could help mitigate the delayed voltage recovery problem as shown in figure 3. Although these devices cannot prevent air conditioners from stalling or subsequent faults, they can help isolate the fault area by literally injecting VARs into the system to prevent the problem from spreading throughout the system. Although a more rudimentary remedy, SVCs and synchronous condensers could help disconnect the stalled air conditioners by raising the units' terminal voltage. The supply VAR raises the terminal voltage subsequently making the thermal protection switch operate much faster. Finally, SVCs and synchronous condensers significantly improve voltage recovery and provide better voltage regulation, particularly in preventing over-voltages by absorbing VARs that decrease voltage.

The main advantage of electrical system-level solutions is that they can be implemented at fewer locations (transmission, subtransmission, or distribution substations) rather than at every air conditioning unit. The disadvantages in utilizing system-level solutions are, they would not

be able to stop the voltage drop in the immediate area of the system problem and would be more costly to implement than air conditioner unit-level solutions.

Figure 24 provides the modeling results. The black plotline simulates an event without using mitigation devices. The red and blue plots simulate the use of SVC and Synchronous Condensers respectively. This shows that each of these two devices help regulate voltage immediately after the fault is cleared by injecting VARs into the system. They also help remedy the over-voltage problem by absorbing VARs.

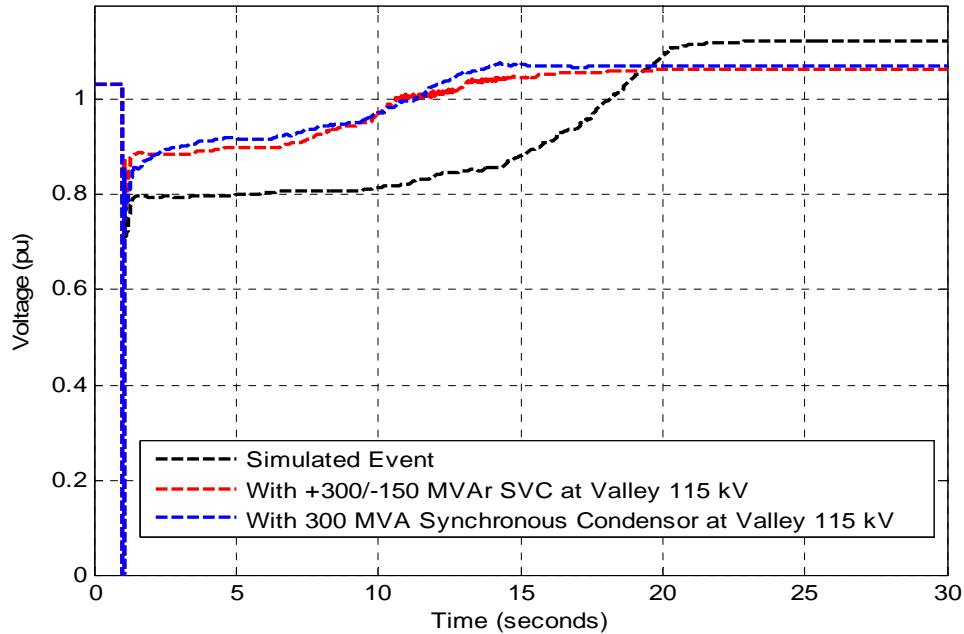


Figure 24 System-Level Solutions Simulations

3.3.3. Economic Assessment

The SCE Valley substation was used as a model for economic assessment because it typifies substations affected by delayed voltage recovery events. The SVCs installed at Devers and Rector Substations were used for cost analysis purposes. The Devers substation SVC has ratings of 605 MVAR reactive (generating) and 110 MVAR inductive (absorbing) and costs approximately \$50 million. The Rector substation SVC has ratings of 200 MVAR reactive (generating) and 100 MVAR inductive (absorbing) and costs approximately \$35 million. In order for SVCs or synchronous condensers to mitigate air conditioner stalling, they need to be installed at approximately 20 Valley 115-kV substations. The total cost for implementing this solution could reach \$100 million as indicated in Table 5.

Mitigating air conditioner stalling is more cost-effective if done at the unit-level. Valley has approximately 300,000 residential and 30,000 industrial, commercial, and agricultural customers with a total peak load of 1,500 MW and 400 MVAR. Assuming each customer has one air conditioner unit, 330,000 under-voltage protection devices would be needed to mitigate the

problem. That leaves two feasible unit-level solutions. The first would be to use under-voltage protection that does not require a certified electrician for a total cost of approximately \$20 million; the second option uses under-voltage protection devices that require an electrician for installation at a cost of approximately \$40 million as indicated in Table 5.

Table 5 Economic Assessment

Unit-Level Solution					
	Customers (Thousands)	Labor & Installation Cost	Material & Installation Cost	Total Material Cost (Millions)	Total Labor & Material Cost (Millions)
Valley	330	\$60	60	\$19.8	\$39.6

System-Level Solution			
	115-kV “B” Substations	SVC Unit Cost (\$ Millions)	Total SVC Cost (\$ Millions)
Valley	~20	~\$5	\$100

3.4. Conclusions and Recommendations

3.4.1. Conclusions

The best way to mitigate the air conditioner stalling problem is to implement a hybrid solution that combines both unit-level and system-level solutions. The under-voltage protection device (unit-level solution) would disconnect air conditioner units during under-voltage events. The SVC (system-level solution) would improve voltage recovery and regulation and prevent over-voltages. By combining unit-level and system-level solutions, Valley would require two SVCs instead of 20, one for each main bus.

3.4.2. Recommendations

For truly effective mitigation of the air conditioner stalling problem, SCE strongly recommends that a standard be created to disconnect stalled air conditioners from the electrical grid. This could be through either a switch at the air conditioner compressor or by action of the thermostat (potentially through the programmable communicating thermostat PCT).

3.4.3. Benefit to California

Adopting a combination of unit-level and system-level solutions to mitigate voltage problems will directly benefit customers and increase the reliability of the California electric grid.

4.0 Load Composition Data Tool

4.1. Introduction

A power system model includes three main elements: the sources of power, the transmission of power, and the loads. Load representation has long been the least accurate of these three elements. The stability of the system depends on whether the balance between supply and demand is maintained. When the system is perturbed by an abrupt change in either supply or demand, the opportunities for part of the system to "fall out of step" increase greatly. Dynamic models are used to examine whether such a risk exists under various conditions, and these models require accurate descriptions of the system interconnections, as well as both the generators and the loads.

Work performed in the early 1990s provided initial guidance regarding load modeling (IEEE Task Force 1993; 1995). The Western Electricity Coordinating Council (WECC) adopted an interim dynamic load model of the California-Oregon Intertie (COI) in early 2002 to address critical operational issues with the COI and formed the WECC Load Modeling Task Force (LMTF) to develop a permanent composite load model to be used for planning and operation studies in the long term (Pereira 2002). The composite load model is nearly complete, and provides a much more accurate representation of the response of load to voltage and frequency disturbances by offering a much more accurate description of the load behavior during transmission faults (Kosterev 2008).

The composite load model structure (see Figure 25) has been previously specified that describes the two salient features of the new model: (a) recognition of the electrical distance between the transmission bus and the end-use loads; and (b) the diversity in the composition and dynamic characteristics of end-use loads. The load model includes data for an equivalent model of the distribution feeder, the load components, and the fractions of the load components.

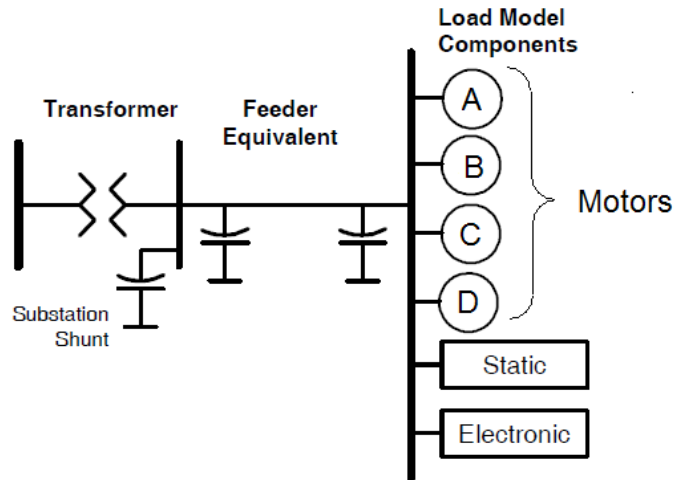


Figure 25. The WECC composite load model structure includes static loads, electronic loads, constant-torque three-phase motors (A), high inertia speed-squared load motors (B), low inertia speed-squared load motors (C), and constant-torque single-phase motors (D).

The methodology adopted by the WECC for identifying the fractions of the load components is specified in Appendix G and summarized in this chapter.

4.2. Task Approach

The approach taken in this development is to meet requirements of three use cases for a load composition data tool. The inputs and outputs for these cases are listed here.

Use Case 1: Feeder Load Composition

Goal

The user seeks to generate a single feeder load model for use with PSLF that incorporates motor A-C, ZIP, and electronic load components based on customer survey data.

Inputs

The user provides the following information

1. City
2. Month
3. Day of week
4. Hour of day

5. Number/type of residential and commercial buildings

Outputs

The total load and the fractions motors A-C, ZIP, and electronic loads.

Use Case 2: Substation Load Composition

Goal

The user seeks to generate a multi-feeder load model for use with PSLF that incorporates motor A-C, ZIP, and electronic load components based on customer survey data.

Inputs

The user provides the following information

1. City
2. Month
3. Day of week
4. Hour of day
5. Number/type of residential and commercial buildings on each feeder

Outputs

The total load and the fractions motors A-C, ZIP, and electronic loads.

Use Case 3: Calibrated Load Composition

Goal

The user seeks to generate a multi-feeder load model for use with PSLF that incorporates motor A-C, ZIP, and electronic load components based on customer meter data.

Inputs

The user provides the following information

1. City
2. Month
3. Day of week
4. Hour of day
5. Number/type of residential and commercial buildings on each feeder
6. Meter scaling results (actual/predicted)

Outputs

The total load and the fractions motors A-C, ZIP, and electronic loads.

The methodology for estimating the fractions of each load component is based on a "bottom-up" approach, coupling information about load types, size, location, time, climate data, and typical building design conditions.

4.3. Task Results

The specifications for the load composition data tool are in Appendix G.

A prototype of the tool can be downloaded from SourceForge (SourceForge.net). The tool provides a numerical reference for validation as well as an illustration of the user input/output requirements. The prototype shall not be considered an authoritative illustration of what the tool must do, rather an example of what it can do. It is expected that developers will improve upon the user interface and data input/output in a substantive way.

Two sample displays from this tool illustrate its function. In Table 6 conditions for a load location are specified. In this case the sample location is Portland, Oregon, and the default conditions are for a summer peak load. The load composition data tool converts this information into parameters needed for the WECC composite load model. This composition is shown in Table 7. The net information needed for the load model is shaded. The compositions for the individual load classes are provided in the table.

Table 6 Prototype Conditions

Conditions Status Check	Ok	Reset			
	Default	Override	Unit	Check	Remarks
Time					
Study type	3			Ok	1=Winter peak, 2=Typical, 3=Summer peak
Month	6			Ok	1=Jan, ... 12=Dec
Day of week	3			Ok	1=Sun, ... 7=Sat, 8=Holiday
Hour of day	15			Ok	0=midnight, ..., 12=noon, ...
Location					
City ST	Portland OR			Ok	Use button to load climate data (see Support col. A)
Latitude	45.5		deg	Ok	Only 25 to 65 N allowed
Climate					
Winter					
Low temperature	20		F	Ok	Determine the heating design conditions
Low month	1			Ok	1=Jan, ... 12=Dec
Low weekday	4			Ok	1=Sun, ... 7=Sat, 8=Holiday
Low hour of day	17			Ok	0=midnight, ..., 12=noon, ...
Summer					
High temperature	92		F	Ok	Determined the cooling design conditions
High month	6			Ok	1=Jan, ... 12=Dec
High weekday	3			Ok	1=Sun, ... 7=Sat, 8=Holiday
High hour of day	15			Ok	0=midnight, ..., 12=noon, ...
Peak solar radiation	301		Btu/sf.h	Ok	Used to establish size of cooling systems
Weather					
Dry Bulb Temperature	92		F	Ok	Determines the load composition conditions
Wind speed	3		mph	Ok	Used to estimate ventilation losses
Relative humidity	87%		%	Ok	Used to estimate latent load
Opaque sky cover	0%		%	Ok	
Diffuse Horizontal Radiation	119		Btu/sf.h	Ok	Used to estimate diffuse window heat gain
Direct normal Radiation	269		Btu/sf.h	Ok	Used to estimate direct solar heat gain

Table 7 Prototype Load Composition

Load composition		Status: Ok													Total power		Update Loadshapes		
Location	Portland OR	Electronic	Motor-A	Motor-B	Motor-C	Motor-D	ZIP Ip	ZIP Iq	ZIP Pp (P)	ZIP Pq (Q)	ZIP Zp (G)	ZIP Zq (B)	ZIP PF			Check	Sensitivity	Unit	
Month	June															Ok	Y	MW	
Weekday	Tuesday																		
Time of day	15:00 - 16:00																		
	Customers																		
Load	583	1.0	1.2	0.9	0.7	2.0	1.3	-0.5	0.0	0.0	1.0	0.1	-0.987	8.0					
Composition	-	12%	14%	12%	8%	25%	16%	-6%	0%	0%	13%	1%	-	100%			Y	%	
Residential	520	366.0	0.0	175.9	352.6	1896.6	14.1	-2.8	0.0	0.0	889.9	0.0	-1.0	3695.0	46%		Y	kW	
Single family	500	231.4	0.0	105.0	222.9	1143.1	8.9	-1.8	0.0	0.0	562.6	0.0	-1.0	2273.8	28%		Y	kW	
Multi family	20	134.6	0.0	70.9	129.7	753.5	5.2	-1.0	0.0	0.0	327.3	0.0	-1.0	1421.2	18%		Y	kW	
Commercial	63	632.3	1152.0	759.8	302.5	104.5	1247.3	-461.1	0.0	0.0	119.6	87.1	-1.0	4334.1	54%		Y	kW	
Small office	25	144.0	170.2	106.1	42.6	49.2	251.9	-90.7	0.0	0.0	24.4	18.0	-1.0	791.7	10%		Y	kW	
Large office	5	349.1	518.8	357.0	132.4	16.0	391.3	-140.9	0.0	0.0	31.5	26.9	-1.0	1799.7	22%		Y	kW	
Retail	15	95.1	280.5	199.0	85.2	6.6	482.4	-173.7	0.0	0.0	34.8	32.2	-1.0	1192.0	15%		Y	kW	
Lodging	5	11.8	31.9	36.6	16.7	21.0	36.1	-13.0	0.0	0.0	6.7	2.3	-1.0	161.1	2%		Y	kW	
Grocery	5	15.9	85.1	13.8	4.0	9.0	36.6	-13.2	0.0	0.0	6.1	2.4	-1.0	171.0	2%		Y	kW	
Restaurant	5	4.7	20.3	14.6	6.7	0.8	14.4	-5.2	0.0	0.0	2.7	0.9	-1.0	64.4	1%		Y	kW	
School	2	6.6	28.5	20.5	9.4	1.1	20.2	-7.3	0.0	0.0	3.8	1.3	-1.0	90.2	1%		Y	kW	
Health	1	5.2	16.7	12.3	5.4	0.7	14.4	-17.3	0.0	0.0	9.6	3.0	-0.9	65.9	1%		Y	kW	
Industrial kW	0	0.0	0.0	0.0	0.0	0.0	0.0	0.0	0.0	0.0	0.0	0.0	1.0	0.0	0%		N	kW	
Agricultural kW	0	0.0	0.0	0.0	0.0	0.0	0.0	0.0	0.0	0.0	0.0	0.0	1.0	0.0	0%		N	kW	

4.4. Conclusions and Recommendations

4.4.1. Conclusions

A prototype load composition data tools has been developed and the specifications for the tool are provided in Appendix G. It was designed to meet the expected use cases needed to specify parameters for the WECC composite load model.

4.4.2. Recommendations

The load model should be used in conjunction with the WECC composite load model. Base case models should be populated with appropriate default values and loads for critical locations may be entered by engineers for specific studies.

4.4.3. Benefits to California

It is understood that load composition varies by location. Previous models greatly simplified analysis by using uniform models. It is expected that more accurate representation for the diversity of load across the West will increase the accuracy of system simulations and increase confidence in reliable system operation in California. Simulations with these improved models will also provide more confidence in system studies that inform decisions concerning power grid investments.

5.0 Load Monitoring

5.1. Introduction

Load monitoring provides an important means to understand load behavior in the actual system. This understanding helps to develop load models to represent the load behavior in simulation studies. Load monitoring provides measured data needed for load model validation, load composition studies, and load uncertainty analysis.

The purpose of load monitoring is to provide better load characterization and better load management, i.e., the core element of load monitoring is focused on applications. Five load monitoring applications were considered in this work, with some preliminary case studies:

- Load monitoring for top-down load composition: The total load profile obtained from load monitoring data can be decomposed to derive fractions of individual load types if load profiles of individual load types are known.
- Load monitoring for load composition validation: Load profiles generated by the load composition model can be validated against load profiles derived from load monitoring data.
- Load monitoring for load model validation: The general approach of model validation is to compare model simulation against measurements, as was applied to WECC generator model validation. Load monitoring provides the basis for load model validation.
- Load monitoring for uncertainty analysis: Statistical analysis can be performed on load monitoring data to quantify load variations over selected time periods.
- Load monitoring for load control performance evaluation: This is the trend that loads will play a more and more active role in managing the power system. Similar to generator performance monitoring, load monitoring can be used to ensure the load behaves as designed for correct credits and control enforcement.

Devices suitable for load monitoring and the details of the case studies are presented in Appendix H. That work is summarized in this chapter.

5.2. Task Approach

Depending on various needs, load monitoring may be implemented differently with different monitoring hardware, different measured quantities, and different requirements for sampling rates, signal types, record length and availability, with different costs. Potential load monitoring options include traditional supervisory control and data acquisition (SCADA), phasor measurement units (PMUs), portable power system monitors (PPSMs), digital fault recorders (DFRs), protective relays, power quality monitors, and a low-cost monitoring device being developed by Western Electricity Coordinating Council (WECC) Disturbance Monitoring Working Group (DMWG). Characteristics of these options are summarized in this Appendix H.

Current load monitoring practices at several utility companies are presented as examples of load monitoring. Each example consists of the following aspects of load monitoring: objective of load monitoring, monitoring location selection, description of monitoring equipment, communication for load monitoring, cost, and use of the data.

5.3. Task Results

5.3.1. Load Monitoring Device Options

There are different devices available for monitoring loads or for event recording in general. Some are even installed in the system, and data are available for load monitoring purposes with minimal efforts. As mentioned earlier, PMUs are excellent general event recording devices. Digital fault recorders (DFRs) can record dynamic behaviors but record lengths are shorter. General supervisory control and data acquisition (SCADA) measurements are more readily available in the system. They are long records, which are good for load composition studies, but contain less dynamic information. This section will address the features of each monitoring option, (i.e., sampling rate, measured quantities, record length, availability, hardware structure, and cost information, when available). A summary is shown in Table 8.

Table 8 Features of Different Monitoring Options

Monitoring Device Options	Sampling Rate (sps)	Measured Quantities	Measurement Type	Record Length	Availability	Cost to Implement
SCADA	Low, ~1/4	V, I, P, Q	RMS	Long	High	Low
PMU	Medium, ~30	V, I, θ , f	Phasor (GPS-synch)	Long	Low	High
PPSM	High, ~960	V, I	POW (GPS-synch)	Long	Low	Moderate
DFR	High, ~5760	V, I	POW	Medium	Moderate	High
Relay	High, >960	V, I	POW	Short	High	Moderate
Power Quality Monitor	High, >960	V, I	POW	Short	Moderate	Moderate
GFA Controller	Medium, ~30	V, I, f	RMS	Long	Low	Low
DMWG Low-cost Monitor	Medium, ~30 for phasor, High, ~960 for POW	V, I, θ , f	Phasor, POW (GPS-synch)	Long	Low	Low

*Note: sps – samples per second.

RMS – Root mean square.

POW – Point-on-wave.

GPS-synch – Global Positioning System time synchronized.

DMWG – Disturbance Monitoring Working Group.

5.3.2. Existing Load Monitoring Examples

This section summarizes several representative examples in load monitoring.

Building Monitoring at BPA

BPA installed monitoring devices (PPSM) for one of its headquarters building. It is intended for characterizing load consumption for energy efficiency applications, as well as for developing and validating load models at the building level.

The recorded data have been used for analyzing building consumption, which leads to a better understanding of load composition at the building level. Further use of the data is planned for the development of the top-down load composition approach. Load model validation at the building level will be explored as well with the recorded data.

Distribution Substation Monitoring at PNM

Starting in 1997, PNM deployed a load monitoring system consisting of six custom-built data loggers at different distribution stations. The primary purpose of this project was to verify load composition assumptions for the design of PNM's Import Contingency Load Shedding Scheme (ICLSS). Specifically, the primary purpose was to estimate the portion of the demand that corresponds to large industrial motors. Sensitivity studies demonstrated that the performance of ICLSS would depend on the portion of the motor load that would disconnect from the system (via under-voltage relays) following the loss of the two principal 345-kV circuits that supply the Albuquerque area. A secondary, but very important objective was to demonstrate the feasibility of identifying parameters for physically-based load models.

The monitors were setup to collect data continuously, hoping to capture naturally occurring disturbances. Actually many natural events were captured over the years. In addition, PNM also performed several tap tests on these stations during specific times and seasons (e.g., summer peak, winter peak, and off peak). The test data proved to be more useful than naturally occurring disturbances. But the one thing learned from naturally occurring disturbances is that modeling the voltage sensitivity of the load is far more important than the frequency sensitivity.

Load Monitoring at IPC

A load monitor was installed at Idaho Power's Grove station to obtain response data from feeder loads to system disturbances and to gain experience with the monitoring device.

Presently the data is not being collected. Remote access has been lost and no information on the status of the device is available. IPC plans to bring it in for inspection as soon as time becomes available. It is expected that in the near future it would be used for load model validation work.

Load Monitoring at PSE

The objective of load monitoring at PSE is to collect load data for validating dynamic and steady state load modeling in the Puget Sound area. Monitoring devices have been installed at several

locations across the Puget Sound region, monitoring primarily 115-kV lines and several 230-kV lines covering a variety of customer classes.

Event recording (phasor data) is used by protection engineers. Disturbance recording (RMS data) will be used for initial and on going load modeling and validation purposes.

Feeder Load Monitoring at PG&E

PG&E has begun installing automated meters that are read by power line carriers from a modem installed at the feeder substation. Domestic customer meters will be read hourly; meters for large energy users will be read every 15 minutes. The data collected by AMI will fundamentally alter many engineering programs now in place at PG&E, resulting in improved load flow studies (for planning and for distribution management system (DMS) – PG&E’s distribution management system for distribution operations), and for transformer load monitoring.

5.4. Conclusions and Recommendations

5.4.1. Conclusions

The purpose of load monitoring is to serve the needs for better load characterization and better load management. Load monitoring can find applications in many aspects, including:

- Load monitoring for top-down load composition
- Load monitoring for load composition validation
- Load monitoring for load model validation
- Load monitoring for uncertainty analysis
- Load monitoring for load control performance evaluation

Load Monitoring for Top-Down Load Composition

The term “top-down” is used in contrast to the “bottom-up” approach, which describes the previous building-simulation-based load composition model. The top-down load composition serves the purpose of estimating load mix and weighting factors that are needed in the bottom-up load composition model. An example shown in Figure 26, assuming typical load profiles for individual building types are known, the top-down approach solves for the weighting factors from the total feeder load profile obtained from SCADA data.

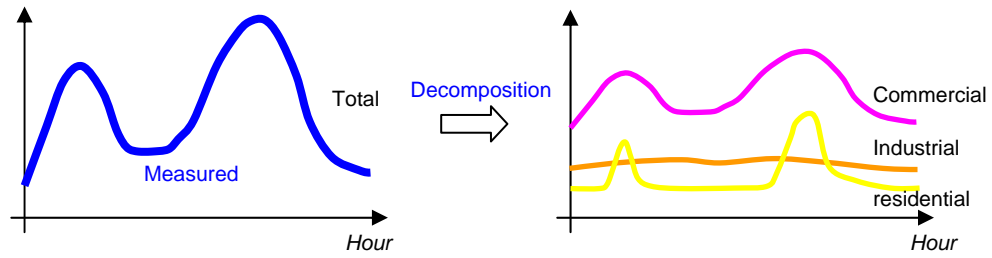


Figure 26 Curve Decomposition for Top-Down Load Composition Analysis

Load Monitoring for Load Composition Validation

Load profiles generated by the load composition model can be compared with load profiles derived from load monitoring data, e.g., historical SCADA data or building monitoring data. If the load composition model captures the right load characteristics, the load profiles should match SCADA data. Otherwise any mismatch can be used to calibrate the load composition model, e.g., tune load mix and adjust weights. The calibration methodology has yet to be developed.

Load Monitoring for Load Model Validation

General approach of model validation is to compare model simulation against measurements, as having been applied to WECC generator model validation. Load monitoring provides the basis for load model validation.

However, load model validation is far more challenging than generator model validation because of extensive uncertainties and variations of loads. It is almost certain that the variations and uncertainties would make the load model not match the next recording.

Therefore, load model validation should not focus on how close the curves would match, but should focus on principal load behaviors to match the impact of loads on system studies. If the load model would produce the right high-level system behaviors, it could be concluded that the load model matches the actual load characteristics in principle.

This “in principle” load model validation can be done in two ways: time-domain load model validation and frequency-domain load model validation. Time-domain load model validation compares the time series curves of simulated system level behavior and recorded monitoring data, while frequency-domain validation compares the frequency/damping contents of the simulation results and actual measurements.

Load monitoring data for this model validation purpose should have enough resolution and time length for capturing system dynamic behaviors. Examples of data sources include phasor measurements (PMUs), PPSM data, and potentially, measurements from the low-cost monitor device DMWG is developing.

Load Monitoring for Uncertainty Analysis

Statistical analysis can be performed on load monitoring data to quantify load variations over selected time periods. Load monitoring data needed for uncertainty analysis can be low resolution data like SCADA measurements or high resolution data like phasor measurements.

Load Monitoring for Load Control Performance Evaluation

It is the trend that loads will play a more and more active role in managing the power system. At the individual end-use level, SCE is developing solutions for prolonged voltage recovery as a result of a/c stalling. At a larger scale, active load control has been studied for the purposes of spinning reserves, damping improvement, frequency and power flow regulation, etc. Similar to generator performance monitoring, there is a need to ensure the load behaves as designed for correct credits and control enforcement.

Load monitoring data for load control performance evaluation range in a wide spectrum, depending on the control objective. High resolution data like phasor measurements are needed for evaluating load performance for damping improvement. Lower resolution data of long records are needed for evaluating load performance for spinning reserves, frequency and power flow regulation.

5.4.2. Recommendations

Continued research on load monitoring to support load modeling activities is needed for purposes of system validation and the potential use of top-down load models. Additionally load monitoring activities associated with direct load control offer opportunities not only for better load models, but also for loads to assist grid reliability.

5.4.3. Benefits to California

Model validation is important for maintaining accurate models that are used to establish reliable operating limits. Use of better models potentially increases reliability in California and the West. Additionally, on-line load monitoring offers the potential for adjusting load composition knowledge in an operating setting. In the long run this could influence operating decision with better information.

6.0 Uncertainty Analysis

6.1. Introduction

Analysis of power system dynamic behavior requires models that capture the phenomena of interest, together with parameter values that ensure those models adequately replicate reality. It is important to distinguish between model fidelity and parameter accuracy. Models are always an approximation. In many cases, the level of approximation is determined by the nature of the study.

The choice of models is a decision that should be made based on knowledge of the actual system composition and the phenomena that are being studied. Determining parameters for those models, on the other hand, usually relies on comparison of model response with actual measured behavior. Parameter estimation processes seek to minimize the difference between measured and simulated behavior. Different choices for model structure will usually result in different parameter values. This is a consequence of the estimation process trying to compensate for unmodeled, or poorly modeled, effects. In all cases, the models and associated parameter sets are approximations, though the goal should always be to obtain the best possible approximations.

Load models are further complicated by the fact that load composition is continually changing. Even if it were possible to obtain a load model that was perfectly accurate at a particular time, it would be inaccurate a short while later. Developing load models is not a futile exercise though, as overall load composition tends to behave fairly predictably. For example, the composition of a residential feeder will (approximately) follow a 24 hour cycle. But, while composition from one day to the next may be roughly equivalent, morning load conditions may well differ greatly from those in the evening. Seasonal variations may be even more pronounced.

As mentioned previously, all models are approximate to some extent. Model structures for large dominant components, such as synchronous generators, are well established, as are procedures for determining the associated parameter values. Furthermore, parameter values for such devices remain fairly constant over their lifetime. Models that represent an aggregation of many distributed components are much more contentious though, given the inherent uncertainty in the overall composition of the model.

This chapter focuses on uncertainty associated with load modeling. The details of this are provided in Appendix I. An extract and summary of that work is presented here.

6.2. Task Approach

Loads form the major source of uncertainty in power system modeling. Loads are highly distributed, and quite variable, so detailed modeling is impossible. Aggregation provides the only practical approach to incorporating loads into power system studies. For static (power

flow) analysis, the approximations inherent in aggregate load models are largely unimportant, as the composition of the load has little impact on results. On the other hand, load composition is very important in the analysis of system dynamic behavior. Different types of loads exhibit quite diverse responses to disturbances.

The approach used in this report, and recommended for uncertainty analysis, is to use a sensitivity model to analyze uncertainties and related quantities of interest. In this report, trajectory sensitivities are calculated and used for the purpose. Trajectory sensitivities will be explained below. With this sensitivity model the following analyses are made possible:

- Uncertainty analysis – characterize the impact of parameter uncertainty on the outcome of a dynamic simulation.
- Parameter ranking – by the sensitivity of the response to parameter values.
- System stress indicator – by increased sensitivity to parameter values.
- Parameter estimation – to aid model validation.

The trajectory sensitivity model is used for these applications.

6.2.1. Trajectory Sensitivities

The time evolution of system quantities following a disturbance is referred to as a trajectory. For power systems, trajectories are driven by a system of switched differential-algebraic equations, with the switching required to capture events such as protection operation or limits being encountered. The details of this underlying model structure are not relevant to this report, and so are not included. A thorough discussion can be found in (Hiskens 2004). The concept of trajectories is important though, so a brief overview is provided.

The trajectory of a dynamical system depends on the initial conditions and the choice of parameter values. This dependence is expressed mathematically as the system *flow*, which can be written

$$x(t) = \phi(t, x_0, \theta)$$

where the initial conditions are given by $x_0 = x(0)$, and θ denotes the parameters. For a particular choice of x_0 and θ , the point on the trajectory at time t , denoted $x(t)$ is given by evaluating the flow ϕ at that time. Generally ϕ cannot be written explicitly, but instead is generated numerically by simulation.

The report focuses on the impact of parameter uncertainty on the trajectory. It will be assumed that the initial conditions remain constant⁵. For notational convenience, the dependence of ϕ on x_0 will therefore be ignored. Accordingly, trajectories will be given by

⁵All subsequent analysis and techniques can be extended to incorporate variations in the initial conditions.

$$x(t) = \phi(t, \theta).$$

Sensitivity concepts are generally associated with the linearization of an input-output relationship. Small changes in inputs map through the linearized relationship to small output changes. Trajectory sensitivities fit this framework by describing the changes in the trajectory (the output) resulting from perturbations in the underlying parameters and/or initial conditions (the inputs). They provide a linearization around the trajectory, as against small disturbance analysis which builds on linearization around the equilibrium point. Trajectory sensitivity concepts are not new (Frank 1998), though until recently progress on practical applications was impeded by:

- Computational inefficiency. Sensitivity to each parameter or initial condition required an additional full simulation.
- Non-smooth behavior. Sensitivities were not well defined for situations where events influenced behavior.

However both these limitations have recently been overcome, with efficient computation of trajectory sensitivities now possible for large-scale, non-smooth systems (Hiskens 2000).

Trajectory sensitivities provide an insightful way of quantifying the effect that individual parameters have on overall system behavior (Hiskens 2006). A trajectory sensitivity is simply the partial derivative of the trajectory, or equivalently the flow, with respect to the p parameters of interest,

$$\begin{aligned} \Phi_i(t, \theta) &= \frac{\partial \phi_i}{\partial \theta}(t, \theta) \\ &= \left[\frac{\partial \phi_i}{\partial \theta_1}(t, \theta) \quad \frac{\partial \phi_i}{\partial \theta_2}(t, \theta) \quad \dots \quad \frac{\partial \phi_i}{\partial \theta_p}(t, \theta) \right] \end{aligned}$$

where ϕ_i refers to the i -th element of the vector function ϕ , or equivalently the i -th state, and θ_j is the j -th parameter.

Trajectories are obtained by numerical integration, which generates a sequence of points at discrete time steps t_0, t_1, \dots, t_N along the actual trajectory. The discretized trajectory will be described using the notation

$$\mathbf{x} = [x(t_0) \quad x(t_1) \quad \dots \quad x(t_N)].$$

Trajectory sensitivities can be calculated efficiently as a byproduct of numerical integration (Hiskens 2000, Feeherey 1997, Li 2000). The corresponding discretized sensitivities can be written,

$$\underline{\Phi}_i(\theta) = \begin{bmatrix} \Phi_i(t_0, \theta) \\ \Phi_i(t_1, \theta) \\ \vdots \\ \Phi_i(t_N, \theta) \end{bmatrix}$$

Unfortunately, few commercial simulation packages currently provide trajectory sensitivity information. Approximate sensitivities must be generated by varying each parameter in turn by a very small amount, re-simulating, determining the difference in trajectories, and thus finding the sensitivity. The disadvantage of this method is that it is computationally expensive, and requires an additional simulation for each parameter.

6.2.2. Test System

Preliminary tests of trajectory sensitivities are applied to the following applications:

- Uncertainty analysis – characterize the impact of parameter uncertainty on the outcome of a dynamic simulation.
- Parameter ranking – by the sensitivity of the response to parameter values.
- System stress indicator – by increased sensitivity to parameter values.
- Parameter estimation – to aid model validation.

The examples throughout the report utilize the IEEE 39 bus system of Figure 27. All generators in this system were represented by a fourth order machine model (Sauer 1998), and were regulated by the IEEE standard AVR/PSS models AC4A and PSS1A (IEEE 1992). All generator and network data were obtained from (Pai 1989).

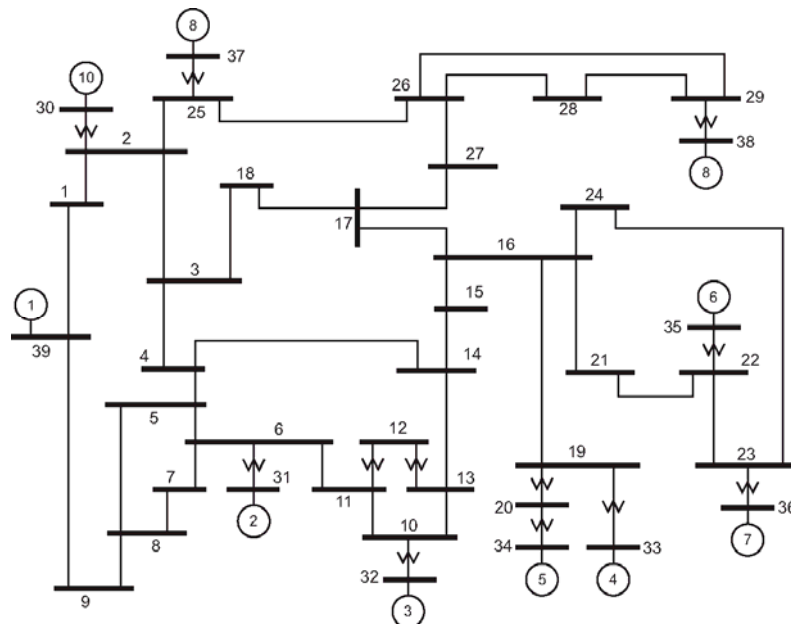


Figure 27 IEEE 39 bus system

6.3. Task Results

Details of results are presented in Appendix I. Here sample results for the applications are presented.

6.3.1. Uncertainty Analysis

The sample disturbance scenario involves a solid three-phase fault on line 16-21, at the bus 21 end. The fault was cleared after 0.15 sec by tripping the faulted line. That left buses 21 and 23, and generators 6 and 7, radially fed over line 23-24.

Figure 28 shows the separation⁶ between the zone 3 mho characteristic (Blackburn 1998) and the apparent impedance seen from bus 23. The dashed line was obtained for a fault clearing time of 0.15 sec, and used the nominal set of load parameters. It remains above zero, suggesting the zone 3 characteristic is not entered.

Uncertainty was introduced into the load composition parameters. They were assumed normally distributed. A Monte-Carlo process was used to generate thirty random parameter sets, with the resulting trajectories shown in Figure 28. The figure also shows the 95% confidence interval⁷. Notice that it is quite probable for trajectories to pass below zero, suggesting the possibility of a zone 3 trip. Knowledge of the load composition is therefore very important in this case.

⁶This distance goes negative when the apparent impedance enters the mho characteristic.

⁷It can be expected that 95% of trajectories lie within that bound.

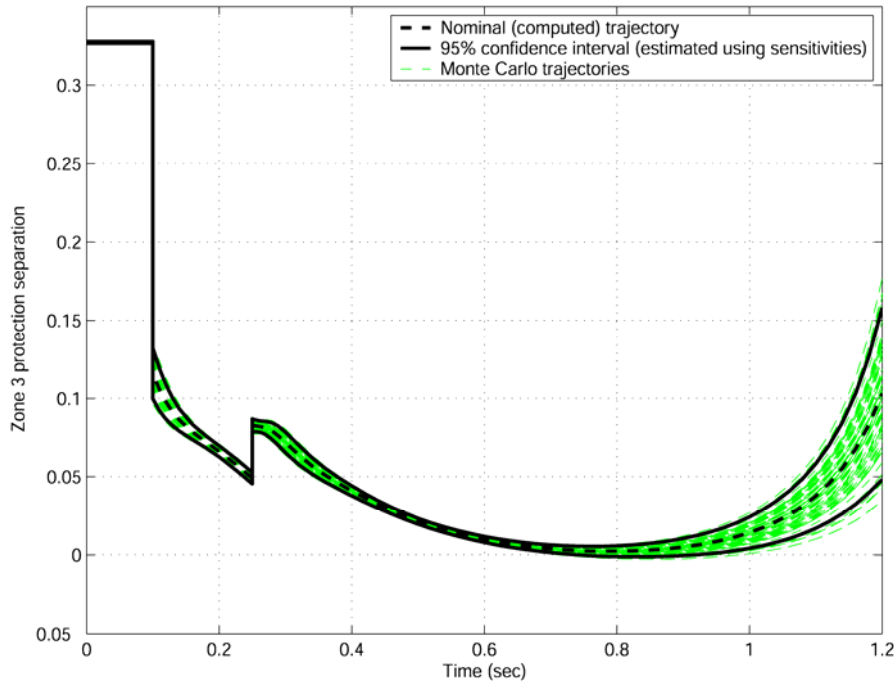


Figure 28 Zone 3 protection on line 23-24, 95% confidence interval bounds.

6.3.2. Parameter Ranking

Trajectory sensitivities provide a basis for ranking the relative influence of parameters. Large sensitivities imply that parameter variations have a large effect on behavior, whereas small sensitivities suggest behavior changes very little with parameter variation. In this example, trajectory sensitivities are used to rank the importance of voltage indices at all loads throughout the IEEE 39 bus system. A three-phase fault was applied at bus 16 at 0.1 sec, and cleared (without any line tripping) 0.2 sec later.

The sensitivities of bus 16 voltage V_{16} to load indices at all buses were computed in conjunction with the nominal trajectory. These trajectory sensitivities are provided in Figure 29, where the vertical axis gives the change in the pu voltage for a unity change in load index values. It is immediately clear that the real power index for bus 20 has a much greater influence on behavior than all other indices. (The reason is that generator 5 is marginally stable for this disturbance scenario, and bus 20 lies on the corridor linking that generator to the rest of the system.) The loads at buses 4, 8 and 23 also display a reasonable, though certainly less pronounced, level of influence. Loads 4 and 8 are influential due to their large size. Load 23 has an important impact on the dynamics of generator 7. The influence of all other loads, for this disturbance scenario, is negligible. Of course a different disturbance could possibly highlight some other set of loads.

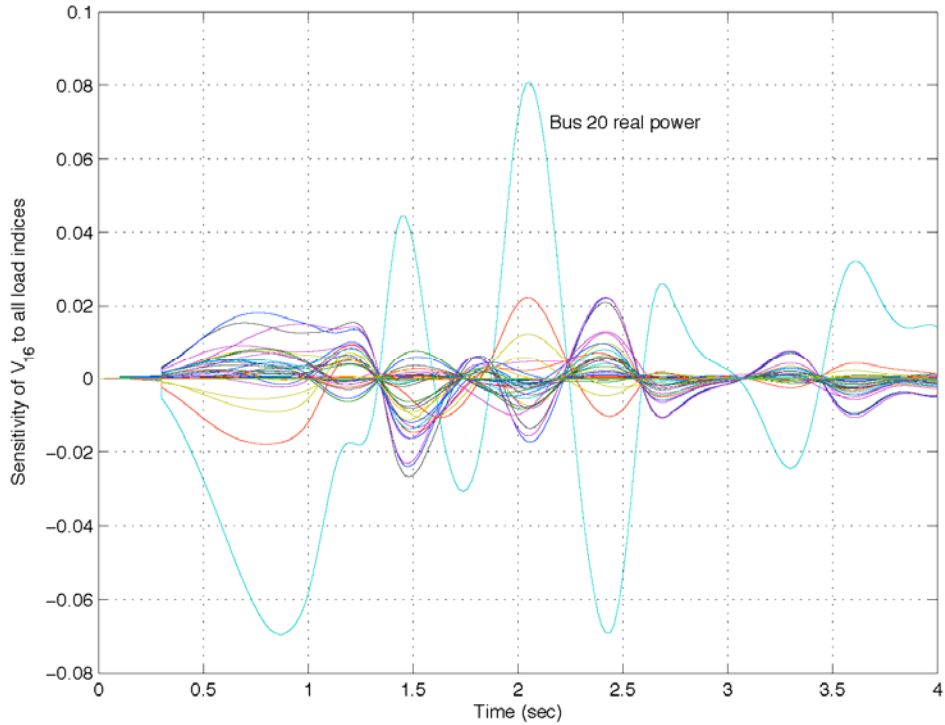


Figure 29 Trajectory sensitivities for all load indices.

6.3.3. System Stress Indicator

It is shown in (Hiskens 2006) that as systems become more heavily stressed, sensitivity to parameter variation increases significantly. This can be illustrated by continuing the previous example. The upper plot of Figure 30 shows the behavior of generator 5 angle (relative to generator 10) for a range of fault clearing times. (The fault clearing time used in the previous example was 0.2 sec.) The critical clearing time is 0.213 sec; slower clearing results in generator 5 losing synchronism. Notice that the angular deviations do not show a great increase, even though instability is imminent.

The sensitivity of V_{16} to the bus 20 load index, for the same range of fault clearing times, is shown in the lower plot of Figure 30. The deviations exhibited by these trajectory sensitivities grow dramatically as critical conditions are approached. This behavior motivated the sensitivity related measures developed in (Hiskens 1999, Nguyen 2002) to predict conditions that induce marginal stability. Further work is required though to fully understand and exploit this phenomenon.

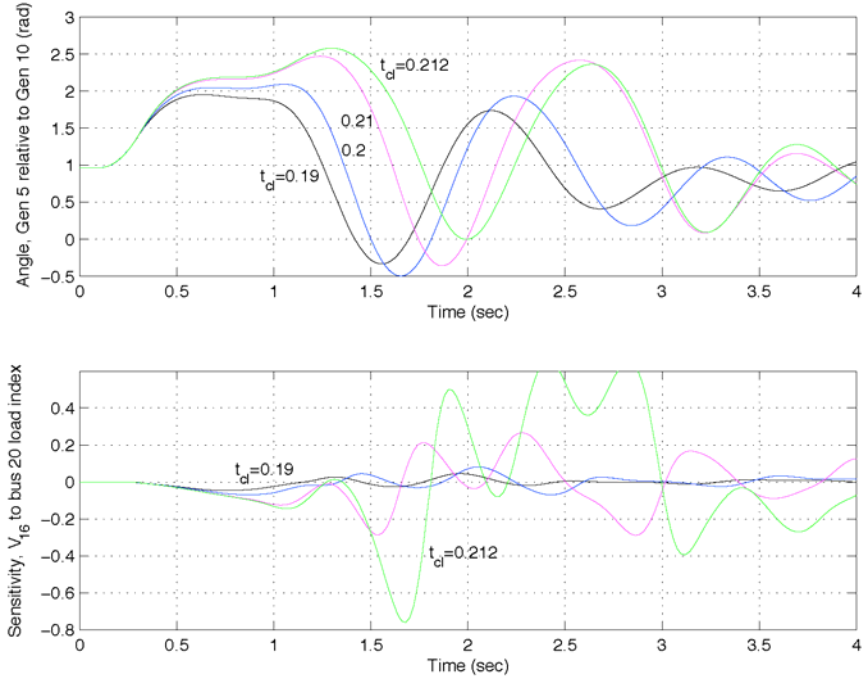


Figure 30 Trajectory and sensitivity variation for increasing system stress.

6.3.4. Parameter Estimation

It is often possible to estimate parameter values from disturbance measurements. For example, simply measuring the active and reactive power consumed by a load during a disturbance may yield sufficient information to accurately estimate several model parameters. The aim of parameter estimation is to determine parameter values that achieve the closest match between the measured samples and the model trajectory.

Disturbance measurements are obtained from data acquisition systems that record sampled system quantities. Let a measurement of interest be given by the sequence of samples

$$m = [m_0 \ m_1 \ \dots \ m_N]$$

with the corresponding simulated trajectory being given by

$$\mathbf{x}_i = [x_i(t_0) \ x_i(t_1) \ \dots \ x_i(t_N)]$$

which is the i -th row of \mathbf{x} . The mismatch between the measurement and its corresponding (discretized) model trajectory can be written in vector form as

$$e(\theta) = \mathbf{x}_i(\theta) - m$$

where a slight abuse of notation has been used to show the dependence of the trajectory on the parameters θ .

The best match between model and measurement is obtained by varying the parameters so as to minimize the error vector $e(\theta)$. It is common for the size of the error vector to be expressed in terms of the 2-norm cost,

$$C(\theta) = \|e(\theta)\|_2^2 = \sum_{k=0}^N e_k(\theta)^2.$$

The desired parameter estimate $\tilde{\theta}$ is then given by

$$\tilde{\theta} = \underset{\theta}{\operatorname{argmin}} C(\theta).$$

This nonlinear least squares problem can be solved using a Gauss-Newton iterative procedure (Hiskens 2001). At each iteration j of this procedure, the parameter values are updated according to

$$\begin{aligned} \underline{\Phi}_i(\theta^j)^T \underline{\Phi}_i(\theta^j) \Delta\theta^{j+1} &= -\underline{\Phi}_i(\theta^j)^T e(\theta^j)^T \\ \theta^{j+1} &= \theta^j + \alpha^{j+1} \Delta\theta^{j+1} \end{aligned}$$

where $\underline{\Phi}_i$ is the trajectory sensitivity matrix previously defined, and α^{j+1} is a suitable scalar step size⁸.

An estimate of θ which (locally) minimizes the cost function $C(\theta)$ is obtained when $\Delta\theta^{j+1}$ is close to zero. Note that this procedure will only locate local minima though, as it is based on a first-order approximation of $e(\theta)$. However if the initial guess for θ is good, which is generally possible using engineering judgement, then a local minimum is usually sufficient.

6.4. Conclusions and Recommendations

All models are an approximation, to some extent. Uncertainty in model-based analysis is therefore unavoidable. Model design should take into account the nature of the phenomena under investigation, with well-designed models minimizing the impact of unmodeled effects and of uncertainty. In power systems, the major source of uncertainty arises from the modeling of loads. Accurate modeling is particularly challenging due to the continual variation in load composition.

Trajectory sensitivities provide a numerically tractable approach to assessing the impact of uncertainty in parameters. Such sensitivities describe the variation in the trajectory resulting from perturbations in parameters. Small sensitivities indicate that uncertainty in the respective parameters has negligible impact on behavior. Large sensitivities, on the other hand, suggest

⁸Numerous line search strategies for determining α are available in (Nocedal 1999) and many other references.

that the respective parameters exert a measurable influence on behavior. It is important to minimize the uncertainty in the latter group of parameters. This can be achieved by estimating parameter values from measurements of system disturbances. The parameter estimation process seeks to minimize the difference between measured behavior and simulated response. This difference can be formulated as a nonlinear least squares problem, with the solution obtained via a Gauss-Newton process. Trajectory sensitivities provide the gradient information that underlies that process.

The impact of uncertain parameters is generally not significant for systems that are unstressed. As the stability margin reduces, however, system behavior becomes much more sensitive to parameter perturbations. It is particularly important to consider cases that are on the verge of protection operation. In such cases, uncertainty may make the difference between protection operating or remaining inactive, with the consequences being vastly different.

Various numerical techniques are available for assessing the impact of parameter uncertainty. Trajectory sensitivities can be used to generate approximate trajectories, which in turn allow parameter uncertainty to be mapped to a bound around the nominal trajectory. The likelihood that uncertain parameters may induce undesirable events, such as reactionary protection operation, can be assessed using these techniques.

6.4.1. Recommendations

Presently, sensitivity models are not routinely used in dynamic system studies.

Sensitivity models have tremendous value for the applications considered here and it is recommended that research be directed towards these topics. Furthermore, it is recommended model sensitivities should be investigated to understand the fidelity of the model being used.

A concrete and high priority recommendation arising from this research is to promote the use of sensitivity models for parameter estimation and model validation. The model validation exercise will serve to reduce the uncertainty in models, and increase confidence in system studies.

6.4.2. Benefits to California

Further research is required to develop the use of sensitivity analyses discussed in this chapter.

In the near term, subject to continued research, model validation efforts will benefit from the use of sensitivity model-based parameter estimation. Increased confidence in the models used to assess system conditions and to establish operating limits will increase system reliability that will benefit California and the West. The identification of most sensitive parameters will serve to flag potentially weak or stressed parts of the grid where the response is most sensitive to local conditions.

In the long term there is considerable potential benefit to the industry and California with increased use of sensitivity models. Similar to the approach advocated here for uncertainty analysis, risk-based decision making procedures will rely on sensitivity models. Such applications will require significant research to better understand the uncertainties involved.

7.0 Solar Generation and Load Models

The complete white paper prepared under this task is Appendix J, from which this Chapter is extracted.

7.1. Introduction

As concerns of climate change intensify, renewable energy technologies such as photovoltaic (PV) generation are being deployed in large scale within the electrical grid dominated by conventional electricity sources such as coal, natural gas, and nuclear generation. Solar power generation has been expanding rapidly. Annual PV installations in the United States increased 42 % from 145 MW in 2006 to 206.5 MW in 2007. Most of the growth occurred in the grid-connected sector – to over 150 MW during 2007. At the State Government level, renewable portfolio standards (RPS) requiring electricity utilities or electricity providers to supply a certain quantity of their delivered energy from renewable energy sources such as PV have been adopted in 25 states and the District of Columbia. These requirements call for as much as 20 % to 30 % of electricity to come from renewable energy sources in the next 15 to 20 years (IEA 2008).

According to a utility solar assessment study, the solar contribution could be quite considerable, realistically reaching 10 percent of total U.S. electricity generation by 2025 by deploying a combination of solar photovoltaic (PV) and concentrating solar power (CSP).

More than 90% of the installed PV capacity is connected to national electric grids (Picault 2009). The increasing connection of distributed generation at distribution levels from a certain penetration level may not only influence the operation and design of distribution systems, but also affect to the operation and stability of transmission system as well. In impact studies for installing these generation systems, the transmission system is generally modeled as a strong – sometimes even as an infinite – voltage source. Thus, the weakening effect that comes with high penetrations of DG therefore has been neglected. Transmission systems in the future however will become weaker and the DG systems may affect significantly the behavior of underlying distribution systems and consequently transmission systems. While there have been some studies of the potential impacts of PV systems on the distribution systems (Thomson 2007), there are no significant works analyzing the impacts of those on transmission systems (Boemer 2009). Investigation impacts of PV systems on power systems become more important as the penetration level increases.

7.2. Task Approach

In this chapter, a state of the art literature survey is conducted, with a goal to establish a simple and accurate empiric modeling of PV systems to complement load representations that are commonly in use for power system load flow and power system stability analysis studies.

Such a PV model may be used to analyze the impact of PV systems on the transmission systems and distribution systems. The desirable model will permit the representation of all PV systems

installed in a distribution area as an equivalent active load by using the source aggregation techniques. To be sure, the model intended will depend on parameters such as installed power, penetration level, location of system, weather condition, rated electrical values etc.

7.3. Task Results

7.3.1. PV System Models

A block diagram of a grid connected PV system is shown in Figure 31. As may be observed from the block diagram, the properties and behavior of the system will be affected on the output I-V characteristics of photovoltaic array, a maximum power point tracking (MPPT) function generally incorporated in the DC-DC converters, and the DC-AC inverter, besides variations in the solar insolation.

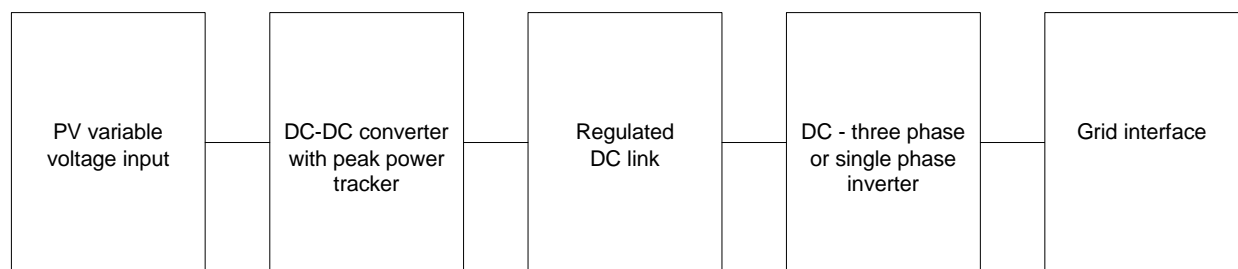


Figure 31 Block diagram of typical grid-connected PV system

There have been parallel efforts to develop models suitable to study their individual impact within the PV generation system and at the grid interface. These models may be classified into three groups: (a) model based on characteristics of PV array, (b) model based on characteristics of specific inverter structure and (c) overall PV system model. The last model is much convenient for interacting with the traditional power flow analysis to obtain steady-state operating status of power grid and PV system. The overall system models use the principle of instantaneous power balance and the principle of power electronic transformation (Wang 2008, Pananikolaou 2009). Model development for study of single PV based generation devices have generally focused on developing tools that enable time-domain simulation using tools such as PSCAD, Matlab-Simulink, EMTP, etc. (Yazdani 2009) provides an excellent overview of the state of the art from this perspective.

On the other hand, among the models that are aimed at studying their collective behavior and investigate the effects of PVs on power systems, most of them are related to impacts on the distribution systems (Azmy 2004, Canova 2009). The few works related studying impacts on transmission systems (Thong 2007, Reza 2003), consider general DG technologies beyond PV systems, with machines such as synchronous and induction generators.

Most of the modeling studies of PV systems have generally been based on analytical methods. Although these models exhibit the behavior of PV systems with certain accuracy, they do not reflect the response of PV systems to variable conditions in irradiance, grid voltage, etc. While there are some studies which present experimental test results in grid-connected PV systems in order to show interaction between PV systems and power systems (Thomson 2007), they have not been generator capable of simulating its response to changes in irradiance and grid voltage is established. However, the effect of variations in grid frequency has not been taken into consideration in the model.

7.3.2. PV System Modeling Issues

When modeling the PV systems in the electric power systems, major issues to be accounted may be grouped into two categories; steady state concerns and transient concerns, as discussed further in the following sub-sections.

Steady State Concerns

The main steady state issue concerning PV generation is the variation of power generation, which is affected by environmental factors such as location, weather, and climate. The single major parameter that affects the output power of PV generator is the irradiance. Since the irradiance is related to latitude, geographical location of PV systems is used to estimate the irradiance consequently output power.

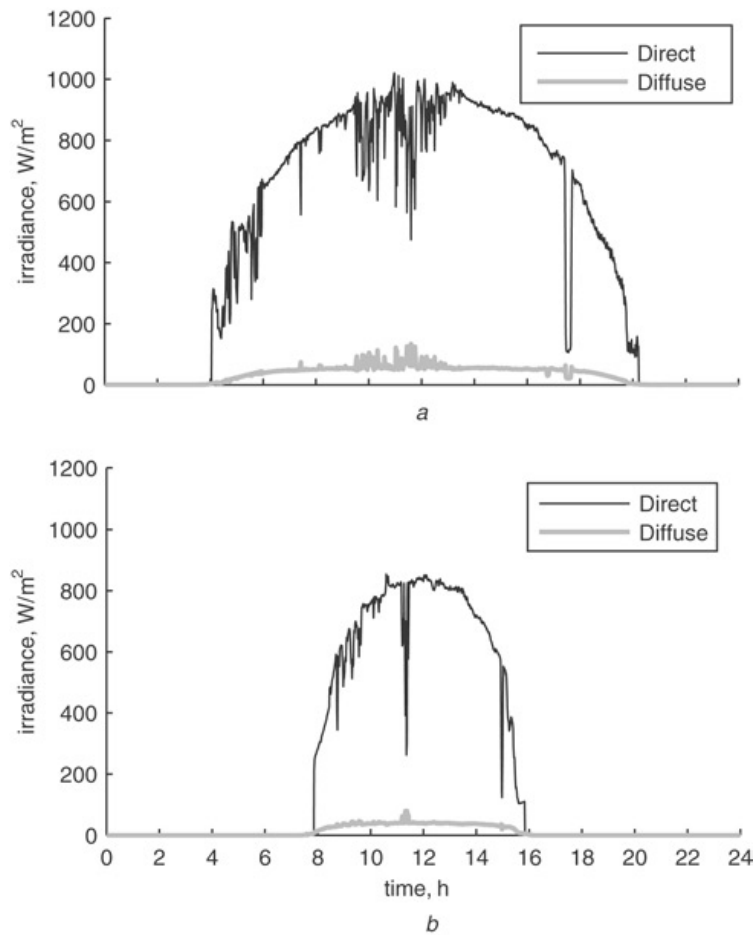


Figure 32 A graph of measured direct and diffuse irradiance on (a) a summer day, and (b) a winter day (From Thomson 2007)

For instance, it has been observed daily average irradiance values ranged from 5.0 to 7.5 kWh/m²/day from a measurement study in which the nineteen monitored systems are located at geographically diverse sites from San Diego County in the South to Willits in the North (Scheuermann 2004). Besides the location, the irradiance changes from hour to hour, day-to-day, or month-to-month, output of the PV system may vary with time. For selected summer and winter days, direct and diffuse irradiance measured in study is shown in Figure 32, (Thomson 2007). As shown from figure, irradiance changes not only during daytime, but also with season.

PV array power output varies depending on module temperature besides irradiance level. It means that PV array output consequently depends on the weather conditions such as ambient temperature and wind speed. Thus, alternative approaches based on weather rather than cell temperatures may be used to develop system capacity estimates (Scheuermann 2004).

The steady state irradiance at the location may be more readily integrated with the power system modeling tools. There are some data sources open to public related to PV generation. European Commission Photovoltaic Geographical Information System has interactive maps for Europe and Africa (PVGIS). National Renewable Energy Laboratory has solar maps for USA

(NREL). These organizations have dynamic solar maps that calculate daily and monthly irradiance throughout the year. Using these data, it may be found the solar insolation for a given location and a specific time.

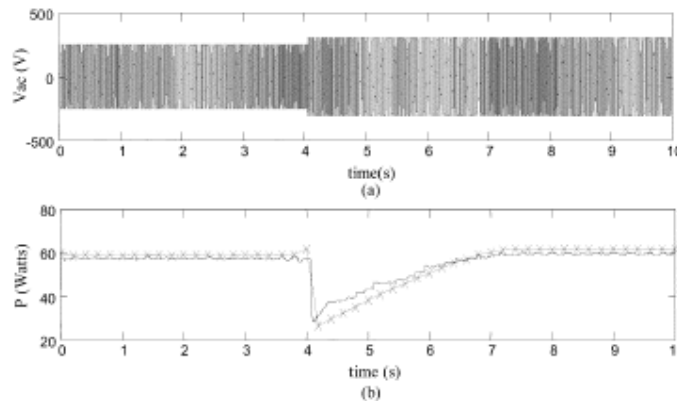
On the other hand, the properties of the PV generation system itself are more difficult to aggregate. The immediate variability conditions of the generation system will depend on the type of solar array, orientation of the solar array, aging of the solar array, dust, dirt, and snow build up on the solar array, microclimate conditions such as local cloud-cover, etc.

Transient Concerns

The properties of the components that comprise the PV generation system contribute to the transient issues that affect the behavior of the generation system in the electric grid. The transient concerns that would to be considered in developing the model may be conveniently represented by the voltage and frequency sensitivity PV array properties, MPPT dynamics, DC-DC converter dynamics, overall power conversion efficiency, anti-islanding protection and decoupling protection which inverters for PV systems should comply with, etc.

Frequency and Voltage Sensitivity

Determining the real power and reactive power sensitivity with respect to grid voltage and frequency is required to model PV system accurately. The response of a commercial PV generator to grid voltage change has been studied in laboratory conditions as reported in (Yun 2004). Figure 33 illustrates the variation of system output real power to voltage variations at the grid connections. In this study, the effect of frequency change has not been considered. While the power factor (PF) of the PV system is typically 1.0 in residential applications, central power stations can be produced reactive power to realize local voltage regulation. The need and impact of such operational variations have not been definitively established and hence a study of the system with respect to voltage and frequency is in order.



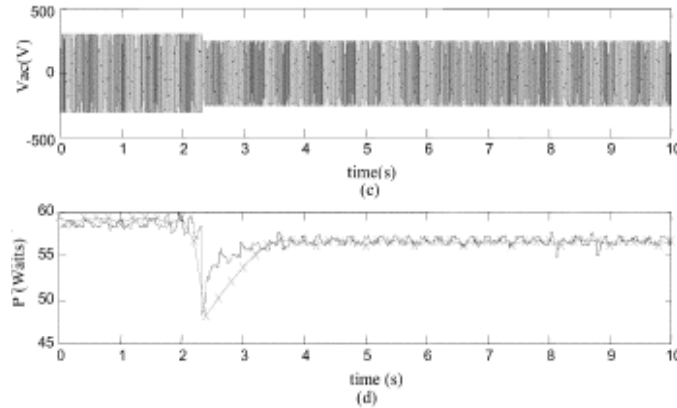


Figure 33 Response of the PV generator to increase and decrease in grid voltage (From Yun 2004)

MPPT Dynamics

A field survey of 387 different models of PV generation systems below 10 kW reported in (Salas 2009), found that all the units contain a MPPT module. Furthermore, the results of experiments carried out with three different inverters have indicated that the response time of PV generating units is significantly affected by MPPT module dynamics and efficiency (Yun 2004). Therefore MPPT dynamics of inverters that form the aggregate representation should be accounted appropriately in the system level models.

Efficiency and derating

While a typical PV system may be rated at a particular power level, equipment dynamics can have drastic impact on output of the system. Power conversion efficiency of the PV system and the de-rating factor of the design together may affect the output power of the system when grid voltage and frequency have variations. The de-rating factors and conversion efficiency may be in 0.1-0.96 ranges, while efficiency may be in the 0.7-0.98 ranges depending on the operating conditions and design cases. Therefore incorporating the collective behavior among these factors is also important in developing an appropriate system level model

Array properties

The solar array of the PV system may vary depending on the crystal used in solar cells; monocrystalline, polycrystalline and amorphous. Since solar cells produced from these materials have different levels of efficiency and aging behavior, consequently efficiencies and behaviors of PV arrays composed various solar cells also show variety.

Protection set points

Islanding is a condition that occurs when a portion of the utility system is disconnected from the remainder of the utility system but remains energized by the distributed resource (DR). Due to concerns associated with islanded system such as safety issues for service personnel and asynchronous reclose which can cause equipments to damage, the islanding is not usually desired (Wang 2009, Kunte 2008). Thus behavior of the anti-island function of the PV inverter should be considered in terms of its behavior during utility disconnection and disturbances.

Furthermore, compliance settings related to standards for distributed energy resources such as IEEE-1547, UL-1741 require decoupling protection requirements besides other regulations. For instance, a survey of the voltage tolerance curves presented in (Kunte 2008) which investigate 9 commercial PV inverters in the range of about 0.2 to 4 kW reports that all inverters except one are highly sensitive to voltage sags. None of them are capable of withstanding any voltage sag deeper than %50, lasting longer than 40 ms, as illustrated in Figure 34. Furthermore, voltage rise may also occur at the point of interconnection to the grid. Since interconnection requirements require disconnection during abnormal voltages, PV systems would disconnect themselves from the power systems under such conditions subject to their protection settings, and variable dynamics in response time. Therefore, it is important to consider and include these aspects in the PV system model representation to ensure faithful predictions from the studies.

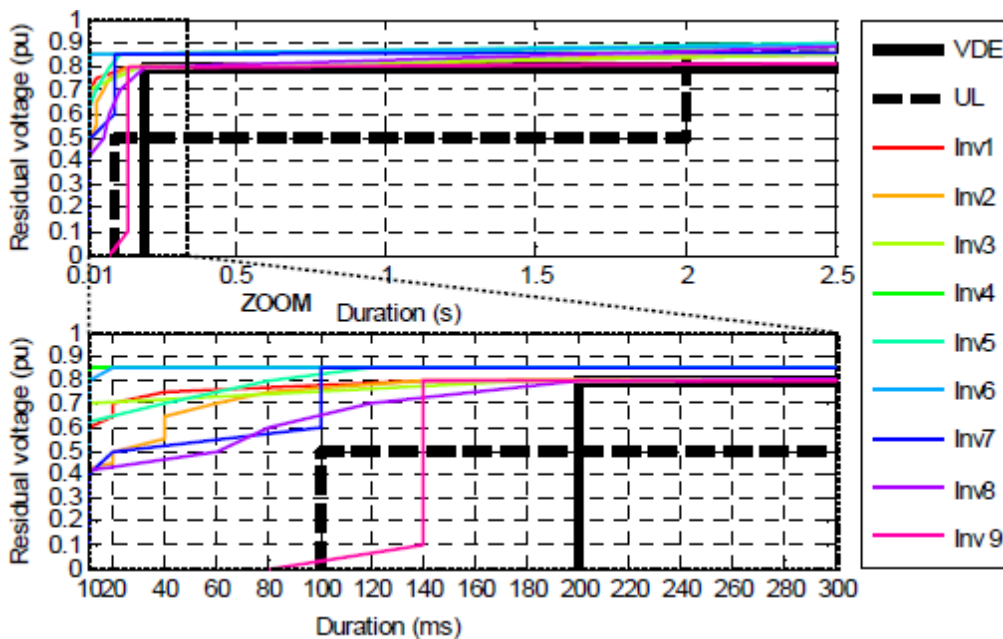


Figure 34 V Voltage tolerance curves of 9 commercial PV inverters (From Kunte 2008)

Penetration and census

Because the effects on the power systems vary with levels of PV penetration and type of PV generation system from among different commercial manufacturers and vendors, these aspects will have to be accounted appropriately in developing the system model.

7.3.3. Candidate System Model

Within the context of power system studies, system components such as power sources, loads, transformers and interconnections are widely modeled in an aggregate manner. In this mix, considering the PV system as an active load that injects energy into power system may provide more convenience, since they have not internal inertia. However, establishing the representative

analytical model that presents accurately the characteristic of grid-connected PV systems is particularly challenging in light of the discussions presented above. Alternatively, empirical model may be a more practical solution, based on laboratory scale experimental results and data from the real field measurements (Yun 2004, Salas 2009, Bletterie 2005). Such load modeling approach in power systems is among the preferred approaches in developing and validating modeling tools (Kosterev 2008).

It should be mentioned that detailed component-level models (such as those including models of PV array, MPPT part, power electronic converter, etc.) are suitable for analysis of specific PV unit or grid-independent PV system. But the precision of such modeling is generally lost in grid-level studies, where wide aggregations are made of large number PV units (such as residential area installed PV units). Therefore grid-level models that reasonably represent of PV units on the power systems should be main motivation of this study. Towards this aim, an appropriate aggregation method similar to that applied in the load aggregation may be used in order to represent the combined effect of the PV systems installed in a distribution area (Price 1988, Nozari 1987).

With such an approach, a simple, practical and faithful PV system model for electrical power systems may be established. The approach should also use an aggregated representation of distribution systems with dynamic and static loads as well as PV systems that is adequate enough for system level studies. Figure 35 illustrates a candidate representation for PV installations within the distribution system by including a ‘PV load model’ to exist the load model structure.

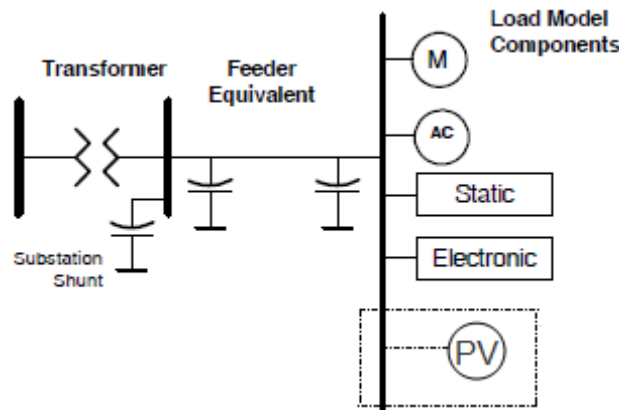


Figure 35 Structure of a candidate PV system model to be incorporated within the framework of load modeling

The heart of the candidate model is the behavioral representation of the inverter component including the various dynamics such as efficiency, MPPT and protection functions. In order to develop this, detailed tests may be carried out using several commercial PV inverters found in the market. The objective of these tests is to investigate the inverter dynamics performance during some events typically found in the grid such as voltage, and frequency fluctuations and oscillations. Additionally, transient response tests may also be carried out. For instance, a switching transient test may be used to determine the time delay when suddenly the inverter is

connected to grid. Inverter anti-island test, short circuit test, rapid power fluctuation test, etc, will provide complementary data to develop a faithful system representation. Based on test data from an array of tests on a variety of inverters, an aggregate representation that provides a weighted average of model parameters depending on the distribution of different devices among the population within the distribution system.

The development of a practical model with a user-friendly interface will be a challenging task, even given all the representative test data. The results from the test data would be classified and correlated for similarities, and differentiated for variations and an appropriate model representation to accurately represent the bulk behavior will need to be developed. On the other hand, based on the model it would be very easy to obtain results needed by entering some parameters, such as installed power, penetration level, population distribution among different manufacturers' inverters as appropriate, location of system, weather conditions, rated electrical values, into the appropriate program interface.

7.4. Conclusions and Recommendations

7.4.1. Conclusions

In this chapter, various issues related to PV generation system representation in power system studies have been discussed. A survey of the state of the art has been presented, highlighting the particular limitations and useful approaches in the literature. A summary conclusion may be stated as,

Though there are several PV modeling studies, none of them are suitable for power flow analysis at the grid-level studies in which wide aggregations are made of large number PV generation sources.

7.4.2. Recommendations

Various parametric and sensitivity aspects of PV generation sources have been identified and discussed on the basis of the literature in the field, and a candidate modeling approach has been presented. The immediate step in developing the approach further is initiating, conducting and completing comprehensive tests on commercial PV generation inverters in laboratories capable of providing grid emulation. It is learned that Southern California Edison is initiating such tests in concert with the National Renewable Energy Labs (Bravo 2009).

On the basis of the results from the tests, an aggregation and representation method may be developed as a follow on activity. Such an approach will lead to useful and practical tools for studying and preparing for high penetration of PV in the electric grid.

7.4.3. Benefit to California

The purpose of the white paper developed under this task was to review PV modeling and recommend further research if needed. PV systems are expanding and will impact the power grid in California. The recommended research, some of which has already been initiated by

SCE, should be considered a high priority. Knowledge of PV impact on the electric grid is necessary for reliable operation of the grid.

8.0 Fault-Induced Delayed Voltage Recovery

This task follows on the potential solutions to the delayed voltage recovery problem presented in Chapter 3. The information in that chapter is based on tests and studies conducted by SCE. The white paper prepared under this task gathered information on this phenomenon from other sources, including the DOE workshops focusing on fault-induced voltage recovery. In other sources, and commonly now, this phenomenon is called, “fault-induced delayed voltage recovery (FIDVR).” The white paper is presented in Appendix K.

8.1. Introduction

Fault-induced delayed voltage recovery is not a new phenomenon. While most reports of events are anecdotal, there are a few published papers describing certain events and studying the causes. In regions with a high percentage of air conditioner loads, the problem persists.

In their 1992 paper (Williams 1992), engineers from Southern California Edison discuss voltage recovery problems they had encountered in the desert regions that they serve. The largest event involved a 1000 square mile region. They also mention other similar incidents at other utilities, including a major blackout in Memphis in 1987.

In his 1997 paper (Shaffer 1997), Florida Power and Light Engineering John Shaffer reports eight incidents of delayed voltage recovery over the preceding decade. These resulted in 200-825 MW of lost load. He mentions a 1988 event with a 10-second voltage recovery. He also points out that most of the load loss was actuated by device protection (in contrast to system controlled protection).

More recent events are not described in journal articles, but have been presented at conferences and workshops. Southern California Edison continues to observe FIDVR events and they are leading research to study causes and propose solutions. One paper presents an undervoltage protection scheme and also shows a plot of a recent disturbance with a 30 second voltage recovery time (Lu 2009).

The state of the art in FIDVR reporting and research has been presented at two recent DOE workshops, in 2008 and 2009. The presentations from these workshops and the related NERC whitepaper summarize present activity in this area⁹ (NERC 2008). Events mentioned in presentations at the 2008 workshop include

⁹ 2008 workshop presentations are available at <http://sites.energetics.com/acstallingworkshop/agenda.html>

The 2009 workshop presentations are not yet posted.

- More than 50 events observed in Southern California Edison (Devers, Antelope, Vally, Lugo, Rector, Villa Park). The Lugo plane crash resulted in 3500 MW lost load.¹⁰
- Several incidences in the Arizona Public Service:¹¹
 - 2 Pinnacle Peak Capacitor Faults. The second resulted in 1000 MW load loss.
 - Hassayampa 500 kV Fault. Loss of 440 MW load and 2600 MW generation.
- Southern Company¹² reported on the Union City event in which 1900 MW of load was lost. Almost all the load was tripped by induction motor protection.

At the 2009 FIDVR workshop emphasized the following items:

- Studies suggest that SVCs help alleviate the problem but does not prevent A/C from stalling therefore the FIDVR events may still occur
- Studies also suggest that undervoltage protection devices in A/C units prevents the FIDVR events but creates another problem that is instantaneous overvoltages at high penetrations for these devices.
- The proper solutions is to have the A/C units ride thru the voltage transient or trip only the A/C units that stalled
- NERC TIS will be creating a site under their website to incorporate FIDVR so that other utilities in the country learn from the California experience.

It is clear that FIDVR events can be consequential, they persist, and they pose a challenge to the reliable operation of the power grid.

8.2. Task Approach

Information is gathered from studies conducted under this project, the literature, meetings and workshops. Researchers examine the underlying causes that drive FIDVR events, predominately the stalling of compressor-driven induction motors, and discuss potential solutions. These include the changes that could be made to units, and system controls that could mitigate FIDVR. The challenges with implementing the solutions are examined.

8.3. Task Results

8.3.1. FIDVR Phenomenon

To consider solutions to avoid or mitigate FIDVR, it is necessary to study the cause. The physical mechanism to explain the phenomenon is related to the end-use load characteristics of

¹⁰ Bob Yinger, "A/C/ Stalling at SCE," DOE Workshop, April 22, 2008.

¹¹ Baj Agrawal, "APS Experience," DOE Workshop, April 22, 2008.

¹² Taylor, "Recent Experience with Fault Induced Delayed Voltage Recovery," DOE Workshop, April 22, 2008.

air conditioners and other motor-driven compressor loads. To understand how these end-use devices react to faults, and how they can effect a slow-to-recover depressed voltage, it is necessary to consider their operation in detail.

For a compressor, the average mechanical load faced by an induction motor increases as it literally drives pistons (reciprocating compressor) or turns a “scroll” (scroll type compressor) to compress a gas. The more it is compressed, the greater the operational motor torque is needed. The electrical torque capability for an induction motor is nonlinear and depends on its operating speed. Figure 36 shows a typical “torque-speed” curve for an induction motor.

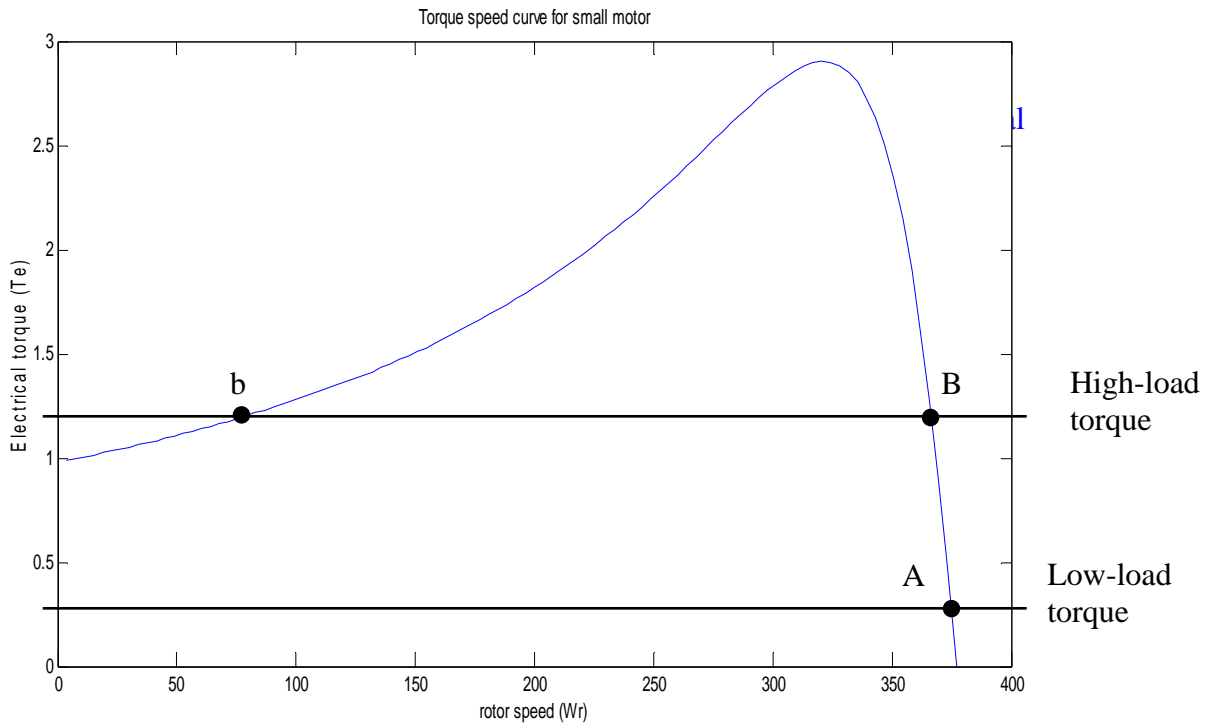


Figure 36. Torque Speed Curve for Motor.

The horizontal axis in Figure 36 is the motor speed expressed in electrical radians/second, and ranges from zero (blocked rotor or stalled) to synchronous speed: $2\pi 60$ (60 Hz). The vertical axis is torque. Superimposed on this plot are two straight-line mechanical load torque curves; one is a low load line meant to represent the compressor when it has been inactive for several minutes. The high load line represents the normal operating load under compression.

Important for this discussion is note that the zero-speed electrical torque is less than mechanical torque load. (This is discussed more below.)

When a compressor initially turns on after a few minutes of inactivity the load torque is low, and the motor quickly accelerates to normal high-speed operation. This is denoted by point “A” in Figure 36. With increased compression the mechanical load torque increases and operation tends to point “B” on the plot. This is the normal operating condition for the compressor, and this torque represents the equality of average load torque and electrical torque. For this level of mechanical load there is a second equilibrium denoted as “b” in the plot. Dynamically this other point is unstable.

For purposes of using Figure 36 to describe the phenomenon of FIDVR, note that this high load torque line intersects the zero-speed axis at a point higher than the electrical load torque. That is, the load torque exceeds the zero-speed torque capability of the motor; if the motor were to stall, it would not be able to restart. And that is exactly what happens: a temporary fault drops the voltage low enough for air conditioner motors to stop, and they are unable to restart when the fault is cleared. The stalled motors draw significant current which causes the observed depressed voltages. Protection equipment eventually remedies this situation.

Motors have two types of protection that are relevant: Contactors that disconnect when the voltage drops below 40%, and an inverse-time characteristic current relay (thermal protection). In practice the stalled voltage is typically larger than the 40% threshold, so the stalled motors stay connected to the grid. The thermal protection does actuate, removing the stalled motors from the grid. As the motors trip off-line, the voltage recovers. The motors don’t trip off simultaneously (3-15 seconds according to one manufacturer¹³), so the recovery appears gradual. The “delay” in “delayed voltage recovery” is due to the delay in motor thermal protection operation.

Once the motors are offline, they will remain offline for some time, until the compressor pressure equilibrates and the motor can restart. (Readers with newer air conditioners, dehumidifiers and other compressor-driven loads may be familiar with this characteristic: these appliances will delay a few minutes to restart after they have been turned off.) The grid response to the accumulated loss of load is to increase the voltage above pre-fault level. As previously noted, network controls will react to then lower the voltage.

The second vulnerable region occurs when air conditioners turn back on. This increased load draws the down the voltage, and without reactive power support the system is potentially susceptible to subsequent events.

The phenomenon as described in the preceding paragraphs is generally accepted as the fundamental mechanism, and it is the mechanism described in the early papers (Williams 1992, Shaffer 1997). More recent testing and model development conducted in the WECC supports this description of the FIDVR mechanism.

¹³ Jayanth, J., and H Pham, “Residential AC Compressor: Low Line Voltage Behavior,” DOE Workshop, April 22, 2008.

There are a few recent additions to the knowledge in this area that are worth mentioning. The models that are examined in the early papers represented an induction motor driving an assumed constant load torque. There are two deficiencies related to the mechanical load in that model: the inertia of the compressor is over-estimated, and the mechanical load torque is not constant. Both of these points help explain the very fast stalling time observed in laboratory tests and in the field. The air conditioner load appears to stall during the fault - measured in cycles. In the models used in the early papers the stalling of the motors is simulated by assertion – when there is voltage drop below a certain threshold, the motor is declared to be in a stalled state. Whereas simulation of the motors using parameters given in the papers do not necessarily capture such a quick stall. In (Shaffer 1997), critical clearing times are given for three motor models subject to faults of varying severity. For those severe faults with a fault voltage of 0 volts, the critical clearing time to avoid a stall ranges from 2 to 6 cycles. For fault voltages in the range of 50-55% nominal, the critical clearing time ranged from 5 to 21 cycles, depending on the initial load torque (with the range of 19-21 cycles for 1.0 pu torque). The tests in (Williams 1992) demonstrated that the air conditioners stalled within 5 cycles (their fastest test) for fault voltages below 60%. Recent laboratory tests note this quick stall - within 3 cycles (their fastest test) (Gaikwad 2008).

The models and measurements can be reconciled. First the assumed inertia in the early simulations is too large ($H = 0.28$ seconds). After recent testing, a compressor was disassembled, the rotor pulled, and its inertia was estimated to be $H = 0.03$ seconds. Laboratory tests suggest an inertia of $H=0.03$ to 0.05 seconds. This suggests a much greater propensity to stall.

Second, the load torque is not constant. One of the comments on the Shaffer paper suggested that the compressor torque may not be constant (Pal 1997). At the time, design engineers had informed the author that the torque could be considered constant for a few seconds after a fault. Recent conversations with air conditioner manufacturers indicate that the load torque is position dependent as the motor drives pistons (reciprocating) or turns the off-center scroll. The compressor load torque resembles a strong triangle wave, and the peak mechanical load torque may exceed peak electrical torque during operation. The compressor relies on the motor inertia to carry through this peak.

The WECC Load Model Task Force has been active in developing improved load models to simulate FIDVR phenomenon. That work has resulted in the development of two models for simulating compressor-driven motors, presented earlier in Chapter 2. The static performance model captures the running and stalled voltage-dependent load characteristics of the motors, with a voltage-specified transition point. A dynamic phasor model suitable for use in positive sequence simulations was developed from a traditional single phase motor model. Both are being incorporated in the standard simulation packages used to study power system behavior in the WECC.

8.3.2. Solutions

Eliminating FIDVR events will be challenging. The NERC whitepaper (NERC 2008) emphasizes this point in its executive summary: **“FIDVR events can – and have – occurred following faults**

cleared in as little as 3 cycles! The number and impact of FIDVR events can be decreased, but their elimination in the near term is unlikely.” (Their emphasis.) To eliminate these events, it would be needed to prevent the air conditioner motors from stalling. Even if new air conditioners were manufactured to avoid stalling, widespread use of new units to replace the existing installed base would take many years to change.

Customer-Level Solutions

The most effective controls may be implemented at the source of the problem: the air conditioning units. There are at least two changes that could reduce FIDVR event or severity of events:

1. Low voltage ride through. Units could be designed to withstand low voltage conditions for a short time to prevent stalling during the fault.
2. Low voltage disconnect. Units could be quickly tripped when the voltage drops to a point at which they would stall. Then, the units would return to operation after random delays, to stagger the return of load.

The first item is ideal in that it would eliminate the problem for normally cleared faults. The application of this solution would require not insignificant changes to the present design of units. One could consider over-sizing motors such that the no-load electrical torque exceeds the normal mechanical torque, with the idea that the motors would be able to restart upon re-excitation after the fault clearing. However, it is not clear that this would be successful – if motors did stall during the fault but attempted to restart simultaneously after the fault, it is likely the voltage would remain low initially. This approach would likely lessen the duration of the event, as some motors trip off-line others may succeed in restarting. Alternatively, one could increase the inertia of the motor/compressor to provide stored mechanical energy with which to ride through the event. Finally, local electrical energy storage coupled through power electronics (also driving the motor), could be implemented to achieve a low voltage ride-through capability. These latter two solutions are technologically feasible, but would increase the cost of such units. It should be expected that manufacturers would be reluctant to implement these without further and equal motivation. Any such changes would likely required modification of standards so that all manufacturers are provided the same objective.

The second item – low voltage disconnect – is practical, and offers the opportunity for effective retrofitting. This type of protection could be implemented on new units, and while it would increase costs, it is not likely be large compared to the solutions mentioned above. Also, this solution could be implemented by under-voltage relays or digital thermostatic control. The low voltage disconnect and delayed reconnect could be programmed into a modern thermostat.¹⁴ A program to retrofit digital thermostats could reduce the FIDVR problem when coordinated with system controls, and it should be considered. (See Lu 2009 for an analysis of under-voltage

¹⁴ To use thermostatic control, the thermostat would need some detection of low line voltage. Otherwise, an under-voltage relay can perform a similar function.

protection schemes in this context.) More generally, new communication and control technologies that enable a customer to actively participate in grid function (i.e., the “smart grid”) could be applied to FIDVR problems.

Unfortunately, the low voltage disconnect solution does not address all of the problem. It should effectively eliminate the delayed voltage recovery portion of the behavior at the expense of immediate loss of load. This will likely result in immediate overvoltages in the system. System level controls would need to be designed to handle this situation.

System Solutions

System solutions are covered in detail in the NERC whitepaper (NERC 2008). These solutions include

1. Reduced fault clearing time. This may reduce the occurrence of events. Given the experience with the very short time to stall for compressor-driven motors, this solution will not eliminate all events.
2. Controlled reactive power support. Generators and SVCs can provide controlled reactive power support to lessen the duration and severity of a delayed voltage recovery event.
3. Limit Impacted Load. Specifically design the system to section the load to limit its size in areas particularly vulnerable to FIDVR events. This should help contain the events.
4. Special Protection Schemes (Remedial Action Schemes). A transmission level protection scheme could be designed to contain the effect of a FIDVR event.
5. Under voltage load shedding
6. Energy Savings devices. Reducing the load could lower the risk of a FIDVR event.

In practice, generators and SVCs have been installed to mitigate these events. APS has installed generation in Phoenix, and plan to install SVCs. Southern Company has installed SVCs.

Further studies are needed to analyze the impact of these solutions. Experience and simulations suggest that reduced clearing times will not eliminate all events – the motors stall during faults. At the grid level, controlled reactive power support seem to be the most promising solution. Appropriate devices are expensive, however, and they may not be able to prevent the events,

though significant reduction in impact should be expected. (See the Pourbeik presentation that includes a simulation with and without SVC or synchronous condenser support.¹⁵)

Items 3-5 in the list above are intended to limit the scope of an event once it occurs. Item 3 is local, item 4 is at a higher level, and item 5 is offered as a measure to stop a fast-acting voltage disturbance from transitioning into a slow-acting voltage collapse. The NERC report notes that item 4 may actually be non-compliant with existing rules, and that this needs attention.

The last item may or may not improve the situation depending the nature of energy savings devices that are used.

In all cases, further study is needed to assess the success of any strategy. Most of the intuition used to consider such options follows balancing power and reactive power under FIDVR scenarios. For those solutions that quickly remove the stalled motors from service, or the feeders that serve them, one needs to be concerned about initiating dynamic instabilities. Detailed studies are needed to ensure there are no unintended consequences.

8.4. Conclusions and Recommendations

8.4.1. Conclusions

Fault Induced Delayed Voltage Recovery is a serious problem threatening the reliability of the electric power grid. Numerous events have already occurred, some with significant load loss. It is a challenging problem whose fundamental characteristics are driven by load behavior that is largely beyond the control of transmission operators. As pointed out in one presentation,¹⁶ “Normally the 12 kV voltage is a slave to the transmission system voltage. However, due to stalled motors, the 12 kV voltage sags heavily and pulls the transmission system voltage lower.”

8.4.2. Recommendations

The most effective solutions are those that can react at the site of the problem. These can also be the hardest to implement. Changes to air conditioner units to provide low voltage ride through would add additional manufacturing expense. Without standards with common requirements for all, manufacturers have a disincentive to implement such changes. Implementing new standards will take time, and even more time will pass before new units dominate the installed base. Digital thermostatic controls are promising; research and perhaps a pilot program should be put in place to determine their effectiveness. One could generalize the use of thermostatic controls to a more distributed use of technology to enable traditional customers to offer valuable grid support. Such efforts fall under the now popular title “smart grid.” As such technologies advance, an eye towards FIDVR mitigation is warranted in those areas susceptible to events.

¹⁵ P.Pourbeik, “Experience with A/C Stalling Behavior and Modeling it for Power System Studies,” DOE Workshop, April 22, 2008.

¹⁶ B. Agrawal, “APS Experience,” DOE Workshop, April 22, 2008.

System level solutions focus on containing and mitigating events. Controlled reactive power sources are essential for this purpose. Studies to assess and quantify their effectiveness are needed. Long term monitoring of events in areas with new generators and SVCs will help determine the value of these resources, and guide additional protection as needed. Research programs for such monitoring and analysis should continue.

It is imperative that California investigates further the way to mitigate the A/C stalling to prevent the FIDVR events that can have a negative impact in the grid.

8.4.3. Benefits to California

California utilities are known to be susceptible to fault-induced delayed voltage recovery. This research improved the fundamental understanding of the phenomenon and the cooperative efforts to discuss the issue will help develop long-term measures to mitigate the problem. A specific benefit of such mitigation is to increase the likelihood that such events will be contained and not lead to widespread outage.

9.0 Motor Protection

9.1. Introduction

Historically, loads in dynamic simulations have been very crudely modeled. The most common models are static functions that relate voltage and frequency to active and reactive powers. The two common voltage functions are exponential and polynomial. The latter is usually truncated at second order and is referred to as the “ZIP” model, where the letters represent impedance (electrical symbol Z), current (electrical symbol I) and power. Motor models have been available in simulation packages but were applied for special studies.

After the study of the 1996 blackout in the West, a necessary interim model was proposed (Pereira 2002) that included 20% induction motor load. The explicit incorporation of motor load was needed to match undamped oscillations that occurred during the event. Initially researchers applied a simpler load model and updated all other information about generators, generator controls, and network conditions. The model failed to capture the undamped oscillations until the load model was changed to include motor load.

The new WECC contains four explicit motor models representing high and low inertia motors, and two different mechanical load characteristics with regard to motor speed: constant torque and torque varying with speed squared. The motor models also allow one to specify voltage trip levels at which the motor will trip off-line. This simple representation for motor protection is disabled by default, but can be set by the user. The exception is the low inertia, constant torque performance model for air conditioners. This model has two protective elements modeled: undervoltage contactors and thermal protection. The thermal protection model is used to determine the amount of stalled air conditioners trip over time.

It is the delay in thermal protection that provides the delay in delayed voltage recovery. Since this characteristic proves critical for this type of motor load, it is reasonable to review motor protection in general to determine whether air conditions are special, or if other motor models should include more sophisticated representations for protection in simulation models.

9.2. Project Approach

In this preliminary white paper study, two primary sources of information are investigated: the air condition test data concerning their protection: contactors and thermal protection. This source provides first-hand details on the characteristics of these types of protection in this context. We also comment on how this information is represented a dynamic load model.

The second source is the National Electric Code (NEC 2002) maintained by the National Fire Protection Association. The NEC offers (advisory) standards for electrical installation that are often adopted by state or local laws. For the purposes of this study, it is expected that motor protection requirements appearing in the NEC are very likely to appear in practice. A review of the code will provide initial guidance into the forms of motor protection that could be included in a load model. Further study may be warranted to determine the range of protection settings in practice – those exceeding code requirements, those that may not adhere to code, and, potentially, types of protection not mentioned in the NEC.

9.3. Project Results

9.3.1. Test Results

As part of this research project, and discussed in Chapter 2, extensive testing of air conditioner units were conducted at Southern California Edison and Bonneville Power Administration. This section focuses only on the results of those tests with respect to the protection equipment on the units.

Contactors

Contactors are undervoltage relays that shut down the compressor (remove its electrical source) when the voltage falls below some value. A plot of contactor voltage drop out is provided in Chapter 2 in Figure 9 (page 28) for the units tested at SCE. It is seen that the drop out voltage ranges from 35% to 55%. Researchers note that the action of the contactor depend also on the rate of change of voltage and suggest the model for a contactor shown below in Figure 37 (LMTF 2006).

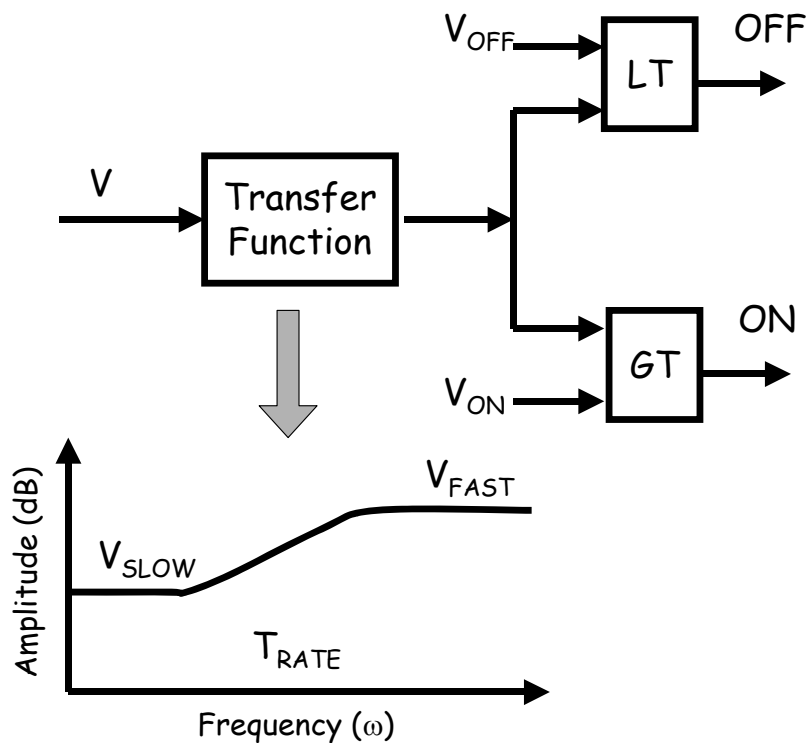


Figure 37 Contactor Model (LMTF 2006)

In the contactor model shown in Figure 37, different voltage thresholds may be specified for the tripping and reconnection, and the effect of rate of change of voltage is captured in the transfer function. In the tests researchers noted that the contactors operate quickly (2 cycles).

Thermal Protection

Thermal protection for the compressor motor is in place to protect the motor from overheating from excessive stall currents. In Chapter 2, Figure 8 (page 27) shows the experimental data for thermal protection operation as a function of stalled voltage. The higher the stall voltage, the higher the stall current and the quicker the thermal protection would operate.

This inverse relation between time delay in operation of thermal protection and stall current is typical for these protective devices. The higher the current the faster the operation. The inverse time characteristic for a sample room air-conditioner is presented below in Figure 38 (LMTF 2006).

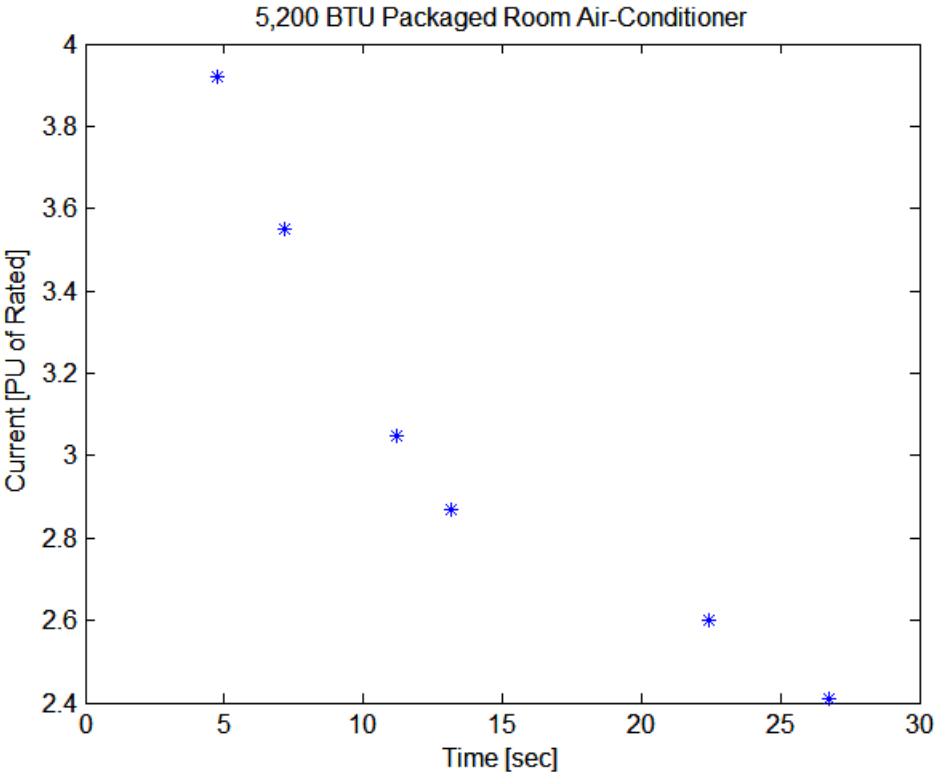


Figure 38. Thermal Relay Characteristic (LMTF 2006)

A block diagram model for a thermal relay is presented below in Figure 39 (LMTF 2006).

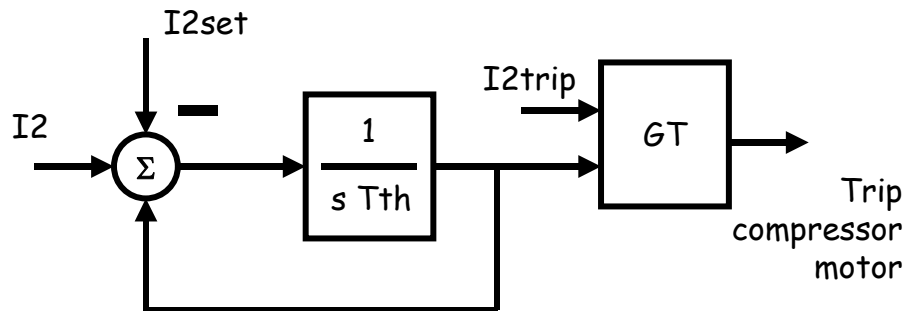


Figure 39. Thermal relay model (LMTF 2006)

The transfer function in Figure 39 delays the response in the operation of the thermal relay. The delay decreases with increased stall current.

It has been noted several times in this report that the delay in the thermal protection explains the delayed voltage recovery observed in practice. There is an initial delay before any unit trips offline. As units trip offline the voltage tends to rise (recover) with decreased load. The increased voltage yields higher stall current which in turn stress the remaining units to trip. The thermal relay model is useful as practical temporal model for approximating the percentage of units that trip.

9.3.2. National Electric Code

This section reviews relevant articles of the NEC pertaining to the protection of motor equipment. The 2002 NEC (NEC 2002) is used for this purpose. While there is a newer version of the NEC issued in 2008, the 2002 version is cited because its codes will be more relevant to the discussion of the existing range of motors that are currently in the field today.

Chapter 4 of the NEC, "Equipment in General Use," has three articles that are potentially relevant to motor protection for load modeling:

- Appliances – Article 422
- Motors, motor circuits, and controllers – Article 430
- Air conditioning and refrigerating equipment - Article 440

Appliances (422)

For motor-operated appliances, Article 422.11(G) specifies that overcurrent protection for motors must be in accordance with the overload protection specified Articles 430 and 440.

A mean must in place to disconnect an appliance. Generally for appliances, the means for disconnection involve switches, cord-and-plugs, and circuit breakers. The first two means do not involve automatic action and are not relevant for modeling loads, and the modeling of circuit breakers are not specific to motor models considered here.

Motors, motor circuits, and controllers (430)

In this examination of the code we focus on protection directly applied to motors. This article in the NEC also deals with motor circuits and their protection, and the protection of electric circuits that provide motor controls. For the purposes of load modeling we presume that the direct motor protection is important for modeling. That is, the circuits supplying the motor are properly sized so that protection of motor overload is local to the motor. This assumption, of course, may not always be true, but provides a basis to start modeling motor protection.

Various means of overload protection are possible depending on the size of motor, and its application. A distinction is made between continuous duty and intermittent duty applications. All applications are treated as continuous duty unless “the nature of the apparatus it drives is such that the motor cannot operate continuously with load under any condition of use.” (NEC 2002, 430.33, p. 70-294.) For example, an elevator can be considered intermittent duty – its time serving load is necessarily bounded.

For continuous duty application, a distinction is made by motor rating. For motors rated above 1 horsepower, overload protection must be one of the following four types

1. Separate overload device that responds to current. The current trip rating should not exceed:
 - a. 125% full load current for those motors marked with service factor 1.15 or above.
 - b. 125% full load current for those motors marked with temperature rise of 40° C or less.
 - c. 115% full load current for all other motors.
2. Thermal protector. The ultimate overload current should not exceed:
 - a. 170% full load current when full load current is 9 amps or less
 - b. 156% full load current for motors with full load current greater than 9 amps and less than or equal to 20 amps.
 - c. 140% full load current for motors with full load current greater than 20 amps.
3. Integral with motor. A device that protects the motor against failure to start is allowed by the NEC provided “the motor is part of an approved assembly that does not normally subject the motor to overloads.” (NEC 2002, 430.32 (A)(3), p. 70-293).

4. Larger than 1500 HP. These larger motors must have embedded temperature sensor that react when the temperature exceeds the nameplate temperature rise in ambient temperature of 40° C.

An exception to type 1 above is allowed if the motor requires greater amperage to start. In this case the three current trip ratings mentioned above for type 1 should not exceed 140%, 140% and 130% respectively.

Similar conditions are specified for motors with ratings lower than 1 horsepower. The details are omitted in this summary. Those listed above provide guidance for the types of protection may need to be considered for load modeling purposes, and specific default values that may be considered for protection types 1 and 2 are provided.

Protection type 3 appears to be special to approved applications and may be treated that way in load models, or ignored as a first step toward typical load models. Protection types 2 and 4 are of the thermal overload type, with type 2 being discussed in the previous section with air conditioners. Type 4 pertains to large motors. It would be inconvenient to introduce simulations for temperature rise for these specific applications; it is likely that the current-based thermal protection model would be suitable for simulation purposes. Type 1 appears to be a protective device acting directly on current and could be easily modeled for those types of load that require it. Further research will be required to identify which typical load applications correspond to the typical protection.

Air Conditioning and Refrigeration Equipment (440)

This article of the NEC deals directly with hermetic refrigerant motor-compressor. Other configurations are handled by articles addressing appliances and motors. As with the general motor loads, for purposes of modeling protection, this summary focuses on the protection requirements for the motor-compressor, recognizing that additional protection is specified in code for connected circuitry. Further research might be warranted to investigate branch circuit requirements; here an assumption is applied that the first step in modeling motor protection is the protection closest to the motor.

Protection of the motor-compressor is specified in Article 440.52 (A) of the NEC. Protection for overload and failure to start should be provided by one of the following types:

1. A separate overload relay designed to trip at no more than 140% rated load current.
2. An integral thermal protector that prevents “dangerous overheating.” This device must be able to operate a current interruption device to interrupt current on overload.
3. Fuse or inverse time circuit breaker. The current rating should not exceed 125% rated load current, and should have a time delay to allow the motor-compressor to start. This protection device can also serve as the branch circuit protection.
4. A protective system designed to protect against “dangerous overheating” and failure to start. This system must be able to operate a current-interrupting device.

Type 1 operates solely on current and is easily implemented in a simulation. Type 2 and type 3 can likely be modeled in a similar fashion for inclusion in a load model, such as presented in Figure 39. The description for Type 4 is vague; modeling would depend on the specific details of the protection system.

9.4. Conclusions and Recommendations

9.4.1. Conclusions

Both contactor and thermal protection are included in the single-phase air-conditioner model in the WECC composite load model. They have been tested in the laboratory and are understood for the purposes of load modeling.

The other three motor models in the WECC composite load model motor protection as a function of voltage. (These are disabled by default.) Two voltage levels with delay settings can be set along with a corresponding amount of motor load to trip. For each voltage trip level, a reconnection level with delay may also be set to restore motor load. No direct distinction is made between the operation of undervoltage contactors or motor overload.

The NEC clearly indicates the need for motors to be equipped with overload protection. (For small motors, this protection might be supplied by the circuit.) It is reasonable then to incorporate an overload protection model in the load model, although it is not entirely clear the best way to do this. For single-phase air conditioners there is an assumption in the models that if all air conditioners stall at a location, and this assumption is largely supported by the test in which all units stall quickly. For other motor loads, however, it is not obvious that they will all simultaneously overload under the same conditions. This issue needs consideration to see if any more sophisticated modeling will offer a better model the presently implemented model.

9.4.2. Recommendations

Further research is warranted to gather specific information on typical motor protection types by motor application, and WECC has initiated a project to do this. With this information, there remains the issue on how to best apply the features of protection in a load model. It is not uniformly applied in the motor models at present.

Overload protection is based on thermal or current characteristics. It is recommended that current-based thermal protection be used in motor models.

9.4.3. Benefit to California

The feature that drives the delayed voltage recovery phenomenon is related to thermal protection in air conditioner units. Proper modeling of this is already incorporated in the improved models discussed in this load modeling report. Similar testing and knowledge of protective action for other motor applications is lacking and not currently modeled in our test systems. This potentially could lead to surprises in operation if motor overload operation were to occur but was not modeled in the dynamic models used in simulation.

Better models for motor protection will benefit California by increasing the confidence in operational planning studies as well as providing knowledge that will help operators understand the impact of motor protection operation when it occurs.

10.0 References

- Azmy, A.M., and I. Erlich. 2004. "Identification of dynamic equivalents for distribution power networks using recurrent ANNs" Power Systems Conference and Exposition, 2004. IEEE PES, vol., no., pp. 348-353 vol.1, 10-13 Oct. 2004
- Blackburn, J.L. 1998. Protective Relaying Principles and Applications, Marcel Dekker, New York, 2nd edition.
- Bletterie, B., R. Brundlinger, and H. Fechner. 2005. "Sensitivity of photovoltaic inverters to voltage sags-test results for a set of commercial products" , IEE Conf. Pub. 2005, v2-67 (2005)
- Boemer, J.C., M. Gibescu, and W.L. Kling. 2009. "Dynamic models for transient stability analysis of transmission and distribution systems with distributed generation: An overview" PowerTech, 2009 IEEE Bucharest, vol., no., pp.1-8, June 28 2009-July 2 2009
- Bravo, R. 2009. Inverter Test Procedures Solar Generation Impact Study Private e-mail communication, 22 Dec 2009.
- Canova, A., L. Giaccone, F. Spertino, and M. Tartaglia. 2009. "Electrical Impact of Photovoltaic Plant in Distributed Network," Industry Applications, IEEE Transactions on , vol.45, no.1, pp.341-347, Jan.-feb. 2009.
- Feehery, W.F., J.E. Tolsma, and P.I. Barton. 1997. "Efficient sensitivity analysis of large-scale differential-algebraic systems," Applied Numerical Mathematics, vol. 25, pp. 41-54, 1997.
- Frank, P.M. 1978. *Introduction to System Sensitivity Theory*, Academic Press, New York, 1978.
- Gaikwad, A.M., R.J. Bravo, D. Kosterev, S. Yang, A. Maitra, P. Pourbeik, B. Agrawal, R. Ying, and D. Brooks. 2008. "Results of Residential Air Conditioner Testing in WECC," IEEE Power Engineering Society General Meeting, 20-24 July, 2008.
- Hiskens, I.A., M.A. Pai, and T.B. Nguyen. 1999. "Dynamic contingency analysis studies for inter-area transfers," in *Proceedings of 13th Power Systems Computation Conference*, Trondheim, Norway, June 1999.
- Hiskens, I.A., and M.A. Pai. 2000 "Trajectory sensitivity analysis of hybrid systems," *IEEE Transactions on Circuits and Systems I: Fundamental Theory and Applications*, vol. 47, no. 2, pp. 204-220, February 2000.
- Hiskens, I.A. 2001. "Nonlinear dynamic model evaluation from disturbance measurements," *IEEE Transactions on Power Systems*, vol. 16, no. 4, pp. 702-710, November 2001.
- Hiskens, I.A. 2004. "Power system modeling for inverse problems," *IEEE Transactions on Circuits and Systems I: Regular Papers*, vol. 51, no. 3, pp. 539-551, March 2004.

Hiskens I.A., and J. Alseddiqui. 2006. "Sensitivity, approximation and uncertainty in power system dynamic simulation," *IEEE Transactions on Power Systems*, vol. 21, no. 4, November 2006.

IEEE Std 421.5-1992. 1992. *IEEE Recommended Practice for Excitation System Models for Power System Stability Studies*, Institute of Electrical and Electronics Engineers, Inc., New York, 1992.

IEEE Task Force on Load Representation for Dynamic Performance. 1993. "Load Representation for Dynamic Performance Analysis." *IEEE Transactions on Power Systems*, vol.8, no.2, (1993): 472-482.

IEEE Task Force on Load Representation for Dynamic Performance. 1995. "Standard Models for Power Flow and Dynamic Performance Simulation." *IEEE Transactions on Power Systems*, vol.10, no.3, (1995): 1302-1313.

International Energy Agency (IEA). 2008. Trends in Photovoltaic Applications Survey report of selected IEA countries between 1992 and 2007, International Energy Agency Report, 2008

Kosterev, D., A. Meklin, J. Undrill, B. Lesieutre, W. Price, D. Chassin, R. Bravo, and S. Yang. 2008. "Load modeling in power system studies: WECC progress update." *2008 IEEE Power and Energy Society General Meeting - Conversion and Delivery of Electrical Energy in the 21st Century*, 20-24. (2008): 1-8.

Kunte, R.S.; W. Gao, 2008. "Comparison and review of islanding detection techniques for distributed energy resources," Power Symposium, 2008. NAPS '08. 40th North American , vol., no., pp.1-8, 28-30 Sept. 2008

Li, S., L. Petzold, and W. Zhu. 2000. "Sensitivity analysis of differential-algebraic equations: A comparison of methods on a special problem," *Applied Numerical Mathematics*, vol. 32, no. 8, pp. 161-174, 2000.

LMTF. 2006. Residential Single-Phase Air Conditioner Modeling, WECC Load Modeling Task Force white paper, October 2006.

Lu, N., B. Yang, Z Huang, and R. Bravo. 2009. "The System Impact of Air Conditioner Under-voltage Protection Schemes," Power System Conference and Exposition, 15-18 March, 2009.

NERC. 2008. Fault-Induced Delayed Voltage Recovery, NERC Transmission Issues Subcommittee Technical Reference Paper, December 2008.

Nguyen, T.B., M.A. Pai, and I.A. Hiskens. 2002. "Sensitivity approaches for direct computation of critical parameters in a power system," *International Journal of Electrical Power and Energy Systems*, vol. 24, pp. 337-343, 2002.

Nocedal, J., and S.J. Wright, 1999. *Numerical Optimization*, Springer-Verlag, New York, 1999.

Nozari, F.; M.D. Kankam, W.W. Price. 1987. "Aggregation of Induction Motors for Transient Stability Load Modeling," *Power Systems, IEEE Transactions on* , vol.2, no.4, pp.1096-1103, Nov. 1987

NREL. U.S. Department of energy, National Renewable Energy Laboratory.
<http://www.nrel.gov/gis/solar.html>.

Pai, M.A. 1989. *Energy Function Analysis for Power System Stability*, Kluwer Academic Publishers, Boston, MA, 1989.

Pal, M.K. 1997. Discussion of "Air Conditioner Response to Transmission Faults." , IEEE Transactions on Power Systems, Vol. 12, No 2, May 1997.

Papanikolaou, N.P., E.C. Tatakis, A.C. Kyritsis. 2009. "Analytical model for PV – Distributed generators, suitable for power systems studies" Power Electronics and Applications, 2009. EPE'09. 13th European Conference on, vol., no., pp.1-10, 8-10 Sept. 2009.

Pereira, L., D. Kosterev, P. Mackin, D. Davies, J. Undrill, and W. Zhu. 2002. "An Interim Dynamic Induction Motor Model for Stability Studies in WSCC." *IEEE Transactions on Power Systems*, vol.17, no.4, (2002): 1108-1115.

Picault, D., B. Raison, and S. Bacha. 2009. "Guidelines for evaluating grid connected PV system topologies," Industrial Technology, 2009. ICIT 2009. IEEE International Conference on , vol., no., pp.1-5, 10-13 Feb. 2009

PVGIS. European Commission, Joint Research Centre, Photovoltaic Geographical Information System. <http://re.jrc.ec.europa.eu/pvgis>.

Price, W.W., K.A. Wirgau, A. Murdoch, J.V. Mitsche, E. Vaahedi, M. El-Kady. 1988. "Load modeling for power flow and transient stability computer studies," Power Systems, IEEE Transactions on , vol.3, no.1, pp.180-187, Feb 1988

Pourbeik, P., A. Maitra, A. Gaikwad, and D. Brooks. 2007. "Developing a Bulk System Load Model in GE PSLF TM for Investigating the Valley Delayed Voltage Recovery Events", December 2, 2007, report issued by EPRI under SCE contract.

Reza, M., J.G. Slootweg, P.H. Schavemaker, W.L. Kling, and L. van der Sluis. 2003. "Investigating impacts of distributed generation on transmission system stability," Power Tech Conference Proceedings, 2003 IEEE Bologna , vol.2, no., pp. 7 pp. Vol.2-, 23-26 June 2003.

Salas, V., P.J. DeBora, and E. Olias. 2009. "Field analysis of commercial PV inverters in the 5 kW power range with respect to MPPT effectively," Power Electronics and Applications, 2009. EPE '09. 13th European Conference on , vol., no., pp.1-7, 8-10 Sept. 2009

Scheuermann, K., D. Boleyn, P. Lilly, and S. Miller. 2004. "Measured Performance of California Buydown Program Residential PV Systems", California Energy Commission, Consultant Report, 2004

Shaffer, J.W. 1997. "Air Conditioner Response to Transmission Faults," IEEE Transactions on Power Systems, Vol. 12, No 2, May 1997.

Sauer, P.W., and M.A. Pai. 1998. *Power System Dynamics and Stability*, Prentice Hall, Upper Saddle River, NJ, 1998.

SourceForge.net. <http://sourceforge.net/projects/gridlab-d/files/load-composition/>.

Thomson, M., and D.G. Infield, D.G. 2007. "Impact of widespread photovoltaics generation on distribution systems" Renewable Power Generation, IET, vol.1, no.1, pp.33-40, March 2007

Thong, V.V., J. Driesen, and R. Belmans. 2007. "Transmission system operation concerns with high penetration level of distributed generation," Universities Power Engineering Conference, 2007. UPEC 2007. 42nd International , vol., no., pp.867-871, 4-6 Sept. 2007

Wang, F., C. Zhang; and Z. Mi. 2009. "Anti-islanding Detection and Protection for Grid Connected PV System Using Instantaneous Power Theory," Industrial and Information Systems, 2009. IIS '09. International Conference on , vol., no., pp.413-416, 24-25 April 2009.

Wang Y.-B.; C.-S. Wu, H. Liao, and H.-H. Xu. 2008. "Steady-state model and power flow analysis of grid-connected photovoltaic power system" Industrial Technology, 2008. ICIT 2008. IEEE International Conference on , vol., no., pp.1-6, 21-24 April 2008.

Williams, B.R., W.R. Schmus, and D.C. Dawson. 1992. "Transmission Voltage Recovery Delayed by Stalled Air Conditioner Compressors," IEEE Transactions on Power Systems, Vol. 7, No. 3, August 1992.

Yazdani, A., A. Difazio, H. Ghoddami, M. Russo, M. Kazerani, and K. Strunz. 2009. "A General Discussion on Modeling and Simulation of Three-Phase Single-Stage Grid-Connected PhotoVoltaic (PV) Systems", Paper presented at IEEE PES General Meeting, July 2009.

Yun Tiam Tan; D.S. Kirschen, N. Jenkins. 2004. "A model of PV generation suitable for stability analysis," Energy Conversion, IEEE Transactions on , vol.19, no.4, pp. 748-755, Dec. 2004

11.0 Glossary

AVR	Automatic Voltage Regulator
BPA	Bonneville Power Administration
CSP	Concentrated Solar Power
DFR	Digital Fault Recorder
DG	Distributed Generation
DSM	Disturbance Management System
DMWG	Disturbance Monitoring Working Group
DOE	Department of Energy
EPRI	Electric Power Research Institute
FIDVR	Fault-Induced Delayed Voltage Recovery
ICLSS	Import Contingency Load Scheduling Scheme
IEEE	Institute of Electrical and Electronic Engineers
IPC	Idaho Power Company
LBNL	Lawrence Berkeley National Laboratory
LMTF	Load Modeling Task Force
MPPT	Maximum Power Point Tracking
MVWG	Modeling and Validation Working Group
NEC	National Electric Code
NERC	North American Electric Reliability Council
NREL	National Renewable Energy Laboratory
PGE	Pacific Gas and Electric
PIER	Public Interest Energy Research
PMU	Phasor Measurement Unit
PNNL	Pacific Northwest National Laboratory
PPSM	Portable Power System Monitor
PSE	Puget Sound Energy

PSLF	Positive Sequence Load Flow
PSS	Power System Stabilizer
PV	Photovoltaic
PVGIS	Photovoltaic Geographical Information System
SCADA	Supervisory Control And Data Acquisition
SCE	Southern California Edison
SEER	Seasonal Energy Efficiency Ratio
SVC	Static Var Compensator
TXV	Thermostatic Expansion Valve
VAR	Volt-Ampere Reactive
WECC	Western Electricity Coordinating Council

FINAL PROJECT REPORT

LOAD MODELING TRANSMISSION RESEARCH

APPENDIX A

AIR CONDITIONER STALLING EFFECTS STUDY

AIR CONDITIONER TESTING PROCEDURES

Prepared for CIEE By:

Lawrence Berkeley National Laboratory



A CIEE Report



Air Conditioner Stalling Effects Study Air Conditioner Testing Procedures

By:
TDBU
**Engineering Advancement
Technology Integration**

Robert Yinger
Richard Bravo
David Martinez

1.0	OBJECTIVE	5
1.1	Measurements	5
2.0	EQUIPMENT REQUIRED	7
3.0	AIR CONDITIONER INSTALLATION AND SETUP.....	9
3.1	Initial Charge	9
3.1.1	Superheat Calculation Method.....	9
3.1.2	Subcooling Calculation Method	9
3.2	Air Conditioner Monitoring Transducers	10
4.0	AIR CONDITIONER SYSTEM PERFORMANCE TESTS	11
4.1	Test 1 - Test the inrush current of the air conditioner unit	11
4.2	Test 2 - Test the compressor contactor critical voltage	11
4.3	Test 3 – Test the compressor stall voltage	13
4.4	Test 4 – Test the compressor over-temperature trip time	13
4.5	Test 5 – Test the compressor stall reaction to short under-voltage transients	14
5.0	AIR CONDITIONER SYSTEM RESEARCH TESTS.....	16
5.1	TEST THE COMPRESSOR UNDER STEADY-STATE CONDITIONS	17
5.1.1	Test 6 – Test the compressor reaction under non-stalling voltages	17
5.1.2	Test 7 –Test compressor reaction under different frequencies.....	18
5.2	TEST THE COMPRESSOR WITH CONTACTOR IN THE CIRCUIT	19
5.2.1	Test 8 – Test the compressor reaction to short under-voltage transients with contactor.....	19
5.2.2	Test 9 – Test the compressor reaction to short under-voltage transients with different recovery voltages	20
5.3	TEST THE COMPRESSOR WITH CONTACTOR BYPASSED	20
5.3.1	Test 10 – Test the compressor reaction to short under-voltage transients	21
5.3.2	Test 11 – Test the compressor reaction to short under-voltage transients with different recovery voltages	21
5.3.3	Test 12 – Test the compressor reaction to ramp-voltage transients	22
5.3.4	Test 13 – Test the compressor reaction to voltage-oscillation transients.....	23
5.3.5	Test 14 – Test the compressor reaction to frequency transients	25
5.3.6	Test 15 – Test the compressor reaction to frequency-oscillation transients	26
6.0	DATA ANALYSIS.....	27
4.1	<i>Volts & Amps versus Time Graph</i>	28
4.2	<i>Watts & VARs versus Time Graph</i>	28
4.3	Start-up Transient <i>Volts & Amps versus Time Graph</i>	29
4.4	Start-up Transient <i>Watts & VARS versus Time Graph</i>	30
7.0	APPENDIX.....	31
7.1	Grid Simulator Controller Programs.....	31
7.2	AC Specifications Data Sheets	31
7.3	AC Testing Data Log Sheets.....	31

1.0 OBJECTIVE

SCE and other utilities have had several occurrences of delayed voltage recovery following faults on the electrical system. Under normal conditions, voltage recovers to normal levels in less than one second after the fault is cleared. In several cases in the past few years, voltage recovery has been delayed for over 30 seconds after normal fault clearing in the Valley Substation area. This delayed voltage recovery is being attributed to stalling of air conditioner units. Testing of air conditioner units is being conducted to determine how they behave when exposed to various under-voltage conditions. These test results will help to properly models the electrical system and determine possible solutions to this problem.

The objective of this testing is to investigate the air conditioner stalling parameters during transient under-voltage conditions. This testing will provide additional understanding of the behavior of the different air conditioner units used in our service territory. It is expected that up to 10 different air conditioner units will be tested.

The following test procedures are required to be performed for each air conditioner unit. Each unit test is composed of fifteen (15) sub-tests (**Test 1** thru **Test 15**).

1.1 Measurements

The air conditioner test shall provide at least four voltages (V_1 , V_2 , V_3 , and V_4) and four currents (I_1 , I_2 , I_3 , and I_4) (see table 1). The voltages and currents need to be captured in the condenser side of the air conditioner (outdoor unit). In addition to the voltages and currents required above, the real power (W) and apparent power (VA) are also required (see Table 2). The Power Analyzer (Yokogawa) can mathematically calculate real, apparent powers and frequency.

TAG	DESCRIPTION	Yokogawa	
		MATH	EXPRESSION
V ₁	Input Voltage	1	Trend(C1)
V ₂	Compressor Motor Running Winding Voltage	3	Trend(C3)
V ₃	Capacitor Voltage	5	Trend(C5)
V ₄	Compressor Motor Start Winding Voltage	7	Trend(C7)
I ₁	Input Current	2	Trend(C2)
I ₂	Compressor Motor Running Winding Current	4	Trend(C4)
I ₃	Fan Motor Current	6	Trend(C6)
I ₄	Compressor Motor Start Winding Current	8	Trend(C8)

Table 1

Tag	Description	Yokogawa	
		MATH	EXPRESSION
W ₁	Total Real Power	9	Trend(C1*C2)
W ₂	Compressor Motor Running Winding Real Power	11	Trend(C3*C4)
W ₃	Compressor Motor Start Winding Real Power	13	Trend(C7*C8)
F	Frequency	15	Trendf(C1)
VA ₁	Total Apparent Power	10	Trend(C1)*Trend(C2)
VA ₂	Compressor Motor Running Winding Apparent Power	12	Trend(C3)*Trend(C4)
VA ₃	Compressor Motor Start Apparent Power	14	Trend(C7)*Trend(C8)

Table 2

All of these required voltages, currents, real power, apparent power, and frequency measurements shall be synchronized. A macro will need to be created to filter the data and calculate the reactive power (VARs) and power factor (PF).

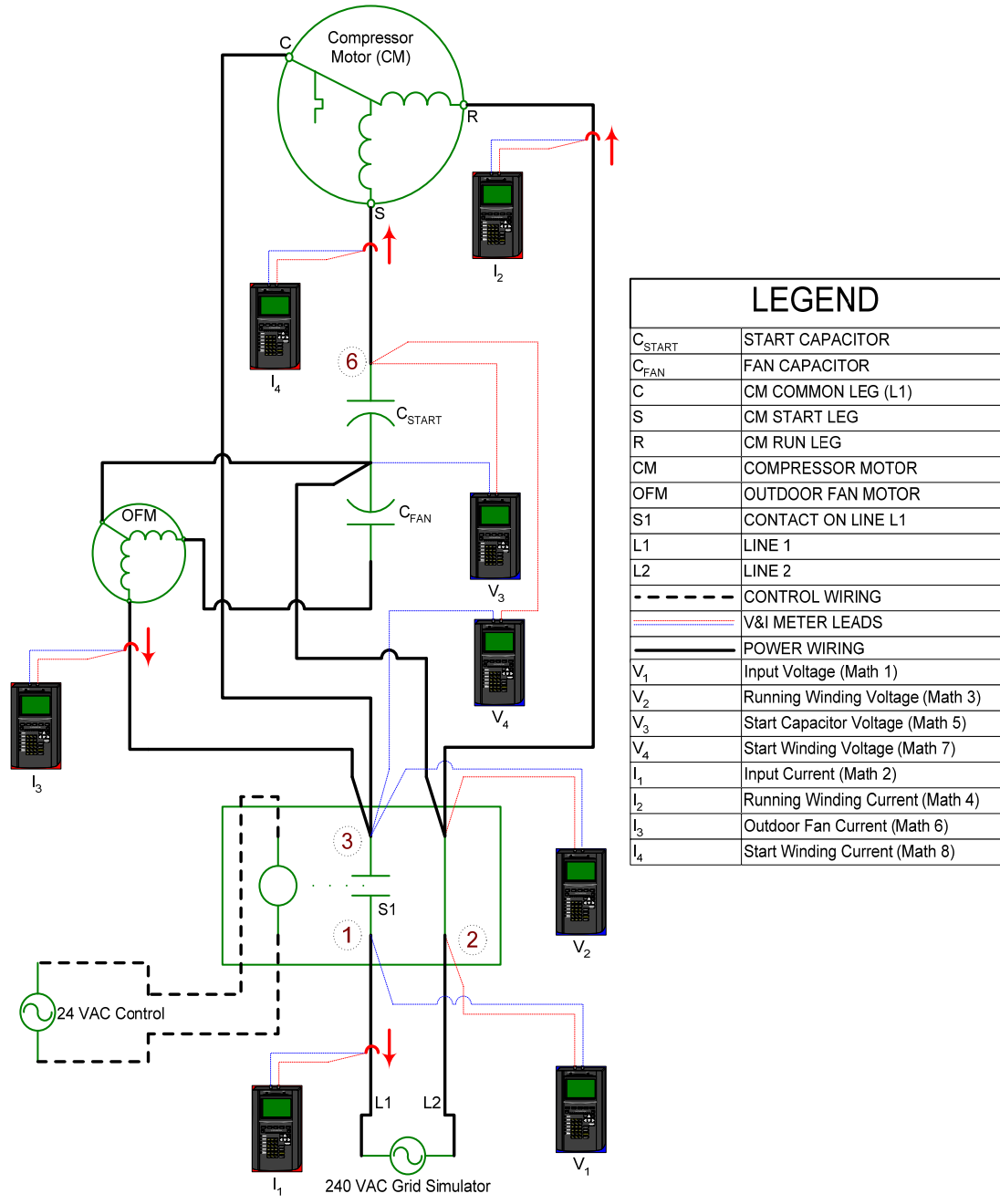


Figure 1

2.0 EQUIPMENT REQUIRED

The equipment required is the following:

- ✓ **Grid Simulator:** A variable power source that simulates different voltages with 1/80 cycle transition time. For these tests, a 62.5 kVA Pacific Power Source System (3060-MS) will be used.
- ✓ **Programmable Controller:** A signal generator that produces the different voltage profiles (sags) for the grid simulator. For these tests, a Pacific Power Source Programmable Transient/Signal Generator (SCU/UPC-32) will be used.
- ✓ **Power Analyzer:** A measuring device to monitor and record voltage, current, power, and power factor. For these tests, a Yokogawa PZ4000 Power Analyzer will be used.
- ✓ **Clamp-on Current Transformers:** Used to reduce current levels so they can be input to the power analyzer. For these tests, IEMC Instruments (SR 632) CTs with a CT ratio of 5000/1 will be used.
- ✓ **Voltage Leads:** Used to supply voltage to the power analyzer
- ✓ **Environmental Test Chamber:** Simulates the different outdoor temperatures ($T_{\text{outdoor}} = 80^{\circ}\text{F}$, 100°F , & 115°F) required for the tests.
- ✓ **Air Flow Transducer:** Monitors airflow of the air conditioner indoor unit. For these tests, an Electronik (EE70) will be used.
- ✓ **Temperature Transducers:** Monitors temperatures in the environmental test chamber, air conditioner outdoor unit, compressor case, and air conditioner indoor unit. For these tests, Omega Type T thermocouples will be used. These temperatures will be recorded at a sample rate of 12 readings per minute.
- ✓ **Pressure Transducers:** Monitors the pressures at both the suction side (in) and the liquid side (out) of the condenser. For these test, SETRA Model 207 (250, 500, 1000 PSI) pressure transducer will be used. These pressure transducers will have a refresh rate of two (2) milliseconds.
- ✓ **Laptop:** Interfaces with the power analyzer, thermocouples, air flow transducer, and records the test data

3.0 AIR CONDITIONER INSTALLATION AND SETUP

The air conditioner's outdoor unit shall be placed in the environmental simulation chamber. This chamber shall simulate different outdoor temperatures ($T_{\text{outdoor}} = 80^{\circ}\text{F}, 100^{\circ}\text{F}, \& 115^{\circ}\text{F}$). The air conditioner's indoor unit shall be placed in a closed and steady-state temperature room (for these tests this closed room will be the temperature controlled EV Technical Center lab space). Both, the air conditioner outdoor unit and indoor unit shall be connected, electrically and mechanically, to perform as one single unit. The temperatures and airflow rate in the indoor unit shall be recorded. The temperature used for the indoor unit is targeted to be in the range of 75°F to 80°F . The power analyzer records the voltage and current at the air conditioner terminals. The programmable controller will generate the transients/signals for the test. The Grid Simulator will amplify the transients/signals generated by the programmable controller to the needed level.

3.1 Initial Charge

It is imperative that all air conditioner units to be tested have the same initial conditions and installation parameters. The initial conditions need to be acquired from the Refrigerant Reference Guide, 4th edition 2004. The new A/C units come with compressed refrigerant in the compressor. The refrigerant need to be released into the air conditioner system. Let the system run for at least 30 minutes at any outdoor simulated temperature (recommended 80F). The charge on the R-22 or R-410A systems need to be back checked by either Superheat and/or Subcooling calculations methods.

3.1.1 Superheat Calculation Method

Superheat calculation method is used only when the air conditioner system is equipped without TXV valve. Read the pressure at the suction (vapor) line and convert it to the saturated temperature, using table 13 below. Read the temperature in the suction (vapor) line. Now, need to compare the saturated temperature with the reading temperature. Superheat normal range is 10°F to 15°F (or otherwise recommended by manufacturer).

Example: Charging an R-22 air conditioner system. The suction (vapor) pressure line reading is 60 PSI. The saturated temperature (table 3) is about 34°F for 60 PSI, see table 3 below. The temperature reading for the suction (vapor) line is 44°F . The difference between the suction (vapor) temperature and the reference saturated temperature is ($44^{\circ}\text{F} - 34^{\circ}\text{F}$) 10°F . The 10°F is in the range of the superheat.

3.1.2 Subcooling Calculation Method

Subcooling calculation method is used only when the air conditioner system is equipped with TXV valve. Read the pressure at the release (liquid) line and convert it to the saturated temperature, using table 13 below. Read the temperature in the release (liquid). Now, need to compare the saturated temperature with the reading temperature. Subcooling normal range is 8°F to 12°F (or otherwise recommended by manufacturer).

Example: Charging an R-22 air conditioner system. The release (liquid) pressure line reading is 254 PSI. The saturated temperature (table 3) is about 118°F for 254 PSI, see table 3 below. The temperature reading for the release (liquid) line is 109°F . The difference between the suction (vapor) temperature and the reference saturated temperature is ($118^{\circ}\text{F} - 109^{\circ}\text{F}$) 9°F . The 9°F is in the range of the subcooling.

T (°F)	R-22 (PSI)	R-410A (PSI)
15	37.8	70.0

20	43.1	78.3
25	48.8	87.3
30	54.9	96.8
35	61.5	107.0
40	68.5	118.0
45	76.1	130.0
50	84.1	142.0
55	92.6	155.0
60	101.6	170.0
65	111.3	185.0
70	121.4	201.0
75	132.2	217.0
80	143.7	235.0
85	155.7	254.0
90	168.4	274.0
95	181.8	295.0
100	196.0	317.0
105	210.8	340.0
110	226.4	365.0
115	242.8	391.0
120	260.0	418.0
125	278.1	446.0
130	297.0	476.0
135	316.7	507.0
140	337.4	539.0

Table 3

3.2 Air Conditioner Monitoring Transducers

In order to test the air conditioner unit at the same initial conditions, it is necessary to install temperature, pressure, and airflow transducers on the unit. The outdoor unit has seven (5) temperature transducers around it, which are averaged during the tests. The suction (vapor) line and the release (liquid) line has (2) two transducers, one for each line. The compressor case has one (1) temperature transducer. The indoor unit's inlet has seven (7) temperature transducers, which are averaged during the tests. The indoor unit's outlet air temperature has (3) temperature transducers, which are averaged as well. The indoor unit's inlet has one (1) airflow transducer. The outdoor unit will have two (2) refrigerant pressure transducers, for the input and output. Each test is launched after all monitored temperatures, pressures, and airflow rate are in steady state conditions.

4.0 AIR CONDITIONER SYSTEM PERFORMANCE TESTS

4.1 Test 1 - Test the inrush current of the air conditioner unit

The air conditioner terminal voltage shall be at zero volts (0 V) before starting this test. The air conditioner terminal voltage shall be raised to nominal voltage (240 V) at t_1 and then dropped back to the off state (0 V) at t_2 4 sec later (see Figure 2). Both voltage switching times 0 V to 240 V and 240 V to 0 V, shall be as quickly as possible (1/80 cycle transition time is used in these tests). The compressor terminal voltage's frequency shall remain constant at 60 Hz. Data will be collected at a voltage and current sampling rate of 10 thousand samples per second for 10 seconds. The inrush test is used to show the characteristics of the air conditioner unit during startup. This information is used to help with the evaluation of the currents observed during later stalling tests.

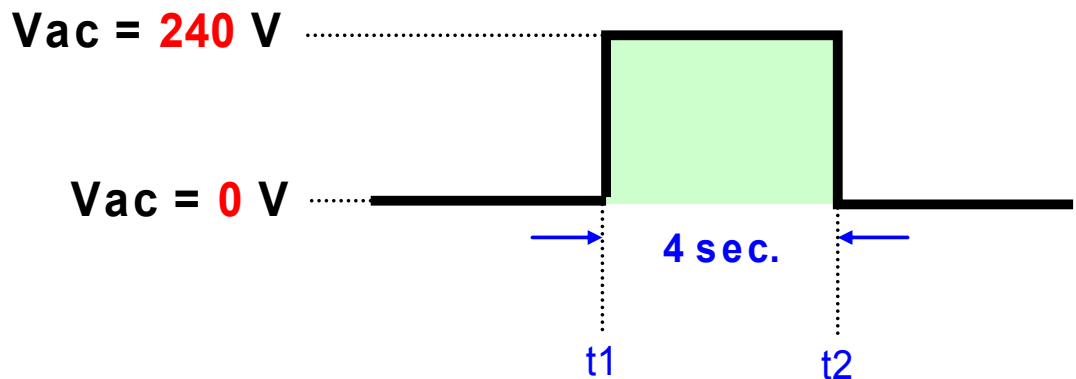


Figure 2

4.2 Test 2 - Test the compressor contactor critical voltage

The air conditioner terminal voltage shall be at its nominal voltage (240 V) before starting this test. This test will provide information where the contactor contacts open. The air conditioner compressor shall be removed from the circuit in order to perform this test. For this test, various step voltage drops (start 60% and go down in voltage steps of 5%) are applied to the contactor coil and held for 4 seconds before the voltage is returned to the nominal voltage, see Table 4. If the contactor contacts open after the voltage step, go back to the previous voltage step and test in voltage steps of 2% until the *contactor threshold voltage* is found. The voltage switching times shall be as quickly as possible (1/80 cycle transition time is used in these tests). The compressor terminal voltage's frequency shall remain constant at 60 Hz. Data will be collected at a voltage and current sampling rate of 25 thousand samples per second for 4 seconds. The voltage where the contactor opens will be the contactor threshold voltage, which will be used to set the lowest test voltage (voltage sag) in subsequent tests. These tests shall be performed at one simulated outdoor temperatures ($T_{\text{outdoor}} = 80^{\circ}\text{F}$).

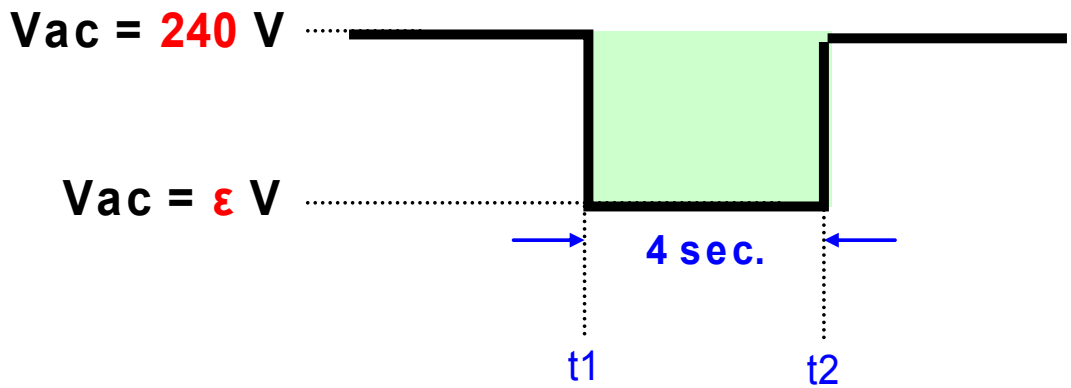


Figure 3

V_{sag}	ϵ
$V_{\text{ac}(60\%)}$	144 V
steps ↓ of 5%	steps ↓ of 5%
$V_{\text{ac}(\text{contactor-open})}$	$V_{\text{ac}(\text{contactor-open})}$

Table 4

4.3 Test 3 – Test the compressor stall voltage

The air conditioner terminal voltage shall be at its nominal voltage (240 V) before starting this test. The air conditioner terminal voltage shall be dropped to the sag voltage (ϵ V) at t_1 and rise back to nominal voltage (240 V) at t_2 30 sec later (see Figure 4). Both voltage switching times 240 V to ϵ V and ϵ V to 240 V, shall be as quickly as possible (1/80 cycle transition time is used in these tests). Testing will be started at 80% of nominal voltage and reduced in increments of 5% until the unit stalls. Once it stalls, go back to the previous voltage step and test in voltage steps of 1% until the stalling threshold voltage is found. After the stalling threshold voltage is found, continue testing lower voltages in steps of 5% until the contactor threshold voltage is reached. The compressor terminal voltage's frequency shall remain constant at 60 Hz. Data will be collected at a voltage and current sampling rate of 2500 samples per second for 40 seconds. These tests shall be performed at different simulated outdoor temperatures ($T_{\text{outdoor}} = 80^\circ\text{F}$, 100°F , & 115°F) as noted in Table 5. The stalling threshold voltage shall be used in Tests 4 and 5.

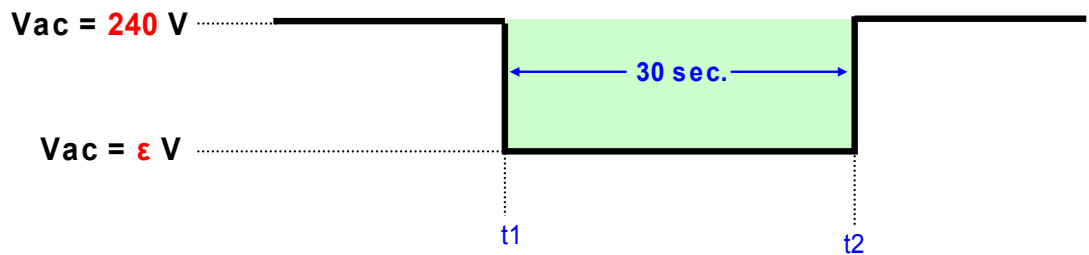


Figure 4

	$T_{\text{outdoor}} = 80^\circ\text{F}$	$T_{\text{outdoor}} = 100^\circ\text{F}$	$T_{\text{outdoor}} = 115^\circ\text{F}$
V_{sag}	ϵ	ϵ	ϵ
$V_{\text{ac}} (80\%)$	192 V	192 V	192 V
$V_{\text{ac}} (75\%)$	180 V	180 V	180 V
steps ↓ of 5%	steps ↓ of 5%	steps ↓ of 5%	steps ↓ of 5%
steps ↓ of 1%	steps ↓ of 1%	steps ↓ of 1%	steps ↓ of 1%
$V_{\text{ac}}(\text{stall}\%)$	$V_{\text{ac}}(\text{stall}\%)$	$V_{\text{ac}}(\text{stall}\%)$	$V_{\text{ac}}(\text{stall}\%)$
steps ↓ of 5%	steps ↓ of 5%	steps ↓ of 5%	steps ↓ of 5%
$V_{\text{ac}}(\text{contactor-open})$	$V_{\text{ac}}(\text{contactor-open})$	$V_{\text{ac}}(\text{contactor-open})$	$V_{\text{ac}}(\text{contactor-open})$

Table 5

4.4 Test 4 – Test the compressor over-temperature trip time

The air conditioner terminal voltage shall be at its nominal voltage (240 V) before starting this test. The air conditioner terminal voltage shall be dropped to the sag voltage (ϵ V) at t_1 and rise back to nominal voltage (240 V) at t_2 30 sec. later (see Figure 5). The voltage switching times 240 V to ϵ V shall be as quickly as possible (1/80 cycle transition time is used in these tests). The voltage switching time ϵ V to 240 V shall be 30 sec. (ramp up). Testing will be started 1% above the stalling threshold voltage (established in Test 3) and reduced in increments of 1% until the unit stalls. After this new stalling threshold voltage is found, continue testing in steps of 5%, starting on the next low multiple of 5, (e.g. if the stall point is 64% then the next test point is 60%) until the contactor threshold voltage is reached. The compressor terminal voltage's frequency shall remain constant at 60 Hz. Data will be collected at a voltage and current sampling rate of 2.5 thousands samples per second for 40 seconds. These tests shall be performed at different simulated outdoor temperatures ($T_{\text{outdoor}} = 80^\circ\text{F}$, 100°F , & 115°F) as noted in Table 6.

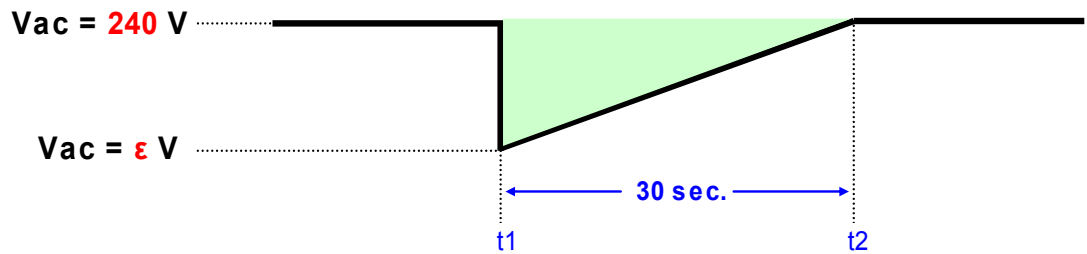


Figure 5

	$T_{\text{outdoor}} = 80^\circ\text{F}$	$T_{\text{outdoor}} = 100^\circ\text{F}$	$T_{\text{outdoor}} = 115^\circ\text{F}$
V_{sag}	ϵ	ϵ	ϵ
$V_{\text{ac(stall\%+1\%)}}$	$V_{\text{ac(stall\%+1\%)}}$	$V_{\text{ac(stall\%+1\%)}}$	$V_{\text{ac(stall\%+1\%)}}$
steps of 1% ↓	steps of 1% ↓	steps of 1% ↓	steps of 1% ↓
$V_{\text{ac(stall\%)}}$	$V_{\text{ac(stall\%)}}$	$V_{\text{ac(stall\%)}}$	$V_{\text{ac(stall\%)}}$
steps of 5% ↓	steps of 5% ↓	steps of 5% ↓	steps of 5% ↓
$V_{\text{ac(contactor-open)}}$	$V_{\text{ac(contactor-open)}}$	$V_{\text{ac(contactor-open)}}$	$V_{\text{ac(contactor-open)}}$

Table 6

*Perform the same ramp-up test above applying a transient with 60% amplitude and 10 sec of duration.

4.5 Test 5 – Test the compressor stall reaction to short under-voltage transients

The air conditioner terminal voltage shall be at its nominal voltage (240 V) before starting this test. The air conditioner terminal voltage shall be dropped to the sag voltage (ϵ V) at t_1 and rise back to nominal voltage (240 V) at t_2 (see Figure 6). These

different sag voltage duration times ($t_2 = 3, 6, 9,$ and 12 cycles) represent switching times for some common circuit breakers. Both changing states, 240 V to $\epsilon\text{ V}$ and $\epsilon\text{ V}$ to 240 V , shall be done as quickly as possible ($1/80$ cycle transition time is used in these tests). Testing will be started right above the stalling threshold voltage (established in Test 3) and reduced in increments of 1% until the unit stalls. After this new stalling threshold voltage is found, continue testing in steps of 5% (e.g. if the stall point is 58% then the next test point is 55%) until the contactor threshold voltage is reached. The compressor terminal voltage's frequency shall remain constant at 60 Hz . Data will be collected at a voltage and current sampling rate of 25 thousand samples per second for 4 seconds. These tests shall be performed at different simulated outdoor temperatures ($T_{\text{outdoor}} = 80^\circ\text{F}, 100^\circ\text{F}, \& 115^\circ\text{F}$) as shown in Table 7, 8, & 9.

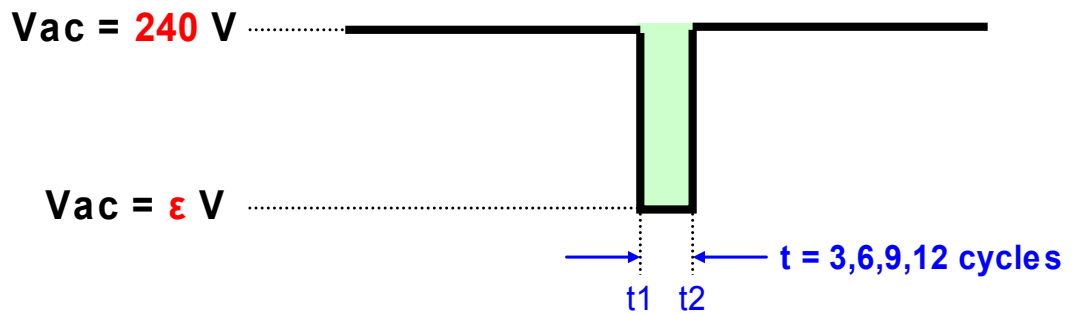


Figure 6

		$T_{\text{outdoor}} = 80^\circ\text{F}$			
V_{sag}		3 cycles	6 cycles	9 cycles	12 cycles
		ϵ	ϵ	ϵ	ϵ
$V_{\text{ac(stall\%+1\%)}}$		$V_{\text{ac(stall\%+1\%)}}$	$V_{\text{ac(stall\%+1\%)}}$	$V_{\text{ac(stall\%+1\%)}}$	$V_{\text{ac(stall\%+1\%)}}$
↓ steps of 1%		↓ steps of 1%	↓ steps of 1%	↓ steps of 1%	↓ steps of 1%
$V_{\text{ac(stall\%)}}$		$V_{\text{ac(stall\%)}}$	$V_{\text{ac(stall\%)}}$	$V_{\text{ac(stall\%)}}$	$V_{\text{ac(stall\%)}}$
↓ steps of 5%		↓ steps of 5%	↓ steps of 5%	↓ steps of 5%	↓ steps of 5%
$V_{\text{ac(contactor-open)}}$		$V_{\text{ac(contactor-open)}}$	$V_{\text{ac(contactor-open)}}$	$V_{\text{ac(contactor-open)}}$	$V_{\text{ac(contactor-open)}}$

Table 7

		$T_{\text{outdoor}} = 100^{\circ}\text{F}$			
		3 cycles ϵ	6 cycles ϵ	9 cycles ϵ	12 cycles ϵ
V_{sag}					
$V_{\text{ac(stall\%+1\%)}}$		$V_{\text{ac(stall\%+1\%)}}$	$V_{\text{ac(stall\%+1\%)}}$	$V_{\text{ac(stall\%+1\%)}}$	$V_{\text{ac(stall\%+1\%)}}$
steps ↓ of 1%		steps ↓ of 1%	steps ↓ of 1%	steps ↓ of 1%	steps ↓ of 1%
$V_{\text{ac(stall\%)}}$		$V_{\text{ac(stall\%)}}$	$V_{\text{ac(stall\%)}}$	$V_{\text{ac(stall\%)}}$	$V_{\text{ac(stall\%)}}$
steps ↓ of 5%		steps ↓ of 5%	steps ↓ of 5%	steps ↓ of 5%	steps ↓ of 5%
$V_{\text{ac(contactor-open)}}$		$V_{\text{ac(contactor-open)}}$	$V_{\text{ac(contactor-open)}}$	$V_{\text{ac(contactor-open)}}$	$V_{\text{ac(contactor-open)}}$

Table 8

		$T_{\text{outdoor}} = 115^{\circ}\text{F}$			
		3 cycles ϵ	6 cycles ϵ	9 cycles ϵ	12 cycles ϵ
V_{sag}					
$V_{\text{ac(stall\%+1\%)}}$		$V_{\text{ac(stall\%+1\%)}}$	$V_{\text{ac(stall\%+1\%)}}$	$V_{\text{ac(stall\%+1\%)}}$	$V_{\text{ac(stall\%+1\%)}}$
steps ↓ of 1%		steps ↓ of 1%	steps ↓ of 1%	steps ↓ of 1%	steps ↓ of 1%
$V_{\text{ac(stall\%)}}$		$V_{\text{ac(stall\%)}}$	$V_{\text{ac(stall\%)}}$	$V_{\text{ac(stall\%)}}$	$V_{\text{ac(stall\%)}}$
steps ↓ of 5%		steps ↓ of 5%	steps ↓ of 5%	steps ↓ of 5%	steps ↓ of 5%
$V_{\text{ac(contactor-open)}}$		$V_{\text{ac(contactor-open)}}$	$V_{\text{ac(contactor-open)}}$	$V_{\text{ac(contactor-open)}}$	$V_{\text{ac(contactor-open)}}$

Table 9

5.0 AIR CONDITIONER SYSTEM RESEARCH TESTS

5.1 TEST THE COMPRESSOR UNDER STEADY-STATE CONDITIONS

These tests will provide information on how air conditioner systems behave under steady state conditions at different voltage and frequency levels.

5.1.1 Test 6 – Test the compressor reaction under non-stalling voltages

The air conditioner terminal voltage shall be at its nominal voltage (240 V) before starting this test. Initially, the air conditioner voltage shall be stepped up to 120% and then stepped down from 110% (264 V) to 70% (168 V) in 5 % intervals and 4 sec step duration (see Figure 7). The voltage switching times between voltage steps shall be as quickly as possible (1/80 cycle transition time is used in these tests). The compressor terminal voltage's frequency shall remain constant at 60 Hz. Data will be collected at a voltage and current sampling rate of 2.5 thousand samples per second for a total of 40 seconds. These tests shall be performed at different simulated outdoor temperatures ($T_{\text{outdoor}} = 80^{\circ}\text{F}, 100^{\circ}\text{F}, \& 115^{\circ}\text{F}$).

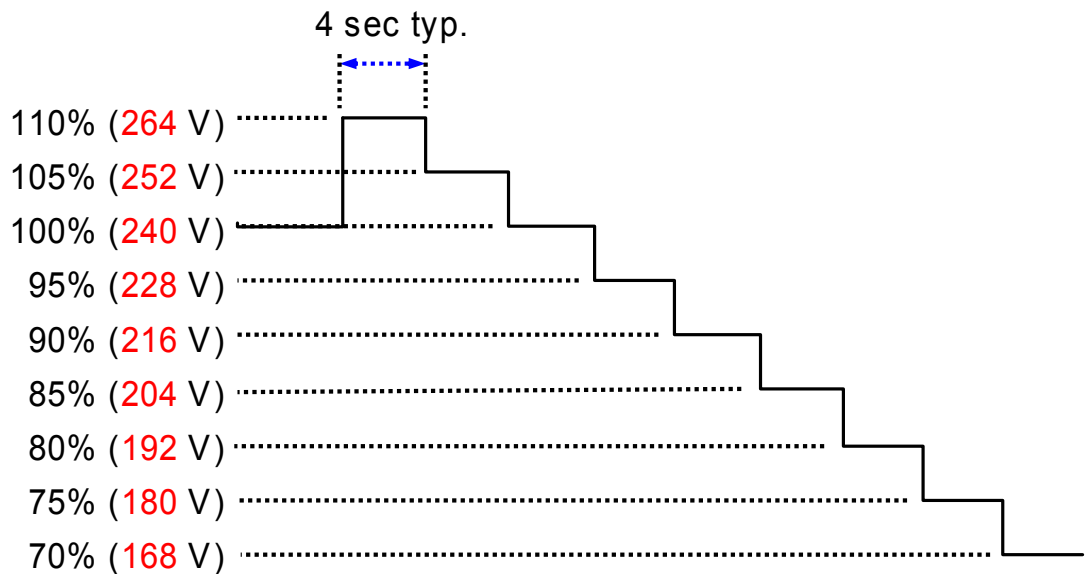


Figure 7

5.1.2 **Test 7** –Test compressor reaction under different frequencies

The air conditioner terminal voltage shall be at its nominal frequency (60 Hz) before starting this test. Initially, the air conditioner frequency shall be stepped up to 63 Hz. Then it shall be stepped down from 63 Hz to 54 Hz in 1 Hz intervals and 4 sec step duration (see Figure 8). The frequency switching time between the frequencies steps shall be as quickly as possible (1/80 cycle transition time is used in these tests). The compressor terminal voltage shall remain constant at 240 V. Data will be collected at a voltage and current sampling rate of 25 thousand samples per second for a total of 40 seconds. These tests shall have a resolution of 1 million samples per test. These tests shall be performed at different simulated outdoor temperatures ($T_{\text{outdoor}} = 80^{\circ}\text{F}, 100^{\circ}\text{F}, \& 115^{\circ}\text{F}$).

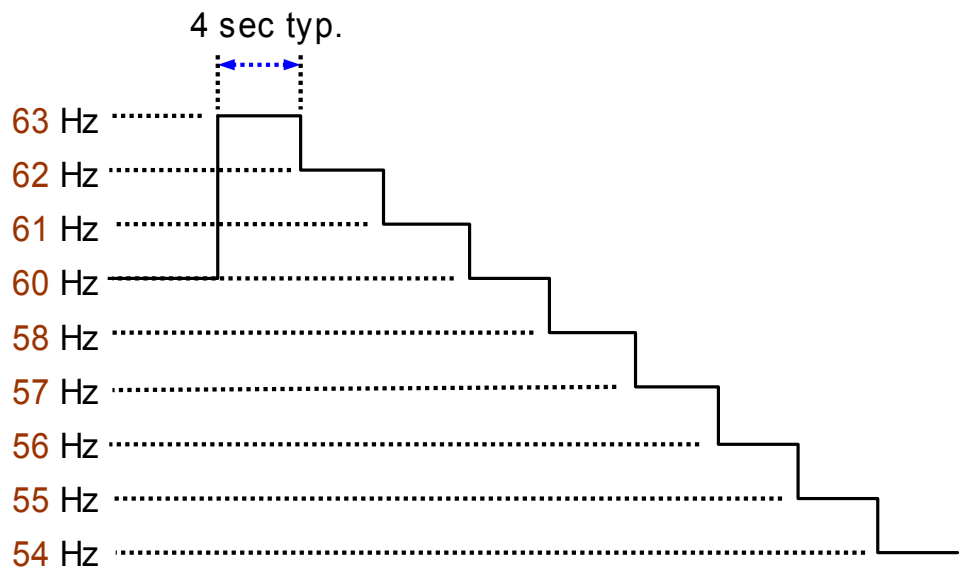


Figure 8

5.2 TEST THE COMPRESSOR WITH CONTACTOR IN THE CIRCUIT

The following tests (Tests 8 and Test 9) will need the contactor coil in the air conditioner system circuitry. This can be accomplished by powering the contactor coil with the air conditioner system's 24 V transformer. These tests will provide information of the air conditioner system behavior under transients.

5.2.1 Test 8 – Test the compressor reaction to short under-voltage transients with contactor

The air conditioner terminal voltage shall be at its nominal voltage (240 V) before starting this test. The air conditioner terminal voltage shall be dropped to the sag voltage (24 V) at t_1 and raised back to nominal voltage (240 V) at t_2 (see Figure 9). These different sag voltage duration times ($t_2 = 3, 6, 9,$ and 12 cycles) represent switching times for some common circuit breakers. Both voltage switching times, 240 V to 24 V and 24 V to 240 V, shall be done as quickly as possible (1/80 cycle transition time is used in these tests). The compressor terminal voltage's frequency shall remain constant at 60 Hz. Data will be collected at a voltage and current sampling rate of 25 thousand samples per second for 4 seconds. These tests shall be performed at different simulated outdoor temperatures ($T_{\text{outdoor}} = 80^{\circ}\text{F}, 100^{\circ}\text{F}, \& 115^{\circ}\text{F}$).

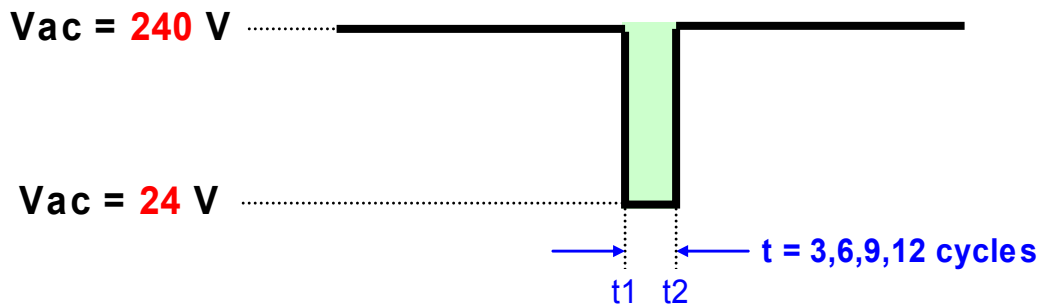


Figure 9

5.2.2 **Test 9** – Test the compressor reaction to short under-voltage transients with different recovery voltages

The air conditioner terminal voltage shall be at its nominal voltage (240 V) before starting this test. The air conditioner terminal voltage shall be dropped to the sag voltage 60% (144 V) at t_1 and raised to 216, 192, & 168 V at t_2 , t cycles later. Once the voltage is raised to 216, 192, & 168 V, it shall be maintained for 4 sec. This test details are in Figure 10. The different sag voltage duration times ($t = 3, 6, 9,$ and 12 cycles) represent switching times for some common circuit breakers. The voltage switching times between the different voltage levels, shall be done as quickly as possible ($1/80$ cycle transition time is used in these tests). The compressor terminal voltage's frequency shall remain constant at 60 Hz. Data will be collected at a voltage and current sampling rate of 25 thousand samples per second for 4 seconds. These tests shall be performed at different simulated outdoor temperatures ($T_{\text{outdoor}} = 80^{\circ}\text{F}, 100^{\circ}\text{F}, \& 115^{\circ}\text{F}$).

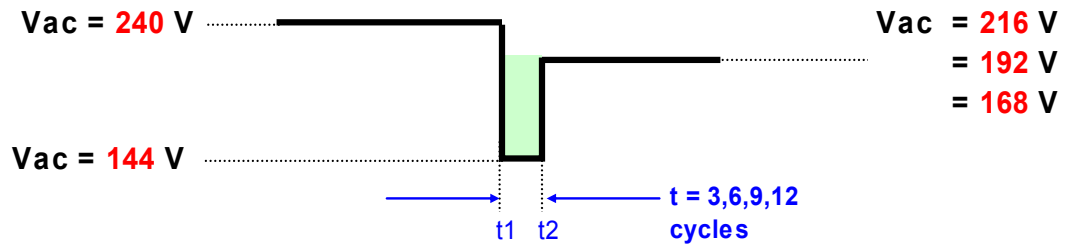


Figure 10

5.3 TEST THE COMPRESSOR WITH CONTACTOR BYPASSED

The following tests (Test 10 thru 15) will need the contactor coil be removed from the air conditioner system circuitry. This can be accomplish either by powering the contactor coil with an independent 24 V constant voltage source or by bypassing the contactor. These tests will provide information of the air conditioner compressor behavior under transients.

5.3.1 Test 10 – Test the compressor reaction to short under-voltage transients

The air conditioner terminal voltage shall be at its nominal voltage (240 V) before starting this test. The air conditioner terminal voltage shall be dropped from nominal voltage (240 V) to the sag voltage (24 V) at t_1 and raised back to nominal voltage (240 V) at t_2 (see Figure 11). These different sag voltage duration times ($t_2 - t_1 = 3, 6, 9,$ and 12 cycles) represent switching times for some common circuit breakers. Both voltage switching times, 240 V to 24 V and 24 V to 240 V, shall be done as quickly as possible (1/80 cycle transition time is used in these tests). The compressor terminal voltage's frequency shall remain constant at 60 Hz. Data will be collected at a voltage and current sampling rate of 25 thousand samples per second for 4 seconds. These tests shall be performed at different simulated outdoor temperatures ($T_{\text{outdoor}} = 80^\circ\text{F}, 100^\circ\text{F}, \& 115^\circ\text{F}$).

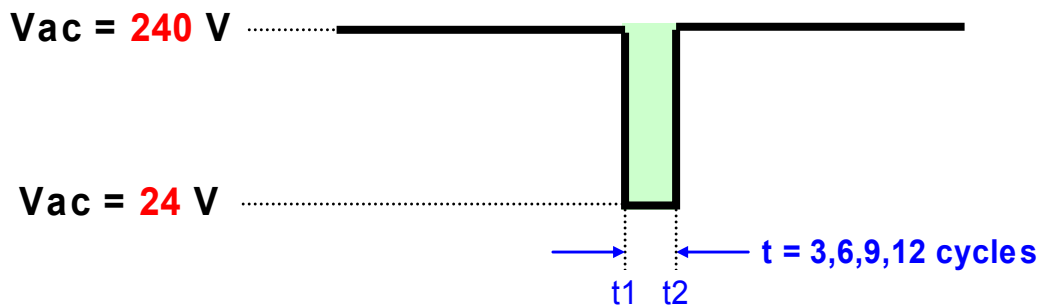


Figure 11

5.3.2 Test 11 – Test the compressor reaction to short under-voltage transients with different recovery voltages

The air conditioner terminal voltage shall be at its nominal voltage (240 V) before starting this test. The air conditioner terminal voltage shall be dropped to the sag voltage 60% (144 V) at t_1 and raised to 216, 192, & 168 V at t_2 , t cycles later. Once the voltage is raised to 216, 192, & 168 V, it shall be maintained for 4 sec. This test details are in Figure 12. The different sag voltage duration times ($t = 3, 6, 9,$ and 12 cycles) represent switching times for some common circuit breakers. The voltage switching times between the different voltage levels, shall be done as quickly as possible ($1/80$ cycle transition time is used in these tests). The compressor terminal voltage's frequency shall remain constant at 60 Hz. Data will be collected at a voltage and current sampling rate of 25 thousand samples per second for 4 seconds. These tests shall be performed at different simulated outdoor temperatures ($T_{outdoor} = 80^{\circ}\text{F}, 100^{\circ}\text{F}, \& 115^{\circ}\text{F}$).

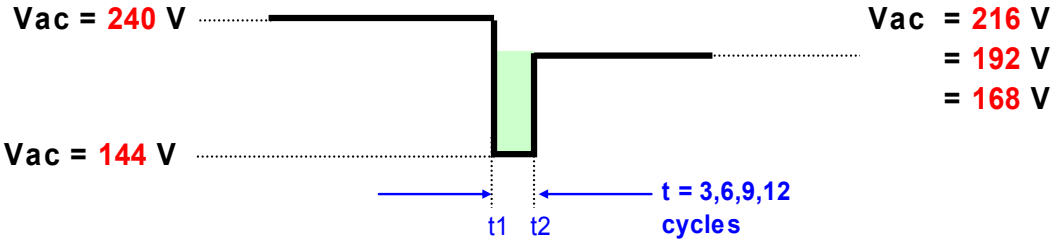


Figure 12

5.3.3 Test 12 – Test the compressor reaction to ramp-voltage transients

The air conditioner terminal voltage shall be at its nominal voltage (240 V) before starting this test. The air conditioner terminal voltage shall be ramped down to the sag voltage (24 V) in 15 sec. and ramped back up to nominal voltage (240 V) in 15 sec.

(see Figure 13). The compressor terminal voltage's frequency shall remain constant at 60 Hz. Data will be collected at a voltage and current sampling rate of 2.5 thousand samples per second for 40 seconds. These tests shall be performed at different simulated outdoor temperatures ($T_{\text{outdoor}} = 80^{\circ}\text{F}$, 100°F , & 115°F).

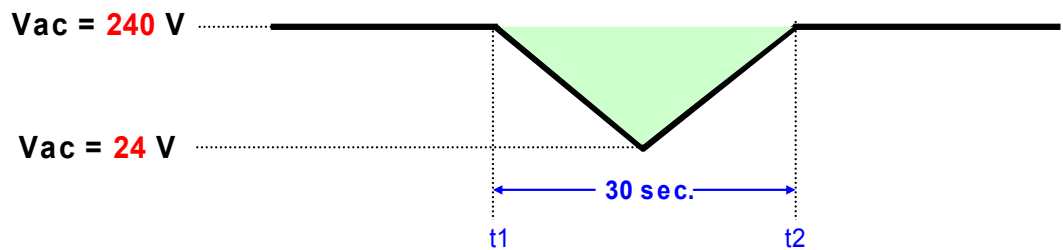


Figure 13

5.3.4 **Test 13** – Test the compressor reaction to voltage-oscillation transients

The air conditioner terminal voltage shall be at its nominal voltage (240 V) before starting this test. The air conditioner terminal voltage amplitude shall be modulated between 100% and 90 % at different envelope frequencies ($f(\text{swing}) = 0.1, 0.25, 0.7, 1, 2 \text{ Hz}$) (See figure 14 and Table 10). These different envelope frequencies ($f(\text{swing})$)

= 0.1, 0.25, 0.7, 1, 2 Hz) represent the oscillation of the system. The compressor terminal voltage's frequency shall remain constant at 60 Hz. Data will be collected at a voltage and current sampling rate of Ψ thousand samples per second for Δ seconds. These tests shall be performed at different simulated outdoor temperatures ($T_{outdoor} = 80^{\circ}\text{F}, 100^{\circ}\text{F}, \& 115^{\circ}\text{F}$).

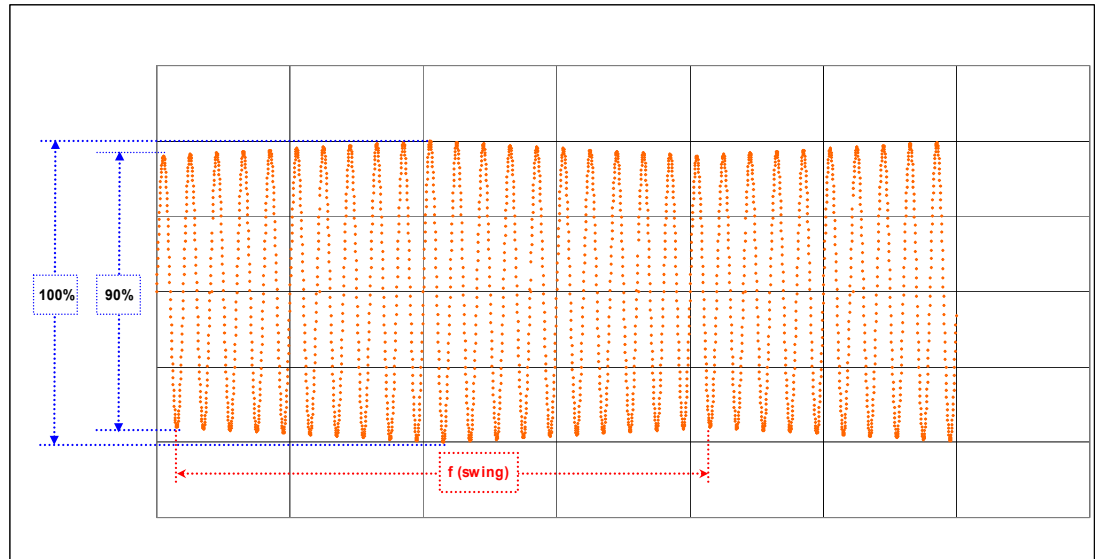


Figure 14

f (swing)	0.10	f (swing)	0.25	f (swing)	0.70	f (swing)	1.00	f (swing)	2.00		
t (swing)	10.0	t (swing)	4.0	t (swing)	1.4	t (swing)	1.0	t (swing)	0.5		
V	t(V)	V	t(V)	V	t(V)	V	t(V)	V	t(V)		
99%	237.6	0.50	99%	237.6	0.20	99%	237.6	0.071	99%	237.6	0.025
98%	235.2	0.50	98%	235.2	0.20	98%	235.2	0.071	98%	235.2	0.025
97%	232.8	0.50	97%	232.8	0.20	97%	232.8	0.071	97%	232.8	0.025
96%	230.4	0.50	96%	230.4	0.20	96%	230.4	0.071	96%	230.4	0.025
95%	228.0	0.50	95%	228.0	0.20	95%	228.0	0.071	95%	228.0	0.025
94%	225.6	0.50	94%	225.6	0.20	94%	225.6	0.071	94%	225.6	0.025
93%	223.2	0.50	93%	223.2	0.20	93%	223.2	0.071	93%	223.2	0.025
92%	220.8	0.50	92%	220.8	0.20	92%	220.8	0.071	92%	220.8	0.025
91%	218.4	0.50	91%	218.4	0.20	91%	218.4	0.071	91%	218.4	0.025
90%	216.0	0.50	90%	216.0	0.20	90%	216.0	0.071	90%	216.0	0.025
91%	218.4	0.50	91%	218.4	0.20	91%	218.4	0.071	91%	218.4	0.025
92%	220.8	0.50	92%	220.8	0.20	92%	220.8	0.071	92%	220.8	0.025
93%	223.2	0.50	93%	223.2	0.20	93%	223.2	0.071	93%	223.2	0.025
94%	225.6	0.50	94%	225.6	0.20	94%	225.6	0.071	94%	225.6	0.025
95%	228.0	0.50	95%	228.0	0.20	95%	228.0	0.071	95%	228.0	0.025
96%	230.4	0.50	96%	230.4	0.20	96%	230.4	0.071	96%	230.4	0.025
97%	232.8	0.50	97%	232.8	0.20	97%	232.8	0.071	97%	232.8	0.025
98%	235.2	0.50	98%	235.2	0.20	98%	235.2	0.071	98%	235.2	0.025
99%	237.6	0.50	99%	237.6	0.20	99%	237.6	0.071	99%	237.6	0.025
100%	240.0	0.50	100%	240.0	0.20	100%	240.0	0.071	100%	240.0	0.025
Total Time	10.00		Total Time	4.00		Total Time	1.43		Total Time	1.00	
$\Delta = 40$			$\Delta = 20$			$\Delta = 10$			$\Delta = 4$		
$\Psi = 2.5$			$\Psi = 5$			$\Psi = 10$			$\Psi = 25$		

Table 10

5.3.5 Test 14 – Test the compressor reaction to frequency transients

The air conditioner terminal voltage's frequency shall be changed according to Figure 15. These frequency changes (sags) shall have 4 sec of duration time and 2 sec of interval time between frequency changes. The frequency switching times between the different frequency levels shall be as quickly as possible (1/80 cycle transition time is used in these tests). The compressor terminal voltage shall remain constant at 240 V. Data will be collected at a voltage and current sampling rate of 25 thousand samples per second for 40 seconds. These tests shall have a resolution of 1 million samples per test. These tests shall be performed at different simulated outdoor temperatures (T_{outdoor} = 80°F, 100°F, & 115°F).

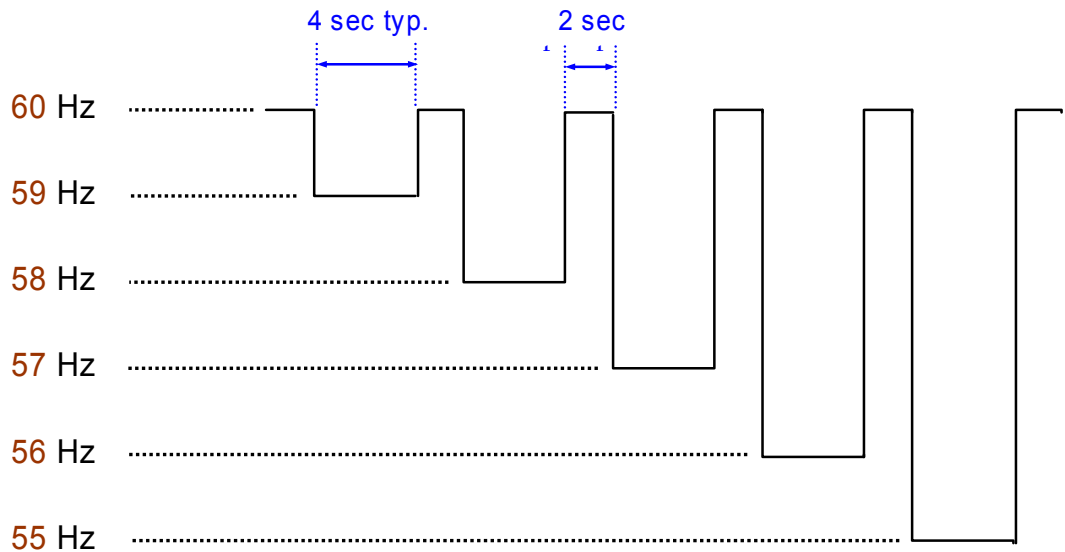


Figure 15

5.3.6 **Test 15** – Test the compressor reaction to frequency-oscillation transients

The air conditioner terminal voltage shall be at its nominal voltage (240 V) before starting this test. The air conditioner terminal voltage's frequency shall be modulated between 61 Hz and 59 Hz at different envelope frequencies ($f(\text{swing}) = 0.1, 0.25, 0.7, 1, 2 \text{ Hz}$) (See figure 16 and Table 11). These different envelope frequencies ($f(\text{swing}) = 0.1, 0.25, 0.7, 1, 2 \text{ Hz}$) represent the oscillation of the system. The compressor terminal voltage shall remain constant at 240 V. Data will be collected at a voltage, current, and frequency sampling rate of Ψ thousand samples per second for Δ seconds, as shown in Table 11. These tests shall have a resolution of 1 million samples per test. These tests shall be performed at different simulated outdoor temperatures ($T_{\text{outdoor}} = 80^\circ\text{F}, 100^\circ\text{F}, \& 115^\circ\text{F}$).

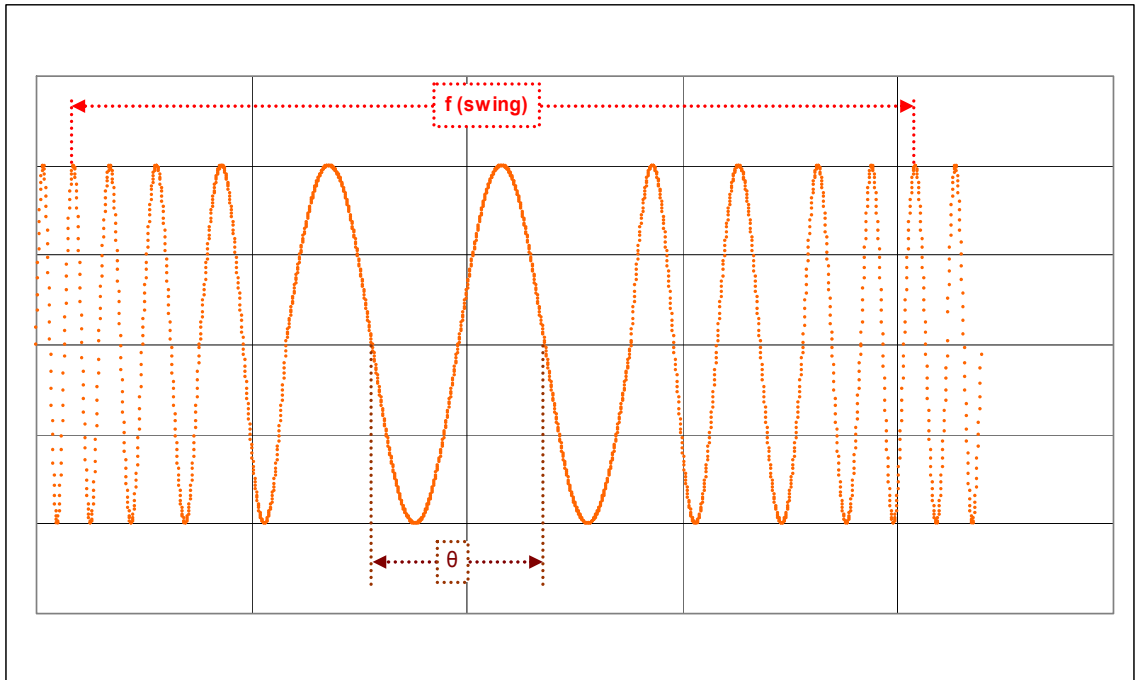


Figure 16

V	240 V								
f (swing)	0.10	f (swing)	0.25	f (swing)	0.70	f (swing)	1.00	f (swing)	2.00
t (swing)	10.0	t (swing)	4.0	t (swing)	1.4	t (swing)	1.0	t (swing)	0.5
θ	t(θ)								
61.0 Hz	0.475	61.0 Hz	0.190	61.0 Hz	0.066	61.0 Hz	0.047	61.0 Hz	0.024
60.8 Hz	0.475	60.8 Hz	0.190	60.8 Hz	0.066	60.8 Hz	0.047	60.8 Hz	0.024
60.6 Hz	0.475	60.6 Hz	0.190	60.6 Hz	0.066	60.6 Hz	0.047	60.6 Hz	0.024
60.4 Hz	0.475	60.4 Hz	0.190	60.4 Hz	0.066	60.4 Hz	0.047	60.4 Hz	0.024
60.2 Hz	0.475	60.2 Hz	0.190	60.2 Hz	0.066	60.2 Hz	0.047	60.2 Hz	0.024
60.0 Hz	0.475	60.0 Hz	0.190	60.0 Hz	0.066	60.0 Hz	0.047	60.0 Hz	0.024
59.8 Hz	0.475	59.8 Hz	0.190	59.8 Hz	0.066	59.8 Hz	0.047	59.8 Hz	0.024
59.6 Hz	0.475	59.6 Hz	0.190	59.6 Hz	0.066	59.6 Hz	0.047	59.6 Hz	0.024
59.4 Hz	0.475	59.4 Hz	0.190	59.4 Hz	0.066	59.4 Hz	0.047	59.4 Hz	0.024
59.2 Hz	0.475	59.2 Hz	0.190	59.2 Hz	0.066	59.2 Hz	0.047	59.2 Hz	0.024
59.0 Hz	0.475	59.0 Hz	0.190	59.0 Hz	0.066	59.0 Hz	0.047	59.0 Hz	0.024
59.2 Hz	0.475	59.2 Hz	0.190	59.2 Hz	0.066	59.2 Hz	0.047	59.2 Hz	0.024
59.4 Hz	0.475	59.4 Hz	0.190	59.4 Hz	0.066	59.4 Hz	0.047	59.4 Hz	0.024
59.6 Hz	0.475	59.6 Hz	0.190	59.6 Hz	0.066	59.6 Hz	0.047	59.6 Hz	0.024
59.8 Hz	0.475	59.8 Hz	0.190	59.8 Hz	0.066	59.8 Hz	0.047	59.8 Hz	0.024
60.0 Hz	0.475	60.0 Hz	0.190	60.0 Hz	0.066	60.0 Hz	0.047	60.0 Hz	0.024
60.2 Hz	0.475	60.2 Hz	0.190	60.2 Hz	0.066	60.2 Hz	0.047	60.2 Hz	0.024
60.4 Hz	0.475	60.4 Hz	0.190	60.4 Hz	0.066	60.4 Hz	0.047	60.4 Hz	0.024
60.6 Hz	0.475	60.6 Hz	0.190	60.6 Hz	0.066	60.6 Hz	0.047	60.6 Hz	0.024
60.8 Hz	0.475	60.8 Hz	0.190	60.8 Hz	0.066	60.8 Hz	0.047	60.8 Hz	0.024
61.0 Hz	0.475	61.0 Hz	0.190	61.0 Hz	0.066	61.0 Hz	0.047	61.0 Hz	0.024
Total Time	9.975 sec.	Total Time	3.99 sec.	Total Time	1.386 sec.	Total Time	0.987 sec.	Total Time	0.504 sec.
$\Delta =$	40	$\Delta =$	20	$\Delta =$	10	$\Delta =$	4	$\Delta =$	4
$\Psi =$	2.5	$\Psi =$	5	$\Psi =$	10	$\Psi =$	25	$\Psi =$	25

Table 11

6.0 DATA ANALYSIS

The Yokogawa Power Analyzer records the voltage and current waveforms during the testing using high-speed sampling. SCE gathers 100 thousand samples in each test (except Test 7, 14, & 15 where gathers 1 million samples per each test). These samples are then processed by the Yokogawa into RMS values for each cycle. These RMS values are further processed by the Yokogawa Power View software to determine the watt and VAR values for each cycle. These RMS values are filtered to one value per cycle and plotted using Excel macros.

4.1 *Volts & Amps versus Time Graph*

The figure below is the *Volts & Amps versus Time graph* (Figure 17). This graph shows that the AC unit has stalled (Volts in blue and Amps in red). The graph also shows that the compressor thermal cut-out switch was activated after about 11 seconds (1 sec/div).

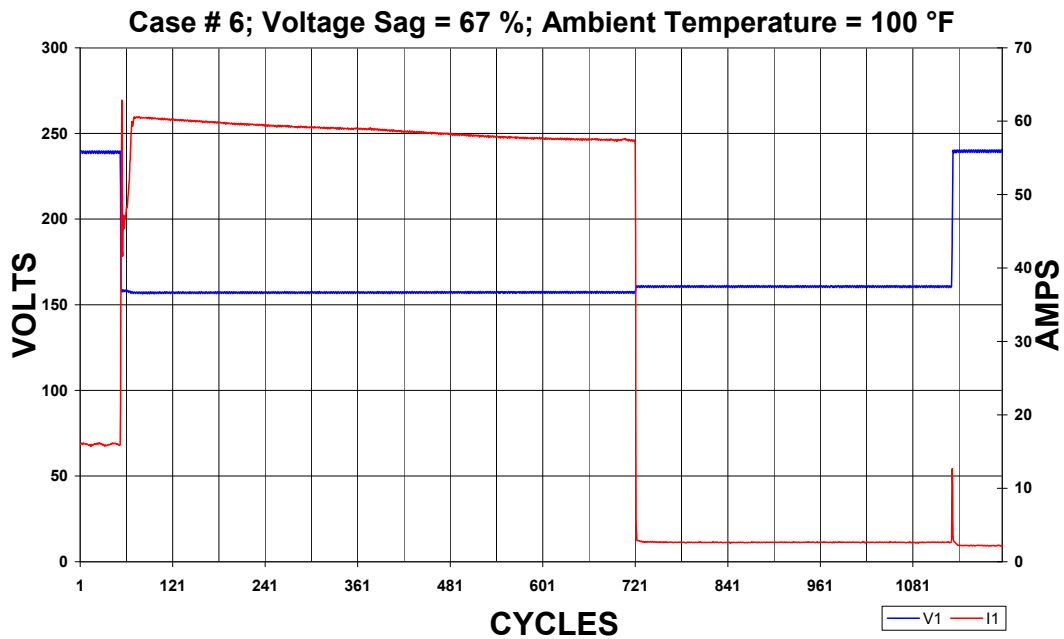


Figure 17

4.2 *Watts & VARs versus Time Graph*

The figure below is the *Watts & VARS versus Time Graph* (Figure 18). This graph shows that the AC unit has stalled (Watts in green and VARS in orange). As in the previous graph, it also shows that the compressor thermal cut-out switch was activated after about 11 seconds (1 sec/div).

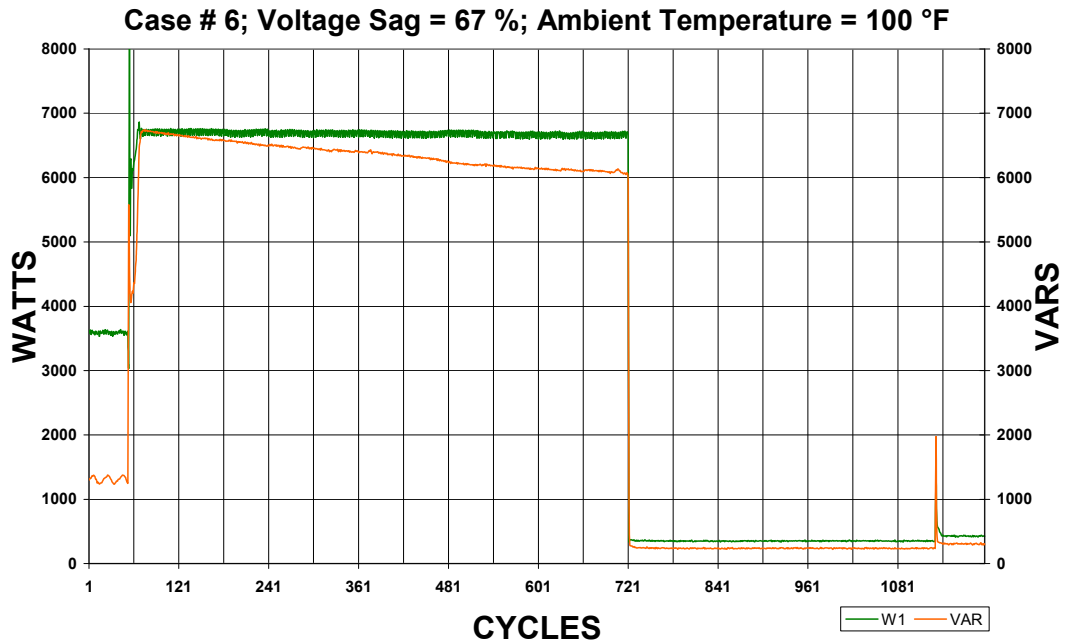


Figure 18

4.3 Start-up Transient Volts & Amps versus Time Graph

The figure below is the initial transient *Volts & Amps versus Time graph* (Figure 19). This graph shows the initial reaction to the applied transient (voltage sag). The graph also shows

that the unit stalled 15 cycles (1 cycles/div) after the transient (Vsag = 67%) was applied and that the current has gone up (16 to 61 Amps).

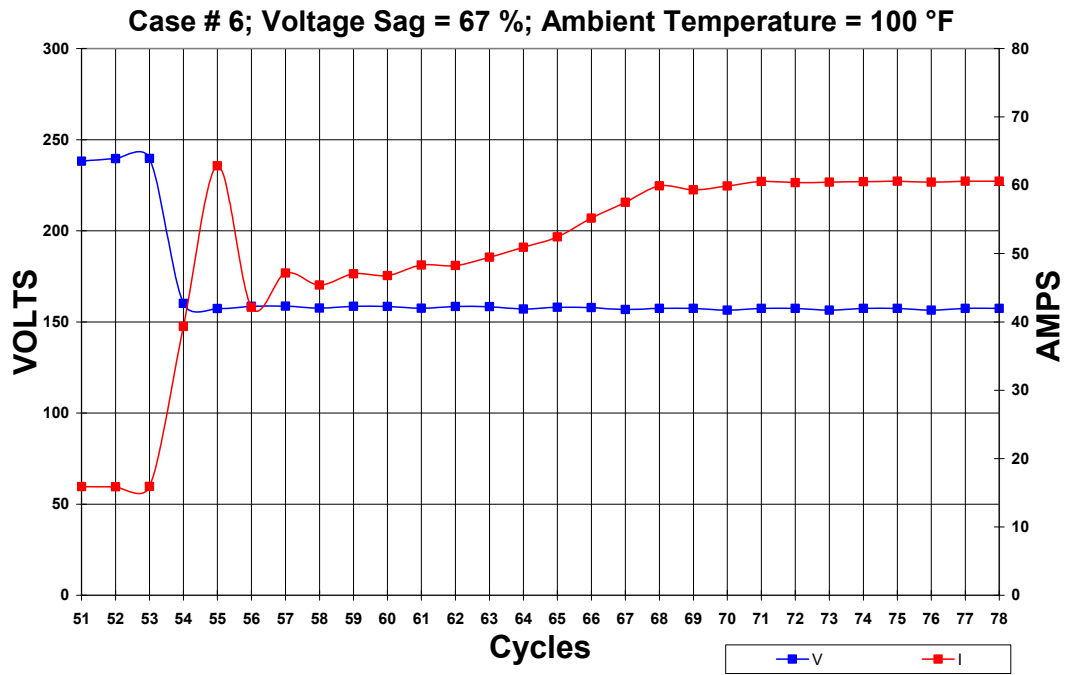


Figure 19

4.4 Start-up Transient Watts & VARS versus Time Graph

The figure below is the Watts & VARS versus Time Graph (Figure 20). This graph shows the initial reaction to the applied transient (voltage sag). The graph also shows that the reactive power has gone up (1200 VARS to 6800 VARS).

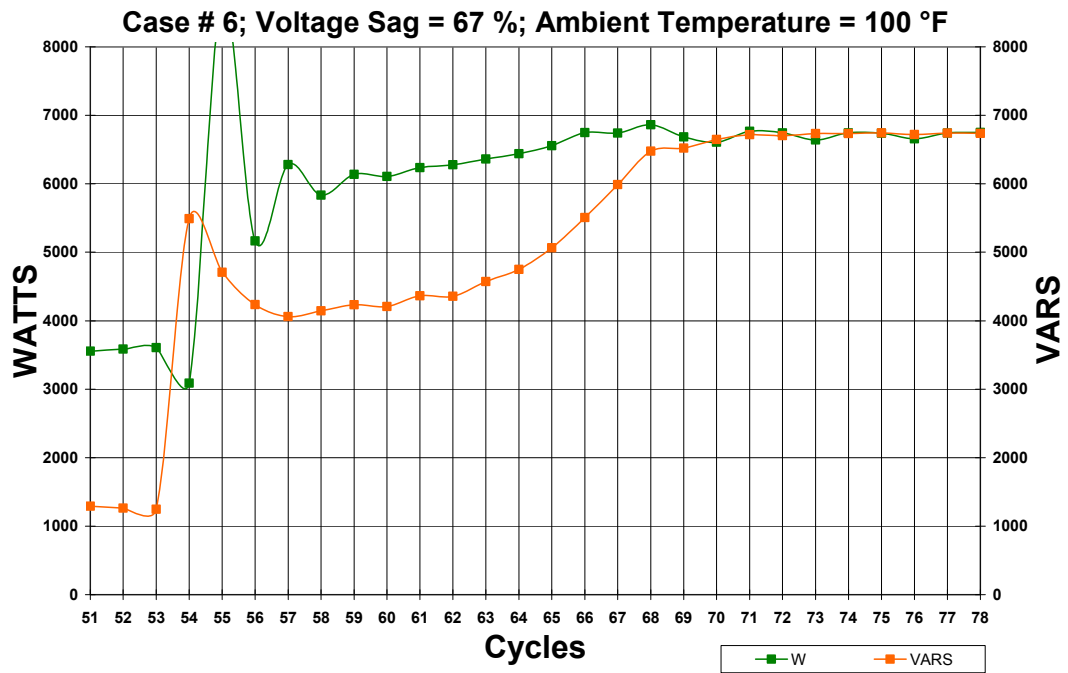


Figure 20

7.0 APPENDIX

7.1 Grid Simulator Controller Programs

7.2 AC Specifications Data Sheets

7.3 AC Testing Data Log Sheets

FINAL PROJECT REPORT

LOAD MODELING TRANSMISSION RESEARCH

APPENDIX B

AIR CONDITIONER TEST REPORT

Prepared for CIEE By:

Lawrence Berkeley National Laboratory



University of California
ciee

A CIEE Report



SOUTHERN CALIFORNIA
EDISON[®]

An *EDISON INTERNATIONAL*[®] Company

Air Conditioner Test Report

By:

TDBU

**Engineering Advancement
Power Systems Technologies**

Richard Bravo
David Martinez
Robert Yinger
Loic Gaillac

1.0	EXECUTIVE SUMMARY	5
1.1	Introduction.....	5
1.2	Work Performed	5
1.3	Testing Results.....	6
1.3.1	Stall Voltage	6
1.3.2	Metering Devices.....	9
1.3.3	Thermal Protection Switch	10
1.3.4	Contactors Dropout	11
2.0	OBJECTIVE	14
2.1.	Measurements	14
3.0	AIR CONDITIONER TEST TRANSIENT	18
3.1	Long Notch Type of Transient.....	18
3.2	Delayed Recovery Type of Transient	18
3.3	Circuit Breaker Clearing Type of Transient	19
4.0	A/C #1- TEST RESULTS.....	20
4.1	SYSTEM SPECIFICATIONS	20
4.2	TEST PARAMETERS	20
4.3	INRUSH TEST RESULTS.....	21
4.4	POWER CONTACTOR TEST RESULTS	21
4.5	<i>30-SECOND LONG NOTCH</i> TYPE OF TRANSIENT TEST RESULTS	22
4.6	<i>DELAYED RECOVERY</i> TYPE OF TRANSIENT TEST RESULTS.....	22
4.7	<i>CIRCUIT BREAKER CLEARING</i> TYPE OF TRANSIENT TEST RESULTS	23
5.0	A/C #2- TEST RESULTS	25
5.1	SYSTEM SPECIFICATIONS	25
5.2	TEST PARAMETERS	25
5.3	INRUSH TEST RESULTS.....	26
5.4	POWER CONTACTOR TEST RESULTS	26
5.5	<i>30-SECOND LONG NOTCH</i> TYPE OF TRANSIENT TEST RESULTS	27
5.6	<i>DELAYED RECOVERY</i> TYPE OF TRANSIENT TEST RESULTS.....	27
5.7	<i>CIRCUIT BREAKER CLEARING</i> TYPE OF TRANSIENT TEST RESULTS	28
6.0	A/C #3- TEST RESULTS	29
6.1	SYSTEM SPECIFICATIONS	29
6.2	TEST PARAMETERS	29
6.3	INRUSH TEST RESULTS.....	30
6.4	POWER CONTACTOR TEST RESULTS	30
6.5	<i>30-SECOND LONG NOTCH</i> TYPE OF TRANSIENT TEST RESULTS	31
6.6	<i>DELAYED RECOVERY</i> TYPE OF TRANSIENT TEST RESULTS.....	32
6.7	<i>CIRCUIT BREAKER CLEARING</i> TYPE OF TRANSIENT TEST RESULTS	32
7.0	A/C #4- TEST RESULTS	34
7.1	SYSTEM SPECIFICATIONS	34
7.2	TEST PARAMETERS	35
7.3	INRUSH TEST RESULTS.....	35

7.4	POWER CONTACTOR TEST RESULTS	36
7.5	<i>30-SECOND LONG NOTCH</i> TYPE OF TRANSIENT TEST RESULTS	36
7.6	<i>DELAYED RECOVERY</i> TYPE OF TRANSIENT TEST RESULTS.....	37
7.7	<i>CIRCUIT BREAKER CLEARING</i> TYPE OF TRANSIENT TEST RESULTS	38
8.0	A/C #5 - TEST RESULTS.....	40
8.1	SYSTEM SPECIFICATIONS	40
8.2	TEST PARAMETERS	41
8.3	INRUSH TEST RESULTS\	41
8.4	POWER CONTACTOR TEST RESULTS	42
8.5	<i>30-SECOND LONG NOTCH</i> TYPE OF TRANSIENT TEST RESULTS	42
8.6	<i>DELAYED RECOVERY</i> TYPE OF TRANSIENT TEST RESULTS.....	43
8.7	<i>CIRCUIT BREAKER CLEARING</i> TYPE OF TRANSIENT TEST RESULTS	44
9.0	A/C #6 - TEST RESULTS	45
9.1	SYSTEM SPECIFICATIONS	45
9.2	TEST PARAMETERS	46
9.3	INRUSH TEST RESULTS.....	47
9.4	POWER CONTACTOR TEST RESULTS	47
9.5	<i>30-SECOND LONG NOTCH</i> TYPE OF TRANSIENT TEST RESULTS	48
9.6	<i>DELAYED RECOVERY</i> TYPE OF TRANSIENT TEST RESULTS.....	49
9.7	<i>CIRCUIT BREAKER CLEARING</i> TYPE OF TRANSIENT TEST RESULTS	50
10.0	A/C #7 - TEST RESULTS.....	51
10.1	SYSTEM SPECIFICATIONS	51
10.2	TEST PARAMETERS	51
10.3	INRUSH TEST RESULTS.....	52
10.4	POWER CONTACTOR TEST RESULTS	52
10.5	<i>30-SECOND LONG NOTCH</i> TYPE OF TRANSIENT TEST RESULTS	53
10.6	<i>DELAYED RECOVERY</i> TYPE OF TRANSIENT TEST RESULTS.....	53
10.7	<i>CIRCUIT BREAKER CLEARING</i> TYPE OF TRANSIENT TEST RESULTS	54
11.0	A/C #8 - TEST RESULTS	55
11.1	SYSTEM SPECIFICATIONS.....	55
11.2	TEST PARAMETERS	55
11.3	INRUSH TEST RESULTS.....	56
11.4	POWER CONTACTOR TEST RESULTS	56
11.5	<i>30-SECOND LONG NOTCH</i> TYPE OF TRANSIENT TEST RESULTS	57
11.6	<i>DELAYED RECOVERY</i> TYPE OF TRANSIENT TEST RESULTS.....	57
11.7	<i>CIRCUIT BREAKER CLEARING</i> TYPE OF TRANSIENT TEST RESULTS	58
12.0	A/C #9 - TEST RESULTS	60
12.1	SYSTEM SPECIFICATIONS.....	60
12.2	TEST PARAMETERS	61
12.3	INRUSH TEST RESULTS.....	61
12.4	POWER CONTACTOR TEST RESULTS	61
12.5	<i>30-SECOND LONG NOTCH</i> TYPE OF TRANSIENT TEST RESULTS	62
12.6	<i>DELAYED RECOVERY</i> TYPE OF TRANSIENT TEST RESULTS.....	63

12.7	CIRCUIT BREAKER CLEARING TYPE OF TRANSIENT TEST RESULTS	64
13.0	A/C #10 - TEST RESULTS	65
13.1	SYSTEM SPECIFICATIONS	65
13.2	TEST PARAMETERS	66
13.3	INRUSH TEST RESULTS.....	66
13.4	POWER CONTACTOR TEST RESULTS	66
13.5	30-SECOND LONG NOTCH TYPE OF TRANSIENT TEST RESULTS	67
13.6	DELAYED RECOVERY TYPE OF TRANSIENT TEST RESULTS.....	68
13.7	CIRCUIT BREAKER CLEARING TYPE OF TRANSIENT TEST RESULTS	68
14.0	APPENDIXES.....	70
14.1	APPENDIX # 1.....	70
14.1.1	ATTACHMENT #1 -- AIR CONDITIONER TESTING PROCEDURES	70
14.2	APPENDIX #2.....	71
14.2.1	AIR CONDITIONER # 1 INTERNAL PERFORMANCE PARAMETERS	71
14.2.2	AIR CONDITIONER # 2 INTERNAL PERFORMANCE PARAMETERS	73
14.2.3	AIR CONDITIONER # 3 INTERNAL PERFORMANCE PARAMETERS	76
14.2.4	AIR CONDITIONER # 4 INTERNAL PERFORMANCE PARAMETERS	79
14.2.5	AIR CONDITIONER # 5 INTERNAL PERFORMANCE PARAMETERS	82
14.2.6	AIR CONDITIONER # 6 INTERNAL PERFORMANCE PARAMETERS	84
14.2.7	AIR CONDITIONER # 7 INTERNAL PERFORMANCE PARAMETERS	87
14.2.8	AIR CONDITIONER # 8 INTERNAL PERFORMANCE PARAMETERS	90
14.2.9	AIR CONDITIONER # 9 INTERNAL PERFORMANCE PARAMETERS	93
14.2.10	AIR CONDITIONER # 10 INTERNAL PERFORMANCE PARAMETERS	95
14.3	APPENDIX #3.....	98
14.3.1	INRUSH REFERENCE GRAPH	98

1.0 EXECUTIVE SUMMARY

1.1 Introduction

SCE and other utilities have been having occurrences of delayed voltage recovery following faults on the electrical system. Under normal conditions, voltage recovers to nominal levels in less than one second after the fault is cleared. In several cases in the past few years, voltage recovery has been delayed for over 30 seconds after normal fault clearing in some substations, especially when the air temperature and electrical system loading was high. This delayed voltage recovery is being attributed to stalling of air conditioner units. Delayed voltage recovery may lead to a system voltage collapse in the worst case.

This delayed undervoltage recovery behavior has been seen in the SCE system since 1989 but has not caused serious problems. In recent years, these delayed undervoltage recovery events have been increasing. During the summer of 2006, SCE experienced 36 delayed voltage recovery events. In some cases, these delayed voltage recoveries are out of compliance with the WECC supply voltage limit, which dictates that voltage should not be more than 20% below nominal for more than 20 cycles.

SCE customers are also affected by the delayed voltage recovery. This causes SCE customers inconvenience and potential loss of business when these events arise. Although there is no indication of an imminent total system voltage collapse at this time, SCE is approaching this problem in a conservative way by studying the phenomenon and exploring potential solutions.

1.2 Work Performed

SCE began air conditioner testing in 2005 to determine how the units would respond when exposed to various under-voltage transient conditions. The test results help SCE to properly model the electrical system and determine possible solutions. SCE tested ten (10) air conditioner units, in its Pomona Electric Vehicle Technical Center (EVTC), typically found in the service territory. The diversity of the tested air conditioner units included sizes (tonnage), compressor technology (reciprocating and scroll), refrigerant technology (R22 and R-410A), vintage (new and old), and efficiencies (10 thru 13 SEER).

The ten (10) air conditioner units were tested under different undervoltage transients including the *Long Notch*, *Delayed Recovery* and *Circuit Breaker Clearing* type of transient. The *Long Notch* transient (drop in voltage that was held for 30 seconds) was used to establish the threshold voltage where the air conditioner compressor stalled. The *Delayed Recovery* transient (drop in voltage followed by a 30 seconds recovery to nominal voltage) simulates the typical delayed voltage recovery event observed in SCE system. The *Circuit Breaker* transient (short duration drop in voltage held for 3, 6, 9, and 12 cycles) simulates the typical transient generated by the tripping and reclosing of circuit breakers commonly used in the SCE system.

In addition, SCE performed additional testing on the air conditioners for the WECC Load Modeling Task Force which included frequency oscillations, voltage oscillations, and different arrangements of undervoltage transients. The WECC is currently developing software models to simulate air conditioners in power system analysis programs. Current models do not properly simulate stalling air conditioner behavior during undervoltage transients. SCE developed the Air

Conditioner Testing Procedures for the testing of air conditioners with input from EPRI Solutions and Bonneville Power Administration (BPA). These procedures were used by EPRI Solutions (under contract with APS) and BPA. Together SCE, BPA, and EPRI Solutions will test more than 40 residential air conditioners and share the test data under the umbrella of the WECC Load Modeling Task Force. The detailed test procedures are attached to this report as Appendix #1.

1.3 Testing Results

This summary section contains the testing results for the air conditioning units when exposed to the *delayed recovery* type of transients, similar to that observed during the delayed voltage recovery events at SCE.

1.3.1 Stall Voltage

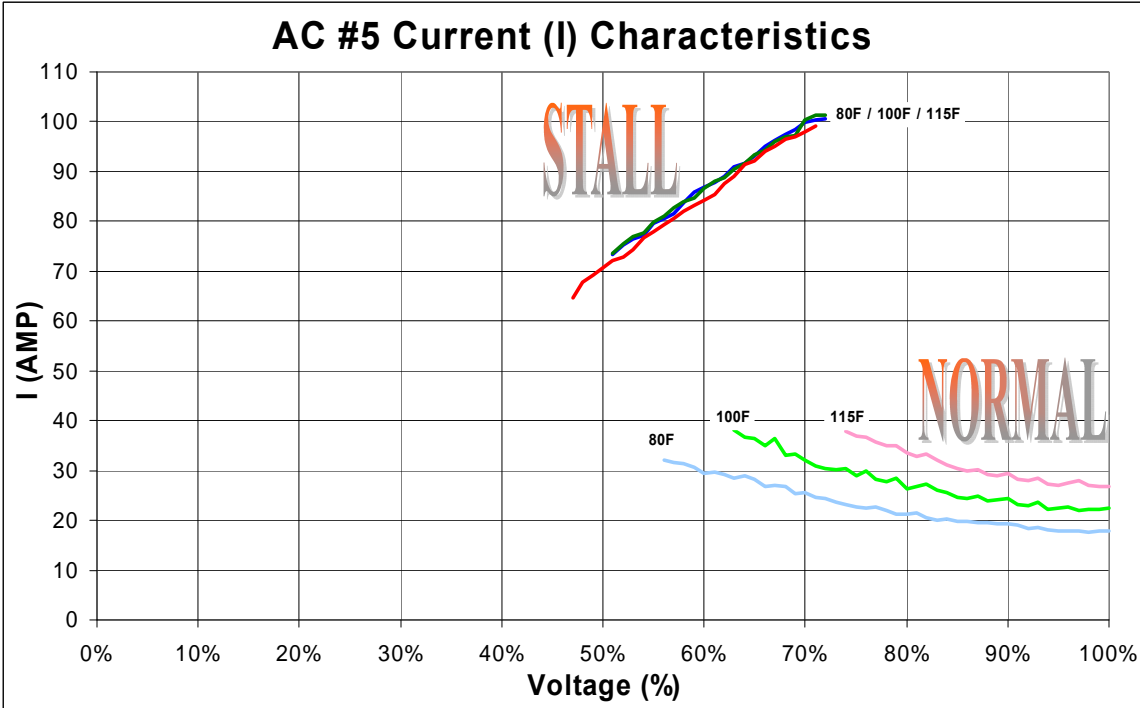
The ten tested air conditioning units had similar stalling voltages within $\pm 5\%$ (voltage level where compressor ceased to turn) at each of the tested temperatures. These voltages varied with the outdoor air temperature that the compressor and condensing coils were subjected to. The stall response time (time it takes the air conditioner compressor to stop turning) on the tested air conditioners was approximately 6 cycles after the under-voltage condition occurred. Test results indicated that the stalling voltage average at 80 °F is 61%, at 100 °F is 65%, and at 115 °F is 69%. Table 1 indicates the stalling windows (voltages between the stall threshold voltage and the contactor dropout voltage) for the ten tested air conditioner units when exposed to the *delayed recovery* type of transients. Air conditioner unit #10 did not stall at 80 °F and it operated down to the voltage where the contactor opened without stalling. Opening of the contactor did not prevent the air conditioner units from stalling; it just delayed stalling until the contactor reclosed (see more details in 1.3.4)

	Stall Window (80°F)		Stall Window (100°F)		Stall Window (115°F)	
	Stall Threshold	Contactor Dropout	Stall Threshold	Contactor Dropout	Stall Threshold	Contactor Dropout
AC #1	64%	50%	66%	50%	68%	50%
AC #2	56%	50%	61%	50%	66%	50%
AC #3	59%	35%	67%	35%	73%	35%
AC #4	62%	50%	67%	50%	75%	50%
AC #5	57%	50%	62%	50%	67%	45%
AC #6	59%	45%	64%	40%	68%	40%
AC #7	57%	50%	61%	50%	67%	50%
AC #8	64%	45%	67%	55%	69%	50%
AC #9	67%	55%	70%	55%	73%	55%
AC #10	none	45%	64%	50%	68%	55%

Table 1 – Stall Window

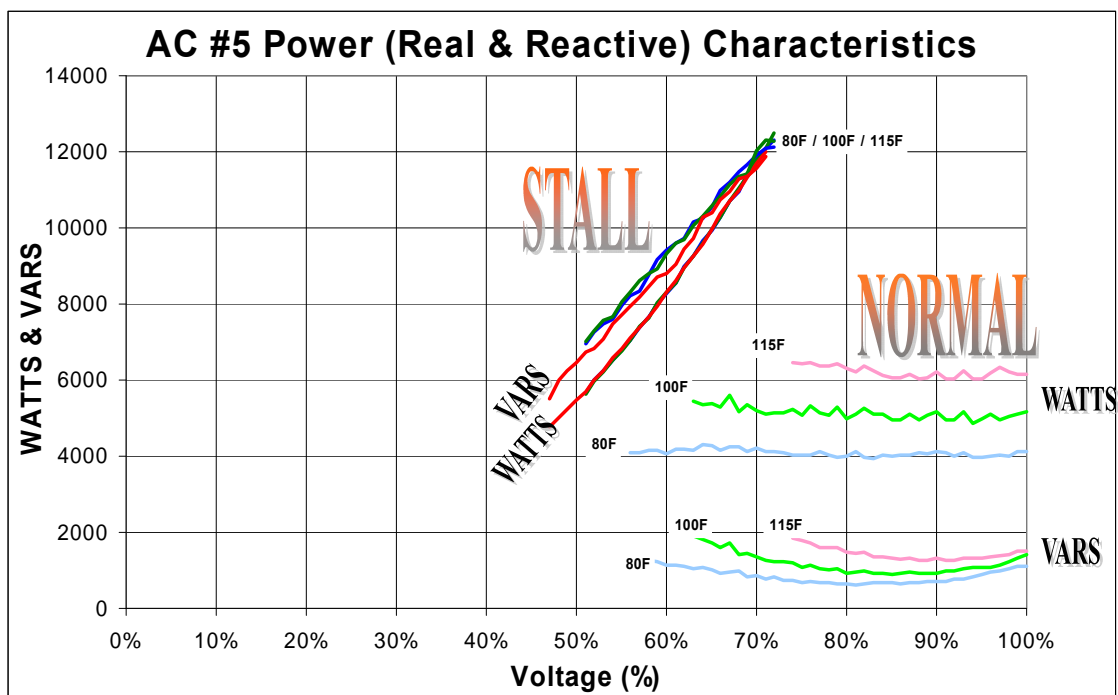
The major influence on the three stall parameters, current (I_{STALL}) and real power (P_{STALL}) and reactive power (Q_{STALL}), was the supply voltage. The higher the terminal voltage when the stall occurs, the higher the stall parameter values. The values of these parameters were also proportional to the unit size.

Graph 1 below indicates the typical current (I) behavior of an air conditioner unit when exposed to the *delayed recovery* type of transient. The normal running current (I_{FLA}) is approximately 17, 22, and 27 Amps at nominal voltage (100% or 240 V) for the three simulated outdoor temperatures 80, 100, 115 °F respectively. The normal running current was found to be inversely proportional to the supply voltage, the lower the voltage the higher the normal running current. This behavior continues down to where the unit starts stalling (stalling threshold voltage). The current jumped from as low as 17 Amps (at nominal voltage and 80 °F) to 100 Amps (at 70% applied voltage) when the unit stalled. The stall current (I_{STALL}) was found to be directly proportional to the applied voltage, the higher the voltage applied to the compressor terminals during the stall the higher the stall current (blue, green, and red plot lines). This behavior continues down to where the contactor drops out (contactor drop out voltage).



Graph 1 – Stall Current

Graph 2 indicates the typical power (real P and reactive Q) behavior of an air conditioner unit when exposed to the *delayed recovery* type of transient. The normal running real power (P) is approximately 4000, 5000, and 6000 Watts and the normal running reactive power (Q) is approximately 900, 1100, and 1300 VARs at nominal voltage (100% or 240 V) for the three simulated outdoor temperatures 80, 100, 115 °F respectively. The normal real power (NORMAL WATTS plot line) did not change significantly when the applied voltage decreased all the way down until the unit stall point. The normal reactive power (NORMAL VARS plot line) was found to be inversely proportional to the applied voltage down to approximately 85% then started being proportional to the applied voltage until the unit stalled (stall threshold voltage). The real power jumped from 4000 Watts (at nominal voltage and 80 °F) to as high as 12,000 Watts (at 70% applied voltage) when the unit stalled. The reactive power jumped from 900 VARs (at nominal voltage and 80 °F) to as high as 12,000 VARs (at 70% applied voltage) when the unit stalled. When stalled, both the real and reactive powers were found to be directly proportional to the applied voltage, the higher the voltage the higher the Watts and VARs. This behavior continues down to where the contactor drops out (contactor drop out voltage).



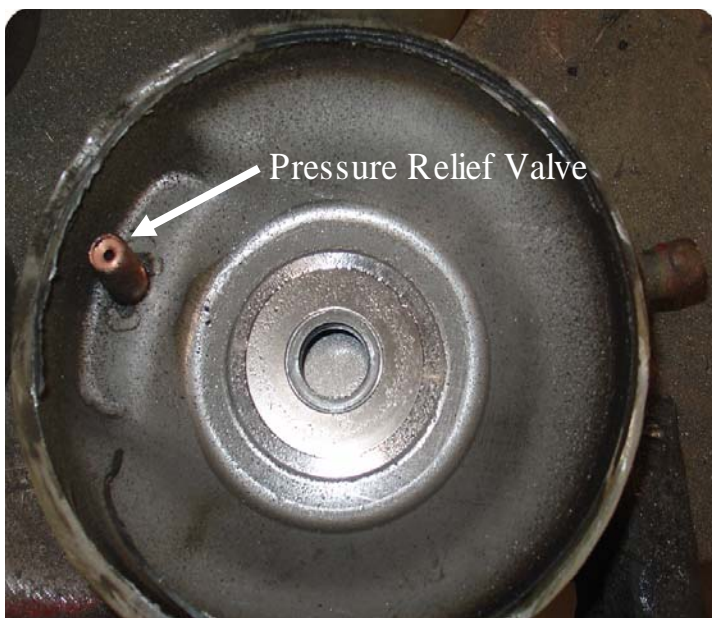
Graph 2 – Stall Real and Reactive Power

1.3.2 Metering Devices

Air conditioner systems usually use either thermostatic expansion valves (TXV) or orifice metering devices to control the proper flow of refrigerant in the high-pressure side of the cooling coil (indoor coil). Controlling the proper flow of refrigerant in the high-pressure side is critical because too much flow can cause the cooling coil to freeze and therefore not produce any cooling. The orifice-metering device has a unique advantage that it brings the pressure quickly into equalization after the compressor shuts down. The TXV helps the cooling coil maintain proper flow using a sophisticated feedback system but pressure equalization is achieved at a much slower rate (1 to 2 minutes) than the orifice. The TXV helps the cooling coil have the proper flow when the system is undercharged, maintaining its efficiency. It offers no improvement when the system is overcharged. Since TXVs are commonly used in new air conditioner installations, most of the air conditioner units tested had TXV valves.

When stalled, the compressor ceases to turn and therefore does not generate pressure. The high-pressure (liquid line) and low-pressure (vapor line) need to equalize in order for the compressors to restart smoothly. Most air conditioners rely on thermostats (which commonly have a 5 minutes delay) to avoid short cycling which allows pressure equalization before a restart is attempted.

Most of the tested air conditioner units with scroll compressors went into IDLE (drawing the same running amps without producing any cooling) or NO-LOAD (drawing about ½ the running amps without producing any cooling) condition after a *circuit breaker clearing* generated type of transient. It seems that some mechanical device prevented them from restarting normally. We opened a scroll compressor and found a pressure relief valve between the high pressure and low-pressure chambers. This valve is designed to prevent too much pressure from building up in the high-pressure side, releasing it into the low-pressure chamber. This valve may have stuck open when the compressor went into either IDLE or NO-LOAD condition because the unit draws current but no pressure is built up, and no cooling is produced. The air conditioner unit had to be turned off and then back on again to resume normal running condition.



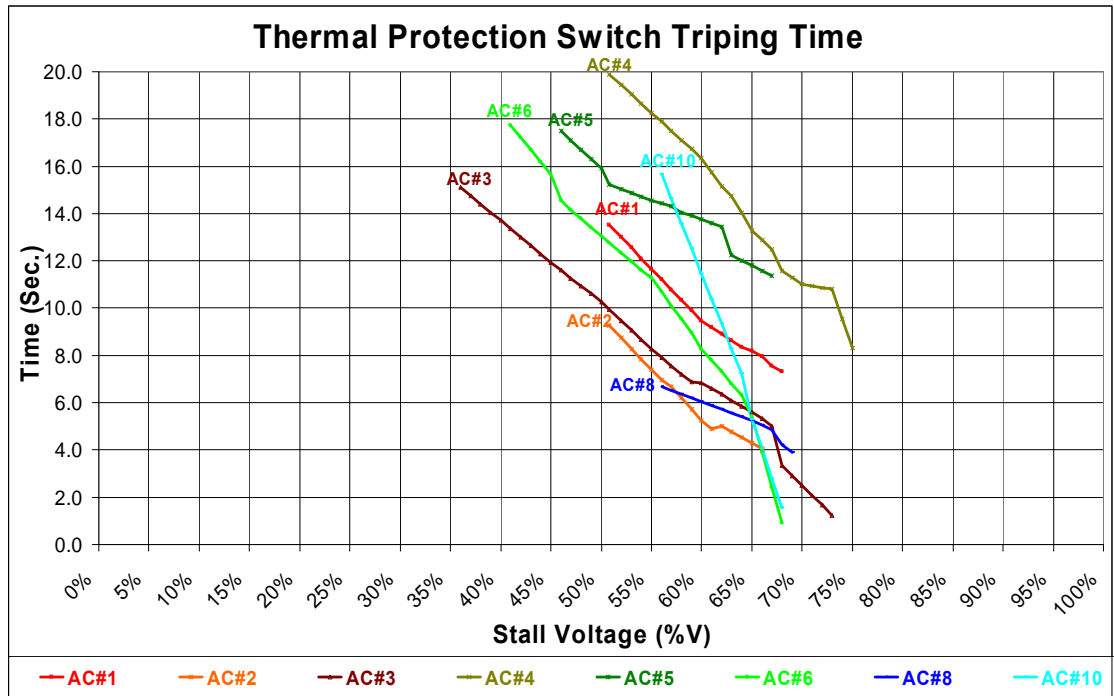
Graph 3 – Pressure Relief Valve

Some air conditioner units have high-pressure and low-pressure switches that are in series with the thermostat circuit to protect the compressor from harmful high-pressure conditions. One of the units (air conditioner unit #5) shut itself down under normal running conditions (at nominal voltage) due to high pressure when the outdoor temperature reached 120°F. This indicated that this particular air conditioner unit, under normal charging conditions, would not work properly at in areas where the temperature reaches 120°F.

1.3.3 Thermal Protection Switch

All of the tested air conditioning units' compressors have a thermal protection switch that opens to protect the motor from overheating due to extended stall currents. Without the thermal protection switch, the motor might overheat and fail when high currents are present for long periods. When exposed to the *delayed recovery* type of transients, most of the tested air conditioner compressors (except A/C #7) stalled for as short as 1.0 second and as long as 20 seconds before the thermal protection switch opened to protect the compressor (as seen in Graph 2). Air conditioner unit #7 stalled for as long as 11.6 seconds without opening the thermal protection switch during the 30 second transient. In this unit, when the voltage rose above 162 V, the compressor resumed normal running condition. Air conditioner unit #9's (used unit) thermal protection switch opened only at the higher test temperatures (100 °F and 115 °F) and only after the compressor stalled for more than 12 seconds. Air conditioner unit #10's thermal protection switch opened only at the highest test temperature (115 °F). All the units restarted normally after the thermal protection switch reclosed except for air conditioner units #6 and #8. These two units needed to be turned off and then on again in order to run normally.

Graph 4 shows the thermal protection switch average tripping time versus the stall voltage for each of the tested air conditioner units except for #7 and #9. Each air conditioner unit had similar linear thermal protection switch tripping time slopes at the three tested temperatures except for unit # 9, which behaved differently for each of the three tested temperatures. The thermal protection tripping time was found to be inversely proportional to the sag voltage, the lower the voltage the longer the thermal protection switch tripping time. The thermal protection tripping time can be as short as 1.0 second and as long as 20 seconds as shown in graph below. The right end of each plot is where the unit started stalling (stall threshold) and the left end is where the contactor opens (contactor dropout voltage).



Graph 4 – Thermal Protection Switch Tripping Time

Table 2 indicates the stalling window (between the stall threshold voltage and contactor dropout voltage). The thermal protection switch (TPS) tripping time for each of the tested units can be calculated with the t_{TPS} formula shown below.

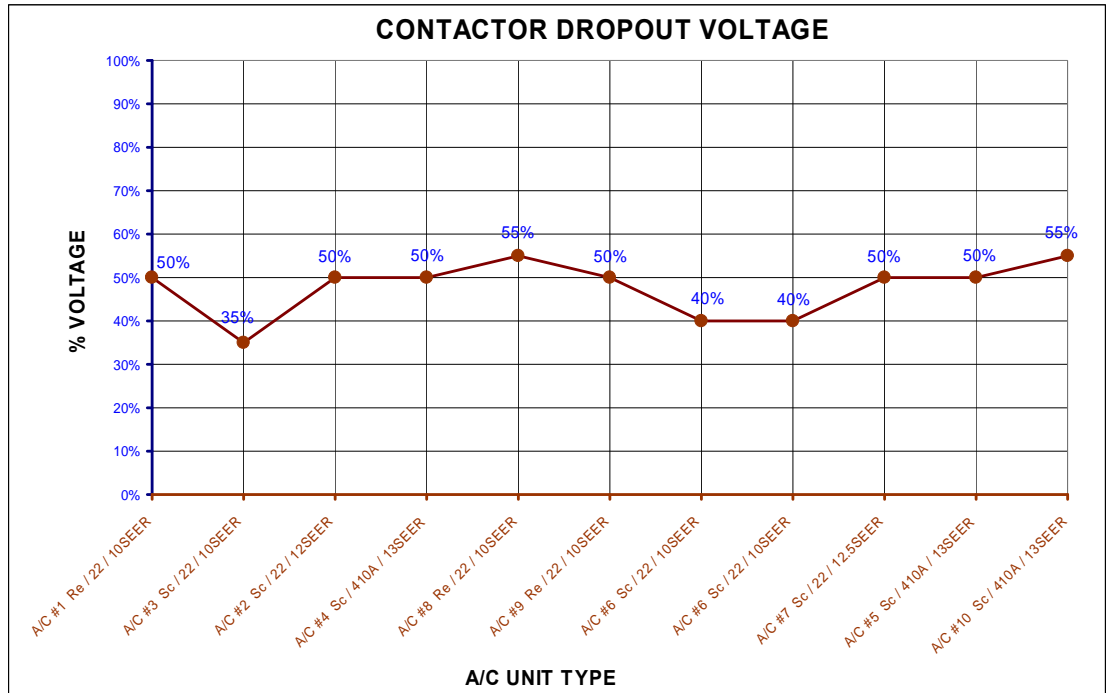
$t_{TPS} = (m * V) + \phi$								
	Stall Window (80°F)		Stall Window (100°F)		Stall Window (115°F)		Slope (m)	Constant (ϕ)
	High	Low	High	Low	High	Low		
AC #1	64%	51%	66%	51%	68%	51%	-44.0000	35.8667
AC #2	56%	51%	61%	51%	66%	51%	-31.2333	24.5817
AC #3	59%	36%	67%	36%	73%	36%	-31.6667	25.8500
AC #4	62%	51%	67%	51%	75%	51%	-49.6667	46.1333
AC #5	57%	51%	62%	51%	67%	46%	-27.3333	30.1500
AC #6	59%	46%	64%	41%	68%	41%	-47.8718	36.9962
AC #7	57%	51%	61%	51%	67%	51%	-68.3333	49.0500
AC #8	64%	46%	67%	56%	69%	51%	-22.7500	20.0442
AC #9	67%	56%	70%	56%	73%	56%	-67.0000	44.1500 @ 80°F
							-62.3077	46.3846 @ 100°F
							-26.0000	22.9000 @ 115°F
AC #10	none	46%	64%	51%	68%	56%	-105.5208	74.7625

Table 2 – Stall Calculation

1.3.4 Contactor Dropout

All the tested air conditioners have a main power contact relay (called the contactor) that has a 24 VAC coil connected in series with the thermostat contact. All of the contactors were found to have a quick response time (2 cycles to open/close when voltage is applied). These units use standard contactors (off the shelf type) which were not specifically designed for air conditioner use. From the tests, the contactor dropout voltage varied from about 55% down to 35% as seen in the Graph 5. This means that

when the supply voltage goes below these values (below brown line on the graph below) the contactor will open tripping off the compressor. While the contactor is open, the compressor is off, but as soon as it recloses, the air conditioner compressor stalls when exposed to the *delayed recovery* type of transient.



Graph 5 – Contactor Dropout Voltage

Opening the contactor did not prevent the air conditioner units from stalling; it just delayed it until the supply voltage reaches the contactor threshold voltage. Table 3 indicates the maximum stalling times after the contactor recloses for all of the tested air conditioner units. This maximum time is when the voltage at the compressor is just above the contactor dropout voltage.

	Contactor Dropout Voltage (%)	Max. Stall Time After Contactor Reclosed (sec.)
A/C #1 Re / 22 / 10SEER	50%	11.5
A/C #3 Sc / 22 / 10SEER	35%	11.8
A/C #2 Sc / 22 / 12SEER	50%	5.5
A/C #4 Sc / 410A / 13SEER	50%	15.9
A/C #8 Re / 22 / 10SEER	55%	5.6
A/C #9 Re / 22 / 10SEER	50%	11.2
A/C #6 Sc / 22 / 10SEER	40%	11.4
A/C #6-OC Sc / 22 / 10SEER	40%	8.1
A/C #7 Sc / 22 / 12.5SEER	50%	6.4
A/C #5 Sc / 410A / 13SEER	50%	8.1
A/C #10 Sc / 410A / 13SEER	55%	6.6

Table 3 –Stalling Time after Contactor Reclosed

2.0 OBJECTIVE

SCE and other utilities have had several occurrences of delayed voltage recovery following faults on the electrical system. Under normal conditions, voltage recovers to normal levels in less than one second after the fault is cleared. In several cases in the past few years, voltage recovery has been delayed for over 30 seconds after normal fault clearing in the Valley Substation area. This delayed voltage recovery is being attributed to stalling of air conditioner units. Testing of air conditioner units is being conducted to determine how they behave when exposed to various under-voltage conditions. These test results will help to properly model the electrical system and determine possible solutions to this problem.

The objective of this testing is to investigate the air conditioner’s response to different under-voltage transient conditions, especially under the *delayed recovery* type of transient. SCE has tested ten air conditioner units typically found in the service territory. The diversity of the tested air conditioner units included size (tonnage), compressor technology (reciprocating and scroll), refrigerant technology (R22 and R-410A), vintage (new and old), and efficiency (10 thru 13 SEER) as seen in Table 4. The test results will help to properly model the electrical system and determine possible solutions to events.

A/C #	Condenser						
	Mfg	Unit	Ton	Comp.	Refrig.	SEER	Vintage
1	Carrier	38CKS036	3	Re	22	10	New
3	Rheem	RAKB036-JAZ	3	Sc	22	10	New
2	Carrier	38BRG036300	3	Sc	22	12	New
4	Carrier	38TXA036-30	3	Sc	410A	13	New
8	Goodman	CLK048	4	Re	22	10	New
9	Day & Night	5680J048	4	Re	22	10	Used
6	Rheem	RAB048-JAZ	4	Sc	22	10	New
6	Rheem (Over-Charged)	RAB048-JAZ	4	Sc	22	10	New
7	Carrier	38TRA-048	4	Sc	22	12.5	New
5	Coleman	AC3B048F1A	4	Sc	410A	13	New
10	Carrier	38TXA060-31	5	Sc	410A	13	New

Table 4 – Tested Air Conditioner Units

The same indoor unit (air handler) was used for all the tests except for the cooling coil, which was replaced, depending on the system tonnage. Three different cooling coils were used for the three different systems tonnages (3, 4, and 5-tons). The air handler’s fan speed was adjusted for the three different system tonnages. Different air conditioner system piping was used for the different refrigerants.

The test procedures described in section 3.0 were performed for each air conditioner unit. Each unit test is composed of fifteen sub-tests from which SCE has analyzed the first five. Others are reviewing the remaining test results.

2.1. Measurements

The air conditioner instrumentation provided four voltages (V_1 , V_2 , V_3 , and V_4) and four currents (I_1 , I_2 , I_3 , and I_4) as noted in Table 5. The voltages and currents were captured at the condenser unit (outdoor unit). In addition to the voltages and currents required above, the real power (W) and apparent power (VA) are also computed (see Table 6). The Yokogawa Power Analyzer can mathematically calculate real, apparent powers and frequency.

TAG	DESCRIPTION	Yokogawa	
		MATH	EXPRESSION
V ₁	Input Voltage	1	Trend(C1)
V ₂	Compressor Motor Running Winding Voltage	3	Trend(C3)
V ₃	Capacitor Voltage	5	Trend(C5)
V ₄	Compressor Motor Start Winding Voltage	7	Trend(C7)
I ₁	Input Current	2	Trend(C2)
I ₂	Compressor Motor Running Winding Current	4	Trend(C4)
I ₃	Fan Motor Current	6	Trend(C6)
I ₄	Compressor Motor Start Winding Current	8	Trend(C8)

Table 5 – Yokogawa Voltage and Current Points

Tag	Description	Yokogawa	
		MATH	EXPRESSION
W ₁	Total Real Power	9	Trend(C1)*C2)
W ₂	Compressor Motor Running Winding Real Power	11	Trend(C3)*C4)
W ₃	Compressor Motor Start Winding Real Power	13	Trend(C7)*C8)
F	Frequency	15	Trendf(C1)
VA ₁	Total Apparent Power	10	Trend(C1)*Trend(C2)
VA ₂	Compressor Motor Running Winding Apparent Power	12	Trend(C3)*Trend(C4)
VA ₃	Compressor Motor Start Apparent Power	14	Trend(C7)*Trend(C8)

Table 6 – Yokogawa Real and Apparent Power Points

All of these voltages, currents, real power, apparent power, and frequency measurements are synchronized. A macro was created to filter the data and calculate the reactive power (VARs) and power factor (PF).

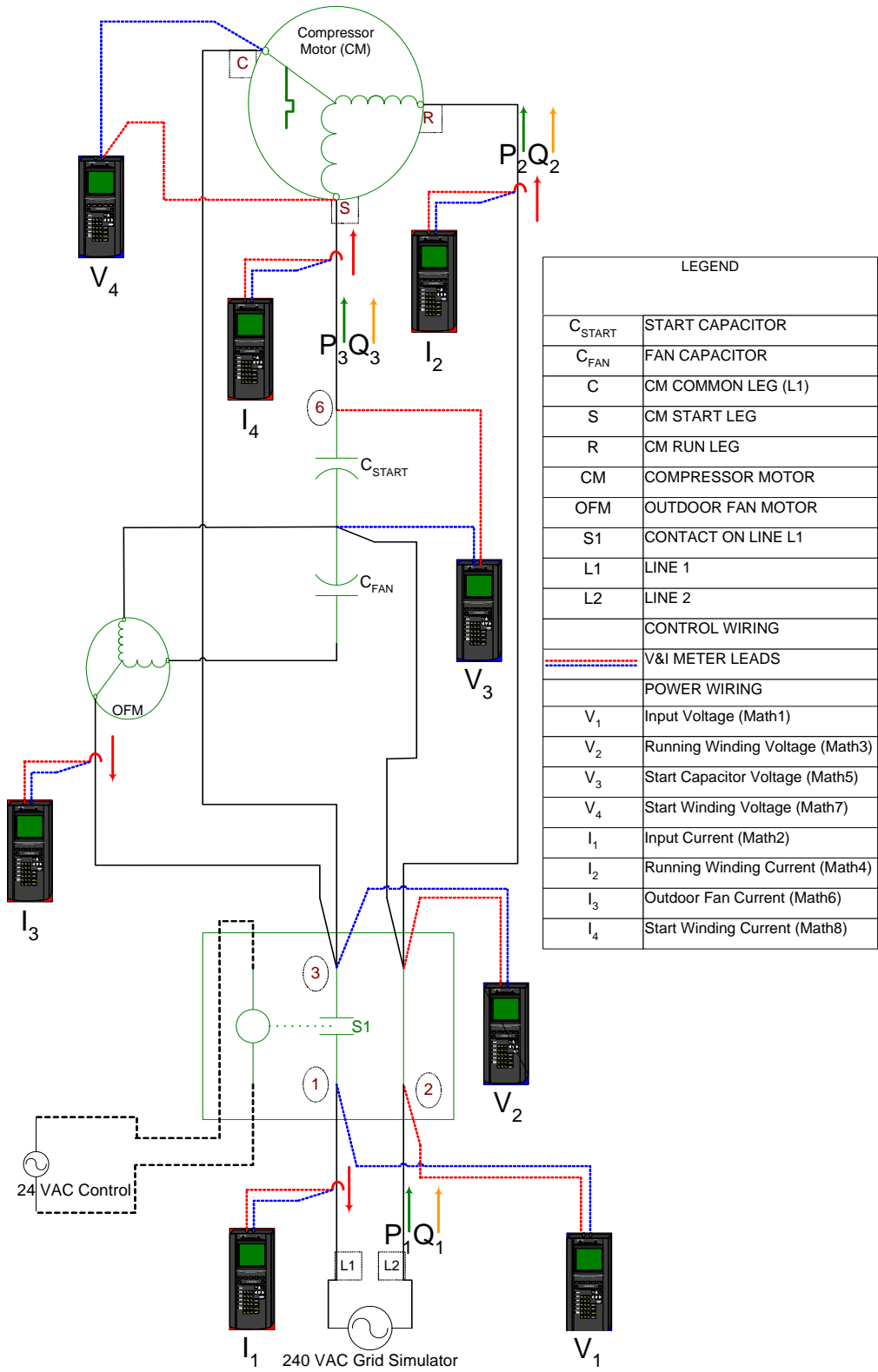


Figure 6 – Typical Air Conditioner Diagram

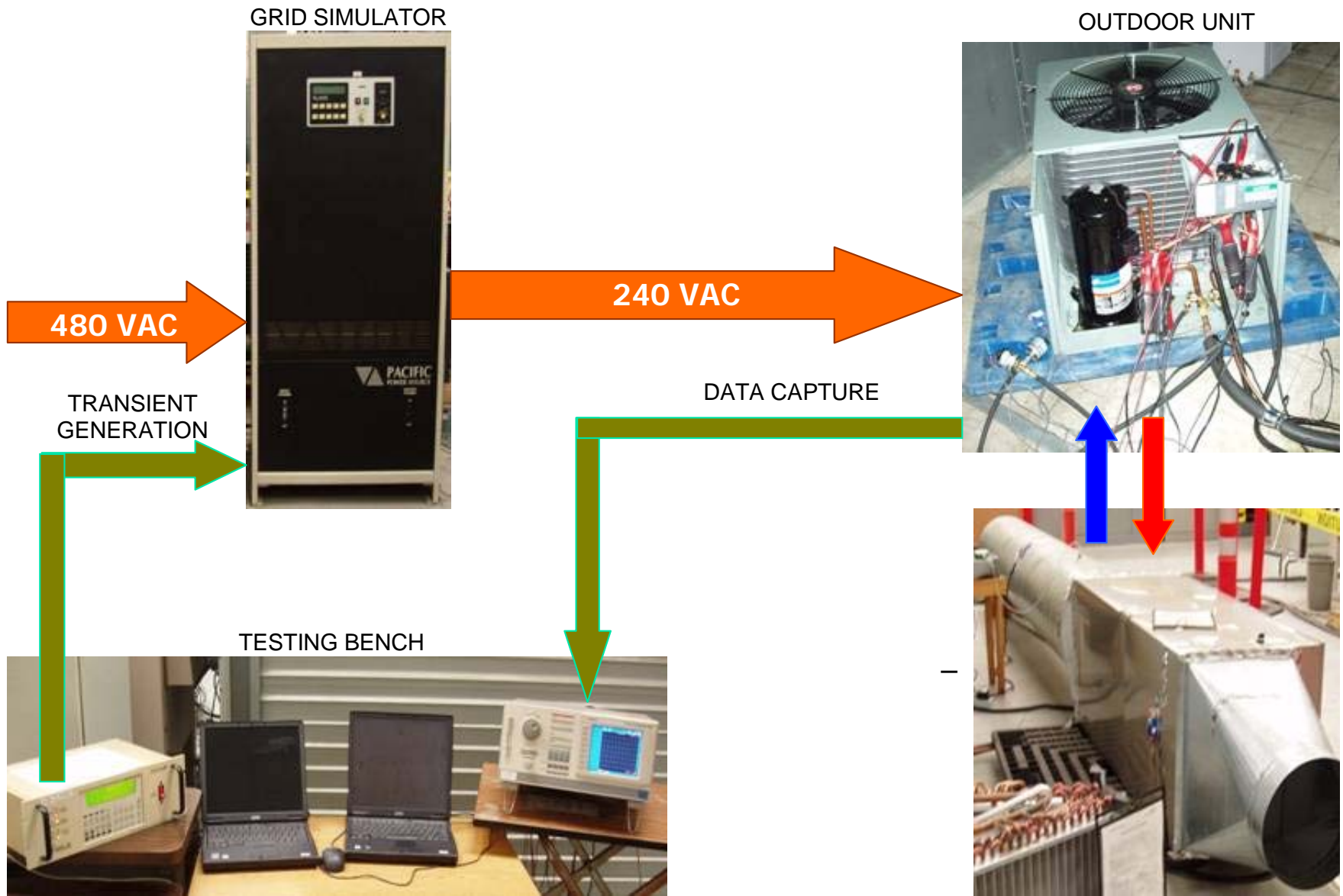


Figure 7 – Testing Layout Diagram

Air Conditioner Stalling Effects Study

Air Conditioner Test Report

3.0 AIR CONDITIONER TEST TRANSIENT

This test report is focused mainly on the response of the air conditioner units to three different types of transients the *Long Notch*, the *Delayed Recovery* and *Circuit Breaker Clearing* type of transients. Other tests were also performed for the WECC Load Modeling Task Force, which included voltage oscillations, frequency oscillations, circuit breaker clearing transients with different voltage recoveries, and tests with the contactor bypassed. The detailed test procedure can be found in APPENDIX # 1.

3.1 Long Notch Type of Transient

The *Long Notch* type of transient was used to determine both the stalling threshold voltage and the contactor dropout voltage. This information was later used to implement the other two types of transients, the *Delayed Recovery* and the *Circuit Breaker Clearing*.

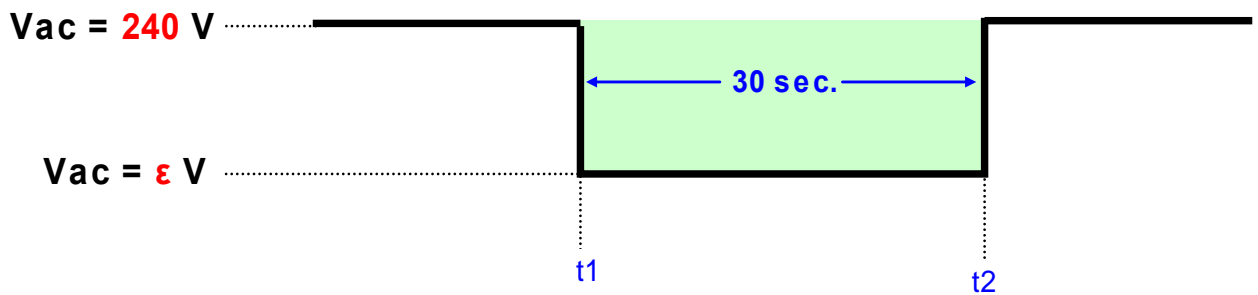


Figure 8

3.2 Delayed Recovery Type of Transient

The *Delayed Recovery* type of transient was used to determine the air conditioners' response to a delayed voltage recovery event in the electrical grid. A 30 second ramp up recovery time was used because this is similar to the transients observed in our system.

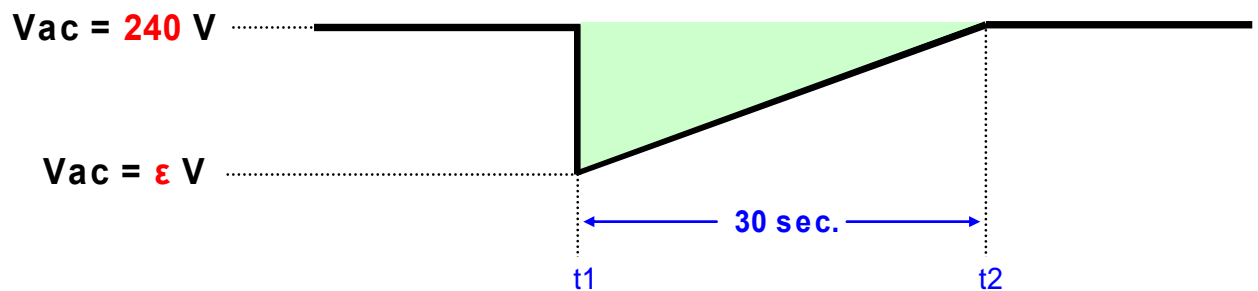


Figure 9

3.3 Circuit Breaker Clearing Type of Transient

The *Circuit Breaker Clearing* type of transients was used to determine the air conditioners response to short interruptions caused by the opening and reclosing of circuit breakers. Transients of 3, 6, 9, and 12 cycles were used because these are the switching times of circuit breakers commonly used on the SCE electrical system.

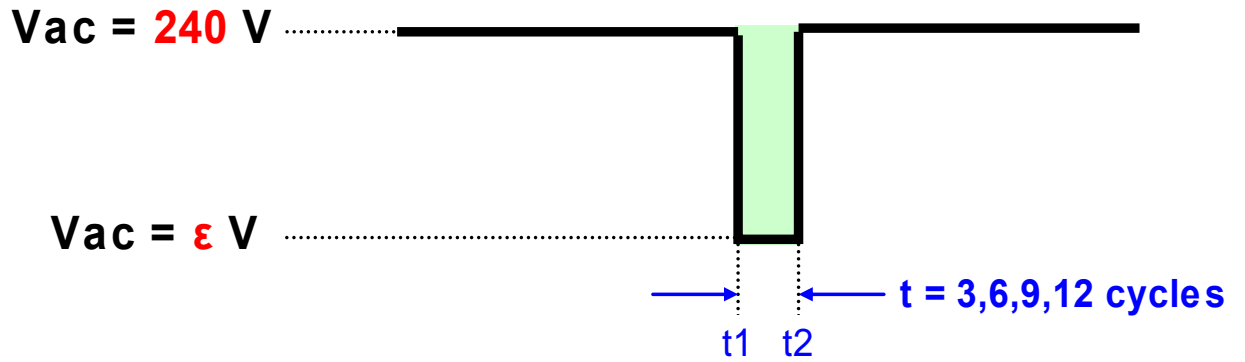


Figure 10

4.0 A/C #1- TEST RESULTS

The air conditioner's compressor stalled when the voltage was in the stalling window (between the stall threshold voltage and contactor dropout voltage) when exposed to any of the three transients. This air conditioner unit stalled, drawing approximately 48 Amps at 129 VAC, for 21.5 seconds before the thermal protection switch opened to protect the compressor when exposed to the *long notch* type of transients. This air conditioner unit stalled, drawing approximately 62 Amps at 175 VAC, for as long as 12.5 seconds before the thermal protection switch opened to protect the compressor when exposed to the *delayed recovery* type of transients. It stalled, drawing approximately 94 Amps at 235 VAC, for as long as 2.9 seconds before the thermal protection switch opened, when exposed to the *circuit breaker clearing* type of transients. Opening the contactor did not help in preventing the compressor from stalling, it just delayed the stall until the contactor reclosed. The good thing about this air conditioner unit is that it restarted normally after any stall. The power contactor drop out voltage was 50%.

4.1 SYSTEM SPECIFICATIONS

The tested air conditioner system has the following specifications:

MAIN SYSTEM	
Manufacturer	Carrier
Condenser Unit	38CKS036
Evaporator Coil	CK3BA036
Size (Tons)	3
Compressor Type	Reciprocating
Refrigerant	R-22
SEER	10
Condition	New
Unit Cost	\$670.00

COMPRESSOR	
Manufacturer	Bristol
Model	739024-1602-00
Type	Reciprocating
FLA (AMPS)	16
LRA (AMPS)	82
Phase	1
Refrigerant	R22
Charge (LBS)	4.6
Voltage (V)	230/208
PMAX High (PSI)	-
PMAXLow (PSI)	-

FAN MOTOR	
Manufacturer	GE
Model	5KCP39EGS070S
Voltage (V)	208/230
Current (I)	1.4
Power (HP)	0.25
RPM	1100
FLA (AMPS)	1.4

CONTACTOR	
Manufacturer	Product Unlimited
Model	HN51KC024
Rating (V)	240/277
FLA (AMPS)	30
LRA (AMPS)	150
Resistance	40

CAPACITOR	
Manufacturer	GE
Model	HC98JA046D
Rating (V)	370
Capacitance (µF)	45

4.2 TEST PARAMETERS

The test parameters for this unit were not captured. The performance parameter table can be found in APPENDIX #2 -- Attachment # 1

	80°F	100°F	115°F
T _{INLET} (°C)	-	-	-
T _{OUTLET} (°C)	-	-	-
T _{COMP. AMB.} (°C)	-	-	-
T _{CASE} (°C)	-	-	-
T _{GAS} (°C)	-	-	-
T _{LIQ} (°C)	-	-	-
R _{FLOW} (Kcfm)	-	-	-
P _{LOW} (PSI)	-	-	-
P _{HIGH} (PSI)	-	-	-
I _{RUNNING} (A)	14.0	16.0	17.0
W _{RUNNING} (W)	3100.0	3500.0	3800.0
VAR _{RUNNING} (VAR)	1300.0	1300.0	1300.0

4.3 INRUSH TEST RESULTS

This air conditioner system took approximately 10 cycles to come to normal steady running state, from which 9 cycles exhibited LOCKED-ROTOR characteristics. The data below was recorded for the air conditioner system.

Inrush	
V _{INRUSH}	233 VAC
I _{INRUSH}	97 A
W _{INRUSH}	16,300 W
VAR _{INRUSH}	15,700 VAR
t	10 cycles

4.4 POWER CONTACTOR TEST RESULTS

The power contactor opened at 50% voltage sag. In general, opening the contactor did not prevent the compressor from stalling; it just delayed the stalling until the contactor reclosed. The compressor had the following responses right after the contactor reclosed:

- ◆ *Long Notch* type of transients
 - The compressor stalled, drawing approximately 94 Amps at 233 VAC, right after the contactor reclosed for as long as 3.0 seconds before the thermal protection switch opened to protect the compressor.
- ◆ *Delayed Recovery* type of transient
 - The compressor stalled, drawing approximately 64 Amps at 176 VAC, right after contactor reclosed for as long as 11.5 seconds before the thermal protection switch opened to protect the compressor.
- ◆ *Circuit Breaker Clearing* type of transients

- The compressor stalled, drawing approximately 94 Amps at 233 VAC, right after the contactor reclosed for as long as 2.9 seconds before the thermal protection switch opened to protect the compressor.

4.5 30-SECOND LONG NOTCH TYPE OF TRANSIENT TEST RESULTS

This compressor has the following threshold voltages 60% at 80 °F, 67% at 100 °F and 115 °F when exposed to the *long notch* type of transients. Therefore, the stalling windows for this compressor are the following: 60% to 50% at 80 °F, 67% to 50% at 100 °F, and 67% to 50% at 115 °F. The thermal protection switch opened after each stall to protect the compressor. The compressor stalled in the stalling window, drawing approximately 48 Amps at 129 VAC, for as long as 21.5 seconds before the thermal protection switch opened to protect the compressor. If the power contactor opened and then reclosed, the compressor stalled drawing approximately 94 Amps at 235 VAC, for as long as 3.0 seconds before the thermal protection opened to protect the compressor. The following are the detail responses of the compressor for each of the temperatures:

- ◆ °At 80 °F
 - The compressors stalled, drawing approximately 48 Amps at 129 VAC, for as long as 16.9 seconds before the thermal protection switch opened to protect the compressor.
 - If the power contactor opened and then reclosed, the compressor stalled for as long as 3.0 seconds, drawing approximately 94 Amps at 237 VAC, characteristics before the thermal protection opened to protect the compressor
- ◆ At 100 °F.
 - The compressor stalled, drawing approximately 48 Amps at 129 VAC, for as long as 21.5 seconds before the thermal protection switch opened to protect the compressor.
 - If the power contactor opened and then reclosed, the compressor stalled for as long as 3.0 seconds, drawing approximately 94 Amps at 235 VAC, before the thermal protection opened to protect the compressor.
- ◆ At 115 °F
 - The compressor stalled, drawing approximately 48 Amps at 130 VAC, for as long as 17.9 seconds before the thermal protection switch opened to protect the compressor.
 - If the power contactor opened and then reclosed, the compressor stalled for as long as 3.0 seconds, drawing approximately 94 Amps at 237 VAC, before the thermal protection switch opened to protect the compressor.

4.6 DELAYED RECOVERY TYPE OF TRANSIENT TEST RESULTS

This compressor has the following stall threshold voltages 64% at 80 °F, 65% at 100 °F, and 68% at 115 °F when exposed to the *delayed recovery* type of transient. Therefore, the stalling windows for this compressor are the following: 65% to 50% at 80 °F, 67% to 50% at 100 °F, and 68% to 50% at 115 °F. The thermal protection switch opened after each stall to protect the compressor. The compressor stalled in the stalling window, drawing approximately 62 Amps at 175 VAC, for as long as 12.5 seconds before the thermal protection switch opened to protect the compressor. If the power contactor opened and then reclosed, the compressor stalled, drawing approximately 63 Amps at 178 VAC, for as long as 11.5 seconds before the thermal protection opened to protect the compressor. The following are the detail responses of the compressor for each of the temperatures:

- ◆ At 80 °F
 - The compressor stalled, drawing approximately 61 Amps at 170 VAC, for as long as 10.9 seconds before the thermal protection switch opened to protect the compressor.
 - If the power contactor opened and then reclosed, the compressor stalled, drawing approximately 62 Amps at 176 VAC, for as long as 10 seconds before the thermal protection switch opened to protect the compressor.
- ◆ At 100 °F
 - The compressor stalled, drawing approximately 62 Amps at 173 VAC, for as long as 11.6 seconds before thermal protection switch opened to protect the compressor.
 - If the power contactor opened and then reclosed, the compressor stalled, drawing approximately 62 Amps at 175 VAC, for as long as 11.0 seconds before the thermal protection opened to protect the compressor.
- ◆ At 115 °F
 - The compressor stalled, drawing approximately 62 Amps at 175 VAC, for as long as 12.5 seconds before thermal protection switch opened to protect the compressor .
 - If the power contactor opened and then reclosed, the unit stalled, drawing approximately 63 Amps at 178 VAC, for as long as 11.5 seconds before the thermal protection opened to protect the compressor.

4.7 *CIRCUIT BREAKER CLEARING* TYPE OF TRANSIENT TEST RESULTS

This compressor has the following threshold voltages 63% at 80 °F, 64% at 100 °F, and 66% at 115 °F when exposed to the *circuit breaker clearing* type of transients. Therefore, the stalling windows are the following: 63% to 50% at 80 °F, 64% to 50% at 100 °F, and 66% to 50% at 115 °F. The thermal protection switch opened after each stall to protect the compressor. The compressor stalled in the stalling window, drawing approximately 94 Amps at 235 VAC, for as long as 2.8 seconds before the thermal protection switch opened to protect the compressor. If the power contactor opened and then reclosed, the compressor stalled, drawing approximately 94 Amps at 235 VAC, for as long as 2.8 seconds before the thermal protection opened to protect the compressor. The following are the detail responses of the compressor for each of the temperatures:

- ◆ At 80 °F
 - The compressor stalled, drawing approximately 95 Amps at 235 VAC, for as long as 2.8 seconds before the thermal protection switch opened to protect the compressor.
 - If the power contactor opened and then reclosed, the compressor stalled, drawing approximately 94 Amps at 235 VAC, for as long as 2.8 seconds before the thermal protection switch opened to protect the compressor.
- ◆ At 100 °F
 - The compressor stalled, drawing approximately 94 Amps at 234 VAC, for as long as 2.8 seconds before the thermal protection switch opened to protect the compressor.
 - If the power contactor opened and then reclosed, the compressor stalled, drawing approximately 94 Amps at 235 VAC, for as long as 2.9 seconds before the thermal protection switch opened to protect the compressor.
- ◆ At 115 °F
 - The compressor stalled, drawing approximately 94 Amps at 235 VAC, for as long as 2.9 seconds before the thermal protection switch opened to protect the compressor.

- If the power contactor opened and then reclosed, the unit stalled, drawing approximately 94 Amps at 235 VAC, for as long as 2.8 seconds before the thermal protection switch opened to protect the compressor.

5.0 A/C #2 - TEST RESULTS

The air conditioner's compressor stalled when the voltage was in the stalling window (between the stall threshold voltage and contactor dropout voltage) when exposed to the *long notch* and *delayed recovery* type of transients. This compressor stalled, drawing approximately 47 Amps at 127 VAC, for as long as 20.2 seconds before the thermal protection switch opened to protect the compressor, when exposed to the *long notch* type of transients. This compressor stalled, drawing approximately 56 Amps at 152 VAC, for as long as 7.7 seconds before the thermal protection switch opened to protect the compressor, when exposed to the *delayed recovery* type of transients. This compressor did not stalled when exposed to the *circuit breaker clearing* type of transients; therefore, this unit is not sensitive to circuit breaker clearing type of transients except when they go below the contactor dropout voltage. Opening the contactor did not help to prevent the compressor from stalling, it just delayed stalling except for the *long notch* type of transient where it did not stall at all. The good thing about this air conditioner unit is that it restarts normally after any stall. The power contactor drop out voltage is 50%.

5.1 SYSTEM SPECIFICATIONS

The tested air conditioner system has the following specifications:

MAIN SYSTEM	
Manufacturer	Carrier
Condenser Unit	38BRG036300
Evaporator Coil	CK3BA036
Size (Tons)	3
Compressor Type	Scroll
Refrigerant	R-22
SEER	12
Condition	New
Unit Cost	\$1,068.00

COMPRESSOR	
Manufacturer	Copeland
Model	ZR34K3-PFV-130
Type	Scroll
FLA (AMPS)	17.6
LRA (AMPS)	88
Phase	1
Refrigerant	R22
Charge (LBS)	6.5
Voltage (V)	230/208
PMAX High (PSI)	398.8
PMAXLow (PSI)	290

FAN MOTOR	
Manufacturer	GE
Model	5KCP39GFSS166S
Voltage (V)	208/230
Current (I)	0.95
Power (HP)	0.2
RPM	825
FLA (AMPS)	1.1

CONTACTOR	
Manufacturer	Product Unlimited
Model	HN51KC024
Rating (V)	240/277
FLA (AMPS)	30
LRA (AMPS)	150
Resistance	40

CAPACITOR	
Manufacturer	Aurora
Model	PRCD 5575
Rating (V)	370
Capacitance (µF)	75

5.2 TEST PARAMETERS

This air conditioner unit has the following testing parameters.

	80°F	100°F	115°F
T_{INLET} (°C)	22.6	23.1	22.9
T_{OUTLET} (°C)	10.9	11.8	12.5
T_{COMP. AMB.} (°C)	27.4	39.2	47.0
T_{CASE} (°C)	78.0	89.9	100.7
T_{GAS} (°C)	-	-	-
T_{LIQ} (°C)	-	-	-
R_{FLOW} (Kcfm)	1.3	1.6	1.4
P_{LOW} (PSI)	54.0	66.3	72.6
P_{HIGH} (PSI)	199.4	261.6	317.5
I_{RUNNING} (A)	12.0	15.0	17.0
W_{RUNNING} (W)	2608.0	3164.0	3884.0
VAR_{RUNNING} (VAR)	823.0	850.0	888.0

A more detail performance parameter table can be found in APPENDIX #2 -- Attachment # 2

5.3 INRUSH TEST RESULTS

This air conditioner unit took approximately 14 cycles to come to normal running state. The data below was recorded for the whole air conditioner system.

Inrush	
V _{INRUSH}	227 VAC
I _{INRUSH}	99 A
W _{INRUSH}	16,000 W
VAR _{INRUSH}	15,700 VAR
t	14 cycles

5.4 POWER CONTACTOR TEST RESULTS

The power contactor opened at 50% voltage sag. In general, opening the contactor did not prevent the compressor from stalling; it just delayed the stalling until the contactor reclosed except when exposed to *long notch* type of transients. The compressor had the following responses right after the contactor reclosed:

- ◆ *Long notch* type of transients
 - The compressor never stalled after the power contactor reclosed.
- ◆ *Delayed Recovery* type of transient
 - The compressor stalled, drawing approximately 61 Amps at 165 VAC, right after the contactor reclosed for as long as 5.5 seconds before the thermal protection switch opened to protect the compressor.

- ◆ *Circuit Breaker Clearing* type of transients
 - The compressor stalled, drawing approximately 90 Amps at 228 VAC, right after the contactor reclosed for as long as 0.3 seconds before resuming the normal running mode.

5.5 30-SECOND LONG NOTCH TYPE OF TRANSIENT TEST RESULTS

This unit has the following threshold voltages 58% at 80 °F, 63% at 100 °F, and 68% at 115 °F when exposed to the *long notch* type of transients. Therefore, the stalling windows are the following: 58% to 50% at 80 °F, 63% to 50% at 100 °F, and 68% to 50% at 115 °F. The thermal protection switch opened after each stall to protect the unit. The unit stalled in the stalling window, drawing approximately 47 Amps at 127 VAC, for as long as 20.2 seconds before the thermal protection switch opened to protect the unit. If the power contactor opened and then reclosed, the compressor would return to the normal running mode. The following are the details for each of the temperatures:

- ◆ At 80 °F
 - The compressor stalled, drawing approximately 47 Amps at 127 VAC, for as long as 20.2 seconds before the thermal protection switch opens to protect the compressor.
 - If the power contactor opened and reclosed, the compressor resumed normal running mode.
- ◆ At 100 °F
 - The compressor stalled, drawing approximately 47 Amps at 127 VAC, for as long as 17.0 seconds before the thermal protection switch opened to protect the compressor.
 - If the power contactor opened and then reclosed, the compressor resumed the normal running mode.
- ◆ At 115 °F
 - The compressor stalled, drawing approximately 47 Amps at 127 VAC, for as long as 14.7 seconds before the thermal protection switch opened to protect the compressor.
 - If the power contactor opened and then reclosed, the compressor resumed the normal running mode.

5.6 DELAYED RECOVERY TYPE OF TRANSIENT TEST RESULTS

This unit has the following threshold voltages 55% at 80 °F, 60% at 100 °F, and 65% at 115 °F when exposed to the *delayed recovery* type of transient. Therefore, the stalling windows are the following: 55% to 50% at 80 °F, 60% to 50% at 100 °F, and 65% to 50% at 115 °F. The thermal protection switch opened after each stall to protect the unit. The compressor stalled in the stalling window, drawing approximately 56 Amps at 152 VAC, for as long as 7.7 seconds before the thermal protection switch opened to protect the compressor. If the power contactor opened and then reclosed, the compressor stalled, drawing approximately 61 Amps at 165 VAC, for as long as 5.5 seconds before the thermal protection switch opened to protect it. The following are the details for each of the temperatures:

- ◆ At 80 °F
 - The compressor stalled, drawing approximately 55 Amps at 148 VAC, for as long as 6.9 seconds before the thermal protection switch opened to protect the compressor.
 - If the power contactor opened and then reclosed, the compressor stalled, drawing approximately 59 Amps at 160 VAC, for as long as 5.2 seconds before the thermal protection opened to protect the compressor.

- ◆ At 100 °F
 - The compressor stalled, drawing approximately 56 Amps at 152 VAC, for as long as 7.7 seconds before the thermal protection switch opened to protect the compressor.
 - If the power contactor opened and then reclosed, the compressor stalled, drawing approximately 60 Amps at 161 VAC, for as long as 5.4 seconds before the thermal protection switch opened to protect the compressor.
- ◆ At 115 °F
 - The compressor stalled, drawing approximately 56 Amps at 154 VAC, for as long as 7.6 seconds before the thermal protection switch opened to protect the compressor.
 - If the power contactor opened and then reclosed, the compressor stalled, drawing approximately 61 Amps at 165 VAC, for as long as 5.5 seconds before the thermal protection switch opened to protect the compressor.

5.7 *CIRCUIT BREAKER CLEARING* TYPE OF TRANSIENT TEST RESULTS

This unit did not stall when exposed to the *Circuit Breaker Clearing* type of transients except when the contactor opened. Then it stalled when the contactor reclosed, drawing approximately 90 Amps at 228 VAC,

6.0 A/C #3 - TEST RESULTS

The air conditioner's compressor stalled when the voltage was in the stalling window (between the stall threshold voltage and contactor dropout voltage) when exposed to any of the three test transients. This compressor stalled, drawing approximately 57 Amps at 138 VAC, for as long as 13.5 seconds before the thermal protection switch opened to protect the compressor, when exposed to the *long notch* type of transients in the stalling window. It stalled, drawing approximately 62 Amps at 156 VAC, for as long as 14.2 seconds before the thermal protection switch opened to protect the compressor, when exposed to the *delayed recovery* type of transients. It stalled, drawing approximately 101 Amps at 227 VAC, for as long as 0.5 seconds then unit restart normally or went into NO-LOAD condition, when exposed to *circuit breaker clearing* type of transients. Opening the contactor did not help to prevent the compressor from stalling, it just delayed it. If the power contactor opened and then reclosed, the compressor stalled for as long as 12.7 seconds before the thermal protection switch opened to protect it except when exposed to the *long notch* type of transients where it returned to normal running mode. If the unit did not restart normally or went into the NO-LOAD condition, then the compressor needed to be turned off and then on again in order to restart normally. At the NO-LOAD condition, the compressor consumed ½ of the normal running power but without producing any cooling. At high temperatures, the compressor is sensitive to the *circuit breaker clearing* type of transients where most of the tests end up in the NO-LOAD condition. The power contactor drop out voltage is 35%.

6.1 SYSTEM SPECIFICATIONS

The tested air conditioner system has the following specifications:

MAIN SYSTEM	
Manufacturer	Rheem
Condenser Unit	RAKB036-JAZ
Evaporator Coil	CK3BA036
Size (Tons)	3
Compressor Type	Scroll
Refrigerant	R-22
SEER	10
Condition	New
Unit Cost	\$925.00

COMPRESSOR	
Manufacturer	Copeland
Model	ZR36X3-PFV-230
Type	Scroll
FLA (AMPS)	19
LRA (AMPS)	95
Phase	1
Refrigerant	R22
Charge (LBS)	4.9
Voltage (V)	230/208
PMAX High (PSI)	398.8
PMAXLow (PSI)	290

FAN MOTOR	
Manufacturer	Emerson
Model	K55HXKYH-9836
Voltage (V)	208/230
Current (I)	1.3
Power (HP)	0.2
RPM	1075
FLA (AMPS)	1.3

CONTACTOR	
Manufacturer	Cutler-Hammer
Model	C25CNY3T
Rating (V)	240/277
FLA (AMPS)	25
LRA (AMPS)	150
Resistance	30

CAPACITOR	
Manufacturer	Digital Tech
Model	43-101665-14
Rating (V)	370
Capacitance (µF)	50

6.2 TEST PARAMETERS

This air conditioner unit has the following testing parameters.

	80°F	100°F	115°F
T_{INLET} (°C)	22.5	23.7	24.7
T_{OUTLET} (°C)	9.1	11.0	12.9
T_{COMP. AMB.} (°C)	26.3	38.5	46.7
T_{CASE} (°C)	67.4	82.2	92.5
T_{GAS} (°C)	-	-	-
T_{LIQ} (°C)	-	-	-
R_{FLOW} (Kcfm)	1.4	1.3	1.3
P_{LOW} (PSI)	62.8	68.1	359.6
P_{HIGH} (PSI)	224.6	300.2	73.7
I_{RUNNING} (A)	14.0	17.0	20.0
W_{RUNNING} (W)	3152.0	3911.0	4583.0
VAR_{RUNNING} (VAR)	1200.0	1250.0	1348.0

A more detail internal performance parameter table can be found in APPENDIX #2 -- Attachment # 3.

6.3 INRUSH TEST RESULTS

This air conditioner unit took approximately 13 cycles to come to the normal steady running state. The data below was recorded for the whole air conditioner system.

Inrush	
V _{INRUSH}	226 VAC
I _{INRUSH}	106 A
W _{INRUSH}	17,200 W
VAR _{INRUSH}	16,800 VAR
t	13 cycles

6.4 POWER CONTACTOR TEST RESULTS

The power contactor opened with a 35% voltage sag. The compressor, at times, goes into a NO-LOAD condition. The compressor had the following responses right after the contactor reclosed:

- ◆ *Long notch* type of transient
 - The compressor never stalled after the power contactor reclosed.
- ◆ *Delayed Recovery* type of transient
 - The compressor stalled, drawing approximately 62 Amps at 154 VAC, for as long as 13 seconds before the thermal protection switch opened to protect the compressor.
- ◆ *Circuit Breaker Clearing* type of transient

- At times the compressor stalled, drawing approximately 102 Amps at 226 VAC, for less than 0.4 seconds right after the power contactor reclosed then return to the normal running mode.
- At times the compressor stalled, drawing approximately 101 Amps at 227 VAC, for less than 0.4 seconds right after the power contactor reclosed then went into a NO-LOAD condition.
- At times the compressor stalled, drawing approximately 102 Amps at 226 VAC, for less than 1 second right after the power contactor reclosed causing the thermal protection switch to open to protect the compressor. The compressor did not go into a NO-LOAD condition.
- At times the compressor returned to the normal running mode after the contactor reclosed.

6.5 30-SECOND LONG NOTCH TYPE OF TRANSIENT TEST RESULTS

This unit has the following threshold voltages 60% at 80 °F, 65% at 100 °F, and 70% at 115 °F when exposed to the *long notch* type of transients. Therefore, the stalling windows are the following: 60% to 35% at 80 °F, 65% to 35% at 100 °F, and 70% to 35% at 115 °F. The thermal protection switch opened to protect the compressor. The compressor did not always restarted normally after the thermal protection switch reclosed and at times it went into the NO-LOAD condition. The compressor needed to be turned off and then on again in order to restart normally. The unit stalled in the stalling window, drawing approximately 57 Amps at 138 VAC, for as long as 13.5 seconds before the thermal protection switch opened to protect the compressor. Sometimes the compressor stalled, drawing approximately 46 Amps at 114 VAC, for the complete transient period without opening the thermal protection switch. If the power contactor opened and then reclosed, the compressor returned to the normal running mode. The following are the details for each of the temperatures:

- ◆ At 80 °F
 - At times the compressor stalled, drawing approximately 57 Amps at 138 VAC, for as long as 13.5 seconds before the thermal protection switch opened to protect the compressor.
 - At times the compressor stalled, drawing approximately 61 Amps at 126 VAC through the complete transient period and then the thermal protection switch opened when the voltage returned to normal at the end of the transient. The unit did not restart normally.
 - At times it stalled, drawing approximately 46 Amps at 114 VAC, for the complete transient period and then returned to the normal running mode.
 - If the power contactor opened and then reclosed, the compressor returned to the normal running mode.
- ◆ At 100 °F
 - At times the compressor stalled, drawing approximately 57 Amps at 138 VAC, for as long as 13.1 seconds before the thermal protection switch opened to protect the compressor.
 - At times, the compressor stalled, drawing approximately 51 Amps at 125 VAC, for as long as 1.1 seconds and then went into the NO-LOAD condition.
 - At times the compressor stalled, drawing approximately 46 Amps at 115 VAC through the complete transient period and the returned to the normal running mode.
 - If the power contactor opened and then reclosed, the compressor returned to the normal running mode.
- ◆ At 115 °F
 - At times the compressor stalled, drawing approximately 61 Amps at 149 VAC, for as long as 6.5 seconds before the thermal protection switch opened. When the thermal switch reclosed the unit stalled for a second time for as long as 4.6 seconds before the thermal protection switch opened again to protect the compressor.

- At times the compressor stalled, drawing approximately 45 Amps at 114 VAC, for the transient period and then returned to the normal running mode.
- If the power contactor opened and then reclosed, the unit returned to the normal running mode.

6.6 *DELAYED RECOVERY* TYPE OF TRANSIENT TEST RESULTS

This compressor has the following threshold voltages 55% at 80 °F, 60% at 100 °F, and 65% at 115 °F when exposed to the *delayed recovery* type of transient. Therefore, the stalling windows are the following: 55% to 35% at 80 °F, 60% to 35% at 100 °F, and 65% to 35% at 115 °F. The thermal protection switch opened after each stall to protect the compressor. The compressor stalled in the stalling window, drawing approximately 62 Amps at 156 VAC, for as long as 14.2 seconds before the thermal protection switch opened to protect the compressor. If the power contactor opened and then reclosed, the compressor stalled, drawing approximately 63 Amps at 157 VAC, for as long as 9.1 seconds before the thermal protection switch opened to protect the compressor. Opening the contactor did not help in preventing the compressor from stalling, it just delayed it. In general, the unit restarted normally after any stalling except in one case where it went into the NO-LOAD condition. The following are the details for each of the temperatures:

- ◆ At 80 °F
 - The compressor stalled, drawing approximately 62 Amps at 156 VAC, for as long as 14.2 seconds before the thermal protection switch opened to protect the compressor.
 - If the power contactor opened and then reclosed, the compressor stalled, drawing approximately 63 Amps at 157 VAC, for as long as 9.1 seconds before the thermal protection switch opened to protect the compressor.
- ◆ At 100 °F
 - The compressor stalled, drawing approximately 61 Amps at 153 VAC, for as long as 12.2 seconds before the thermal protection switch opened to protect the compressor.
 - In one test, the compressor stalled, drawing approximately 57 Amps at 137 VAC, for as long as 0.8 seconds before the thermal protection switch opened. When the thermal protection switch closed, the unit went into NO-LOAD condition.
- ◆ At 115 °F
 - The compressor stalled, drawing approximately 60 Amps at 154 VAC, for as long as 12.9 seconds before the thermal protection switch opened to protect the compressor.
 - If the power contactor opened and then reclosed, the compressor stalled, drawing approximately 63 Amps at 159 VAC, for as long as 8.8 seconds before the thermal protection opened to protect the compressor.

6.7 *CIRCUIT BREAKER CLEARING* TYPE OF TRANSIENT TEST RESULTS

This unit had the following threshold voltages 50% at 80 °F, 60% at 100 °F, and 65% at 115 °F when exposed to the *circuit breaker clearing* type of transients. Therefore, the stalling windows are the following: 50% to 35% at 80 °F, 60% to 35% at 100 °F, and 65% to 35% at 115 °F. The thermal protection switch rarely opened after stalling to protect the compressor. The unit stalled in the stalling window, drawing approximately 101 Amps at 227 VAC, for as long as 0.5 seconds before return to the normal running state or the NO-LOAD condition. If the power contactor opened and then reclosed the compressor stalled, drawing approximately 102 Amps at 227 VAC, long as 0.5 seconds. Then it either resumed the normal running state or went into the NO-LOAD

condition. Opening the contactor did not prevent the compressor from stalling, it just delayed it. The following are the details for each of the temperatures:

- ◆ At 80 °F
 - The compressor stalled, drawing approximately 101 Amps at 227 VAC, for as long as 0.5 seconds before it returned to the normal running mode.
 - If the power contactor opened and then reclosed, the compressor stalled, drawing approximately 102 Amps at 227 VAC, for as long as 0.5 seconds. Then it either the thermal protection switch opened or it went into the NO-LOAD condition. In both cases, the compressor did not restart normally.
- ◆ At 100 °F
 - At times the compressor stalled, drawing approximately 102 Amps at 226 VAC, for as long as 0.5 seconds before it returned to the normal running state.
 - At times the compressor stalled, drawing approximately 103 Amps at 227 VAC, for as long as 0.4 seconds before it went into the NO-LOAD condition.
 - If the power contactor opens and then recloses, the unit stalled for as long as 0.3 seconds , drawing approximately 101 Amps at 226 VAC. It then went into the NO-LOAD condition.
- ◆ At 115 °F
 - Usually the compressor stalled, drawing approximately 102 Amps at 226 VAC, for as long as 0.5 seconds and then went into the NO-LOAD condition.
 - At times the unit stalled, drawing approximately 102 Amps at 226 VAC, for as long as 0.5 seconds before it returned to the normal running mode.
 - If the power contactor opened and then reclosed, the compressor stalled for as long as 0.4 seconds, drawing approximately 103 Amps at 227 VAC. Then either the unit returned to the normal running state or it went into the NO-LOAD condition.

7.0 A/C #4 - TEST RESULTS

The air conditioner's compressor stalled when the voltage was in the stalling window (between the stall threshold voltage and contactor dropout voltage) when exposed to any of the three test transients. When exposed to the *long notch* type of transients in the stalling window, this compressor stalled, drawing approximately 44 Amps at 140 VAC, for as long as 28.2 seconds before the thermal protection switch opened to protect the compressor but sometimes it stalled for the complete 30 second transient period without opening the thermal protection switch. At times, the compressor stalled for a short period of time (1.0 second) then went into the NO-LOAD condition. The compressor stalled, drawing approximately 60 Amps at 195 VAC, for as long as 19.6 seconds before the thermal protection switch opened to protect the compressor, when exposed to the *delayed recovery* type of transient. It stalled, drawing approximately 82 Amps at 229 VAC, for as long as 0.5 seconds then the compressor either returned to normal running mode or went into the NO-LOAD condition, when exposed to the *circuit breaker clearing* type of transients. In general, opening the contactor did not prevent the compressor from stalling; it just delayed it except when exposed to the *long notch* transient where it resumed normal running mode. If the power contactor opened and then reclosed, the compressor stalled for as long as 21.0 seconds before the thermal protection switch opened to protect it except when exposed to the *long notch* type of transients where it resumed the normal running mode. When the contactor opened under the *circuit breaker clearing* type of transients, the compressor stalled for as long as 0.5 second then usually went into the NO-LOAD condition. If the unit did not restart normally or went into the NO-LOAD condition, then the compressor needed to be turned off and then on again in order to restart normally. The compressor in the NO-LOAD condition consumed $\frac{1}{2}$ of the normal running power but without producing any work (cooling). At high temperatures, the compressor is more sensitive to the *circuit breaker clearing* type of transients where most of the tests end up in the NO-LOAD condition. The power contactor drop out voltage is 55%.

7.1 SYSTEM SPECIFICATIONS

The tested air conditioner system has the following specifications:

MAIN SYSTEM	
Manufacturer	Carrier
Condenser Unit	38TXA036-30
Evaporator Coil	CK3BA036
Size (Tons)	3
Compressor Type	Scroll
Refrigerant	R-410A
SEER	13
Condition	New
Unit Cost	\$1,687.00

COMPRESSOR	
Manufacturer	Copeland
Model	ZP31K5-PFV-130
Type	Scroll
FLA (AMPS)	16.7
LRA (AMPS)	79
Phase	1
Refrigerant	R410A
Charge (LBS)	6.88
Voltage (V)	230/208
P _{MAX} High (PSI)	623.7
P _{MAX} Low (PSI)	406.1

FAN MOTOR	
Manufacturer	GE
Model	5KCP39GF
Voltage (V)	208/230
Current (I)	0.95
Power (HP)	0.2
RPM	825
FLA (AMPS)	1.1

CONTACTOR	
Manufacturer	Product Unlimited
Model	HN51KC024
Rating (V)	240/277
FLA (AMPS)	30
LRA (AMPS)	160
Resistance	40

CAPACITOR	
Manufacturer	GE
Model	97F9969
Rating (V)	370
Capacitance (µF)	45

7.2 TEST PARAMETERS

This air conditioner unit has the following testing parameters.

	80°F	100°F	115°F
T _{INLET} (°C)	22.4	22.9	22.9
T _{OUTLET} (°C)	10.8	10.9	12.1
T _{COMP. AMB.} (°C)	27.8	39.0	47.8
T _{CASE} (°C)	89.5	94.8	108.7
T _{GAS} (°C)	-	-	-
T _{LIQ} (°C)	-	-	-
R _{FLOW} (Kcfm)	1.6	1.2	1.2
P _{LOW} (PSI)	106.9	117.8	127.1
P _{HIGH} (PSI)	351.9	471.5	579.4
I _{RUNNING} (A)	12.0	15.0	18.0
W _{RUNNING} (W)	2763.0	3507.0	4272.0
VAR _{RUNNING} (VAR)	647.0	700.0	846.0

A more detail internal performance parameter table can be found in APPENDIX #2 -- Attachment # 4.

7.3 INRUSH TEST RESULTS

It would take approximately 14 cycles to come to the normal steady running state. The data below was recorded for the whole air conditioner system.

Inrush	
V_{INRUSH}	228 VAC
I_{INRUSH}	84 A
W_{INRUSH}	14,400 W
VAR_{INRUSH}	13,100 VAR
t	14 cycles

7.4 POWER CONTACTOR TEST RESULTS

The power contactor opened with a 50% voltage sag. In one instance, the unit did not restart normally and needed to be turned off and then on again in order to return to the normal running mode. The compressor had the following responses right after contactor reclosed:

- ◆ *Long notch* type of transient
 - Never stalled after power contactor reclosed.
- ◆ *Delayed Recovery* type of transient
 - The compressor stalled, drawing approximately 62 Amps at 202 VAC, right after contactor reclosed for as long as 15.9 seconds before the thermal protection switch opened to protect the compressor.
 - Restarted normally after thermal protection switch reclosed except for one case where it did not restart normally and needed to be turned off and then on again in order to return to the normal running state.
- ◆ *Circuit Breaker Clearing* type of transient
 - At 80 °F
 - The compressor stalled, drawing approximately 84 Amps at 229 VAC, right after the contactor reclosed for as long as 1.4 seconds before it returned to the normal running mode.
 - At 100 °F
 - At times the compressor stalled, drawing approximately 85 Amps at 229 VAC right after the contactor reclosed for as long as 0.4 seconds before it went into the NO-LOAD condition.
 - At times the compressor returned to the normal running mode.
 - At 115 °F
 - At times the compressor stalled, drawing approximately 83 Amps at 229 VAC right after the contactor reclosed for as long as 0.4 seconds before it went into the NO-LOAD condition.
 - At times the compressor returned to the normal running mode.

7.5 30-SECOND LONG NOTCH TYPE OF TRANSIENT TEST RESULTS

This compressor has the following threshold voltages 62% at 80 °F, 68% at 100 °F, and 75% at 115 °F when exposed to the *long notch* type of transients. Therefore, the stalling windows are the following: 62% to 50% at 80 °F, 68% to 50% at 100 °F, and 75% to 50% at 115 °F. The thermal

protection switch opens to protect the compressor. The unit stalled in the stalling window, drawing approximately 44 Amps at 140 VAC, for as long as 28.2 seconds before the thermal protection switch opened to protect the compressor. At times, it also stalled for as long as 0.9 seconds before it went into the NO-LOAD condition. In this condition, the compressor will never restart normally, it will always consume ½ the normal running power but without producing any work (no cooling). If the power contactor opened and then reclosed the compressor did not return to the normal running state. The compressor needed to be turned off and then on again in order to restart normally. The following are the details for each of the temperatures:

- ◆ At 80 °F
 - At times the compressor stalled, drawing approximately 42 Amps at 128 VAC, for the complete transient period and then returned to the normal running state.
 - At times the compressor stalled, drawing approximately 44 Amps at 140 VAC, for as long as 28.2 seconds before the thermal protection switch opened to protect the compressor. The compressor did not restart normally.
 - If the power contactor opened and then reclosed, the compressor returned to normal running mode.
- ◆ At 100 °F
 - At times the compressor stalled, drawing approximately 51 Amps at 159 VAC, for as long as 0.9 seconds then went into the NO-LOAD condition.
 - At times the compressor stalled, drawing approximately 51 Amps at 151 VAC, for as long as 23.8 seconds before the thermal protection switch opened to protect the compressor.
 - At times the compressor stalled, drawing approximately 41 Amps at 126 VAC, for the complete transient period without opening the thermal protection switch.
 - If the power contactor opened and then reclosed, the compressor returned to normal running mode.
- ◆ At 115 °F
 - At times the compressor stalled, drawing approximately 56 Amps at 174 VAC, for as long as 1.0 second and then went into the NO-LOAD condition.
 - At times the compressor stalled, drawing approximately 49 Amps at 151 VAC, for as long as 16.5 seconds before the thermal protection switch opened to protect the compressor.
 - At times the compressor stalled, drawing approximately 40 Amps at 128 VAC, for the complete transient period without opening the thermal protection switch.
 - If the power contactor opened and then reclosed the unit returned to the normal running state.

7.6 DELAYED RECOVERY TYPE OF TRANSIENT TEST RESULTS

This compressor had the following threshold voltages 60% at 80 °F, 65% at 100 °F, and 75% at 115 °F when exposed to the *delayed recovery* type of transient. Therefore, the stalling windows are the following: 60% to 50% at 80 °F, 65% to 50% at 100 °F, and 75% to 50% at 115 °F. The thermal protection switch opened after each stall to protect the compressor. The unit stalled in the stalling window, drawing approximately 60 Amps at 195 VAC, for as long as 19.6 seconds before the thermal protection switch opened to protect the compressor. At high temperatures, this compressor at times did not restarted normally after the thermal protection switch reclosed. It needed to be turned off and then on again in order to restart normally. If the power contactor opened and then reclosed, the compressor stalled, drawing approximately 62 Amps at 200 VAC, for as long as 15.9 seconds before the thermal protection switch opened to protect the compressor. The following are the details for each of the temperatures:

- ◆ At 80 °F
 - The compressor stalled, drawing approximately 58 Amps at 186 VAC, for as long as 16.8 seconds before the thermal protection switch opened to protect the compressor.
 - If the power contactor opened and then reclosed, the compressor stalled, drawing approximately 58 Amps at 185 VAC, for as long as 13.2 seconds before the thermal protection switch opened to protect the compressor. The compressor did not restart normally.
- ◆ At 100 °F
 - The compressor stalled, drawing approximately 60 Amps at 195 VAC, for as long as 19.6 seconds before the thermal protection switch opened to protect the compressor.
 - If the power contactor opened and then reclosed, the compressor stalled, drawing approximately 61 Amps at 194 VAC, for as long as 13.4 seconds before the thermal protection switch opened to protect the compressor.
- ◆ At 115 °F
 - At times the compressor stalled, drawing approximately 59 Amps at 193 VAC, for as long as 18.4 seconds before the thermal protection switch opened to protect the compressor.
 - At times the compressor stalled, drawing approximately 60 Amps at 191 VAC, for as long as 16.9 seconds before the thermal protection switch opened to protect the compressor. The compressor did not restart normally.
 - If the power contactor opened and then reclosed, the compressor stalled, drawing approximately 62 Amps at 200 VAC, for as long as 15.9 seconds before the thermal protection switch opened to protect the compressor.

7.7 *CIRCUIT BREAKER CLEARING* TYPE OF TRANSIENT TEST RESULTS

This compressor had the following threshold voltages 55% at 80 °F, 65% at 100 °F, and 70% at 115 °F when exposed to the *Circuit Breaker Clearing* type of transients. Therefore, the stalling windows are the following: 55% to 50% at 80 °F, 60% to 50% at 100 °F, and 70% to 50% at 115 °F. At times the thermal protection switch opened after stalling to protect the compressor. The unit stalled in the stalling window, drawing approximately 82 Amps at 229 VAC, for as long as 0.5 seconds before it either returned to the normal running state or it went into the NO-LOAD condition. If the power contactor opened and then reclosed, the compressor stalled for as long as 1.4 seconds drawing approximately 84 Amps at 229 VAC then either resumed the normal running state or went into the NO-LOAD condition. The following are the details for each of the temperatures:

- ◆ At 80 °F
 - The compressor did not stall in the 3 and 6 cycle tests.
 - At times the compressor stalled, drawing approximately 82 Amps at 229 VAC, for as long as 0.5 seconds before it returned to the normal running mode.
 - At times the compressor stalled, drawing approximately 82 Amps at 229 VAC, for as long as 0.3 seconds before the thermal protection switch opened to protect the compressor. The compressor did not restart normally.
 - If the power contactor opened and then reclosed, the compressor stalled, drawing approximately 84 Amps at 229 VAC, for as long as 1.4 seconds before it returned to the normal running state.
- ◆ At 100 °F

- The compressor stalled, drawing approximately 84 Amps at 229 VAC, for as long as 0.4 seconds and then went into the NO-LOAD condition.
- If the power contactor opened and then reclosed, the compressor stalled, drawing approximately 85 Amps at 229 VAC, for as long as 0.3 seconds. At times it went into the NO-LOAD condition but at other times it returned to the normal running mode.
- ◆ At 115 °F
 - Usually the compressor stalled, drawing approximately 80 Amps at 229 VAC, for as long as 0.4 seconds and then went into the NO-LOAD condition.
 - At times the compressor stalled, drawing approximately 81 Amps at 229 VAC, for as long as 0.5 seconds before it returned to the normal running state
 - If the power contactor opened and then reclosed, the compressor stalled, drawing approximately 83 Amps at 229 VAC, for as long as 0.4 seconds before it returned to the normal running mode.

8.0 A/C #5 - TEST RESULTS

The air conditioner's compressor stalled when the voltage was in the stalling window (between the stall threshold voltage and contactor dropout voltage) when exposed to any of the three types of transients. When exposed to the *long notch* type of transients in the stalling window, this compressor stalled, drawing approximately 81 Amps at 135 VAC, for as long as 26.0 seconds before the thermal protection switch opened to protect the compressor for as long as 30.0 seconds (drawing approximately 73 Amps at 124 VAC) before resuming the normal running mode. The compressor did not restart normally after the thermal protection switch opened and needed to be turned off and then on again in order to resume the normal running mode. The compressor stalled, drawing approximately 99 Amps at 172 VAC, for as long as 15.9 seconds before returning to the normal running mode, when exposed to the *delayed recovery* type of transients in the stalling window. The compressor stalled, drawing approximately 87 Amps at 145 VAC, for the complete 30 second transient time before going into the IDLE condition, when exposed to the *circuit breaker clearing* type of transients in the stalling window. When the contactor opened under the *delayed recovery* type of transients and then reclosed, the compressor stalled, drawing approximately 115 Amps at 193 VAC, for as long as 8.1 seconds before returning to the normal running mode. In general, opening the contactor did not help prevent the compressor from stalling; it just delayed the stall. If the unit did not restart normally or went into the IDLE condition, then the compressor needed to be turned off and then on again in order to return to the normal running mode. The compressor in the IDLE condition consumed the same power as with normal running but without producing any work (cooling). The compressor was more prone to go into the IDLE condition when it stalled during the *circuit breaker clearing* type of transients.

8.1 SYSTEM SPECIFICATIONS

The tested air conditioner system has the following specifications:

MAIN SYSTEM		FAN MOTOR	
Manufacturer	Coleman	Manufacturer	Motor Division
Condenser Unit	AC3B048F1A	Model	K55HXKWQ-9803
Evaporator Coil	CK3BA048	Voltage (V)	208/230
Size (Tons)	4	Current (I)	1.5
Compressor Type	Scroll	Power (HP)	0.25
Refrigerant	R-410A	RPM	850
SEER	13	FLA (AMPS)	1.5
Condition	New		
Unit Cost	\$1,630.00		
COMPRESSOR		CONTACTOR	
Manufacturer	Benchmark	Manufacturer	GE
Model	H83R413ABCA	Model	CR453CE3HBLAY
Type	Scroll	Rating (V)	240/277
FLA (AMPS)	21.1	FLA (AMPS)	40
LRA (AMPS)	150	LRA (AMPS)	180
Phase	1	Resistance	50
Refrigerant	R410A	CAPACITOR	
Charge (LBS)	8.75	Manufacturer	CSC
Voltage (V)	230/208	Model	328P7005H37P37A5X
P _{MAX} High (PSI)	-	Rating (V)	370
P _{MAX} Low (PSI)	-	Capacitance (µF)	70

8.2 TEST PARAMETERS

This air conditioner unit has the following testing parameters.

	80°F	100°F	115°F
T _{INLET} (°C)	22.0	23.2	23.2
T _{OUTLET} (°C)	9.4	11.2	12.2
T _{COMP. AMB.} (°C)	26.7	38.1	46.2
T _{CASE} (°C)	71.8	88.9	107.1
T _{GAS} (°C)	-	-	-
T _{LIQ} (°C)	-	-	-
R _{FLOW} (Kcfm)	1.7	1.5	1.5
P _{LOW} (PSI)	105.9	116.5	123.9
P _{HIGH} (PSI)	353.5	474.7	693.6
I _{RUNNING} (A)	17.0	22.0	26.0
W _{RUNNING} (W)	4030.0	5047.0	6106.0
VAR _{RUNNING} (VAR)	1100.0	1225.0	1443.0

A more detail internal performance parameter table can be found in APPENDIX #2 -- Attachment # 5.

8.3 INRUSH TEST RESULTS\

It would take approximately 13 cycles to come to the normal steady running state. The data below was recorded for the whole air conditioner system.

Inrush	
V_{INRUSH}	221 VAC
I_{INRUSH}	148 A
W_{INRUSH}	22,000 W
VAR_{INRUSH}	24,200 VAR
t	13 cycles

8.4 POWER CONTACTOR TEST RESULTS

The power contactor opened at 50% voltage sag. The compressor had the following responses right after contactor reclosed:

- ◆ *Long notch* type of transient
 - At 80 °F and 100 °F, the compressor restarted normally after the contactor reclosed.
 - At 115 °F, the compressor stalled, drawing approximately 146 Amps at 223 VAC, for as long as 2 seconds after the contacts reclosed before returned to the normal running state.
- ◆ *Delayed Recovery* type of transient
 - The compressor stalled, drawing approximately 116 Amps at 193 VAC, right after the contactor reclosed for as long as 8.1 seconds before it returned to the normal running condition.
- ◆ *Circuit Breaker Clearing* type of transient
 - At 80 °F
 - At times the compressor went into the IDLE condition.
 - At times the compressor returned to the normal running mode.
 - At 100 °F
 - At times the compressor stalled, drawing approximately 141 Amps at 221 VAC, for 2.0 seconds right after the power contactor reclosed before the thermal protection switch open to protect the compressor.
 - At times the compressor returned to the normal running mode.
 - At 115 °F
 - The compressor stalled for a couple of cycles right after the power contactor reclosed and then went into the IDLE condition.

8.5 30-SECOND LONG NOTCH TYPE OF TRANSIENT TEST RESULTS

This compressor had the following threshold voltages 58% at 80 °F, 63% at 100 °F, and 70% at 115 °F when exposed to the *long notch* type of transients. Therefore, the stalling windows are the following: 58% to 50% at 80 °F, 63% to 50% at 100 °F, and 70% to 50% at 115 °F. The thermal protection switch opened to protect the compressor but not always after the unit stalled. The compressor did not always restart normally after the thermal protection switch reclosed and needed to be turned off and then on again in order to restart normally. The compressor stalled in the stalling window, drawing approximately 81 Amps at 135 VAC, for as long as 26.0 seconds before the thermal protection switch opened to protect the compressor and at times stalled for the

complete transient period (30 seconds drawing approximately 73 Amps at 124 VAC) without opening the thermal protection switch. If the power contactor opened and then reclosed, the compressor returned to the normal running mode. The following are the details for each of the temperatures:

- ◆ At 80 °F
 - At times the compressor stalled, drawing approximately 143 Amps at 224 VAC, for as long as 6.6 seconds before the thermal protection switch opened to protect the compressor.
 - At times the compressor stalled, drawing approximately 73 Amps at 124 VAC, for the complete transient period without opening the thermal protection switch.
 - If the power contactor opened and then reclosed, the unit returned to normal running mode.
- ◆ At 100 °F
 - At times the compressor stalled, drawing approximately 81 Amps at 135 VAC, for as long as 26.0 seconds before the thermal protection switch opened to protect the compressor. The unit did not restart normally.
 - At times the compressor stalled, drawing approximately 74 Amps at 124 VAC, for the complete transient period without opening the thermal protection switch.
 - If the power contactor opened and then reclosed, the compressor returned to the normal running mode.
- ◆ At 115 °F
 - At times the compressor stalled, drawing approximately 78 Amps at 135 VAC, for as long as 19.6 seconds before the thermal protection switch opened to protect the compressor. The unit did not restart normally.
 - At times the compressor stalled, drawing approximately 75 Amps at 123 VAC, for the complete transient period without opening the thermal protection switch.
 - If the power contactor opened and then reclosed, the unit returned to the normal running mode.

8.6 DELAYED RECOVERY TYPE OF TRANSIENT TEST RESULTS

This compressor had the following threshold voltages 55% at 80 °F, 60% at 100 °F, and 65% at 115 °F when exposed to the *delayed recovery* type of transient. Therefore, the stalling windows are the following: 55% to 50% at 80 °F, 60% to 50% at 100 °F, and 65% to 50% at 115 °F. The thermal protection switch opened to protect the compressor after stalling except when the compressor stalled right after the contactor reclosed. The compressor stalled in the stalling window, drawing approximately 99 Amps at 172 VAC, for as long as 15.9 seconds before the thermal protection switch opened to protect the compressor. If the power contactor opened and then reclosed, the compressor stalled, drawing approximately 115 Amps at 193 VAC, for as long as 8.1 seconds before returned to normal running mode. Opening the contactor did not help in preventing the compressor from stalling, it just delayed it until the contactor reclosed. The following are the details for each of the temperatures:

- ◆ At 80 °F
 - The compressor stalled, drawing approximately 101 Amps at 172 VAC, for as long as 14.6 seconds before the thermal protection switch opened to protect the compressor.
 - If the power contactor opened and then reclosed, The compressor stalled, drawing approximately 108 Amps at 180 VAC, for as long as 6.8 seconds before it returned to the normal running mode.
- ◆ At 100 °F

- The compressor stalled, drawing approximately 101 Amps at 174 VAC, for as long as 15.1 seconds before the thermal protection switch opened to protect the unit.
- If the power contactor opened and then reclosed, the compressor stalled, drawing approximately 108 Amps at 180 VAC, for as long as 6.8 seconds before it returned to the normal running mode.
- ◆ At 115 °F
 - The compressor stalled, drawing approximately 99 Amps at 172 VAC, for as long as 15.9 seconds before the thermal protection switch opened to protect the unit.
 - If the power contactor opened and then reclosed, the compressor stalled for as long as 8.1 seconds, drawing approximately 115 Amps at 193 VAC, before it returned to the normal running mode.

8.7 *CIRCUIT BREAKER CLEARING* TYPE OF TRANSIENT TEST RESULTS

This compressor had the following threshold voltages at 80 °F, 60% at 100 °F, and 65% at 115 °F when exposed to the *Circuit Breaker Clearing* type of transients. Therefore, the stalling windows are the following: 60% to 50% at 100 °F, and 65% to 50% at 115 °F. The thermal protection switch never opened after stalling to protect the compressor. The compressor stalled in the stalling window, drawing approximately 87 Amps at 145 VAC, for the complete transient time then went into the IDLE condition, except at 80 °F where it did not stall. If the power contactor opened and then reclosed, the compressor usually went into the IDLE condition and at times returned to the normal running state. The following are the details for each of the temperatures:

- ◆ At 80 °F
 - The compressor did not stall in the stalling window.
 - If the power contactor opened and then reclosed, the compressor at times went into the IDLE condition and at other times resumed the normal running state.
- ◆ At 100 °F
 - The compressor stalled, drawing approximately 80 Amps at 134 VAC, for the complete transient period then the compressor went into the IDLE condition.
 - If the power contactor opened and then reclosed, the compressor usually stalled, drawing approximately 147 Amps at 221 VAC, for as long as 2 seconds before going into the IDLE condition.
- ◆ At 115 °F
 - The compressor stalled, drawing approximately 87 Amps at 145 VAC, for the complete transient period then the compressor went into the IDLE condition.
 - If the power contactor opened and then reclosed, the compressor went into the IDLE condition.

9.0 A/C #6 - TEST RESULTS

The air conditioner's compressor stalled when the voltage was in the stalling window (between the stall threshold voltage and contactor dropout voltage) when exposed to any of the three types of transients. When exposed to the *long notch* type of transients in the stalling window, this compressor stalled, drawing approximately 64 Amps at 124 VAC, for as long as 30.0 seconds before either the thermal protection switch opened to protect the compressor or it resumed the normal running mode. At times, the compressor stalled, drawing approximately 64 Amps at 123 VAC, for short period of time (1.0 second) and then went into the NO-LOAD condition. The compressor stalled, drawing approximately 80 Amps at 166 VAC, for as long as 14.8 seconds before the thermal protection switch opened to protect the compressor, when exposed to the *delayed recovery* type of transients in the stalling window. At times, the compressor stalled, drawing approximately 50 Amps at 103 VAC, for a short period of time (1.0 second) then went into the NO-LOAD condition. The compressor stalled, drawing approximately 128 Amps at 223 VAC, for about 0.5 seconds before either returning to the normal running mode or went into the NO-LOAD condition, when exposed to the *circuit breaker clearing* type of transients in the stalling window. In general, opening the contactor did not help to prevent the compressor from stalling; it just delayed it except when exposed to the *long notch* transient where it did not stall and returned to normal running mode. When the contactor opened under the *delayed recovery* type of transients and then reclosed, the compressor stalled for as long as 11.4 seconds before the thermal protection switch opened to protect the compressor. When the contactor opened under the *circuit breaker clearing* type of transients and then reclosed, the compressor stalled and then either returned to normal running mode or went into the NO-LOAD condition. If the unit did not restart normally or went into the NO-LOAD condition, then the compressor needed to be turned off and then on again in order to restart normally. The compressor at the NO-LOAD condition consumed $\frac{1}{2}$ of the normal running power but without producing any work (cooling). At high temperatures, the compressor is more sensitive to transients where most of the tests ended up in NO-LOAD condition or the unit did not restart normally after the thermal protection switch reclosed.

This air conditioner unit was also tested under overcharge conditions. The stalling behavior was similar for all cases except that the stalling threshold voltage increased to 60% at 80 °F, 70% at 100 °F, and 78% at 115 °F. The power contactor dropout voltage did not change and is 45%.

9.1 SYSTEM SPECIFICATIONS

The tested air conditioner system has the following specifications:

MAIN SYSTEM		FAN MOTOR	
Manufacturer	Rheem	Manufacturer	GE
Condenser Unit	RAB048-JAZ	Model	5KCP39GG
Evaporator Coil	CK3BA048	Voltage (V)	220/240
Size (Tons)	4	Current (I)	1.5
Compressor Type	Scroll	Power (HP)	1.5
Refrigerant	R-22	RPM	1075
SEER	10	FLA (AMPS)	1.5
Condition	New		
Unit Cost	\$1,171.00	CONTACTOR	
		Manufacturer	Cutler-Hammer
		Model	C25CNY42
		Rating (V)	240/277
		FLA (AMPS)	30
		LRA (AMPS)	150
		Resistance	40
		CAPACITOR	
		Manufacturer	CSC
		Model	328P4505H37N37P5X
		Rating (V)	370
		Capacitance (µF)	50

COMPRESSOR	
Manufacturer	Copeland
Model	ZR47KC-PFV-235
Type	Scroll
FLA (AMPS)	26.5
LRA (AMPS)	131
Phase	1
Refrigerant	R22
Charge (LBS)	6.4
Voltage (V)	230/208
P _{MAX} High (PSI)	398.8
P _{MAX} Low (PSI)	290

9.2 TEST PARAMETERS

This air conditioner unit has the following testing parameters.

#6	80°F	100°F	115°F
T _{INLET} (°C)	74.2	96.4	118.6
T _{OUTLET} (°C)	90.8	118.8	147.2
T _{COMP. AMB.} (°C)	107.5	141.2	175.7
T _{CASE} (°C)	124.2	163.6	204.3
T _{GAS} (°C)	-	-	-
T _{LIQ} (°C)	-	-	-
R _{FLOW} (Kcfm)	1.7	1.5	1.5
P _{LOW} (PSI)	59.2	62.0	67.1
P _{HIGH} (PSI)	210.0	275.5	340.2
I _{RUNNING} (A)	19.0	22.0	25.0
W _{RUNNING} (W)	3846.0	4670.0	5434.0
VAR _{RUNNING} (VAR)	2511.0	2550.0	2600.0

A more detailed internal performance parameter table can be found in APPENDIX #2 -- Attachment # 6.

Overcharged)			
	80°F	100°F	115°F
T_{INLET} (°C)	74.2	96.4	118.6
T_{OUTLET} (°C)	90.8	118.8	147.2
T_{COMP. AMB.} (°C)	107.5	141.2	175.7
T_{CASE} (°C)	124.2	163.6	204.3
T_{GAS} (°C)	-	-	-
T_{LIQ} (°C)	-	-	-
R_{FLOW} (Kcfm)	1.6	1.5	1.6
P_{LOW} (PSI)	55.4	59.2	67.3
P_{HIGH} (PSI)	258.6	354.0	444.4
I_{RUNNING} (A)	21.0	26.0	31.0
W_{RUNNING} (W)	4410.0	5642.0	6908.0
VAR_{RUNNING} (VAR)	2550.0	2626.0	2767.0

9.3 INRUSH TEST RESULTS

This unit took approximately 13 cycles to come to the normal steady running state. The data below was recorded for the whole air conditioner system.

Inrush	
V _{INRUSH}	222 VAC
I _{INRUSH}	137 A
W _{INRUSH}	21,300 W
VAR _{INRUSH}	21,900 VAR
t	15 cycles

9.4 POWER CONTACTOR TEST RESULTS

The power contactor opened at 45% voltage sag. The compressor had the following responses right after contactor reclosed:

- ◆ *Long notch* type of transient
 - The compressor returned to the normal running state after the power contactor reclosed.
- ◆ *Delayed Recovery* type of transient

The compressor restarted normally right after the power contactor reclosed or after the thermal protection switch reclosed.

 - At 80 °F
 - The compressor stalled, drawing approximately 82 Amps at 167 VAC, right after contactor reclosed for as long as 11.4 seconds before the compressor returned to the normal running mode.
 - At 100 °F

- The compressor stalled, drawing approximately 83 Amps at 166 VAC, right after contactor reclosed for as long as 11.4 seconds before the thermal protection switch opened to protect the unit.
- At 115 °F
 - The compressor stalled, drawing approximately 81 Amps at 160 VAC, right after contactor reclosed for as long as 9.5 seconds before the thermal protection switch opened to protect the unit.
- ◆ *Circuit Breaker Clearing* type of transient
 - At 80 °F
 - Usually the compressor returned to normal running state after power contactor reclosed.
 - Occasionally the compressor stalled, drawing approximately 127 Amps at 223 VAC, then returned to the normal running mode.
 - At 100 °F
 - At times the compressor returned to the normal running state after the power contactor reclosed.
 - At times the compressor stalled, drawing approximately 124 Amps at 224 VAC, then went into a NO-LOAD condition.
 - At 115 °F
 - At times the compressor returned to the normal running state after power contactor reclosed.
 - At times the compressor stalled, drawing approximately 122 Amps at 224 VAC, then went into a NO-LOAD condition.

9.5 30-SECOND LONG NOTCH TYPE OF TRANSIENT TEST RESULTS

The compressor had the following threshold voltages 58% at 80 °F, 63% at 100 °F, and 70% at 115 °F when exposed to the *long notch* type of transients. Therefore, the stalling windows are the following: 58% to 45% at 80 °F, 63% to 45% at 100 °F, and 45% to 50% at 115 °F. The thermal protection switch opened to protect the compressor but did not always open after the compressor stalled. The compressor did not always restarted normally after either the thermal protection switch reclosed or the unit stalled. It needed to be turned off and then on again in order to restart normally. The compressor stalled in the stalling window, drawing approximately 57 Amps at 112 VAC, for as long as 30 seconds before the thermal protection switch opened to protect the compressor. If the power contactor opened and then reclosed, the compressor returned to normal running mode. The following are the details for each of the temperatures:

- ◆ At 80 °F
 - At times the compressor stalled, drawing approximately 51 Amps at 102 VAC, for the complete transient time and then returned to the normal running mode.
 - At times the compressor stalled, drawing approximately 69 Amps at 131 VAC, for as long as 25.5 seconds before the thermal protection switch opened to protect the compressor. The unit did not restart normally.
 - At times the compressor stalled, drawing approximately 64 Amps at 123 VAC, for as long as 1.0 second and then the unit went into the NO-LOAD condition.
 - If the power contactor opened and then reclosed the compressor returned to the normal running mode.
- ◆ At 100 °F
 - At times the compressor stalled, drawing approximately 54 Amps at 109 VAC, for the complete transient time and then returned to the normal running mode.

- At times the compressor stalled, drawing approximately 64 Amps at 124 VAC, for the complete transient time and then at recovery the thermal protection switch opened to protect the compressor. The unit did not restart normally.
 - At times the compressor stalled, drawing approximately 69 Amps at 136 VAC, for as long as 0.7 seconds and then the compressor went into the NO-LOAD condition.
 - If the power contactor opened and then reclosed again the compressor returned to the normal running mode.
- ◆ At 115 °F
- At times the compressor stalled, drawing approximately 57 Amps at 112 VAC, for the complete transient time and then returned to the normal running mode.
 - At times the compressor stalled, drawing approximately 79 Amps at 160 VAC, for as long as 7.1 seconds and then the compressor went into the NO-LOAD condition.
 - If the power contactor opened and then reclosed, the compressor returned to the normal running mode.

9.6 DELAYED RECOVERY TYPE OF TRANSIENT TEST RESULTS

This compressor had the following threshold voltages 58% at 80 °F, 63% at 100 °F, and 70% at 115 °F when exposed to the *long notch* type of transients. Therefore, the stalling windows are the following: 58% to 45% at 80 °F, 63% to 45% at 100 °F, and 70% to 45% at 115 °F. The thermal protection switch opened to protect the compressor but did not always open after stalling and instead went into the NO-LOAD condition. At times, the compressor did not return to normal running state after the thermal protection switch reclosed and need it to be turned off and then on again in order to return to the normal running mode. The compressor stalled in the stalling window, drawing approximately 80 Amps at 166 VAC, for as long as 14.8 seconds before the thermal protection switch opened to protect the compressor. At times the compressor stalled as long as 1 second, drawing approximately 50 Amps at 103 VAC, then went into the NO-LOAD condition. If the power contactor opened and then reclosed, the compressor stalled for as long as 11.4 seconds , drawing approximately 82 Amps at 167 VAC, before the thermal protection switch opened to protect the compressor. The following are the details for each of the temperatures:

- ◆ At 80 °F
 - The compressor stalled, drawing approximately 81 Amps at 165 VAC, for as long as 12.9 seconds before the thermal protection switch opened to protect the compressor. The unit did not restart normally.
 - If the power contactor opened and then reclosed, the compressor stalled, drawing approximately 82 Amps at 167 VAC, for as long as 11.4 seconds before it returned to the normal running mode.
- ◆ At 100 °F
 - At times the compressor stalled, drawing approximately 82 Amps at 165 VAC, for as long as 14.0 seconds before the thermal protection switch opened to protect the compressor. The compressor did not restart normally.
 - At times the compressor stalled, drawing approximately 50 Amps at 103 VAC, for as long as 1.0 second. It then went into the NO-LOAD condition.
 - If the power contactor opened and then reclosed, the compressor stalled, drawing approximately 83 Amps at 166 VAC, for as long as 11.4 seconds before the thermal protection switch opened to protect the compressor.
- ◆ At 115 °F

- At times the compressor stalled, drawing approximately 80 Amps at 166 VAC, for as long as 14.8 seconds before the thermal protection switch opened to protect the compressor. The compressor did not restart normally.
- At times the compressor stalled, drawing approximately 78 Amps at 153 VAC, for as long as 0.9 seconds before the compressor went into the NO-LOAD condition.
- If the power contactor opened and then reclosed, the compressor stalled, drawing approximately 81 Amps at 160 VAC, for as long as 9.5 seconds before the thermal protection switch opened to protect the compressor.

9.7 *CIRCUIT BREAKER CLEARING* TYPE OF TRANSIENT TEST RESULTS

This compressor had the following threshold voltages 55% at 80 °F, 60% at 100 °F, and 65% at 115 °F when exposed to the *Circuit Breaker Clearing* type of transients. Therefore, the stalling windows are the following: 55% to 45% at 80 °F, 60% to 45% at 100 °F, and 65% to 45% at 115 °F. The thermal protection switch never opened after stalling to protect the compressor. This compressor stalled in the stalling window, drawing approximately 127 Amps at 223 VAC then either it returned to the normal running mode or went into the NO-LOAD condition. This compressor did not stall with the 3 cycle transient at 80 °F. If the power contactor opened and then reclosed, the compressor usually stalled and went into the IDLE condition and at other times it returned to the normal running mode. The following are the details for each of the temperatures:

- ◆ At 80 °F
 - The compressor did not stall with the 3 cycle transients.
 - At times, the compressor stalled, drawing approximately 127 Amps at 223 VAC, for as long as 0.6 seconds and then the compressor went into the NO-LOAD condition.
 - At times, the compressor stalled, drawing approximately 128 Amps at 223 VAC for as long as 0.5 seconds before it returned to the normal running mode.
 - If the power contactor opened and then reclosed, the unit either returned to the normal running mode or stalled, drawing approximately 127 Amps at 223 VAC, for 0.5 seconds before returning to the normal running mode.
- ◆ At 100 °F
 - Usually the compressor stalled, drawing approximately 124 Amps at 224 VAC, for as long as 0.4 seconds before the compressor went into the NO-LOAD condition.
 - Sometime the compressor stalled, drawing approximately 124 Amps at 224 VAC, for as long as 0.4 seconds before it returned to the normal running mode.
 - If the power contactor opened and then reclosed, the compressor either returned to the normal running mode or stalled, drawing approximately 124 Amps at 224 VAC, for a couple of cycles and then went into the NO-LOAD condition.
- ◆ At 115 °F
 - Usually the compressor stalled, drawing approximately 122 Amps at 224 VAC, for as long as 0.4 seconds and then the compressor went into the NO-LOAD condition.
 - Sometime the compressor stalled, drawing approximately 122 Amps at 224 VAC, for as long as 0.5 seconds before it returned to the normal running mode.
 - If the power contactor opened and then reclosed, the compressor either returned to the normal running mode or stalled, drawing approximately 122 Amps at 224 VAC, for 0.3 seconds before it went into the NO-LOAD condition.

10.0 A/C #7- TEST RESULTS

The air conditioner's compressor stalled when the voltage was in the stalling window (between the stall threshold voltage and contactor dropout voltage) when exposed to any of the three types of transients. When exposed to the *long notch* type of transients in the stalling window, this compressor stalled, drawing approximately 74 Amps at 135 VAC, for as long as 30.0 seconds before returning to the normal running mode. The compressor stalled, drawing approximately 85 Amps at 163 VAC, for as long as 11.0 seconds before returning to the normal running mode, when exposed to the *delayed recovery* type of transients in the stalling window. The compressor stalled, drawing approximately 130 Amps at 223 VAC except at 80 °F, for about 0.5 seconds before returning to the normal running mode, when exposed to the *circuit breaker clearing* type of transients in the stalling window. There were a couple of cases where the unit went into the NO-LOAD condition at the *circuit breaker clearing* type of transient. If the power contactor opened under the *delayed recovery* transient and then reclosed, the compressor stalled, drawing approximately 83 Amps at 163 VAC, for as long as 6 seconds before returning to the normal running mode. In general, opening the contactor did not help to prevent the compressor from stalling; it just delayed it. If the compressor went into the IDLE condition, then the compressor needed to be turned off and then on again in order to return to the normal running mode. The compressor at the NO-LOAD condition consumed ½ of the normal running power but without producing any work (cooling).

10.1 SYSTEM SPECIFICATIONS

The tested air conditioner system has the following specifications:

MAIN SYSTEM	
Manufacturer	Carrier
Condenser Unit	38TRA-048
Evaporator Coil	CK3BA048
Size (Tons)	4
Compressor Type	Scroll
Refrigerant	R-22
SEER	12.5
Condition	New
Unit Cost	\$1,930.00

COMPRESSOR	
Manufacturer	Copeland
Model	ZR47K3-PFV-135
Type	Scroll
FLA (AMPS)	22.7
LRA (AMPS)	137
Phase	1
Refrigerant	R22
Charge (LBS)	9.75
Voltage (V)	230/208
PMAx High (PSI)	398.8
PMAxLow (PSI)	290

FAN MOTOR	
Manufacturer	GE
Model	5KCP39GFS166S
Voltage (V)	208/230
Current (I)	0.95
Power (HP)	0.2
RPM	825
FLA (AMPS)	1.1

CONTACTOR	
Manufacturer	Product Unlimited
Model	HN51KCF024
Rating (V)	240/277
FLA (AMPS)	30
LRA (AMPS)	150
Resistance	40

CAPACITOR	
Manufacturer	GE
Model	97F9898
Rating (V)	440
Capacitance (µF)	60

10.2 TEST PARAMETERS

This air conditioner unit has the following testing parameters.

	80°F	100°F	115°F
T_{INLET} (°C)	21.7	22.2	21.7
T_{OUTLET} (°C)	10.1	10.0	10.5
T_{COMP. AMB.} (°C)	26.1	37.4	46.0
T_{CASE} (°C)	67.5	84.3	98.4
T_{GAS} (°C)	-	-	-
T_{LIQ} (°C)	-	-	-
R_{FLOW} (Kcfm)	1.9	1.6	1.5
P_{LOW} (PSI)	59.7	60.3	63.3
P_{HIGH} (PSI)	192.4	254.6	312.9
I_{RUNNING} (A)	15.0	19.0	22.0
W_{RUNNING} (W)	3525.0	4279.0	5029.0
VAR_{RUNNING} (VAR)	1050.0	1098.0	1159.0

A more detail internal performance parameter table can be found in APPENDIX #2 -- Attachment # 7.

10.3 INRUSH TEST RESULTS

This unit took approximately 12 cycles before entering its normal steady running state. The data below was recorded for the whole air conditioner system.

Inrush	
V _{INRUSH}	222 VAC
I _{INRUSH}	133 A
W _{INRUSH}	22,000 W
VAR _{INRUSH}	19,700 VAR
t	12 cycles

10.4 POWER CONTACTOR TEST RESULTS

The power contactor opened at 50% voltage sag. The compressor had the following responses right after contactor reclosed:

- ◆ *Long notch* type of transient
 - The compressor never stalled after the power contactor reclosed.
- ◆ *Delayed Recovery* type of transient
 - The compressor stalled, drawing approximately 83 Amps at 163 VAC, right after the contactor reclosed for as long as 6 seconds before it returned to the normal running mode.
- ◆ *Circuit Breaker Clearing* type of transient

- The compressor returned to the normal running mode after the power contactor reclosed except in one case where it stalled. In this case, it drew approximately 121 Amps at 233 VAC, for a couple of cycles and then went into the NO-LOAD condition.

10.5 30-SECOND LONG NOTCH TYPE OF TRANSIENT TEST RESULTS

This compressor had the following threshold voltages 55% at 80 °F, 60% at 100 °F, and 68% at 115 °F when exposed to the *long notch* type of transients. Therefore, the stalling windows are the following: 55% to 50% at 80 °F, 60% to 50% at 100 °F, and 68% to 50% at 115 °F. The thermal protection switch seldom opened to protect the compressor and the compressor did not restart normally after the thermal protection switch reclosed. The compressor stalled in the stalling window, drawing approximately 74 Amps at 135 VAC, for as long as 30 seconds before it returned to the normal running state. On one occasion, the thermal protection switch opened to protect the compressor after stalling for 21 seconds and the compressor did not restart normally. If the power contactor opened and then reclosed, the compressor returned to the normal running mode. The following are the details for each of the temperatures:

- ◆ At 80 °F
 - The compressor stalled, drawing approximately 68 Amps at 123 VAC, for as long as 30 seconds before it returned to the normal running mode.
 - If the power contactor opened and then reclosed, the compressor returned to the normal running mode.
- ◆ At 100 °F
 - The compressor stalled, drawing approximately 74 Amps at 135 VAC, for as long as 30 seconds before it returned to the normal running mode.
 - If the power contactor opened and then reclosed the compressor returned to the normal running mode.
- ◆ At 115 °F
 - The compressor stalled, drawing approximately 72 Amps at 135 VAC, for as long as 30 seconds before it returned to the normal running mode except in one case where the thermal protection switch opened to protect the compressor. The unit did not restart normally.
 - If the power contactor opened and then reclosed, the compressor returned to the normal running mode.

10.6 DELAYED RECOVERY TYPE OF TRANSIENT TEST RESULTS

This compressor had the following threshold voltages 55% at 80 °F, 60% at 100 °F, and 65% at 115 °F when exposed to the *delayed recovery* type of transient. Therefore, the stalling windows are the following: 55% to 50% at 80 °F, 60% to 50% at 100 °F, and 65% to 50% at 115 °F. The thermal protection switch never opened to protect the compressor and it returned to the normal running mode after any stall. The compressor stalled in the stalling window, drawing approximately 85 Amps at 163 VAC, for as long as 11 seconds before it returned to the normal running mode. If the power contactor opened and then reclosed, the compressor stalled, drawing approximately 83 Amps at 163 VAC, for as long as 6 seconds before it returned to the normal running mode. In general, opening the contactor did not prevent the compressor from stalling, it just delayed the stall. The following are the details for each of the temperatures:

- ◆ At 80 °F

- The compressor stalled, drawing approximately 85 Amps at 163 VAC, for as long as 11 seconds before it returned to the normal running mode.
- If the power contactor opened and then reclosed, the compressor stalled, drawing approximately 85 Amps at 159 VAC, for as long as 6 seconds before returning to the normal running mode.
- ◆ At 100 °F
 - The compressor stalled, drawing approximately 81 Amps at 158 VAC, for as long as 10 seconds before returning to the normal running mode.
 - If the power contactor opened and then reclosed, the compressor stalled, drawing approximately 85 Amps at 164 VAC, for as long as 6 seconds before returning to the normal running mode.
- ◆ At 115 °F
 - The compressor stalled, drawing approximately 79 Amps at 160 VAC, for as long as 10 seconds before returning to normal running mode.
 - If the power contactor opened and then reclosed, the compressor stalled, drawing approximately 83 Amps at 163 VAC, for as long as 6 seconds before returning to the normal running mode.

10.7 *CIRCUIT BREAKER CLEARING* TYPE OF TRANSIENT TEST RESULTS

This compressor had the following threshold voltages 55% at 80 °F, 60% at 100 °F, and 65% at 115 °F when exposed to the *circuit breaker clearing* type of transients. Therefore, the stalling windows are the following: 55% to 50% at 80 °F, 60% to 50% at 100 °F, and 65% to 50% at 115 °F. The thermal protection switch never opened to protect the compressor. This compressor did not stall at 80 °F. In general, the compressor did not stall except in a couple of cases where it stalled in the stalling window, drawing approximately 130 Amps at 223 VAC, for as long as 0.5 seconds and then went into a NO-LOAD condition. If the power contactor opened and then reclosed, the compressor returned to the normal running mode except in couple cases. In these cases, it stalled, drawing approximately 121 Amps at 233 VAC, and then went into the NO-LOAD condition. The following are the details for each of the temperatures:

- ◆ At 80 °F
 - The compressor did not stall in the stalling window.
- ◆ At 100 °F
 - The compressor stalled, drawing approximately 130 Amps at 223 VAC, for as long as 0.5 seconds before it returned to the normal running mode.
 - If the power contactor opened and then reclosed, the compressor mostly returned to the normal running mode except in one case where it stalled. In this case it drew approximately 121 Amps at 233 VAC, for couple of cycles and then went into the NO-LOAD condition.
- ◆ At 115 °F
 - The compressor stalled, drawing approximately 127 Amps at 123 VAC, for as long as 0.4 seconds before it went into the NO-LOAD condition.
 - If the power contactor opened and then reclosed, the compressor returned to a normal running mode.

11.0 A/C #8 - TEST RESULTS

The air conditioner's compressor stalled when the voltage was in the stalling window (between the stall threshold voltage and contactor dropout voltage) when exposed to any of the three types of transients. When exposed to the *long notch* type of transients in the stalling window, this compressor stalled, drawing approximately 64 Amps at 137 VAC, for as long as 8.1 seconds before the thermal protection switch opened to protect the compressor but the unit did not restart normally. When exposed to the *delayed recovery* type of transients in the stalling window, this compressor stalled, drawing approximately 69 Amps at 154 VAC, for as long as 6.3 seconds before the thermal protection switch opened to protect the compressor but the unit did not restart normally. When exposed to the *circuit breaker clearing* type of transients in the stalling window, this compressor stalled, drawing approximately 111 Amps at 225 VAC, before the thermal protection switch opened to protect the compressor but the unit did not restart normally. When the contactor opened under the *delayed recovery* type of transients and then reclosed, the compressor stalled, drawing approximately 77 Amps at 169 VAC, for as long as 5.6 seconds before the thermal protection switch opened to protect the compressor but did not restart normally. In general, opening the contactor did not help to prevent the compressor from stalling; it just delayed the stall.

11.1 SYSTEM SPECIFICATIONS

The tested air conditioner system has the following specifications:

MAIN SYSTEM	
Manufacturer	Goodman
Condenser Unit	CLK048
Evaporator Coil	CK3BA048
Size (Tons)	4
Compressor Type	Reciprocating
Refrigerant	R-22
SEER	10
Condition	New
Unit Cost	\$953.00

COMPRESSOR	
Manufacturer	Copeland
Model	CR42K6-PFV-223
Type	Reciprocating
FLA (AMPS)	18.3
LRA (AMPS)	102
Phase	1
Refrigerant	R22
Charge (LBS)	7
Voltage (V)	230/208
PMAH High (PSI)	-
PMAH Low (PSI)	-

FAN MOTOR	
Manufacturer	A.O. Smith
Model	F48F97A76
Voltage (V)	208/230
Current (I)	1.5
Power (HP)	0.25
RPM	1075
FLA (AMPS)	1.8

CONTACTOR	
Manufacturer	GE
Model	CR453CCHBAFG
Rating (V)	240/277
FLA (AMPS)	30
LRA (AMPS)	180
Resistance	40

CAPACITOR	
Manufacturer	GE
Model	97F9638
Rating (V)	440
Capacitance (µF)	40

11.2 TEST PARAMETERS

This air conditioner unit has the following testing parameters.

	80°F	100°F	115°F
T_{INLET} (°C)	22.0	21.9	21.9
T_{OUTLET} (°C)	10.9	11.8	13.0
T_{COMP. AMB.} (°C)	26.6	37.6	45.9
T_{CASE} (°C)	43.2	41.9	47.2
T_{GAS} (°C)	7.9	9.3	11.7
T_{LIQ} (°C)	33.0	44.5	52.5
R_{FLOW} (Kcfm)	1.7	1.5	1.7
P_{LOW} (PSI)	65.3	69.0	74.3
P_{HIGH} (PSI)	205.3	270.9	324.5
I_{RUNNING} (A)	17.0	19.0	20.0
W_{RUNNING} (W)	3762.0	4221.0	4535.0
VAR_{RUNNING} (VAR)	1700.0	1750.0	1750.0

A more detail internal performance parameter table can be found in APPENDIX #2 -- Attachment # 8.

11.3 INRUSH TEST RESULTS

This unit took approximately 12 cycles before entering its normal steady running state. The data below was recorded for the whole air conditioner system.

Inrush	
V _{INRUSH}	223 VAC
I _{INRUSH}	119 A
W _{INRUSH}	19,200 W
VAR _{INRUSH}	18,500 VAR
t	12 cycles

11.4 POWER CONTACTOR TEST RESULTS

The power contactor opened with a 53% voltage sag. In general, opening the contactor made the compressor stall harder after the contactor reclosed with the unit not returning to the normal running state. The compressor needed to be turned off and then on again in order to return to the normal running state. The compressor had the following responses right after contactor reclosed:

- ◆ *Long notch* type of transient
 - The compressor stalled, drawing approximately 115 Amps at 226 VAC, right after contactor reclosed for as long as 2.2 seconds before the thermal protection switch opened to protect the compressor. The unit did not restart normally.
- ◆ *Delayed Recovery* type of transient

- The compressor stalled, drawing approximately 77 Amps at 169 VAC, right after the contactor reclosed for as long as 5.6 seconds before the thermal protection switch opened to protect the compressor. The unit did not restart normally.
- ◆ *Circuit Breaker Clearing* type of transient
 - The compressor stalled, drawing approximately 112 Amps at 225 VAC, right after the contactor reclosed for as long as 1.7 seconds before the thermal protection switch opened to protect the compressor. The unit did not restart normally.

11.5 30-SECOND LONG NOTCH TYPE OF TRANSIENT TEST RESULTS

This compressor had the following threshold voltages 65% at 80 °F, 65% at 100 °F, and 68% at 115 °F when exposed to the *long notch* type of transients. Therefore, the stalling windows are the following: 65% to 53% at 80 °F, 65% to 53% at 100 °F, and 68% to 53% at 115 °F. The thermal protection switch opened after each stall to protect the compressor but the compressor never restarted normally. The compressor stalled in the stalling window, drawing approximately 64 Amps at 137 VAC, for as long as 8.1 seconds before the thermal protection switch opened to protect the compressor. If the power contactor opened and then reclosed, the compressor stalled, drawing approximately 115 Amps at 226 VAC, for as long as 2.2 seconds. The unit did not restart normally. The following are the details for each of the temperatures:

- ◆ At 80 °F
 - The compressor stalled, drawing approximately 64 Amps at 137 VAC, for as long as 7.5 seconds before the thermal protection switch opened to protect the compressor. The unit did not restart normally.
 - If the power contactor opened and then reclosed, the compressor stalled, drawing approximately 115 Amps at 226 VAC, for as long as 2.2 seconds before the thermal protection opened to protect the compressor. The unit did not restart normally.
- ◆ At 100 °F
 - The compressor stalled, drawing approximately 64 Amps at 137 VAC, for as long as 8.1 seconds before the thermal protection switch opened to protect the compressor. The unit did not restart normally.
 - If the power contactor opened and then reclosed, the compressor stalled, drawing approximately 114 Amps at 227 VAC, for as long as 1.9 seconds before the thermal protection opened to protect the compressor. The unit did not restart normally.
- ◆ At 115 °F
 - The compressor stalled, drawing approximately 63 Amps at 137 VAC, for as long as 7.3 seconds before the thermal protection switch opened to protect the compressor. The unit did not restart normally.
 - If the power contactor opened and then reclosed, the compressor stalled, drawing approximately 112 Amps at 226 VAC, for as long as 2.0 seconds before the thermal protection switch opened to protect the compressor. The unit did not restart normally.

11.6 DELAYED RECOVERY TYPE OF TRANSIENT TEST RESULTS

This compressor had the following threshold voltages 65% at 80 °F, 65% at 100 °F, and 68% at 115 °F when exposed to the *delayed recovery* type of transient. Therefore, the stalling windows are the following: 65% to 53% at 80 °F, 65% to 53% at 100 °F, and 68% to 53% at 115 °F. The thermal protection switch opened after each stall to protect the compressor but the unit never

restarted normally after the thermal protection switch reclosed. The compressor stalled in the stalling window, drawing approximately 69 Amps at 154 VAC, for as long as 6.3 seconds before the thermal protection switch opened to protect the compressor. If the power contactor opened and then reclosed, the compressor stalled, drawing approximately 77 Amps at 169 VAC, for as long as 5.6 seconds. The unit did not restart normally. In general, opening the contactor did not prevent the compressor from stalling it just delayed it. The following are the details for each of the temperatures:

- ◆ At 80 °F
 - The compressor stalled, drawing approximately 70 Amps at 151 VAC, for as long as 6.0 seconds before the thermal protection switch opened to protect the compressor. The unit did not restart normally.
 - If the power contactor opened and then reclosed, the compressor stalled, drawing approximately 77 Amps at 166 VAC, for as long as 1.3 seconds before the thermal protection switch opened to protect the compressor. The unit did not restart normally.
- ◆ At 100 °F
 - The compressor stalled, drawing approximately 70 Amps at 153 VAC, for as long as 5.9 seconds before the thermal protection switch opened to protect the compressor. The unit did not restart normally.
 - If the power contactor opened and then reclosed, the compressor stalled, drawing approximately 77 Amps at 169 VAC, for as long as 5.6 seconds before the thermal protection switch opened to protect the compressor. The unit did not restart normally.
- ◆ At 115 °F
 - The compressor stalled, drawing approximately 69 Amps at 154 VAC, for as long as 6.3 seconds before the thermal protection switch opened to protect the compressor. The unit did not restart normally.
 - If the power contactor opened and then reclosed, the compressor stalled, drawing approximately 75 Amps at 168 VAC, for as long as 5.0 seconds before the thermal protection switch opened to protect the compressor. The unit did not restart normally.

11.7 *CIRCUIT BREAKER CLEARING* TYPE OF TRANSIENT TEST RESULTS

This compressor had the following threshold voltages 65% at 80 °F, 65% at 100 °F, and 68% at 115 °F when exposed to the *Circuit Breaker Clearing* type of transients. Therefore, the stalling windows are the following: 65% to 50% at 80 °F, 65% to 50% at 100 °F, and 68% to 50% at 115 °F. The thermal protection switch opened after each stall to protect the compressor but never restarted normally after the thermal protection switch reclosed. The compressor stalled in the stalling window, drawing approximately 111 Amps at 225 VAC, for as long as 1.9 seconds before the thermal protection switch opened to protect the compressor. If the power contactor opened and then reclosed, the compressor stalled, drawing approximately 112 Amps at 225 VAC, for as long as 1.7 seconds. The unit did not restart normally. In general, opening the contactor did not prevent the compressor from stalling it just delayed it. The following are the details for each of the temperatures:

- ◆ At 80 °F
 - The compressor stalled, drawing approximately 113 Amps at 225 VAC, for as long as 1.5 seconds before the thermal protection switch opened to protect the compressor. The unit did not restart normally.

- If the power contactor opened and then reclosed, the compressor stalled, drawing approximately 114 Amps at 225 VAC, for as long as 1.7 seconds before the thermal protection switch opened to protect the compressor. The unit did not restart normally.
- ◆ At 100 °F
 - The compressor stalled, drawing approximately 112 Amps at 225 VAC, for as long as 1.7 seconds before the thermal protection switch opened to protect the compressor. The unit did not restart normally.
 - If the power contactor opened and then reclosed, the compressor stalled, drawing approximately 113 Amps at 225 VAC, for as long as 1.7 seconds before the thermal protection switch opened to protect the compressor. The unit did not restart normally.
- ◆ At 115 °F
 - The compressor stalled, drawing approximately 111 Amps at 225 VAC, for as long as 1.9 seconds before the thermal protection switch opened to protect the compressor. The unit did not restart normally.
 - If the power contactor opened and then reclosed, the compressor stalled, drawing approximately 112 Amps at 225 VAC, for as long as 1.7 seconds before the thermal protection switch opened to protect the compressor. The unit did not restart normally.

12.0 A/C #9 - TEST RESULTS

The air conditioner's compressor stalled when the voltage was in the stalling window (between the stall threshold voltage and contactor dropout voltage) when exposed to any of the three types of transients. When exposed to the *long notch* type of transients at the stalling window, this compressor stalled, drawing approximately 64 Amps at 49 VAC, for as long as 25.3 seconds before the thermal protection switch opened to protect the compressor. In a particular test, the compressor stalled twice, the first for 5.3 seconds and the second for 1.0 second, and in both cases the thermal protection switch opened to protect the compressor. When exposed to the *delayed recovery* type of transients in the stalling window, this compressor stalled, drawing approximately 67 Amps at 166 VAC, for as long as 11.9 seconds before the thermal protection switch opened to protect the compressor or it stalled drawing approximately 66 Amps at 147 VAC, for as long as 10.9 seconds before returning to the normal running mode. When exposed to the *circuit breaker clearing* type of transients in the stalling window except at 80 °F, this compressor stalled, drawing approximately 114 Amps at 224 VAC, for as long as 1.7 seconds before the thermal protection switch opened to protect the compressor. It also stalled, drawing approximately 113 Amps at 225 VAC, for as long as 0.9 seconds before returning to the normal running mode. When the contactor opened under the *delayed recovery* type of transients and then reclosed, the compressor stalled, drawing approximately 72 Amps at 157 VAC, for as long as 11.2 seconds before the thermal protection switch opened to protect the compressor or stalled, drawing approximately 82 Amps at 175 VAC, for as long as 3.0 before returning to the normal running mode. In general, opening the contactor did not help to prevent the compressor from stalling; it just delayed it.

12.1 SYSTEM SPECIFICATIONS

The tested air conditioner system has the following specifications:

MAIN SYSTEM	
Manufacturer	Day & Night
Condenser Unit	5680J048
Evaporator Coil	CK3BA048
Size (Tons)	4
Compressor Type	Reciprocating
Refrigerant	R-22
SEER	10
Condition	Used
Unit Cost	\$0.00

COMPRESSOR	
Manufacturer	Copeland Weld
Model	CRL1-0350-PFV
Type	Reciprocating
FLA (AMPS)	24
LRA (AMPS)	114
Phase	1
Refrigerant	R22
Charge (LBS)	11.25
Voltage (V)	230/208
PMAX High (PSI)	-
PMAXLow (PSI)	-

FAN MOTOR	
Manufacturer	GE
Model	5KCP39GJ352S
Voltage (V)	208/230
Current (I)	1
Power (HP)	0.1
RPM	825
FLA (AMPS)	1

CONTACTOR	
Manufacturer	Cutler-Hammer
Model	C35BNB 240T
Rating (V)	240
FLA (AMPS)	40
LRA (AMPS)	240
Resistance	50

CAPACITOR	
Manufacturer	SPRAGUE/GE/GE
Model	HC95DE208 / 97F5362 / 97F5341
Rating (V)	320 / 440 / 440
Capacitance (µF)	- / 25 / 15

12.2 TEST PARAMETERS

This air conditioner unit has the following testing parameters.

	80°F	100°F	115°F
T_{INLET} (°C)	22.4	22.8	24.1
T_{OUTLET} (°C)	12.4	13.1	15.0
T_{COMP. AMB.} (°C)	25.7	37.9	46.5
T_{CASE} (°C)	31.1	42.0	51.5
T_{GAS} (°C)	8.4	9.5	12.9
T_{LIQ} (°C)	22.7	29.3	37.0
R_{FLOW} (Kcfm)	1.5	1.5	1.5
P_{LOW} (PSI)	67.4	70.7	77.6
P_{HIGH} (PSI)	198.0	261.9	313.0
I_{RUNNING} (A)	20.0	23.0	25.0
W_{RUNNING} (W)	4347.0	4892.0	5380.0
VAR_{RUNNING} (VAR)	2124.0	2221.0	2330.0

A more detail internal performance parameter table can be found in APPENDIX #2 -- Attachment # 9.

12.3 INRUSH TEST RESULTS

This unit took approximately 5 cycles before entering its normal steady running state. The data below was recorded for the whole air conditioner system.

Inrush	
V _{INRUSH}	224 VAC
I _{INRUSH}	119 A
W _{INRUSH}	23,050 W
VAR _{INRUSH}	13,200 VAR
t	5 cycles

12.4 POWER CONTACTOR TEST RESULTS

The power contactor opened with a 55% voltage sag. Opening the contactor did not help to prevent stalling, it just delayed it. The compressor had the following responses right after the contactor reclosed:

- ◆ *Long notch* type of transient
 - The compressor never stalled after the contactor reclosed.
- ◆ *Delayed Recovery* type of transient
 - At 80 °F

- The compressor stalled, drawing approximately 71 Amps at 152 VAC, right after the contactor reclosed for as long as 2.0 seconds before it returned to the normal running mode.
- At 100 °F
 - The compressor stalled, drawing approximately 72 Amps at 157 VAC, right after the contactor reclosed for as long as 11.2 seconds before the thermal protection switch opened to protect the compressor.
- At 115 °F
 - The compressor stalled, drawing approximately 82 Amps at 175 VAC, right after the contactor reclosed for as long as 3.0 seconds before it returned to the normal running mode.
- ◆ *Circuit Breaker Clearing* type of transient
 - At 80 °F
 - The compressor never stalled after the contactor reclosed.
 - At 100 °F
 - The compressor stalled, drawing approximately 115 Amps at 224 VAC, right after the contactor reclosed for as long as 0.9 seconds then the unit returned to the normal running mode.
 - At 115 °F
 - The compressor stalled, drawing approximately 113 Amps at 225 VAC, right after the contactor reclosed for as long as 0.9 seconds before it returned to the normal running mode.

12.5 30-SECOND LONG NOTCH TYPE OF TRANSIENT TEST RESULTS

This compressor had the following threshold voltages 65% at 80 °F, 70% at 100 °F, and 75% at 115 °F when exposed to the *long notch* type of transients. Therefore, the stalling windows are the following: 65% to 55% at 80 °F, 70% to 55% at 100 °F, and 75% to 55% at 115 °F. The thermal protection switch opened after each stall to protect the compressor. The compressor stalled in the stalling window, drawing approximately 64 Amps at 49 VAC, for as long as 25.3 seconds before the thermal protection switch opened to protect the compressor. If the power contactor opened and then reclosed, the compressor returned to the normal running mode. The following are the details for each of the temperatures:

- ◆ At 80 °F
 - The compressor stalled, drawing approximately 54 Amps at 138 VAC, for as long as 22.0 seconds before the thermal protection switch opened to protect the compressor.
 - In a particular test, the compressor stalled, drawing approximately 70 Amps at 148 VAC, for as long as 5.3 seconds before the thermal protection switch opened to protect the compressor. Then the thermal protection switch reclosed and the unit stalled again, drawing approximately 69 Amps at 148 VAC, for 1.0 second before it returned to the normal running mode.
 - If the power contactor opened and then reclosed, the compressor returned to the normal running mode.
- ◆ At 100 °F
 - The compressor stalled, drawing approximately 64 Amps at 49 VAC, for as long as 25.3 seconds before the thermal protection switch opened to protect the compressor.

- In a particular test the unit stalled, drawing approximately 68 Amps at 163 VAC, for the complete transient period without opening the thermal protection switch to protect the compressor.
- If the power contactor opened and then reclosed, the compressor returned to normal running mode.
- ◆ At 115 °F
 - The compressor stalled, drawing approximately 63 Amps at 148 VAC, for as long as 17.7 seconds before the thermal protection switch opened to protect the compressor.
 - If the power contactor opened and then reclosed, the compressor returned to the normal running mode.

12.6 DELAYED RECOVERY TYPE OF TRANSIENT TEST RESULTS

This compressor had the following threshold voltages 60% at 80 °F, 70% at 100 °F, and 70% at 115 °F when exposed to the *delayed recovery* type of transient. Therefore, the stalling windows are the following: 60% to 55% at 80 °F, 70% to 55% at 100 °F, and 70% to 55% at 115 °F. The thermal protection switch rarely opened to protect the compressor. The compressor stalled in the stalling window, drawing approximately 75 Amps at 164 VAC, for as long as 11.9 seconds before the thermal protection switch opened to protect the compressor. At times, the compressor stalled, drawing approximately 66 Amps at 147 VAC, for as long as 10.9 seconds without opening the thermal protection switch and then returned to the normal running mode. If the power contactor opened and then reclosed, the compressor either stalled, drawing approximately 72 Amps at 157 VAC, for as long as 3.0 seconds before returned to the normal running mode or stalled, drawing approximately 82 Amps at 175 VAC, for as long as 11.2 seconds before the thermal protection switch opened to protect the compressor. In general, opening the contactor did not prevent the compressor from stalling it just delayed it. The following are the details for each of the temperatures:

- ◆ At 80 °F
 - The compressor stalled, drawing approximately 66 Amps at 147 VAC, for as long as 10.9 seconds before it returned to the normal running mode.
 - If the power contactor opened and then reclosed, the compressor stalled, drawing approximately 71 Amps at 152 VAC, for as long as 2.0 seconds before returning to the normal running mode.
- ◆ At 100 °F
 - The compressor stalled, drawing approximately 67 Amps at 166 VAC, for as long as 9.0 seconds before returning to the normal running mode.
 - The compressor stalled, drawing approximately 75 Amps at 164 VAC, for as long as 11.9 seconds before thermal protection switch opened to protect the compressor.
 - If the power contactor opened and then reclosed, the compressor stalled, drawing approximately 72 Amps at 157 VAC, for as long as 11.2 seconds before the thermal protection switch opened to protect the compressor.
- ◆ At 115 °F
 - The compressor stalled, drawing approximately 72 Amps at 169 VAC, for as long as 4.7 seconds before it returned to the normal running mode.
 - The compressor stalled, drawing approximately 72 Amps at 156 VAC, for as long as 7.3 seconds before the thermal protection switch opened to protect the compressor.

- If the power contactor opened and then reclosed, the compressor stalled, drawing approximately 82 Amps at 175 VAC, for as long as 3.0 seconds before returning to the normal running state.

12.7 CIRCUIT BREAKER CLEARING TYPE OF TRANSIENT TEST RESULTS

This compressor had the following threshold voltages no-stall at 80 °F, 60% at 100 °F, and 65% at 115 °F when exposed to the *circuit breaker clearing* type of transients. Therefore, the stalling windows are the following: NONE at 80 °F, 60% to 45% at 100 °F, and 65% to 50% at 115 °F. The thermal protection switch rarely opened to protect the compressor furthermore the compressor restarted normally after each stall. This compressor never stalled at 80 °F. The compressor stalled in the stalling window, drawing approximately 114 Amps at 224 VAC, for as long as 1.7 seconds before the thermal protection switch opened to protect the compressor. At times, the compressor stalled, drawing approximately 113 Amps at 225 VAC, for as long as 0.9 seconds before returning to the normal running mode. If the power contactor opened and then reclosed, the compressor either stalled, drawing approximately 115 Amps at 224 VAC, for as long as 0.9 seconds or returned to the normal running mode. In general, opening the contactor did not prevent the compressor from stalling it just delayed it. The following are the details for each of the temperatures:

- ◆ At 80 °F
 - The compressor never stalled in the stalling window.
- ◆ At 100 °F
 - The compressor only stalled with the 12 cycles transient, drawing approximately 114 Amps at 224 VAC, for as long as 1.7 seconds before the thermal protection switch opened to protect the compressor.
 - If the power contactor opened and then reclosed, the compressors either stalled, drawing approximately 115 Amps at 224 VAC, for as long as 0.9 seconds before it returned to the normal running mode.
- ◆ At 115 °F
 - The compressor only stalled at the 6 and 12 cycle transients, drawing approximately 113 Amps at 225 VAC, for as long as 0.9 seconds before it returned to the normal running mode.
 - If the power contactor opened and then reclosed, the compressor stalled, drawing approximately 113 Amps at 225 VAC, for as long as 0.8 seconds before it returned to the normal running mode.

13.0 A/C #10 - TEST RESULTS

The air conditioner's compressor stalled when the voltage was in the stalling window (between the stall threshold voltage and contactor dropout voltage) when exposed to any of the three types of transients except at 80 °F with the *delayed recovery* type of transients. When exposed to the *long notch* type of transients in the stalling window, this compressor stalled, drawing approximately 88 Amps at 133 VAC, for as long as 27.3 seconds before the thermal protection switch opened to protect the compressor or stalled, drawing approximately 88 Amps at 128 VAC, for 30 seconds before returning to the normal running mode. When exposed to the *delayed recovery* type of transients in the stalling window, this compressor stalled, drawing approximately 103 Amps at 165 VAC, for as long as 11.5 seconds before either the thermal protection switch opened to protect the compressor or it returned to the normal running mode. When exposed to the *circuit breaker clearing* type of transients in the stalling window except at 80 °F, this compressor stalled, drawing approximately 153 Amps at 219 VAC, for as long as 0.9 seconds before returning to the *normal running* mode. When the contactor opened under the *delayed recovery* type of transients and then reclosed, the compressor stalled, drawing approximately 120 Amps at 180 VAC, for as long as 6.6 seconds before the thermal protection switch opened to protect the compressor or stalled for as long as 0.7 before returning to the normal running mode. In general, opening the contactor did not help to prevent the compressor from stalling; it just delayed it.

13.1 SYSTEM SPECIFICATIONS

The tested air conditioner system has the following specifications:

MAIN SYSTEM	
Manufacturer	Carrier
Condenser Unit	38TXA060-31
Evaporator Coil	TBD
Size (Tons)	5
Compressor Type	Scroll
Refrigerant	R-410A
SEER	13
Condition	New
Unit Cost	\$2,253.00

COMPRESSOR	
Manufacturer	Copeland
Model	ZP54K3E-PFV-130
Type	Scroll
FLA (AMPS)	27.6
LRA (AMPS)	158
Phase	1
Refrigerant	R410A
Charge (LBS)	11.5
Voltage (V)	230/208
PMAX High (PSI)	623.7
PMAXLow (PSI)	406.1

FAN MOTOR	
Manufacturer	GE
Model	5KCP39FG S071 S
Voltage (V)	208/230
Current (I)	1.4
Power (HP)	0.25
RPM	1100
FLA (AMPS)	1.4

CONTACTOR	
Manufacturer	Product Unlimited
Model	3100-30Q1028TT
Rating (V)	240
FLA (AMPS)	40
LRA (AMPS)	240
Resistance	-

CAPACITOR	
Manufacturer	GE
Model	27L681
Rating (V)	370
Capacitance (µF)	80

13.2 TEST PARAMETERS

This air conditioner unit has the following testing parameters.

	80°F	100°F	115°F
T_{INLET} (°C)	22.6	22.4	22.2
T_{OUTLET} (°C)	12.9	13.5	15.3
T_{COMP. AMB.} (°C)	26.3	38.0	46.5
T_{CASE} (°C)	86.6	109.0	130.7
T_{GAS} (°C)	15.8	18.2	21.8
T_{LIQ} (°C)	25.2	37.0	44.8
R_{FLOW} (Kcfm)	2.3	2.0	2.2
P_{LOW} (PSI)	90.4	95.8	105.8
P_{HIGH} (PSI)	310.6	415.4	490.8
I_{RUNNING} (A)	21.0	26.0	32.0
W_{RUNNING} (W)	4561.0	5948.0	7234.0
VAR_{RUNNING} (VAR)	1602.0	1750.0	1941.0

A more detail internal performance parameter table can be found in APPENDIX #2 -- Attachment # 10.

13.3 INRUSH TEST RESULTS

It would take approximately 22 cycles to come into its normal steady running state. The data below was recorded for the whole air conditioner system.

Inrush	
V _{INRUSH}	218 VAC
I _{INRUSH}	163 A
W _{INRUSH}	25,950 W
VAR _{INRUSH}	24,300 VAR
t	22 cycles

13.4 POWER CONTACTOR TEST RESULTS

The power contactor opened at a 55% voltage sag. In general, the thermal protection switch never opened to protect the unit from stalling after the contactor reclosed. The compressor had the following responses right after contactor reclosed:

- ◆ *Long notch type of transient*
 - The compressor never stalled after contactor reclosed.
- ◆ *Delayed Recovery type of transient*
 - At 80 °F

- The compressor stalled, drawing approximately 120 Amps at 180 VAC, right after the contactor reclosed for as long as 6.6 seconds before the thermal protection opened to protect the compressor.
- At 100 °F
 - The compressor stalled, drawing approximately 111 Amps at 161 VAC, right after the contactor reclosed for as long as 0.7 seconds before it returned to the normal running mode.
- At 115 °F
 - The compressor stalled, drawing approximately 110 Amps at 165 VAC, right after the contactor reclosed for as long as 0.7 seconds before it returned to the normal running mode.
- ◆ *Circuit Breaker Clearing* type of transient
 - At 80 °F
 - The compressor stalled, drawing approximately 162 Amps at 219 VAC, right after the contactor reclosed for as long as 4.0 seconds before it returned to the normal running mode.
 - At 100 °F
 - The compressor stalled, drawing approximately 159 Amps at 219 VAC, right after the contactor reclosed for as long as 0.9 seconds before it returned to the normal running mode.
 - At 115 °F
 - The compressor stalled, drawing approximately 155 Amps at 219 VAC, right after the contactor reclosed for as long as 0.6 seconds before it returned to the normal running mode.

13.5 30-SECOND LONG NOTCH TYPE OF TRANSIENT TEST RESULTS

This compressor had the following threshold voltages 58% at 80 °F, 63% at 100 °F, and 70% at 115 °F when exposed to the *long notch* type of transients. Therefore, the stalling windows are the following: 58% to 55% at 80 °F, 63% to 55% at 100 °F, and 70% to 55% at 115 °F. The thermal protection switch opened to protect the compressor, except in some cases where the compressor stalled for the complete transient period and the thermal protection switch never opened. The unit stalled in the stalling window, drawing approximately 88 Amps at 133 VAC, for as long as 27.3 seconds before the thermal protection switch opened to protect the compressor. In some cases the compressor stalled, drawing approximately 88 Amps at 128 VAC, for the complete transient period before it returned to the normal running mode. If the power contactor opened and then reclosed, the compressor returned to the normal running mode. In general, opening the contactor helped the unit by keeping it out of stalling under this type of transient. The following are the details for each of the temperatures:

- ◆ At 80 °F
 - The compressor stalled, drawing approximately 88 Amps at 128 VAC, for the complete transient period (30.0 seconds) before returned to normal running mode.
 - If the power contactor opened and then reclosed, the compressor returned to the normal running mode.
- ◆ At 100 °F
 - The compressor stalled, drawing approximately 88 Amps at 133 VAC, for as long as 27.3 seconds before the thermal protection switch opened to protect the compressor.

- If the power contactor opened and then reclosed, the compressor returned to the normal running mode.
- ◆ At 115 °F
 - The compressor stalled, drawing approximately 86 Amps at 134 VAC, for as long as 22.3 seconds before the thermal protection switch opened to protect the compressor. In one instance the compressor stalled, drawing approximately 104 Amps at 155 VAC, four (4) times without opening the thermal protection switch.
 - If the power contactor opened and then reclosed, the compressor returned to the normal running mode.

13.6 DELAYED RECOVERY TYPE OF TRANSIENT TEST RESULTS

This compressor had the following threshold voltages 63% at 100 °F and 68% at 115 °F when exposed to the *delayed recovery* type of transient. Therefore, the stalling windows are the following: 63% to 55% at 100 °F, and 68% to 55% at 115 °F. The unit did not stall at 80 °F. The thermal protection switch opened to protect the compressor. The compressor stalled in the stalling window, drawing approximately 103 Amps at 165 VAC, for as long as 11.5 seconds before the thermal protection switch opened to protect the compressor. If the power contactor opened and then reclosed, the compressor stalled, drawing approximately 120 Amps at 180 VAC, for as long as 6.6 seconds before the thermal protection switch opened to protect the compressor. There were a couple cases where the compressor stalled and then returned to the normal running mode. In general, opening the contactor did not help keep the unit out of stalling under these transients. The following are the details for each of the temperatures:

- ◆ At 80 °F
 - The compressor never stalled in the stalling window.
 - If the power contactor opened and then reclosed, the compressor stalled, drawing approximately 120 Amps at 180 VAC, for as long as 6.6 seconds before the thermal protection switch opened to protect the compressor.
- ◆ At 100 °F
 - The compressor stalled, drawing approximately 106 Amps at 167 VAC, for as long as 11.4 seconds before returning to the normal running mode.
 - If the power contactor opened and then reclosed, the compressor stalled for as long as 0.7 seconds, drawing approximately 111 Amps at 161 VAC, before returning to the normal running mode.
- ◆ At 115 °F
 - The compressor stalled, drawing approximately 103 Amps at 165 VAC, for as long as 11.5 seconds before the thermal protection switch opened to protect the compressor.
 - If the power contactor opened and then reclosed, the compressor stalled, drawing approximately 110 Amps at 165 VAC, for as long as 0.7 seconds before returning to the normal running mode.

13.7 CIRCUIT BREAKER CLEARING TYPE OF TRANSIENT TEST RESULTS

This compressor had the following threshold voltages: none at 80 °F, 60% at 100 °F, and 68% at 115 °F when exposed to the *Circuit Breaker Clearing* type of transients. Therefore, the stalling windows are the following: none at 80 °F, 60% to 50% at 100 °F, and 68% to 50% at 115 °F. The

thermal protection switch never opened to protect the compressor, furthermore the compressor restarted normally after any stall conditions. This compressor never stalled at 80 °F. The compressor stalled in the stalling window, drawing approximately 153 Amps at 219 VAC, for as long as 0.9 seconds before it returned to a normal running mode. If the power contactor opened and then reclosed, the compressor at times stalled, drawing approximately 162 Amps at 219 VAC, for as long as 4.0 seconds before returned to normal running mode. In general, opening the contactor did not prevent the compressor from stalling it just delayed it. The following are the details for each of the temperatures:

- ◆ At 80 °F
 - The compressor never stalled in the stalling window.
 - If the power contactor opened and then reclosed, the compressor stalled, drawing approximately 162 Amps at 219 VAC, for as long as 4.0 seconds before it returned to the normal running mode.
- ◆ At 100 °F
 - Only stalled at the 12 cycle transients, drawing approximately 159 Amps at 219 VAC, for as long as 0.8 seconds before it returned to the normal running mode.
 - If the power contactor opened and then reclosed, the compressor stalled for as long as 0.9 seconds, drawing approximately 159 Amps at 219 VAC, before it returned to the normal running mode.
- ◆ At 115 °F
 - Only stalled at 6, 9, and 12 cycle transients, drawing approximately 153 Amps at 219 VAC, for as long as 0.9 seconds before it returned to the normal running mode.
 - If the power contactor opened and then reclosed, the compressor stalled, drawing approximately 155 Amps at 219 VAC, for as long as 0.6 seconds before it returned to the normal running mode.

Air Conditioner Stalling Effects Study

Air Conditioner Test Report

14.0 APPENDIXES

14.1 APPENDIX # 1

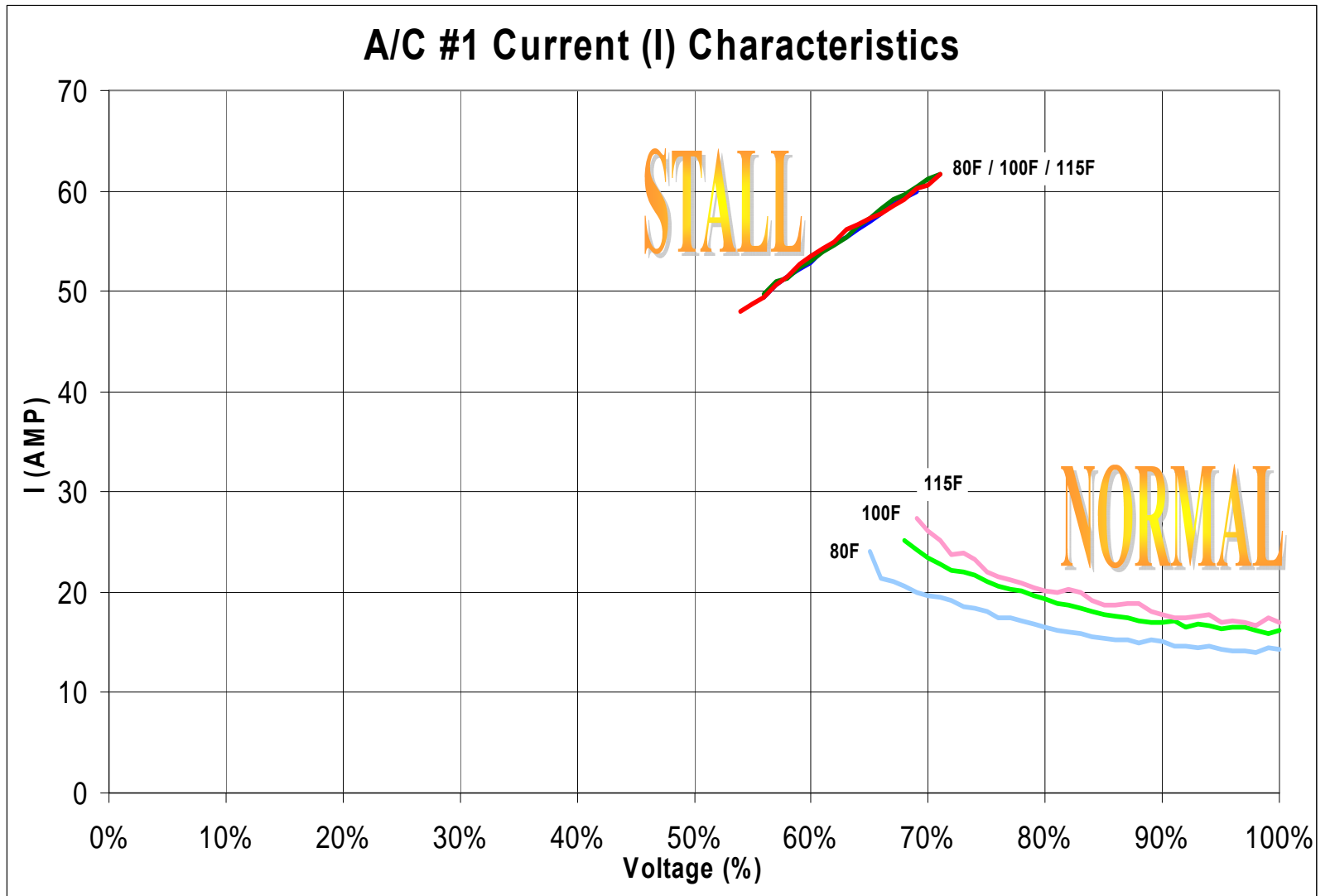
14.1.1 ATTACHMENT #1 -- AIR CONDITIONER TESTING PROCEDURES

Air Conditioner Stalling Effects Study

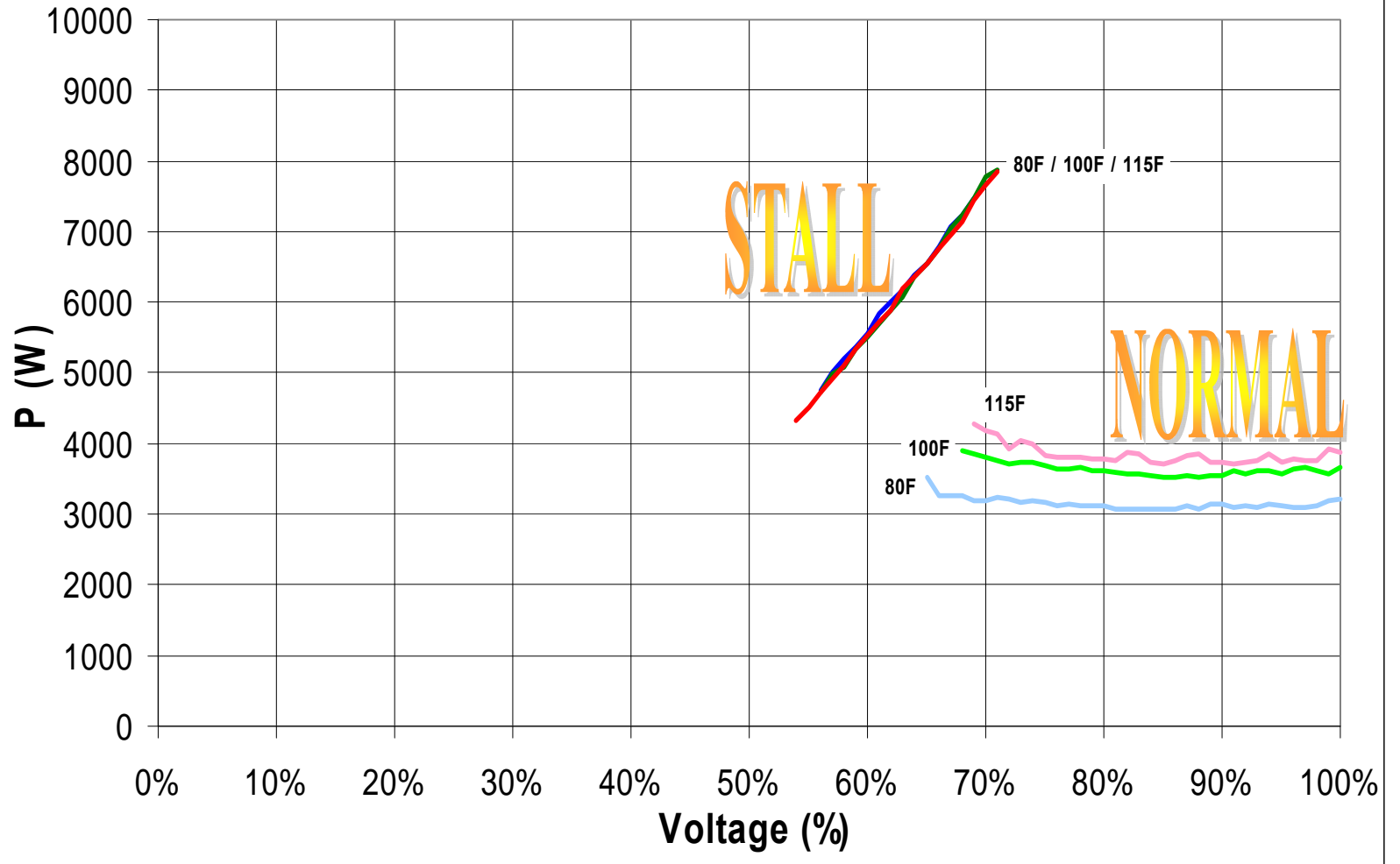
Air Conditioner Test Report

14.2 APPENDIX #2

14.2.1 AIR CONDITIONER # 1 INTERNAL PERFORMANCE PARAMETERS



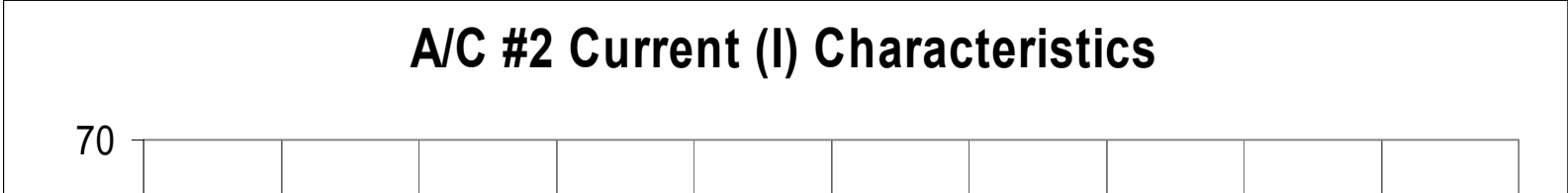
A/C #1 Real Power (P) Characteristics



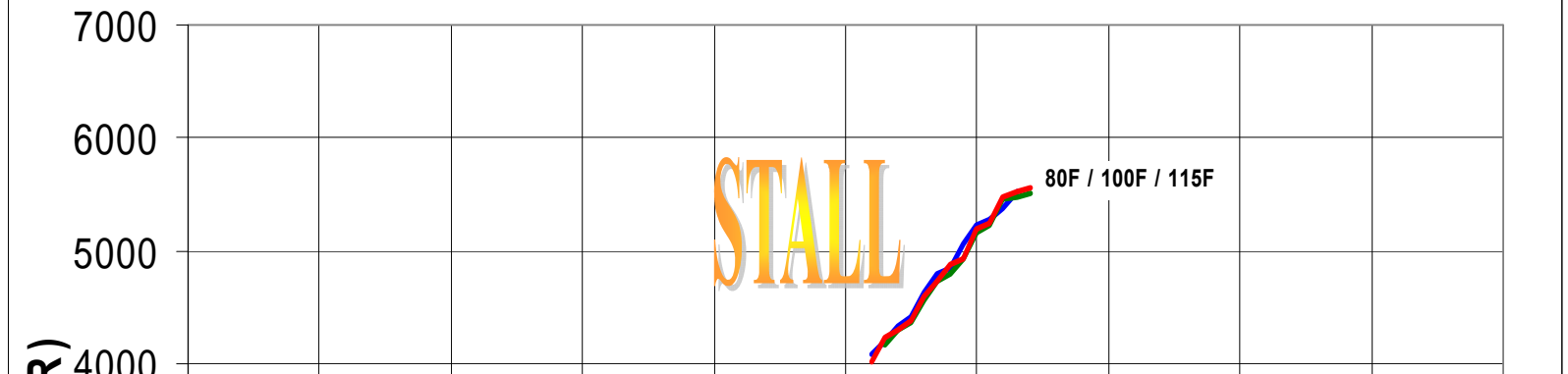
A/C #1 Reactive Power (Q) Characteristics



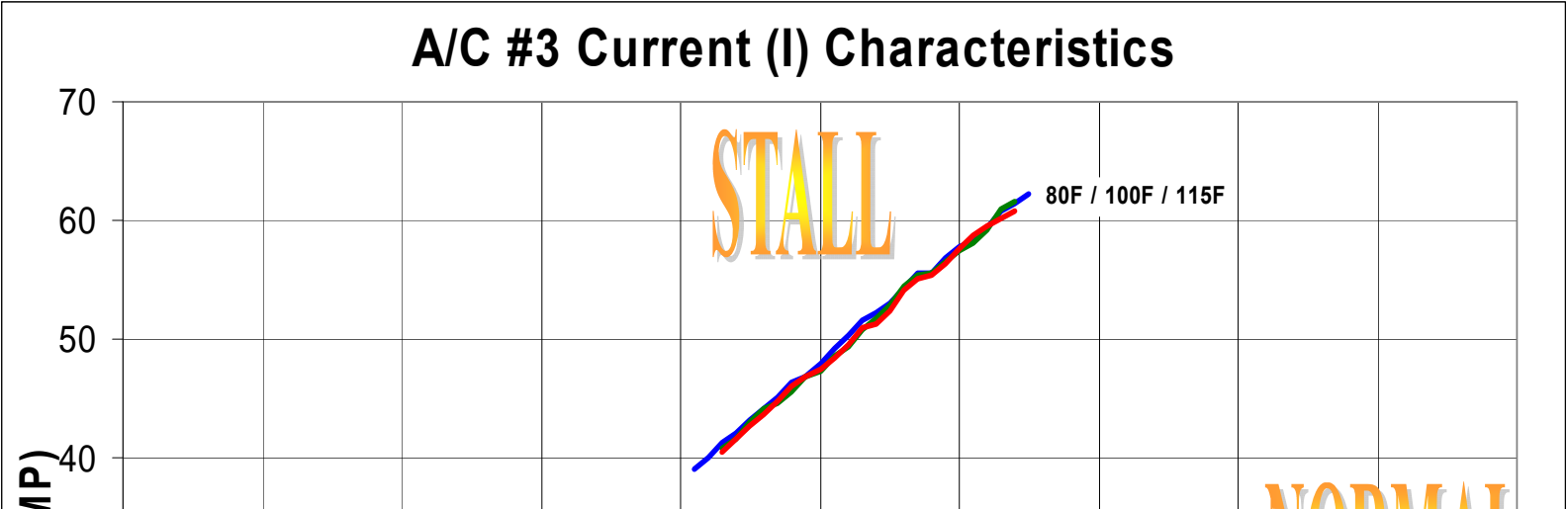
14.2.2 AIR CONDITIONER # 2 INTERNAL PERFORMANCE PARAMETERS



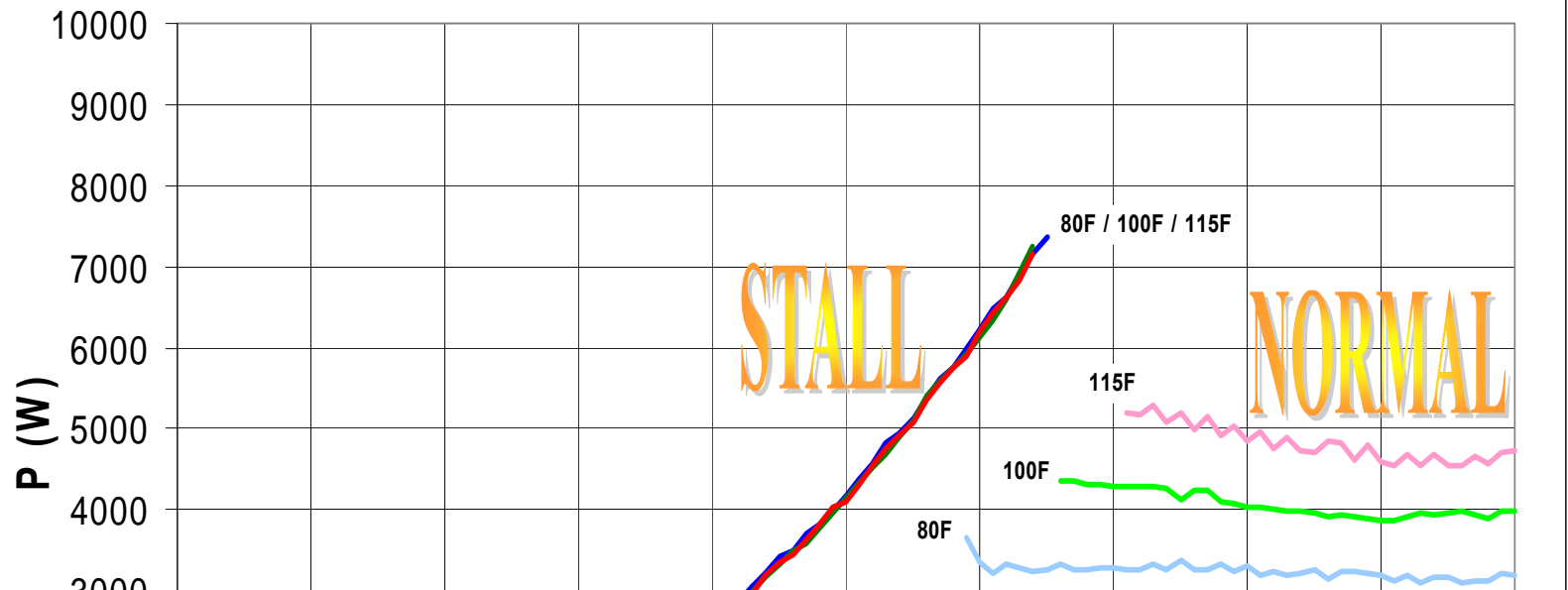
A/C #2 Reactive Power (Q) Characteristics



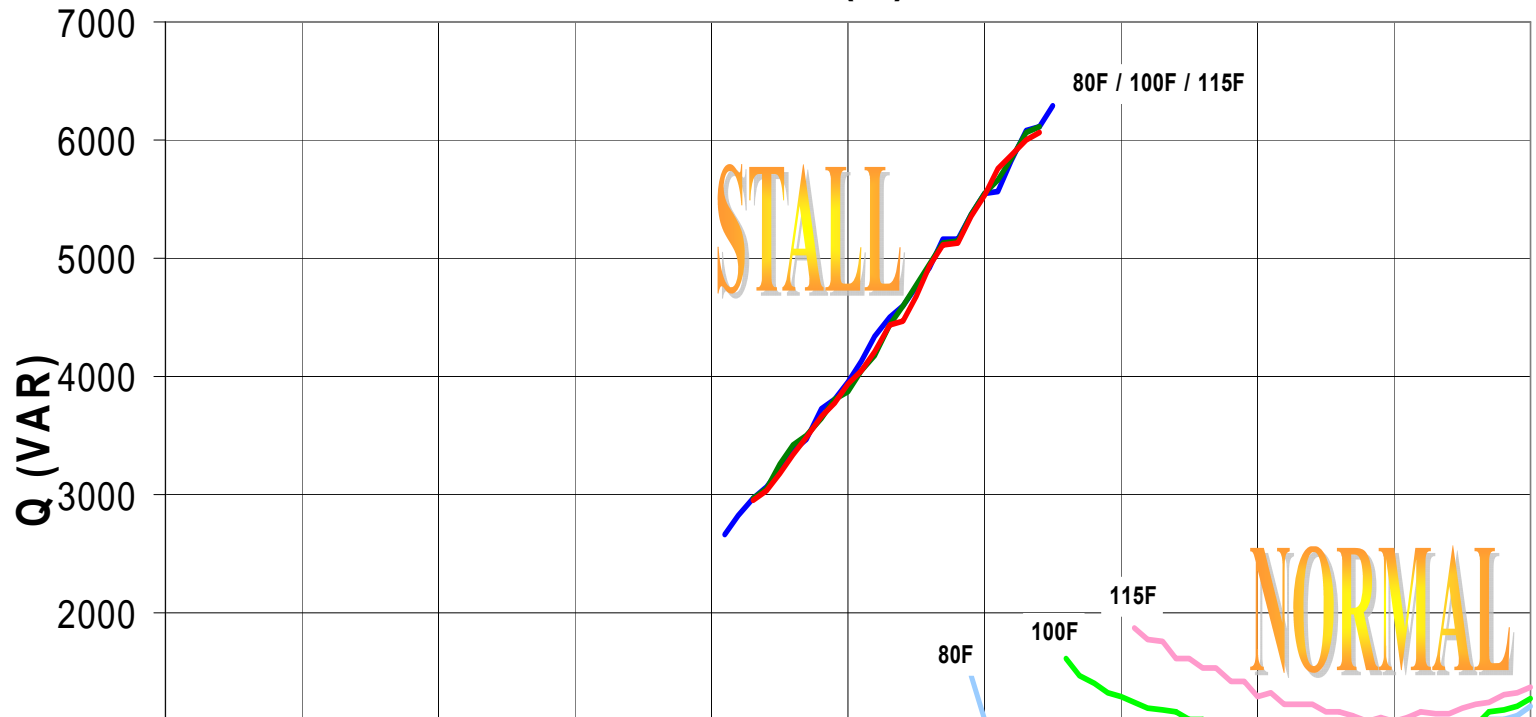
14.2.3 AIR CONDITIONER # 3 INTERNAL PERFORMANCE PARAMETERS



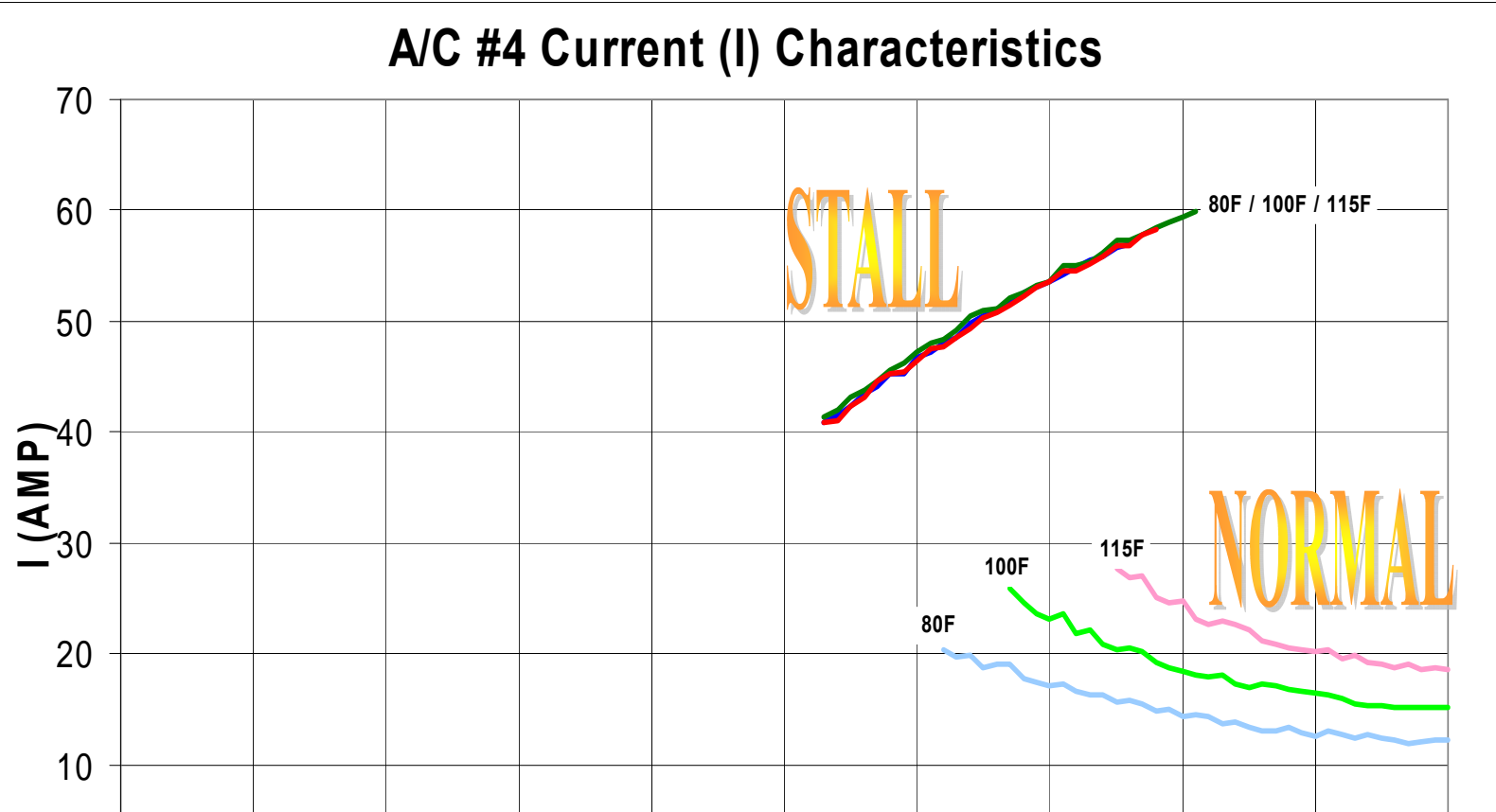
A/C #3 Real Power (P) Characteristics



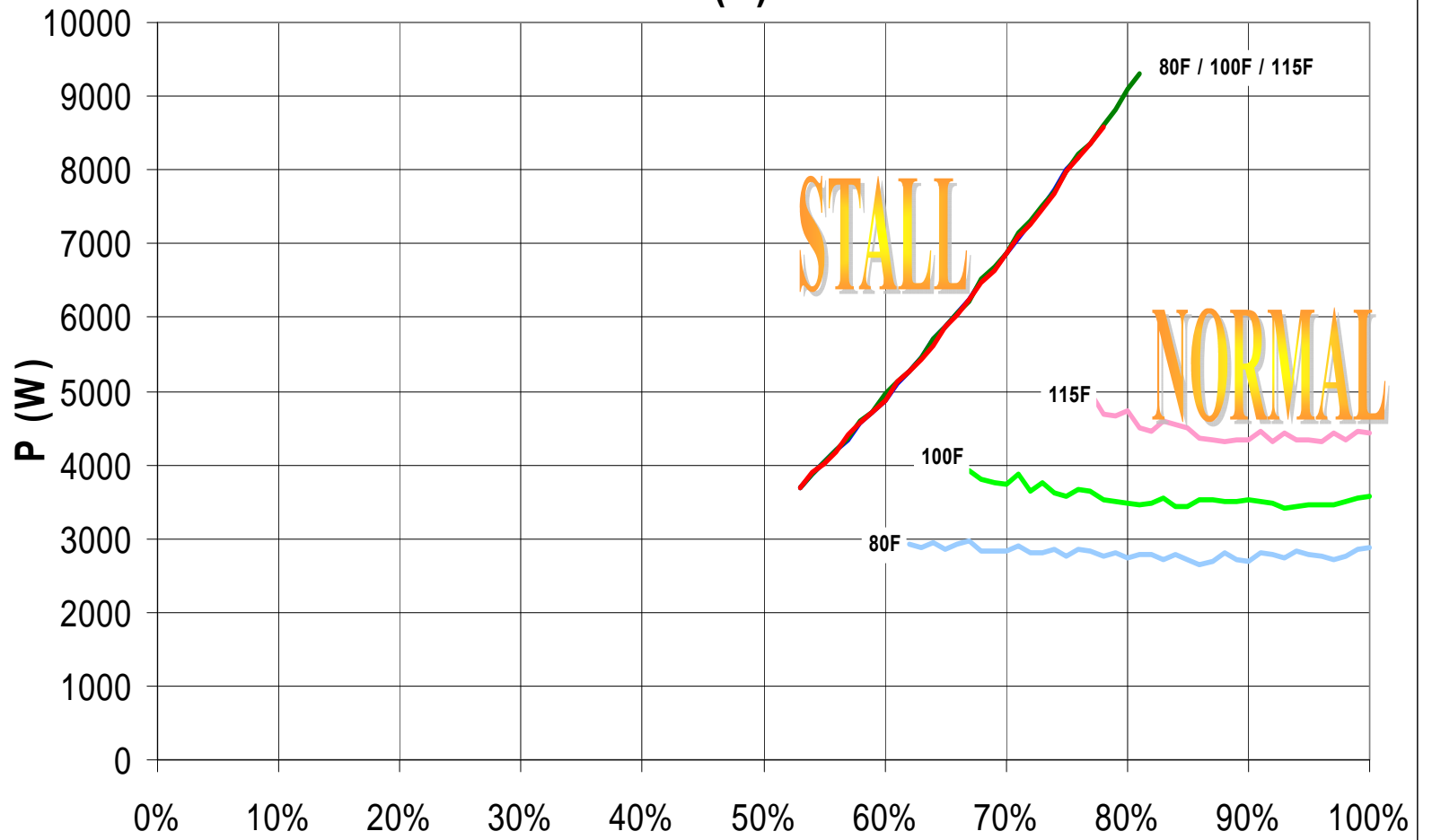
A/C #3 Reactive Power (Q) Characteristics



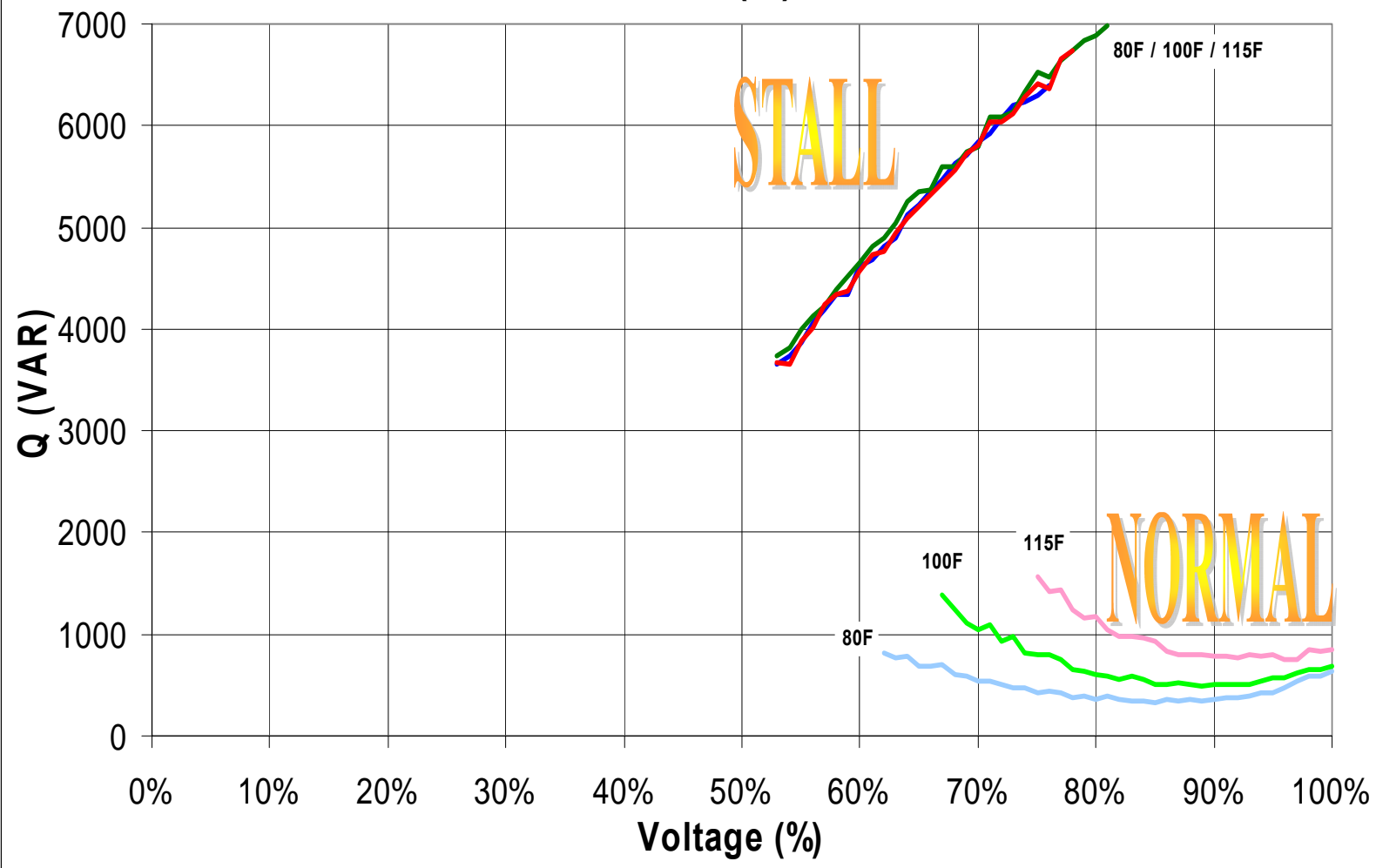
14.2.4 AIR CONDITIONER # 4 INTERNAL PERFORMANCE PARAMETERS



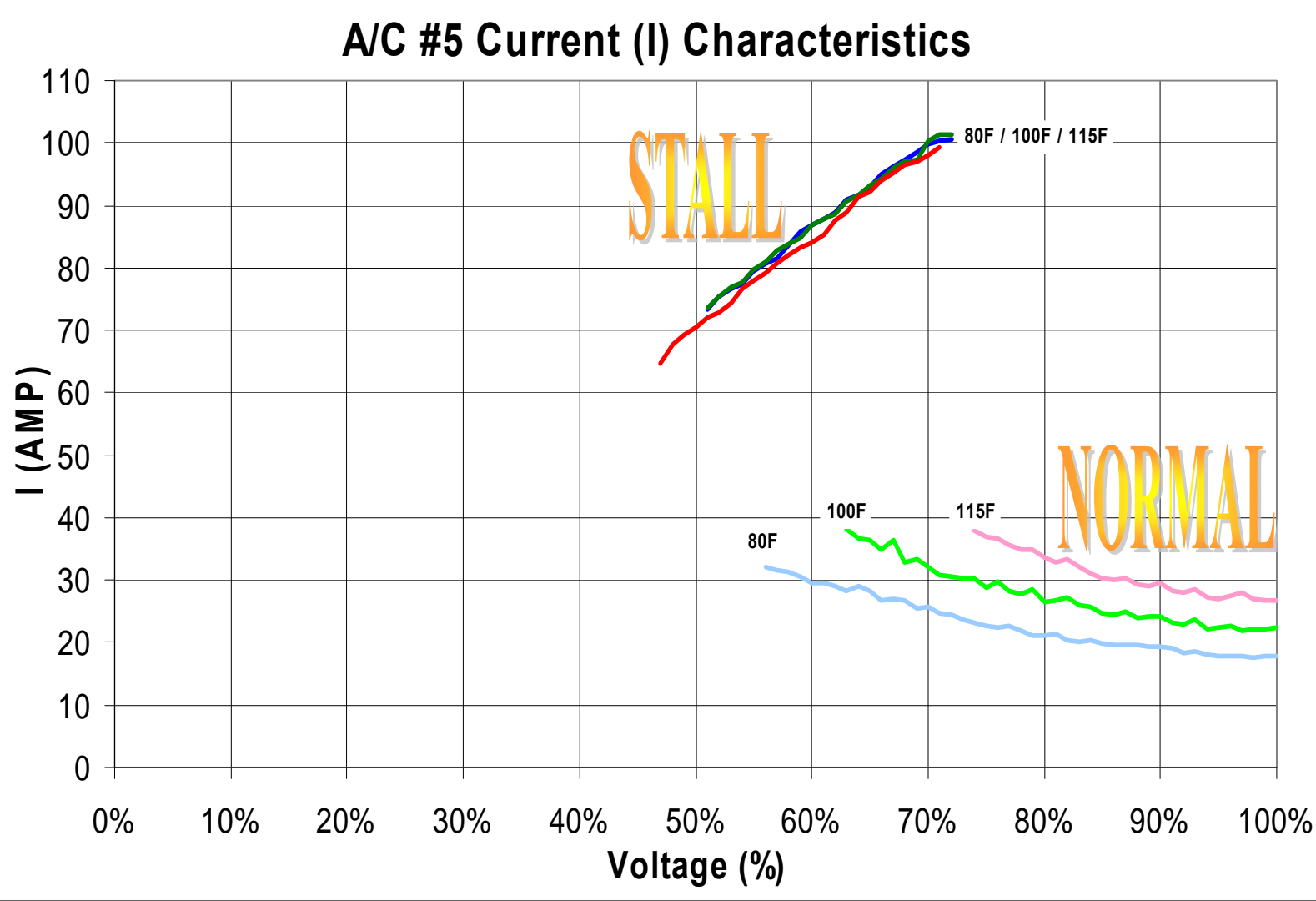
A/C #4 Real Power (P) Characteristics



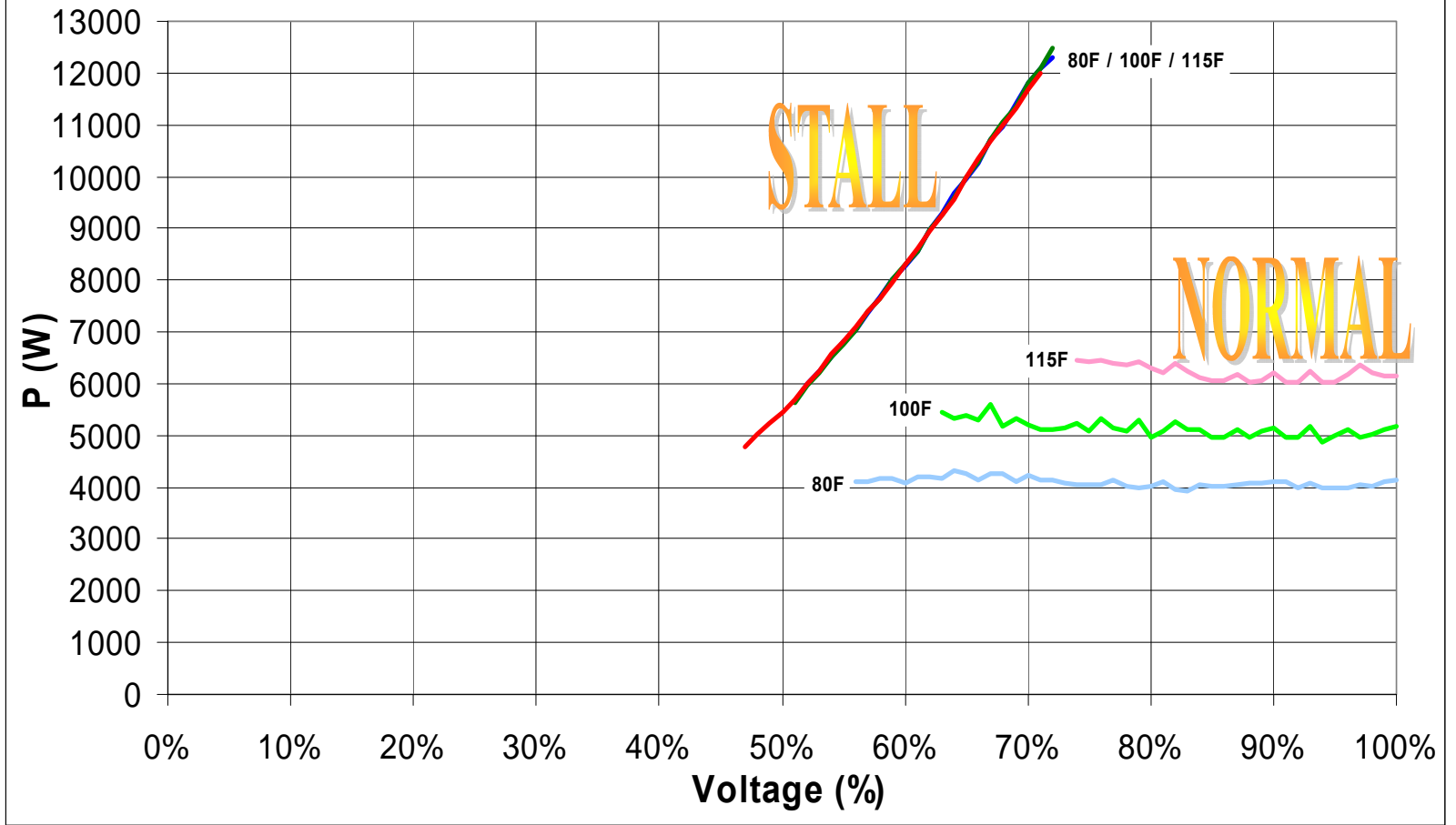
A/C #4 Reactive Power (Q) Characteristics

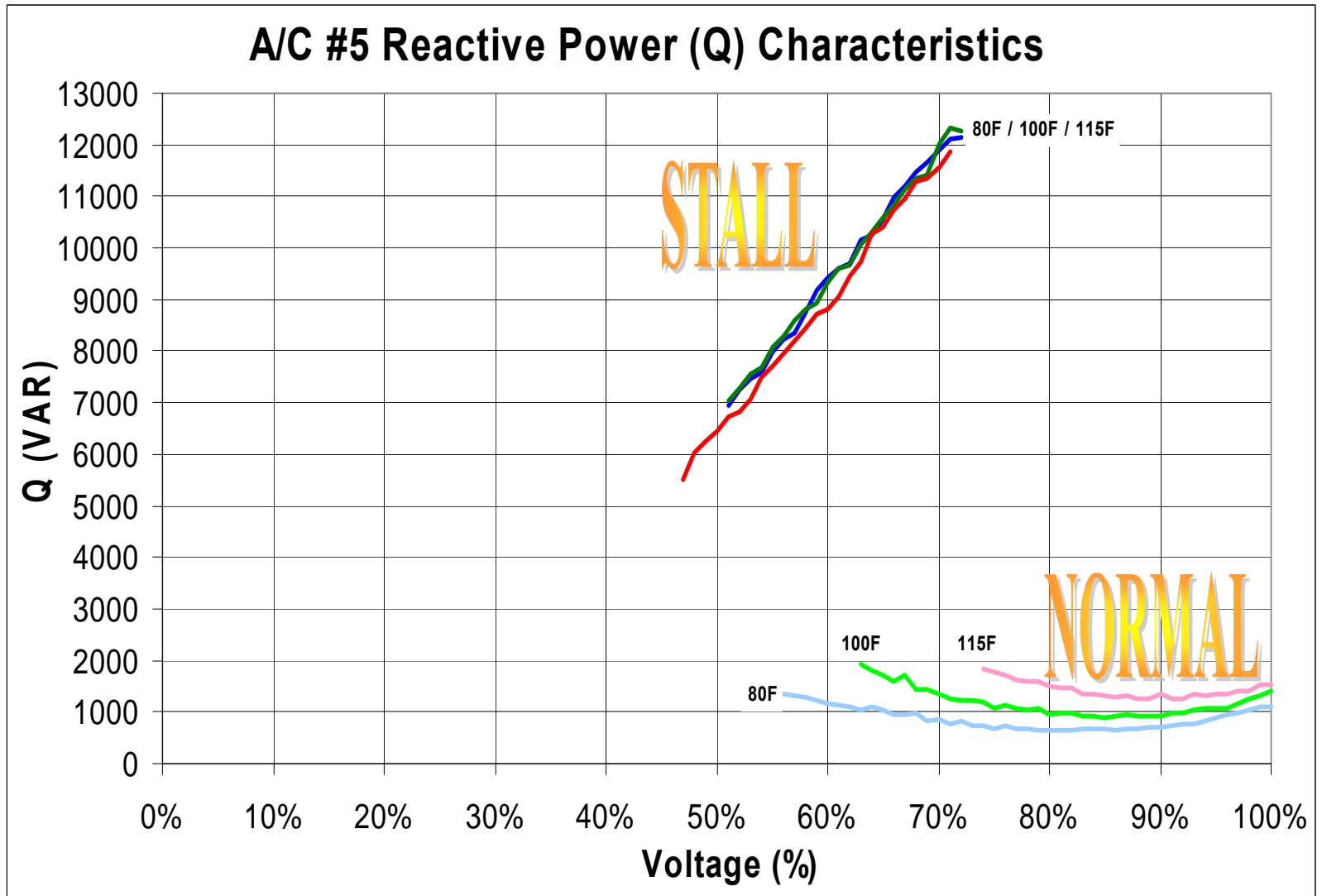


14.2.5 AIR CONDITIONER # 5 INTERNAL PERFORMANCE PARAMETERS

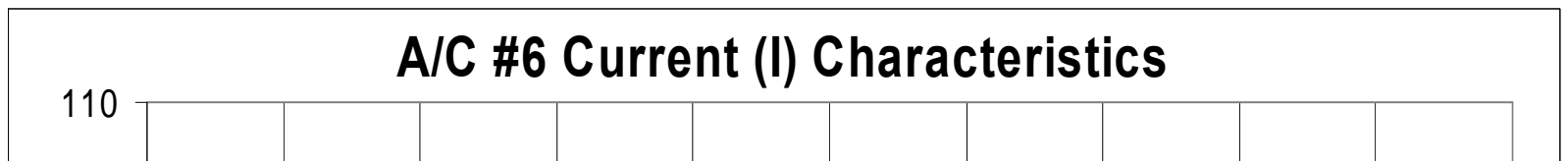


A/C #5 Real Power (P) Characteristics





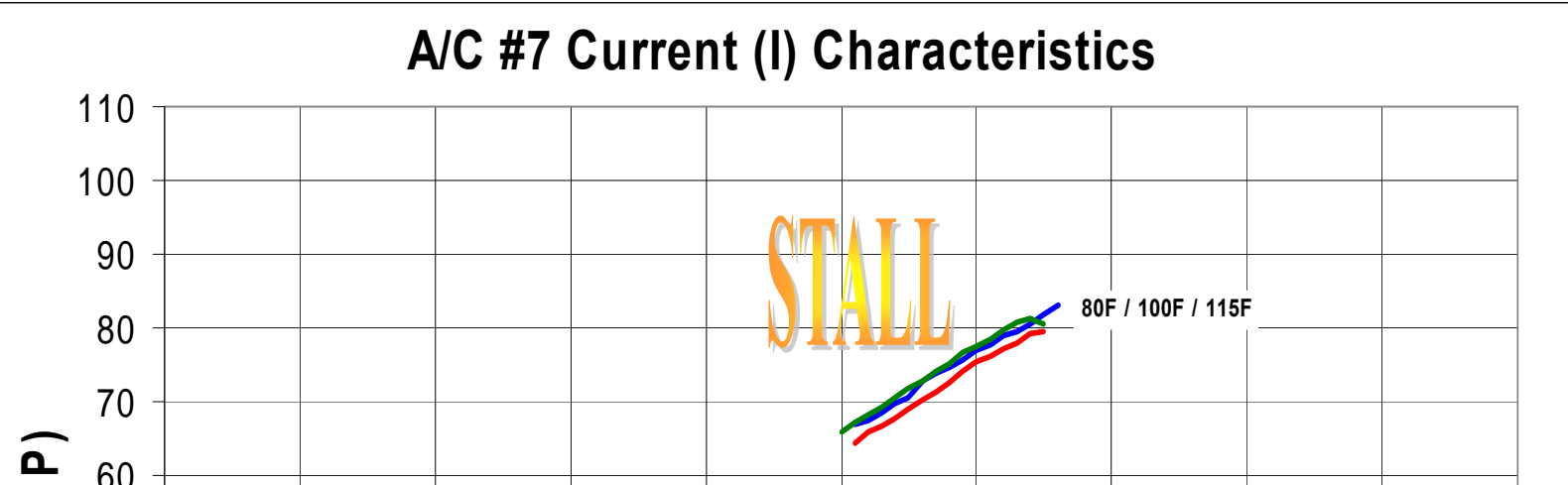
14.2.6 AIR CONDITIONER # 6 INTERNAL PERFORMANCE PARAMETERS



A/C #6 Real Power (P) Characteristics

13000										
12000										
11000								80F / 100F / 115F		

14.2.7 AIR CONDITIONER # 7 INTERNAL PERFORMANCE PARAMETERS



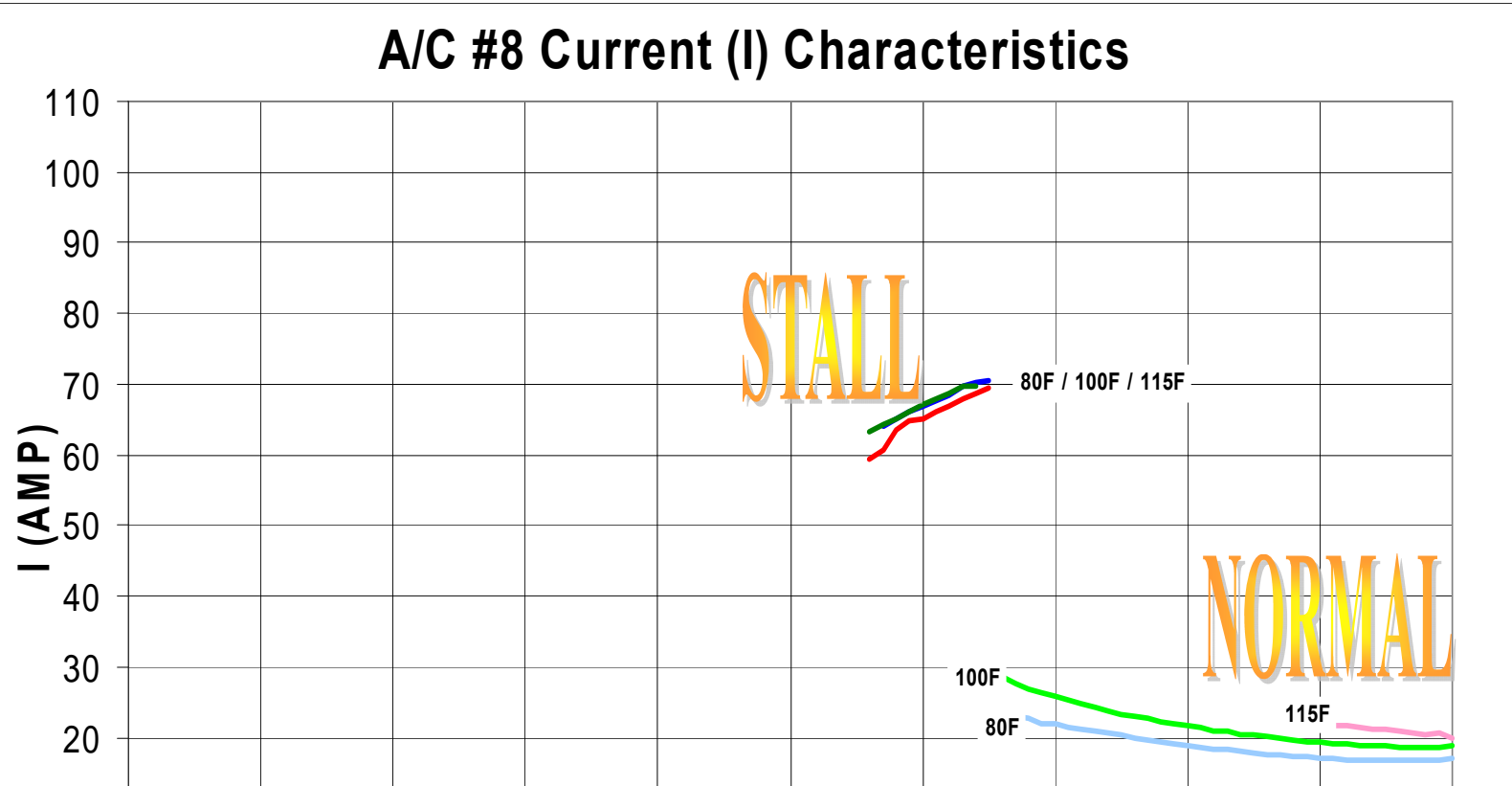
A/C #7 Real Power (P) Characteristics



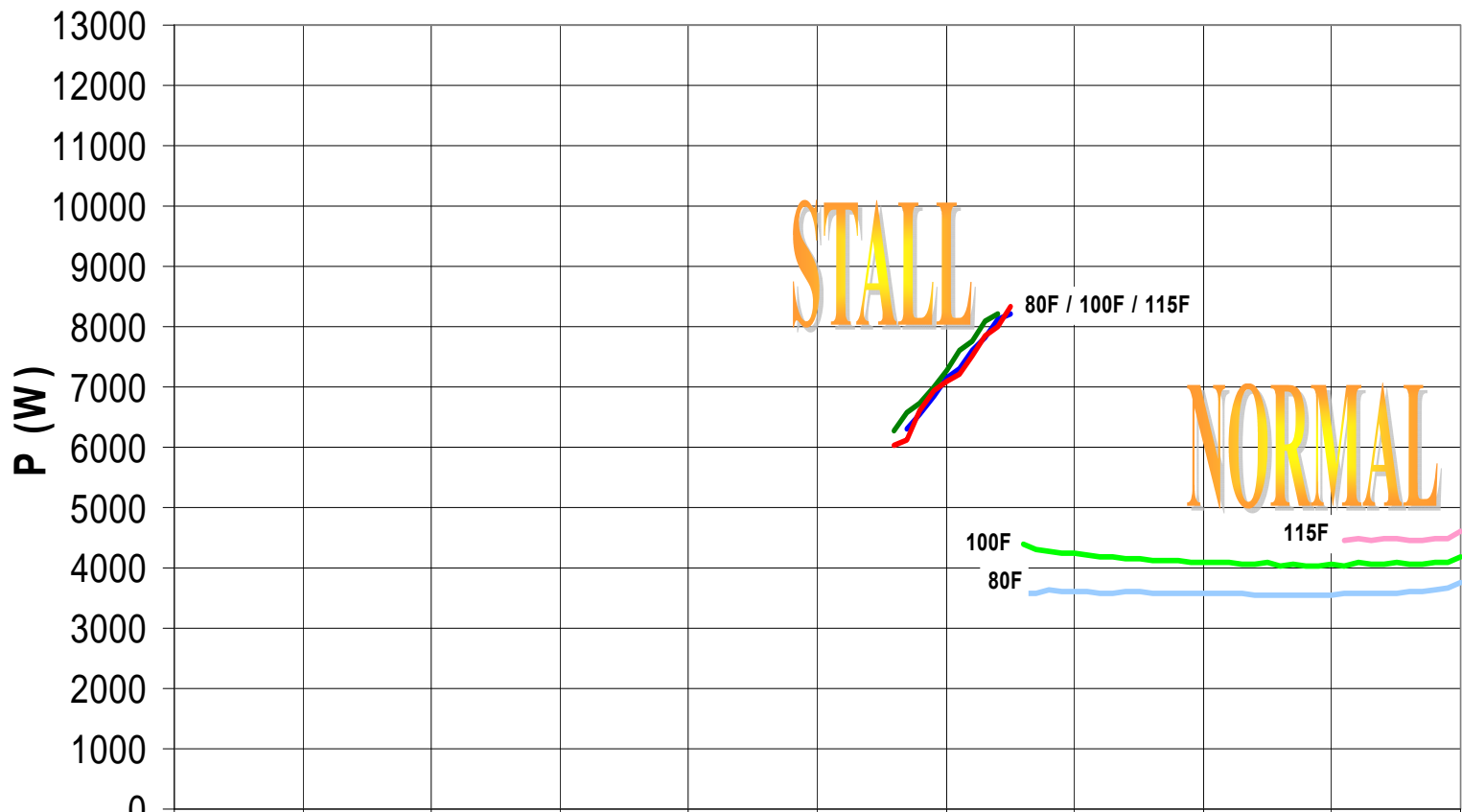
A/C #7 Reactive Power (Q) Characteristics



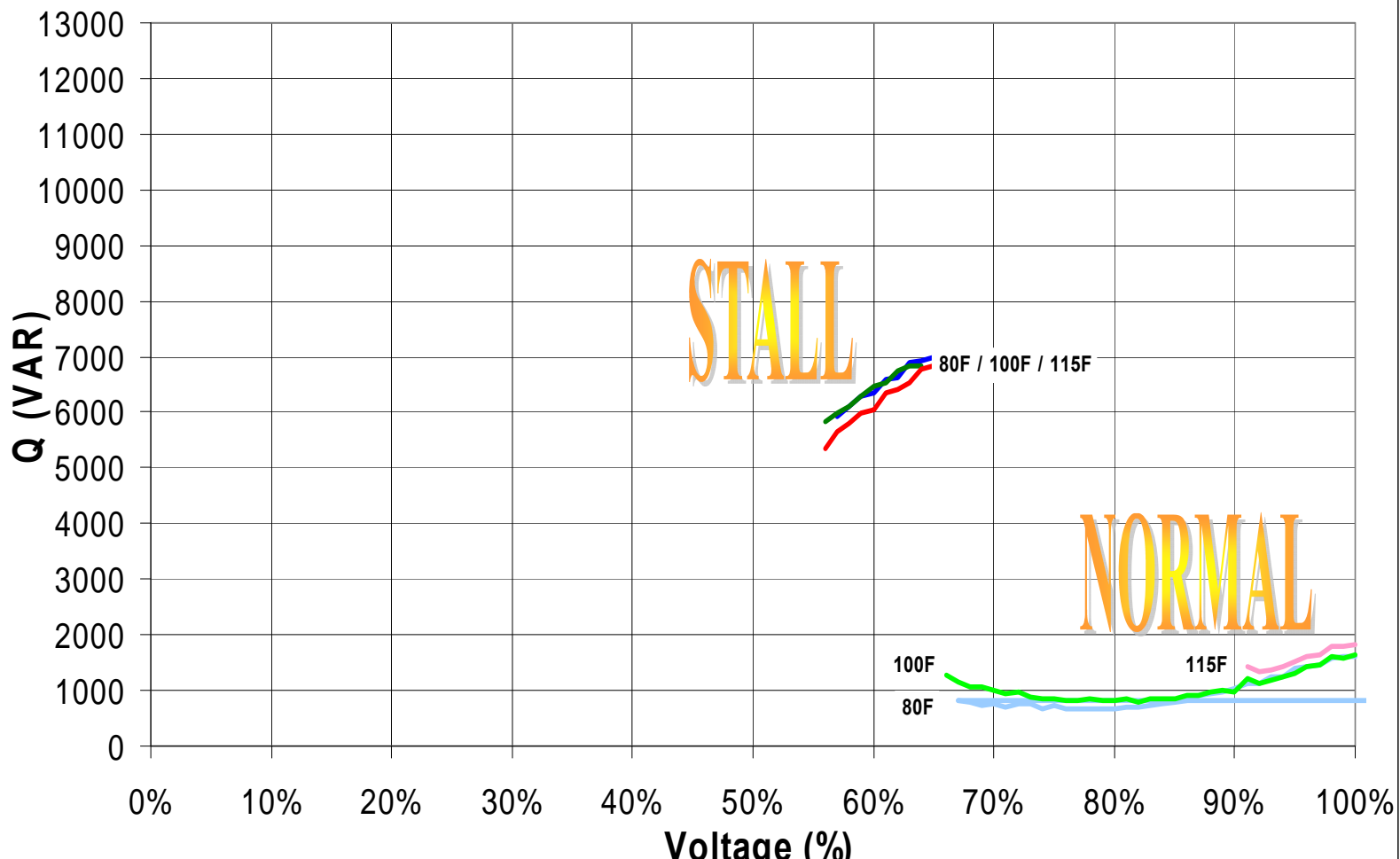
14.2.8 AIR CONDITIONER # 8 INTERNAL PERFORMANCE PARAMETERS



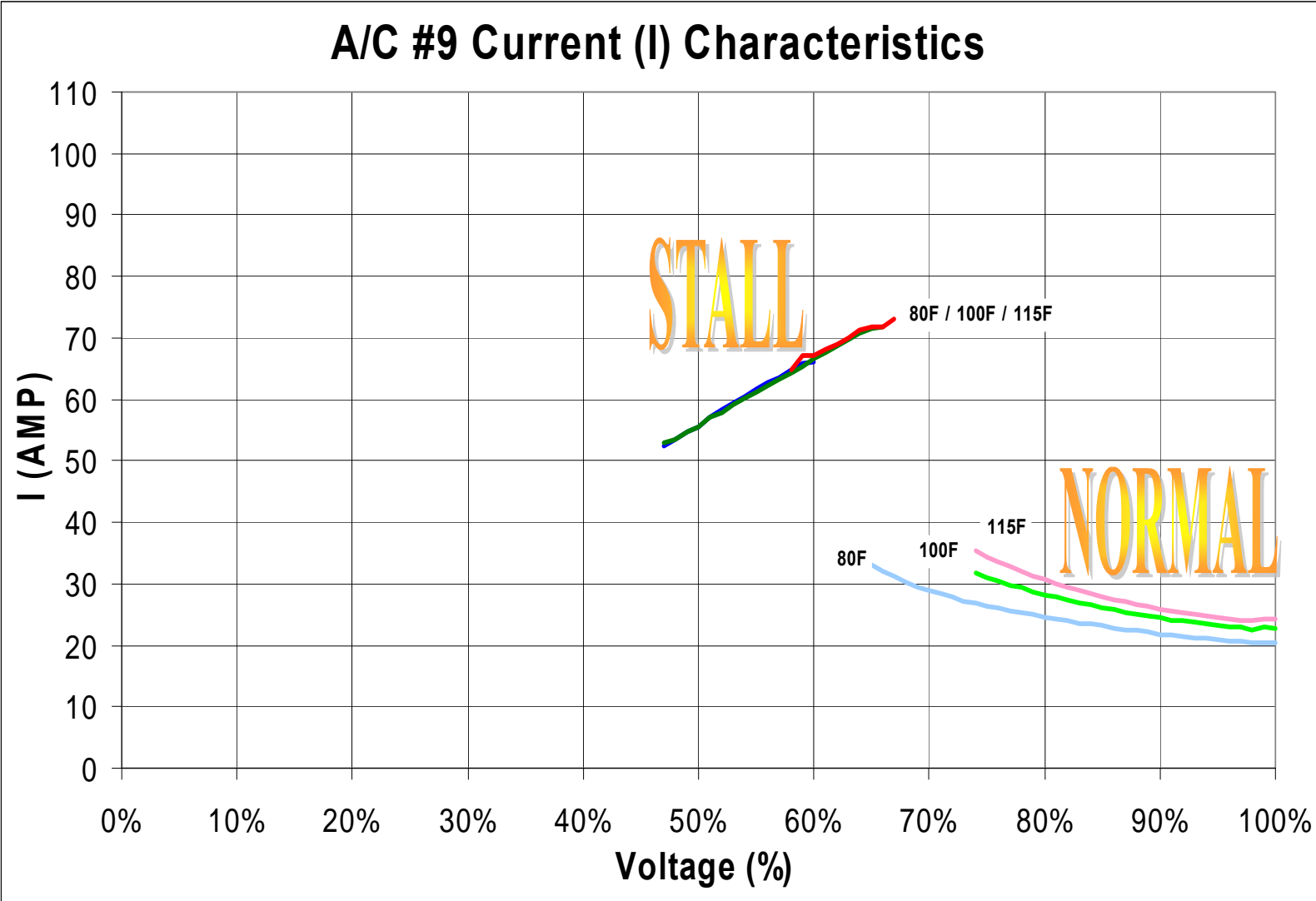
A/C #8 Real Power (P) Characteristics



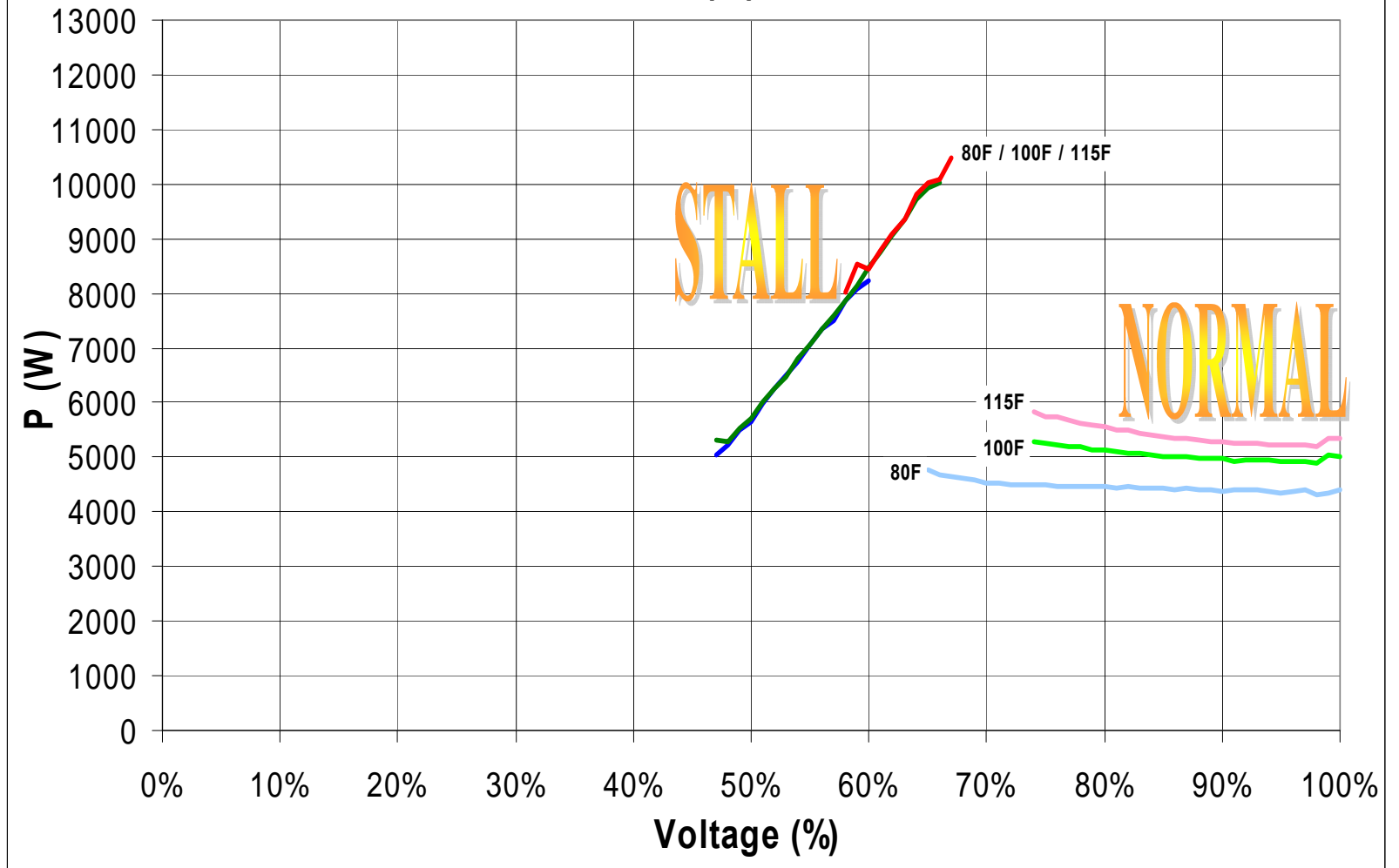
A/C #8 Reactive Power (Q) Characteristics

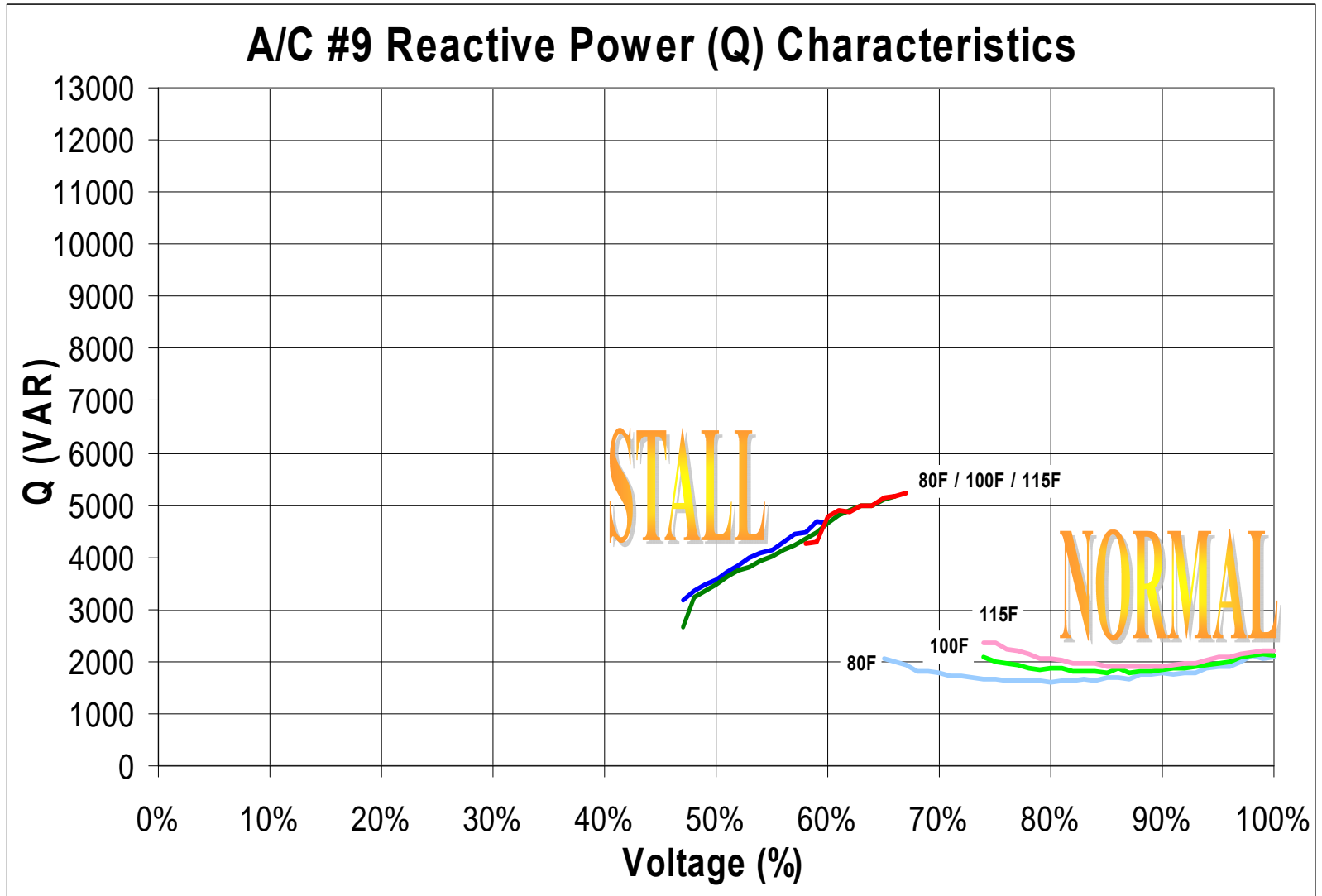


14.2.9 AIR CONDITIONER # 9 INTERNAL PERFORMANCE PARAMETERS

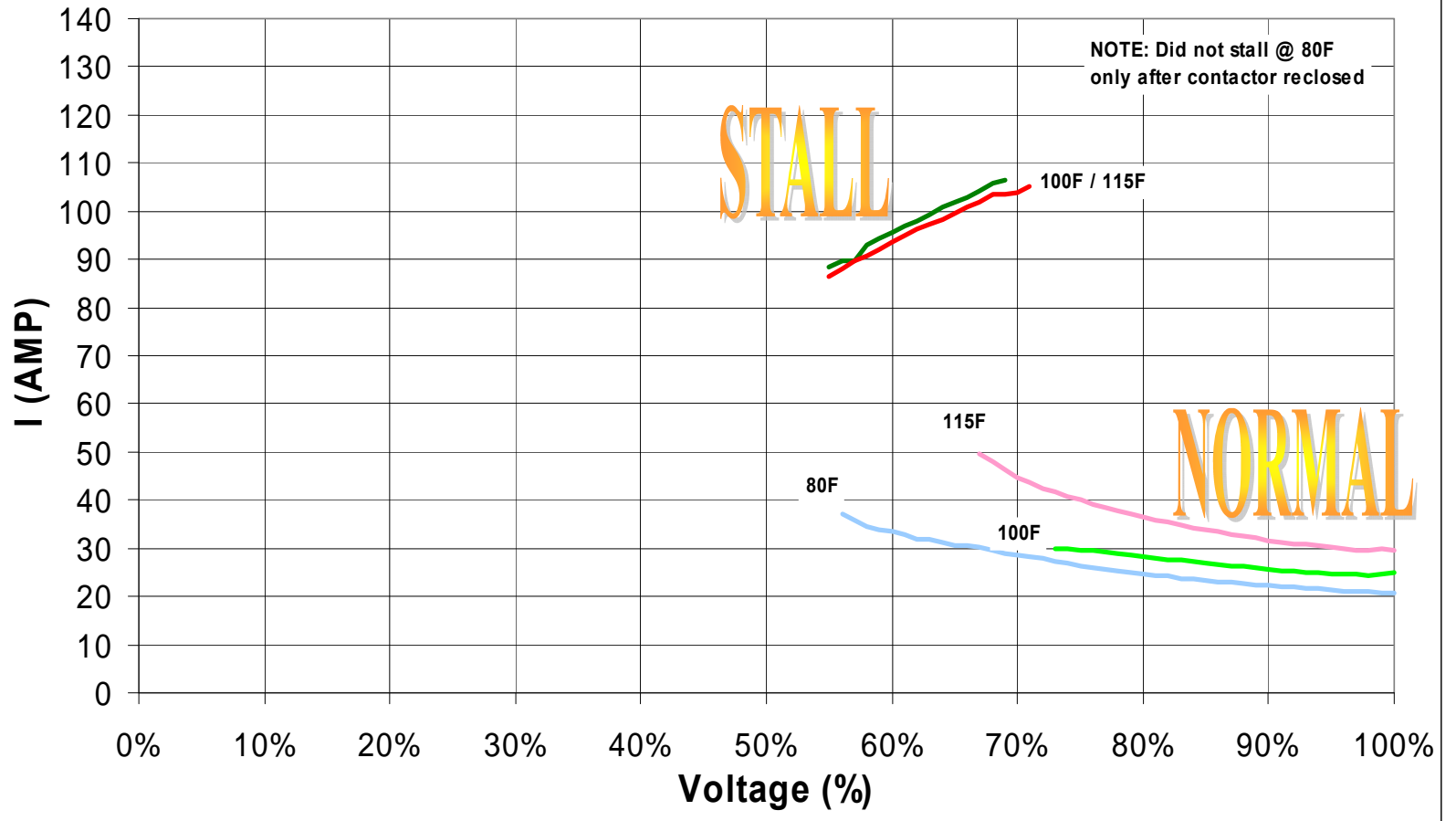


A/C #9 Real Power (P) Characteristics





A/C #10 Current (I) Characteristics



A/C #10 Real Power (P) Characteristics

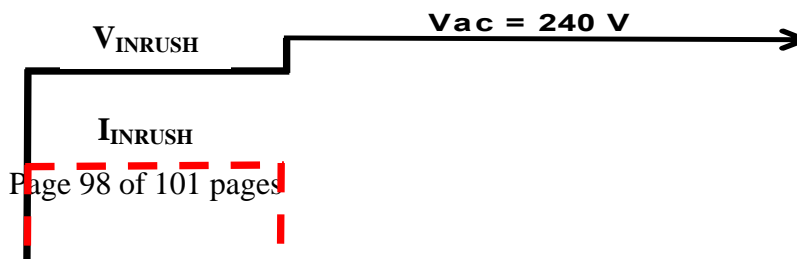


A/C #10 Reactive Power (Q) Characteristics



14.3 APPENDIX #3

14.3.1 INRUSH REFERENCE GRAPH



FINAL PROJECT REPORT

LOAD MODELING TRANSMISSION RESEARCH

APPENDIX C

PERFORMANCE MODEL EVALUATION

Prepared for CIEE By:

Lawrence Berkeley National Laboratory



A CIEE Report

Performance Model Evaluation

Pacific Northwest National Laboratory

Ning Lu and Henry Huang

April 5, 2007

The performance model has been evaluated under the following fault conditions:

- Voltage rampdown and rampup
- Voltage sags
- Voltage oscillations
- Voltage humps (over voltages)

- Frequency oscillations
- Frequency sags
- Frequency rampdown and rampup

The system diagram is shown in Figure 1.

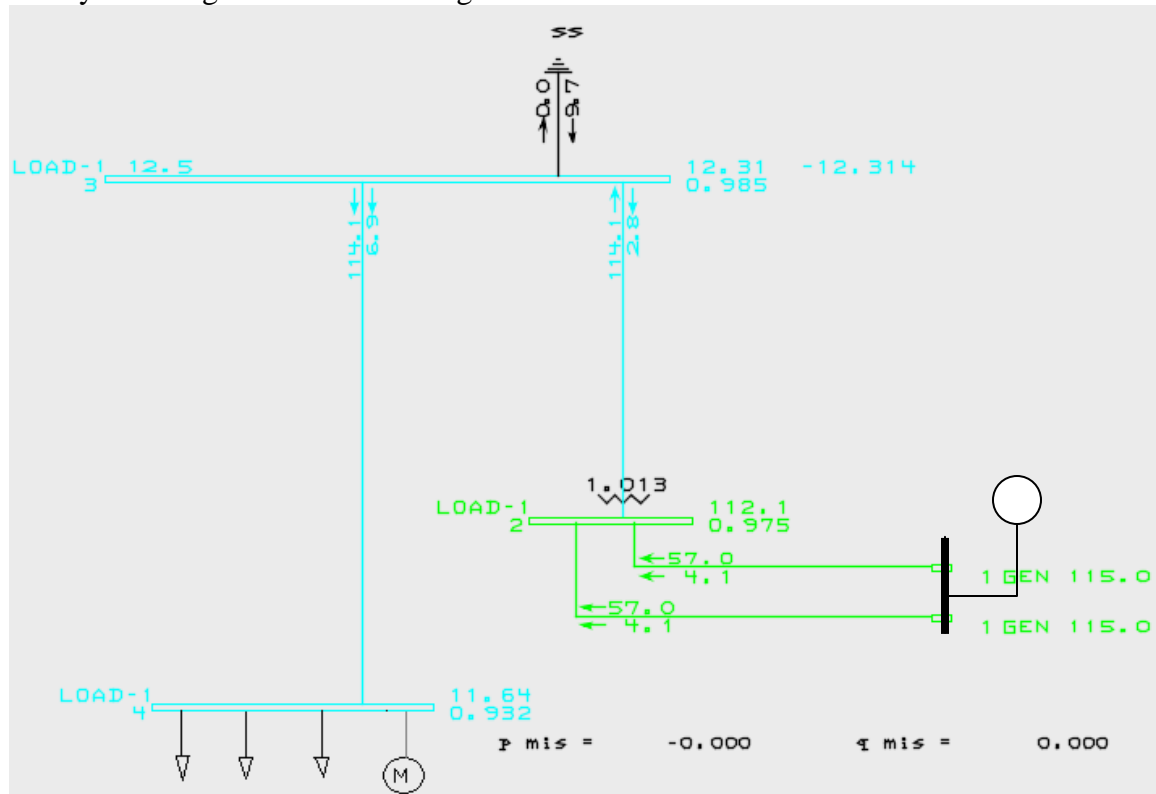


Figure 1: The system diagram of the testing system

The settings are listed in the acTestcsv.dyd. The simulations are done by replaying voltage profiles from the CSV files. The comments and the observations for the model performance are provided in this report.

Conclusions:

- 1) The performance model is numerically robust.
- 2) The model can reasonably simulate voltage recovery caused by stalling. The voltage recovery process is mainly determined by thermal relay parameters.
- 3) The model simulates the worst case scenario. The key assumption is that once the voltage is below V_{stall} , all the motors at the feeder will stall. Because of the

cascaded effect, the assumption is valid for most cases. That is, once the motors at the end of the feeder stall, it will draw huge current and bring the voltage down along the feeder. This will cause the other motors along the feeder to stall.

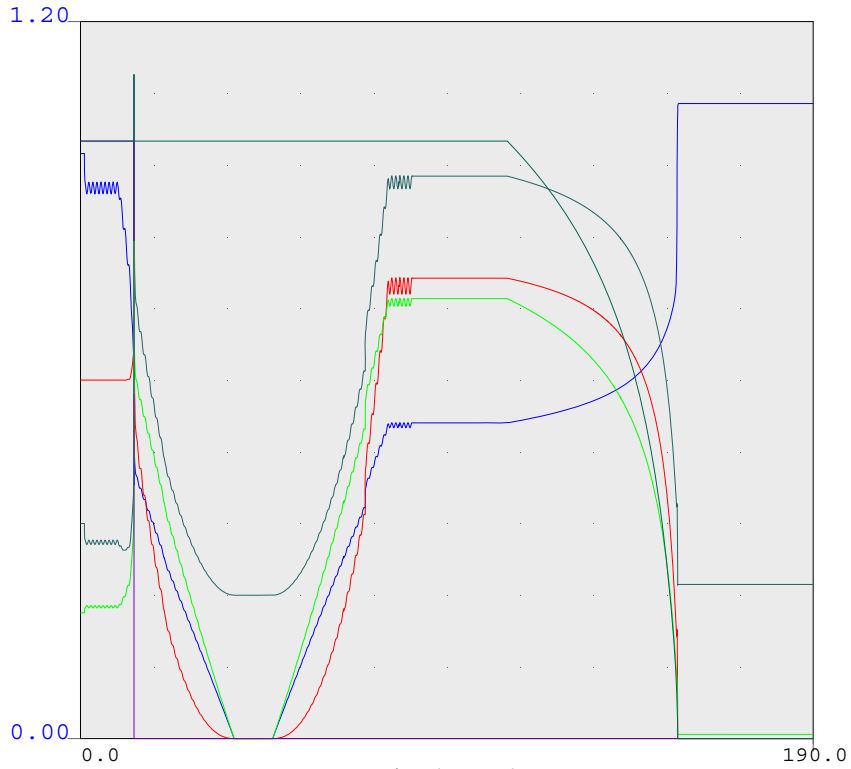
- 4) There are two potential numerical problems:
- the frequency dependency calculation. The default settings are 1.0 and -3. Unless the frequency calculation is off too much, numerically, the model will function well. However, the model will be more stable if a maximum frequency change allowed is used to cap the maximum P and Q changes.

 - the discontinuity in the running and stalling curves. So far we didn't find the model fail to function properly because of this, but it might be an issue for weak systems where instantaneous real and reactive power increases are limited by their regulating capabilities.

acTestcsv.dyd

```
#
# AC unit model tests
#
models
monit 1 "GEN " 115.0 "1" : #9 9999.00
vmeta 1 "GEN " 115.0 "1" : #9 0.0 0.0
fmeta 1 "GEN " 115.0 "1" : #9 0.0 0.0 0.050000
#
#
lodrep
#
motorw 4 "LOAD-1 " 12.5 "M1" : #9 mva=-0.85 1.0 3.58 0.177 0.02 0.56 0.3 2 0.6 99999 0 0.5 0.177 0.02 10 0.75
motorw 4 "LOAD-1 " 12.5 "M2" : #9 mva=-0.85 1.0 3.58 0.177 0.02 0.56 0.3 2 0.6 0.1 0 0.5 0.177 0.02 10 0.75
#
blwsc 4 "LOAD-1 " 12.5 "ZP" : #9 0.05 0.5 1 0.5 0 0 0 0.0 0.0 0.0 1.0 -1.0
#
#
models
#
#gencls 1 "GEN " 115.0 "1" : #9 mva=10000 5.0 0.0 0.0 0.2 0.0 0.0 0.0
#gencls 1 "GEN " 12.50 "1" : #9 mva=10000 5.0 0.0 0.0 0.2 0.0 0.0 1.0 vramp100.csv 0 0 0 0
#gencls 1 "GEN " 12.50 "1" : #9 mva=10000 5.0 0.0 0.0 0.2 0.0 0.0 1.0 vsag.csv 0 0 0 0
#gencls 1 "GEN " 12.50 "1" : #9 mva=10000 5.0 0.0 0.0 0.2 0.0 0.0 1.0 fosci59hz.csv 0 0 0 0
#gencls 1 "GEN " 12.50 "1" : #9 mva=10000 5.0 0.0 0.0 0.2 0.0 0.0 1.0 Vosci.csv 0 0 0 0
#gencls 1 "GEN " 12.50 "1" : #9 mva=10000 5.0 0.0 0.0 0.2 0.0 0.0 1.0 fsag.csv 0 0 0 0
gencls 1 "GEN " 12.50 "1" : #9 mva=10000 5.0 0.0 0.0 0.2 0.0 0.0 1.0 framp.csv 0 0 0 0
#gencls 1 "GEN " 12.50 "1" : #9 mva=10000 5.0 0.0 0.0 0.2 0.0 0.0 1.0 vsag1.csv 0 0 0 0
#
epcgen 4 "LOAD-1 " 12.5 "AC" : #9 "epcACcomp.p" 12 "rsrc" 0.0 "xsrc" 0.0 "tv" 0.016 "tf" 0.1 /
"CompLF" 1.0 "CompPF" 0.97 "Kps" 5.57 "Nps" 2.3 "Kqs" 5.2 "Nqs" 2.0 "Kp1" 0.0 "Np1" 1.0 "Kq1" 6.0 "Nq1" 2.0 "Kp2" 12.0
"Np2" 3.2 "Kq2" 11.0 "Nq2" 2.5 /
"Vstall" 0.59 "Vbrk" 0.86 "LFadj" 0.3 "Vrest" 999.0 "Prest" 0.0 "CmpKpf" 1.0 "CmpKqf" -3.3 /
"rth" 0.11 "kth" 0.08 "ith" 2.75 "tth1" 5.2 "tth2" 13 /
"vcoff" 0.0 "vcon" 0.0 "vvt" 0.75 "pcoff" 0.0
```

Voltage Ramp down and ramp up



0.0	vt	4	LOAD-1	12.5	AC	1	1.2
0.0	pac	4	LOAD-1	12.5	AC	1	80.0
-20.0	qac	4	LOAD-1	12.5	AC	1	80.0
0.0	iac	4	LOAD-1	12.5	AC	1	6.0
0.0	spd	4	LOAD-1	12.5	AC	1	1.2
0.0	gth	4	LOAD-1	12.5	AC	1	1.2

TASMO MODEL; OUTPUT GENERATED 2002-07-16 11:52:05
 SWINGBUS 1520 FOR FC-2001-1:2003-07-14:17:4F--1--1-0-0



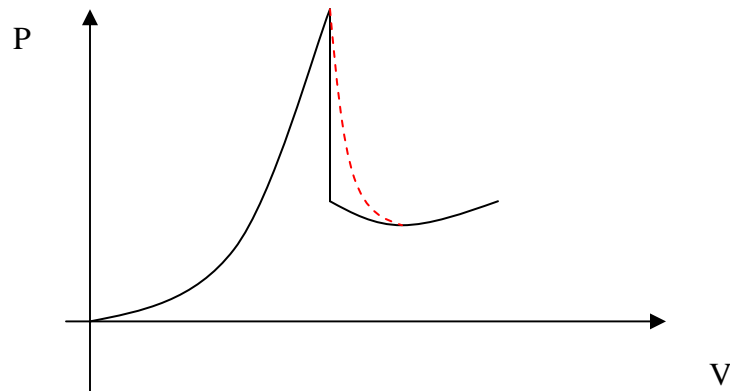
pslf.chf

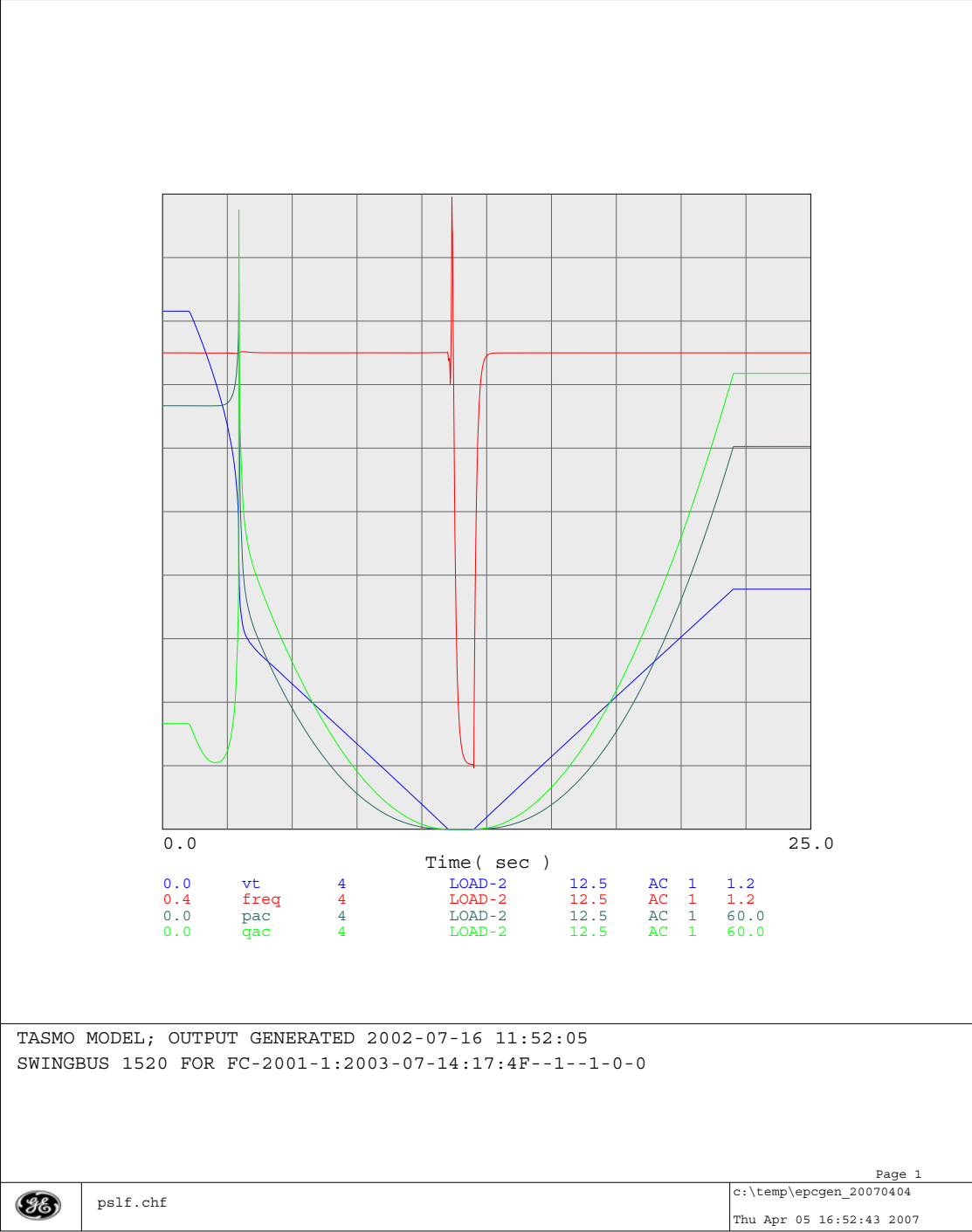
Page 1

pslf152\myps1f\ningtest01
 Tue Apr 03 17:01:22 2007

Observations:

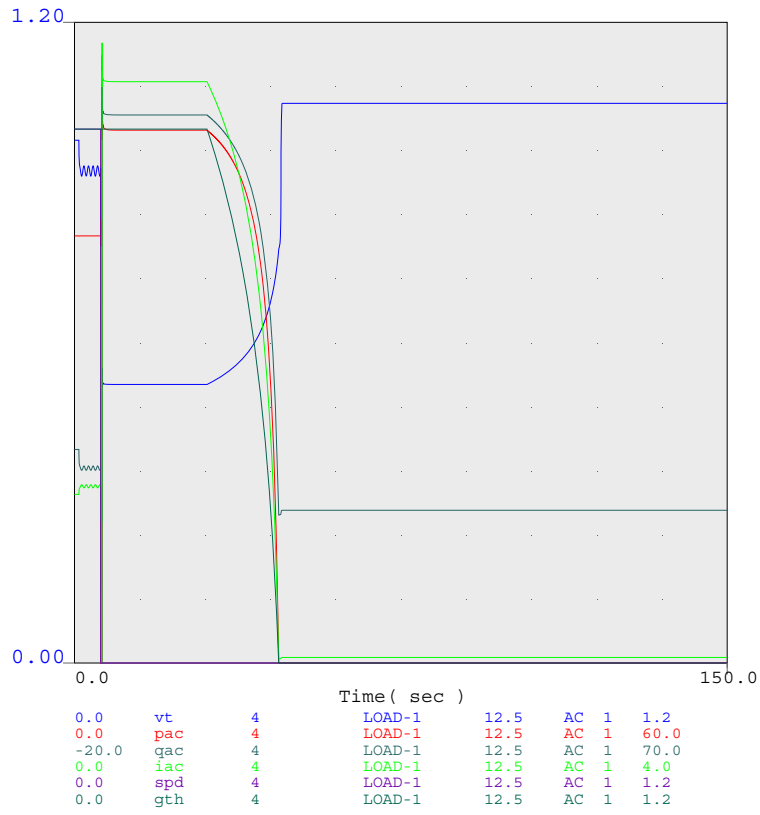
- 1) Note that the voltage profile was loaded in from a CSV file. The small voltage oscillation observed is not due to the motor initialization.
- 2) The motor stalled when voltage ramped down below 0.59V. Therefore, when generator voltage recovered, the load bus voltage remained low because of the huge current draw by the stalled compressor.
- 3) After the compressor thermal relay temperature reached Threshold 1, compressors started to be tripped offline by their thermal relays. After the thermal relay temperature reached threshold 2, all the compressors are tripped offline. Voltage then recovered to a value higher than the normal running voltage because of the capacitive loading after the trip of the compressors.
- 4) The motor model behavior is as expected.
- 5) As observed, the voltage recovery is determined by the thermal relay settings.
 - By adjusting TTH1 and TTH2, one can adjust the rate at which the motors are tripped offline.
 - The stalling threshold will be purely determined by V_{stall} . The stalling is insensitive to the fault duration for the performance model.
 - Abrupt changes of P and Q were always observed when voltage crossed the V_{stall} . This is because the switching between the running curve and stalling curve is not continuous. The discontinuity in P and Q running and stalling curves caused the jump of P and Q when the motor change states. This might not be an issue for a strong system but might be an issue for weak systems, because the P and Q will change instantaneously instead of smoothly.



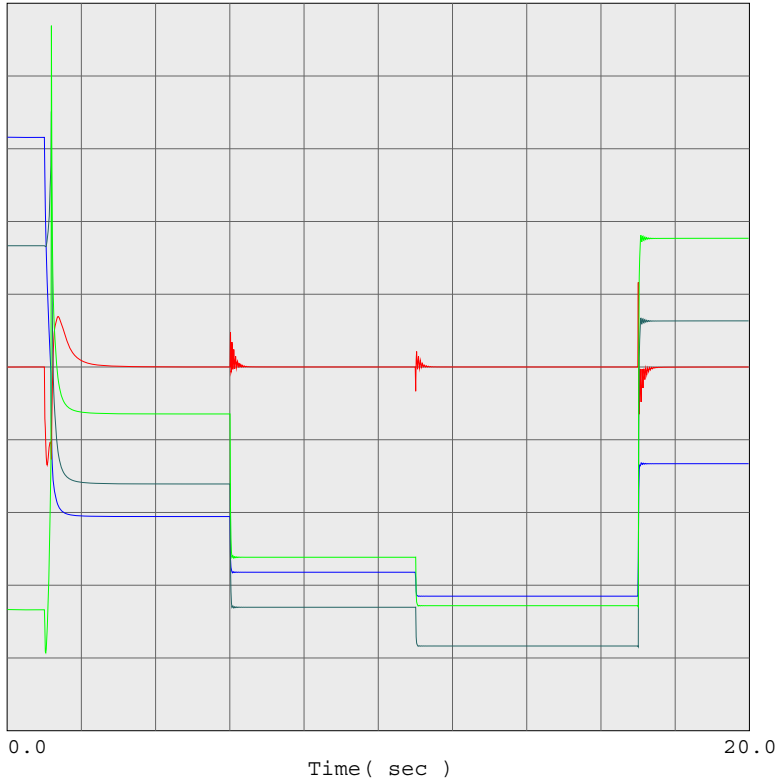


As observed, frequency calculation may have an error. To avoid possible problems, a cap might be set for a maximum power change caused by frequency change.

Voltage Sag



TASMO MODEL; OUTPUT GENERATED 2002-07-16 11:52:05
 SWINGBUS 1520 FOR FC-2001-1:2003-07-14:17:4F--1--1-0-0

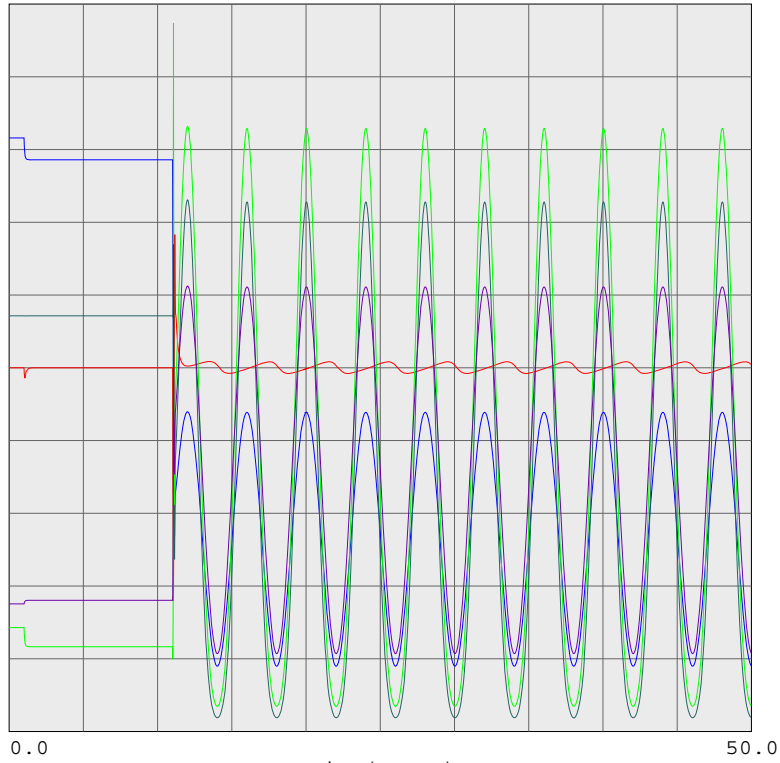


0.0	vt	4	LOAD-2	12.5	AC	1	1.2
0.99	freq	4	LOAD-2	12.5	AC	1	1.01
0.0	pac	4	LOAD-2	12.5	AC	1	60.0
0.0	qac	4	LOAD-2	12.5	AC	1	60.0

TASMO MODEL; OUTPUT GENERATED 2002-07-16 11:52:05
 SWINGBUS 1520 FOR FC-2001-1:2003-07-14:17:4F--1--1-0-0



Voltage oscillation

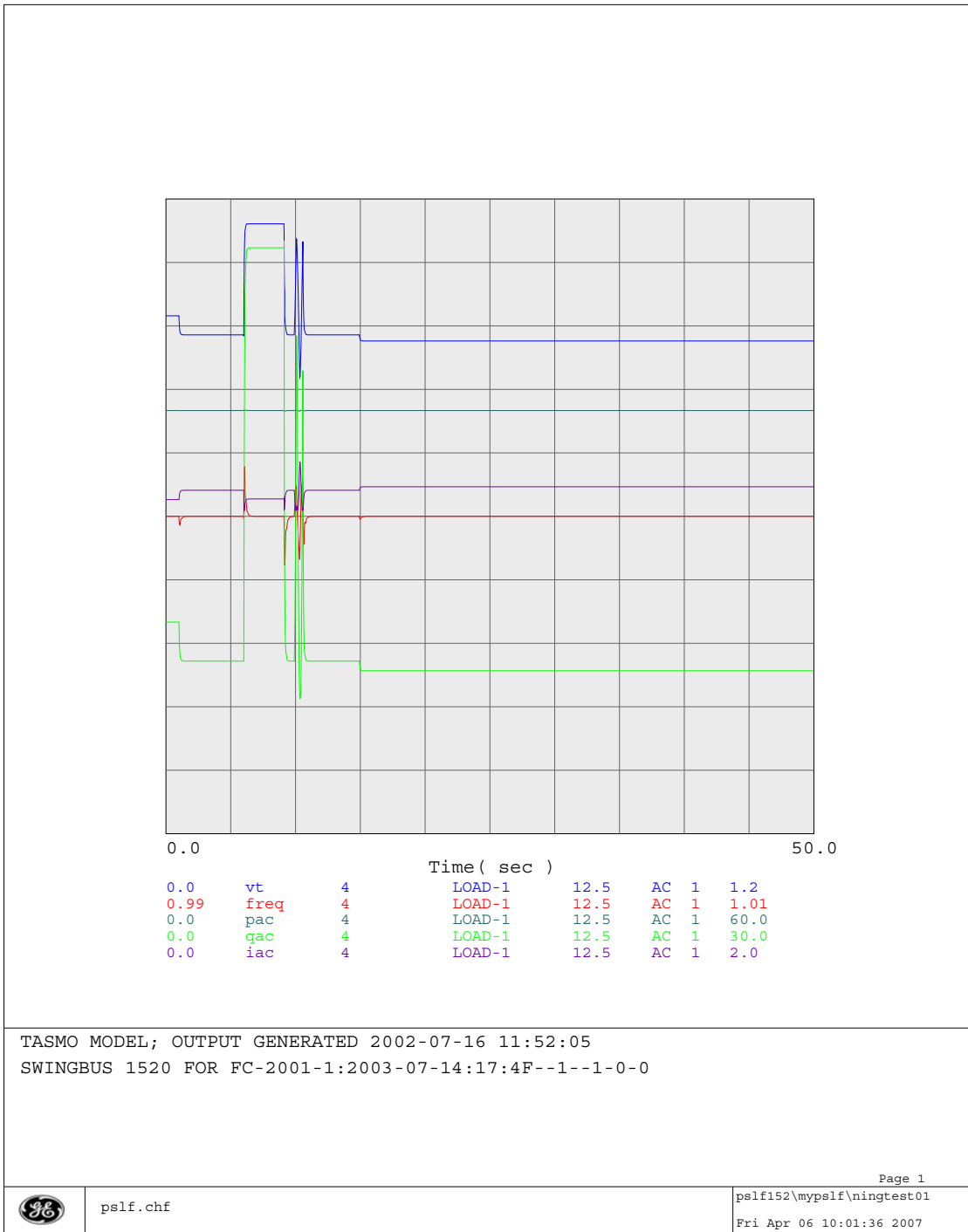


0.0	vt	4	LOAD-1	12.5	AC	1	1.2
0.99	freq	4	LOAD-1	12.5	AC	1	1.01
0.0	pac	4	LOAD-1	12.5	AC	1	70.0
0.0	qac	4	LOAD-1	12.5	AC	1	70.0
0.0	iac	4	LOAD-1	12.5	AC	1	6.0

TASMO MODEL; OUTPUT GENERATED 2002-07-16 11:52:05
 SWINGBUS 1520 FOR FC-2001-1:2003-07-14:17:4F--1--1-0-0



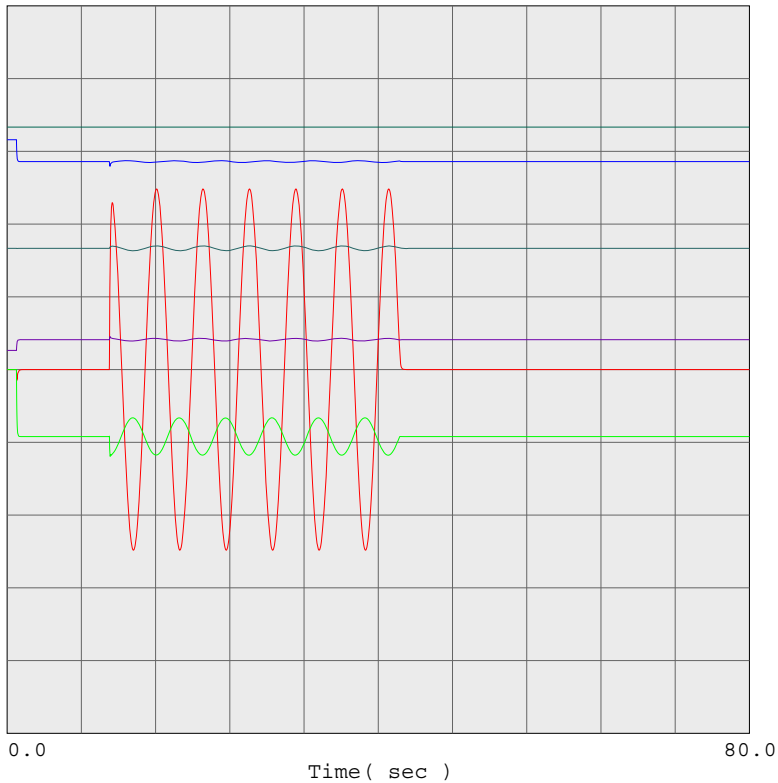
Voltage humps (simulate A/C unit over voltage behaviors)



Observations:

The default $K_{p1} = 0$, so P is insensitive to voltage humps.
 The default $K_{q1} = 6$, which caused the jump of Q.

Frequency Oscillation



0.0	vt	4	LOAD-1	12.5	AC	1	1.2
0.99	freq	4	LOAD-1	12.5	AC	1	1.01
0.0	pac	4	LOAD-1	12.5	AC	1	60.0
0.0	qac	4	LOAD-1	12.5	AC	1	20.0
0.0	iac	4	LOAD-1	12.5	AC	1	2.0
0.0	spd	4	LOAD-1	12.5	AC	1	1.2

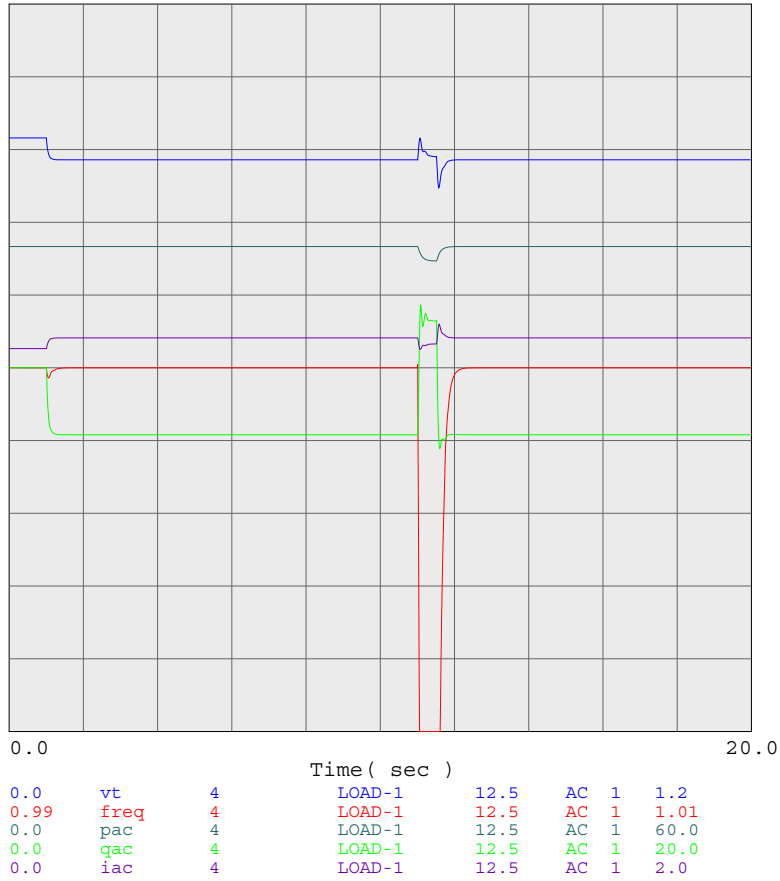
TASMO MODEL; OUTPUT GENERATED 2002-07-16 11:52:05
 SWINGBUS 1520 FOR FC-2001-1:2003-07-14:17:4F--1--1-0-0



pslf.chf

Page 1
 pslf152\mypslf\ningtest01
 Wed Apr 04 11:33:26 2007

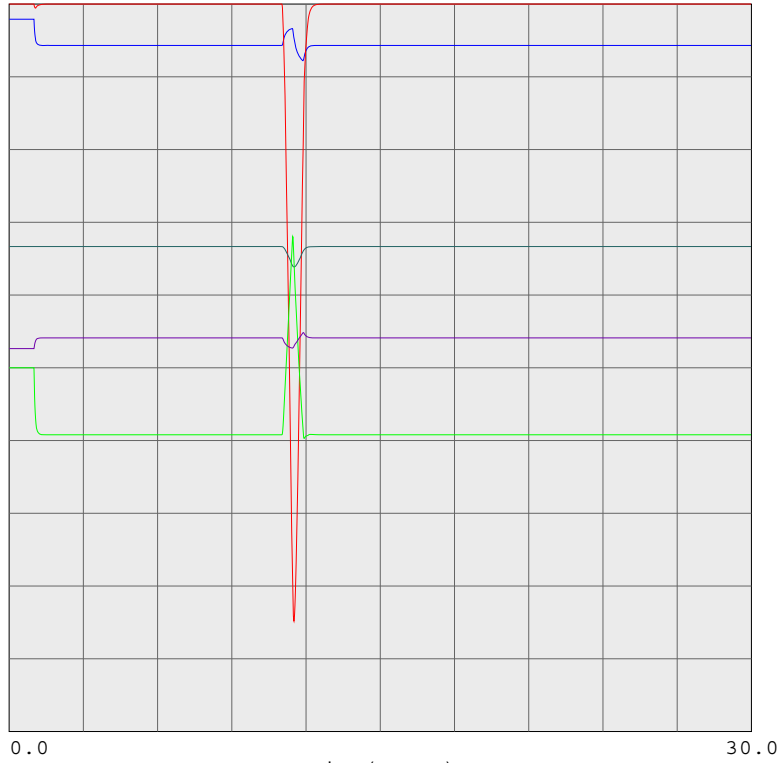
Frequency sag



TASMO MODEL; OUTPUT GENERATED 2002-07-16 11:52:05
 SWINGBUS 1520 FOR FC-2001-1:2003-07-14:17:4F--1--1-0-0



Frequency rampdown and ramp up



0.0	vt	4	LOAD-1	12.5	AC	1	1.0
0.95	freq	4	LOAD-1	12.5	AC	1	1.0
0.0	pac	4	LOAD-1	12.5	AC	1	60.0
0.0	qac	4	LOAD-1	12.5	AC	1	20.0
0.0	iac	4	LOAD-1	12.5	AC	1	2.0

TASMO MODEL; OUTPUT GENERATED 2002-07-16 11:52:05
 SWINGBUS 1520 FOR FC-2001-1:2003-07-14:17:4F--1--1-0-0



APPENDIX

WECC Air Conditioner Load Model Performance Model Specifications

Prepared by
Ning Lu and Henry Huang
Jan. 01, 2007

1. Overall Specifications

The overall structure of the air conditioner performance model is shown in Figure 1. The PV and QV curves are shown in Figure 2.

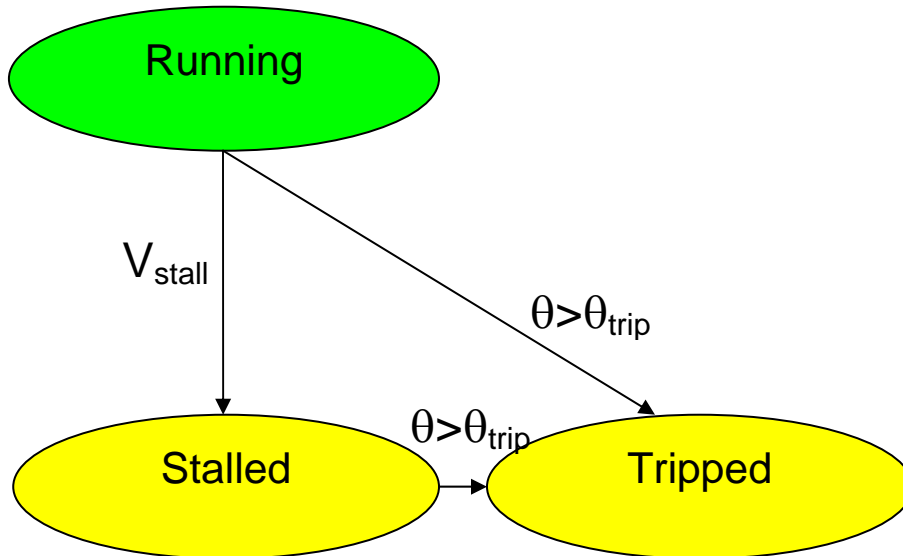


Figure1: The states of the a/c motor model

Static Load Model equations:

Running:

$$P_{run} = a_1 + \frac{a_2}{V - a_0} + a_3(V - a_0) + a_4(V - a_0)^4$$

$$Q_{run} = b_1 + \frac{b_2}{V - b_0} + b_3(V - b_0) + b_4(V - b_0)^4$$

Stalling:

$$P_{stall} = K_{p1}V^3 + K_{p2}V^2$$

$$Q_{stall} = K_{q1}V^3 + K_{q2}V^2$$

Temperature for each parameters a and b in the above equations of P_{run} , Q_{run} , P_{stall} and Q_{stall} :

$$a(T) = c_2T^2 + c_1T + c_0$$

$$b(T) = d_2T^2 + d_1T + d_0$$

2) For each a/c motor performance load model, input data will be:

- Location – bus number, (name, kV), load ID.
- MVA=xxx – feeder & xfmr MVA base.
- Temperature/Loading factor.
- Flag – indicating if the motor is in service.
- Thermal relay parameters.
- Static load parameters,
 - If not considering temperature or loading condition: $a_0 \sim a_4$, $b_0 \sim b_4$, K_{p1} , K_{p2} , K_{q1} , K_{q2} .
 - If considering temperature or loading condition: $c_0 \sim c_2$, $d_0 \sim d_2$, K_{p1} , K_{p2} , K_{q1} , K_{q2} .

3) Output variables will be:

- Real and Reactive Power
 - P– Total MW at system bus
 - Q– Total MVar at system bus
- Motor State
 - Motor stalled
 - Motor in operation
 - Motor not in service

4) Initialization process: determine parameters a and b if considering temperature.

5) Calculations during normal running:

Check voltage for stalling and switch the motor state from RUNNING to STALLED if voltage is below V_{stall} .

Check thermal relay temperature and switch the motor state from RUNNING/STALLED to TRIPPED.

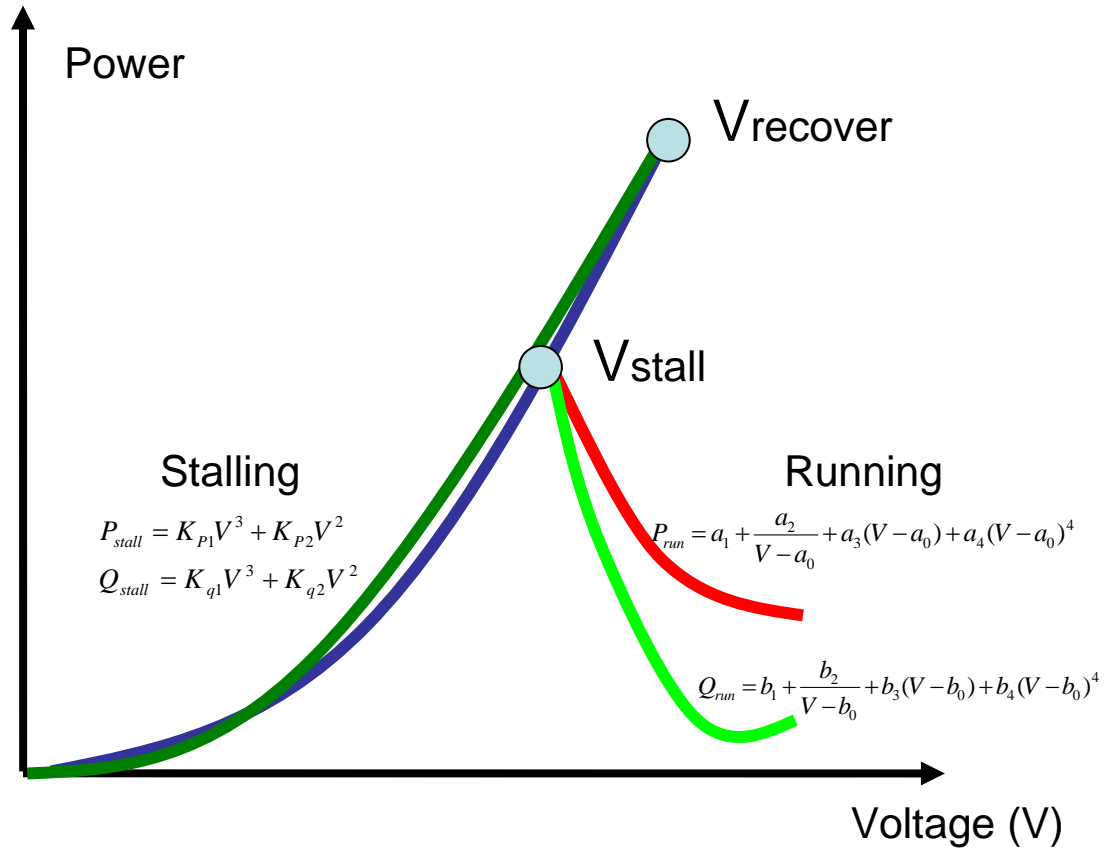


Figure 2: The PV and QV curves

FINAL PROJECT REPORT

LOAD MODELING TRANSMISSION RESEARCH

APPENDIX D

RECOMMENDED MODEL FOR SINGLE PHASE COMPRESSOR

Prepared for CIEE By:

Lawrence Berkeley National Laboratory



University of California
ciee

A CIEE Report

Table of Contents

<i>1. Introduction</i>	<i>1</i>
<i>2. Model Derivation</i>	<i>2</i>
<i>4. Examples</i>	<i>12</i>
<i>4. Conclusions</i>	<i>27</i>

1. Introduction

Single-phase induction motors in residential air conditioners are believed to be the cause of prolonged voltage dips in the Southwest, Florida, and likely elsewhere. During these events, a short fault (properly cleared) cause these motors to stall. The resulting depressed voltage this causes, persists until the air conditioners trip off line by individual thermal protection. A number of such delayed voltage recovery events has been increasing in Southern California in past several years.

In this paper we report on our activities to develop a dynamic model for compressor-driving single-phase induction motors. This focus is warranted because (a) these are the most common type of motor in residential air conditioners, and (b) all their features and effects on the grid are not mimicked by three phase motor models. It is our goal to develop a model for use in a positive sequence power system simulator. A new model is necessary because three phase motor models, which are common in simulation packages, do not adequately represent all the observed behavior of single phase motors.

Our objective is to develop a model that represents the impact of residential air-conditioners on power system dynamic performance. Our particular interest is in modeling the air-conditioner impact on dynamic voltage stability and oscillation damping. The model is expected to:

- accurately capture the sensitivities of motor real and reactive power requirements as a function of its voltage and frequency
- represent the motor impact on damping of low frequency inter-area oscillations
- reasonably predict the stalling phenomenon, as well as accurately represent motor current, real and reactive power during the stalled state

In this document we present a detailed report on the development of a mathematical model to represent a single-phase induction motor driving a compressor load. This model is derived from first principles and verified using data from laboratory tests conducted by Bonneville Power Administration.

In the next section, Section 2, we step through a detailed derivation of the recommended model. In Section 3, we use the data collected from laboratory tests to calibrate the model. Using a consistent set of parameters for the model, we validate voltage ramp tests, voltage oscillation, frequency deviation, and voltage sag tests. We conclude that the model structure is rich enough to model this important type of load both during steady-state operation and transients.

This work is limited to the derivation and verification of the model structure. We do not report on preliminary system-wide studies using this model, nor do we provide comprehensive details on a method for calibrating the model to tests. These remain the subject of continuing research.

2. Model Derivation

Here we present a derivation of the model from first principles. First we write the equations for the single phase induction motor directly applying Faraday's Law for the winding electrical dynamics and Newton's Law for the rotational dynamics.

A. Original Coordinates

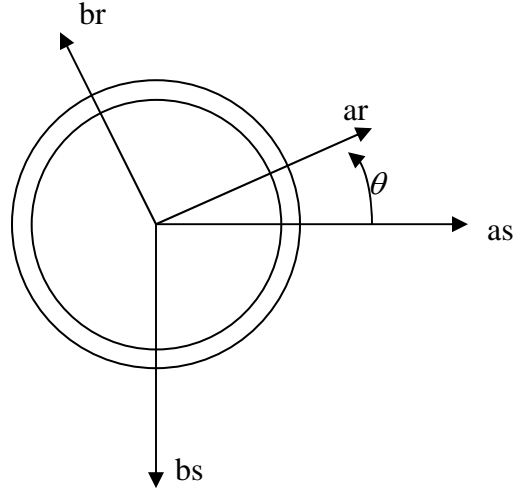


Figure 1. Orientation of magnetic axes

$$v_{bs} = r_{bs} i_{bs} + \frac{d\lambda_{bs}}{dt}$$

$$0 = r_r i_{ar} + \frac{d\lambda_{ar}}{dt}$$

$$0 = r_r i_{br} + \frac{d\lambda_{br}}{dt}$$

$$J \frac{d\omega_r}{dt} = T_{elec} - T_{mech}$$

where:

v_{as}	stator main winding voltage
v_{bs}	stator auxiliary winding voltage
i_{as}	stator main winding current
i_{bs}	stator auxiliary winding current
λ_{as}	stator main winding flux
λ_{bs}	stator auxiliary winding flux
i_{ar}	rotor main winding current
i_{br}	rotor auxiliary winding current
λ_{ar}	rotor main winding flux
λ_{br}	rotor auxiliary winding flux
θ	rotor angle
ω_r	rotor speed

Currents and fluxes are related as follows, assuming linear magnetic characteristics

$$\begin{bmatrix} \lambda_{as} \\ \lambda_{bs} \\ \lambda_{ar} \\ \lambda_{br} \end{bmatrix} = \begin{bmatrix} L_{as} & 0 & L_m \cos(\theta) & -L_m \sin(\theta) \\ 0 & L_{bs} & -nL_m \sin(\theta) & -nL_m \cos(\theta) \\ L_m \cos(\theta) & -nL_m \sin(\theta) & L_r & 0 \\ -L_m \sin(\theta) & -nL_m \cos(\theta) & 0 & L_r \end{bmatrix} \begin{bmatrix} i_{as} \\ i_{bs} \\ i_{ar} \\ i_{br} \end{bmatrix}$$

where the inductances are defined as:

$$L_{as} = L_{las} + L_m$$

$$L_{bs} = L_{lbs} + n^2 L_m$$

$$L_r = L_{lr} + L_m$$

and

n

is the ratio of stator auxiliary winding turns to stator main winding turns. Note that the rotor quantities have already been referred to the stator relative to the main winding turns ratio.

The electrical torque is given by

$$T_{elec} = \begin{bmatrix} i_{as} & i_{bs} \end{bmatrix} \begin{bmatrix} L_m & 0 \\ 0 & nL_m \end{bmatrix} \begin{bmatrix} -\sin(\theta) & -\cos(\theta) \\ -\cos(\theta) & \sin(\theta) \end{bmatrix} \begin{bmatrix} i_{ar} \\ i_{br} \end{bmatrix}$$

B. Transform variables to a stationary reference frame.

In this reference frame the fundamental frequency for all electrical quantities will be the same, and equal to the source frequency. This transformation also eliminates the angle from the model representation.

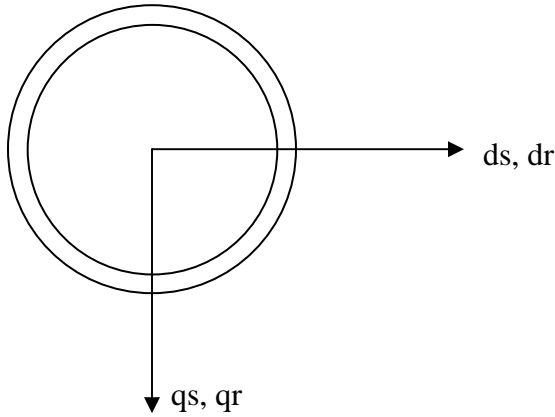


Figure 2. Magnetic axes in stationary reference frame

Apply transformation to a stationary reference frame:

$$\begin{bmatrix} ds \\ qs \end{bmatrix} = \begin{bmatrix} 1 & 0 \\ 0 & 1 \end{bmatrix} \begin{bmatrix} as \\ bs \end{bmatrix} \quad \begin{bmatrix} dr \\ qr \end{bmatrix} = \begin{bmatrix} \cos(\theta) & -\sin(\theta) \\ -\sin(\theta) & -\cos(\theta) \end{bmatrix} \begin{bmatrix} ar \\ br \end{bmatrix}$$

Then

$$v_{ds} = r_{ds} i_{ds} + \frac{d\lambda_{ds}}{dt}$$

$$v_{qs} = r_{qs} i_{qs} + \frac{d\lambda_{qs}}{dt}$$

$$0 = r_r i_{dr} - \omega_r \lambda_{qr} + \frac{d\lambda_{dr}}{dt}$$

$$0 = r_r i_{qr} + \omega_r \lambda_{dr} + \frac{d\lambda_{qr}}{dt}$$

$$J \frac{d\omega_r}{dt} = T_{elec} - T_{mech}$$

where

$$r_{ds} = r_{as}$$

$$r_{qs} = r_{bs}$$

The flux current relation may be rewritten as follows, using a little linear algebra that will allow us to remove the rotor currents from the differential equations later.

$$\begin{bmatrix} \lambda_{ds} \\ \lambda_{qs} \\ i_{dr} \\ i_{qr} \end{bmatrix} = \begin{bmatrix} L'_{ds} & 0 & \frac{L_m}{L_r} & 0 \\ 0 & L'_{qs} & 0 & n \frac{L_m}{L_r} \\ -\frac{L_m}{L_r} & 0 & \frac{1}{L_r} & 0 \\ 0 & -n \frac{L_m}{L_r} & 0 & \frac{1}{L_r} \end{bmatrix} \begin{bmatrix} i_{ds} \\ i_{qs} \\ \lambda_{dr} \\ \lambda_{qr} \end{bmatrix}$$

where

$$L'_{ds} = L_{as} - \frac{L_m^2}{L_r}$$

$$L'_{qs} = L_{bs} - n^2 \frac{L_m^2}{L_r}$$

The electrical torque transforms to

$$\begin{aligned} T_{elec} &= \begin{bmatrix} i_{ds} & i_{qs} \end{bmatrix} \begin{bmatrix} L_m & 0 \\ 0 & nL_m \end{bmatrix} \begin{bmatrix} -\sin(\theta) & -\cos(\theta) \\ -\cos(\theta) & \sin(\theta) \end{bmatrix} \begin{bmatrix} \cos(\theta) & -\sin(\theta) \\ -\sin(\theta) & -\cos(\theta) \end{bmatrix} \begin{bmatrix} i_{dr} \\ i_{qr} \end{bmatrix} \\ &= L_m i_{ds} i_{qr} - nL_m i_{qs} i_{dr} \\ &= \frac{L_m}{L_r} i_{ds} \lambda_{qr} - \frac{nL_m}{L_r} i_{qs} \lambda_{dr} \end{aligned}$$

C. Scale Fluxes and Inductances, use phasors, and express in per-unit quantities

$$\Psi = \omega_b \lambda \quad X = \omega_b L$$

The differential equations may be written (substituting in for rotor currents)

$$\begin{aligned} v_{ds} &= r_{ds} i_{ds} + \frac{1}{\omega_b} \frac{d\Psi_{ds}}{dt} \\ v_{qs} &= r_{qs} i_{qs} + \frac{1}{\omega_b} \frac{d\Psi_{qs}}{dt} \\ 0 &= -\frac{r_r}{X_r} X_m i_{ds} + \frac{r_r}{X_r} \Psi_{dr} - \frac{\omega_r}{\omega_b} \Psi_{qr} + \frac{1}{\omega_b} \frac{d\Psi_{dr}}{dt} \\ 0 &= -\frac{r_r}{X_r} nX_m i_{qs} + \frac{r_r}{X_r} \Psi_{qr} + \frac{\omega_r}{\omega_b} \Psi_{dr} + \frac{1}{\omega_b} \frac{d\Psi_{qr}}{dt} \\ J \frac{d\omega_r}{dt} &= \frac{1}{\omega_b} \frac{X_m}{X_r} i_{ds} \Psi_{qr} - \frac{1}{\omega_b} \frac{nX_m}{X_r} i_{qs} \Psi_{dr} - T_{mech} \end{aligned}$$

All electrical variables can be represented by fundamental frequency phasors. For example,

$$\begin{aligned} i_{ds} &= \sqrt{2} I_{ds}^R \cos(\omega_b t + \phi) - \sqrt{2} I_{ds}^I \sin(\omega_b t + \phi) \\ &= \frac{1}{\sqrt{2}} (I_{ds}^R - j I_{ds}^I) e^{-j(\omega_b t + \phi)} + \frac{1}{\sqrt{2}} (I_{ds}^R + j I_{ds}^I) e^{+j(\omega_b t + \phi)} \end{aligned}$$

where the angle ϕ is a convenient reference angle. In this model we find it useful to specify this angle to be the phasor angle of the applied single phase voltage. We argue below that this allows us to treat represent frequency in a straightforward way.

Now we express the variables in per-unit quantities.

Per Unit:

$$\begin{aligned} P_B &= V_B I_B & V_B &= \Psi_B \\ Z_B &= \frac{V_B}{I_B} & T_B &= \frac{P_B}{\omega_b} \\ H &= \frac{J \omega_b^2}{2 P_B} & T'_o &= \frac{X_r}{\omega_b r_r} \end{aligned}$$

The equations for the resulting model are show below in Model 1. In this model the single phase voltage is applied to the main winding. As mentioned above, the phasor angle of this voltage is used for our reference, so the voltage magnitude is applied to the model and the frequency appears as

$$\omega_s = \omega_b + \frac{d\phi}{dt}$$

$$\frac{1}{\omega_b} \frac{d}{dt} (\Psi_{ds}^R + j\Psi_{ds}^I) = |V_{ds}| - r_{ds} (I_{ds}^R + jI_{ds}^I) - j \frac{\omega_s}{\omega_b} (\Psi_{ds}^R + j\Psi_{ds}^I)$$

$$\frac{1}{\omega_b} \frac{d}{dt} (\Psi_{qs}^R + j\Psi_{qs}^I) = (V_{qs}^R + jV_{qs}^I) - r_{qs} (I_{qs}^R + jI_{qs}^I) - j \frac{\omega_s}{\omega_b} (\Psi_{qs}^R + j\Psi_{qs}^I)$$

$$T_o' \frac{d}{dt} (\Psi_{dr}^R + j\Psi_{dr}^I) = X_m (I_{ds}^R + jI_{ds}^I) - (1 + j\omega_s T_o') (\Psi_{dr}^R + j\Psi_{dr}^I) + \omega_r T_o' (\Psi_{qr}^R + j\Psi_{qr}^I)$$

$$T_o' \frac{d}{dt} (\Psi_{qr}^R + j\Psi_{qr}^I) = nX_m (I_{qs}^R + jI_{qs}^I) - (1 + j\omega_s T_o') (\Psi_{qr}^R + j\Psi_{qr}^I) - \omega_r T_o' (\Psi_{dr}^R + j\Psi_{dr}^I)$$

$$\frac{2H}{\omega_b} \frac{d\omega_r}{dt} = \frac{X_m}{X_r} (I_{ds}^R \Psi_{qr}^R + I_{ds}^I \Psi_{qr}^I) - \frac{nX_m}{X_r} (I_{qs}^R \Psi_{dr}^R + I_{qs}^I \Psi_{dr}^I) - T_{mech}$$

Model 1. Dynamic Phasor Model

D. Resolve into forward- and backward-rotating fields

We recognize that this machine is not symmetrical and the applied winding voltages are not balanced (one being fed off the other through a capacitor), and so it should not be expected that the rotating magnetic field will be spatially uniform. To highlight this in the model it is convenient to resolve the rotor flux variables into forward and backward rotating components. This will also serve to highlight a time-scale separation that otherwise may not be apparent.

First, express the rotor d-axis field as the sum of the forward and backward rotating field components:

$$(\Psi_{dr}^R + j\Psi_{dr}^I) = (\Psi_f^R + j\Psi_f^I) + (\Psi_b^R + j\Psi_b^I)$$

The relation above should be interpreted as follows: with the rotor winding referenced to the stator, both the forward-backward rotating fields will induce currents in the winding. The rotating fields contribute to the q-axis winding in a different way; the forward rotating field will lead in the q-axis compared to the d-axis, and the backward field will lag in the in the q-axis compared to the d-axis:

$$(\Psi_{qr}^R + j\Psi_{qr}^I) = j(\Psi_f^R + j\Psi_f^I) - j(\Psi_b^R + j\Psi_b^I)$$

More compactly, these phasor relations may be written

$$\begin{bmatrix} (\Psi_{dr}^R + j\Psi_{dr}^I) \\ (\Psi_{qr}^R + j\Psi_{qr}^I) \end{bmatrix} = \begin{bmatrix} 1 & 1 \\ j & -j \end{bmatrix} \begin{bmatrix} (\Psi_f^R + j\Psi_f^I) \\ (\Psi_b^R + j\Psi_b^I) \end{bmatrix}$$

$$\begin{bmatrix} (\Psi_f^R + j\Psi_f^I) \\ (\Psi_b^R + j\Psi_b^I) \end{bmatrix} = \left(\frac{1}{2}\right) \begin{bmatrix} 1 & -j \\ 1 & j \end{bmatrix} \begin{bmatrix} (\Psi_{dr}^R + j\Psi_{dr}^I) \\ (\Psi_{qr}^R + j\Psi_{qr}^I) \end{bmatrix}$$

It is likewise convenient to transform the stator currents for the rotor relations

$$\begin{bmatrix} (I_f^R + jI_f^I) \\ (I_b^R + jI_b^I) \end{bmatrix} = \left(\frac{1}{2}\right) \begin{bmatrix} 1 & -jn \\ 1 & jn \end{bmatrix} \begin{bmatrix} (I_{ds}^R + jI_{ds}^I) \\ (I_{qs}^R + jI_{qs}^I) \end{bmatrix}$$

In terms of these new variables, the model may be expressed as

$$\frac{1}{\omega_b} \frac{d}{dt} (\Psi_{ds}^R + j\Psi_{ds}^I) = |V_{ds}| - r_{ds} (I_{ds}^R + jI_{ds}^I) - j \frac{\omega_s}{\omega_b} (\Psi_{ds}^R + j\Psi_{ds}^I)$$

$$\frac{1}{\omega_b} \frac{d}{dt} (\Psi_{qs}^R + j\Psi_{qs}^I) = (V_{qs}^R + jV_{qs}^I) - r_{qs} (I_{qs}^R + jI_{qs}^I) - j \frac{\omega_s}{\omega_b} (\Psi_{qs}^R + j\Psi_{qs}^I)$$

$$\begin{bmatrix} (\Psi_f^R + j\Psi_f^I) \\ (\Psi_b^R + j\Psi_b^I) \end{bmatrix} = \left(\frac{1}{2}\right) \begin{bmatrix} 1 & -j \\ 1 & j \end{bmatrix} \begin{bmatrix} (\Psi_{dr}^R + j\Psi_{dr}^I) \\ (\Psi_{qr}^R + j\Psi_{qr}^I) \end{bmatrix} \quad \begin{bmatrix} (\Psi_{dr}^R + j\Psi_{dr}^I) \\ (\Psi_{qr}^R + j\Psi_{qr}^I) \end{bmatrix} = \begin{bmatrix} 1 & 1 \\ j & -j \end{bmatrix} \begin{bmatrix} (\Psi_f^R + j\Psi_f^I) \\ (\Psi_b^R + j\Psi_b^I) \end{bmatrix}$$

$$\begin{bmatrix} (I_f^R + jI_f^I) \\ (I_b^R + jI_b^I) \end{bmatrix} = \left(\frac{1}{2}\right) \begin{bmatrix} 1 & -jn \\ 1 & jn \end{bmatrix} \begin{bmatrix} (I_{ds}^R + jI_{ds}^I) \\ (I_{qs}^R + jI_{qs}^I) \end{bmatrix} \quad \begin{bmatrix} (I_{ds}^R + jI_{ds}^I) \\ (I_{qs}^R + jI_{qs}^I) \end{bmatrix} = \begin{bmatrix} 1 & 1 \\ j/n & -j/n \end{bmatrix} \begin{bmatrix} (I_f^R + jI_f^I) \\ (I_b^R + jI_b^I) \end{bmatrix}$$

$$T_o' \frac{d}{dt} (\Psi_f^R + j\Psi_f^I) = X_m (I_f^R + jI_f^I) - (1 + j(\omega_s - \omega_r) T_o') (\Psi_f^R + j\Psi_f^I)$$

$$T_o' \frac{d}{dt} (\Psi_b^R + j\Psi_b^I) = X_m (I_b^R + jI_b^I) - (1 + j(\omega_s + \omega_r) T_o') (\Psi_b^R + j\Psi_b^I)$$

$$\frac{2H}{\omega_b} \frac{d\omega_r}{dt} = \frac{X_m}{X_r} 2(I_f^I \Psi_f^R - I_f^R \Psi_f^I - I_b^I \Psi_b^R + I_b^R \Psi_b^I) - T_{mech}$$

Model 2. Represented with forward and backward rotating fields

E. Neglect Fast Transients

Next we neglect the effects of fast transients. These may be either fast decaying transients, or fast oscillatory dynamics that are attenuated by slow dynamics that essentially act as a nonlinear low-pass filter. The dynamics suitable for this simplification include the stator transients, the capacitor transients (which we have not shown yet). The rotor dynamics are explicitly related to machine speed. Under normal high speed operation, the backward field dynamics appear fast and should be neglected along with the stator transients. When the motor is at low speed, all electrical dynamics may contribute to the response, and an argument could be made to represent all the dynamics. However, this would be inconsistent with the quasi-static approximation used for other machine models and the network representation. Neglecting stator transients, neglecting rotor backward-rotating field transients, and neglecting capacitor transients and lumping the capacitor into the q-axis stator equation, we obtain the following model.

$$\begin{aligned}
 |V_s| &= \left(r_{ds} + j \frac{\omega_s}{\omega_b} X'_{ds} \right) (I_{ds}^R + j I_{ds}^I) + j \left(\frac{\omega_s}{\omega_b} \right) \frac{X_m}{X_r} (\Psi_{dr}^R + j \Psi_{dr}^I) \\
 |V_s| &= \left(r_{qs} + j \frac{\omega_s}{\omega_b} X'_{qs} + j \frac{\omega_b}{\omega_s} X_c \right) (I_{qs}^R + j I_{qs}^I) + j \left(\frac{\omega_s}{\omega_b} \right) \frac{n X_m}{X_r} (\Psi_{qr}^R + j \Psi_{qr}^I) \\
 \begin{bmatrix} \Psi_f^R + j \Psi_f^I \\ \Psi_b^R + j \Psi_b^I \end{bmatrix} &= \begin{pmatrix} 1 & -j \\ 2 & j \end{pmatrix} \begin{bmatrix} \Psi_{dr}^R + j \Psi_{dr}^I \\ \Psi_{qr}^R + j \Psi_{qr}^I \end{bmatrix} \quad \begin{bmatrix} \Psi_{dr}^R + j \Psi_{dr}^I \\ \Psi_{qr}^R + j \Psi_{qr}^I \end{bmatrix} = \begin{bmatrix} 1 & 1 \\ j & -j \end{bmatrix} \begin{bmatrix} \Psi_f^R + j \Psi_f^I \\ \Psi_b^R + j \Psi_b^I \end{bmatrix} \\
 \begin{bmatrix} I_f^R + j I_f^I \\ I_b^R + j I_b^I \end{bmatrix} &= \begin{pmatrix} 1 & -jn \\ 2 & jn \end{pmatrix} \begin{bmatrix} I_{ds}^R + j I_{ds}^I \\ I_{qs}^R + j I_{qs}^I \end{bmatrix} \quad \begin{bmatrix} I_{ds}^R + j I_{ds}^I \\ I_{qs}^R + j I_{qs}^I \end{bmatrix} = \begin{bmatrix} 1 & 1 \\ j/n & -j/n \end{bmatrix} \begin{bmatrix} I_f^R + j I_f^I \\ I_b^R + j I_b^I \end{bmatrix} \\
 T'_o \frac{d}{dt} (\Psi_f^R + j \Psi_f^I) &= X_m (I_f^R + j I_f^I) - (1 + j(\omega_s - \omega_r) T'_o) (\Psi_f^R + j \Psi_f^I) \\
 (\Psi_b^R + j \Psi_b^I) &= \frac{X_m (I_b^R + j I_b^I)}{(1 + j(\omega_s + \omega_r) T'_o)} \\
 \frac{2H}{\omega_b} \frac{d\omega_r}{dt} &= \frac{X_m}{X_r} 2 (I_f^I \Psi_f^R - I_f^R \Psi_f^I - I_b^I \Psi_b^R + I_b^R \Psi_b^I) - T_{mech}
 \end{aligned}$$

Model 3. Phasor Model neglecting fast transients

In this model we have introduced a new notation for the applied voltage phasor: V_s . This voltage is directly connected to the d-axis stator winding, and it is separated from the q-axis winding by the capacitor.

F. Saturation

We model the impact of magnetizing saturation by adjusting the magnetizing reactance as a function of the rotor fluxes. The saturation scaling function is computed as follows

$$\text{define } \Psi = \sqrt{(\Psi_f^R)^2 + (\Psi_f^I)^2 + (\Psi_b^R)^2 + (\Psi_b^I)^2}$$

Then

$$\text{sat}(\Psi_f, \Psi_b) = \begin{cases} 1 & \text{for } \Psi \leq b_{sat} \\ 1 + A_{sat} (\Psi - b_{sat})^2 & \text{for } \Psi > b_{sat} \end{cases}$$

In this model we note that the effect of saturation in the ratio of (X_m/X_r) is negligible and is not applied. We also note that the definition of T'_o includes X_r and is affected by saturation. The transient reactances are largely insensitive to saturation. Careful examination of the equations in Model 2 shows that the saturation scaling term only shows up in two places; once in each of the rotor flux equations. The final model is shown below in Model 4; it also includes the output current phasor relative to the applied voltage angle reference.

$$\begin{aligned}
|V_s| &= \left(r_{ds} + j \frac{\omega_s}{\omega_b} X'_{ds} \right) (I_{ds}^R + jI_{ds}^I) + j \left(\frac{\omega_s}{\omega_b} \right) \frac{X_m}{X_r} (\Psi_{dr}^R + j\Psi_{dr}^I) \\
|V_s| &= \left(r_{qs} + j \frac{\omega_s}{\omega_b} X'_{qs} + j \frac{\omega_b}{\omega_s} X_c \right) (I_{qs}^R + jI_{qs}^I) + j \left(\frac{\omega_s}{\omega_b} \right) \frac{nX_m}{X_r} (\Psi_{qr}^R + j\Psi_{qr}^I) \\
\begin{bmatrix} \Psi_f^R + j\Psi_f^I \\ \Psi_b^R + j\Psi_b^I \end{bmatrix} &= \begin{pmatrix} 1 & -j \\ 1 & j \end{pmatrix} \begin{bmatrix} \Psi_{dr}^R + j\Psi_{dr}^I \\ \Psi_{qr}^R + j\Psi_{qr}^I \end{bmatrix} \quad \begin{bmatrix} \Psi_{dr}^R + j\Psi_{dr}^I \\ \Psi_{qr}^R + j\Psi_{qr}^I \end{bmatrix} = \begin{bmatrix} 1 & 1 \\ j & -j \end{bmatrix} \begin{bmatrix} \Psi_f^R + j\Psi_f^I \\ \Psi_b^R + j\Psi_b^I \end{bmatrix} \\
\begin{bmatrix} I_f^R + jI_f^I \\ I_b^R + jI_b^I \end{bmatrix} &= \begin{pmatrix} 1 & -jn \\ 1 & jn \end{pmatrix} \begin{bmatrix} I_{ds}^R + jI_{ds}^I \\ I_{qs}^R + jI_{qs}^I \end{bmatrix} \quad \begin{bmatrix} I_{ds}^R + jI_{ds}^I \\ I_{qs}^R + jI_{qs}^I \end{bmatrix} = \begin{bmatrix} 1 & 1 \\ j/n & -j/n \end{bmatrix} \begin{bmatrix} I_f^R + jI_f^I \\ I_b^R + jI_b^I \end{bmatrix} \\
T'_o \frac{d}{dt} (\Psi_f^R + j\Psi_f^I) &= X_m (I_f^R + jI_f^I) - (\text{sat}(\Psi_f, \Psi_b) + j(\omega_s - \omega_r)T'_o) (\Psi_f^R + j\Psi_f^I) \\
(\Psi_b^R + j\Psi_b^I) &= \frac{X_m (I_b^R + jI_b^I)}{(\text{sat}(\Psi_f, \Psi_b) + j(\omega_s + \omega_r)T'_o)} \\
\frac{2H}{\omega_b} \frac{d\omega_r}{dt} &= \frac{X_m}{X_r} 2(I_f^I \Psi_f^R - I_f^R \Psi_f^I - I_b^I \Psi_b^R + I_b^R \Psi_b^I) - T_{mech} \\
I_s &= \left[(I_{ds}^R + jI_{ds}^I) + (I_{qs}^R + jI_{qs}^I) \right] e^{j\phi}
\end{aligned}$$

Model 4. Final model including saturation, forward- and backward-rotating field representations, and neglecting fast transients. The model is driven by the magnitude of the applied voltage and its frequency: $|V_s|$ and ω_s . The output current phasor I_s is the sum of the two winding current phasors relative to the applied voltage phasor angle, ϕ .

4. Examples

The parameters used in all test are

P_{base} : 3500	V_{base} : 240	n : 1.2200
R_{ds} : 0.0365	R_{qs} : 0.0729	R_r : 0.0486
X_m : 2.2800	X_r : 2.3300	
H : 0.0400	T'_o : 0.1212	
X'_d : 0.1033	X'_q : 0.1489	X_{cap} : -2.7790
b_{sat} : 0.7212	A_{sat} : 5.6000	

The mechanical torque is set to match initial conditions on power drawn by the motor.

A. Voltage Ramp Test

The initial power is 1.0960 pu. The mechanical torque is initially 1.0448 pu. The torque model used throughout these test applies 0.85 to constant torque and 0.15 to speed to the fourth power. This speed variation helps marginally with the voltage oscillation tests. A constant torque model gives high quality, consistent results as well. (In the ramp test, the constant torque model stalls slightly before the speed dependent model.)

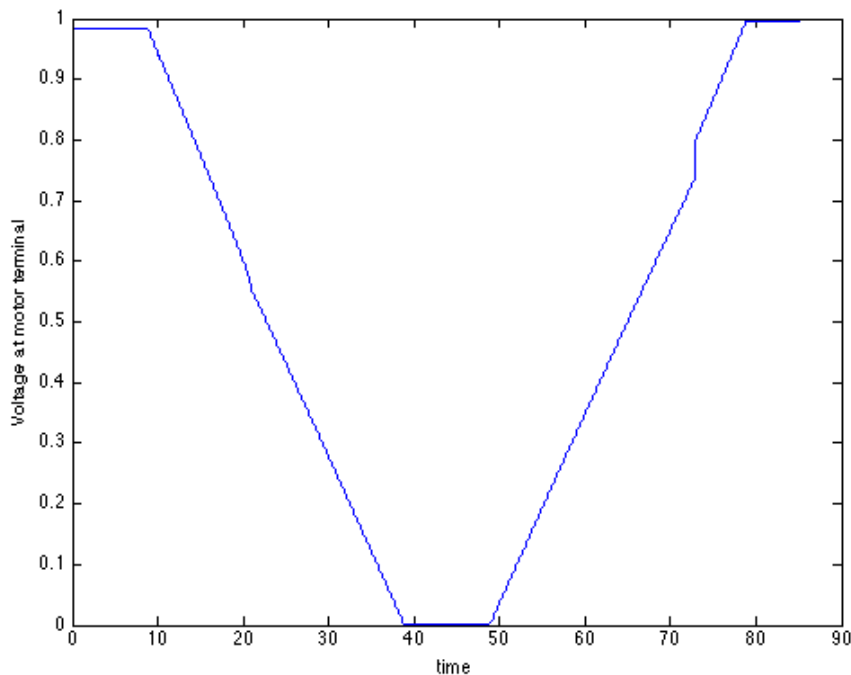


Figure 3. Voltage ramp measured at terminal of motor. The voltage initially is 0.98 pu.

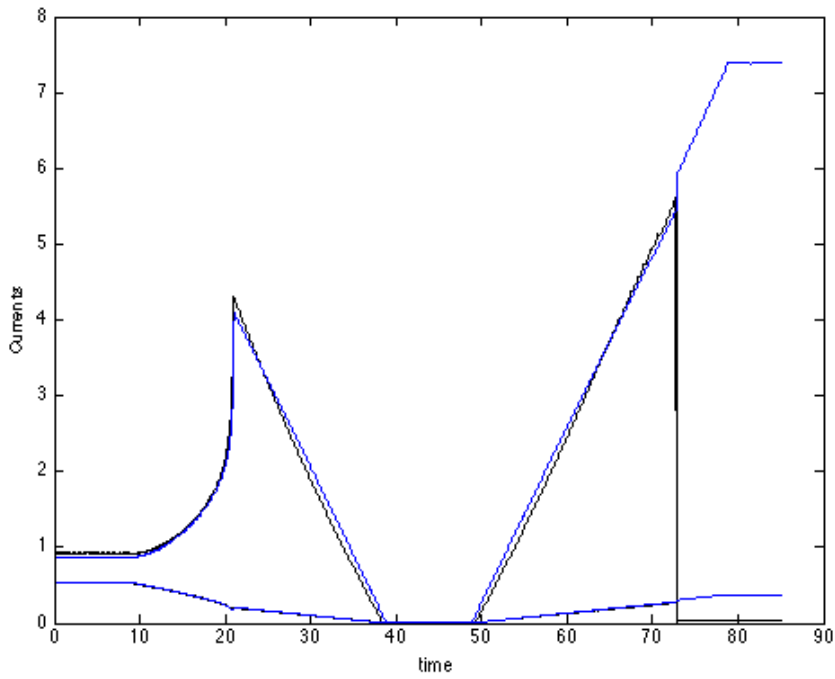


Figure 4. Measured and simulated currents. The main winding current is the larger of the two.

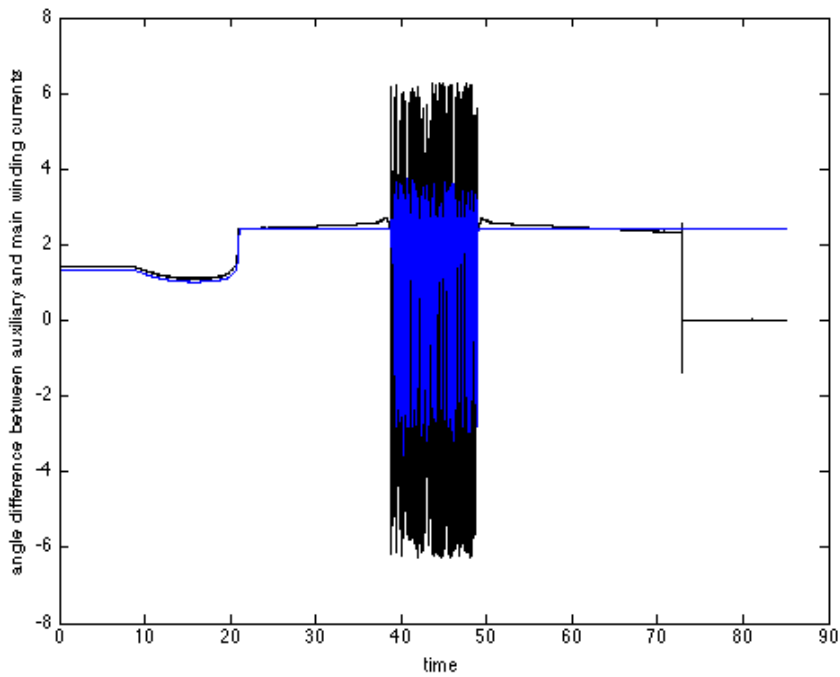


Figure 5. A plot of the angle difference between the auxiliary winding and the main winding. The measured difference at full voltages is about 82 degrees, the simulated difference is about 77 degrees. (When the voltage and current are zero, the angle is not defined and its calculation jumps around randomly.)

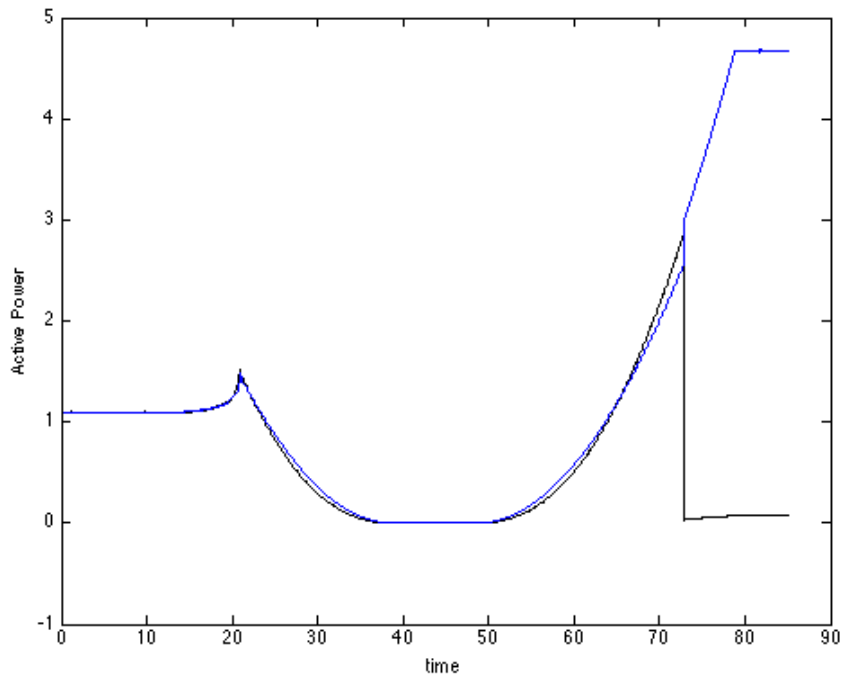


Figure 6. Measured and simulated active power.

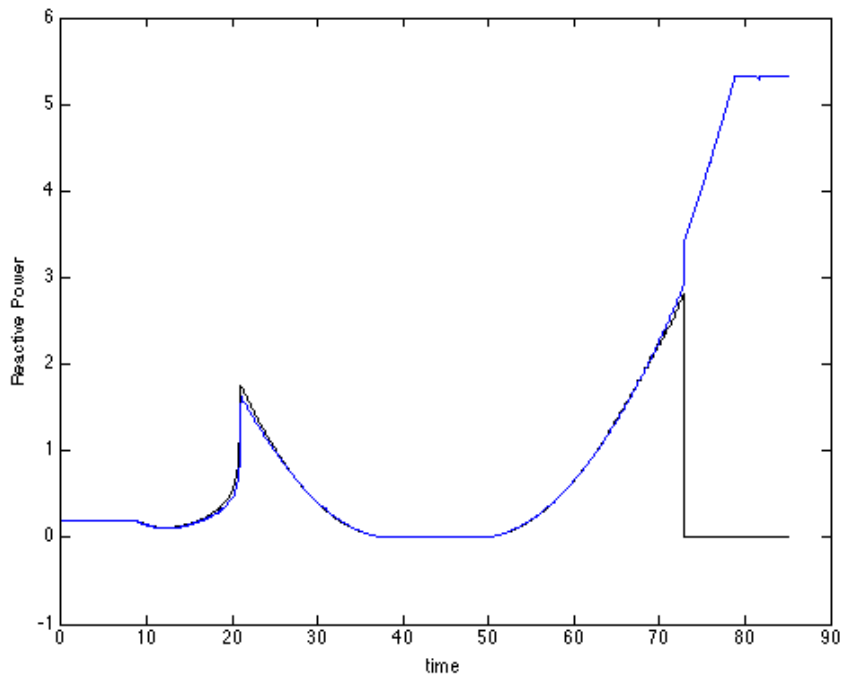


Figure 7. Measured and simulated reactive power

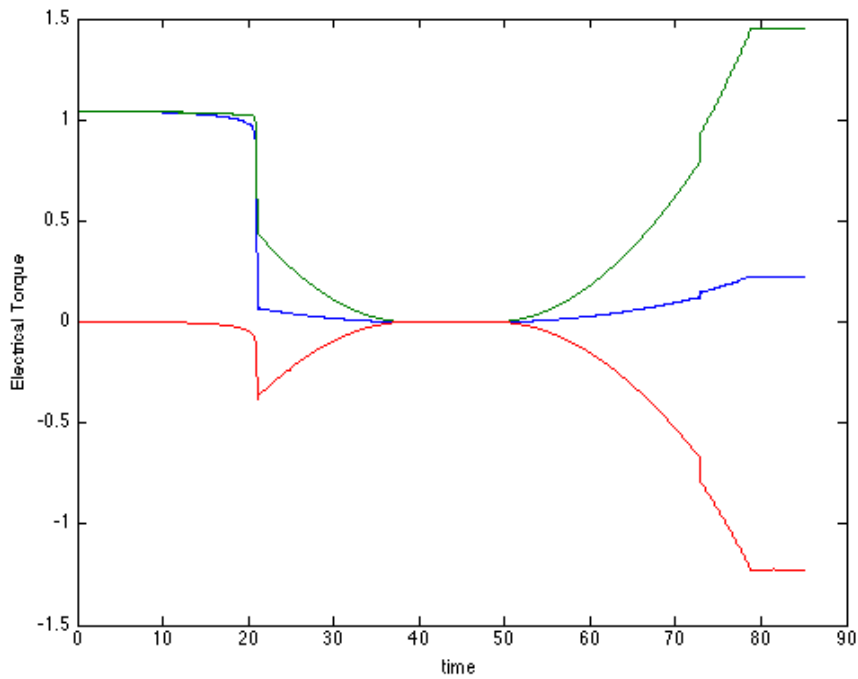
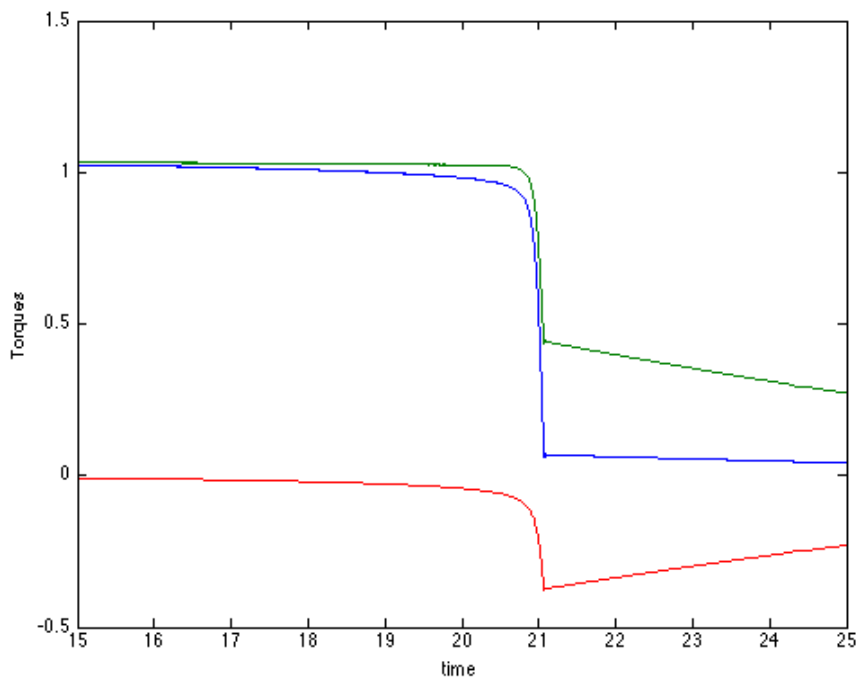


Figure 8. Simulated electric torque. Total (blue), forward component (green) and backward component (red). See close up during stall in next figure.



Figures 8. Electrical torque around stall point. Note that the green line (forward component) remains almost constant right up to stall point, suggesting that the backward component 's contribution (red) to the total torque (blue) is needed to accurately capture the stall.

B. Voltage Oscillation Test

In this test, the magnitude of the applied voltage oscillations between 90% and 110% of the nominal value. The applied oscillations are at frequencies of 0.1Hz, 0.25Hz, 0.7Hz, 1.5Hz, and 2Hz. The initial power at nominal power is 1.067, and the corresponding torque is 1.018. The mechanical torque model used in these simulations is 85% constant torque and 15% speed raised to the fourth power.

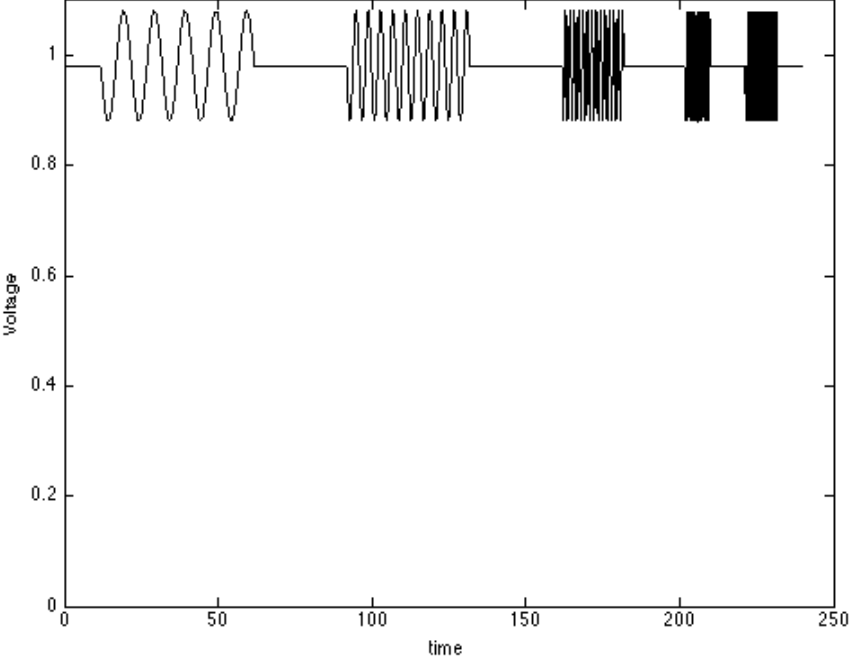


Figure 10. Voltage Oscillation Test. The applied voltage varies between 90% and 110% of nominal at frequencies: 0.1 Hz, 0.25 Hz, 0.7 Hz, 1.5Hz, and 2 Hz.

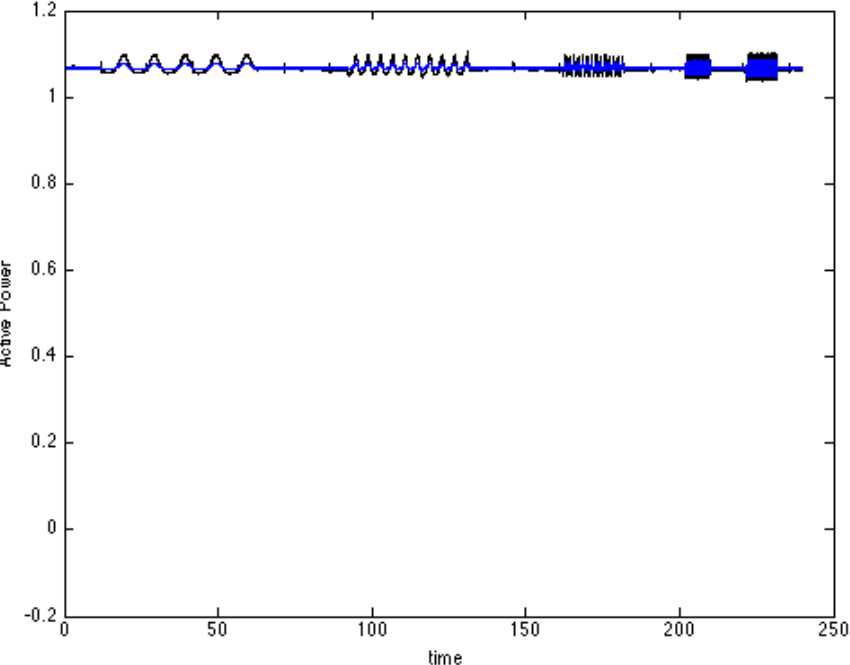


Figure 11. Active Power, simulated and calculated from measurements for the voltage oscillation test.

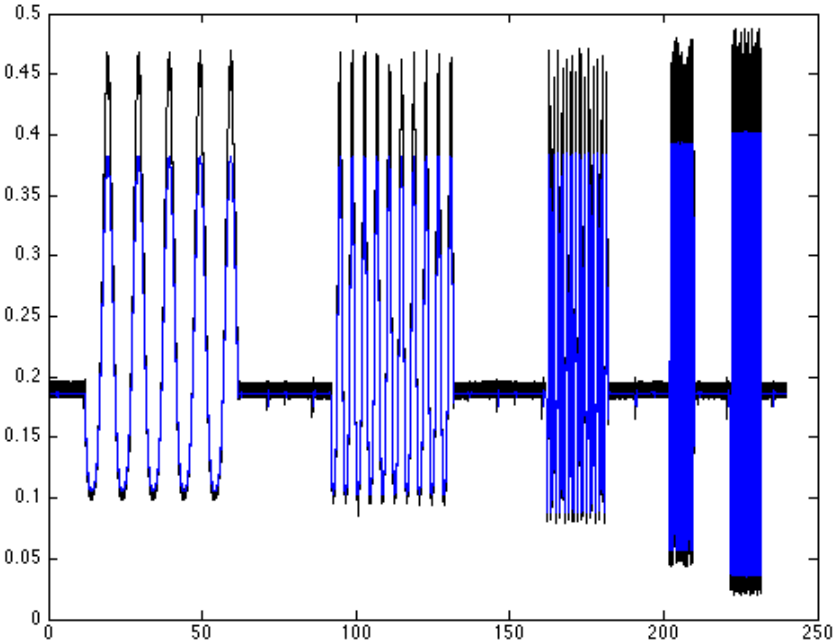


Figure 12. Reactive Power, simulated and calculated from measurements for the voltage oscillation test.

The simulated reactive power and calculated reactive power match very well during the low voltage portion of the oscillation. The simulation underestimates the peaks during the high voltage portion of the oscillation. The active power only changes slightly during these oscillations. Some speed dependence in the torque equation model is necessary for the simulation to qualitatively move in the same direction as the calculated values. The overall variations are small, so this detail may not be critical for modeling.

C. Frequency Tests

In the next test, the supply frequency is decreased from 60Hz to 58.5Hz in 0.25Hz increments, and then increased back again to 60Hz. Care must be taken to accurately calculate the active and reactive powers of the fundamental frequency components as the frequency changes. Calculating values assuming 60Hz - modulating by 60Hz sinusoids and averaging over integer periods - results in oscillations and *bias*. In our calculation we find it convenient to modulate by signals of the correct frequencies, but averaged using a fixed window length. This results in oscillations, but removes the bias. Then a 1sec average is applied to smooth out the oscillations. Also, the applied voltage as seen from the terminal of the single phase motor changes with frequency. The voltage drop from the laboratory supply to motor depends on frequency.

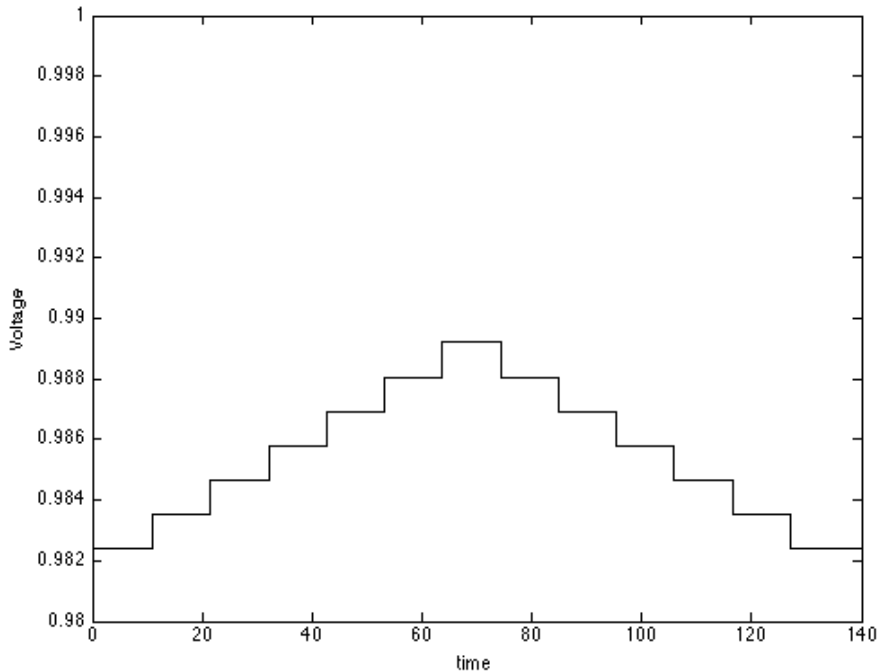


Figure 13. Simulation voltage consistent with laboratory voltage. The voltage magnitude increases as frequency decreases because the supply line voltage drop decreases.

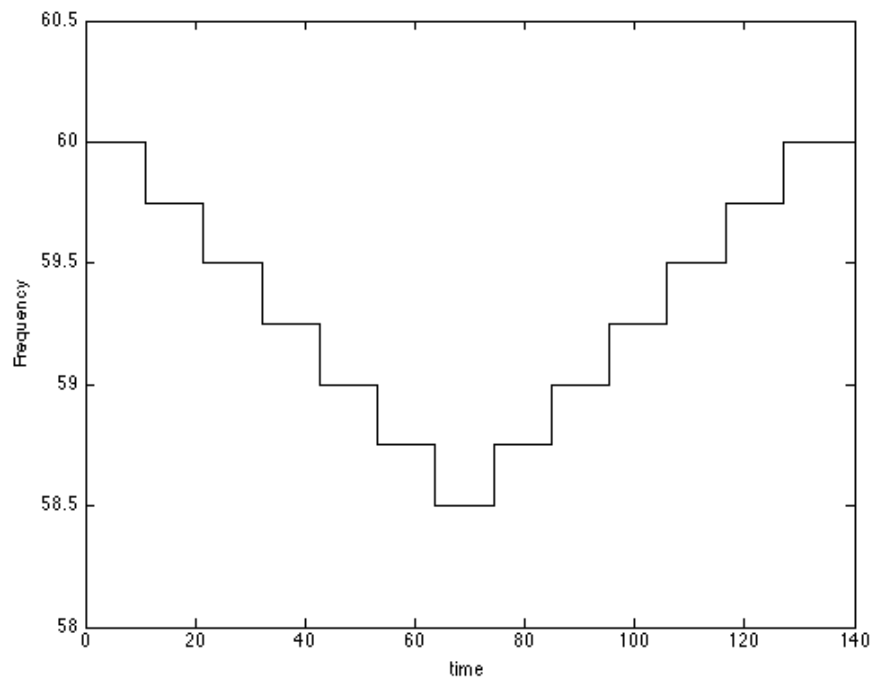


Figure 14. Frequency. The frequency drops from 60Hz to 58.5Hz and returns to 60Hz in 0.25Hz increments.

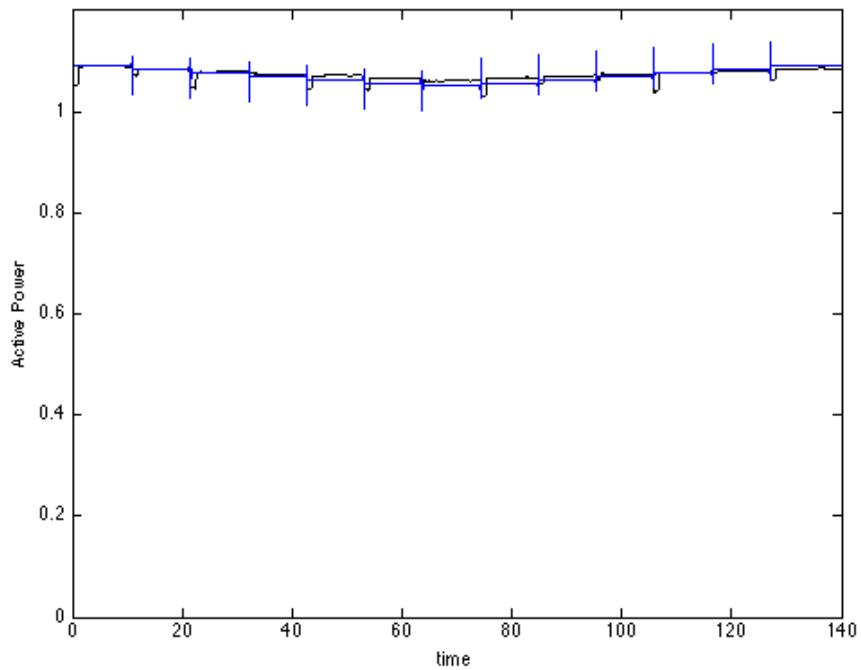


Figure 15. Calculated and simulated active power. The response is small and proportional to frequency.

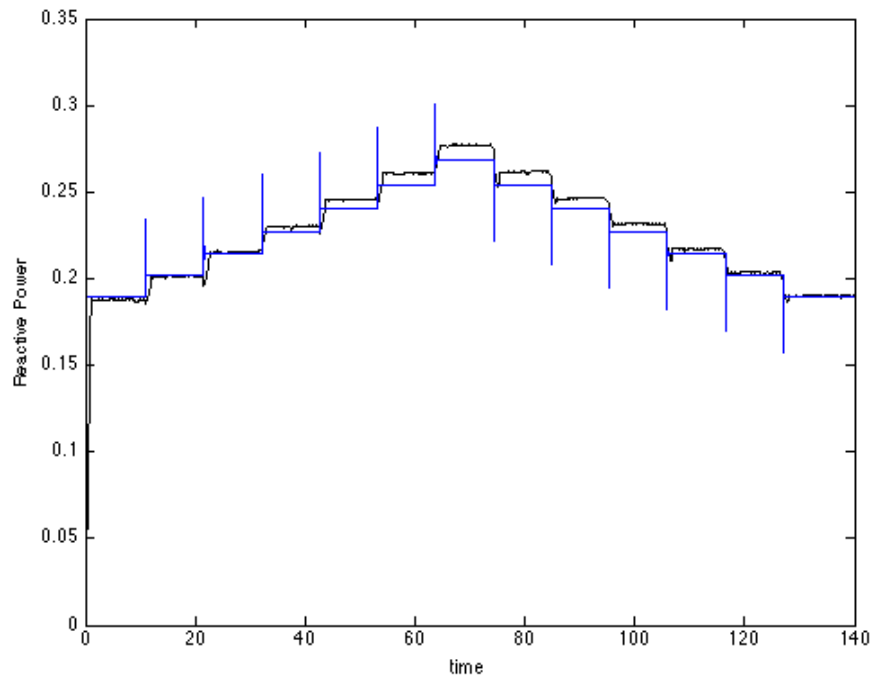


Figure 16. Calculated and simulated eactive powers. The reactive power increases with decrease in frequency.

The simulated responses are close to the measured responses. The applied frequency variation down to 58.5 Hz is large. The model should accurately represent the load frequency response for even large events.

D. Voltage Sag Tests

The voltage sag tests characterizes the response of the air conditioner to faults in the network. The voltage profile for these tests has three parts, a pre-fault voltage at 100% nominal, a sag level for some specified fault duration, and a post-fault recovery level. The output of a particular test is simply whether or not the motor stalled. We use our simulation model to attempt to repeat the results, and in this case we tune our model's Inertia constant, H , to best match the data.

We note again an important point about the voltage levels in the test: there is a small voltage drop from the laboratory supply source to the terminal of the motor. While the difference is usually small, it is important to account for these few percent when trying to match the results with simulations. The particular tests we examine here are those that distinguish between motor recovery and motor stall. We note the terminal voltages when discussing these tests.

Six-cycle fault tests

The sag voltage was decreases to 0 pu and raised to various recovery voltages including 100%. The motor remained stalled in all cases.

Three-cycle fault, 100% recover tests

In these tests the recovery voltage was returned to 100% after a 3-cycle voltage sag. Repeated tests determined that the motor remained stalled for a voltage sag of 0.52 per unit, but recovered for a voltage sag of 0.54 pu.

For simulation purposes we account for the voltage drop in the supply line. The terminal voltage at 100% supply is 0.98 pu. The voltage sags of 0.52 and 0.54, correspond to terminal voltages of 0.49 pu and 0.51 pu, respectively. For the case when the motor stalled, the high current kept the terminal voltage around 0.90 pu. In the recovery case, the terminal voltage recovered initially to around 0.90 pu and increased to 0.98 as the motor quickly returned to speed. In the simulation we used a pre-fault voltage of 0.98 pu, sag voltages of 0.49 pu and 0.51 pu, and a recovery voltage of 0.90 pu.

Keeping all other parameters constant, and modeling the mechanical load as constant torque, the inertia constant is found to be $H = 0.0219$ sec. The following four plots compare the active and reactive powers computed from measurements and simulated using the model described here. The model distinguishes between the stall/non stall conditions, and follows the dynamics reasonably well.

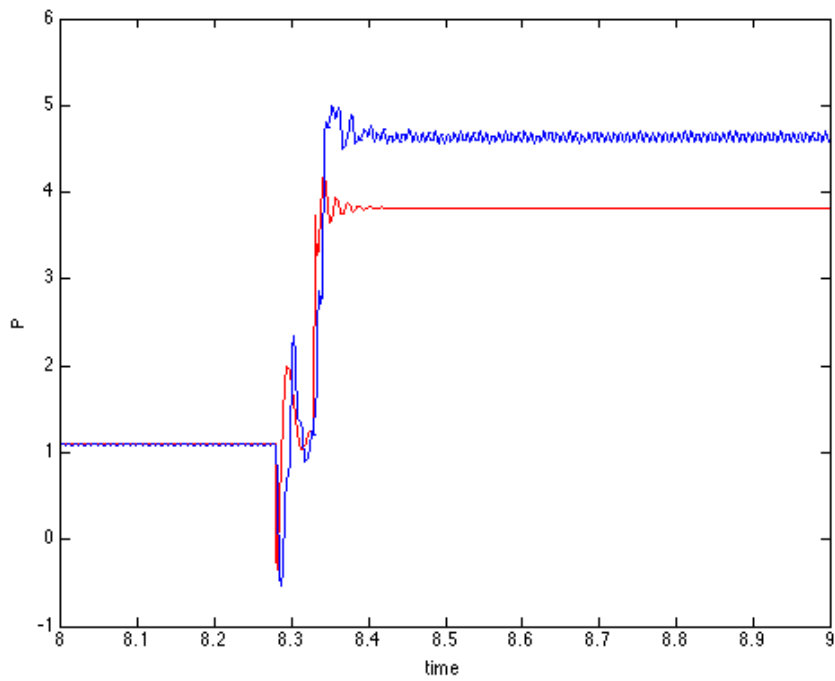


Figure 17. Plot of active power for 3-cycle 52% voltage sag test. The motor stalls.

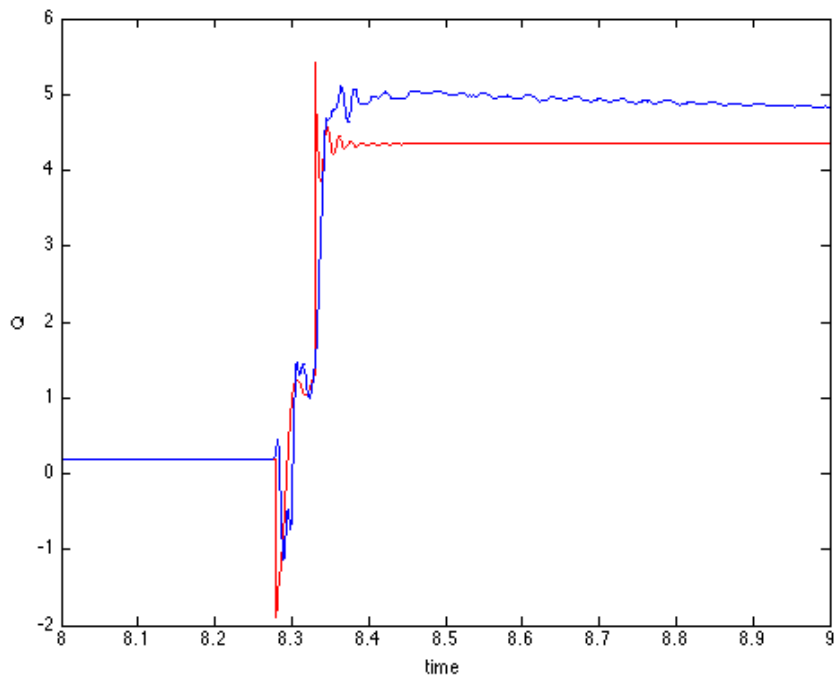
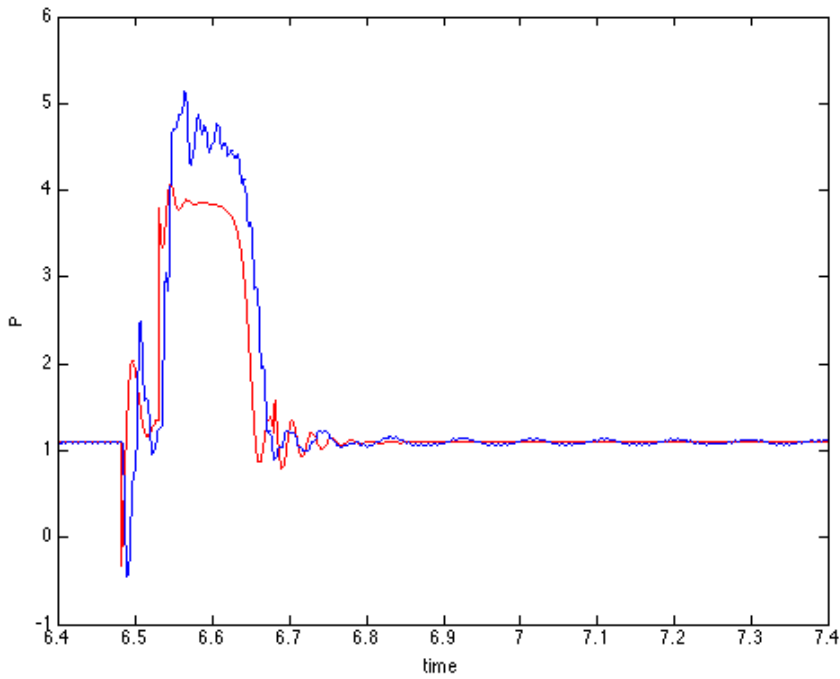
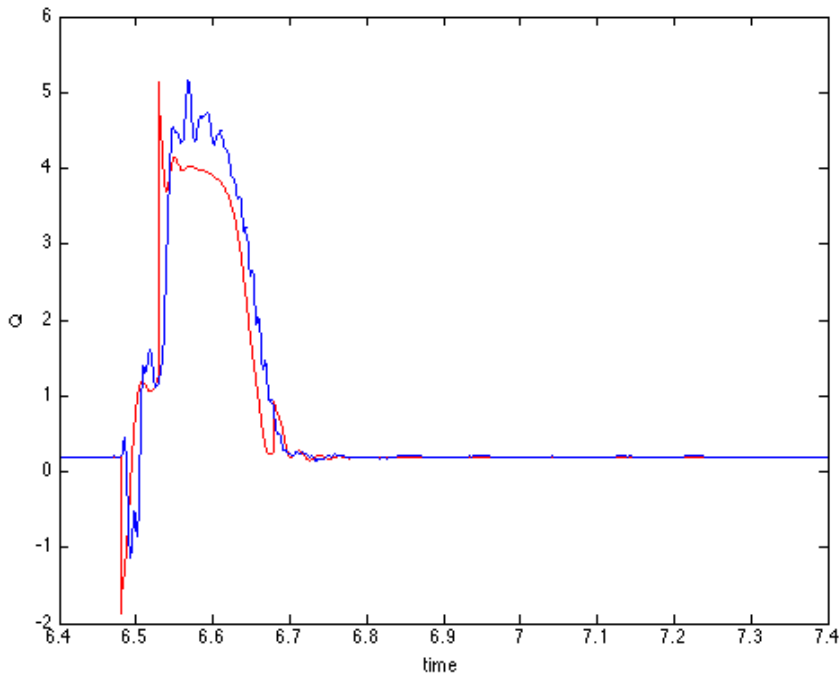


Figure 18. Plot of reactive power for 3-cycle, 52% voltage sag test. The motor stalls.



Plot 19. Plot of active power for 3-cycle, 54% voltage sag test. The motor recovers. (Note that the apparent delay in measured response, approximately 1 cycle, is due to calculation of power from data – using a 1-cycle window.)

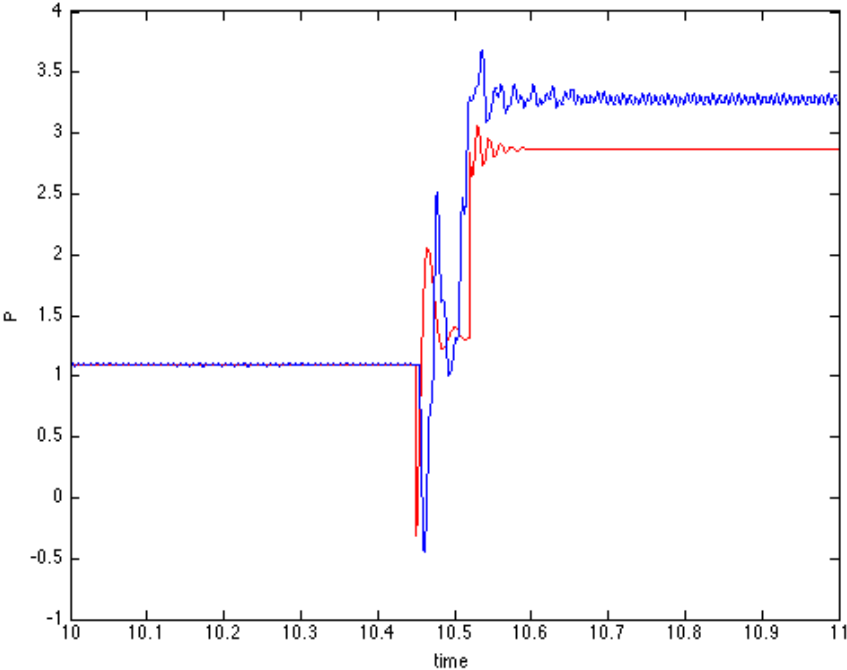


Plot 20. Plot of reactive power for 3-cycle, 54% voltage sag test. The motor recovers. (Note that the apparent delay in measured response, approximately 1 cycle, is due to calculation of power from data – using a 1-cycle window.)

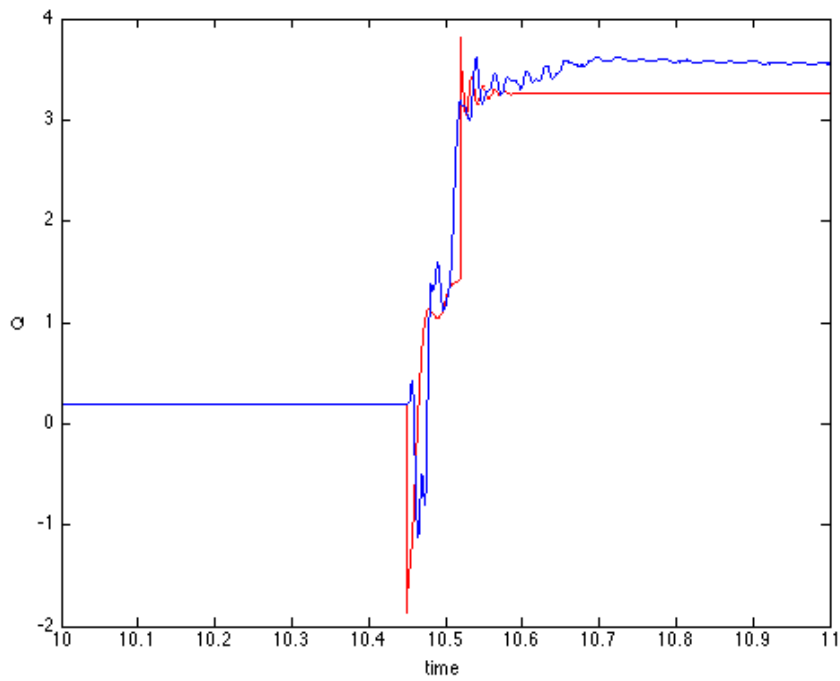
Three-cycle 55% sag, variable recovery voltage

In this test, the voltage sag is fixed at 55% (0.52 terminal) for three cycles and recovery voltages are sought to distinguish between stall and nonstall results. At a recovery voltage of 85% (0.78 terminal) the motor stalls. At a recovery voltage of 90% (0.82 pu rising to 0.88 pu) the motor does not stall.

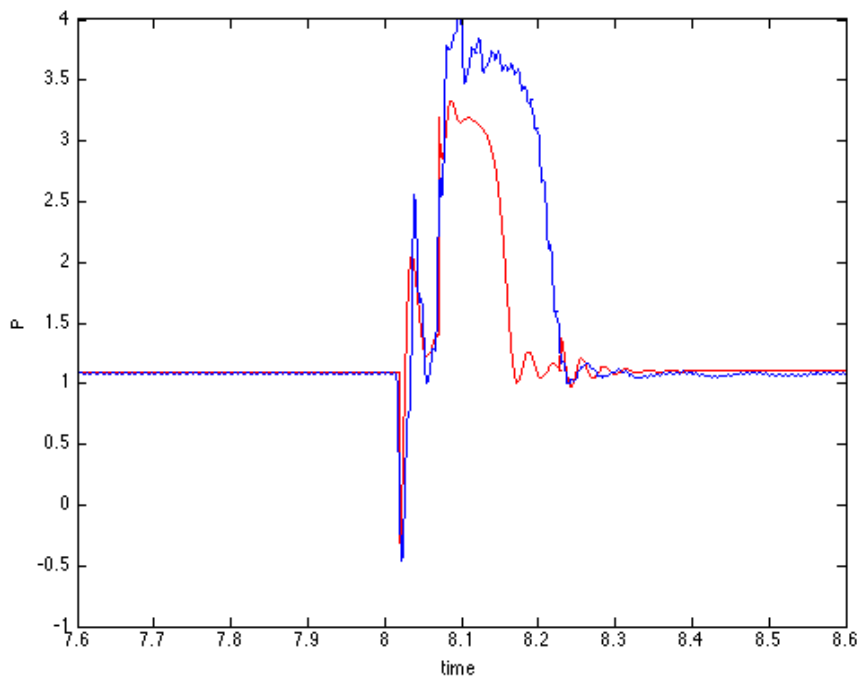
Simulations with $H = 0.0219$ sec. match these results. The following four plots compare the active and reactive powers computed from measurements and simulated using the model described here. The model distinguishes between the stall/non stall conditions, and follows the dynamics reasonably well. The simulated motor response reaccelerates a little more quickly than the test.



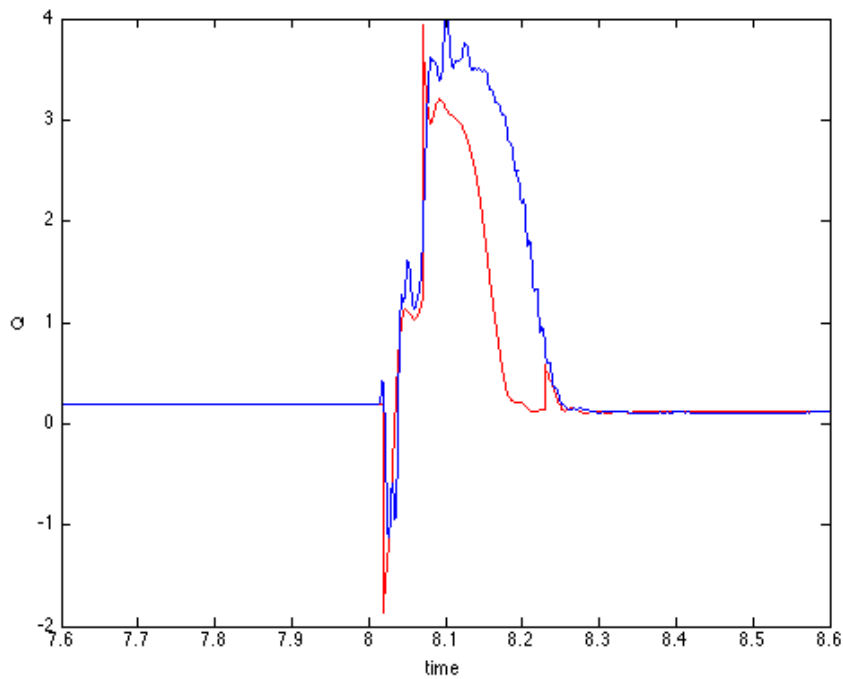
Plot 21. Plot of active power for 3-cycle, 55% voltage sag test with recovery voltage equal to 80%. The motor stalls.



Plot 22. Plot of reactive power for 3-cycl3, 55% voltage sag test with recovery voltage equal to 80%. The motor stalls.



Plot 23. Plot of active power for 3-cycl3, 55% voltage sag test with recovery voltage equal to 90%. The motor recovers.



Plot 24. Plot of reactive power for 3-cycl3, 55% voltage sag test with recovery voltage equal to 80%. The motor recovers

30-cycle, 80% recovery voltage

In this test, the sag voltage is varied to determine the threshold between stall and non-stall. For a sag voltage of 63% (0.58 pu terminal at 30 cycles, and decreasing), and recovery voltage of 80% (0.73 terminal), the motor stalls. For a sag voltage of 64% (0.61 pu at 30 cycles, and increasing), the motor does not stall. Thirty cycles is a long time for a fault, and this test comes close to identifying a steady-state stall voltage for the specified load.

Simulations with $H = 0.0219$ sec. match these results.

Summary:

From these simulations it appears that an inertia constant of $H = 0.0219$ sec. is appropriate for this simulation model.

4. Conclusions

The model presented here is clearly capable of representing the behavior observed in the laboratory tests. The laboratory tests are comprehensive. The voltage ramp tests operating conditions between full and zero voltage – identifying the motor stall voltage along the way. The voltage oscillation tests for the response that may be observed in the system under certain conditions, as does the frequency test. Both, in fact, test for frequencies beyond those typically observed in the system. The voltage sag tests confirm that the model can capture the stall/recover characteristics of these motors.

Continuing work involves the application of the model in system-wide studies, and the development of an automated procedure for parameters estimation to match laboratory tests.

FINAL PROJECT REPORT

LOAD MODELING TRANSMISSION RESEARCH

APPENDIX E

**AIR CONDITIONER STALLING UNIT LEVEL SOLUTIONS TEST
REPORT**

Prepared for CIEE By:

Lawrence Berkeley National Laboratory



University of California
ciee

A CIEE Report



SOUTHERN CALIFORNIA
EDISON[®]

An *EDISON INTERNATIONAL*[®] Company

Air Conditioner Stalling Unit Level Solutions Test Report

By:

TDBU

**Engineering Advancement
Power Systems Technologies**

Richard Bravo
Robert Yinger
Loic Gaillac

The preparation of this white paper was conducted with support from the California Energy Commission's (CEC) Public Interest Energy Research (PIER) Program, WA# MR-049, through the California Institute of Energy and the Environment, Award Number MTX-06-01, and support from Southern California Edison (SCE).

Legal Notice

This report was prepared as a result of work sponsored by the CEC, SCE, and the University of California (UC). It does not necessarily represent the views of the CEC, SCE, UC, the State of California, or their employees. The CEC, SCE, UC, and the State of California or any of these entities' employees, make no warranty, expressed or implied, and assume no legal liability for the information in this report; nor does any party represent that the use of this information will not infringe upon privately owned rights. This report has not been approved or disapproved by the CEC, SCE, or UC, nor has the CEC, SCE, or UC passed upon the accuracy or adequacy of the information in this report.

1.0	EXECUTIVE SUMMARY	5
1.1	Introduction.....	5
1.2	Work Performed.....	5
1.3	Testing Results.....	6
1.3.1	Digital Thermostats Test Results	6
1.3.2	Under-Voltage Relays Test Results	6
1.3.3	Load Control Switch Test Results	7
1.3.4	Conclusion	7
2.0	OBJECTIVE	9
3.0	SCE PROPOSED STALL PROTECTION PARAMETERS.....	10
	Short Cycle Protection Time:.....	11
	Cold Load Pickup Protection:.....	11
4.0	DIGITAL PROGRAMMABLE THERMOSTATS TESTING.....	13
4.1	Honeywell Digital Programmable Thermostat Test Results	14
4.1.1	Specifications.....	14
4.1.2	Non-Installed Testing.....	15
4.1.3	Installed Testing.....	15
4.2	Totaline Digital Programmable Thermostat Test Results.....	19
4.2.1	Specifications.....	19
4.2.2	Non-Installed Testing.....	20
4.2.3	Installed Testing.....	20
4.3	Ritetemp Digital Programmable Thermostat Test Results	23
4.3.1	Specifications.....	23
4.3.2	Non-Installed Testing.....	24
4.3.3	Installed Testing.....	25
5.0	UNDER-VOLTAGE PROTECTION DEVICES	27
5.1	ICM Controls Under-Voltage Relay Test Results	29
5.1.1	Specifications.....	29
5.1.2	Non-Power Test	30
5.1.3	Under-Voltage Protection.....	31
5.1.4	Electronics Shutdown	31
5.1.5	Short Cycle Protection Time.....	31
5.1.6	Test Details	31
5.2	Diversified Electronics 240-VAC Plug-in Under-Voltage Relay Test Results	33
5.2.1	Specifications.....	33
5.2.2	Non-Power Test	34
5.2.3	Under-Voltage Protection.....	35
5.2.4	Electronics Shutdown	35
5.2.5	Short Cycle Protection Time.....	35
5.2.6	Test Details	35
5.3	Diversified Electronics CV-100RS Plug-In Under-Voltage Relay Test Results.....	37
5.3.1	Specifications.....	37
5.3.2	Non-Power Test	38
5.3.3	Under-Voltage Protection.....	39
5.3.4	Electronics Shutdown	39
5.3.5	Short Cycle Protection Time.....	39
5.3.6	Test Details	39

5.4	Diversified Electronics Mount-In Under-Voltage Relay Test Results	41
5.4.1	Specifications	41
5.4.2	Non-Power Test	42
5.4.3	Under-Voltage Protection	42
5.4.4	Electronics Shutdown	43
5.4.5	Short Cycle Protection Time	43
5.4.6	Test Details	43
5.5	Kriwan Under-Voltage Relay Test Results	44
5.5.1	Specifications	44
5.5.2	Non-Power Test	45
5.5.3	Under-Voltage Protection	46
5.5.4	Electronics Shutdown	46
5.5.5	Short Cycle Protection Time	46
5.5.6	Test Details	46
5.6	CSE Under-Voltage Relay Test Results	48
5.6.1	Specifications	48
5.6.2	Non-Power Test	49
5.6.3	Under-Voltage Protection	49
5.6.4	Electronics Shutdown	50
5.6.5	Short Cycle Protection Time	50
5.6.6	Test Details	50
5.7	PNNL Grid-Friendly Device Test Results	52
5.7.1	Specifications	52
5.7.2	Under-Voltage Protection	52
5.7.3	Electronics Shutdown	52
5.7.4	Short Cycle Protection Time	53
5.7.5	Test Details	53
5.8	Cannon Technologies Load Control Switch (LCS) Test Results	55
5.8.1	Specifications	55
5.8.2	Under-Voltage Protection	55
5.8.3	Electronics Shutdown	56
5.8.4	Short Cycle Protection Time	56
5.8.5	Test Details	56
6.0	CONCLUSION	56

1.0 EXECUTIVE SUMMARY

1.1 Introduction

Southern California Edison (SCE) and other utilities have been experiencing occurrences of delayed voltage recovery following faults on the electrical system (see figure 1). Under normal conditions, voltage recovers to nominal levels less than one second after the fault is cleared. In several incidents the past few years, voltage recovery has been delayed for more than 30 seconds after normal fault clearing at some SCE substations. These cases usually occur at substations located in areas with hot climates and new housing developments. This delayed voltage recovery can be attributed to the stalling of air conditioner units. SCE tested 10 residential air conditioning units to assess their response to delayed voltage recovery transients. The tests indicated that all 10 air conditioning units stalled when exposed to these types of transients. This study proposes that the installation of under-voltage protection devices such as under-voltage relays or digital programmable thermostats are possible solutions to the air conditioner stalling problem.

Figure 1 is a typical delayed voltage recovery profile on a SCE 220 KV circuit. This figure indicates that immediately after the fault, the voltage decreases to 79 percent of nominal voltage (point 1); the voltage on the distribution circuits dips even lower. This drop in voltage causes air conditioner units to stall and the stalled air conditioner units prevent the voltage from recovering to a nominal level (point 2). When the air conditioning units' thermal overload protection switches trip, the voltage recovers but overshoots the nominal voltage (in this case 6 percent above) because the capacitor banks are still connected to the circuit (point 3). This over-voltage causes another problem, the capacitor banks tripping off due to over-voltage (point 4). With the capacitors tripped off and the load (air conditioners) returning, the voltage dips below the nominal voltage (points 5 & 6). This could lead to additional problems because it makes the circuit more vulnerable to similar chains of events.

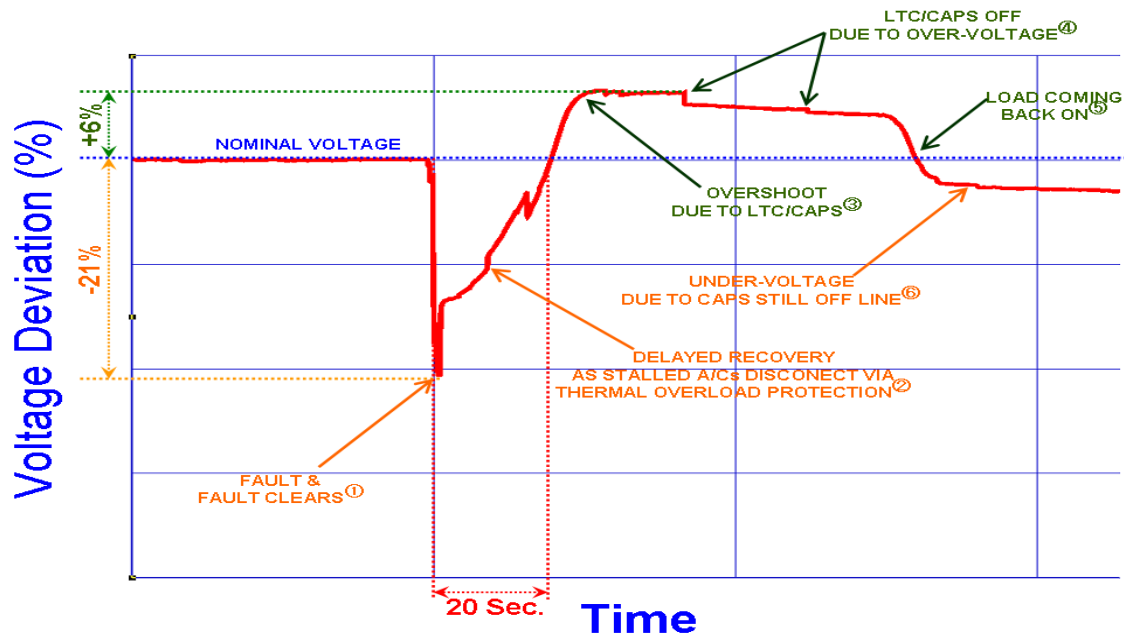


Figure 1 - Typical Delayed Voltage Recovery

1.2 Work Performed

SCE tested under-voltage protection devices and digital programmable thermostats to determine their response during under-voltage events and assess their ability to mitigate the air conditioner stalling problem. The test results will help SCE determine the best possible solutions to address the problem at its source, air conditioner units installed along the SCE power grid. SCE tested three digital programmable thermostats, seven under-voltage relays, and one load control switch (refer Table 3). All testing was conducted at its Pomona Electric Vehicle Technical Center (EVTC).

1.3 Testing Results

This summary section contains the under-voltage transients test results for selected under-voltage protection devices, load control switches, and digital programmable thermostats.

1.3.1 Digital Thermostats Test Results

Three digital programmable thermostats were tested to assess their response during under-voltage transients. The test results determined that only one thermostat had under-voltage protection, the Honeywell thermostat. Although this thermostat's under-voltage protection and response time do not currently meet SCE's proposed stall protection specifications, it may help mitigate the air conditioner stalling problem. To meet SCE's proposed stall protection specifications, this thermostat would need the following reconfigurations:

- ◆ Raise the under-voltage protection threshold to 78 percent of rated voltage
- ◆ Quicken the under-voltage response time to 250 milliseconds (15 cycles)
- ◆ Randomly time (3 to 5 minutes) the short cycle protection

A recommended additional modification is to allow the air handler fan to run when the thermostat trips off the compressor due to an under-voltage transient. This will help dissipate the stored cooling while the compressor is off.

The use of thermostats to mitigate the air conditioner stalling problem is one of the easiest retrofit solutions. In most cases retrofitting thermostats would not require a qualified electrician because in California, only branch circuits rated greater than 100 VA require a qualified electrician and most residential thermostats circuits are rated below 24 VA.

The disadvantage of using the Honeywell thermostat to mitigate the air conditioner stalling problem is that it needs the common "C" wire. This wire is used to provide power to the thermostat's electronics. The common "C" wire started being used after the release of digital programmable thermostats in the mid-1990s.

1.3.2 Under-Voltage Relays Test Results

Seven under-voltage protection relays were tested to assess their response during under-voltage transients. Test results indicate that two of the tested relays (CSE and PNNL) have the under-voltage protection needed to mitigate the air conditioner stalling problem but will require minor adjustments to meet SCE's proposed stall protection specifications. These two relays are still in developmental stages; therefore, their implementation may be delayed due to the need for further testing, certifications, mass production, and retrofit time.

The test results also indicate that three other under-voltage protection devices manufactured by Diversified Electronics (DE) have under-voltage protection that may help mitigate the air conditioner stalling problem. These three relays are off-the-shelf devices, but clearly have some disadvantages. First, they do not have a randomly distributed short cycle-prevention allowing them to restart at the same time after voltage is restored to normal conditions. This might keep the voltage depressed and cause further stalling of air conditioners. Second, they use normally open (N.O.) contacts that prevents the units from restarting if the under-voltage relay fails. All other tested under-voltage protection devices provided limited stall protection, which may help to some degree, but will not alleviate the air conditioner stalling problem. The installation of any of these under-voltage protection relays in California would require a qualified electrician for retrofit because the served circuits will be rated at more than 100-VA.

1.3.3 Load Control Switch Test Results

Cannon Technologies' load control switch was tested. These switches are mainly used to remotely control motor load during times of high system load demand. Initial testing of this device indicated it did not have the desired stall protection. Cannon Technologies claims it reconfigured this load control switch's software to meet SCE's proposed stall protection specifications. Our recent tests indicate that this device was indeed reconfigured and it now meets SCE stall protection specifications. Its disadvantage is that it will be more expensive than the average under-voltage relay; it has extra features (such as load control and demand response) and will require additional retrofitting labor because California law requires a qualified electrician when served circuits are more than 100-VA.

1.3.4 Conclusion

The most viable solution to the air conditioner stalling problem is the use of digital programmable thermostats with stall protection capability. The challenge will be working with various thermostat manufacturers to ensure that their products meet SCE's proposed stall protection specifications. It must be noted: this solution may not protect older units (those installed prior to the mid-1990s) because many do not have the common "C" wire used to power today's thermostat electronics. This remedy's effectiveness will only be realized as older air conditioners are replaced with new units having the common "C" wire. Another viable solution is the use of plug-in under-voltage protection relays that meet SCE's proposed stall protection specifications. This fix offers easy installation on window air conditioners and plug-in air handlers. Either of these solutions would be relatively simple and less costly remedies because they will not require a certified electrician for implementation.

The next most viable solution is the use of devices such as under-voltage relays or load control switches with SCE’s proposed stall protection specifications. This solution is less attractive than the others because it would require qualified electricians to perform the retrofits, adding a labor cost of \$90 to \$100 per installation.

Table 1 shows the test results for the various devices in our study. The potential column is an SCE assessment of how viable each device is in protecting air conditioners from stalling. Notice that the devices with the highest score are those in developmental stages.

	Manuf.	Model	UV Threshold (%V)	Response Time (sec.)	Electronics Shutdown (%V)	Re-close Delay (sec.)	Control Contacts	Potential (%)
Thermostats	Honeywell	RTH7400D100 §	60%	0.760	can't tell	290	N.O.	Medium-High
	Totaline	P374-1800	none	none	can't tell	none	N.O.	none
	Ritetemp	8022C	none	none	can't tell	none	N.O.	none
Under-Voltage Relays	ICM	ICM491	86%	5.100	75%	6	N.O.	Low
	DE	CV-200RS-20 Plug-in	83%	0.300	can't tell	300	N.O.	Medium
	DE	CV-100RS Plug-in	78%	0.232	can't tell	300	N.O.	Medium
	DE	CV-240-AFN Mount-in	83%	0.483	can't tell	300	N.O.	Medium
	Kriwan	JNT369	68%	0.294	can't tell	120	N.O.	Medium-Low
	CSE	N/A	78%	0.25	15%	180 ~ 300	N.C.	High
	PNNL	N/A	77%	0.033	40%	180 ~ 300	N.C.	High
LCS	Cannon	N/A	80%	0.264	33%	180 ~ 300	N.C.	High

Table 1 - Test Results

2.0 OBJECTIVE

The objective of this testing is to investigate how under-voltage protection devices and digital programmable thermostats respond to under-voltage transients. SCE tested seven under-voltage relays, one load control switch, and three digital programmable thermostats (Table 2) to assess their stall protection capabilities.

	Manufacturer	Model Number	Name	Cost
Digital Programmable Thermostats				
1	Honeywell	RTH7400D1008	Digital Thermostat	\$100
2	Totaline	P374-1800	Digital Thermostat	\$70
3	Rittemp	8022C	Digital Thermostat	\$80
Under-voltage protection Relays				
1	ICM Controls	ICM491	Single Phase Line Monitor	\$50
2	Diversified Electronics	CV-200RS-20 Plug-in	Voltage Band Monitor with Short Cycle Protector	\$80
3	Diversified Electronics	CV-100RS Plug-in	Voltage Band Monitor with Short Cycle Protector	\$80
4	Diversified Electronics	CV-240-AFN Mount-in	Under-voltage Short Cycle Protector	\$80
5	CMP Corporation – Kriwan Division	JNT369	Motor Protector	\$80
6	Corporate Systems Engineering	N/A	A/C Under Voltage Relay	\$10 *
7	Pacific Northwest National Laboratory	N/A	Grid Friendly Device	N/A
Load Control Switch				
1	Cannon	N/A	Load Control Switch	N/A

Table 2 - Tested Devices

3.0 SCE PROPOSED STALL PROTECTION PARAMETERS

Air conditioner testing performed by SCE, Electric Power Research Institute (EPRI) and the Bonneville Power Administration (BPA) indicates that air conditioners stall very quickly, within a mere 6 cycles. The stall threshold (voltage point where air conditioners start stalling) is dependent on temperature – the warmer the temperature, the higher the stalling threshold. SCE found that the average stall threshold voltage is 73 percent when outdoor temperatures reach 115 °F. The stalling threshold could be even higher when the air conditioner unit is overcharged. SCE decided to use a 78 percent stalling threshold voltage, 5 percent higher than the average and 2 percent below a typical compressor’s lowest voltage nameplate rating.

Figure 2 shows the voltages of the SCE proposed stall protection parameters chosen after analyzing the air conditioner testing results.

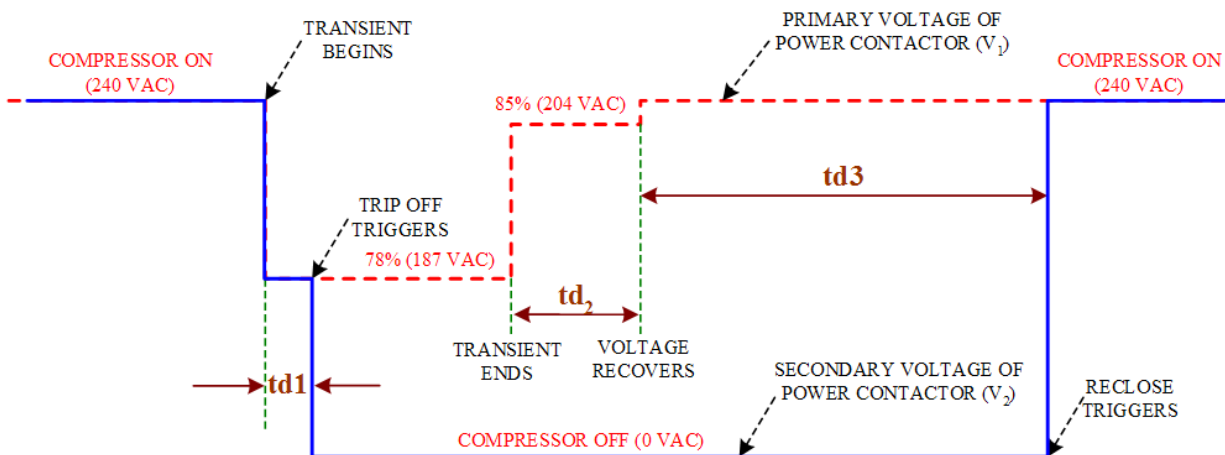


Figure 2 - Proposed Stall Protection Parameters

Table 3 provides the ideal parameters and their corresponding SCE specifications:

1	Under-voltage trip level	78 % of nominal voltage
2	Trip response time (td_1)	6 – 15 cycles
3	Voltage recovery condition	85% for at least 15 sec (td_2)
4	Contacts re-close delay time (td_3) or short cycle protection	3 to 5 minutes, random
5	Lowest operation voltage	40% of nominal voltage
6	Contacts type	Normally closed (N.C.) contacts
7	Cold load pick up	After loss of power during an under-voltage event

Table 3 - SCE Proposed Stall Protection Specifications

In order to minimize false tripping SCE recommends measuring currents to confirm the stalling conditions. The test results indicate that when the air conditioner stalls, the current quickly (within 2 - 3

cycles) exceeds 3.0 p.u. When stall protection devices fail the use of normally closed contacts (N.C.) will not lockout the air conditioner.

Short Cycle Protection Time:

Short cycle protection time prevents the air conditioner from turning back on before the pressure bleeds off (releases). If the air conditioner is allowed to turn back on when pressure is built up, it might stall because the electrical torque would not be able to overcome the built up mechanical torque.

Cold Load Pickup Protection:

Cold load pickup protection waits for a predetermined time after power is restored before it allows the compressor to restart. This avoids high inrush currents in the distribution feeders immediately following power restoration. The high inrush currents cause a voltage drop which can result in air conditioner stalling or circuit tripping.

3.1. TRANSIENT TEST TYPE

This test report focuses on the response of under-voltage protection relays and digital programmable thermostats to under-voltage events such as the long-notch transient. The nominal rated voltage used for all the tests is 240 VAC.

Figure 3 shows the long-notch type transient used to determine how the thermostats, under-voltage protection relays, and load control switches behave during under-voltage transients. The characteristics to be examined are: under-voltage protection threshold, under-voltage response time, electronics shutdown voltage and time, short cycle protection, and cold load pickup.

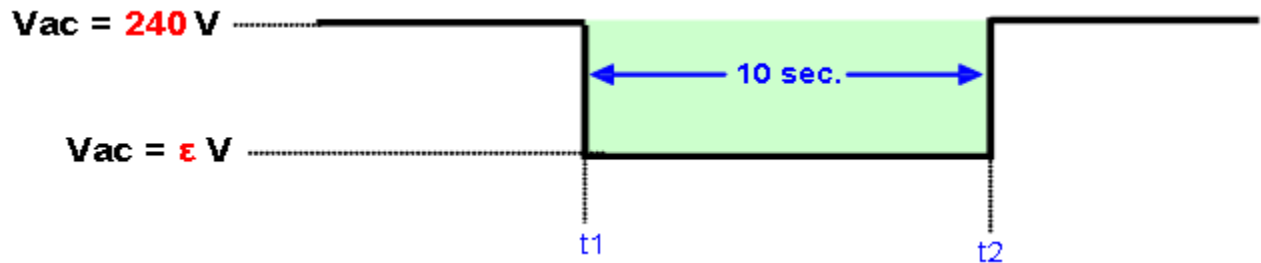


Figure 3 - Long-Notch Transient

Figure 4 shows the short-fast type of transient used to determine how the thermostats, under-voltage protection relays, and load control switches, behave during short and fast under-voltage transients such as typical transmission circuit breakers' clearing times.

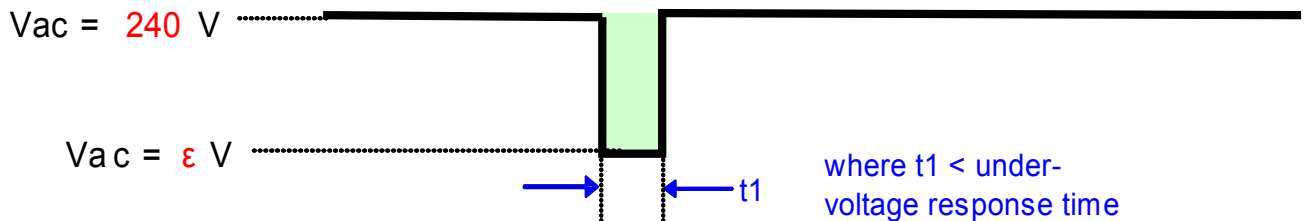


Figure 4 - Short-Fast Transient

4.0 DIGITAL PROGRAMMABLE THERMOSTATS TESTING

Testing was performed on the Honeywell, Totaline and Ritetemp devices to assess how digital programmable thermostats perform during under-voltage transients. Digital programmable thermostats are used to control the indoor temperature by turning the air conditioner compressor on and off. Thermostats also have a fan switch that turns the indoor fan on and off providing cooled airflow to the served area. They also have a system switch with three settings (cool, off and heat). Of the three, we are most interested in the cool setting, the standard setting when an air conditioner is turned on. Thermostats also have a temperature setting switch that allows selection of the desired temperature. The tests were performed when the air conditioner was running properly (system switch = cool & fan switch = auto & TSET < TACTUAL), cooling down the desired area. Figure 5 refers to the typical installation of a digital programmable thermostat. The common “C” wire (purple) that runs from the air handler unit to the digital programmable thermostat came into standard use for residential air conditioners in the mid-1990s. This wire provides power to the digital programmable thermostat electronics.

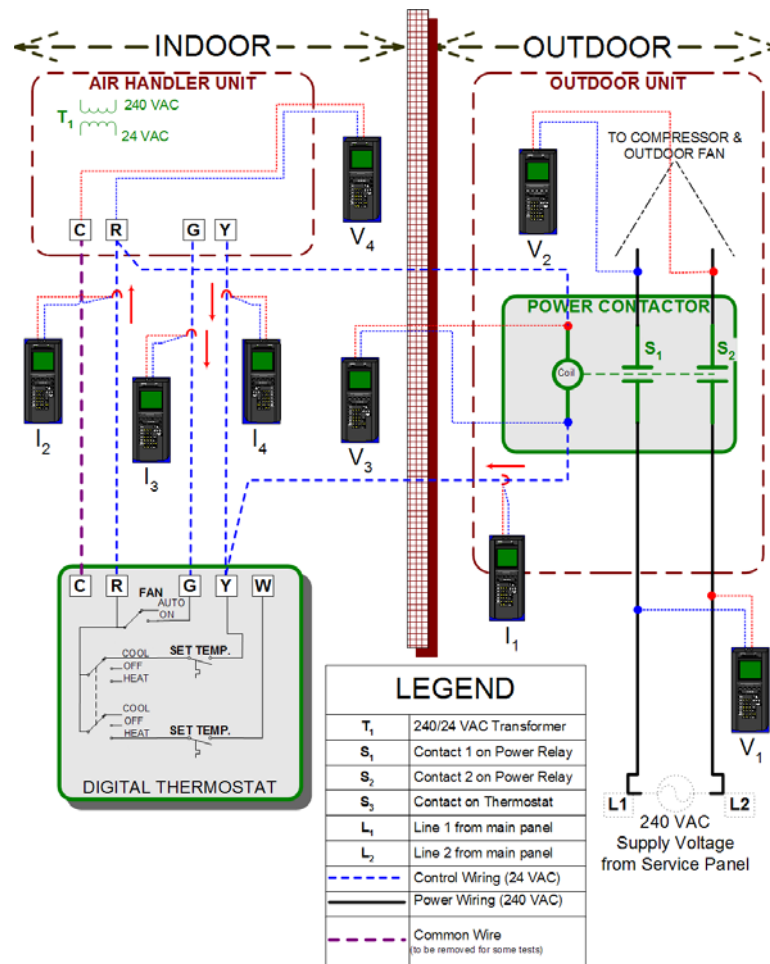


Figure 5 - Programmable Digital Thermostat Typical Installation

4.1 Honeywell Digital Programmable Thermostat Test Results

This high-end off-the-shelf digital programmable thermostat was purchased at a popular local warehouse store. The Honeywell Digital Programmable thermostat's system-button has cool, off, and heat modes. Its fan-button has on and auto positions. Its temperature-button ranges from 50°F to 99°F. This thermostat also has schedule and clock buttons. The under-voltage testing was done in the cool position (system-button = cool & fan-button = on & TSET < TACTUAL).

Test results indicate that this thermostat's:

- ◆ Under-voltage protection threshold is 60 percent, but only works with the common wire "C"
- ◆ Under-voltage protection response is 1.2 seconds at the voltage threshold and 0.4 seconds at lower under-voltages
- ◆ Short cycle protection time is approximately 5 minutes and the compressor is not protected when the under-voltage transient persists longer than 5 minutes, allowing the compressor to restart, which can cause the compressor to stall for 6 cycles
- ◆ Short cycle protection is activated by:
 - Under-voltage trip off
 - Change in system-button positions
 - Actual temperature increases above the set temperature
 - Power loss and initial electronics power on (cold load pick up protection)
- ◆ Cold load pickup protection is 5 minutes after power is restored

Although this thermostat's under-voltage protection is lower and the under-voltage response time is longer than SCE's proposed stall protection specifications, this thermostat could help mitigate the air conditioner stalling problem. But, in order for this thermostat to meet SCE's specifications for stall protection, it would need the following changes:

- Raise the under-voltage threshold to 78 percent
- Shorten its response time to about 6 to 15 cycles (100 to 300 milliseconds)
- Randomize the cycle protection time
- Prevent the compressor from restarting during under-voltages

Additional improvements needed for this thermostat include:

- The fan should be allowed to run when the thermostat trips off the compressor due to an under-voltage transient. This will allow the fan to dissipate any coolant stored in the cooling coil
- The compressor should not be allowed to restart during under-voltages lower than 85 percent
- The internal energy storage device (capacitor) should be enlarged. This will allow the thermostat to work at lower voltages for longer periods of times; it currently takes 0.5 seconds but needs at least 4 seconds

4.1.1 Specifications

Table 4 provides the specifications for the tested Honeywell digital programmable thermostat.

Manufacturer		Honeywell		
Model Number		RTH7400D1008		
Name		Digital Programmable Thermostat		
Line Terminals Ratings				
Voltage		24 VAC		
Frequency		50/60 Hz		
Time Delay		Not specified		
Cycle Protection Time		5 minutes		
Selector Buttons				
System	Fan	Temperature Selector	Schedule	Clock
Terminals				
Common "C"	Return "R"	Green "G"	Yellow "Y"	White "W"
Contacts				
Cooling		Heating		Fan
"R" and "Y" terminals		"R" and "W" terminals		"R" and "G" terminals
Picture				

Table 4 - Honeywell Digital Programmable Thermostat Specifications

4.1.2 Non-Installed Testing

These tests monitored the Honeywell thermostat's response to different settings without any external connections. The following observations were noted:

- When the thermostat had no batteries the thermostat electronics shut down and its resistance among all terminals was infinity
- When the batteries were installed, the thermostat went into short cycle protection (wait state), which took approximately 5 minutes to clear
- With batteries installed and the thermostat in cool mode (system switch = cool & fan switch = on & TSET < TACTUAL) the short cycle protection timed out. This caused:
 - The R-G (fan switch) terminal's resistance to lower, indicating the fan switch was in the "on" position
 - The short cycle protection wait state to be enabled only if:
 - There were any change in the system's switch position ending in the "cool" position
 - The actual temperature equaled or surpassed the set temperature (TSET > TACTUAL) indicating no further cooling was needed at the time

4.1.3 Installed Testing

The following tests were performed on the Honeywell thermostat with all the standard residential connections (including the common wires, batteries) and after the short cycle protection “wait” state timed out.

4.1.3.1 System, Fan and Temperature Buttons Testing

The system fan and temperature buttons are used to control the cooling and heating functions of the thermostat. They were tested to assess their functionality. With the thermostat in cool mode (system switch = cool & fan switch = auto & TSET < TACTUAL) and the compressor and fan running normally, the following observations were made:

- ◆ The fan switch changes did not activate any function while the compressor was running
- ◆ When the system switch was turned off the compressor shut down and cycle protection activated immediately, the fan ran normally
- ◆ When the system switch was turned to ‘off’ or ‘heat’ and then back to ‘cool’ the short cycle protection activated immediately, the fan ran normally
- ◆ When the actual temperature equaled the set temperature, the compressor shut down immediately and the short cycle protection activated immediately, the fan ran normally
- ◆ The fan only ran when the system switch was in the cool position or the fan switch was on

4.1.3.2 Under-Voltage Transient Testing

Tests were done to assess how the thermostat behaves during under-voltage transients. The under-voltage transients were applied with the thermostat in ‘cool’ mode (system switch = cool & fan switch = auto & TSET < TACTUAL) and the compressor running normally. The following observations were made:

- ◆ Its under-voltage threshold is 60 percent of the rated voltage
- ◆ Its under-voltage protection response time is 1.2 seconds at 60 percent of the rated voltage and 0.6 seconds at 50 percent of the rated voltage
- ◆ Its short cycle protection timed out in approximately 5 minutes
- ◆ Allowed the compressor to restart for 6 cycles during under-voltage transients but only after short cycle protection timed out
- ◆ It has no protection for transients faster than 0.65 seconds
- ◆ Its electronics never shut down because it had batteries; therefore, it had under-voltage protection even at total power loss

Table 5 provides the test results for the Honeywell Digital Programmable Thermostat.

V _{SAG} (%)	t _{SAG} (Sec.)	t _{RESPONSE} (Sec.)	Comments
Long Under-voltage Transient Test			
62	10	N/A	Nothing
60	10	1.2	* Compressor and fan tripped off
60	10	1.26	* Short cycle-protection "wait" mode was enabled
60	10	1.28	* Compressor came back on in approx. 5 min.
55	10	0.6	NOTE: The indoor fan was shut down after compressor tripped off by an under-voltage transient. The fan remained off until the short cycle-prevention timed out.
50	10	0.6	
Short-Fast Under-voltage Transient Test			
40	0.45	0.45	* Power contactor opened * The compressor and the fan tripped off at end of transient * Short cycle-protection "wait" mode was enabled * Compressor came back on in approx. 5 min.
0	0.40	0.40	NOTE: The indoor fan was shut down after compressor tripped off by an under-voltage transient. The fan remained off until the short cycle-prevention timed out.
60	0.80	0.283	* Compressor and fan tripped off * Short cycle-protection "wait" mode was enabled * Compressor came back on in approx. 5 min.
60	0.50	none	No under-voltage protection, transient too fast
60	0.65	none	
40	0.25	none	* Power contactor opened * No thermostat protection, Transient too fast * Electronics did not die
40	0.35	none	
0	0.10	none	
0	0.20	none	
0	0.30	none	
0	0.30	none	

Table 5 - Honeywell Digital Programmable Thermostat Test Results

4.1.3.3 Under-Voltage Testing without Batteries

This test was performed maintaining all the previous connections and settings with one exception; the batteries were removed. The common "C" and return "R" wires powered the thermostat electronics. The tests indicate this thermostat's under-voltage threshold was 58 percent of the rated voltage. The tests also indicate that it had an energy storage device allowing it to work for some time (0.5 seconds) at low voltages before its electronics shutdown. The thermostat's cycle protection was activated at voltage recovery to protect the compressor. Table 6 summarizes the test results.

V _{SAG} (%)	t _{SAG} (Sec.)	t _{HOLD-ON} (Sec.)	Comments
60	10	N/A	Electronics did not shutdown
58	10	0.44	* Electronics shutdown in 0.5 sec after applying the transient
55	10	0.66	* Short cycle-protection was activated at voltage recovery
50	10	0.40	* Restart in approximately 5 minutes after voltage recovery

Table 6 - Honeywell Digital Programmable Thermostat without Batteries Test Results

4.1.3.4 Under-Voltage Testing with Batteries and without Common “C” Wire

The removal of the “C” wire causes the thermostat to have no under-voltage protection.

4.1.3.5 Under-Voltage Testing without Batteries and Common “C” Wire

The removal of the “C” wire and batteries makes the thermostat inoperable. The thermostat electronics are powered by batteries and/or the 24-volt transformer with common “C” and return “R” wires. Without a source of energy to operate its electronics this thermostat becomes inoperable.

4.2 Totaline Digital Programmable Thermostat Test Results

This high-end off-the-shelf digital programmable thermostat was purchased from a local air conditioner contractor. The Totaline Digital Programmable thermostat's system switch has cool, off, and heat positions. Its fan switch has on and auto settings. Its temperature-setting button has ranges from 35°F to 90°F. It has additional buttons for programming temperatures and setting the clock. Under-voltage testing was done with the button set to the cool position (system switch = cool & fan switch = on & TSET < TACTUAL). This thermostat did not have a battery compartment; therefore, does not require batteries.

Test results indicated the Totaline thermostat:

- ◆ Does not have any under-voltage protection
- ◆ Short cycle protection
 - Did not activate with total power loss or electronics shutdown
 - Activated when the actual temperature rose above the set temperature or with changes to the system switch settings
 - Lasted approximately 5.5 minutes
- ◆ Does not have a cold load pickup protection after its electronics shuts down

Testing concluded that this thermostat provides no under-voltage protection; therefore, it would not mitigate the air conditioner stalling problem.

4.2.1 Specifications

Table 7 provides the specifications for the tested Totaline digital programmable thermostat.

Manufacturer		Totaline			
Model Number		P374-1800			
Name		Digital Programmable Thermostat			
Line Terminals Ratings					
Voltage		24 VAC			
Frequency		50/60 Hz			
Time Delay		Not specified			
Cycle Protection Time		5 minutes			
Selector Buttons					
Mode (System)	Fan	Temperature Selector	Outside Temperature	Humidity	Program/Clock
Terminals					
Common "C"	Return "R"	Green "G"	Yellow "Y"	White "W"	
Contacts					
Cooling		Heating		Fan	
"R" and "Y" terminals		"R" and "W" terminals		"R" and "G" terminals	
Picture					

Table 7 - Totaline Digital Programmable Thermostat Specifications

4.2.2 Non-Installed Testing

These tests were performed to observe the thermostat's response to setting changes without any external connections. Since this thermostat does not have batteries, it needs no power to turn on its electronics. All its terminals had infinite resistance among each other.

4.2.3 Installed Testing

These tests were performed with all the standard residential connections including the common "C" wire. The short cycle protection caused by power loss clears this thermostat's memory and allows the compressor to restart following the power loss.

4.2.2.1 System, Fan, and Temperature Setting Buttons Testing

Tests were performed to assess the functionality of the system, fan, and temperature-setting buttons used for controlling the cooling and heating functions of the thermostat. When the thermostat was in the cool mode (system switch = cool & fan switch = auto & TSET < TACTUAL) and the compressor was running normally, the following observations were made:

- ◆ The compressor and indoor fan ran normally
- ◆ Fan switch changes did not change anything while the compressor was running
- ◆ When the system switch was turned off, the compressor shut down and the short cycle protection activated immediately, the fan ran normally
- ◆ When the system switch was turned to 'off' or 'heat' and then back to the 'cool' position, the short cycle protection activated immediately, the fan ran normally
- ◆ When the actual temperature reached the set temperature, the compressor shut down and the short cycle protection activated immediately, the fan ran normally
- ◆ The fan ran when the system switch was in the 'cool' position and/or the fan switch was in the 'on' position

4.2.2.2 Under-Voltage Testing

These tests were performed to assess how the Totaline thermostat behaves during under-voltage transients. The under-voltage transients were applied when the thermostat was in the cool mode (system switch = cool & fan switch = auto & TSET < TACTUAL) and the compressor was running normally. Table 8 shows the test results indicating this thermostat's lack of under-voltage protection. We also found that neither total power loss nor electronics shutdown protected the compressor when power was restored.

V_{SA} G (%)	t_{SAC} (Sec.)	$t_{RESPONSE}$ (Sec.)	Comments
Long Under-voltage Transient Test			
60	10	none	Nothing
50	10	none	* Power contactor opened for all of the transient period
45	10	none	* No short cycle-protection after voltage recovery
43	10	none	* Electronics shutdown in 0.6 sec for the duration of the transient period
40	10	none	* Power contactor opened for transient period and approx. 3.1 sec after recovery
			* No short cycle-protection after voltage recovery
Short-Fast Under-voltage Transient Test			
40	0.70	none	* Electronics shutdown in 0.6 sec for the duration of the transient period
			* Power contactor opened for transient period and approx. 3.1 sec after recovery
40	1.00	none	* No short cycle-protection after voltage recovery
40	0.30	none	* Electronics did not shutdown
40	0.50	none	* Power contactor opened for the duration of the transient period
0	0.30	none	* No short cycle-protection after voltage recovery

Table 8 - Totaline Digital Programmable Thermostat Test Results

4.2.2.3 Under-Voltage Testing Without Batteries

This test was not possible because this thermostat does not require batteries.

4.2.2.4 Under-Voltage Testing without Common "C" Wire

The removal of the “C” wire causes the thermostat to be inoperable because this wire powers this thermostat’s electronics.

4.3 Ritetemp Digital Programmable Thermostat Test Results

This high-end off-the-shelf digital programmable thermostat was purchased from a local air conditioner contractor. The thermostat's mode (system) switch has cool mode, off, and heat positions. Its fan switch has on and auto positions. Its temperature-setting button has ranges from 35°F to 90°F. It has additional buttons for programming temperatures and setting the clock. Under-voltage testing was done with the button settings in the cool position (system switch = cool & fan switch = on & TSET < TACTUAL).

Test results indicate the Ritetemp thermostat:

- ◆ Does not have any under-voltage protection
- ◆ Short cycle protection
 - Lasted approximately 5 minutes
 - Activates with changes to system switch settings or when temperature settings equal the actual temperature
- ◆ Does not have a cold load pickup protection after its electronics shut down

This thermostat does not have any under-voltage protection; therefore, it would not help mitigate the air conditioner stalling problem.

4.3.1 Specifications

Table 9 provides specifications for the tested Ritetemp digital programmable thermostat.

Manufacturer	Ritetemp			
Model Number	8022C			
Name	Digital Programmable Thermostat			
Line Terminals Ratings				
Voltage	24 VAC			
Frequency	50/60 Hz			
Time Delay	Not specified			
Cycle Protection Time	5 minutes			
Selector Buttons				
Mode (System)	Fan			
Select Buttons				
Outside Temperature	Filter	Program	Time	Temperature Selector
Terminals				
Common "C"	Return "R"	Green "G"	Yellow "Y"	White "W"
Contacts				
Cooling		Heating		Fan
"R" and "Y" terminals		"R" and "W" terminals		"R" and "G" terminals
Picture				

Table 9 - Ritetemp Digital Programmable Thermostat Specifications

4.3.2 Non-Installed Testing

These tests were performed to observe the thermostat's response to different settings without any external connections. The thermostat did not work without a battery installed because its electronics were shut down. Without batteries, the resistance between "R" (return) and "G" (green) terminals follow the fan switch settings. The resistance among all other terminals is infinite, meaning they are isolated from each other.

When the batteries were removed the electronics took about 1.5 minutes to shut down. The short cycle protection activates immediately when batteries are installed or when the cool temperature is lower than the actual temperature. It took approximately 5.5 minutes for the short cycle protection to clear. With the batteries installed and thermostat settings in cool mode (system switch = cool & fan switch = on & TSET < TACTUAL), the following observations were made:

- ◆ The R and G fan switch terminals had low resistance indicating the fan switch was in the "on" position

- ◆ The short cycle protection (wait state) enabled immediately if the actual temperature reached or surpassed the set temperature ($TSET > TACTUAL$) and cooling of the desired area was accomplished
- ◆ Short cycle protection was not enabled by any system switch position changes

4.3.3 Installed Testing

These tests were performed on the Ritetemp thermostat with all the standard residential connections including the common wire “C” and batteries.

4.3.2.1 System, Fan, and Temperature Setting Switches Testing

These tests were performed to assess the functionality of the system, fan, and temperature-setting switches used to control the cooling and heating functions of the thermostat. When the thermostat was in the cool mode (system switch = cool & fan switch = auto & $TSET < TACTUAL$) with the compressor running normally, it was observed:

- ◆ The compressor and indoor fan ran normally
- ◆ Fan switch changes did not activate any function while the compressor was running
- ◆ When the system switch was turned off, the compressor shut down and the short cycle protection activated immediately, the fan ran normally
- ◆ When the system switch was turned to ‘off’ or ‘heat’ and then back to the ‘cool’ position, the short cycle protection activated immediately, the fan ran normally
- ◆ When the actual temperature equaled the set temperature, the compressor shut down immediately and the short cycle protection activated immediately, the fan ran normally
- ◆ The fan only ran when the system switch was in the cool position or the fan switch was on

4.3.2.2 Under-Voltage Testing

These tests were performed to assess how the thermostat behaves during under-voltage transients. The under-voltage transients were applied when the thermostat had batteries in place, was in ‘cool’ mode (system switch = cool & fan switch = auto & $TSET < TACTUAL$) and the compressor was running normally. Table 10 provides the test results, revealing that this thermostat does not have any under-voltage protection and neither total power loss nor electronics shutdown activated the cycle protection.

V_{SA} C (%)	t_{SAG} (Sec.)	$t_{RESPONSE}$ (Sec.)	Comments
Power contactor opened			
70	10	none	Nothing
65	10	none	
60	10	none	
50	10	none	* Power Contactor opened for all of the transient period * Electronics did not shutdown * Cycle protection did not activate at voltage recovery
40	10	none	
20	10	none	
0	10	none	

Table 10 - Ritetemp Digital Programmable Thermostat Test Results

4.3.2.3 Under-Voltage Testing with Batteries and without Common “C” Wire

This test revealed that the thermostat did not provide any under-voltage protection even with both batteries and the “C” wire installed.

4.3.2.4 Under-Voltage Testing without Batteries and Common “C” Wire

The thermostat electronics shut down; therefore, the thermostat does not function without batteries and without the “C” wire.

5.0 UNDER-VOLTAGE PROTECTION DEVICES

Under-voltage protection devices were tested to assess how well they perform during under-voltage transient events. These devices are used to protect motors from dangerously high currents that can damage the compressor windings. Eight under-voltage protection devices were tested, two of which were prototypes.

Figure 6 shows a typical wire-in under-voltage protection relay connection in the control circuit loop. The under-voltage protection device monitors the supply voltage and disconnects the control circuit when a predetermined under-voltage condition is present. The device has four terminals: two are connected to the supply voltage (240 VAC) for monitoring the voltage, and two (contact S4) are connected in series with the control circuit loop and serve to open the air conditioner power contactor. These under-voltage relays typically have a normally open (N.O.) and/or a normally closed (N.C.) contact. This loop usually begins at the 24 VAC side of the potential transformer, goes through the thermostat contact and power contactor coil, and then returns to the power transformer. For testing purposes, the thermostat relay contact was omitted from the control circuit loop as shown in Figure 6. The under-voltage protection device's contacts will only open if a predetermined under-voltage condition is present in the supply voltage. Digital programmable thermostats were not used in this test because they were evaluated in a separate set of tests.

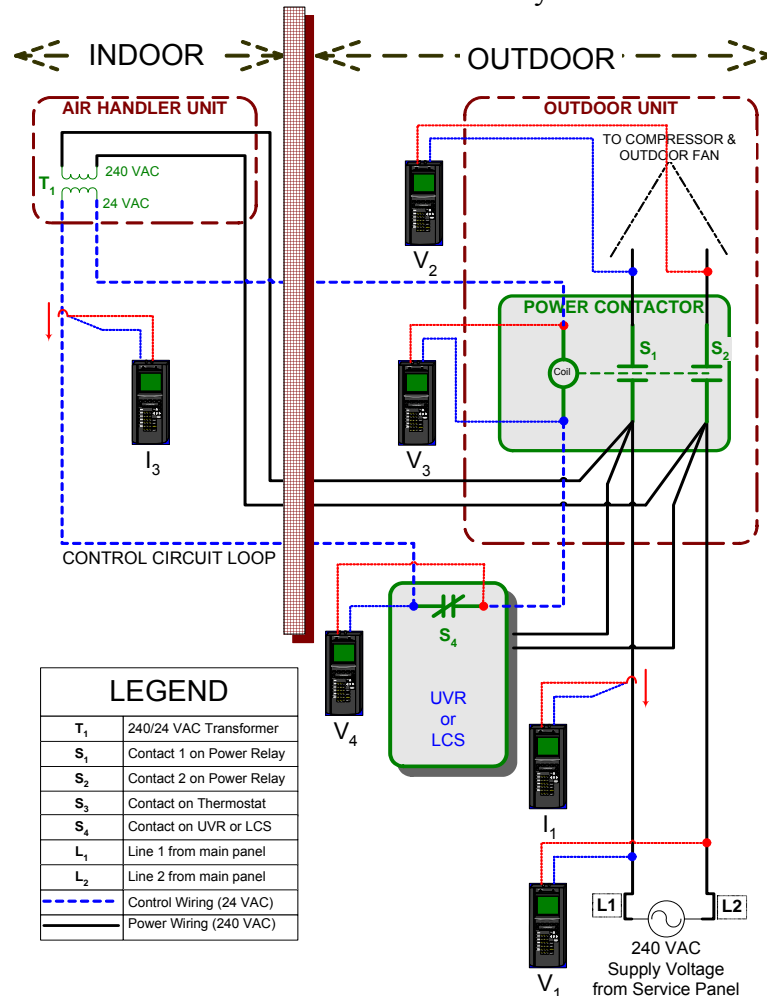


Figure 6 - Under-Voltage Protection Device Test Setup Installation

Figure 7 shows the typical plug-in under-voltage protection connection used for this test. This type of under-voltage protection device does not have control contacts; it only has power contacts in line with the supply voltage. This under-voltage relay monitors the supply voltage and disconnects its output voltage when a predetermined under-voltage condition is present. This type of relay has a plug-in side which is connected to a power outlet and has a outlet side where the loads are connected. For this test, a load will not be needed to determine proper operation. In an actual installation the load would be in the air handler unit, window air conditioner, or the power transformer because the contacts have low amperage ratings and would not be able to handle the normal full motor load of split A/C compressors.

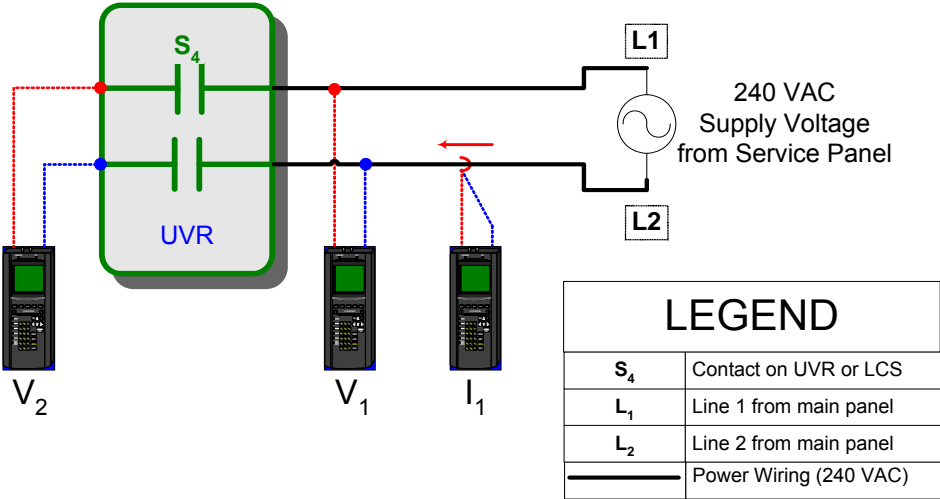


Figure 7 - Plug-in Type Under-Voltage Protection Device Test Setup Installation

5.1 ICM Controls Under-Voltage Relay Test Results

The ICM Controls under-voltage relay has two knobs that can be manually adjusted. The first is the voltage tripping set point knob with a range of 190 VAC (80 percent) to 270 VAC (110 percent) of the full rated voltage. We set this knob to the lowest set point, 190 VAC for all the performed tests. The second knob is the under-voltage delay time knob and its settings go from 6 seconds to 10 minutes. We set this knob to the lowest set point, 6 seconds, for most of the performed tests. This under-voltage relay has two sets of contacts, normally closed (N.C.) and normally open (N.O.), for under-voltage protection. We used the normally closed (N.C.) contacts for this test.

Test results indicate this device's:

- ◆ Under-voltage protection threshold is 86 percent
- ◆ Under-voltage protection response time is approximately 4.8 seconds
- ◆ Short cycle protection time is 6 seconds
- ◆ Cold load pickup protection does not work

- ◆ This under-voltage protection device does not have adequate under-voltage protection logic to mitigate the air conditioner stalling problem.

5.1.1 Specifications

Table 11 provides the specifications for the tested ICM Controls under-voltage relay.

Manufacturer	ICM Controls	
Model Number	ICM491	
Part Number	ICM491	
Name	Single Phase Line Monitor	
Line Terminals Ratings		
Voltage	240 VAC	
Frequency	50/60 Hz	
Time Delay	0.045 seconds	
Short Cycle Time Delay	0.1 to 10 minutes	
Selector Voltage Switch	190 to 270 VAC	95 – 135 VAC
High Voltage cut-out	Selected + 12%	
High Voltage cut-in	Selected + 8%	
Low Voltage cut-out	Selected - 12%	
Low Voltage cut-in	Selected - 8%	
Control Contacts Terminals Ratings		
Amperage	5 Amps @ 277 VAC	
Contacts Type	Normally Open (N.O.) & Normally closed (N.C.)	
Picture		

Table 11 - ICM Controls Under-Voltage Relay Specifications

5.1.2 Non-Power Test

This test was performed on the ICM relay to find out the type of control contacts this under-voltage protection relay has and to assess whether it was safe to install the device and initiate testing. Table 12 lists the impedance measurements taken from the tested unit. The resistance for the line terminals (L1 and L2) was infinite making it safe for installation. The resistance among the control contacts terminals was infinite and 3.9 Ω, normally open and normally closed contacts respectively.

Power Terminals Resistance L1 – L2 ₂₄₀	2.63 MΩ
Power Terminals Resistance L1 – L2 ₁₂₀	2.67 MΩ
N.O. Control Contacts Terminals Resistance NO – COM	Infinite Ω
N.C. Control Contacts Terminals Resistance NC – COM	3.9 Ω
Power Line 1 (L1)- Control Contacts Terminal Resistance L1 – NO L1 – NC L1 – COM	Infinite Ω
Power Line 2 @ 240 (L2 ₂₄₀)- Control Contacts Terminal Resistance L2 ₂₄₀ – NO L2 ₂₄₀ – NC L2 ₂₄₀ – COM	Infinite Ω
Power Line 2 @ 120 (L2 ₁₂₀)- Control Contacts Terminal Resistance L2 ₁₂₀ – NO L2 ₁₂₀ – NC L2 ₁₂₀ – COM	Infinite Ω

Table 12 - ICM Under-Voltage Relay Impedance

5.1.3 Under-Voltage Protection

Tests indicate this under-voltage relay’s threshold is 86 percent of the full rated voltage (240 VAC). The ICM under-voltage relay provided protection from 86 percent down to 78 percent with the equal protection response times of 4.8 seconds.

The device has a time delay knob that can be adjusted from 6 seconds to 10 minutes. The test results reveal that this knob was not accurate because its response time was 5.28 seconds when set at 6 seconds and its response time measured 4.97 seconds when set at 120 seconds.

5.1.4 Electronics Shutdown

The electronics shut down when the voltage dipped below 76 percent of the full rated voltage for more than 100 milliseconds. With the electronics shut down, this device did not open its control contacts to protect the compressor against under-voltages.

5.1.5 Short Cycle Protection Time

Testing indicates that this under-voltage protection device has a short cycle protection time of 5 seconds when its control contacts open due to an under-voltage. This device did not have any short cycle protection when the electronics came back on following an under-voltage shutdown. This device does not have cold load pickup protection after its electronics shut down.

5.1.6 Test Details

Table 13 provides test details for the ICM Controls under-voltage relay.

V_{SAG} (%)	t_{SAG} (sec.)	$t_{DELAY-SETTING}$ (sec.)	$t_{RESPONSE}$ (sec.)	Comments
Long Under-voltage Protection Test				
88	10	6	none	Nothing happened
86	10	6	4.8	* Control contacts opened * Control contacts re-closed 4.8 sec after voltage recovery * No short cycle protection (only 6 seconds)
80	140	120	4.97	
80	20	6	6	
78	10	6	4.8	
0	30	6	N/A	* Allowed the compressor to restart * No startup delay time, therefore no cold load pickup protection
80	20	120	none	* Nothing because the transient was shorter than the set delay time (120 sec)
75	10	6	none	* Control contacts did not open because electronics died * No short cycle protection
60	10	6	none	
55	10	6	none	* Control contacts did not open because electronics died * Power contactor opened for all of the transient period * No short cycle protection
50	10	6	none	
Short-Fast Long Under-voltage Protection Test				
<50	>0.1	6	none	* Control contacts did not open because electronics died * Power contactor opened for all of the transient period * No short cycle protection
40	2.5	6	none	
0	2.5	6	none	
60	2.5	6	none	* Control contacts did not open because electronics died * No short cycle protection

Table 13 - ICM Under-Voltage Relay Test Results

5.2 Diversified Electronics 240-VAC Plug-in Under-Voltage Relay Test Results

The Diversified Electronics CV-200RS-20 Plug-in under-voltage relay is suitable for use in window type air conditioner units and air conditioner air handlers equipped with 240 VAC plug-in type cords. It does not have control loop contacts but instead has high amperage rating contacts (20 amperes at 240 VAC) between the input and output line terminals. This device can withstand a locked rotor current of 72 amperes for a short period of time. It has a voltage selector switch used to choose voltages rated 240 VAC or 230 VAC. All tests performed on this device were done with the selector switch at 240 VAC, the standard SCE residential voltage.

Test results indicate that this device's:

- ◆ Under-voltage protection threshold is 83 percent and does not work for voltage transients faster than 4 cycles
- ◆ Under-voltage response time is approximately 300 to 100 milliseconds, with longer response times at the higher voltages
- ◆ Short cycle protection time is 5 minutes, without randomization
- ◆ Cold load pickup protection is approximately 5 minutes
- ◆ Contacts are normally open (N.O.)
- ◆ Protects the air conditioner from really low under-voltage transients

Although this device has a higher under-voltage threshold than SCE's proposed stall protection specifications, it could help to mitigate the air conditioner stalling problem. Its under-voltage protection threshold and response delay time are close to SCE's proposed stall protection parameters. Additionally, this device has a good short cycle protection time, similar to what SCE suggests, but without randomization.

It has two disadvantages; first, it has N.O. contacts, which locks out the air conditioner when the under-voltage relay fails. Second, implementation could be difficult because the protected device must have a plug-in electric cord.

5.2.1 Specifications

Table 14 provides the specifications for the tested Diversified Electronics CV-200RS-20 Plug-in under-voltage relay.

Manufacturer	Diversified Electronics	
Model Number	CV-200RS-20	
Part Number	CV-200RS-20	
Name	Voltage Band Monitor with Short Cycle Protector	
Line Terminals Ratings		
Voltage	240 VAC	
Frequency	50/60 Hz	
Short Cycle Time Delay	5 min.	
Selector Voltage Switch	230 VAC	240 VAC
Drop-out Under-voltage	190 VAC	202 VAC
Pick-up Under-voltage	198 VAC	210 VAC
Drop-out Over-voltage	243 VAC	258 VAC
Pick-up Over-voltage	253 VAC	268 VAC
Contacts Terminals Ratings		
Amperage	20 Amps @ 240 VAC	
Lock Rotor Amps (LRA)	72 Amps	
Contacts Type	Normally Open (N.O.)	
Receptacle Type		
Picture		

Table 14 - Diversified Electronics CV-200RS-20 Plug-in Under-Voltage Relay Specifications

5.2.2 Non-Power Test

This test was performed on this relay to determine what type of control contacts the under-voltage protection has and assess whether it was safe to install the device and initiate its testing. Table 15 lists the impedance readings for this device. The resistance among the input power terminals (H1, N1, G1) was infinite, just as it was with the output power terminals (H2, N2, G2). The resistance between the input and output line terminals was infinite, as they were normally open contacts. All the resistance readings indicated it was safe for installation.

Input/Output L1 Power Terminal Resistance L1H1 – L1H2	Infinite Ω
Input/Output L2 Power Terminal Resistance L2H1 – L2H2	4.0 Ω
Input/Output Ground (G) Power Terminal Resistance G1 – G2	4.0 Ω
Input Power (L1 and L2) Terminals Resistance L1H1 – L2H1	Infinite Ω
Input Power (L1) - Ground Terminals Resistance L1H1 – G	Infinite Ω
Input Power (L2) - Ground Terminals Resistance L2H1 – G	Infinite Ω
Output Power (L1 and L2) Terminals Resistance L1H2 – L2H2	Infinite Ω
Output Power (L1) - Ground Terminals Resistance L1H2 – G	Infinite Ω
Output Power (L2) - Ground Terminals Resistance L2H2 – G	Infinite Ω

Table 15 - Diversified Electronics CV-200RS-20 Plug-in Under-Voltage Relay Impedances

5.2.3 Under-Voltage Protection

Tests indicate this relay’s under-voltage threshold is 83 percent of the full rated voltage (240 VAC). It protects from 83 percent down to 50 percent with response times varying from 100 to 300 milliseconds; the longest response time being at the under-voltage threshold. It also protects for voltages below 50% with about the same response time of the power contactor, 2 cycles. This under-voltage relay did not respond to transients faster than 6 cycles (100 milliseconds).

5.2.4 Electronics Shutdown

It was hard to determine the electronics shutdown threshold for this device because it has normally open (N.O.) contacts. When the electronics shut down, the line contacts open and as soon as the voltage recovers the cold load pickup protection activates.

5.2.5 Short Cycle Protection Time

Tests indicate this device has a short cycle protection time of approximately 290 sec (~ 5 minutes). This short cycle protection time is activated by almost any under-voltage event (except transients faster than 6 cycles) including total power loss for any period.

5.2.6 Test Details

Table 16 provides test details for the Diversified Electronics CV-200RS-20 Plug-in under-voltage relay.

V _{SAG} (%)	t _{SAG} (sec.)	t _{RESPONSE} (sec.)	Comments
Long Under-voltage Protection Test			
85	40	N/A	Nothing happened
83	40	0.300	* Control contacts opened * Control contacts re-closed 5 minutes after voltage recovery * Good short cycle-protection
80	40	0.190	
70	40	0.132	
60	40	0.100	
55	40	0.100	
50	40	0.100	* Control contacts opened * Power Contactor opened * Control contacts re-closed 5 minutes after voltage recovery * Good short cycle-protection
Short-Fast Under-voltage Protection Test			
60	0.065	none	Nothing because transient too fast
60	0.100	0.084	* Control contacts opened * Control contacts re-closed 5 minutes after voltage recovery * Good short cycle-protection
40	0.100	0.067	* Control contacts opened * Power Contactor opened * Control contacts re-closed 5 minutes after voltage recovery * Good short cycle-protection
40	0.065	0.067	
0	0.250	0.032	
0	0.100	0.650	
0	0.065	0.087	
0	0.065	0.087	

Table 16 - Diversified Electronics CV-200RS-20 Plug-in Under-Voltage Relay Test Results

5.3 Diversified Electronics CV-100RS Plug-In Under-Voltage Relay Test Results

Diversified Electronics CV-100RS plug-in under-voltage relay is suitable for use in window type air conditioner units or for air conditioner air handlers equipped with 120 VAC plug-in type cords. It does not have control loop contacts; instead, it has high amperage rating contacts 15 amperes at 240 VAC. This device can withstand a locked rotor current of 40 amperes for short period of time. It has a voltage selector switch used to select the rated voltage, 120 VAC or 110 VAC. All tests performed on this device were done with the selector switch at 120 VAC, an SCE residential voltage.

Test results indicate that this device's:

- ◆ Under-voltage protection threshold is 78 percent and does not work for voltage transients faster than 3 cycles
- ◆ Under-voltage response time is approximately 233 milliseconds at the threshold and faster for lower voltage transients
- ◆ Short cycle protection time is 5 minutes, without randomization
- ◆ Cold load pickup protection activates after its electronics shut down
- ◆ Contacts are normally open (N.O.)

Its under-voltage threshold and response delay time are close to SCE's proposed stalled protection parameters. This device has a good short cycle protection time and could be used to protect air handler units rated 120 VAC.

This relay has good under-voltage protection logic to mitigate the air conditioner stalling problem. It has two disadvantages. First, it can only be used in air conditioners rated 120 VAC. Second, it has N.O. contacts, which locks out the air conditioner when the under-voltage relay fails.

5.3.1 Specifications

Table 17 provides the specifications for the tested Diversified Electronics CV-100RS plug-in under-voltage relay.

Manufacturer	Diversified Electronics	
Model Number	CV-100RS	
Part Number	CV-100RS	
Name	Voltage Band Monitor with Short Cycle Protector	
Line Terminals Ratings		
Voltage	120 VAC	
Frequency	50/60 Hz	
Short Cycle Time Delay	5 min.	
Selector Voltage Switch	110 VAC	120 VAC
Drop-out Under-voltage	87 VAC	95 VAC
Pick-up Under-voltage	95 VAC	103 VAC
Drop-out Over-voltage	120 VAC	131 VAC
Pick-up Over-voltage	128 VAC	140 VAC
Contacts Terminals Ratings		
Amperage	15 Amps @ 120 VAC	
Lock Rotor Amps (LRA)	40 Amps	
Contacts Type	Normally Open (N.O.)	
Receptacle Type		
Picture		

Table 17 - Diversified Electronics CV-100RS Plug-in Under-voltage Relay Specifications

5.3.2 Non-Power Test

This test was performed on this relay to determine what type of control contacts the under-voltage protection the device has and assess whether it was safe to install and initiate testing. Table 18 lists the impedance readings for this device. The resistance among the input power terminals (H1, N1, G1) was infinite, just as it was with the output power terminals (H2, N2, G2). The resistance between the input and output hot terminals was infinite, as they were normally open contacts. All the resistance readings indicated it was safe for installation.

Input/Output Hot Terminals Resistance H1 – H2	Infinite Ω
Input/Output Neutral Terminals Resistance N1 – N2	7.2 Ω
Input/Output Ground Terminal Resistance G1 – G2	4.0 Ω
Input Hot and Neutral Terminals Resistance H1 – N1	Infinite Ω
Input Hot and Ground Terminals Resistance H1 – G1	Infinite Ω
Input Neutral and Ground Terminals Resistance N1 – G1	Infinite Ω
Output Hot and Neutral Terminals Resistance H2 – N2	Infinite Ω
Output Hot and Ground Terminals Resistance H2 – G2	Infinite Ω
Output Neutral and Ground Terminals Resistance N2 – G2	Infinite Ω

Table 18 - Diversified Electronics CV-100RS Plug-In Under-Voltage Relay Impedances

5.3.3 Under-Voltage Protection

Tests indicate that this under-voltage relay's threshold is 78 percent of the full rated voltage (240 VAC). The DE 120 relay works from 78 percent down to 0 percent and its response times range from 17 to 232 milliseconds; the longest response time is at the under-voltage threshold. This under-voltage relay does not respond for transients faster than 3 cycles (50 milliseconds). This device's response time is good because it quickens as the voltage decreases.

5.3.4 Electronics Shutdown

It is hard to determine the electronics shutdown threshold because it has normally open (N.O.) contacts. This is because when the electronics shut down, the line contacts open and as soon as the voltage recovers the cold load pickup protection activates.

5.3.5 Short Cycle Protection Time

Tests indicate that this device has a short cycle protection time of approximately 290 sec (~ 5 minutes). This short cycle protection time is activated by almost any under-voltage event (except transients faster than 3 cycles) including total power loss for any period.

5.3.6 Test Details

Table 19 provides test details for the Diversified Electronics CV-100RS plug-in under-voltage relay.

V_{SAG} (%)	t_{SAG} (sec.)	t_{RESPONSE} (sec.)	Comments
Long Undervoltage Transient Test			
80	10	N/A	Nothing happened
78	10	0.232	* Control contacts opened * Control contacts re-closed 5 minutes after voltage recovery * Good short cycle-protection
75	10	0.150	
70	10	0.117	
60	10	0.084	
50	10	0.067	* Control contacts opened * Power Contactor opened * Control contacts re-closed 5 minutes after voltage recovery * Good short cycle-protection
40	10	0.050	
Short-Fast Undervoltage Transient Test			
60	0.100	0.084	* Control contacts opened * Control contacts re-closed 5 minutes after voltage recovery * Good short cycle-protection
60	0.050	none	Nothing because transient was too fast
40	0.050	0.033	* Control contacts opened * Power Contactor opened * Control contacts re-closed 5 minutes after voltage recovery * Good short cycle-protection
0	0.050	0.017	
0	0.100	0.017	

Table 19 - Diversified Electronics CV-100RS Plug-In Under-Voltage Relay Test results

5.4 Diversified Electronics Mount-In Under-Voltage Relay Test Results

The Diversified Electronics CV-240-AFN mount-in under-voltage relay can be installed into the air conditioner outdoor unit using quick connectors. Its contacts have a high amperage rating making it suitable for circuits drawing fewer than 20 amperes at 240 VAC, especially for control loop circuits. This device can withstand a locked rotor current of 52 amperes for a short period of time.

Test results indicate that this device's:

- ◆ Under-voltage protection threshold is 83 percent and does not work for voltage transients faster than 15 cycles
- ◆ Under-voltage response time is approximately 500 milliseconds
- ◆ Short cycle protection time is 5 minutes, without randomization
- ◆ Cold load pickup protection activates after its electronics shut down
- ◆ Contacts are normally open (N.O.)

This under-voltage protection device can help mitigate the air conditioner stalling problem if its under-voltage protection threshold and response time are adjusted to meet SCE's proposed specifications.

5.4.1 Specifications

Table 20 provides the specifications for the tested Diversified Electronics CV-240-AFN mount-in under-voltage relay.

Manufacturer	Diversified Electronics
Model Number	CV-240-AFN
Part Number	CV-240-AFN
Name	Under-voltage Short Cycle Protector
Line Terminals Ratings	
Voltage	240 VAC
Frequency	50/60 Hz
Short Cycle Time Delay	5 min.
Pick-up and Drop-out Voltages	
Drop-out Under-voltage	202 VAC
Pick-up Under-voltage	210 VAC
Drop-out Over-voltage	N/A
Pick-up Over-voltage	N/A
Control Contacts Terminals Ratings	
Amperage	20 Amps @ 240 VAC
LRA	52 Amps
Type	Normally Open (N.O.)
Picture	

Table 20 - Diversified Electronics CV-240-AFN Mount-in Under-Voltage Relay Specifications

5.4.2 Non-Power Test

This test was performed on the this relay to determine what type of control contacts this device has and assess whether it was safe to install and initiate testing. Table 21 lists the impedance readings for this device. The line terminal (L1 and L2) resistance was infinite making it safe for installation. The resistance among the control contacts terminals was infinite, as they were normally open contacts. All the resistance readings indicated it was safe for installation.

Power Line (L1 and L2) Terminals Resistance L1 - L2	Infinite Ω
Control Contacts Terminals Resistance M1 - M2	Infinite Ω
Power - Control Contacts Terminal Resistance L1 - M1 L1 - M2 L2 - M2	Infinite Ω

Table 21 - Diversified Electronics CV-240-AFN Mount-in Under-Voltage Relay Impedance

5.4.3 Under-Voltage Protection

Tests indicated that this under-voltage relay's threshold is 83 percent of the full rated voltage (240 VAC). The Diversified Electronics mount-in relay works from 83 percent down to 30 percent voltage with equal response times of 500 milliseconds. The response time varies for voltages below 30 percent – from the long end at 140 milliseconds, to the shortest at 100 milliseconds. This under-voltage relay does not respond to transients faster than 12 cycles (250 milliseconds).

5.4.4 Electronics Shutdown

It was hard to determine the electronics shutdown threshold for this device because it has normally open (N.O.) contacts, but it seems to be at 30 percent of full rated voltage. If the electronics shut down, the control contacts open. As soon as the voltage recovers the cold load pickup protection activates.

5.4.5 Short Cycle Protection Time

Tests indicated this device has a short cycle protection time of approximately 290 sec (~ 5 minutes). This short cycle protection time is activated by almost any under-voltage event (except transients faster than 3 cycles) including when there is total power loss for any period of time.

5.4.6 Test Details

Table 22 provides test details for the Diversified Electronics CV-240-AFN mount-in under-voltage relay.

V _{SAG} (%)	t _{SAG} (sec.)	t ^{POWER} _{CONTACTOR-OPEN} (sec.)	t ^{RESPONSE} (sec.)	Comments
Long Under-voltage Transient Test				
85	10	N/A	N/A	Nothing happened
83	10	N/A	0.483	* Control contacts opened * Control contacts re-closed 5 minutes after voltage recovery * Good cycle protection
80	10	N/A	0.483	
70	10	N/A	0.516	
60	10	N/A	0.483	
55	10	0.033	0.462	* Power contactor (P.C.) opened * Control contacts opened * Control contacts re-closed 5 minutes after voltage recovery * Good cycle protection * Impossible to tell where electronics start failing
50	10	0.033	0.483	
40	10	0.033	0.440	
30	10	0.016	0.424	
20	10	0.016	0.140	
10	10	0.033	0.100	
Short-Fast Under-voltage Transient Test				
60	<0.250	N/A	N/A	Nothing because transient was too fast
40	<0.240	N/A	N/A	* Power contactor opened for the transient time then re-closed normally
0	<0.250	N/A	N/A	* Control contacts did not get tripped off * No cycle protection

Table 22 - Diversified Electronics CV-240-AFN Mount-in Under-Voltage Relay Test Results

5.5 Kriwan Under-Voltage Relay Test Results

The Kriwan mount-in under-voltage relay can be installed into the compressor unit using quick connectors. This device is commonly used on high-end air conditioner units with Copeland compressors. Its contacts have a low amperage rating of 2.5 amperes at 240 VAC making it only suitable for control circuits. This device also has thermal protection capabilities; its three thermocouples connections protect the compressors against high temperature conditions. These thermocouples were not used during testing instead three resistors were installed to simulate normal temperature conditions.

The test results indicate that this device's:

- ◆ Under-voltage protection threshold is 68 percent and does not work for voltage transient faster than 9 cycles
- ◆ Under-voltage response protection time is approximately 300 milliseconds
- ◆ Short cycle protection time is 2 minutes, without randomization
- ◆ Cold load pickup protection activates after its electronics shut down
- ◆ Contacts are normally open (N.O.)

This under-voltage protection device can help mitigate the air conditioner stalling problem if its under-voltage protection threshold and short cycle protection time are adjusted to meet SCE's proposed stall protection parameters.

5.5.1 Specifications

Table 23 provides the specifications for the tested Kriwan mount-in under-voltage relay.

Manufacturer	CMP Corporation – Kriwan Division	
Model Number	INT369	
Part Number	22A276S21	
Name	Motor Protector	
Line Terminals Ratings		
Voltage	240 VAC	
Frequency	50/60 Hz	
Short Cycle Time Delay	120 ± 20 seconds	
Selector Voltage Switch	120 VAC Automatic	240 VAC Automatic
Drop-out Under-voltage	85 VAC	170 VAC
Contacts Terminals Ratings		
Amperage	2.5 Amps @ 240 VAC	
Contacts Type	Normally Open (N.O.)	
Receptacle Type	N/A	
Picture		

Table 23 - Kriwan Under-Voltage Relay Specifications

5.5.2 Non-Power Test

This test was performed on this relay to determine what type of control contacts this under-voltage protection device has and to assess whether it was safe to install and initiate testing. Table 24 lists the impedance readings for this device. The line terminals (L1 and L2) resistance was 4-K Ω , a high resistance value making it safe for installation. The resistance among the control contacts terminals was infinite, as they have normally open contacts (N.O.). The resistance between each temperature sensor terminal and the common and temperature sensor terminals was 8.04 K- Ω and 6.36 K- Ω respectively. All the resistance readings indicate it was safe for installation.

Power Line (L1 and L2) Terminals Resistance L1 – L2	4 K Ω
Control Contacts Terminals Resistance M1 – M2	Infinite Ω
Power - Control Contacts Terminal Resistance L1 – M1 L1 – M2 L2 – M2	Infinite Ω
Temperature Sensor Terminals Resistance S1 – S2 S1 – S3 S2 – S3	8.04 K Ω
Common - Temperature Sensor Terminals Resistance C – S1 C – S2 C – S3	6.36 K Ω

Table 24 - Kriwan Under-Voltage Relay Impedance

This under-voltage relay also provides temperature protection for events brought on by under-voltage transients or other factors. Temperature sensors located in the motor casing are used to monitor the motor temperature. Because the device didn't have temperature sensors, installation of three resistors (560 Ω) was necessary before testing. These three resistors were installed connecting each of the temperature terminals to the common terminal in the under-voltage protection relay.

5.5.3 Under-Voltage Protection

Tests indicate that the under-voltage protection threshold of this device was 68 percent of the full rated voltage (240 VAC). The Kriwan relay's under-voltage protection works from 68 percent down to 40 percent with equal response times of 300 milliseconds. The response time varies for voltages below 40 percent. This under-voltage protection relay does not respond to transients faster than 9 cycles (150 milliseconds).

5.5.4 Electronics Shutdown

Since this device has normally open contacts it is difficult to tell where the electronics begin to fail. The electronics seem to start failing at approximately 40 percent for transients longer than 300 milliseconds.

5.5.5 Short Cycle Protection Time

The short cycle protection time for this device was 2 minutes. Under-voltage transients lower than the under-voltage threshold and longer than 300 milliseconds activate cycle protection. This cycle protection is also activated at initial power-up and 2 minutes pass before it allows the compressor to start up.

5.5.6 Test Details

Table 25 provides test details for the Kriwan under-voltage relay.

V _{SAG} (%)	t _{SAG} (sec.)	t _{POWER CONTACTOR-OPEN} (sec.)	t _{RESPONSE} (sec.)	Comments
Long Under-voltage Transient Test				
70	10	N/A	N/A	Nothing happened
68	10	N/A	0.440	* Control contacts opened * Control contacts re-closed 2 minutes after voltage recovery * Cycle protection (2 minutes)
65	10	N/A	0.350	
60	10	N/A	0.300	
55	10	N/A	0.300	
50	10	0.016	0.300	* Power contactor opened * Control contacts opened * Control contacts re-closed 2 minutes after voltage recovery * Cycle protection (2 minutes) * Impossible to tell where electronics shutdown (might be 40% because there the response time changes drastically)
45	10	0.016	0.300	
40	10	0.016	0.300	
40	20	0.016	0.300	
35	10	0.016	0.241	
10	10	0.016	0.200	
5	10	0.033	0.200	
Short-Fast Under-voltage Transient Test				
60	0.250	0.016	0.300	* Control contacts opened * Control contacts re-closed 2 minutes after voltage recovery * Cycle protection (2 minutes)
20	0.500	0.016	0.200	* Power contactor opened * Control contacts opened
0	0.500	0.016	0.500	* Control contacts re-closed 2 minutes after voltage recovery * Cycle protection (2 minutes)
0	0.150	0.016	0.067	* Impossible to tell where electronics shutdown (might be 40% because there the response time changes drastically)
60	0.100	N/A	N/A	Nothing because transient was too fast
60	0.150	N/A	N/A	
40	0.150	N/A	N/A	
0	0.100	N/A	N/A	

Table 25 - Kriwan Under-Voltage Relay Test Results

5.6 CSE Under-Voltage Relay Test Results

Corporate Systems Engineering (CSE) developed this device using SCE's proposed stall protection specifications, yielding the proper under-voltage protection logic to mitigate the air conditioner stalling problem. The CSE under-voltage relay can be installed by connecting quick connectors into the compressor unit. Its contacts have a low amperage rating of 3 amperes at 240 VAC making it suitable only for control circuits.

Test results indicated that this device's:

- ◆ Under-voltage protection threshold was 78 percent and does not work for voltage transients faster than 15 cycles
- ◆ Under-voltage response time is approximately 250 milliseconds
- ◆ Short cycle protection time is 3 to 5 minutes, with randomization
- ◆ Cold load pickup protection activates after its electronics shut down
- ◆ Contacts are normally closed (N.C.),

This device's electronics shut down too quickly. Its electronics need to remain active at 40 percent for at least 20 seconds and it must have a cold load pickup to meet SCE's proposed stall protection specifications. Overall, with the recommended adjustments, this device has the capability to mitigate the air conditioner stalling problem. It must be noted that this is a prototype and not yet a commercially available product.

5.6.1 Specifications

Table 26 provides the specifications for the tested CSE under-voltage relay.

Manufacturer	Corporate Systems Engineering
Model Number	N/A
Part Number	N/A
Name	A/C Under Voltage Relay
Line Terminals Ratings	
Voltage	240 VAC
Frequency	50/60 Hz
Short Cycle Time Delay	3~5 minutes in with randomization
Selector Voltage Switch	
Drop-out Under-voltage	187 VAC
Contacts Terminals Ratings	
Amperage	3 Amps @ 24 VAC
Contacts Type	Normally closed (N.C.)
Receptacle Type	N/A
Picture	

Table 26 - CSE Under-Voltage Relay Specifications

5.6.2 Non-Power Test

This test was performed on the CSE relay to determine what type of control contacts this under-voltage protection device has and to assess whether it was safe to install for testing. Table 27 lists the impedance readings for this device. The line terminals (L1 and L2) resistance was infinite Ω , a high resistance value, making it safe for installation. The resistance among the control contacts terminals was 1.4 Ω . It has normally closed (N.C.) contacts.

Power Terminals Resistance L1 – L2	Infinite Ω
Control Contacts Terminals Resistance M1 – M2	4 K Ω
Power - Control Contacts Terminal Resistance L1 – M1 L1 – M2 L2 – M2	Infinite Ω

Table 27 - CSE Under-Voltage Relay Impedance

5.6.3 Under-Voltage Protection

Tests indicate the under-voltage protection threshold of this device was 78 percent of the full rated voltage (240 VAC). The CSE relay's under-voltage protection works from 78 percent down to 15

percent with equal response times of 250 milliseconds. This under-voltage protection relay does not respond to transients faster than 15 cycles (250 milliseconds).

5.6.4 Electronics Shutdown

The electronics started failing at approximately 15 percent for 10-second transients. This device does not have cold load pickup protection after its electronics shut down.

5.6.5 Short Cycle Protection Time

The short cycle protection time of this device was 3 to 5 minutes with randomization. Under-voltage transients lower than the under-voltage threshold and initial startup activate this short cycle protection.

5.6.6 Test Details

Table 28 provides the test details for the CSE under-voltage relay.

V _{SAG} (%)	t _{SAG} (sec.)	t _{POWER CONTACTOR- OPEN} (sec.)	t _{RESPONSE} (sec.)	Comments
Long Under-voltage Transient Test				
80	10	N/A	N/A	Nothing happened
78	10	N/A	0.500	* Control contacts opened * Control contacts re-closed 3~5 minutes randomly after voltage recovery * Good short cycle-protection
75	10	N/A	0.250	
70	10	N/A	0.250	
65	10	N/A	0.250	
60	10	N/A	0.250	
55	10	N/A	0.250	
50	10	0.016	0.250	* Power contactor opened in 1 cycle
40	20	0.016	0.250	* Control contacts opened
40	10	0.016	0.250	* Control contacts re-closed 3~5 minutes randomly after voltage recovery
30	10	0.016	0.250	* Good short cycle-protection
20	10	0.016	0.250	* Electronics OK
15	10	0.016	0.250	
10	10	0.016	0.250	* Power contactor opened in 1 cycle * Control contacts chat then opened. Re-closed 3~5 minutes randomly after voltage recovery * Good short cycle-protection * Electronics start dying
Short-Fast Under-voltage Transient Test				
60	0.250	N/A	N/A	Nothing because transient was too fast
60	0.132	N/A	N/A	
60	0.100	N/A	N/A	
40	0.132	0.016	N/A	* Power contactor opened for the transient time then re-closed normally
0	0.132	0.016	N/A	* Control contacts did not opened * No cycle protection
0	0.100	0.016	N/A	* No cold load pickup -- at 0 VAC the memory clears and there is no cycle protection at start up

Table 28 - CSE Under-Voltage Relay Test Results

5.7 PNNL Grid-Friendly Device Test Results

The PNNL grid-friendly device (GFD) contains a grid-friendly appliance (GFA) chip with circuitry that reduces the 240 VAC to a circuit board voltage level of 5 VDC. The GFA is an electronics chip mainly used to mitigate frequency transients. PNNL has reconfigured the GFA using SCE’s proposed stall protection specifications.

Test results indicated this device’s:

- ◆ Under-voltage protection threshold is 78 percent
- ◆ Under-voltage response time is approximately 33 milliseconds
- ◆ Short cycle protection time is 3 to 4 minutes, with randomization
- ◆ Cold load pickup protection is not available
- ◆ Contacts are normally closed (N.C.) and normally opened (N.O.), in this test N.C. contacts were used
- ◆ Electronics shut down 20 seconds after the voltage reached 40 percent

This device needs a cold load pickup to meet SCE’s proposed stall protection specifications. Overall, with the recommended adjustments, this device has the capability to mitigate the air conditioner stalling problem. It is important to mention that most of this device’s parameters can be adjusted as needed but it is a prototype device needing further testing and certifications.

5.7.1 Specifications

Table 29 provides the specifications for the tested PNNL grid-friendly device.

Manufacturer	Pacific Northwest National Laboratory
Model Number	N/A
Part Number	N/A
Name	Grid Friendly Device
Line Terminals Ratings	
Voltage	240 VAC
Frequency	50/60 Hz
Short Cycle Time Delay	3~5 minutes in with randomization
Selector Voltage Switch	
Drop-out Under-voltage	185 VAC
Contacts Terminals Ratings	
Contacts Type	Normally closed (N.C.) & Normally Open (N.O.)
Receptacle Type	N/A
Picture	Final product is under design

Table 29 - PNNL Grid-Friendly Device Specifications

5.7.2 Under-Voltage Protection

Tests indicated the under-voltage protection threshold for this device was 77 percent of the full rated voltage (240 VAC). The PNNL grid-friendly device’s under-voltage protection works from 77 percent down to 40 percent with equal response times of 33 milliseconds (2 cycles).

5.7.3 Electronics Shutdown

The electronics started failing at approximately 40 percent for 10-second transients. If the electronics shut down, the compressor is allowed to restart immediately after voltage recovery; therefore, this device does not have cold load pickup protection.

5.7.4 Short Cycle Protection Time

The short cycle protection time for this device was 3 to 5 minutes with randomization. Under-voltage transients lower than the under-voltage threshold and initial startup activate this cycle protection.

5.7.5 Test Details

Table 30 provides the test details for the PNNL grid-friendly device.

V_{SAG} (%)	t_{SAG} (sec.)	t_{POWER} CONTACTOR- OPEN(sec.)	t_{RESPONSE} (sec.)	Comments
Long Under-voltage Transient Test				
78	10	N/A	N/A	Nothing happened
77	10	N/A	0.033	* Control contacts opened
75	10	N/A	0.033	* Control contacts re-closed 3~5 minutes randomly after voltage recovery
60	10	N/A	0.033	* Good short cycle-protection
50	10	0.016	0.033	* Power contactor (P.C.) opened in 1 cycle
				* Control contacts opened
40	10	0.016	0.033	* Control contacts re-closed 3~5 minutes randomly after voltage recovery
40	20	0.016	0.033	* Good short cycle-protection
				* Electronics OK
35	10	0.016	N/A	* Power contactor (P.C.) opened in 1 cycle
				* Control contacts did not open
30	10	0.016	N/A	* No short cycle-protection after voltage recovery
				* Electronics shutdown threshold
Short-Fast Under-voltage Transient Test				
Not needed because the under-voltage response time of this device was 2 cycles				

Table 30 - PNNL Grid-Friendly Device Test Results

5.8 Cannon Technologies Load Control Switch (LCS) Test Results

The Cannon Technologies load control switch (LCS) is used to remotely control motor load. Initial testing of this device indicated it can provide limited under-voltage protection. Cannon Technologies was asked to update the LCS software to meet SCE’s proposed stall protection parameters. Recent tests indicate that the device was indeed reconfigured to SCE’s specifications

Test results indicate this device’s:

- ◆ Under-voltage protection threshold is 80 percent and does not work for voltage transients faster than 15 cycles
- ◆ Under-voltage protection response time is approximately 280 milliseconds
- ◆ Short cycle protection time is 4 minutes to 4.5 minutes, with randomization
- ◆ Cold load pickup protection activates after electronics shutdown

This device has normally closed contacts (N.C.), as proposed by SCE; therefore, an N.C. contact failure would not lockout the air conditioner. The electronics shut down at 33 percent (a good reading), which is below SCE’s proposed stall protection parameters. This device has the capability to mitigate the air conditioner stalling problem. It is important to mention that all parameters can be adjusted if needed.

5.8.1 Specifications

Table 31 provides the specifications for the tested Cannon Technologies load control switch.

Manufacturer	Cannon Technologies
Name	Load Control Switch
Line Terminals Ratings	
Voltage	240 VAC
Frequency	50/60 Hz
Short Cycle Time Delay	3~4 minutes in with randomization
Selector Voltage Switch	N/A
Drop-out Under-voltage	192 VAC
Contacts Terminals Ratings	
Amperage	N/A
Contacts Type	Normally closed (N.C.) & Normally Open (N.O.)
Receptacle Type	N/A
Picture	

Table 31 - Cannon Technologies Load Control Switch Specifications

5.8.2 Under-Voltage Protection

Tests indicate the under-voltage protection threshold of this device was 80 percent of the full rated voltage (240 VAC). The under-voltage protection works from 80 percent down to 35 percent with a response time between 200 and 280 milliseconds, the fastest response occurring at the lower voltages.

5.8.3 Electronics Shutdown

The electronics started failing at approximately 33 percent for 10-second transients. This device has cold load pickup protection after its electronics shut down and at startup.

5.8.4 Short Cycle Protection Time

The short cycle protection time of this device was 3 to 4 minutes with randomization. This short cycle-prevention was activated either by under-voltage transients lower than the under-voltage threshold or initial startup.

5.8.5 Test Details

Table 32 provides the test details for the Cannon Technologies load control switch.

V_{SAG} (%)	t_{SAG} (sec.)	t_{POWER} CONTACTOR- OPEN (sec.)	$t_{RESPONSE}$ (sec.)	Comments
Long Under-voltage Transient Test				
85%	10	N/A	N/A	Nothing happened
80%	10	N/A	2.000	* Control contacts opened * Control contacts re-closed 3~5 minutes randomly after voltage recovery * Good short cycle protection
75%	10	N/A	0.250	
70%	10	N/A	0.350	
65%	10	N/A	0.332	
60%	10	N/A	0.267	
55%	10	N/A	0.232	
50%	10	0.033	0.282	* Power contactor (P.C.) opened in ~2 cycles
45%	10	0.033	0.216	* Control contacts opened
40%	10	0.033	0.200	* Control contacts re-closed 3~5 minutes randomly after voltage recovery
35%	10	0.033	0.250	* Good short cycle protection
33%	10	0.033	0.335	* Power contactor (P.C.) opened in ~2 cycles
30%	10	0.033	0.267	* Control contacts opened for couple cycles then re-closed
				* Electronics shutdown
100%	10	N/A	0.500	* No short cycle protection after voltage recovery
				* It has Cold load pickup

Table 32 - Cannon Technologies Load Control Switch Specifications

6.0 CONCLUSION

Comprehensive testing of selected digital programmable thermostats, under-voltage protection devices, and load control switches has led to the following conclusions regarding the air conditioner stalling problem.

Of the three digital programmable thermostats tested for their response to under-voltage transients only one thermostat had under-voltage protection, the Honeywell. This thermostat may help mitigate the air conditioner stalling problem, but its under-voltage protection and response times do not currently meet SCE's proposed stall protection specifications. The use of digital programmable thermostats with proposed under-voltage protection is one of the easiest retrofitting solutions because it would not require a certified electrician. Here in California, retrofitting thermostats would not require a qualified electrician because only branch circuits rated greater than 100 VA require a qualified electrician and most residential thermostats circuits are rated below 24 VA.

The tests revealed that with minor adjustments, two of the seven under-voltage protection relays tested would be able to satisfy SCE's proposed stall protection specifications to mitigate the air conditioner stalling problem. The CSE and PNNL relays have good under-voltage protection. These two relays are prototypes and still in developmental stages; therefore, their implementation may be delayed due to the need for further testing, certifications, mass production, and retrofit time.

Three under-voltage protection devices manufactured by Diversified Electronics (DE) were tested that may have the under-voltage protection that help mitigate the air conditioner stalling problem. These three relays are off-the-shelf devices making them conveniently attainable, but they also come with disadvantages. First, two of them are plug-in devices making them suitable only for window air conditioners and maybe plug-in air handler units. Second, they do not have a randomly distributed short cycle-prevention to allow them to restart at different times after voltage is restored to normal conditions. Third, they use normally open (N.O.) contacts that prevent the units from restarting if the under-voltage relay fails. All other tested under-voltage protection devices provided limited stall protection; while helping to some degree, they will not alleviate the air conditioner stalling problem. Another disadvantage is the retrofit cost – installing any of these under-voltage protection relays in California would require a qualified electrician for retrofit because the served circuits are rated at more than 100-VA, except for the plug-in devices.

One load control switch manufactured by Cannon Technologies was tested. These switches are primarily used to remotely control motor load during times of high system load demand. Initial testing of the device indicated it did not have the desired stall protection, but Cannon Technologies responded and reconfigured the load control switch's software to meet SCE's proposed stall protection specifications. This switch would be the most expensive remedy due to its special features (such as load control and demand response) and retrofit labor costs – its served circuits exceed 100-VA requiring retrofitting by a qualified electrician.

The tests revealed that the most viable solution to the air conditioner stalling problem would be realized by using digital programmable thermostats with stall protection capability. This would require working with various thermostat manufacturers to ensure that their products meet SCE's proposed stall protection specifications. It must be noted: this solution may not protect older units (those installed prior to the mid-1990s) because many do not have the common "C" wire used to power today's thermostat electronics. This remedy's effectiveness will only be realized as older air conditioners are replaced with new units having the common "C" wire. Another viable solution is the use of plug-in under-voltage protection relays that meet SCE's proposed stall protection specifications. This fix offers easy installation on window air

conditioners and plug-in air handlers. Either of these solutions would be relatively simple and less costly remedies because they will not require a certified electrician for implementation.

The next most effective solution is the use of devices such as under-voltage relays or load control switches with SCE's proposed stall protection specifications. This solution is less attractive than the others because it would require qualified electricians to perform the retrofits adding a labor cost of \$90 to \$100 per installation.

FINAL PROJECT REPORT

LOAD MODELING TRANSMISSION RESEARCH

APPENDIX F

AIR CONDITIONER STALLING SOLUTIONS SUMMARY REPORT

Prepared for CIEE By:

Lawrence Berkeley National Laboratory



A CIEE Report



SOUTHERN CALIFORNIA
EDISON[®]

An *EDISON INTERNATIONAL*[®] Company

Air Conditioner Stalling Solutions Summary Report

CEC Load Modeling Project

By:

TDBU

**Engineering Advancement
Power Systems Technologies**

Richard Bravo
Robert Yinger
Deborah Catanese

The preparation of this white paper was conducted with support from the California Energy Commission's (CEC) Public Interest Energy Research (PIER) Program, WA# MR-049, through the California Institute of Energy and the Environment, Award Number MTX-06-01, and support from Southern California Edison (SCE).

Legal Notice

This report was prepared as a result of work sponsored by the CEC, SCE, and the University of California (UC). It does not necessarily represent the views of the CEC, SCE, the UC system, the State of California, or any of these entities' employees. The CEC, the State of California, SCE, and UC make no warranty, expressed or implied, and assume no legal liability for the information in this report; nor does any party represent that the use of this information will not infringe upon privately owned rights. This report has not been approved or disapproved by the CEC, SCE, or UC, nor has the CEC, SCE, or UC passed upon the accuracy or adequacy of the information in this report.

1.0	EXECUTIVE SUMMARY	4
1.1	Introduction.....	4
1.2	Work Performed	5
1.2.1	Air Conditioner Unit-Level Solutions	5
1.2.2	System-Level Solutions	7
1.3	Economic Assessment	8
1.4	Conclusion	9
2.0	REFERENCES.....	10

1.0 EXECUTIVE SUMMARY

1.1 Introduction

SCE and other utilities experience occurrences of delayed voltage recovery following faults on their electrical systems as shown in figure 1. Under normal conditions voltage recovers to nominal levels less than one second after the fault is cleared, but the past few years there have been several instances at some SCE substations when voltage recovery was delayed for more than 30 seconds after normal fault clearing. These events primarily occurred during the heavy summer load at substations located in hot climates and serving new housing developments. Stalling air conditioner units were believed to be causing the delayed voltage recoveries, so SCE tested ten residential air conditioning units to assess their response to these types of transients. All ten air conditioning units stalled when exposed to under-voltage transients.

Figure 1 is a typical delayed voltage recovery profile on a SCE 220 KV circuit. This figure indicates that right after the fault, voltage decreased to 79 percent of nominal voltage (point 1). The radial distribution circuit voltage being much lower, the dip in voltage caused air conditioning units to stall; the stalled air conditioning units kept the voltage from recovering to a nominal level (point 2). When the air conditioner units' thermal overload protection switches tripped, the voltage recovered, but overshoot the nominal voltage (in this case 6 percent above). Because the capacitor banks were still connected to the circuit an over-voltage occurred (point 3). This over-voltage caused another problem, the capacitor banks tripping off (point 4). With the capacitors tripped off and the load (including air conditioners) returning, the voltage went below the nominal voltage (points 5 & 6) making the circuit more vulnerable to other similar chains of events.

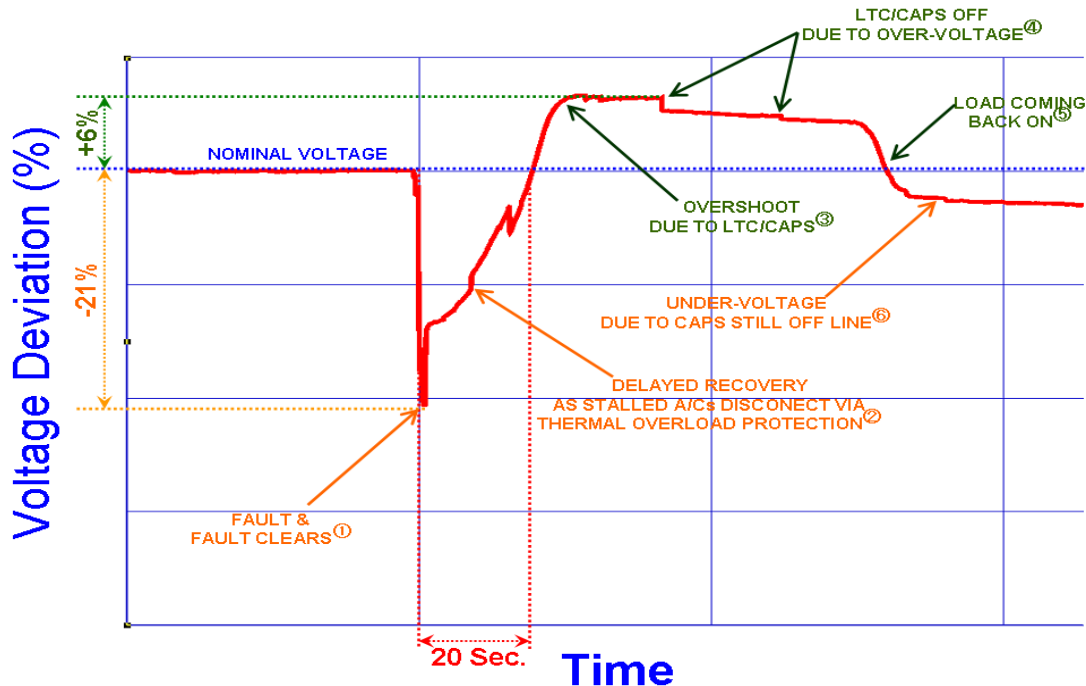


Figure 1 – Typical Delayed Voltage Recovery

Western Electricity Coordinating Council (WECC) dynamic load models do not replicate the observed system response of the delayed voltage recovery events. The WECC's motor model does

not accurately represent the behavior of small induction motors used in air conditioner compressors. This mismatch of real measurements versus the WECC model is shown in figure 2.

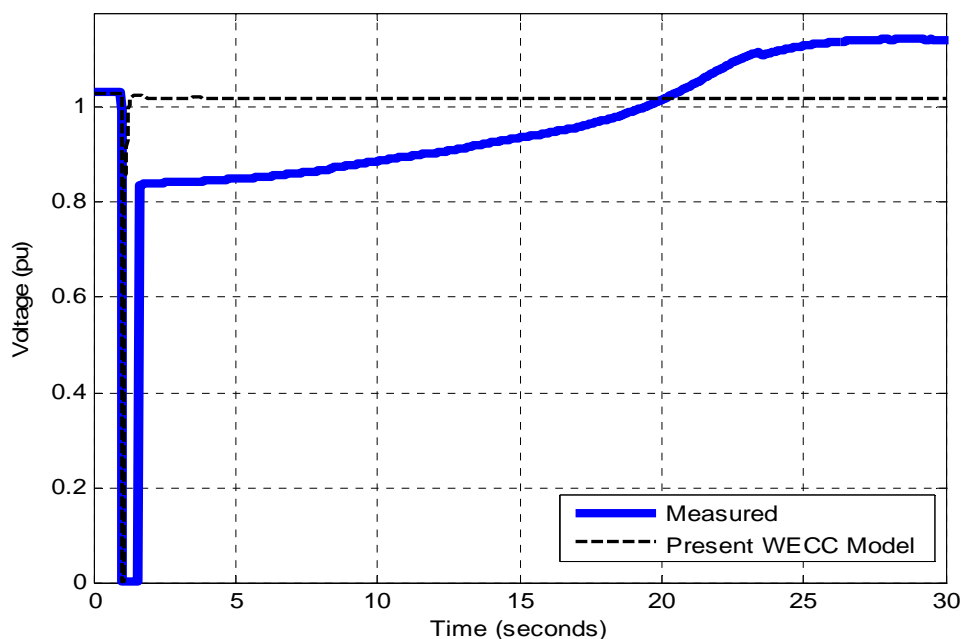


Figure 2 – Delayed Voltage Recovery

1.2 Work Performed

SCE's investigation focused on two approaches for mitigating the air conditioner stalling problem. The first approach was solving the problem at its source, the individual air conditioner units. SCE tested various digital thermostats, under-voltage protection devices, and load control switches to assess their ability to mitigate the air conditioner stalling problem. The second approach attempted to mitigate the problem at the power systems grid. SCE contracted the Electric Power Research Institute (EPRI) to perform simulations to assess the effectiveness of voltage support devices, static VAR compensators (SVC) and synchronous condensers to resolve the air conditioner stalling problem.

1.2.1 Air Conditioner Unit-Level Solutions

SCE tested selected digital programmable thermostats, under-voltage protection devices, and load control switches to determine their ability to mitigate the air conditioner stalling problem.

Of the three digital programmable thermostats tested for response to under-voltage transients, only one thermostat had under-voltage protection, the Honeywell. This thermostat may help mitigate the air conditioner stalling problem, but its under-voltage protection and response times do not currently meet SCE's proposed stall protection specifications.

The use of digital programmable thermostats with proposed under-voltage protection is one of the easiest retrofitting solutions because it does not require a certified electrician. In California, retrofitting thermostats requires a certified electrician only when branch circuits

are rated 100 VA or greater and most residential thermostats circuits are rated below 24 VA. It is important to mention that this solution would not protect older units, those installed prior to the mid-1990s, because they lack the common “C” wire. This wire powers the thermostat electronics used for measuring voltage. The effectiveness of this solution will only become evident as new air conditioner units having the common “C” wire, replace older air conditioners.

Three under-voltage protection devices manufactured by Diversified Electronics (DE) were tested that may have the under-voltage protection to help mitigate the air conditioner stalling problem. These three relays are off-the-shelf devices making them conveniently attainable, but they also come with disadvantages. First, two are plug-in devices, making them suitable only for window air conditioners and possibly some plug-in air handler units. Second, they do not have randomly distributed short cycle-prevention allowing them to restart at different times after voltage are restored to normal conditions. Third, they use normally open (N.O.) contacts that prevent the units from restarting if the under-voltage relay fails. Another disadvantage is the retrofit cost – installing any of these under-voltage protection relays in California would require a qualified electrician for retrofit.

All other tested under-voltage protection devices provided limited stall protection; while helping to some degree, they will not alleviate the air conditioner stalling problem.

SCE worked with other entities such as Corporate System Engineering (CSE), Pacific Northwest National Laboratory (PNNL), and Cannon Technologies to modify their devices to mitigate the air conditioner stalling problem. The first two entities, CSE and PNNL agreed to modify their devices to meet SCE’s proposed under-voltage protection scheme; both devices were prototypes. Cannon’s off-the-shelf device (load control switch) required software modifications to meet SCE’s proposed under-voltage protection scheme. Because the state of California requires a certified electrician when servicing circuits rated 100 VA or more, implementation of all three of these devices will require an additional labor cost of \$70 to \$100 per installation, making it a less attractive solution.

Table 1 provides the test results for each device and assesses how well they mitigate air conditioner stalling. The *Potential* column is an SCE assessment of how viable these devices are for protecting air conditioners from stalling.

	Manuf.	Model	UV Threshold (%V)	Response Time (sec.)	Electronics Shutdown (%V)	Re-close Delay (sec.)	Control Contacts	Potential (%)
Thermostats	Honeywell	RTH7400D100 ‡	60%	0.760	can't tell	290	N.O.	Medium-High
	Totaline	P374-1800	none	none	can't tell	none	N.O.	none
	Rttemp	8022C	none	none	can't tell	none	N.O.	none
Under-Voltage Relays	ICM	ICM491	86%	5.100	75%	6	N.O.	Low
	DE	CV-200RS-20 Plug-in	83%	0.300	can't tell	300	N.O.	Medium
	DE	CV-100RS Plug-in	78%	0.232	can't tell	300	N.O.	Medium
	DE	CV-240-AFN Mount-in	83%	0.483	can't tell	300	N.O.	Medium
	Kriwan	INT369	68%	0.294	can't tell	120	N.O.	Medium-Low
	CSE	N/A	78%	0.25	15%	180 ~ 300	N.C.	High
	PNNL	N/A	77%	0.033	40%	180 ~ 300	N.C.	High
LCS	Cannon	N/A	80%	0.264	33%	180 ~ 300	N.C.	High

Table 1 – Unit Level Devices Test Results

1.2.2 System-Level Solutions

EPRI was contracted by SCE to develop a more representative load model for use in dynamic studies as well as the study of mitigation field equipment such as Static VAR Compensators (SVC), and synchronous condensers [2].

EPRI modeling indicated that SVCs and synchronous condensers at the system level could help mitigate the delayed voltage recovery problem as shown in figure 3. Although these devices cannot prevent air conditioners from stalling or subsequent faults, they can help isolate the fault area by literally injecting VARs into the system to prevent the problem from spreading throughout the system. Although a more rudimentary remedy, SVCs and synchronous condensers could help disconnect the stalled air conditioners by raising the units' terminal voltage. The supply VAR raises the terminal voltage subsequently making the thermal protection switch operate much faster. Finally, SVCs and synchronous condensers significantly improve voltage recovery and provide better voltage regulation; particularly in preventing over-voltages by absorbing VARs that decrease voltage.

The main advantage of electrical system-level solutions is that they can be implemented at fewer locations (transmission, subtransmission, or distribution substations) rather than at every air conditioning unit. The disadvantages in utilizing system-level solutions are, they would not be able to stop the voltage drop in the immediate area of the system problem and would be more costly to implement than air conditioner unit-level solutions.

Figure 3 provides the modeling results. The black plotline simulates an event without using mitigation devices. The red and blue plots simulate the use of SVC and Synchronous Condensers respectively. This shows that each of these two devices help regulate voltage

immediately after the fault is cleared by injecting VARs into the system. They also help remedy the over-voltage problem by absorbing VARs.

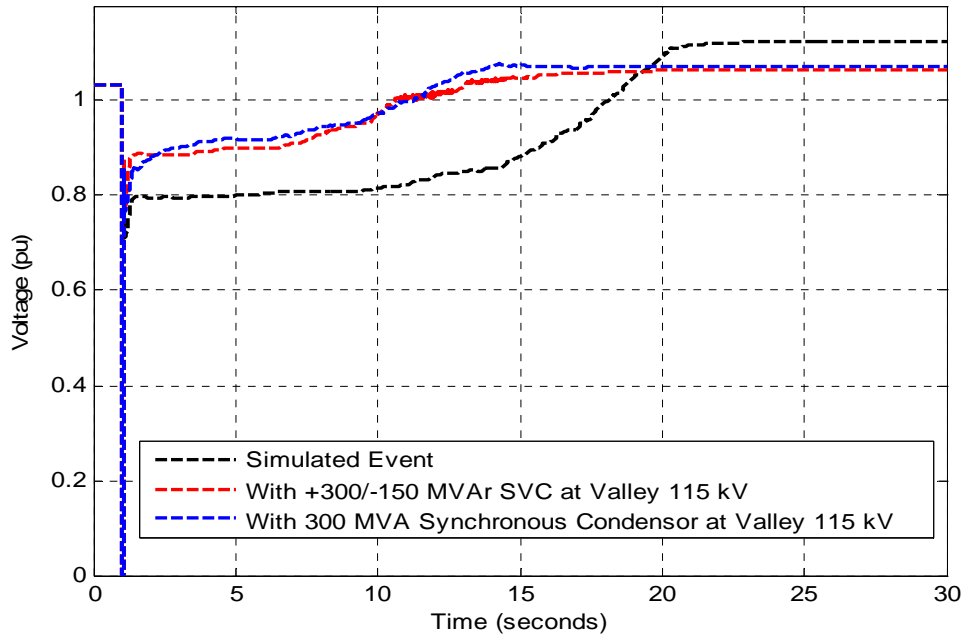


Figure 3 – System-Level Solutions Simulations

1.3 Economic Assessment

The SCE Valley substation, was used as a model for economic assessment because it typifies substations affected by delayed voltage recovery events. The SVCs installed at Devers and Rector Substations were used for cost analysis purposes. The Devers substation SVC has ratings of 605 MVAR reactive (generating) and 110 MVAR inductive (absorbing) and costs approximately \$50 million. The Rector substation SVC has ratings of 200 MVAR reactive (generating) and 100 MVAR inductive (absorbing) and costs approximately \$35 million. In order for SVCs or synchronous condensers to mitigate air conditioner stalling, they need to be installed at approximately 20 Valley 115-kV substations. The total cost for implementing this solution could reach \$100 million as indicated in table 2.

Mitigating air conditioner stalling is more cost-effective if done at the unit-level. Valley has approximately 300,000 residential and 30,000 industrial, commercial, and agricultural customers with a total peak load of 1,500 MW and 400 MVAR. Assuming each customer has one air conditioner unit, 330,000 under-voltage protection devices would be needed to mitigate the problem. That leaves two feasible unit-level solutions. The first would be to use under-voltage protection that does not require a certified electrician for a total cost of approximately \$20 million; the second option uses under-voltage protection devices that require an electrician for installation at a cost of approximately \$40 million as indicated in table 2.

Unit-Level Solution					
	Customers (Thousands)	Labor & Installation Cost	Material & Installation Cost	Total Material Cost (Millions)	Total Labor & Material Cost (Millions)
Valley	330	\$60	60	\$19.8	\$39.6
System-Level Solution					

	115-kV “B” Substations	SVC Unit Cost (\$ Millions)	Total SVC Cost (\$ Millions)
Valley	~20	~\$5	\$100

Table 2 – Economic Assessment

1.4 Conclusion

The best way to mitigate the air conditioner stalling problem is to implement a hybrid solution that combines both unit-level and system-level solutions. The under-voltage protection device (unit-level solution) would disconnect air conditioner units during under-voltage events. The SVC (system-level solution) would improve voltage recovery and regulation and prevent over-voltages. By combining unit-level and system-level solutions, Valley would require two SVCs instead of 20, one for each main bus.

For truly effective mitigation of the air conditioner stalling problem, SCE strongly recommends that a standard be created to disconnect stalled air conditioners from the electrical grid. This could be through either a switch at the air conditioner compressor or by action of the thermostat (potentially through the programmable communicating thermostat PCT).

SCE will continue its pursuit of the ideal stall protection device and establishment of air conditioner stall protection standards.

2.0 REFERENCES

- [1] R. Bravo, R. Yinger, and L. Gaillac, "Air Conditioner Solutions Test Report", December 2, 2007, report issued by SCE.
- [2] P. Pourbeik, A. Maitra, A. Gaikwad, and D. Brooks, "Developing a Bulk System Load Model in GE PSLF TM for Investigating the Valley Delayed Voltage Recovery Events", December 2, 2007, report issued by EPRI under SCE contract.
- [3] R. Bravo, R. Yinger, D. Martinez, and L. Gaillac, "Air Conditioner Test Report", November 27, 2006, report issued by SCE.

FINAL PROJECT REPORT

LOAD MODELING TRANSMISSION RESEARCH

APPENDIX G

WECC LOAD COMPOSITION DATA TOOL SPECIFICATION

Prepared for CIEE By:

Lawrence Berkeley National Laboratory



A CIEE Report

Table of Contents

Abstract	vii
1.0 Nomenclature	1
2.0 Introduction	3
3.0 Use Cases.....	5
3.1. Use Case 1: Feeder Load Composition	5
3.2. Use Case 2: Substation Load Composition.....	5
3.3. Use Case 3: Calibrated Load Composition.....	6
4.0 Requirements.....	7
4.1. Location	8
4.2. Study Information.....	9
4.3. Climate Data	9
4.4. Building Design Conditions	11
4.5. Substation/Feeder Composition.....	12
4.6. Residential Model	13
4.6.1. Single-Family Dwellings.....	13
4.6.2. Multi-Family Dwellings.....	27
4.7. Commercial Model	28
4.7.1. Floor Area	29
4.7.2. Load Shapes.....	29
4.7.3. Rules of Association	30
4.8. Industrial.....	31
4.9. Agricultural.....	31
4.10. Load Composition	31
4.10.1. Feeder Composition	32
4.11. Loadshapes	32
4.12. Sensitivities	33
4.13. System-Wide Results	34
5.0 Prototype.....	37
5.1. Conditions.....	37
5.2. Composition	38
5.3. Feeders.....	39
5.4. Loadshapes	39

5.5.	Sensitivity.....	40
5.6.	Residential.....	41
5.7.	Commercial.....	43
5.8.	Industrial.....	43
5.9.	Agricultural.....	44
6.0	References	45

Figures

Figure 1. Typical delayed voltage-recovery profile on a 230 kV transmission circuit. The fault occurs at (a) and is cleared at (b) after the voltage has dropped to 79% of the nominal voltage. The dip causes air-conditioner motors to stall, during which time their current draw is significantly higher than normal. This situation lasts through (c) until the motors' thermal protection interrupts the current and the voltage gradually recovers by (d). Meanwhile, other voltage controls such as load tap changers and capacitor banks cause the voltage to overshoot (e) and settle out too low (f)..... 4

Figure 2. The WECC composite load model structure includes static loads, electronic loads, constant-torque three-phase motors (A), high inertia speed-squared load motors (B), low inertia speed-squared load motors (C), and constant-torque single-phase motors (D)..... 4

Figure 3. Diversified single-family air-conditioning load curves. 22

Figure 4. The prototype conditions page..... 37

Figure 5. The prototype feeder composition page. 38

Figure 6. The prototype substation composition page. 38

Figure 7. The prototype feeder composition table page..... 39

Figure 8. The prototype loadshapes graphs page. 39

Figure 9. The prototype sensitivity table page..... 40

Figure 10. The prototype residential single-family design page..... 41

Figure 11. The prototype residential multi-family design page..... 42

Figure 12. The prototype residential design page..... 43

Figure 13. The prototype commercial design page..... 43

Figure 14. The prototype industrial design page. 43

Figure 15. The prototype agricultural design page..... 44

Tables

Table 1. Building types.....	7
Table 2. End-use electrification by city (fraction of homes having electric end-use)	18
Table 3. Installed end-use capacities for single-family residential dwelling.....	20
Table 4. Residential air-conditioner size weighting factors	21
Table 5. SEER model calibration results	21
Table 6. Residential end-use load shapes	23
Table 7. Single-family residential rules of association.....	26
Table 8. Multi-family residential rules of association.....	28
Table 9. Commercial building default floor area.....	29
Table 10. Rules of association for commercial buildings (except health facilities).....	30
Table 11. Rules of association for health facilities	31
Table 12. Customer class load composition scalar	32
Table 13. Customer type on feeders	32
Table 14. Temperature sensitivities	34

Abstract

This document specifies the methodology used by the Load Composition Data Tool developed for the Western Electricity Coordinating Council (WECC). A composite load model structure has been previously specified that describes the two salient features of the new model:

(a) recognition of the electrical distance between the transmission bus and the end-use loads; and (b) the diversity in the composition and dynamic characteristics of end-use loads. The load model includes data for an equivalent model of the distribution feeder, the load components, and the fractions of the load components. The methodology adopted by the WECC for identifying the fractions of the load components is specified in this document.

1.0 Nomenclature

<i>A</i>	area
<i>CEUS</i>	California End Use Survey data
<i>COP</i>	coefficient of performance
<i>D</i>	duty cycle
<i>E</i>	electric energy
<i>EER</i>	energy efficiency ratio
<i>F</i>	fraction
<i>H</i>	hour, height
<i>k</i>	load basis
<i>L</i>	load
<i>LS</i>	load shape
<i>m</i>	TMY index, month
<i>M</i>	motor
<i>N</i>	number
<i>P</i>	power
<i>PF</i>	power factor
<i>Q</i>	heat load, capacity
<i>q</i>	load density
<i>R</i>	thermal resistance value
<i>RH</i>	relative humidity
<i>S</i>	solar gain, shading
<i>SEER</i>	seasonal energy efficiency ratio
<i>T</i>	temperature

t	time
TMY	typical meteorological year
U_A	thermal conductance
v	velocity
V	volume
W	power
Z	impedance
ZIP	impedance, current, and power

2.0 Introduction

A power system model includes three main elements: the sources of power, the transmission of power, and the loads. Load representation has long been the least accurate of these three elements. The stability of the system depends on whether the balance between supply and demand is maintained. When the system is perturbed by an abrupt change in either supply or demand, the opportunities for part of the system to "fall out of step" increase greatly. Dynamic models are used to examine whether such a risk exists under various conditions, and these models require accurate descriptions of the system interconnections, as well as both the generators and the loads.

Work performed in the early 1990s provided initial guidance regarding load modeling (IEEE Task Force 1993; 1995). The Western Electricity Coordinating Council (WECC) adopted an interim dynamic load model of the California-Oregon Intertie (COI) in early 2002 to address critical operational issues with the COI and formed the WECC Load Modeling Task Force (LMTF) to develop a permanent composite load model to be used for planning and operation studies in the long term (Pereira 2002). The composite load model is nearly complete, and provides a much more accurate representation of the response of load to voltage and frequency disturbances by offering a much more accurate description of the load behavior during transmission faults (Kosterev 2008).

Of greatest importance for WECC in this context is the ability to perform dynamic voltage-stability studies, the outcomes of which are strongly influenced by the dynamic behavior of loads. The interim load model is unable to represent delayed voltage recovery from transmission faults, such as those observed in Southern California since 1990 and reported by Florida Power and Light (Williams 1992; Shaffer 1997).

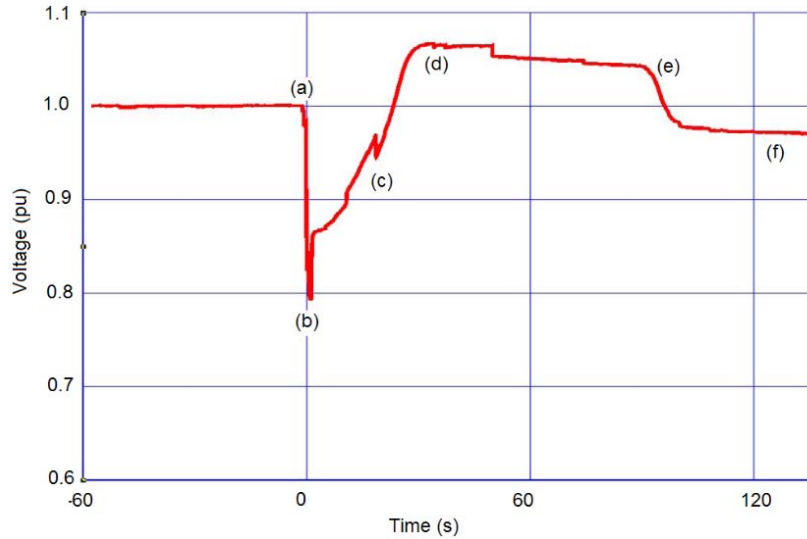


Figure 1. Typical delayed voltage-recovery profile on a 230 kV transmission circuit. The fault occurs at (a) and is cleared at (b) after the voltage has dropped to 79% of the nominal voltage. The dip causes air-conditioner motors to stall, during which time their current draw is significantly higher than normal. This situation lasts through (c) until the motors' thermal protection interrupts the current and the voltage gradually recovers by (d). Meanwhile, other voltage controls such as load tap changers and capacitor banks cause the voltage to overshoot (e) and settle out too low (f).

It is generally accepted that delayed voltage recovery is related to stalling of residential single-phase air conditioners in areas close to the fault. Simulations of these events show instantaneous post-fault voltage recovery, in sharp contrast to the observed behavior shown in Figure 1 (Chinn 2006).

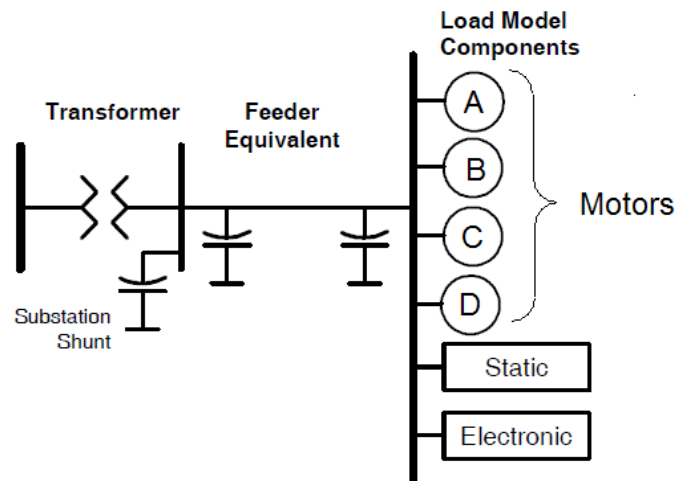


Figure 2. The WECC composite load model structure includes static loads, electronic loads, constant-torque three-phase motors (A), high inertia speed-squared load motors (B), low inertia speed-squared load motors (C), and constant-torque single-phase motors (D).

3.0 Use Cases

The following use-cases shall be considered by software developers.

3.1. Use Case 1: Feeder Load Composition

Goal

The user seeks to generate a single feeder load model for use with PSLF that incorporates motor A-C, ZIP, and electronic load components based on customer survey data.

Inputs

The user provides the following information

1. City
2. Month
3. Day of week
4. Hour of day
5. Number/type of residential and commercial buildings

Outputs

The total load and the fractions motors A-C, ZIP, and electronic loads.

3.2. Use Case 2: Substation Load Composition

Goal

The user seeks to generate a multi-feeder load model for use with PSLF that incorporates motor A-C, ZIP, and electronic load components based on customer survey data.

Inputs

The user provides the following information

1. City
2. Month
3. Day of week
4. Hour of day
5. Number/type of residential and commercial buildings on each feeder

Outputs

The total load and the fractions motors A-C, ZIP, and electronic loads.

3.3. Use Case 3: Calibrated Load Composition

Goal

The user seeks to generate a multi-feeder load model for use with PSLF that incorporates motor A-C, ZIP, and electronic load components based on customer meter data.

Inputs

The user provides the following information

1. City
2. Month
3. Day of week
4. Hour of day
5. Number/type of residential and commercial buildings on each feeder
6. Meter scaling results (actual/predicted)

Outputs

The total load and the fractions motors A-C, ZIP, and electronic loads.

4.0 Requirements

The methodology for estimating the fractions of each load component is based on a "bottom-up" approach. For single-family and multi-family residential buildings, the model is based on a thermal and equipment performance model described in Residential Model (Section 4.6).

Table 1. Building types

Load class	Building type	Floor area
Residential	Single-family home	all
	Multi-family dwelling	all
Commercial	Small office	≤ 30,000 sf
	Large office	> 30,000 sf
	Retail	all
	Lodging	all
	Grocery	all
	Restaurant	all
	School	all
	Health	all

For commercial buildings, the California Commercial End Use Survey (CEUS) is used as the primary source for the load shapes of each commercial building type listed in Table 1. These are described in Commercial Model (Section 4.7).

4.1. Location

The location shall be requested from the user and shall be a city chosen from among the supported cities. The default location shall be *Portland OR*. The supported cities shall include at least the following

1. Albuquerque NM
2. Bakersfield CA
3. Barstow CA
4. Boise ID
5. Cheyenne WY
6. Denver CO
7. Eugene OR
8. Eureka CA
9. Fresno CA
10. Helena MT
11. Las Vegas NV
12. Long Beach CA
13. Los Angeles CA
14. Phoenix AZ
15. Portland OR
16. Prince George BC
17. Redmond OR
18. Reno NV
19. Richland WA
20. Sacramento CA
21. Salt Lake City UT
22. San Diego CA
23. San Francisco CA
24. Santa Maria CA
25. Seattle WA
26. Spokane WA
27. Yakima WA

4.2. Study Information

A study is a scenario or case that a user wishes to examine.

All the information pertaining to a study shall be stored in a study file that can be retrieved later. The data storage requirements must be verifiably repeatable, i.e., a user shall be able to send a study file to another user, who shall be able to load the study file and produce an identical result without any additional data entry.

The study information shall include the data needed to determine when and where the load composition is being evaluated. The default study shall be a summer-peak weekday.

The following study information shall be requested from the user:

Study type

The study type shall specify the general time of the condition for which the load composition is being evaluated. It shall be chosen from among the set of allowed study conditions, including *winter peak*, *typical*, and *summer peak*. The default study type shall be *summer peak*.

Month

The month, M_{study} , shall be the month for which the study is being evaluated. If the study type is *winter peak*, the default month shall be the month during which the lowest temperature is observed at the location. If the study type is *typical*, the default month shall be the month with the minimum cooling and heating degree days. If the study type is *summer peak*, the default month shall be the month during which the highest temperature is observed.

Day of week

The day of week, D_{study} , shall be the day for which the study is being evaluated. If the study is *winter peak*, the default day of week shall be Monday. If the study is *typical* or *summer peak*, the default day of week shall be Wednesday. In cases where the week day is specified or used as a digit, Sunday shall be week day 0, Monday day 1, etc.

Hour of day

The hour of day, H_{study} , shall be the hour for which the study is being evaluated. The hour of day shall be specified as an integer between 0 and 23. If the study is *winter peak*, the default hour of day shall be the early morning hour of the coldest day at which the Monday morning setup occurs (typically between 5am and 8am). If the study is *typical* or *summer peak*, the default hour of day shall be the afternoon hour at which the peak load is observed (typically between 3pm and 6pm).

4.3. Climate Data

The climate data shall be that which is given by the Typical Meteorological Year version 2 data for the feeder location. The default climate data shall be for the current study city (NREL TMY2).

The weather data for the study conditions shall be based on the climate data at the time of the study. The following data shall be obtained from the TMY2 data:

Dry-bulb temperature

The dry-bulb outdoor air temperature shall be specified in degrees Fahrenheit(°F), and the default dry-bulb air temperature shall be TMY drybulb temperature at the cooling design condition

$$T_{out} = T_{cool} = 95 \text{ F.} \quad (1)$$

Wind speed

The wind speed shall be specified in miles per hour (mph) and the default wind speed shall be the TMY wind speed at the cooling design condition

$$v_{wind} = \text{windspeed of } \max(T_{drybulb}) = 3 \text{ mph.} \quad (2)$$

When more than one maximum temperature is found in the TMY temperature data, then the maximum wind speed for all those observations is to be used.

Relative humidity

The relative humidity shall be specified in percent(%), and the default relative humidity shall be the TMY relative humidity at the cooling design condition

$$Rh_{out} = \text{humidity of } \max(T_{drybulb}) = 87 \%. \quad (3)$$

When more than one maximum temperature is found in the TMY temperature data, then the maximum relative humidity for all those observations is to be used.

Opaque sky cover

The opaque sky cover shall be specified in %, and the default opaque sky cover shall be the TMY opaque sky cover at the cooling design condition

$$F_{sky} = \text{skycover of } \max(T_{drybulb}) = 0 \%. \quad (4)$$

Diffuse horizontal radiation

The diffuse horizontal radiation shall be specified in 'Btu/sf.h', and the default diffuse horizontal radiation shall be the TMY diffuse horizontal radiation at the cooling design condition

$$S_{diffuse} = \text{radiation}_{diffuse} \text{ of } \max(T_{drybulb}) = 120 \text{ Btu/sf.h.} \quad (5)$$

Direct normal radiation

The direct normal radiation shall be specified in BTU per square foot per hour (Btu/sf.h), and the default direct normal radiation shall be the TMY direct normal radiation at the cooling design condition

$$S_{normal} = radiation_{normal} \text{ of } max(T_{drybulb}) = 270 \text{ Btu/sf.h.} \quad (6)$$

Design heating hour

The peak heating hour, h_{heat} shall be the hour of year (0 to 8760) at which the design heating condition is observed.

Design cooling hour

The peak cooling hour, h_{cool} shall be the hour of year (0 to 8760) at which the design cooling condition is observed.

TMY index

The index, TMY_{row} , shall be the TMY lookup index (the climate data row number), such that

$$TMY_{row} = m_{study} * 100 + h_{study} \quad (7)$$

Note that up to 31 TMY records will match a single TMY_{row} index lookup.

4.4. Building Design Conditions

The design conditions shall be specified as follows

Heating design temperature

The heating design temperature shall be the minimum temperature for which building heating equipment is designed, i.e., heating equipment shall run at 100% duty cycle when the outdoor air temperature is at or below the heating design temperature. The heating design temperature shall be specified in °F, and the default heating design temperature shall be determined from the TMY2 data at the building location such that

$$T_{heat} = \check{T}_{drybulb} = 20 \text{ F.} \quad (8)$$

Heating design month

The heating design month shall be the month during which the heating design temperature occurs. The heating design month shall be specified as an integer value between 1 and 12 or as the name of the month. The default heating design month shall be the month during which the default heating design temperature is observed in the TMY2 data, i.e.,

$$M_{low} = month(\check{T}_{drybulb}) = 1 \text{ (January=1, February=2, ...).} \quad (9)$$

Heating design hour

The heating design hour shall be the hour during which the heating design temperature occurs. The heating design hour shall be specified as an integer value between 0 and 23. The default heating design hour shall be the hour during which the default heating design temperature is observed in the TMY2 data, i.e.,

$$H_{low} = hour(\check{T}_{drybulb}) = 4 : 00. \quad (10)$$

Cooling design temperature

The cooling design temperature shall be the maximum temperature for which building cooling equipment is designed, i.e., cooling equipment shall run at 100% duty cycle when the outdoor air temperature is at or above the cooling design temperature. The cooling design temperature shall be specified in °F, and the default cooling design temperature shall be determined from the TMY2 data at the building location such that

$$T_{cool} = \hat{T}_{drybulb} = 95\text{F}. \quad (11)$$

Cooling design month

The cooling design month shall be the month during which the cooling design temperature occurs. The cooling design month shall be specified as an integer value between 1 and 12 or as the name of the month. The default cooling design month shall be the month during which the default cooling design temperature is observed in the TMY2 data, i.e.,

$$M_{high} = month(\hat{T}_{drybulb}) = 7 \text{ (July)}. \quad (12)$$

Cooling design hour

The cooling design hour shall be the hour during which the cooling design temperature occurs. The cooling design hour shall be specified as an integer value between 0 and 23. The default cooling design hour shall be the hour during which the default cooling design temperature is observed in the TMY2 data, i.e.,

$$t_{high} = hour(\hat{T}_{drybulb}) = 16 : 00. \quad (13)$$

Peak solar gain

The peak solar gain shall be the largest value for direct normal solar radiation that occurs during the year, excluding diffuse radiation and the effects of sky cover. The peak solar gain shall be specified in Btu/sf.h, and the default peak solar gain shall be the largest direct normal radiation observed in the TMY2.

4.5. Substation/Feeder Composition

The method for computing a substation load composition shall be the same as for a single feeder, except that the user shall be able to provide separate customer counts for each

building type in each load class for each of up to 8 feeders, as illustrated in Figure 6. Each building type count shall be multiplied by the load for that building type before being added to the load composition, as shown in Figure 5.

Furthermore, the user shall be permitted to provide scalar adjustment to the load classes, such that the total load composition is scale by that factor. The scalars shall be any real number greater than 0.

4.6. Residential Model

The residential model shall consider single-family and multi-family dwellings only. Mobile homes shall not be considered.

4.6.1. Single-Family Dwellings

The basic building design parameters shall be as follows:

Floor area

The floor area shall be specified in units of square feet (sf), and the default floor area shall be

$$A_{floor} = 2200 \text{ sf.} \quad (14)$$

Building height

The building height shall be specified in ft and the default building height shall be

$$H_{building} = 10 \text{ ft.} \quad (15)$$

Wall area

The exterior wall area shall be specified in sf, and the default exterior wall area shall be

$$A_{wall} = 3H_{building}\sqrt{2A_{floor}} = 1990 \text{ sf.} \quad (16)$$

Wall R-value

The exterior wall R-value shall be specified in °F.h/Btu.sf, and the default wall R-value shall be

$$R_{wall} = 19 \text{ °F.h/Btu.sf.} \quad (17)$$

Roof R-value

The roof R-value shall be specified in °F.h/Btu.sf, and the default roof R-value shall be

$$R_{roof} = 60 \text{ °F.h/Btu.sf.} \quad (18)$$

Window-wall ratio

The window-to-wall ratio shall be specified in %, and the default window wall ratio shall be

$$F_{window} = 15\%. \quad (19)$$

Window R-value

The window R-value shall be specified in °F.h/Btu.sf, and the default window R-value shall be

$$R_{window} = 3.5 \text{ °F.h/Btu.sf.} \quad (20)$$

Ventilation rate

The ventilation rate shall be specified in air changes per hour (ach), and the default ventilation rate shall be

$$\dot{V}_{vent} = \frac{0.65 \times 3600 A_{wall} \sqrt{2 \times 32.17 H_{building} \frac{|T_{in} - T_{out}|}{T_{in}}}}{10000 V_{air}} + \frac{A_{window} v_{wind}}{100000} = 0.3 \text{ ach.} \quad (21)$$

where

- $A_{window} = A_{wall} F_{window}$ is the window area
- $V_{air} = A_{floor} H_{building}$ is the indoor air volume

Balance temperature

The balance temperature shall be specified in °F, and the default balance temperature shall be

$$T_{bal} = T_{set} - \frac{Q_{internal} + Q_{solar}}{U_A} \text{ °F,} \quad (22)$$

where

- Q_{solar} is defined below
- U_A is defined below.

The balance temperature must be between - 50 °F and the cooling design temperature (see below).

Heating design temperature

The heating design temperature shall be specified in °F, and the default heating design temperature shall be

$$T_{heat_design} = \check{T}_{drybulb} \text{ °F.} \quad (23)$$

Cooling design temperature

The cooling design temperature shall be specified in °F, and the default cooling design temperature shall be

$$T_{cool_{design}} = \hat{T}_{drybulb} \text{ °F.} \quad (24)$$

Heating design capacity

The heating design capacity shall be specified in Btu/h, and the default heating design capacity shall be

$$Q_{heat} = U_A \times (T_{set} - T_{heat_{design}}) \text{ Btu/h.} \quad (25)$$

The heating design capacity must be a positive number.

Cooling design capacity

The cooling design capacity shall be specified in Btu/h, and the default cooling design capacity shall be

$$Q_{cool} = U_A(T_{cooling_{design}} - T_{set}) + 0.25\hat{Q}_{solar} A_{windows} (1 - S_{external}) S_{solar} + Q_{internal_{design}} \text{ Btu/h.} \quad (26)$$

where

- $S_{external}$ is the external shading coefficient,
- S_{solar} is the solar exposure fraction, and
- $Q_{internal_{design}}$ is the internal design heat load.

Thermostat setpoint

The thermostat setpoint shall be specified in °F, and the default thermostat setpoint shall be 75°F.

Building UA

The building UA shall be specified in Btu/°F.h, and the default building UA shall be

$$U_A = Q_{vent} + \frac{A_{wall}}{R_{wall}}(1 - F_{window}) + \frac{A_{floor}}{R_{roof}} + \frac{A_{wall}}{R_{window}} F_{window} \text{ Btu/°F.h.} \quad (27)$$

where

- $Q_{vent} = 0.182\dot{V}_{vent}V_{air}$.

Internal heat gain

The internal heat gain shall be specified in Btu/h, and the default internal heat gain shall be

$$Q_{internal} = 3412 (0.8L_{cooking} + 0.1L_{hotwater} + L_{lighting} + 0.25L_{washing} + L_{plugs} + L_{refrigeration}) \text{ Btu/h.} \quad (28)$$

External shading

The external shading coefficient shall describe the fraction of sunlight that is blocked by foliage and other means external to the building, in '%'. The default external shading coefficient shall be

$$F_{shading} = 20\%. \quad (29)$$

Solar gains

The solar gains shall be given in Btu/h and the default solar gains shall be

$$Q_{solar} = S_{normal} A_{window} / 4 (1 - F_{shading}) F_{solar} / 2 \quad (30)$$

where

- $A_{window} = A_{wall} F_{window}$;
- $F_{solar} = \begin{cases} 0.7 \cos(E_{solar}) \sin(E_{solar}) & E_{solar} > 0 \\ 0 & E_{solar} \leq 0 \end{cases}$;
- $E_{solar} = \sin^{-1} (\cos(H_{solar}) \cos(D_{solar}) \cos(\text{Solar Latitude}) + \sin(D_{solar}) \sin(L_{solar}))$;
- $H_{solar} = 2\pi(H_{study} - 12) / 24$;
- $D_{solar} = (-23.45/360)2\pi \cos(2\pi(30.6M_{study} - 15 + 10)/365)$; and
- $L_{solar} = 2\pi \text{latitude} / 360$.

Latent load

The latent load shall be the load caused by moisture condensation on the cooling coils in 'Btu/h'. The default latent load shall be estimated as

$$Q_{latent} = 0.3 \frac{Q_{internal} + Q_{solar}}{1 + e^{4-10RH_{out}}} \quad (31)$$

Heating duty cycle

The heating duty cycle shall be the fraction of time under the study condition that the heating system is operating, in %. The default heating duty cycle shall be

$$D_{heat} = \frac{100}{0} \left| \frac{T_{balance} - T_{out}}{T_{balance} - T_{heat}} \right| \quad (32)$$

Cooling duty cycle

The cooling duty cycle shall be the fraction of time under the study condition that the cooling system is operating, in %. The default cooling duty cycle shall be

$$D_{cool} = \frac{100}{0} \left| \frac{T_{out} - T_{balance}}{T_{cool} - T_{balance}} \right. \quad (33)$$

End-Use Electrification

The end-use electrification shall specify the fraction of residential end uses that use electricity. The default values shall be obtained from a look-up table for the available study cities, as provided in the following table.

Table 2. End-use electrification by city (fraction of homes having electric end-use)

City	Resistance heat	Heat pumps	Hot water	Cooking	Drying	Air conditioning
Albuquerque NM	25%	25%	30%	30%	75%	90%
Bakersfield CA	25%	25%	30%	30%	75%	90%
Barstow CA	25%	25%	30%	30%	75%	90%
Boise ID	75%	25%	70%	70%	75%	75%
Cheyenne WY	75%	25%	70%	70%	75%	50%
Denver CO	75%	25%	30%	30%	75%	80%
Eugene OR	75%	25%	70%	70%	75%	30%
Eureka CA	25%	50%	70%	70%	75%	20%
Fresno CA	25%	50%	30%	30%	75%	75%
Helena MT	75%	25%	70%	70%	75%	20%
Las Vegas NV	25%	75%	30%	30%	75%	95%
Long Beach CA	75%	75%	30%	30%	75%	50%
Los Angeles CA	75%	75%	30%	30%	75%	30%
Phoenix AZ	25%	50%	30%	30%	75%	95%
Portland OR	50%	25%	30%	30%	75%	60%
Prince George BC	75%	25%	70%	70%	75%	10%
Redmond OR	50%	25%	30%	30%	75%	75%
Reno NV	50%	25%	70%	70%	75%	90%
Richland WA	50%	25%	70%	70%	75%	75%
Sacramento CA	25%	25%	30%	30%	75%	75%
Salt Lake City UT	50%	25%	70%	70%	75%	75%
San Diego CA	25%	25%	30%	30%	75%	25%
San Francisco CA	25%	25%	30%	30%	75%	25%
Santa Maria CA	25%	25%	30%	30%	75%	50%
Seattle WA	25%	25%	30%	30%	75%	25%
Spokane WA	75%	25%	70%	70%	75%	60%
Yakima WA	75%	25%	70%	70%	75%	50%

Resistive heating fraction

The resistive heating fraction, $EF_{resistive}$, shall be the fraction of single-family dwellings that use electric resistive heating. The default resistive heating fraction shall be obtained from the End-use Electrification table above for the study city.

Heat pump fraction

The heat pump heating fraction, $EF_{heatpump}$, shall be the fraction of single-family dwellings that use electric heat pump heating. The default heat pump heating fraction shall be obtained from the End-use Electrification table above for the study city.

Electric hot water fraction

The electric hot water heating fraction, $EF_{hotwater}$, shall be the fraction of single-family dwellings that use electric hot water heating. The default electric hot water heating fraction shall be obtained from the End-use Electrification table above for the study city.

Electric cooking fraction

The electric cooking fraction, $EF_{cooking}$, shall be the fraction of single-family dwellings that use electric cooking heating. The default electric cooking fraction shall be obtained from the End-use Electrification table above for the study city.

Electric drying fraction

The electric drying fraction, EF_{drying} , shall be the fraction of single family dwellings that use electric drying heating. The default electric drying fraction shall be obtained from the End-use Electrification table above for the study city.

Air-conditioning fraction

The electric cooling fraction, $EF_{cooling}$, shall be the fraction of single family dwellings that use electric cooling. The default electric cooling fraction shall be obtained from the End-use Electrification table above for the study city.

Efficiency

Heating and cooling efficiency shall be defaulted and entered by the user such that they can be adjusted as appropriate.

Heating efficiency

The heating efficiency, ρ_{heat} shall specify the average coefficient of performance (COP) of the electric heating system. The heating efficiency shall be 1.0 when no heat pumps are in use, and shall be greater than 1.0 when heat pumps are in use. The default heating efficiency shall be

$$\rho_{heat} = \frac{EF_{resistive} + COP_{HP} EF_{heatpump}}{EF_{resistive} + EF_{heatpump}}, \quad (34)$$

where COP_{HP} is provided by the user.

Cooling efficiency

The cooling efficiency shall given in (SEER) and the default cooling efficiency shall be

$$\rho_{cool} = 11.5 \text{ SEER (seasonally energy efficiency ratio)}. \quad (35)$$

Installed Capacity

The end-use installed capacity shall be the power density of each end use, described as follows:

Table 3. Installed end-use capacities for single-family residential dwelling

Cooking	$q_{cooking} = 3.00 \text{ W/sf}$
Hot water	$q_{hotwater} = 2.50 \text{ W/sf}$
Lighting	$q_{lighting} = 1.00 \text{ W/sf}$
Plugs	$q_{plugs} = 1.50 \text{ W/sf}$
Washing	$q_{washing} = 2.50 \text{ W/sf}$
Heating	$q_{heat} = \frac{Q_{heat}}{3.412 A_{floor} \rho_{heat}} \quad (36)$
Cooling	$q_{cool} = \frac{Q_{cool}}{3.412 A_{floor} EER_{model}} \quad (37)$
Refrigeration	$q_{refrigeration} = 0.2 \text{ W/sf}$

The maximum EER (energy efficiency ratio in Btu/W.h) is typically used to calculate the SEER value using the assumption $SEER = 0.875 EER_{max}$. The EER is determined as follows:

$$EER_{max} = EER_{coeff} \times 3.412 \frac{T_{set} + 459.7}{T_{cooldesign} - T_{set}}, \quad (38)$$

where the EER_{coeff} is typically around 0.1. This is the relatively invariant ratio of the Carnot efficiency to the actual efficiency and can be used to compute EER_{coeff} .

$$EER_{coeff} = \frac{SEER}{0.875} \frac{T_{cooldesign} - T_{set}}{3.412(T_{set} + 459.7)}. \quad (39)$$

The theoretical EER, $EER_{theoretical}$ can thus be computed for any outdoor temperature

$$EER_{theoretical} = EER_{coeff} \times 3.412 \frac{T_{set} + 459.7}{T_{out} - T_{set}}. \quad (40)$$

However, actual ERR values do not show such a large variation in EER, and $EER_{theoretical}$ must be adjusted using the following formula to obtain the EER_{model} :

$$EER_{model} = EER_{theoretical} (1 - E_{factor} (T_{cool\,design} - T_{out})), \quad (41)$$

where

- E_{factor} is estimated by minimizing the weighted root-mean-square (RMS) error between the observed power used in the tests and the model's prediction at various cooling design temperatures, using the weights for the equipment sizes, as shown in Table 1. The results for the model calibration are shown in Table 4.

Note

If the outdoor temperature is below 83°F then the SEER values for 83 °F are used.

Table 4. Residential air-conditioner size weighting factors

Size (tons)	Weight
2.5	10%
3.0	20%
3.5	30%
4.0	20%
5.0	20%

Table 5. SEER model calibration results

T_{design} (°F)	E_{factor}
90	0.05914
95	0.04613
100	0.03782
105	0.03197
110	0.02764
115	0.02433

A quadratic fit of this data yields the following relation

$$E_{factor} = 4.6 \times 10^{-5} T_{cool\,design}^2 - 1.08 \times 10^{-2} T_{cool\,design} + 0.656 \quad (41a)$$

with $R^2 = 0.9969$ Figure 3 shows the diversified AC load curves (in kWh/h) as a function of outdoor temperature (in °F) for various cooling design conditions.

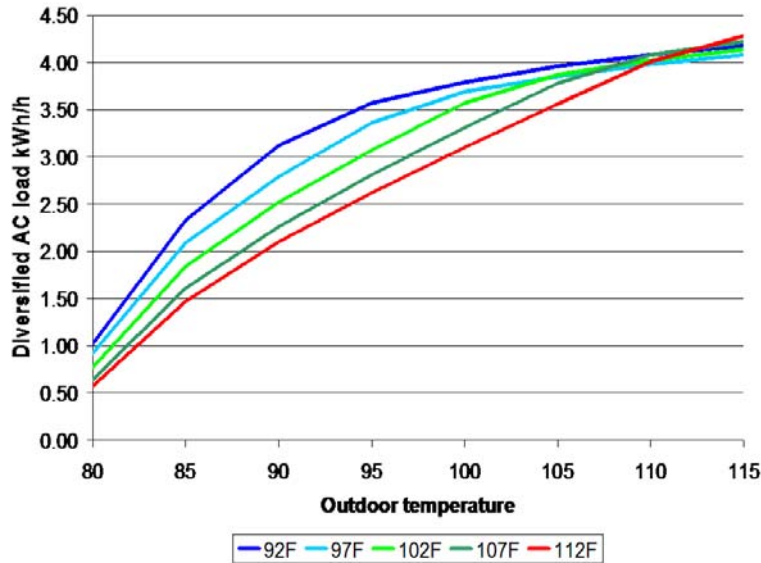


Figure 3. Diversified single-family air-conditioning load curves

Caveat

This approach assumes that the thermostat setpoint is maintained. If the duty cycle is 100%, that assumption is not valid and the efficiency may be better than that predicted based on the change in outdoor temperature alone.

Diversified Load

The *diversified end-use load* shall describe the average end-use load, per home, of a population of single-family homes, in kW.

Table 6. Residential end-use load shapes

	Winter weekday					Winter weekend					Summer weekday					Summer weekend				
Hour	Cooking	Hotwater	Lighting	Plugs	Washing	Cooking	Hotwater	Lighting	Plugs	Washing	Cooking	Hotwater	Lighting	Plugs	Washing	Cooking	Hotwater	Lighting	Plugs	Washing
0	0.01	0.25	0.42	0.82	0.0444	0.013	0.29	0.49	0.95	0.0497	0.009	0.21	0.38	1.02	0.0437	0.009	0.23	0.41	0.48	0.0484
1	0.009	0.19	0.38	0.74	0.0193	0.01	0.22	0.42	0.79	0.0245	0.008	0.16	0.34	0.91	0.0188	0.007	0.17	0.36	0.41	0.0234
2	0.009	0.16	0.37	0.69	0.0116	0.01	0.17	0.38	0.72	0.0143	0.007	0.13	0.32	0.85	0.011	0.007	0.14	0.33	0.39	0.0134
3	0.009	0.15	0.36	0.68	0.0092	0.01	0.15	0.38	0.7	0.0095	0.007	0.12	0.32	0.84	0.0086	0.007	0.13	0.32	0.38	0.0087
4	0.009	0.18	0.37	0.68	0.0108	0.01	0.16	0.37	0.69	0.0094	0.008	0.15	0.32	0.86	0.01	0.007	0.13	0.32	0.37	0.0085
5	0.016	0.34	0.42	0.78	0.0297	0.012	0.19	0.38	0.71	0.0116	0.012	0.26	0.35	0.95	0.0283	0.009	0.17	0.32	0.38	0.0111
6	0.032	0.74	0.58	1.01	0.0757	0.018	0.27	0.43	0.77	0.0236	0.025	0.51	0.41	1.22	0.075	0.017	0.26	0.34	0.42	0.0233
7	0.05	1.2	0.69	1.29	0.1317	0.04	0.47	0.51	0.95	0.0634	0.04	0.76	0.45	1.33	0.1325	0.038	0.45	0.39	0.48	0.0633
8	0.045	1.1	0.61	1.22	0.1677	0.073	0.82	0.6	1.21	0.1387	0.044	0.77	0.45	1.25	0.1681	0.06	0.69	0.44	0.56	0.1399
9	0.043	0.94	0.56	1.18	0.2098	0.094	1.08	0.63	1.43	0.2295	0.042	0.76	0.45	1.25	0.2095	0.068	0.85	0.47	0.6	0.2271
10	0.045	0.82	0.53	1.18	0.2299	0.091	1.15	0.63	1.52	0.3009	0.042	0.71	0.45	1.26	0.2313	0.065	0.84	0.47	0.62	0.2957
11	0.059	0.71	0.51	1.13	0.2266	0.1	1.08	0.61	1.51	0.3251	0.053	0.61	0.45	1.29	0.2279	0.067	0.76	0.47	0.62	0.3179
12	0.063	0.62	0.49	1.11	0.2052	0.117	0.98	0.6	1.49	0.3202	0.057	0.54	0.45	1.28	0.2069	0.076	0.65	0.47	0.63	0.3125
13	0.053	0.55	0.47	1.04	0.1913	0.109	0.87	0.59	1.49	0.3079	0.046	0.49	0.44	1.23	0.1928	0.066	0.58	0.46	0.65	0.3011
14	0.052	0.48	0.47	1.05	0.1702	0.1	0.77	0.59	1.45	0.2809	0.044	0.43	0.44	1.19	0.1714	0.061	0.49	0.46	0.67	0.2744
15	0.072	0.47	0.51	1.15	0.1645	0.108	0.69	0.61	1.46	0.2623	0.053	0.41	0.45	1.2	0.165	0.067	0.46	0.46	0.71	0.2556
16	0.138	0.54	0.63	1.38	0.1729	0.153	0.72	0.71	1.62	0.2521	0.094	0.43	0.47	1.31	0.1719	0.091	0.46	0.47	0.78	0.2462
17	0.242	0.68	0.84	1.81	0.1835	0.215	0.78	0.88	1.93	0.2399	0.168	0.52	0.51	1.55	0.1818	0.134	0.5	0.49	0.88	0.2347
18	0.182	0.83	0.97	2.02	0.1934	0.161	0.83	0.96	2.03	0.2343	0.148	0.6	0.54	1.71	0.1913	0.121	0.54	0.52	0.95	0.2296
19	0.088	0.82	0.98	1.95	0.1997	0.085	0.79	0.97	1.95	0.2306	0.086	0.6	0.56	1.75	0.1981	0.08	0.55	0.54	0.95	0.2268
20	0.051	0.74	0.96	1.88	0.2033	0.05	0.72	0.94	1.86	0.2247	0.053	0.59	0.63	1.86	0.2025	0.052	0.56	0.61	0.93	0.2223
21	0.034	0.68	0.89	1.77	0.2063	0.033	0.64	0.88	1.74	0.2152	0.038	0.6	0.71	1.96	0.2055	0.035	0.56	0.68	0.88	0.2149
22	0.022	0.57	0.74	1.47	0.1684	0.022	0.53	0.76	1.5	0.1726	0.023	0.55	0.65	1.73	0.1684	0.022	0.49	0.63	0.76	0.171
23	0.014	0.4	0.55	1.09	0.0986	0.014	0.43	0.58	1.14	0.1078	0.013	0.37	0.49	1.32	0.0983	0.011	0.38	0.5	0.58	0.107
kWh/day	0.6735	7.08	7.15	14.56	1.66185	0.824	7.4	7.45	15.805	2.02435	0.56	5.64	5.515	15.56	1.6593	0.5885	5.52	5.465	7.54	1.9884
Basis	31.12535					33.50335					28.9343					21.1019				

Cooking

The cooking diversified load shall be given in kilowatts (kW) and the default diversified load shall be

$$\tilde{Q}_{\text{cooking}} = \left(F_{\text{winter}} \frac{LS_{\text{cooking}}[H_{\text{study}}, D_{\text{study}}, \text{winter}]}{k_{\text{cooking}}[D_{\text{study}}, \text{winter}]} + F_{\text{summer}} \frac{LS_{\text{cooking}}[H_{\text{study}}, D_{\text{study}}, \text{summer}]}{k_{\text{cooking}}[D_{\text{study}}, \text{summer}]} \right) q_{\text{cooking}} A_{\text{floor}} / 1000 \text{ kW} \quad (42)$$

where

- $LS_{\text{cooking}}[H_{\text{study}}, D_{\text{study}}]$ is the cooking loadshape value from Table 6 in kW;
- $k_{\text{cooking}}[H_{\text{study}}, D_{\text{study}}]$ is the cooking load basis in kWh/day;
- $F_{\text{winter}} = 1 - F_{\text{summer}}$; and
- $F_{\text{summer}} = \left| \sin \left(\frac{\pi (M_{\text{study}} - 1.5)}{12} \right) \right|$.

Hot water

The hot-water diversified load shall be given in kW and the default diversified load shall be

$$\tilde{Q}_{\text{hotwater}} = \left(F_{\text{winter}} \frac{LS_{\text{hotwater}}[H_{\text{study}}, D_{\text{study}}, \text{winter}]}{k_{\text{hotwater}}[D_{\text{study}}, \text{winter}]} + F_{\text{summer}} \frac{LS_{\text{hotwater}}[H_{\text{study}}, D_{\text{study}}, \text{summer}]}{k_{\text{hotwater}}[D_{\text{study}}, \text{summer}]} \right) q_{\text{hotwater}} A_{\text{floor}} / 1000 \text{ kW} \quad (43)$$

where

- $LS_{\text{hotwater}}[H_{\text{study}}, D_{\text{study}}]$ is the hotwater loadshape value from Table 6 in kW; and
- $k_{\text{hotwater}}[H_{\text{study}}, D_{\text{study}}]$ is the hotwater load basis in kWh/day.

Lighting

The lighting diversified load shall be given in kW and the default diversified load shall be

$$\tilde{Q}_{\text{lighting}} = \left(F_{\text{winter}} \frac{LS_{\text{lighting}}[H_{\text{study}}, D_{\text{study}}, \text{winter}]}{k_{\text{lighting}}[D_{\text{study}}, \text{winter}]} + F_{\text{summer}} \frac{LS_{\text{lighting}}[H_{\text{study}}, D_{\text{study}}, \text{summer}]}{k_{\text{lighting}}[D_{\text{study}}, \text{summer}]} \right) q_{\text{lighting}} A_{\text{floor}} / 1000 \text{ kW} \quad (44)$$

where

- $LS_{\text{lighting}}[H_{\text{study}}, D_{\text{study}}]$ is the lighting loadshape value from Table 6 in kW; and
- $k_{\text{lighting}}[H_{\text{study}}, D_{\text{study}}]$ is the lighting load basis in kWh/day.

Plugs

The plugs diversified load shall be given in kW and the default diversified load shall be

$$\tilde{Q}_{\text{plugs}} = \left(F_{\text{winter}} \frac{LS_{\text{plugs}}[H_{\text{study}}, D_{\text{study}}, \text{winter}]}{k_{\text{plugs}}[D_{\text{study}}, \text{winter}]} + F_{\text{summer}} \frac{LS_{\text{plugs}}[H_{\text{study}}, D_{\text{study}}, \text{summer}]}{k_{\text{plugs}}[D_{\text{study}}, \text{summer}]} \right) q_{\text{plugs}} A_{\text{floor}} / 1000 \text{ kW} \quad (45)$$

where

- $LS_{plugs}[H_{study}, D_{study}]$ is the plugs loadshape value from Table 6 in kW; and
- $k_{plugs}[H_{study}, D_{study}]$ is the plugs load basis in kWh/day.

Washing

The washing diversified load shall be given in kW and the default diversified load shall be

$$\tilde{Q}_{washing} = \left(F_{winter} \frac{LS_{washing}[H_{study}, D_{study}, winter]}{k_{washing}[D_{study}, winter]} + F_{summer} \frac{LS_{washing}[H_{study}, D_{study}, summer]}{k_{washing}[D_{study}, summer]} \right) q_{washing} A_{floor} / 1000 \text{ kW} \quad (46)$$

where

- $LS_{washing}[H_{study}, D_{study}]$ is the washing loadshape value from Table 6 in kW; and
- $k_{washing}[H_{study}, D_{study}]$ is the washing load basis in kWh/day.

Heating

The diversified heating load shall be $\tilde{Q}_{heat} = D_{heat} q_{heat} A_{floor} / 1000 \text{ kW}$.

Cooling

The diversified cooling load shall be $\tilde{Q}_{cool} = D_{cool} q_{cool} A_{floor} / 1000 F_{airconditioning} \text{ kW}$.

Refrigeration

The refrigeration diversified load shall include freezer loads and shall be

$$\tilde{Q}_{refrigeration} = q_{refrigeration} A_{floor} / 1000 \text{ kW}. \quad (47)$$

Single-Family Rules of Association

The single-family residential rules of association (RoA) table shall be used to convert diversified end-use load to model component loads.

Table 7. Single-family residential rules of association

End-use	Non-ZIP component					ZIP component					
	Electronic (E)	Motor-A (M _A)	Motor-B (M _B)	Motor-C (M _C)	Motor-D (M _D)	I _p	I _q	P _p (P)	P _q (Q)	Z _p (G)	Z _q (B)
Cooking	0.3			0.1						0.6	
Hotwater										1	
Lighting						0.1	-0.02			0.9	
Plugs	0.9									0.1	
Washing				0.7						0.3	
Heating			0.1F _{heatpump}		0.3F _{heatpump}					0.6F _{heatpump} +F _{resistive}	
Cooling			0.1		0.9						
Refrigeration	0.1				0.9						

In addition to the model load components, the user shall be provided the following results to assist in input quality assurance:

Power Factor

The power factor shall be computed for each end use for which the ZIP components are non-zero in real-power, such that

$$PF_{enduse} = \frac{S_{penduse}}{\sqrt{S_{penduse}^2 + S_{qenduse}^2}} \frac{S_{qenduse}}{|S_{qenduse}|} \quad (48)$$

where

- $S_{penduse} = Z_{penduse} + I_{penduse} + P_{penduse}$; and
- $S_{qenduse} = Z_{qenduse} + I_{qenduse} + P_{qenduse}$.

Total real power

The total real power for each end use shall be

$$P_{enduse} = \tilde{Q}_{enduse} (E + M_A + M_B + M_C + M_D + S_{penduse}) \quad (49)$$

Total real power fraction

The total real power fraction for each end-use shall be

$$F_{P_{enduse}} = \frac{P_{enduse}}{\sum_{i \in enduses} P_i} \quad (50)$$

Total reactive power

The total reactive power for each end-use shall be

$$Q_{enduse} = \tilde{Q}_{enduse} S_{q_{enduse}} \quad (51)$$

Total reactive power fraction

The total reactive power fraction for each end-use shall be

$$F_{q_{enduse}} = \frac{Q_{enduse}}{\sum_{i \in enduses} Q_i} \quad (52)$$

Checksum

The rules of association shall be verified for each end-use so that the following constraints are not violated:

- $F_{P_{enduse}} \leq 1.0$, and
- $F_{q_{enduse}} \leq 1.0$.

4.6.2. Multi-Family Dwellings

Multi-family dwelling load composition shall be computed in a manner identical to that used for single family dwellings, with the following exceptions.

Floor Area per Unit

The floor area per unit shall be specified in 'sf/unit' and describe the net floor area of each dwelling unit. The default value of $A_{unit} = 800$ sf/unit.

Floors per Building

The default number of floors per building shall be $N_{floors} = 4$.

Units per Floor

The default number of units per floor shall be $N_{units} = 10$.

Floor Area

The default floor area shall be computed as

$$A_{floor} = A_{unit} N_{units} N_{floors} \text{ sf.} \quad (53)$$

Floor-to-Floor Height

The default floor-to-floor height shall be $H_{floor} = 10$ ft.

Exterior Wall Area

The exterior wall area of a building shall be

$$A_{wall} = A_{unitwall} N_{units} N_{floors} \text{ sf.} \quad (54)$$

Multi-Family Rules of Association

The multi-family residential rules of association (RoA) table shall be used to convert diversified end-use load to model component loads.

Table 8. Multi-family residential rules of association

End-use	Non-ZIP component					ZIP component					
	Electronic (E)	Motor-A (M _A)	Motor-B (M _B)	Motor-C (M _C)	Motor-D (M _D)	I _p	I _q	P _p (P)	P _q (Q)	Z _p (G)	Z _q (B)
Cooking	0.3			0.1						0.6	
Hotwater										1	
Lighting						0.1	-0.02			0.9	
Plugs	0.9									0.1	
Washing				0.7						0.3	
Heating			0.025		0.075					0.65	
Cooling			0.1		0.9						
Refrigeration	0.1				0.9						

4.7. Commercial Model

The commercial building end-use model shall be based on the California End-Use Survey (CEUS) data collected for the California Energy Commission by Itron (California End-use Survey 2006).

The building types that shall be considered shall include at least the following

1. Small office (up to 30,000 sf)
2. Large office (above 30,000 sf)
3. Retail
4. Lodging
5. Grocery
6. Restaurant

- 7. School
- 8. Health

4.7.1. Floor Area

Default values for the floor area for each building type shall be as shown in Table 9.

Table 9. Commercial building default floor area

Type	Default A_{floor} (ksf)
Small office	10
Large office	50
Retail	15
Lodging	25
Grocery	15
Restaurant	10
School	35
Health	50

4.7.2. Load Shapes

The load shape data from the CEUS data shall be used to determine the electric load density

$$Q_{enduse} = \frac{CEUS [code_{CEUS}, enduse]}{\sum_{x \in enduse} CEUS [code_{CEUS}, x]} \quad (55)$$

where

- $enduse \in \{small\ office, large\ office, retail, lodging, grocery, restaurant, school, health\}$,
and

- $CEUS_{code} = 1000 E \left(\frac{M_{study} - 1}{3} + 1 \right) + 100 CEUS_{daycode} + H_{study} + 1$

- $CEUS_{daycode} = \begin{cases} 1 & : \bar{T}[TMY_{row}] - 10 \leq T_{out} \leq \bar{T}[TMY_{row}] + 10 \\ 2 & : T_{out} > \bar{T}[TMY_{row}] + 10 \\ 3 & : T_{out} < \bar{T}[TMY_{row}] - 10 \\ 4 & : D_{study} \in \{Saturday, Sunday\} \end{cases}$

The CEUS data shall be obtained from the Commercial sheet in the Load Composition Excel spreadsheet delivered with this report.

4.7.3. Rules of Association

The rules of association for all commercial building types, except health facilities, shall be as provided in Table 10

Table 10. Rules of association for commercial buildings (except health facilities)

	Electronic	Motor-A	Motor-B	Motor-C	Motor-D	ZIP Ip	ZIP Iq	ZIP Pp (P)	ZIP Pq (Q)	ZIP Zp (G)	ZIP Zq (B)
Heating		0.70			0.20					0.10	0.015
Cooling		0.75			0.25						
Vent	0.30		0.70								
WaterHeat										1.00	0.15
Cooking	0.20		0.20							0.6	
Refrig	0.10	0.30			0.60						
ExtLight						1.00	-0.36				0.06
IntLight						1.00	-0.36				0.06
OfficeEquip	1.00										
Misc			0.50	0.50							
Process	0.5		0.25	0.25							
Motors		0.3	0.4	0.3							
AirComp		1									

The rules of association for health facilities shall be as provided in Table 11

Table 11. Rules of association for health facilities

	Electronic	Motor-A	Motor-B	Motor-C	Motor-D	ZIP Ip	ZIP Iq	ZIP Pp (P)	ZIP Pq (Q)	ZIP Zp (G)	ZIP Zq (B)
Heating		0.75			0.15					0.10	0.015
Cooling		1.00									
Vent	0.30		0.70								
WaterHeat										1.00	0.15
Cooking	0.20		0.20							0.60	
Refrig	0.20	0.70			0.10						
ExtLight						1.00	-1.20				0.20
IntLight						1.00	-1.2				0.20
OfficeEquip	1.00										
Misc										1.00	
Process			0.50	0.50							
Motors			0.50	0.50							
AirComp		1.00									

4.8. Industrial

Industrial loads shall be described without rules of association. The default values for industrial loads shall be zero for all load components.

When non-zero loads are described, the total real power and the power factor of the ZIP load shall be computed (see above) and displayed.

4.9. Agricultural

Agricultural loads shall be described without rules of association. The default values for industrial loads shall be zero for all load components.

When non-zero loads are described, the total real power and the power factor of the ZIP load shall be computed and displayed.

4.10. Load Composition

The load composition shall be calculated for each model component by summing all the feeder compositions and multiplying resulting totals for residential, commercial, industrial, and agricultural loads by scalars, the defaults of which shall be as shown in Table 12.

Table 12. Customer class load composition scalar

Customer class	Default load scalars
Residential	1.0
Commercial	1.0
Industrial	1.0
Agricultural	1.0

4.10.1. Feeder Composition

The user shall be permitted to enter the composition for up to 8 feeders by providing the number of customers of each type. The default number of customers of each type shall be as shown in Table 13.

Table 13. Customer type on feeders

Customer type	Default number of customer
Single family	500
Multi family	20
Small office	25
Large office	5
Retail	15
Lodging	5
Grocery	5
Restaurant	5
School	2
Health	1
Industrial	0
Agricultural	0

4.11. Loadshapes

The user shall be permitted to display and output four loadshapes of the study.

The customer-class shape shall display a stacked bar graph of the customer loads (in MW) for each hour of the study day from 0 (midnight to 1am) to 23 hours of the load for all customer classes (residential, commercial, industrial, and agricultural).

The customer-class composition shall display a stacked bar graph of the customer load fractions (in %) for each hour of the study day from 0 to 23 hours of the load for all customer classes (residential, commercial, industrial, and agricultural).

The load component shape shall display a stacked bar graph of the load components (in MW) for each hour of the study day from 0 to 23 hours of the load for all components (electronic, motors A-D, and ZIP).

The load component composition shall display a stacked bar graph of the load composition (in %) for each of the study day from 0 to 23 hours of the load for all components (electronic, motors A-D, and ZIP).

4.12. Sensitivities

A temperature sensitivity report shall be generated upon request of the user. The temperature sensitivity of each load component shall be estimated by lowering the outdoor temperature one degree when cooling and raising the outdoor temperature one degree when heating and then calculating the difference in load.

The temperature sensitivities shall be reported as shown in Table 14 for each load component, the power factor, and the total power.

Table 14. Temperature sensitivities

Sensitivity	Unit
Total Load	MW/°F
Composition	%/°F
Residential	kW/°F
Single family	kW/°F
Multi family	kW/°F
Commercial	kW/°F
Small office	kW/°F
Large office	kW/°F
Retail	kW/°F
Lodging	kW/°F
Grocery	kW/°F
Restaurant	kW/°F
School	kW/°F
Health	kW/°F

The following notation conventions shall be observed and a legend to this effect shall be included.

- All numbers shall be displayed to 3 significant digits;
- A hyphen (-) shall be displayed when the difference is between loads that are both exactly zero;
- A zero (0) shall be displayed when the difference between the loads is exactly the zero;
- A zero with precision (0.00) shall be displayed when the difference between the two load is less than the precision.

4.13. System-Wide Results

The system-wide results report shall be generated upon request of the user. The load composition (including power factor) shall be reported for the following combinations of conditions:

1. winter peak, typical, and summer peak day

2. 6 am, 9 am, 3 pm, and 6 pm (note that noon is not included)

3. each city

4. 100% residential, 100% commercial, and 50/50 mixed residential/commercial

All quantities in the report (except for power factor) shall be provided as % of total power.

5.0 Prototype

A prototype of the tool can be downloaded from SourceForge (SourceForge.net). The tool provides a numerical reference for validation as well as an illustration of the user input/output requirements. The prototype shall not be considered an authoritative illustration of what the tool must do, rather an example of what it can do. It is expected that developers will improve upon the user interface and data input/output in a substantive way.

5.1. Conditions

Conditions Status Check	Ok	Reset			
	Default	Override	Unit	Check	Remarks
Time					
Study type	3			Ok	1=Winter peak, 2=Typical, 3=Summer peak
Month	6			Ok	1=Jan, ... 12=Dec
Day of week	3			Ok	1=Sun, ... 7=Sat, 8=Holiday
Hour of day	15			Ok	0=midnight, ..., 12=noon, ...
Location					
City ST	Portland OR			Ok	Use button to load climate data (see Support col. A)
Latitude	45.5		deg	Ok	Only 25 to 65 N allowed
Climate					
<i>Winter</i>					
Low temperature	20		F	Ok	Determine the heating design conditions
Low month	1			Ok	1=Jan, ... 12=Dec
Low weekday	4			Ok	1=Sun, ... 7=Sat, 8=Holiday
Low hour of day	17			Ok	0=midnight, ..., 12=noon, ...
<i>Summer</i>					
High temperature	92		F	Ok	Determined the cooling design conditions
High month	6			Ok	1=Jan, ... 12=Dec
High weekday	3			Ok	1=Sun, ... 7=Sat, 8=Holiday
High hour of day	15			Ok	0=midnight, ..., 12=noon, ...
Peak solar radiation	301		Btu/sf.h	Ok	Used to establish size of cooling systems
Weather					
Dry Bulb Temperature	92		F	Ok	Determines the load composition conditions
Wind speed	3		mph	Ok	Used to estimate ventilation losses
Relative humidity	87%		%	Ok	Used to estimate latent load
Opaque sky cover	0%		%	Ok	
Diffuse Horizontal Radiation	119		Btu/sf.h	Ok	Used to estimate diffuse window heat gain
Direct normal Radiation	269		Btu/sf.h	Ok	Used to estimate direct solar heat gain

Figure 4. The prototype conditions page

5.2. Composition

Load composition		Status: Ok																	
Location	Portland OR													Total power		Update Loadshapes			
Month	June															Update Sensitivities			
Weekday	Tuesday																		
Time of day	15:00 - 16:00																		
	Customers	Electronic	Motor-A	Motor-B	Motor-C	Motor-D	ZIP Ip	ZIP Iq	ZIP Pp (P)	ZIP Pq (Q)	ZIP Zp (G)	ZIP Zq (B)	ZIP PF	Total power	Check	Sensitivity	Unit		
Load	583	1.0	1.2	0.9	0.7	2.0	1.3	-0.5	0.0	0.0	1.0	0.1	-0.987	8.0	Ok	Y	MW		
Composition	-	12%	14%	12%	8%	25%	16%	-6%	0%	0%	13%	1%	-	100%		Y	%		
Residential	520	366.0	0.0	175.9	352.6	1896.6	14.1	-2.8	0.0	0.0	889.9	0.0	-1.0	3695.0	46%	Y	kW		
Single family	500	231.4	0.0	105.0	222.9	1143.1	8.9	-1.8	0.0	0.0	562.6	0.0	-1.0	2273.8	28%	Y	kW		
Multi family	20	134.6	0.0	70.9	129.7	753.5	5.2	-1.0	0.0	0.0	327.3	0.0	-1.0	1421.2	18%	Y	kW		
Commercial	63	632.3	1152.0	759.8	302.5	104.5	1247.3	-461.1	0.0	0.0	119.6	87.1	-1.0	4334.1	54%	Y	kW		
Small office	25	144.0	170.2	106.1	42.6	49.2	251.9	-90.7	0.0	0.0	24.4	18.0	-1.0	791.7	10%	Y	kW		
Large office	5	349.1	518.8	357.0	132.4	16.0	391.3	-140.9	0.0	0.0	31.5	26.9	-1.0	1799.7	22%	Y	kW		
Retail	15	95.1	280.5	199.0	85.2	6.6	482.4	-173.7	0.0	0.0	34.8	32.2	-1.0	1192.0	15%	Y	kW		
Lodging	5	11.8	31.9	36.6	16.7	21.0	36.1	-13.0	0.0	0.0	6.7	2.3	-1.0	161.1	2%	Y	kW		
Grocery	5	15.9	85.1	13.8	4.0	9.0	36.6	-13.2	0.0	0.0	6.1	2.4	-1.0	171.0	2%	Y	kW		
Restaurant	5	4.7	20.3	14.6	6.7	0.8	14.4	-5.2	0.0	0.0	2.7	0.9	-1.0	64.4	1%	Y	kW		
School	2	6.6	28.5	20.5	9.4	1.1	20.2	-7.3	0.0	0.0	3.8	1.3	-1.0	90.2	1%	Y	kW		
Health	1	5.2	16.7	12.3	5.4	0.7	14.4	-17.3	0.0	0.0	9.6	3.0	-0.9	65.9	1%	Y	kW		
Industrial kW	0	0.0	0.0	0.0	0.0	0.0	0.0	0.0	0.0	0.0	0.0	0.0	1.0	0.0	0%	N	kW		
Agricultural kW	0	0.0	0.0	0.0	0.0	0.0	0.0	0.0	0.0	0.0	0.0	0.0	1.0	0.0	0%	N	kW		

Figure 5. The prototype feeder composition page

Substation composition		Residential		Commercial								Other		Total
Reset	Scalars:	Single family	Multi family	Small office	Large office	Retail	Lodging	Grocery	Restaurant	School	Health	Industrial kW	Agricultural kW	
Feeder														
Defaults		500	20	25	5	15	5	5	5	2	1	0	0	583
Total		500	20	25	5	15	5	5	5	2	1	0	0	583
1														0
2														0
3														0
4														0
5														0
6														0
7														0
8														0
Square footage (ksf)		1,100	640	250	250	225	125	75	50	70	50	-	-	2,835

Figure 6. The prototype substation composition page

5.3. Feeders

Update																
Winter peak	06:00	City ST	Residential											Zp	Zq	PF
			Electronic	Motor-A	Motor-B	Motor-C	Motor-D	Ip	Iq	Pp	Pq					
		Albuquerque NM	8.3%	0.0%	3.0%	3.6%	14.8%	0.8%	-0.2%	0.0%	0.0%	69.5%	0.0%	-1.000		
		Bakersfield CA	10.6%	0.0%	2.4%	4.6%	14.8%	1.0%	-0.2%	0.0%	0.0%	66.6%	0.0%	-1.000		
		Boise ID	4.7%	0.0%	1.9%	2.0%	9.1%	0.4%	-0.1%	0.0%	0.0%	81.8%	0.0%	-1.000		
		Cheyenne WY	4.0%	0.0%	2.0%	1.7%	8.9%	0.4%	-0.1%	0.0%	0.0%	83.0%	0.0%	-1.000		
		Denver CO	4.0%	0.0%	2.0%	1.7%	8.9%	0.4%	-0.1%	0.0%	0.0%	83.0%	0.0%	-1.000		
		Eugene OR	6.5%	0.0%	1.7%	2.8%	9.7%	0.6%	-0.1%	0.0%	0.0%	78.7%	0.0%	-1.000		
		Eureka CA	9.8%	0.0%	3.6%	4.1%	17.5%	0.9%	-0.2%	0.0%	0.0%	64.1%	0.0%	-1.000		
		Fresno CA	8.0%	0.0%	4.4%	1.4%	21.2%	0.8%	-0.2%	0.0%	0.0%	64.2%	0.0%	-1.000		
		Helena MT	3.5%	0.0%	2.1%	1.5%	8.7%	0.3%	-0.1%	0.0%	0.0%	83.8%	0.0%	-1.000		
		Las Vegas NV	7.2%	0.0%	4.8%	3.1%	19.7%	0.7%	-0.1%	0.0%	0.0%	64.4%	0.0%	-1.000		
		Long Beach CA	8.2%	0.0%	3.1%	3.5%	14.9%	0.7%	-0.1%	0.0%	0.0%	69.7%	0.0%	-1.000		
		Los Angeles CA	10.1%	0.0%	2.6%	4.3%	14.8%	0.9%	-0.2%	0.0%	0.0%	67.3%	0.0%	-1.000		
		Phoenix AZ	8.3%	0.0%	4.3%	1.5%	21.3%	0.8%	-0.2%	0.0%	0.0%	63.9%	0.0%	-1.000		
		Portland OR	7.1%	0.0%	2.2%	3.1%	11.6%	0.7%	-0.1%	0.0%	0.0%	75.4%	0.0%	-1.000		
		Redmond OR	4.5%	0.0%	2.6%	2.0%	11.0%	0.4%	-0.1%	0.0%	0.0%	79.4%	0.0%	-1.000		
		Reno NV	5.1%	0.0%	2.5%	2.2%	11.1%	0.5%	-0.1%	0.0%	0.0%	78.6%	0.0%	-1.000		
		Sacramento CA	12.1%	0.0%	2.0%	5.2%	14.7%	1.1%	-0.2%	0.0%	0.0%	64.8%	0.0%	-1.000		
		Salt Lake City UT	5.5%	0.0%	2.4%	2.4%	11.2%	0.5%	-0.1%	0.0%	0.0%	77.9%	0.0%	-1.000		
		San Diego CA	15.0%	0.0%	1.4%	6.3%	14.8%	1.4%	-0.3%	0.0%	0.0%	61.1%	0.0%	-1.000		
		San Francisco CA	11.6%	0.0%	2.5%	2.1%	19.6%	1.2%	-0.2%	0.0%	0.0%	63.1%	0.0%	-1.000		
		Santa Maria CA	10.9%	0.0%	2.4%	4.6%	14.8%	1.0%	-0.2%	0.0%	0.0%	66.3%	0.0%	-1.000		
		Seattle WA	9.0%	0.0%	3.1%	1.6%	18.0%	0.9%	-0.2%	0.0%	0.0%	67.4%	0.0%	-1.000		
		Spokane WA	3.8%	0.0%	2.0%	1.6%	8.8%	0.4%	-0.1%	0.0%	0.0%	83.4%	0.0%	-1.000		
		Yakima WA	3.4%	0.0%	2.1%	0.6%	9.9%	0.3%	-0.1%	0.0%	0.0%	83.7%	0.0%	-1.000		

Figure 7. The prototype feeder composition table page

5.4. Loadshapes

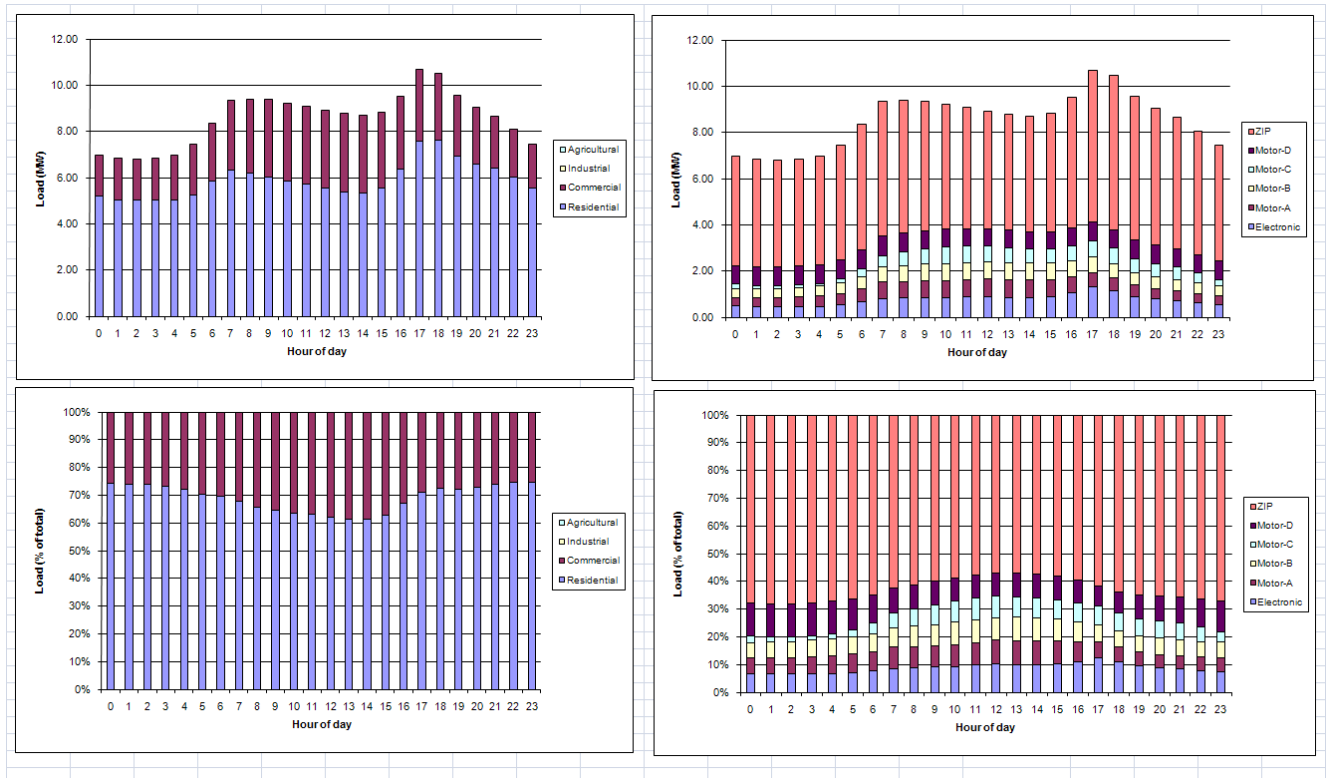


Figure 8. The prototype loadshapes graphs page

5.5. Sensitivity

Temperature sensitivities	Electronic	Motor-A	Motor-B	Motor-C	Motor-D	ZIP Ip	ZIP Iq	ZIP Pp (P)	ZIP Pq (Q)	ZIP Zp (G)	ZIP Zq (B)	ZIP PF	Total powe
Load [MW/F]	0	0	0.0072	0	0.0645	0	0	-	-	0	0	0	0.0716
Composition [%/F]	-0.11%	-0.13%	-0.01%	-0.07%	0.59%	-0.14%	0.05%	-	-	-0.11%	-0.01%		0
Residential [kW/F]	0	-	7.17	0	64.5	0	0	-	-	0	-	0	71.7
Single family [kW/F]	0	-	3.39	0	30.5	0	0	-	-	0	-	0	33.9
Multi family [kW/F]	0	-	3.78	0	34.0	0	0	-	-	0	-	0	37.8
Commercial [kW/F]	0	0	0	0	0	0	0	-	-	0	0	0	0
Small office [kW/F]	0	0	0	0	0	0	0	-	-	0	0	0	0
Large office [kW/F]	0	0	0	0	0	0	0	-	-	0	0	0	0
Retail [kW/F]	0	0	0	0	0	0	0	-	-	0	0	0	0
Lodging [kW/F]	0	0	0	0	0	0	0	-	-	0	0	0	0
Grocery [kW/F]	0	0	0	0	0	0	0	-	-	0	0	0	0
Restaurant [kW/F]	0	0	0	0	0	0	0	-	-	0	0	0	0
School [kW/F]	0	0	0	0	0	0	0	-	-	0	0	0	0
Health [kW/F]	0	0	0	0	0	0	0	-	-	0	0	0	0
Numeric legend:													
- Both loads are exactly zero													
0 The load difference is exactly zero													
0.00 The load difference is nearly zero													

Figure 9. The prototype sensitivity table page

5.6. Residential

Residential model check	Ok				
	Default	Override	Unit	Check	Remarks
Single Family					
<i>Design</i>					
Floor area	2200		sf	Ok	
Building height	10		ft	Ok	
Wall area	1990		sf	Ok	
Wall R-value	19		F.h/Btu.sf	Ok	Recommend using local code
Roof R-value	60		F.h/Btu.sf	Ok	Recommend using local code
Window-wall ratio	15%		%	Ok	Recommend using local code
Window R-value	3.5		F.h/Btu.sf	Ok	Recommend using local code
Ventilation rate	0.3		ac/h	Ok	
Balance temperature	50		F		Should be below 92F
Heating design temperature	20		F		Should be above -50F
Cooling design temperature	92		F	Ok	
Heating design capacity	17598		Btu/h	Ok	
Cooling design capacity	35221		Btu/h	Ok	
Thermostat setpoint	75		F	Ok	Should be between 55F and 85F
Building UA	320		Btu/F.h	Ok	
Internal heat gain	5302		Btu/h	Ok	
External shading	20%		%	Ok	
Solar gains	2804		Btu/h	Ok	
Latent load	2410		Btu/h	Ok	
Heating duty cycle	0%		%	Ok	
Cooling duty cycle	100%		%	Ok	
<i>Enduse electrification</i>					
					Fraction of customers that use electric...
Resistive heating fraction	50%		%	Ok	...resistive heating
Heatpump fraction	25%		%	Ok	...heatpumps
Electric hotwater fraction	30%		%	Ok	...electric waterheaters
Electric cooking fraction	30%		%	Ok	...electric range
Electric drying fraction	75%		%	Ok	...electric dryers
Air-conditioning fraction	60%		%	Ok	...air-conditioning
<i>Efficiency</i>					
Heating efficiency	3.0		COP	Ok	>1.0 when heat pumps present
Cooling efficiency	11.5		SEER	Ok	Must be between 0 and 25
<i>Installed capacity</i>					
Cooking	3.00		W/sf	Ok	
Hotwater	2.50		W/sf	Ok	
Lighting	1.00		W/sf	Ok	
Plugs	1.50		W/sf	Ok	
Washing	2.50		W/sf	Ok	
Heating	0.78		W/sf	Ok	
Cooling	1.59		W/sf	Ok	
Refrigeration	0.2		W/sf	Ok	
<i>Diversified load</i>					
Cooking	0.63		kW	Ok	
Hotwater	0.40		kW	Ok	
Lighting	0.18		kW	Ok	
Plugs	0.25		kW	Ok	
Washing	0.55		kW	Ok	
Heating	0.00		kW	Ok	
Cooling	2.10		kW	Ok	
Refrigeration	0.44		kW	Ok	

Figure 10. The prototype residential single-family design page

Multi Family					
Design					
Floor area per unit	800		sf	Ok	Must be positive
Floors per building	4			Ok	Must be positive
Units per floor	10			Ok	Must be positive
Floor-to-floor height	10		ft	Ok	Must be 8 ft or more
External unit wall area	160		sf	Ok	Must be positive
External wall R-value	9		F.h/Btu.sf	Ok	Recommend using local code
Roof R-value	30			Ok	Recommend using local code
Window-wall ratio	60%		%	Ok	Recommend using local code
Window R-value	3.5		F.h/Btu.sf	Ok	Recommend using local code
Ventilation rate	0.2		ac/h	Ok	
Balance temperature	61		F		Should be below 92F
Heating design temperature	20		F		Should be above -50F
Cooling design temperature	92		F	Ok	Should be between 50F and 150F
Heating design capacity	392014		Btu/h	Ok	
Cooling design capacity	517138		Btu/h	Ok	
Thermostat setpoint	78		F	Ok	Should be between 55F and 85F
Building UA	6752		Btu/F.h	Ok	
Internal heat gain	77114		Btu/h	Ok	
External shading	20%		%	Ok	
Solar gains	36066		Btu/h	Ok	
Latent load	33648		Btu/h	Ok	
Heating duty cycle	0%		%	Ok	
Cooling duty cycle	100%		%	Ok	
Enduse electrification					
					Fraction of customers that use electric...
Resistive heating fraction	50%		%	Ok	...resistive heating
Heatpump fraction	25%		%	Ok	...heatpumps
Electric hotwater fraction	30%		%	Ok	...electric waterheaters
Electric cooking fraction	30%		%	Ok	...electric range
Electric drying fraction	75%		%	Ok	...electric dryers
Air-conditioning fraction	60%		%	Ok	...air-conditioning
Efficiency					
Heating efficiency	3.0		COP	Ok	>1.0 when heat pumps present
Cooling efficiency	10.0		SEER	Ok	Must be between 0 and 25
Installed capacity					
Cooking	3.00		W/sf	Ok	
Hotwater	2.50		W/sf	Ok	
Lighting	1.00		W/sf	Ok	
Plugs	1.50		W/sf	Ok	
Washing	2.50		W/sf	Ok	
Heating	1.20		W/sf	Ok	
Cooling	1.85		W/sf	Ok	
Refrigeration	0.2		W/sf	Ok	
Diversified load					
Cooking	9.18		kW	Ok	
Hotwater	5.78		kW	Ok	
Lighting	2.59		kW	Ok	
Plugs	3.71		kW	Ok	
Washing	7.95		kW	Ok	
Heating	0.00		kW	Ok	
Cooling	35.46		kW	Ok	
Refrigeration	6.40		kW	Ok	

Figure 11. The prototype residential multi-family design page

	Demand	Electronic	Motor-A	Motor-B	Motor-C	Motor-D	ZIP Ip	ZIP Iq	ZIP Pp (P)	ZIP Pq (Q)	ZIP Zp (G)	ZIP Zq (B)	PF	P		Q		Check
														Total	Fraction	Total	Fraction	
Single-family loads	4.55	0.46	0.00	0.21	0.45	2.29	0.02	0.00	0.00	0.00	1.13	0.00	-1.00	4.55	100%	0.00	0%	Ok
Cooking	0.63	0.30			0.10						0.60		1.00	0.63	14%	0.00	0%	Ok
Hotwater	0.40										1.00		1.00	0.40	9%	0.00	0%	Ok
Lighting	0.18						0.10	-0.02			0.90		-1.00	0.18	4%	0.00	0%	Ok
Plugs	0.25	0.90									0.10		1.00	0.25	6%	0.00	0%	Ok
Washing	0.55				0.70						0.30		1.00	0.55	12%	0.00	0%	Ok
Heating	0.00			0.03		0.08					0.65		1.00	0.00	0%	0.00	0%	Ok
Cooling	2.10			0.10		0.90							1.00	2.10	46%	0.00	0%	Ok
Refrigeration	0.44	0.10				0.90							1.00	0.44	10%	0.00	0%	Ok

Figure 12. The prototype residential design page

5.7. Commercial

Commercial model check		Ok																	P		Q		Check	
	Default	Override	Unit	Check	Remarks	Demand	Electronic	Motor-A	Motor-B	Motor-C	Motor-D	ZIP Ip	ZIP Iq	ZIP Pp (P)	ZIP Pq (Q)	ZIP Zp (G)	ZIP Zq (B)	PF	Total	Fraction	Total	Fraction		
Small office																								
Floor area	10		ksf	Ok	Must be less than 30,000 sf																			
Electric load density						21	6	7	4	2	2	10	4	0	0	1	1	-0.97	21	100%	-3	100%		
Heating	0.02		W/sf	Ok	Heating	0.2	0.70				0.20						0.10	0.02	0.99	0	1%	0	0%	Ok
Cooling	0.59		W/sf	Ok	Cooling	5.9	0.75				0.25								1.00	6	28%	0	0%	Ok
Vent	0.32		W/sf	Ok	Vent	3.2	0.30	0.70											1.00	3	15%	0	0%	Ok
WaterHeat	0.08		W/sf	Ok	WaterHeat	0.8										1.00	0.15		0.99	1	4%	0	-4%	Ok
Cooking	0.03		W/sf	Ok	Cooking	0.3	0.20	0.20											1.00	0	2%	0	0%	Ok
Refrig	0.08		W/sf	Ok	Refrig	0.8	0.10	0.30			0.60						0.60		1.00	1	4%	0	0%	Ok
ExtLight	0.00		W/sf	Ok	ExtLight	0.0						1.00	-0.36					0.06	-0.96	0	0%	0	0%	Ok
IntLight	1.01		W/sf	Ok	IntLight	10.1						1.00	-0.36					0.06	-0.96	10	47%	-3	104%	Ok
OfficeEquip	0.46		W/sf	Ok	OfficeEquip	4.6	1.00												1.00	5	22%	0	0%	Ok
Misc	0.22		W/sf	Ok	Misc	2.2		0.50	0.50										1.00	2	10%	0	0%	Ok
Process	0.01		W/sf	Ok	Process	0.1	0.50		0.25	0.25									1.00	0	0%	0	0%	Ok
Motors	0.20		W/sf	Ok	Motors	2.0		0.30	0.40	0.30									1.00	2	10%	0	0%	Ok
AirComp	0.14		W/sf	Ok	AirComp	1.4													1.00	1	7%	0	0%	Ok

Figure 13. The prototype commercial design page

5.8. Industrial

Industrial model check	Ok	
Total electric	1515	kW
Electronic	200	kW
Motor-A	300	kW
Motor-B	500	kW
Motor-C	500	kW
Motor-D	0	kW
ZIP Ip	10	kW
ZIP Iq		kW
ZIP Pp (P)		kW
ZIP Pq (Q)		kW
ZIP Zp (G)	5	kW
ZIP Zq (B)		kW
Power factor	1.00	

Figure 14. The prototype industrial design page

5.9. Agricultural

Agricultural model check	Ok		
Total electric	0	kW	
Electronic		kW	
Motor-A		kW	
Motor-B		kW	
Motor-C		kW	
Motor-D		kW	
ZIP Ip		kW	
ZIP Iq		kW	
ZIP Pp (P)		kW	
ZIP Pq (Q)		kW	
ZIP Zp (G)		kW	
ZIP Zq (B)		kW	
Power factor		1.00	

Figure 15. The prototype agricultural design page

6.0 References

California End-use Survey. March 2006. <http://capabilities.itron.com/ceusweb/>.

Chinn, Garry. "Modeling Stalled Induction Motors," presented at the *IEEE Transmission and Distribution Conference*. Dallas TX, 2006.

IEEE Task Force on Load Representation for Dynamic Performance. "Load Representation for Dynamic Performance Analysis." *IEEE Transactions on Power Systems*, vol.8, no.2, (1993): 472-482.

IEEE Task Force on Load Representation for Dynamic Performance. "Standard Models for Power Flow and Dynamic Performance Simulation." *IEEE Transactions on Power Systems*, vol.10, no.3, (1995): 1302-1313.

Kosterev, D., A. Meklin, J. Undrill, B. Lesieutre, W. Price, D. Chassin, R. Bravo, and S. Yang. "Load modeling in power system studies: WECC progress update." *2008 IEEE Power and Energy Society General Meeting - Conversion and Delivery of Electrical Energy in the 21st Century*, 20-24. (2008): 1-8.

NREL TMY2 archive. http://rredc.nrel.gov/solar/old_data/nsrdb/tmy2/.

Pereira, Les, Dmitry Kosterev, Peter Mackin, Donald Davies, John Undrill, and Wenchun Zhu. "An Interim Dynamic Induction Motor Model for Stability Studies in WSCC." *IEEE Transactions on Power Systems*, vol.17, no.4, (2002): 1108-1115.

Shaffer, John. "Air Conditioner Response to Transmission Faults." *IEEE Transactions on Power Systems*, vol.12, no.2, (1997): 614-621.

SourceForge.net. <http://sourceforge.net/projects/gridlab-d/files/load-composition/>.

Williams, Bradley, Wayne Schmus, and Douglas Dawson. "Transmission Voltage Recovery Delayed by Stalled Air Conditioner Compressors." *IEEE Transactions on Power Systems*, vol.7, no.3, (1992): 1173-1181.

FINAL PROJECT REPORT

LOAD MODELING TRANSMISSION RESEARCH

APPENDIX H

LOAD MONITORING

CEC/LMTF LOAD RESEARCH PROGRAM

Prepared for CIEE By:

Lawrence Berkeley National Laboratory



A CIEE Report

Pacific Northwest National Laboratory

Operated by Battelle for the
U.S. Department of Energy

Load Monitoring

CEC/LMTF Load Research Program

Z. Huang	J. Phillips
B. Lesieutre	D. Kosterev
S. Yang	M. Hoffman
A. Ellis	O. Ciniglio
A. Meklin	R. Hartwell
B. Wong	P. Pourbeik
A. Gaikwad	A. Maitra
D. Brooks	N. Lu
D. Hammerstrom	

November 2007



Prepared for
Lawrence Berkeley National Laboratory
for the California Energy Commission
under Contract DE-AC05-76RL01830

DISCLAIMER

This report was prepared as an account of work sponsored by an agency of the United States Government. Neither the United States Government nor any agency thereof, nor Battelle Memorial Institute, nor any of their employees, makes **any warranty, express or implied, or assumes any legal liability or responsibility for the accuracy, completeness, or usefulness of any information, apparatus, product, or process disclosed, or represents that its use would not infringe privately owned rights**. Reference herein to any specific commercial product, process, or service by trade name, trademark, manufacturer, or otherwise does not necessarily constitute or imply its endorsement, recommendation, or favoring by the United States Government or any agency thereof, or Battelle Memorial Institute. The views and opinions of authors expressed herein do not necessarily state or reflect those of the United States Government or any agency thereof.

PACIFIC NORTHWEST NATIONAL LABORATORY
operated by
BATTELLE
for the
UNITED STATES DEPARTMENT OF ENERGY
under Contract DE-AC0576RL01830

Printed in the United States of America

Available to DOE and DOE contractors from the
Office of Scientific and Technical Information,
P.O. Box 62, Oak Ridge, TN 37831-0062;
ph: (865) 576-8401, fax: (865) 576-5728
email: reports@adonis.osti.gov

Available to the public from the National Technical Information Service,
U.S. Department of Commerce, 5285 Port Royal Rd., Springfield, VA 22161
ph: (800) 553-6847, fax: (703) 605-6900
email: orders@ntis.fedworld.gov
online ordering: <http://www.ntis.gov/ordering.htm>

LEGAL NOTICE

This report was prepared as a result of work sponsored by the California Energy Commission (CEC) and the University of California (UC), and performed by Pacific Northwest National Laboratory (PNNL). It does not necessarily represent the views of CEC, PNNL, UC, their employees, or the State of California. CEC, the State of California, its employees, PNNL, and UC make no warranty, expressed or implied,

and assume no legal liability for the information in this report; nor does any party represent that the use of this information will not infringe upon privately owned rights. This report has not been approved or disapproved by CEC, PNNL, or UC, nor has CEC, PNNL, or UC passed upon the accuracy or adequacy of the information in this report.



This document was printed on recycled paper.

(8/00)

Load Monitoring

CEC/LMTF Load Research Program

Z. Huang (1)	John Phillips (2)
B. Lesieutre (3)	D. Kosterev (4)
S. Yang (4)	M. Hoffman (4)
A. Ellis (5)	O. Ciniglio (6)
A. Meklin (7)	R. Hartwell (7)
B. Wong (7)	P. Pourbeik (8)
A. Gaikwad (8)	A. Maitra (8)
D. Brooks (8)	N. Lu (1)
D. Hammerstrom (1)	

November 2007

Prepared for
Lawrence Berkeley National Laboratory
for the California Energy Commission
under Contract DE-AC05-76RL01830

-
- (1) Pacific Northwest National Laboratory
 - (2) Puget Sound Energy
 - (3) Lawrence Berkeley National Laboratory
 - (4) Bonneville Power Administration
 - (5) Public Service Company of New Mexico
 - (6) Idaho Power Company
 - (7) Pacific Gas & Electric
 - (8) Electric Power Research Institute

SUMMARY

This report is intended to serve as a reference for future load monitoring projects. The identification of specific vendor's equipment/software, etc. in this document is for research documentation only and does not constitute an endorsement of these items.

Load monitoring provides an important means to understand load behavior in the actual system. This understanding helps to develop load models to represent the load behavior in simulation studies. Load monitoring provides measured data needed for load model validation, load composition studies, and load uncertainty analysis.

Depending on various needs, load monitoring may be implemented differently with different monitoring hardware, different measured quantities, and different requirements for sampling rates, signal types, record length and availability, with different costs. Potential load monitoring options include traditional supervisory control and data acquisition (SCADA), phasor measurement units (PMUs), portable power system monitors (PPSMs), digital fault recorders (DFRs), protective relays, power quality monitors, and a low-cost monitoring device being developed by Western Electricity Coordinating Council (WECC) Disturbance Monitoring Working Group (DMWG). Characteristics of these options are summarized in this report.

Current load monitoring practices at several utility companies are presented as examples of load monitoring. Each example consists of the following aspects of load monitoring: objective of load monitoring, monitoring location selection, description of monitoring equipment, communication for load monitoring, cost, and use of the data.

The purpose of load monitoring is to provide better load characterization and better load management, i.e., the core element of load monitoring is focused on applications. Five load monitoring applications are proposed in this report, with some preliminary case studies:

- Load monitoring for top-down load composition: The total load profile obtained from load monitoring data can be decomposed to derive fractions of individual load types if load profiles of individual load types are known.
- Load monitoring for load composition validation: Load profiles generated by the load composition model can be validated against load profiles derived from load monitoring data.
- Load monitoring for load model validation: The general approach of model validation is to compare model simulation against measurements, as was applied to WECC generator model validation. Load monitoring provides the basis for load model validation.
- Load monitoring for uncertainty analysis: Statistical analysis can be performed on load monitoring data to quantify load variations over selected time periods.
- Load monitoring for load control performance evaluation: This is the trend that loads will play a more and more active role in managing the power system. Similar to generator performance monitoring, load monitoring can be used to ensure the load behaves as designed for correct credits and control enforcement.

The case studies show promising results of the use of load monitoring for the above purposes. Based on these results, recommendations on future load monitoring work are presented. It is important to point out

that load monitoring efforts should be consistent with and driven by load research needs. Given the current ongoing load modeling work in WECC, a roadmap for load monitoring is proposed.

ACKNOWLEDGEMENT

The preparation of this report was conducted with support from the California Energy Commission's Public Interest Energy Research Program, WA# MR-049, through the California Institute of Energy and Environment, Award Number MTX-06-01, and support from Pacific Northwest National Laboratory.

CONTENTS

SUMMARY	iii
ACKNOWLEDGEMENT	v
1.0 BACKGROUND	1
2.0 LOAD MONITORING NEEDS	1
2.1 Load Model Validation	1
2.2 Load Composition.....	3
2.3 Load Uncertainty Analysis.....	4
2.4 Load Control Performance Evaluation.....	4
3.0 LOAD MONITORING DEVICE OPTIONS	5
3.1 SCADA	6
3.2 Phasor Measurement Units (PMUs)	6
3.3 Portable Power System Monitors (PPSM).....	8
3.4 Digital Fault Recorders (DFRs)	8
3.5 Protective Relays	8
3.6 Power Quality Monitors.....	8
3.7 Low-cost Monitoring Device being Developed by WECC DMWG	9
3.8 Grid Friendly™ Controller	9
3.9 Custom Recorders	11
4.0 EXISTING LOAD MONITORING EXAMPLES	12
4.1 Building Monitoring at BPA.....	12
4.1.1 Objective	12
4.1.2 Location	12
4.1.3 Description of Monitoring Equipment	12
4.1.4 Communication.....	13
4.1.5 Cost	13
4.1.6 Use of the Data.....	13
4.2 Distribution Substation Monitoring at PNM.....	13
4.2.1 Objective	13
4.2.2 Location	13
4.2.3 Description of Monitoring Equipment	13
4.2.4 Communication.....	14
4.2.5 Cost	14
4.2.6 Use of the Data.....	14
4.2.7 Other Aspects	14
4.3 Load Monitoring at IPC	14
4.3.1 Objective	14
4.3.2 Location	15
4.3.3 Description of Monitoring Equipment	15
4.3.4 Communication.....	15
4.3.5 Cost	15
4.3.6 Use of the Data.....	15
4.4 Load Monitoring at PSE	15
4.4.1 Objective	15
4.4.2 Location	16
4.4.3 Description of Monitoring Equipment	16
4.4.4 Communication.....	16

4.4.5 Cost	16
4.4.6 Use of the Data.....	16
4.5 Feeder Load Monitoring at PG&E.....	16
4.5.1 Objective	16
4.5.2 Locations.....	17
4.5.3 Description of Monitoring Equipment	18
4.5.4 Communication.....	18
4.5.5 Cost	18
4.5.6 Use of the Data.....	19
4.5.7 Other Issues affecting Consumer Loads	19
4.6 Load Modeling Based on Monitored System Disturbance Data.....	19
4.6.1 Motivation.....	19
4.6.2 Locations.....	19
4.6.3 Description of Monitoring Equipment	20
4.6.4 Cost	22
4.6.5 Use of the Data.....	22
4.6.6 Summary	24
4.7 Load Monitoring via Commercial or Residential Load Control Systems.....	24
4.7.1 Objective	24
4.7.2 Location	25
4.7.3 Description of Monitoring Equipment	25
4.7.4 Communication.....	26
4.7.5 Cost	26
4.7.6 Use of the Data.....	26
5.0 LOAD MONITORING APPLICATIONS	28
5.1 Load Monitoring for Top-Down Load Composition	28
5.2 Load Monitoring for Load Composition Validation.....	30
5.3 Load Monitoring for Load Model Validation	33
5.4 Load Monitoring for Uncertainty Analysis.....	34
5.5 Load Monitoring for Load Control Performance Evaluation.....	34
6.0 LOAD MONITORING RECOMMENDATIONS	37
6.1 Site Selection	37
6.2 Load Monitoring Levels.....	37
6.3 Load Monitoring Equipment.....	38
7.0 REFERENCES	40
APPENDIX A – PMU Specifications and Technical Data.....	A.1
APPENDIX B – PPSM Cost Breakdown	B.1

FIGURES

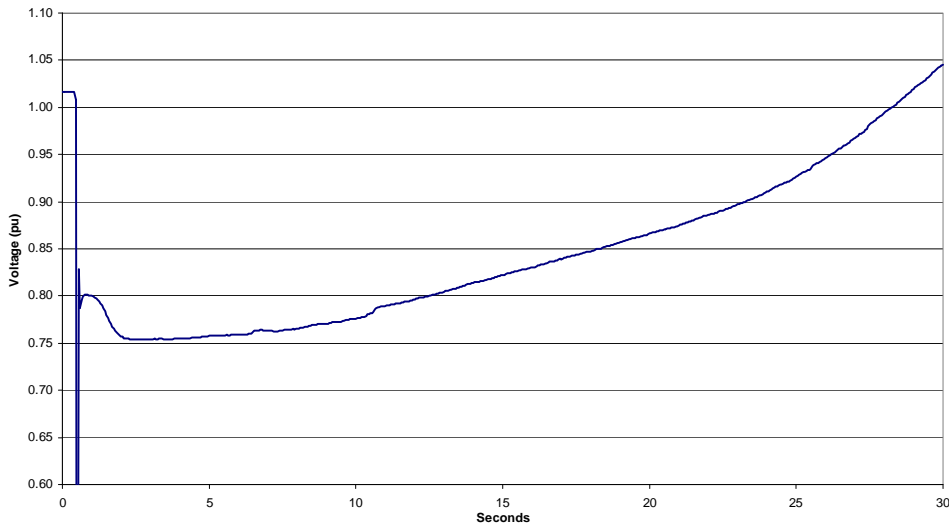
Figure 1 Voltage at Valley Substation during a Fault Event in Southern California.....	1
Figure 2 General Composite Load Model Structure	2
Figure 3 WECC WAMS Network	2
Figure 4 Load Model Validation by Playing Back Voltage at the Feeder Head.....	2
Figure 5 Average Hardware Cost of one PMU Installation (response to the question: What is the average cost of hardware, including PMU, for one installation?)	7
Figure 6 Average Labor Cost of one PMU Installation (response to the question: What is the average cost of labor for one PMU installation?)	7
Figure 7 Average Total Cost of one PMU Installation (response to the question: What is the average Total cost for one PMU installation?).....	7
Figure 8 Grid Friendly Controller	11
Figure 9 PPSM Monitoring Unit at BPA’s Portland Headquarters	12
Figure 10 Commercially Available IEDs.....	21
Figure 11 Example Parameter Estimation using an Optimization Algorithm to fit Load Model Parameters to a Specified “Aggregated” Load Model Structure.	23
Figure 12 Load Model Structure used for Parameter Estimation.....	24
Figure 13 Value Proposition of Load Monitoring via Load Control Systems	25
Figure 14 A potential data architecture for load monitoring.....	26
Figure 15 Demand Response and Market Analysis Studies of Commercial Load	27
Figure 16 Demand Response and Market Analysis Studies of Residential Load	27
Figure 17 Illustration of the Top-Down Approach for Load Composition Analysis.....	28
Figure 18 Curve Decomposition for Top-Down Load Composition Analysis	29
Figure 19 The Setup of a Virtual Feeder.....	30
Figure 20 Example Results of the Top-Down Approach for Load Composition Analysis	31
Figure 21 Example Typical Load Profiles for Sit-Down Restaurants.	32
Figure 22 Summer and Winter Typical Load Profiles for Residential Loads.....	32
Figure 23 Example Result of Load Composition Validation for a Portland Feeder Supplying Mainly Residential Loads and Some Small Commercial Loads.	33
Figure 24 Example Data Logged from Active Project Dryer during an Under-Frequency Event.....	35
Figure 25 Percentages of Grid Friendly Controllers responding at Various Frequency Depths.....	36
Figure 26. Load Monitoring Roadmap	39

TABLES

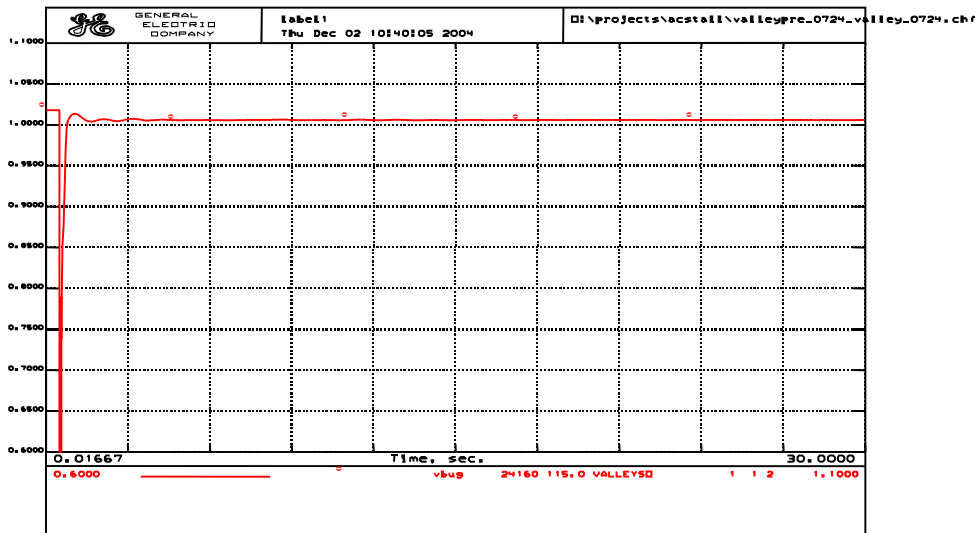
Table 1 Features of Different Monitoring Options	5
Table 2 Technical Requirements of DMWG Low-Cost Monitoring Devices	10
Table 3 Performance Matrix for Commercially Available IEDs	20
Table A-1 PMU Specifications and Technical Data	A-1
Table B-1 Cost Estimate for PXI-based Centralia PPSM	B-1

1.0 BACKGROUND

The Load Modeling Task Force (LMTF) is nearing completion of defining a new composite load model to be implemented in both GE PSLF and Siemens PTI PSS/E for use in Western Electricity Coordinating Council (WECC) dynamic simulation studies. Currently the default load model for dynamic simulations is to replace 20% of the bus load with a three-phase induction motor and use a ZIP model (a combination of constant impedance, constant current, and constant power elements) for the other 80% of the load (Pereira et al. 2002). While this model has been successfully used to validate several large system-wide disturbances including the August 1996 outage, it has failed to simulate several other significant outages that resulted in slow voltage recovery and the loss of significant load (Figure 1).



(a) Real Event – voltage recovers in almost 30 seconds after the fault, load tripping, stalled air-conditioners



(b) Simulations – voltage recovers almost instantaneously after the fault, no load tripped
Figure 1 Voltage at Valley Substation during a Fault Event in Southern California

Through studies performed by Southern California Edison (SCE), Pacific Gas & Electric (PG&E), California Independent System Operators (CALISO), and Bonneville Power Administration (BPA), the basic requirements for an improved load model were determined. These requirements included modeling the substation transformer and feeder impedances, as well as more detailed motor modeling that included both large and small motor dynamics. All of these parameters have been included in the new composite model (Figure 2). The composite load model is to be used for transmission-level system dynamic simulation, so it should represent, at a relative high voltage level (e.g., 60 kV), the aggregated behavior of all the load components on a feeder system.

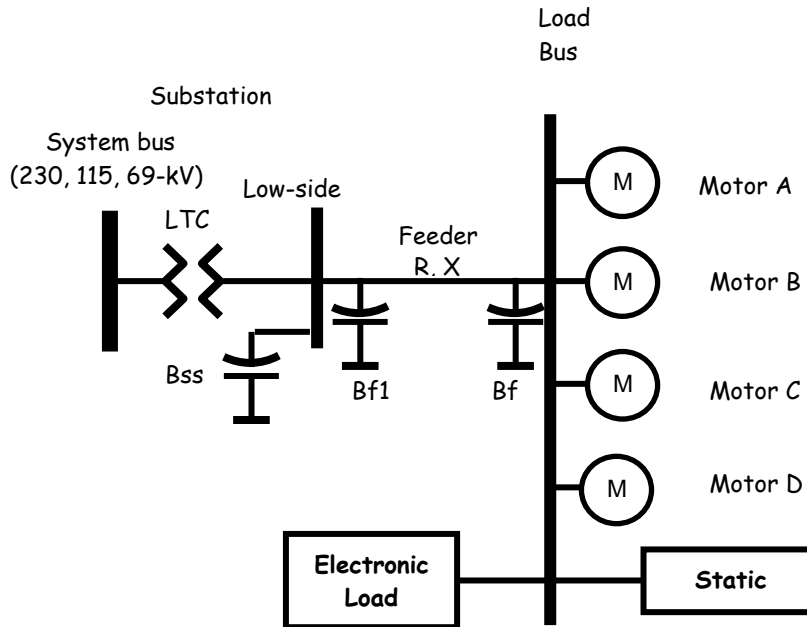


Figure 2 General Composite Load Model Structure

Following development of the composite load model, the next step will be to develop data for the model that will represent the characteristics of each load. The California Energy Commission (CEC) and the WECC Load Modeling Task Force (LMTF) joined forces and set up a load research program. One task in this program is to test air-conditioning (a/c) units in a laboratory environment and use the testing data to develop a/c models. A/c units are of great concern because they slow voltage recovery events. Good progress has been made in the testing and model development. Laboratory tests of a/c units were performed by Bonneville Power Administration (BPA), by Southern California Edison (SCE) and by the Electric Power Research Institute (EPRI). Bonneville Power Administration (BPA) is also conducting laboratory tests of other residential appliances including lighting, refrigerators, dishwashers, clothes washers, dryers, fans, and electronic equipment for developing model databases for individual load components. Besides laboratory tests of individual load components, there is another aspect of data for load model development – load monitoring. Load monitoring generates data of actual load behaviors and reveals insights about load representations in power system simulation studies. Load monitoring is of importance for load model validation, load model composition and load uncertainty studies. This document will address the needs, options and examples of load monitoring, followed by recommendations for further work in this area.

2.0 LOAD MONITORING NEEDS

Load monitoring provides a means to understand load behavior in the actual system. The understanding helps to develop load models to represent the load behavior in simulation studies. Three aspects of load monitoring needs are addressed below: load model validation, load composition, and load uncertainty analysis.

2.1 Load Model Validation

The CEC/LMTF load research program takes a bottom-up approach to develop models for individual load components and then aggregate them at a higher voltage level for transmission system simulation studies. The individual load component models are being developed and validated via laboratory testing. However, the aggregated load model, shown as a composite load model in Figure 2, needs to be validated as well. It is expected that this development effort will generate better quality load models which matches recorded events, especially those delayed voltage recovery disturbances. If the validation process is successful, one can conclude that the model is an improvement over the existing modeling procedure. With the new composite load models populated with data, validation studies will be run on selected major WECC disturbances identified by the LMTF by comparing model simulation against recorded load behavior, as shown in Figure 1. This WECC-wide validation needs to have monitoring devices to record system response. Currently there are about 60 phasor measurement units (PMUs) installed, most at high voltage levels (500 kV and 230 kV) across the WECC power grid for event recording purposes (Figure 3). These PMUs provide good data for model validation in general. To better validate load models, one would need to have monitoring devices at lower voltage levels to better capture load behavior. If monitoring data are available, one can even validate load models at different levels using the “playback” function developed during previous model validation studies (Kosterev 2004; Huang et al. 2006). This multi-level validation would provide a way to identify how the model performance would evolve because the models are gradually aggregated at higher levels, so load aggregation techniques can be validated. Figure 4 provides an example of “playback”-based load model validation.

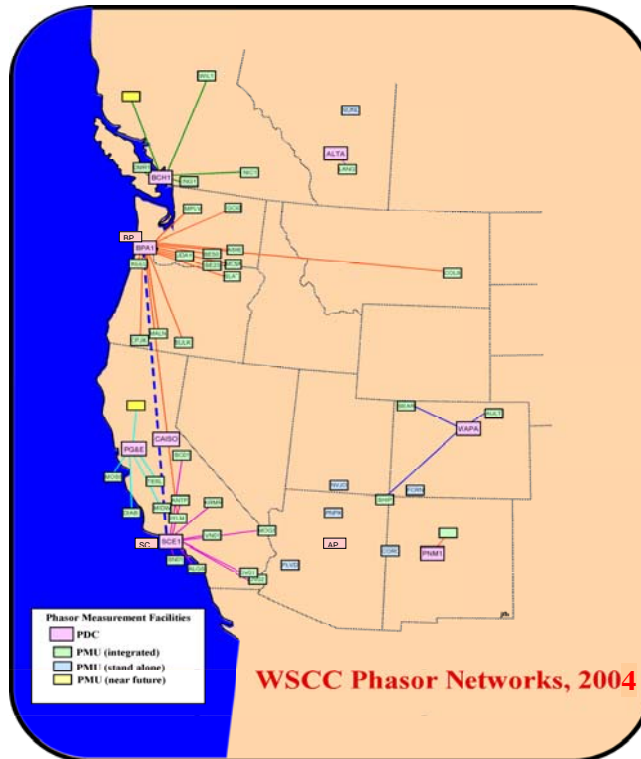


Figure 3 WECC WAMS Network

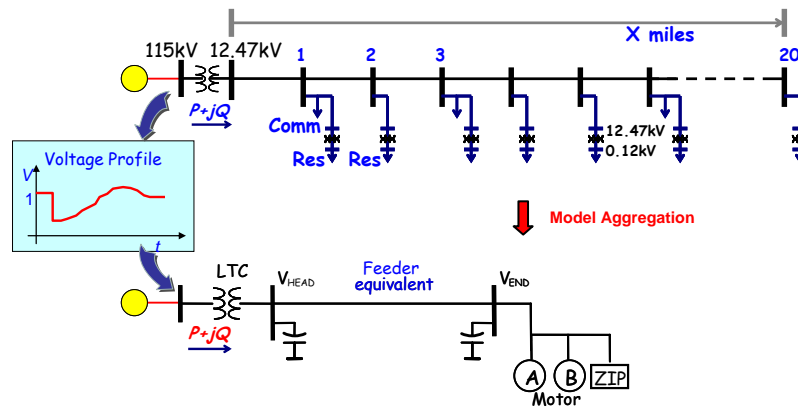


Figure 4 Load Model Validation by Playing Back Voltage at the Feeder Head

The benefits of load modeling may be impacted by the customer type: industrial, commercial, agricultural, and residential. As noted above, if a broad spectrum of load is being modeled only at higher voltage levels (e.g. 230-kV level), then the broader system monitoring devices such as PMUs are likely sufficient for validating the model. However, for smaller discrete modeling, the monitoring needs may vary by customer type:

- Industrial loads: These loads typically are motor dominated and should be relatively straight forward to a model based on the type of industrial processes involved. BPA has already done validation studies on industrial loads in the Pacific Northwest.
- Commercial loads: Purely commercial loads would be found where substations serve commercial buildings or large business/warehouse parks. Commercial loads should be fairly consistent across

the entire system so validation of primarily commercial loads should be beneficial to all of WECC.

- Agricultural loads: Agricultural loads are primarily pumps used for irrigation. They vary depending on region's climate.
- Residential loads: Residential dominated loads will show the greatest regional and seasonal variations. Air conditioning modeling is of prime concern to the summer peaking WECC members, especially in California (as shown in Figure 1).
- Mixed commercial and residential loads: These will be the most common loading type across the system and again will vary by region as a result of air conditioning needs.

To capture load dynamic characteristics, load monitoring devices are necessary to have high sampling rates and data records in the seconds to minutes range, like phasor data.

2.2 Load Composition

Load composition plays a critical role as modeling techniques in the outcomes of power system simulation studies. The type of load modeled at each individual bus varies throughout the system and in addition, the detail of how this load is modeled also varies. In the Pacific Northwest, for instance, each substation is modeled down to 55-kV systems. This allows the distribution of customer types to be determined at a fairly granular level (i.e., approximately <25 MW per bus). This also allows industrial customers with dedicated substations to be modeled separate from commercial and residential loads. In other areas, loads are aggregated up to the 230-kV level, which results in modeling a broader distribution of customer types, including industrial customers in some cases.

It is recognized that load composition will be dependant on the customer class being served, as well as the season and loading level. For load composition, one can use customer billing data if available as monitored load behavior and try to derive typical customer mix by zone or owner or where available, at a bus-by-bus basis. Once the initial load composition for zones/buses is determined, assumptions based on input from current on-going studies by PNNL will be used to determine model parameters based on seasons and loading levels.

Besides the derivation of initial load composition from billing data, load monitoring also provides data necessary for developing load composition methods and validating load composition results.

There are basically two approaches for determining load composition – bottom-up approach and top-down approach. The bottom-up approach is based on individual load profiles and aggregates them into a load mix – motor, lighting, electronics, etc., from which the load composition is determined. Monitoring at individual end use would provide excellent insight about individual load profiles. On the other hand, the top-down approach decomposes recorded load data into different load “elements”, similar to spectrum-analysis-like decomposition. The elements would indicate the percentage of a certain load mix, so load composition is determined. Load monitoring plays a crucial role, providing recorded data for this top-down approach.

For the bottom-up approach, load monitoring devices can have slow sampling rates, like metering data, but need to have long records of days or months to capture load behavior over different times and seasons. The monitoring devices should be installed at the end use level.

For the top-down approach, the requirement for load monitoring depends on the specific method. It is possible that very high sampling rates are required to have the fine granularity to derive load composition. The monitoring devices are at the feeder level.

2.3 Load Uncertainty Analysis

Loads are known for their diversity and uncertainties, which adds to the challenging job of load modeling. No model is complete without uncertainty analysis. Uncertainty analysis can reveal how the uncertainties would affect the model performance and identify what is not modeled so the models can be used with confidence. The goal of uncertainty analysis is to minimize the impact of the uncertainty in the load model data on the decisions that engineers make on grid operating limits and capital investments. First hand load uncertainty information comes from actual load behavior, which requires monitoring data of typical loads. One example is to continuously record load data for a selected time period and compare daily load profiles to show the range of load changes over a day. Load models may be adjusted based on the time of the day to reduce the impact of load uncertainty. However, the uncertainty at this specific time is not modeled; but, its impact on load model performance can be quantified based on the range of load changes.

2.4 Load Control Performance Evaluation

Load solutions for delayed voltage recovery caused by stalled air-conditioning units are being identified under the current CEC/LMTF load research program, and various load controls are expected to be implemented by utilities like SCE and BPA to improve load response to adverse system conditions. To validate the load response and evaluate the performance of load controls, load monitoring devices need to be installed in the system (e.g., at the feeder level) to monitor load behavior. For this purpose, a technical approach similar to generator performance monitoring can be developed. Analysis of the load monitoring data shall be conducted to confirm the performance improvement of the load solution implementation.

3.0 LOAD MONITORING DEVICE OPTIONS

Good load monitoring will provide required data (real and reactive power, voltage, frequency, etc.) at necessary sampling rates. Ideally it will also be remotely accessible. To save on data storage, event triggering would be beneficial. For dynamic validation, event recording would be the main focus, although there is an interest in seeing if steady state data would be helpful in determining load composition.

There are different devices available for monitoring loads or for event recording in general. Some are even installed in the system, and data are available for load monitoring purposes with minimal efforts. As mentioned earlier, PMUs are excellent general event recording devices (Figure 3). Digital fault recorders (DFRs) can record dynamic behaviors but record lengths are shorter. General supervisory control and data acquisition (SCADA) measurements are more readily available in the system. They are long records, which are good for load composition studies, but contain less dynamic information. This section will address the features of each monitoring option, (i.e., sampling rate, measured quantities, record length, availability, hardware structure, and cost information, when available). A summary is shown in Table 1.

Table 1 Features of Different Monitoring Options

Monitoring Device Options	Sampling Rate (sps)	Measured Quantities	Measurement Type	Record Length	Availability	Cost to Implement
SCADA	Low, ~1/4	V, I, P, Q	RMS	Long	High	Low
PMU	Medium, ~30	V, I, θ , f	Phasor (GPS-synch)	Long	Low	High
PPSM	High, ~960	V, I	POW (GPS-synch)	Long	Low	Moderate
DFR	High, ~5760	V, I	POW	Medium	Moderate	High
Relay	High, >960	V, I	POW	Short	High	Moderate
Power Quality Monitor	High, >960	V, I	POW	Short	Moderate	Moderate
GFA Controller	Medium, ~30	V, I, f	RMS	Long	Low	Low
DMWG Low-cost Monitor	Medium, ~30 for phasor, High, ~960 for POW	V, I, θ , f	Phasor, POW (GPS-synch)	Long	Low	Low

*Note: sps – samples per second.

RMS – Root mean square.

POW – Point-on-wave.

GPS-synch – Global Positioning System time synchronized.

DMWG – Disturbance Monitoring Working Group.

3.1 SCADA

Traditionally, power system operators primarily rely on SCADA measurements to understand power system status and guide system operations. Redundant SCADA measurements are available for the major portion of power systems. SCADA systems measure RMS values of bus voltage and line current, and in turn, real power and reactive power on a transmission line. These quantities are measured at an interval of seconds (typically 4 seconds), so these measurements will reflect slow changes (quasi steady state) in the system, but typical dynamic behaviors are not captured. For load monitoring purposes, SCADA measurements are good for deriving load composition, and possibly for load uncertainty analysis. One advantage of using SCADA measurements is that the additional cost is minimal because they are already available. In addition, SCADA measurements are continuous recordings, and they are good data sources for identifying load changes over a long period of time.

3.2 Phasor Measurement Units (PMUs)

PMUs are a relatively new type of measurements in power systems. Phasor measurement technologies emerged about 2 decades ago (Phadke et al. 1983), and currently there are a number of companies manufacturing PMUs, the hardware device that measures phasors. Appendix A provides an incomplete list of PMU manufacturers. Output of a PMU includes voltage and current phasors (including phase angles) and frequency. Real and reactive power quantities can then be derived from phasors. Phasor measurements are GPS-time synchronized and have a higher sampling rate (typically 30 samples per second), which makes phasor measurements a data source for constructing a more accurate real-time picture of system dynamic status, compared with traditional SCADA measurements. A phasor measurement network – wide area measurement systems (WAMS) – is being developed in both the Western and Eastern Interconnections, with between 60 and 70 PMUs, respectively. These WAMS systems perform well for collecting data for large system-wide events and local events at high voltage levels (500 kV/230 kV) near the recorders. PMUs can have long data records with continuous recording functions, or at least the event length as defined by triggering functions.

Most PMUs are installed at high voltage level substation or power plant points of connection to the transmission system. From load monitoring perspective, these PMUs provide good data for system-wide load model validation studies. There are also some PMUs in lower voltage systems, which can be good data sources for specific load model validation or load composition development. However, cost to install new PMUs at desired load locations can be significant. The cost includes several aspects like hardware (PMU), software and data communication. The Eastern Interconnection Phasor Project (EIPP) Performance Requirements Task Team (PRTT) conducted a survey on PMU installation in 2006, and 11 responses were received. Figure 5 through Figure 7 are the PMU cost information excerpted from the survey summary (Centeno et al. 2006). More specific PMU hardware cost information can be found in Appendix A. Actual cost varies depending on specific situations.

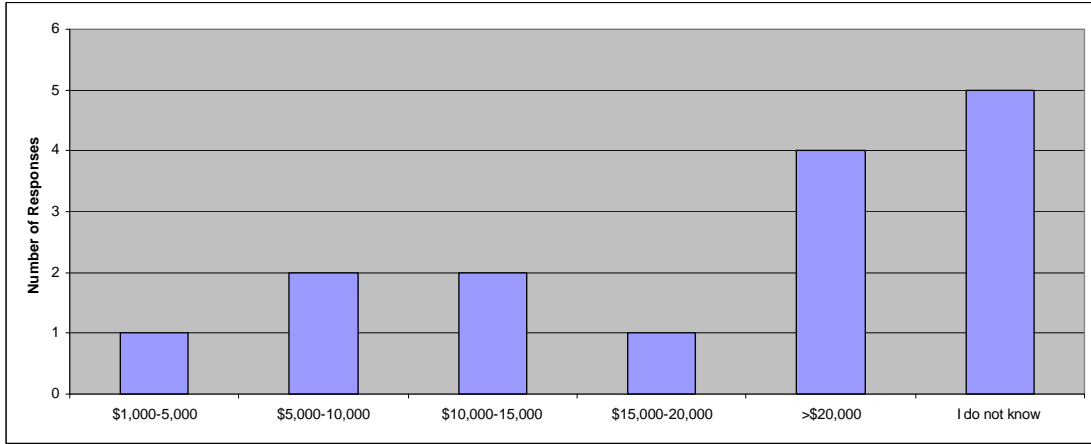


Figure 5 Average Hardware Cost of one PMU Installation (response to the question: What is the average cost of hardware, including PMU, for one installation?)

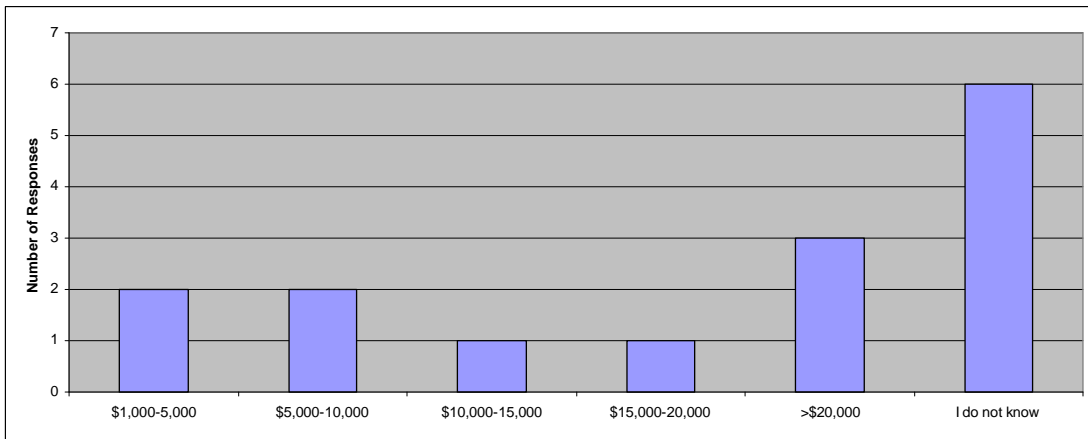


Figure 6 Average Labor Cost of one PMU Installation (response to the question: What is the average cost of labor for one PMU installation?)

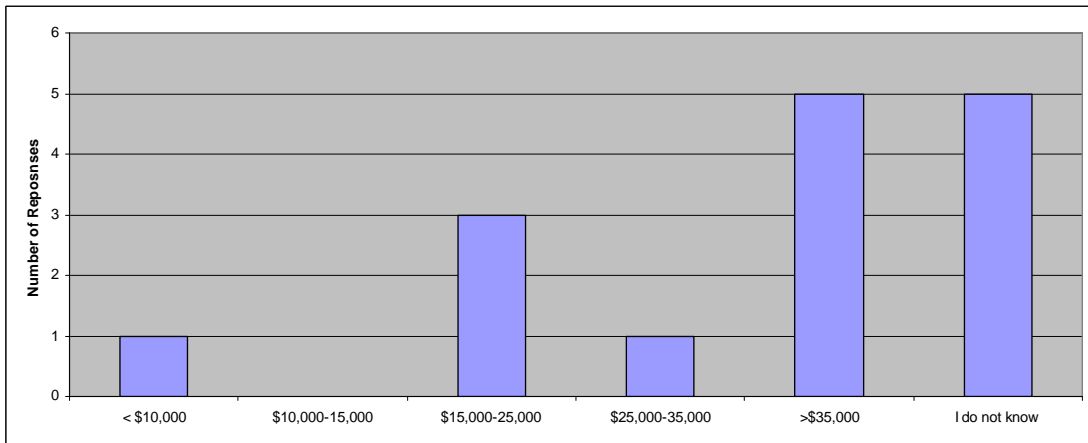


Figure 7 Average Total Cost of one PMU Installation (response to the question: What is the average Total cost for one PMU installation?)

3.3 Portable Power System Monitors (PPSM)

PPSMs have been developed and used for about 15 years at Bonneville Power Administration (BPA). Currently, there are 14 PPSMs within the BPA region, 3 of them in power plants, 6 of them at point-of-connection to power plants, 1 at the commercial building (BPA's Headquarters) and rest of them at different parts of the system. Data from these PPSMs have been used for generator model validation, system model validation, and system studies. PPSMs collect point-on-wave data for voltages, currents and other signals at a very high sampling rate. These PC-based PPSMs consist of off-the-shelf signal conditionings and transducers. This makes PPSM very versatile and easy to modify for different types of signals. It also has the capability to synchronize to GPS-time and can sample data in multiples of 60 using an external clock source, which can be useful for the analysis. PPSMs are most desirable for temporary monitoring or testing. However, it can also be designed for permanent monitoring. PPSMs use a circular buffering for continuous recording, and also have a triggering function. PPSM file formats can be selected from LabView, MATLAB or Excel.

3.4 Digital Fault Recorders (DFRs)

Digital fault recorders are installed throughout most major utility systems, and newer ones may have the capability to provide good validation data for local faults, with triggering and sampling rate capabilities separate from those used for protection. DFRs record point-on-wave voltage and current signals at very high sampling rate (e.g., 5760 samples per second) and at a typical length of several seconds. They usually have communication back to the main office. Concerns have been expressed that the CTs may not be suitable, and that protection engineering may not be willing to open their system for planning purposes.

Where newer units are installed with suitable sampling rates and event durations, DFRs can provide data for system-wide load model validation studies. They are also more likely to be found in lower voltage systems, and can be good data sources for specific load model validation or load composition development.

3.5 Protective Relays

Protective relays are widely installed in power systems for various protection purposes, e.g., under/over voltage protection, reverse time line overloading protection, generator under/over frequency protection, and grounding protection. Protective relays can record point-on-wave voltage and current at very high sampling rates (>960 samples per second). Their record length is usually short as tens of cycles because of their designed purposes. Similar to DFRs, a concern is that protection engineers may not be willing to open their protective relay system for planning purposes.

3.6 Power Quality Monitors

Most utilities have power quality monitors used by substation field personnel for testing and monitoring. Most power quality monitors can store only tens of cycles of data at sampling rates higher than 960 samples/second. They are typically mobile units that are used on an as-needed basis. While they may not

work well for event recording, they could be used for short term steady state recording, if it is determined that there is modeling value in the steady state data.

3.7 Low-cost Monitoring Device being Developed by WECC DMWG

WECC Disturbance Monitoring Working Group (DMWG) intends to obtain standardized low-cost performance monitors for WECC members to use. The design of the basic unit shall be such that it can be installed and used without specialized technical expertise for the following test practices:

- Connection within a member system's substation to monitor generator output quantities (V, I, P, Q and frequency)
- Connection within a member system's substation to monitor load feeder quantities (same as above)
- Connection within a member's substation to measure SVC, STATCOM, FACTS device quantities (same as above)

Specific technical requirements of the low-cost monitoring device are listed in Table 2. This device is expected to provide high-sampling-rate long-length records of voltage and current signals. Time synchronization is included as part of the functionality.

3.8 Grid Friendly™ Controller

Grid Friendly™ Controllers are an emerging technology developed at the Pacific Northwest National Laboratory (PNNL) in Richland, Washington (Grid Friendly™ Appliances 2007). The Grid Friendly concept focuses on demand side management (DSM), but it goes beyond traditional DSM technologies like under frequency and under voltage load shedding. Unlike load shedding, which would interrupt power supply to entire feeders, the Grid Friendly controller focuses on interruptible load. The Grid Friendly technology enables active load control so electrical loads can be used as an active resource, participating in stabilizing power grids, rather than just be passive components in the power grids.

Central to the Grid Friendly technology is a small digital controller that can continually monitor frequency or voltage of the power grid at the local point and process this information to control electrical loads based on pre-defined control strategies (see Figure 8). The Grid Friendly controller can be integrated into appliances like water heaters and refrigerators, and it is very cost-effective (batch production is estimated to be \$2-5 per controller). When the grid experiences an emergency condition, the Grid Friendly controller would identify this situation within milliseconds and adjust the load for a short period of time.

Table 2 Technical Requirements of DMWG Low-Cost Monitoring Devices

Element		Minimum
Frequency response (calculated data)	FR	40 Hz
Maximum rolloff at frequency response (FR)	Rfr	-3dB
Maximum deviation from 0 to 1/2 FR		-0.5dB (-0.1dB preferred)
Rejection above Nyquist frequency	Rnq	40dB (60 dB preferred)
Rejection at 60 Hz harmonics	R60	60dB
Step response ringing		not excessive (see details in text)
Sampling rate	Sm	3600 Hz
A/D sampling resolution		16 bits
Full scale range adjustment	AC voltage AC current DC coupled	50 - 600 V peak 1 - 20 A peak 100 mV – 600V
Active bits (as determined by full scale adjustment)		12-14
Measurement noise		see text
Documentation		Required
Continuous storage capability	overwriting	10 days
Continuous storage capability	non-overwriting	60 days
Triggered event retention		60 days
Measurement synchronization to UTC		100x10-E6
Data access alternatives	A	Network
	B	leased line
	C	dial up
Data format		see text
Minimum record length		300 seconds
Pre-disturbance time for triggered events		60 seconds
Availability		99.99%
Power supply		125 VAC or VDC

* Note:UTC – Universal Time Coordinates

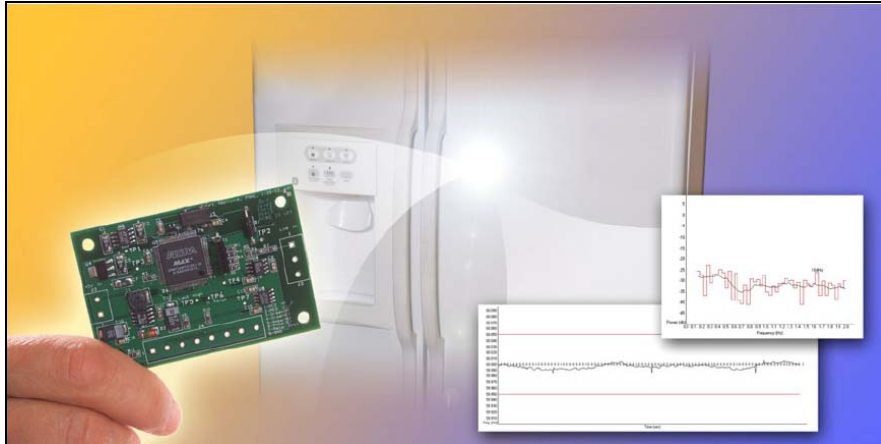


Figure 8 Grid Friendly Controller

Recent development of the Grid Friendly controller hardware features a more compact design and expands recording capabilities to store RMS voltage, current and frequency signals at a sampling rate of between 10 and 30 samples per second. As a result of research on the Grid Friendly concept, PNNL and major appliance manufacturers have begun to define a simple appliance interface based on successful implementation of such an interface during the Pacific Northwest GridWise™ Demonstration [Hammerstrom et al. 2007]. This interface will guide not only appliance manufacturers but designers of any residential product in developing a standard way to receive communications and respond to a load reduction request from an advanced load management system. And including the Grid Friendly controller in appliances at the manufacture stage would make the monitoring capability ubiquitously available at the appliance level. This type of data can be used for developing and verifying models of individual appliances.

3.9 Custom Recorders

Several utilities have developed individual recording units based around either PC or laptops and installed them in individual substations. The units have typically monitored feeder loading on a continuous basis with some form of communication back to the main office. These monitors have typically cost approximately \$5K per installation for hardware plus the cost to establish the communication link. These monitors provide good data but do require upfront costs and effort to install and maintain.

4.0 EXISTING LOAD MONITORING EXAMPLES

This section summarizes several representative examples in load monitoring. The purpose is to provide reference information for future load monitoring projects. Each example addresses the following aspects of load monitoring:

- Objective of load monitoring
- Monitoring location selection
- Description of monitoring equipment (make and model, quantities measured, record length, sampling rate, etc.)
- Communication for load monitoring
- Cost (if available)
- Use of the data.

4.1 Building Monitoring at BPA

4.1.1 Objective

Recently, BPA installed monitoring devices for one of its headquarters building. It is intended for characterizing load consumption for energy efficiency applications, as well as for developing and validating load models at the building level.

4.1.2 Location

For the load monitoring purposes, BPA has a PPSM installed at their headquarters. It is monitoring main distribution of the building (see Figure 9).



Figure 9 PPSM Monitoring Unit at BPA's Portland Headquarters

4.1.3 Description of Monitoring Equipment

The PPSM has 18 channels and is sampling at 2500 sps. With 150-GB memory, its record length is about 16 days.

4.1.4 Communication

This PPSM unit uses a dial-up link to transfer data.

4.1.5 Cost

The cost of the PPSM monitoring system was about \$ 14,000, which includes PC, A/D board, SCXI signal conditioning, current transformers (CTs), cables, etc. Detailed cost information for PPSMs can be found in Appendix B – PPSM Cost Breakdown.

4.1.6 Use of the Data

The recorded data have been used for analyzing building consumption, which leads to a better understanding of load composition at the building level. Further use of the data is planned for the development of the top-down load composition approach. Load model validation at the building level will be explored as well with the recorded data.

4.2 Distribution Substation Monitoring at PNM

4.2.1 Objective

Starting in 1997, PNM deployed a load monitoring system consisting of six custom-built data loggers at different distribution stations. The primary purpose of this project was to verify load composition assumptions for the design of PNM's Import Contingency Load Shedding Scheme (ICLSS). Specifically, the primary purpose was to estimate the portion of the demand that corresponds to large industrial motors. Sensitivity studies demonstrated that the performance of ICLSS would depend on the portion of the motor load that would disconnect from the system (via under-voltage relays) following the loss of the two principal 345-kV circuits that supply the Albuquerque area. A secondary, but very important objective was to demonstrate the feasibility of identifying parameters for physically-based load models.

4.2.2 Location

Monitors were deployed at the following distribution unit stations: Reeves, Iron, Prager, North#2, Juan Tabo, and Rodeo. The former five are in the Albuquerque area, and Rodeo is in the Santa Fe area. Each monitor was setup to monitor all distribution feeders at 12.5 kV (four in each station). In total, 24 feeders were monitored. The feeders were selected to provide a sample of industrial, commercial and residential customer classes. The class mix of each feeder was known a priori. Physically, the monitors were installed at the relay panels of the unit station, where access to all secondary potential transformers (PT) and CT signals was relatively easy. In addition, PNM developed a portable monitor with the same specifications, which was used to capture voltage sensitivity data at several other stations, primarily using manual tap changes.

4.2.3 Description of Monitoring Equipment

Each monitor consists of a National Instruments® signal conditioning stage and a ruggedized Windows PC. For the first three installations, a calibrated shunt was inserted in each phase of the CT secondary. The last three monitors had clamp-on CTs for ease of installation. DataTake was used to handle high-speed point-on-wave data sampling (1200 samples per second) of per-phase, per-feeder voltage and current. A separate custom application was developed to perform additional data processing (calculation of RMS voltage, current and power at 10 samples per second; RMS triggering; data compression; local data storage); and communications. Each monitor produced 15 point-on-wave signals: 12-phase currents

(three per feeder) and 3- phase voltages. For each feeder and for each phase, RMS current, voltage, real power and reactive power were calculated. Frequency was also calculated and included in the RMS data table.

The monitors were setup to collect data continuously, hoping to capture naturally-occurring disturbances. Actually many natural events were captured over the years. In addition, PNM also performed several tap tests on these stations during specific times and seasons (e.g., summer peak, winter peak, and off peak). The test data proved to be more useful than naturally-occurring disturbances. But the one thing learned from naturally-occurring disturbances is that modeling the voltage sensitivity of the load is far more important than the frequency sensitivity.

4.2.4 Communication

Communications from the monitors was via telephone/modem link. Each monitor was programmed to initiate an FTP session once a day to transfer triggered data (both RMS and corresponding point-on-wave data) to an FTP server. Users could access the data from the FTP server as needed. Data stored in the local rolling buffer could also be accessed manually using PC Anywhere¹.

4.2.5 Cost

The PNM load monitors were custom-built for approximately \$8,000 each. This does not include installation and the cost of DataTake and other custom software development. The cost of commercial alternatives would be much higher, considering the number of signals collected and the sampling rate.

4.2.6 Use of the Data

Custom software was developed for data post-processing. The primary purpose of the software is to perform model identification; however, various extensions such as automated data mining were later added. The project was discontinued in 2002, after the primary research objectives were achieved.

4.2.7 Other Aspects

Reliability has been a major issue. Because unit stations are not climate-controlled, several equipment failures occurred as a result of high temperatures (140°F during the summer). Telephone communication was difficult because of the slow data rates and service quality (high noise). The custom software and operating system performance was inconsistent, often resulting in outages and requiring manual equipment restart. As stated before, alternative off-the-shelf equipment and software to accomplish the same job would cost much higher. These factors played a role in PNM's decision not to continue the load-monitoring program after the primary research objectives were accomplished.

4.3 Load Monitoring at IPC

4.3.1 Objective

A load monitor was installed at Idaho Power's Grove station to obtain response data from feeder loads to system disturbances and to gain experience with the monitoring device.

¹ Manufactured by Symantec, Cupertino, CA.

4.3.2 Location

The first (and the only one so far) load monitor was installed in IPC's Grove station. The location was chosen because it had a fast communication link, it was relatively close to the office, and its feeders represented a different mix of commercial and residential customers.

4.3.3 Description of Monitoring Equipment

The "load monitor" was assembled by IPC staff with components purchased separately from a company by the name "Chassis Plans", outside of San Diego, CA. The load monitor is basically a PC mounted inside a special chassis with an alternate power supply for the station 48Vdc source, an A/D card and a timing card (by Symmetricom) used for providing synchronized timing with the rest of the WAMS system. This particular unit is set for ½ msec sampling cycle and a record length of ~ 5 minutes. All three-phase currents and voltages for three different feeders are continuously monitored and recorded by this equipment.

4.3.4 Communication

Communication is via a broadband internet connection. File management, archiving and retrieval are done through PC Anywhere, while the triggering and PC to A/D control are implemented with LabView (original routines provided by BPA).

4.3.5 Cost

The load monitor is basically a refurbished PC, with the following additional parts (most of the components listed below were obtained from www.chassis-plans.com):

- Chassis ~ \$300 (by Chassis Plan)
- Alternate power supply for substation 48VDC Source ~ \$200
- A/D card ~ \$750
- Timing card (for GPS) by Symmetricom ~ \$1500 (presently not used for synchronizing monitor with other similar devices, but to obtain a more stable sampling rate).
- Clamp type CTs ~\$60 each
- Signal conditioning module (used to reduce PT and CT signal levels to fit the A/D card)
- Terminal Block (for conditioning module)
- Cable (from terminal block to PC) ~ \$200
- Total: ~\$3,000.

4.3.6 Use of the Data

Presently the data is not being collected. Remote access has been lost and no information on the status of the device is available. IPC plans to bring it in for inspection as soon as time becomes available. It is expected that in the near future it would be used for load model validation work.

4.4 Load Monitoring at PSE

4.4.1 Objective

The objective of load monitoring at PSE is to collect load data for validating dynamic and steady state load modeling in the Puget Sound area.

4.4.2 Location

Monitoring devices have been installed at several locations across the Puget Sound region, monitoring primarily 115-kV lines and several 230-kV lines covering a variety of customer classes.

4.4.3 Description of Monitoring Equipment

The monitoring device is AMETEK's DFR model TR2000 with disturbance monitoring capability of two samples/cycle for up to 5 minutes.

4.4.4 Communication

Two units currently can be poled from a central office with the remaining units to be connected by the end of 2007.

4.4.5 Cost

Units have been installed in association with substation control house upgrades at the request of the protection group. The estimated installed cost is approximately \$100K.

4.4.6 Use of the Data

Event recording (phasor data) is used by protection engineers. Disturbance recording (RMS data) will be used for initial and on going load modeling and validation purposes.

4.5 Feeder Load Monitoring at PG&E

Feeder load monitoring at PG&E is undergoing fundamental changes. An Automated Meter Initiative (AMI) at PG&E resulted in the selection of a vendor (DSI) and PG&E has begun installing automated meters that are read by power line carriers from a modem installed at the feeder substation. Domestic customer meters will be read hourly; meters for large energy users will be read every 15 minutes. The data collected by AMI will fundamentally alter many engineering programs now in place at PG&E, resulting in improved load flow studies (for planning and for distribution management system (DMS) – PG&E's distribution management system for distribution operations), and for transformer load monitoring.

4.5.1 Objective

In the future, customers will be able to monitor their daily energy usage (collected via AMI) over the Web.

In the near term, hourly usage data, combined with meter-transformer connectivity, means transformer-load-profiles can be generated in near real-time for transformer load monitoring. This will fundamentally change the transformer loading program at PG&E, which currently relies on average daily usage collected from monthly reads to estimate peak demand on the transformer. (While individual customer's power factor and harmonics will still be unknowns, these parameters are less variable than hourly usage.)

Transformer load profiles at the transformer level will also provide the P,Q (watt and Var) inputs to the DMS and other planning programs. DMS applications include calculation of line and equipment loading, and analysis of normal and emergency switching analysis. Other planning programs at PG&E that require

load data are ASPEN DistriView – used by PG&E planners for setting distributed generation relays, for fault analysis, and for phasing studies.

4.5.2 Locations

While AMI addresses energy usage at the customer's panel, other load parameters still require load monitoring. The power quality group at PG&E is addressing current and voltage harmonics, power factor, displacement power factor, surge amps, etc. at individual customers with power monitors (from PMI) placed at the customer's panel.

Many PG&E customers are considering installing solar panels or have installed solar panels. Consumer products for measuring instantaneous watts, current and voltage are now available (i.e., the “kill-a-watt” monitor available in some consumer catalogues for less than \$35) -- to help acquaint customers with the load demands of individual appliances. For off-grid applications, solar installers size the number of panels and batteries based on daily demand (appliances and usage rate) and will provide customers with suggested alternatives – e.g., energy efficient, and highly insulated refrigerators – to reduce size and cost of the solar installation. The “kill-a-watt” monitor can tell the customer how much energy the appliance uses, and whether that appliance might be an inappropriate load for an off-grid solar system.

Increased awareness of energy costs by consumers, together with more stringent energy standards for appliances -- has affected feeder demand and feeder power factor. PG&E has found that the power factor on feeders has risen (improved) over the last 15 years.

In 2004, PG&E redid its power factor study for domestic customers. To get an initial sense of what the power factor range might be on a domestic residence, a PG&E engineer took a power quality meter home, and attached it to his house panel. To his utter surprise, the meter indicated a “leading” power factor. Stunned by this observation, the meter was placed on individual home appliances, until the source of the leading power factor was found. The source of the leading power factor turned out to be the compact fluorescent bulbs (CFBs) that the engineer had installed throughout the house when he first moved in.

Another “load” surprise was when the engineer placed a “kill-a-watt” meter on the home's energy efficient refrigerator. Measured running amps were around 1 amp, instantaneous watts were around 115, and power factor was a remarkable .95. (During the defrost cycle, usage spiked to around 400 Watts. Two-day kWh usage at an average room temperature of approximately 64°F was 1.62 kWh. This included one defrost cycle. Nevertheless, the refrigerator's power factor was higher than the engineer anticipated, and the refrigerator's daily usage was far less than the engineer expected.)

The efficiency of home lighting continues to improve. Consumer awareness of the benefits of replacing incandescent bulbs with compact fluorescent bulbs (CFBs) continues to grow. (Improved LED bulbs may make home lighting a once a decade or more purchase in the future.)

The rising efficiency and power factor of major appliances such as refrigerators is believed to be one of the factors behind the improvement in power factor PG&E has seen on its distribution system.

Considering the recent success governmental efforts have had on energy use and energy efficiency, national laboratories should continue to focus on the nature (harmonics, power factor), demand (kW) and daily usage (kWh/day) of lighting and appliances with the aim of improving all of these factors in the future.

In particular, the replacement of compression a/c with evaporative coolers (swamp coolers) in areas with dry climates – such as Arizona, Nevada and California should be researched by the government together

with appliance manufacturers, with the aim of providing home owners with a less energy intensive means of space cooling.

4.5.3 Description of Monitoring Equipment

PG&E has an extensive SCADA system, with data accessed by radio, microwave, and telephone. Consolidation of multiple frequencies and standardization of equipment is on-going.

AMI is the power line for electric meters; gas meters are wireless.

For power quality, PG&E has purchased two Eagle 120 meters from PMI (Power Monitors, Inc.) for single-phase monitoring. These monitors plug directly into 120-V wall receptacles and have the option of connecting a single-phase load to it. A typical use would be at a residential customer facility. For detail information, please see <http://www.powermonitors.com/products/eagle120.htm>

All of PG&E's power quality monitors are portable as opposed to permanent installations. This is because they are used for three-phase commercial/industrial customer site investigations. The majority of the monitors are reliable power meters (RPM), now part of Fluke Corporation. The RPMs have a sampling rate of 128 samples per cycle per channel and are capable of recording voltage, current, harmonics, transients, waveform capture, and power consumption. The intended use is primarily to investigate voltage problems, i.e., sags, spikes, and power outages (momentary and sustained). For detail information, please see [http://us.fluke.com/usen/products/PMPwrRcdr.htm?catalog_name=FlukeUnitedStates&Category=PQTTOP\(FlukeProducts\)](http://us.fluke.com/usen/products/PMPwrRcdr.htm?catalog_name=FlukeUnitedStates&Category=PQTTOP(FlukeProducts))

Commercial and industrial customers have the option of installing their own revenue-grade meter at the main service panel. This allows them to monitor their own distribution system and collect loading information. However, special facility charges apply. An example of a few vendors includes Power Monitor Limited (PML), Dranetz-BMI, Square-D, and GE.

4.5.4 Communication

Communication with the RPMs is accomplished through the use on an Ethernet cable between the monitor and laptop. Remote forms of communication include high-speed DSL, lease line, and wireless connections.

There is one communication system that PG&E has had some experience with in a past collaborative power quality project involving EPRI-PEAC and that is the PASS Signature System from Dranetz-BMI. For detail information, please see <http://www.dranetz-bmi.com/products/prod2.cfm?prodcats=5>.

4.5.5 Cost

The base cost of the RPM monitor is approximately \$10,000 and up to \$15,000 with accessories, i.e., 100A, 1000A, or 5000A current transformers. Repair costs are a flat rate of about \$1,200.

The cost of an Eagle 120 monitor from PMI, as mentioned above, is approximately \$2,000.

4.5.6 Use of the Data

The monitoring data provide insightful information to understand consumer load behavior and characteristics. The insight has helped to develop the composite load model structure, and some of the findings have been applied in the development of load composition.

4.5.7 Other Issues affecting Consumer Loads

The California Solar Initiative provides incentives for residential customers to install solar panels. Besides increasing photovoltaic (PV) (“green”) generation, the California Solar Initiative may have other significant and beneficial consequences:

1. Grid connected solar systems in general, and off-grid solar systems in particular, require a “high-efficiency approach” to energy consumption. This approach often will mean that inefficient appliances must be replaced. As the demand for more efficient lights and appliances grows, the cost for improved energy efficient devices should diminish, benefiting all consumers.
2. Education: PV systems are very visible. As more and more consumers install PV, education about PV generation and home energy consumption should increase, improving consumer’s knowledge about the benefits of PV and home energy efficiency.
3. Energy independence: PV systems provide consumers with a measure of energy independence, and may displace the combustion of fossil fuels.

4.6 Load Modeling Based on Monitored System Disturbance Data

4.6.1 Motivation

The motivation for improved modeling of load is clear, based on the discussion in the previous sections . However, to truly assess the efficacy of new and more sophisticated load models being developed through the WECC efforts, one needs to be able to compare the simulated performance of these models to actual recorded system response. Even more beneficial is the ability to use recorded system behavior to directly derive parameters for the various load model structures being developed through the WECC efforts. This has multiple benefits:

- It assesses the adequacy of the composite load model structure.
- It helps to identify potential limitation in load models and helps to fine tune and improve load models.
- It provides a direct means of estimating load model parameters for “aggregated” load models without the need for guess work.

For these reasons, the ability to systematically deploy monitoring equipment (or utilize existing monitoring equipment such as DFRs and power quality meters) to record the behavior of system loads during system disturbance is an extremely beneficial exercise. It is also important to establish a range of realistic parameters for “aggregated” load behavior on the power system for various seasons, regions, types of load, etc.

4.6.2 Locations

To assess the “aggregated” behavior of system loads, the most effective place to deploy monitoring equipment is at the distribution substations that are considered representative of commercial, industrial, and residential loads. A typical monitoring installation would involve installing data acquisitions systems

on the low-voltage side of a distribution transformer. The need is to monitor the three-phase voltage and three-phase current on the low-voltage side of the distribution transformer at a sampling rate of at least several hundred samples to a few thousand samples per second. Typical sampling rates of commercially available devices are 7680, 5760, 2880, 1920, and 1440 samples/second. These sampling rates can be considered adequate to capture time-domain data. Also, to capture slow voltage recovery events, the recorded length of the data during and following a system event should be large enough for the time scale of interest – typically around 30 seconds.

The need for high sampling frequency is to fully capture the system dynamic response (down to sub-cycle phenomena) and to be able to perform various signal processing and parameter fitting exercises with the collected data (e.g., high sampling rates help numerical stability while solving machine differential equations for parameter optimization). Typical power quality meters, as deployed by utilities, can be effectively used for this purpose. Presently EPRI is engaged in this type of work with many Eastern Interconnection utilities.

Ideally, one would want to monitor several locations throughout the system, which represent the diversity of loads in the utility. For example, a few residential feeders, a few commercial feeders, one or two typical industrial feeders of different load types (heavy industry, agricultural industry, light manufacturing, etc.). In this way data can be collected on a variety of load types. In addition, patience is needed because the load monitoring effort may have to continue for several months to capture sufficiently good measurement data for deriving load model parameters, as well as sufficient variety in load composition for capturing parameter sensitivity. That is, to account for regional, seasonal and daily variations in load composition. In the work that EPRI has been doing over the past couple of years, it has been found that the most fruitful data is that recorded during severe and relatively balanced voltage dips – e.g., as caused by a three-phase fault in the transmission system. This is clearly a rare event and at times data have been collected for months before such an event could be captured.

Often the tendency could be to use existing monitors in the system without having to purchase and install a new device for collecting data. In these cases, existing data acquisitions systems (power quality meters, digital fault recorders and other recording equipment) may exist already and may be used to serve the required purpose. A detailed study to assess the applicability of commercially available monitoring systems for load modeling purposes was performed as a part of EPRI’s Power System Load Modeling (PSLM) Phase #1 collaborative R&D effort. Some of the key findings of that study are summarized in the next section. For detailed information, please refer to the EPRI report “Measurement Based Load Modeling” (EPRI 2006).

4.6.3 Description of Monitoring Equipment

Common types of monitoring equipment that can be used for acquiring load modeling data include: power quality monitors, digital fault recorders (portable as well as permanently installed), and digital relays. These devices are commonly referred as intelligent electronics devices (IEDs). There are a large number of commercially available IEDs that are already deployed by numerous utilities for monitoring power system data. However, significant differences exist in the way individual IEDs are configured to capture natural system disturbance data. To capture natural system disturbances using commercially available IEDs and make sure the available data is suitable for load modeling, the requirements and guidelines of load monitoring functions should be defined. As part of a study, EPRI developed a performance matrix such that measurement data from these devices can be used in load modeling development and validation. Main performance indicators to look for in an IED are shown in Table 3.

Table 3 Performance Matrix for Commercially Available IEDs

Performance Criteria	Description
Type of data acquired	Should be capable of acquiring time domain data
Number of input analog channels	6/9/12/15 At least six channels (three for phase voltages and three for phase currents to monitor one feeder). The more the better ,especially if one desires to record individual feeder currents as well as the total substation current
Number of input digital channels	Optional, not needed most of the time
Sampling rate	Should have at least 960 samples/second/channel, Many IEDs especially DFRs have adjustable sampling rates
Trigger	Programmable triggers (voltage and current), user should be able to set trigger and reset thresholds
Pre-fault and post-fault recording time	It is necessary to capture a few cycles of pre-fault data to obtain steady state conditions before the fault. Post-fault recording duration is a function of reset threshold and maximum storage capability
Memory storage (RAM)	Ideally, the device should be able to store up to tens of seconds worth of data to capture slow voltage recovery events
Hardware requirements	Should have peripheral ports for networking, data transfer, user interface, etc.
Data format	Data could be stored in various data formats such as COMTRADE, comma separated, etc.

A list of commercially available IEDs that meet most of the performance criteria are shown in Figure 10.

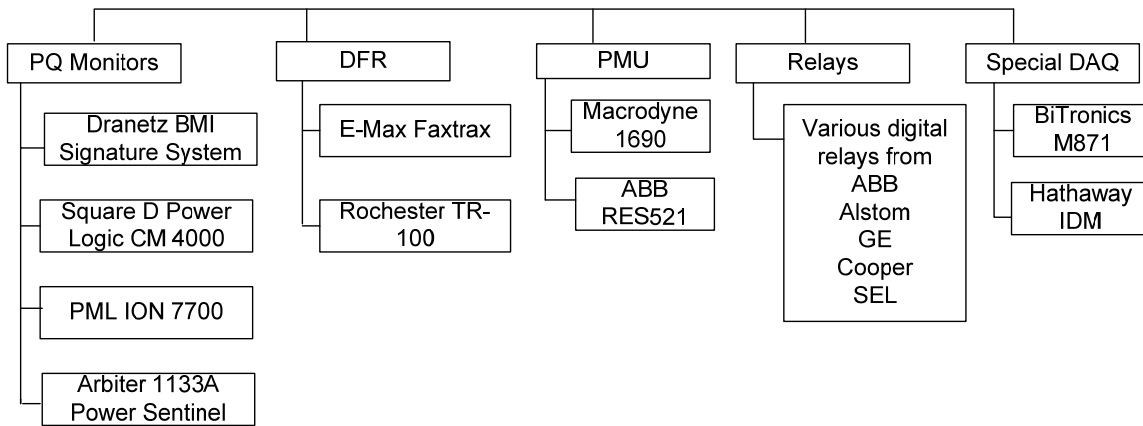


Figure 10 Commercially Available IEDs

Note that many power quality monitors can store only tens of cycles of data at sampling rates higher than 960 samples/second. If a power-quality (PQ) monitor does not have an adequate number of channels, more devices can be installed (which will increase the overall cost) for monitoring multiple feeders coming out of a substation. The PQ monitors mentioned in the table typically cost between \$5,000 to \$8,000. All of them have dial up and/or Ethernet ports, which enable remote data access.

All the digital fault recorders (DFRs) mentioned in Figure 10 are portable DFRs that do not need elaborate mounting cabinets. DFRs are more flexible than PQ monitors because they have adjustable sampling rates, more analog input channels, and bigger RAM to store longer disturbances. They also have dial up and Ethernet ports for remote data access. Portable DFRs typically cost between \$9,000 to \$11,000. One issue with DFRs is that protection engineers typically configure them for recording fault current and not load response. This specifically affects current measurements. Therefore, even though

there might be an existing DFR installed at a distribution substation, it may not record “suitable” data for load modeling purposes.

The EPRI load modeling team has not worked with either PMU or digital relay data. All the data being used for the various load-modeling projects is either from PQ monitors or DFRs. The primary reason for this is that PMUs are typically installed at major transmission substations, whereas for load-modeling purposes, data is required at the distribution level, where PQ monitors and DFRs are more prevalent. .

4.6.4 Cost

PQ devices capable of waveform data capture required for load modeling applications:

- PQ instrument costs: \$5,000 - \$12,000
- Other costs associated with installing permanent monitoring devices: Additional costs of 2 to 10 times the cost of the monitoring equipment can be incurred for the installation and maintenance of a permanent substation instrument. These costs vary depending on whether the substation has available PT/CT measurement points, whether the station has communications capability, etc. Potential installation cost components could include
 - Engineering and line crew labor
 - Instrument costs
 - Calibration and other maintenance costs
 - Purchase of ancillary equipments (CTs and PTs)
 - Provision of necessary communications in the substation

Example Costs:

Instrument Costs – \$10,000

Installation costs (available metering points and communications) - \$25,000

TOTAL = \$10,000+\$25,000 = \$35,000

- Installing portable monitoring devices: Additional costs of 1 to 1.5 times the cost of the monitoring equipment is typically incurred for new installation and maintenance of any portable instruments.

Example Costs:

TOTAL = \$10,000 + \$10,000 = \$20,000

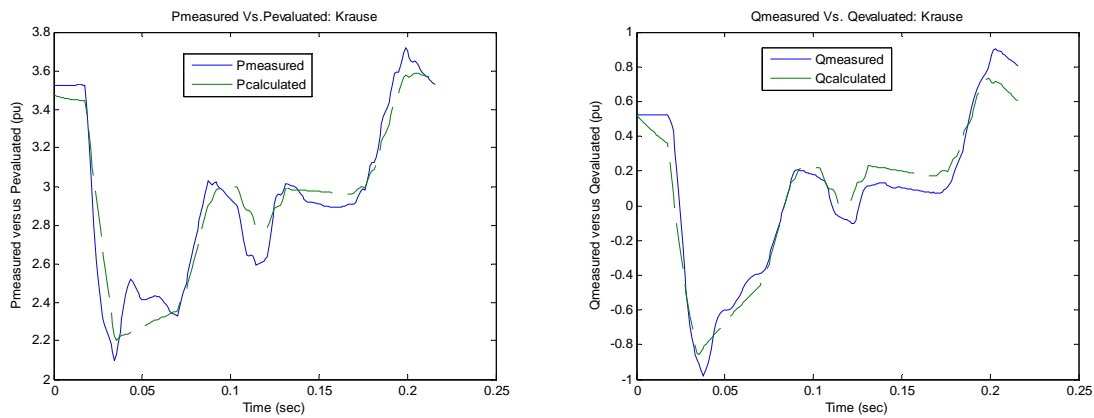
4.6.5 Use of the Data

The main use of the load monitoring data is to

- Estimate load composition (percentages for motor load versus other load types) and load model parameters (parameters for each type of load)
- Identify which parameters can be estimated reliably from available measurements
- Evaluate different parameter estimation techniques and load model structures
- Identify variations in load model parameters and composition over time (seasonally etc.) and for different types of loads in the system

In this way one can develop a pool of information on the behavior of various “aggregated” loads (residential, commercial and industrial) for different times of the year and day.

Presently, EPRI is engaged in a research project funded by several utilities in the Eastern Interconnection related to this type of work. The outcomes of that project can be leveraged to the Western System. EPRI’s load model structure is based on positive sequence representation of loads and uses balanced three-phase disturbance data. The positive sequence representation incorporates both static and dynamic characteristics of the loads. The parameters obtained can be easily incorporated in various load models in Siemens PSS/ETM and GE PSLFTM programs. As an example, Figure 11 shows a sample result from the work being done by EPRI to illustrate the use of load monitoring data for model validation. Figure 12 shows the model structure used in this case to derive estimated parameters for the model. The load model parameter estimation is done using an optimization algorithm developed in MATLAB®. EPRI is currently testing the algorithm using field events collected by various member utilities.



(The solid blue lines are positive sequence real and reactive powers of the feeder calculated using monitored three-phase feeder voltage and current. The dashed green lines are simulated results based on optimally estimated parameters.)

Figure 11 Example Parameter Estimation using an Optimization Algorithm to fit Load Model Parameters to a Specified “Aggregated” Load Model Structure.

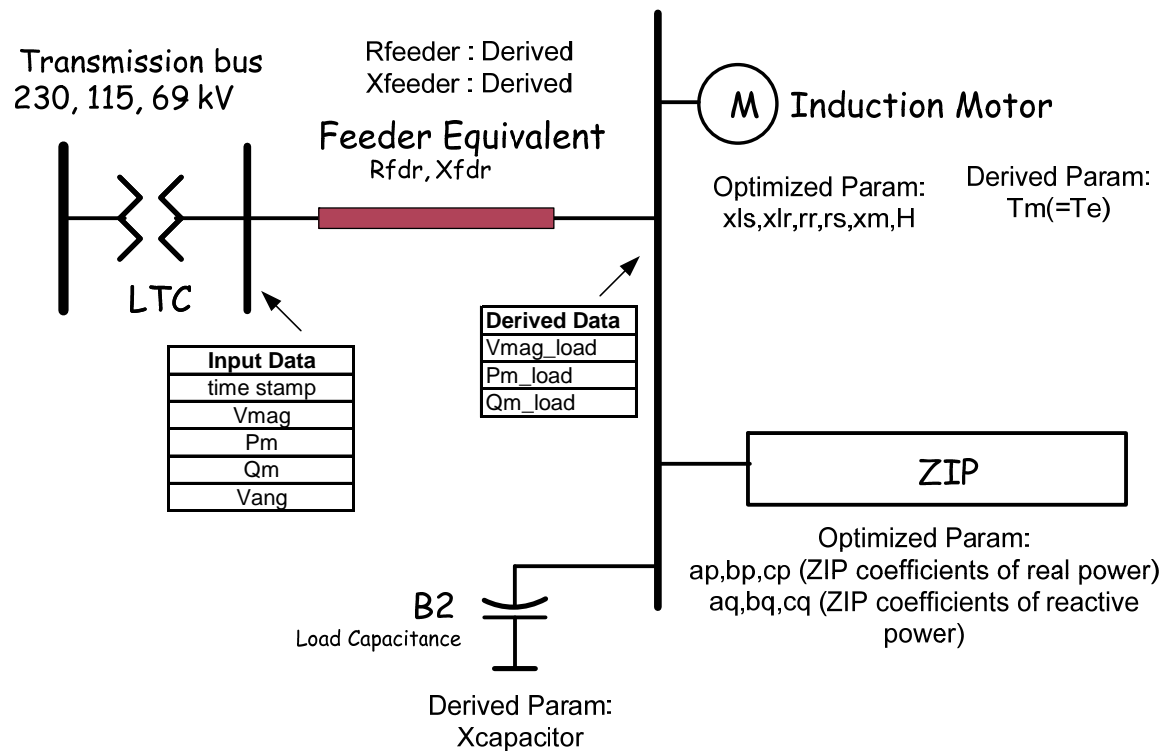


Figure 12 Load Model Structure used for Parameter Estimation.

4.6.6 Summary

Ideally, one would like to obtain a load model that would be accurate across a wide spectrum of system conditions. In reality this level of generality may be insurmountable as a result of the wide variation in load composition both geographically and hourly/daily/seasonally. In general, the results of any study should be evaluated to determine how much they can change if assumptions regarding load model structures or parameters change. Thus, a key requirement of load modeling for system studies is the ability to reasonably capture the variations in load model parameters for sensitivity analysis. Load monitoring (over wide geographical areas and various seasons of the year) and subsequent estimation of “aggregated” load model parameters is a key exercise in facilitating this approach.

4.7 Load Monitoring via Commercial or Residential Load Control Systems

4.7.1 Objective

Commercial and residential load monitors for demand response studies have been used by BPA and PNNL for data gathering for several years (see Figure 13). These load monitors use commercially available equipment to sense, record and control home devices. The monitoring data can be provided online in real time for utility and public use in stability studies, energy efficiency studies and demand response studies. The data are already available and only needs to be put online and additional sites could be added to cover various building types and climate zones.

- Where is the value?
 - If there were a market transformation effort or mandated inclusion of the under voltage and under frequency capabilities in appliances, it could give utilities “instant” spinning reserves and allow sale of what is now spinning reserve from thermal plants
- What issue could kill the value?
 - Autonomous response – could make system events worse depending on settings and where the devices are located
- How could this response be made to work?
 - Add 2 way communications, broadband is becoming ubiquitous, use a Zigbee gateway that talks to all home appliances Zigbee, and a programmable communicating thermostat (PCT) and with the Zigbee gateway using under voltage and under frequency capabilities – there is sensing, recording and control



Slide 5

Figure 13 Value Proposition of Load Monitoring via Load Control Systems

4.7.2 Location

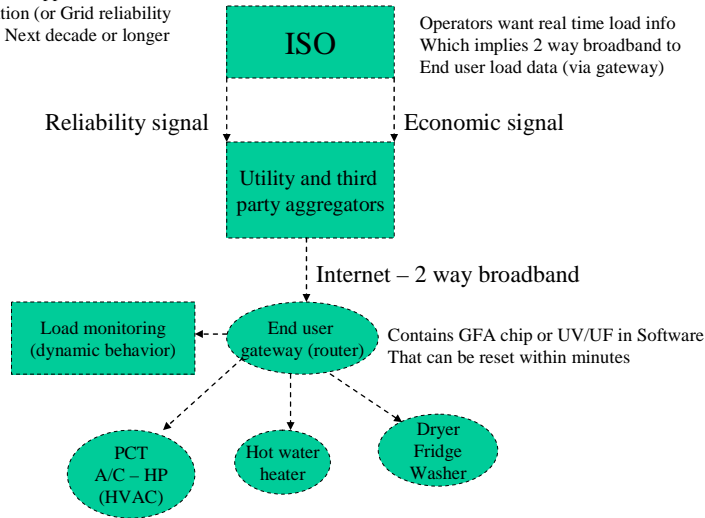
Demonstration locations have been Ashland (100 homes), Oregon and the Olympic Peninsula (150 homes) in Washington. Project descriptions are available at:

http://energypriorities.com/entries/2006/04/bpa_ashland_goodwatts.php
<http://electricdistribution.ctc.com/pdfs/ED06/Hammerstrom.pdf>

4.7.3 Description of Monitoring Equipment

Both commercial and residential monitoring systems used wireless communications to a gateway connected to broadband via Ethernet. Systems could gather down to 1 second data but used 1 minute increments for data gathering of voltage and current signals. Both systems could add frequency data for minimal cost and software tweaks. A potential architecture for use is shown in Figure 14.

Potential Architecture Appliance control via Market transformation (or Grid reliability standard of future) Next decade or longer



Slide 6

Figure 14 A potential data architecture for load monitoring

4.7.4 Communication

Communication is via a broadband internet connection. Data are collected in real time using an online data base (Oracle and SQL). No special data collection systems are needed over a broadband connection.

4.7.5 Cost

A residential data system costs about \$2,000 per home originally, but will soon be available for \$299. The installation cost of the thermostat is estimated at about \$150.

A unique source for commercial building data has already been used by the Load Composition Study group. The cost for using the data from existing sites would be a monthly service charge for data hosting, with no incremental hardware cost, except to add new sites where utilities want data.

4.7.6 Use of the Data

Data has been used for demand response and market analysis studies. Some examples of the studies are presented in Figure 15 and Figure 16. In Figure 15, the composition of various end uses is shown during a 24-hour period, as individual end uses are separately metered. Figure 16 gives the HVAC load in percentage of the total residential load, clearly showing the thermostat setback period at night and the high activity period in the late afternoon and early evening.

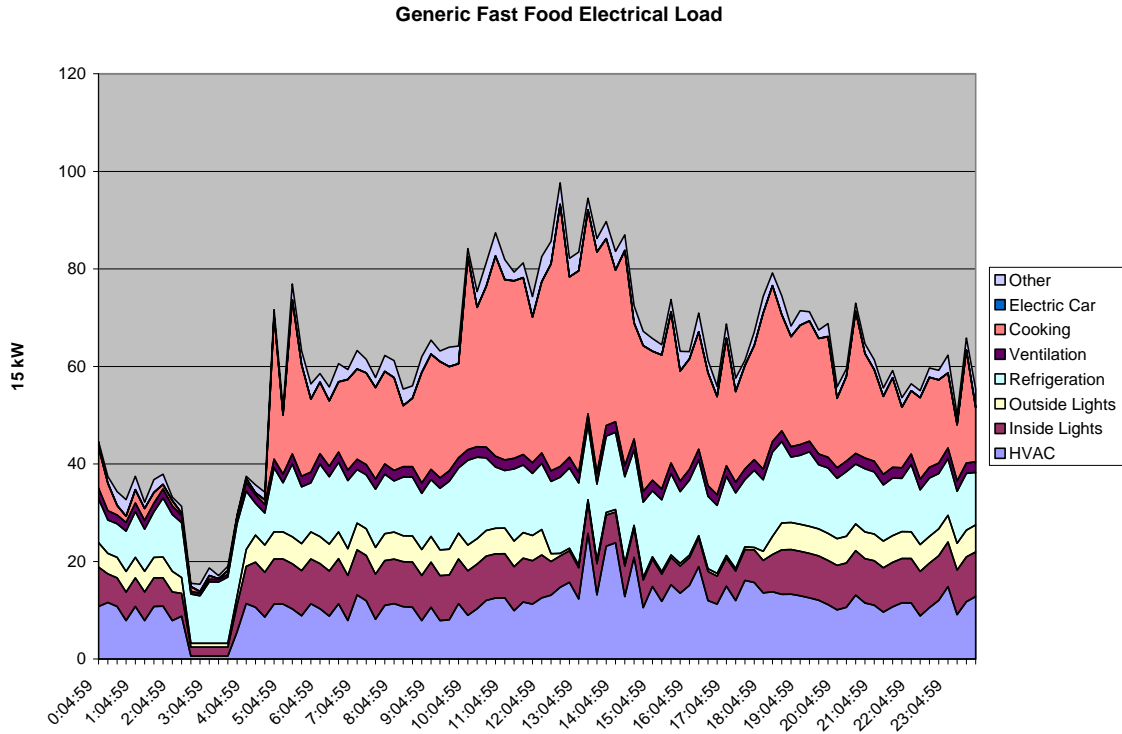


Figure 15 Demand Response and Market Analysis Studies of Commercial Load

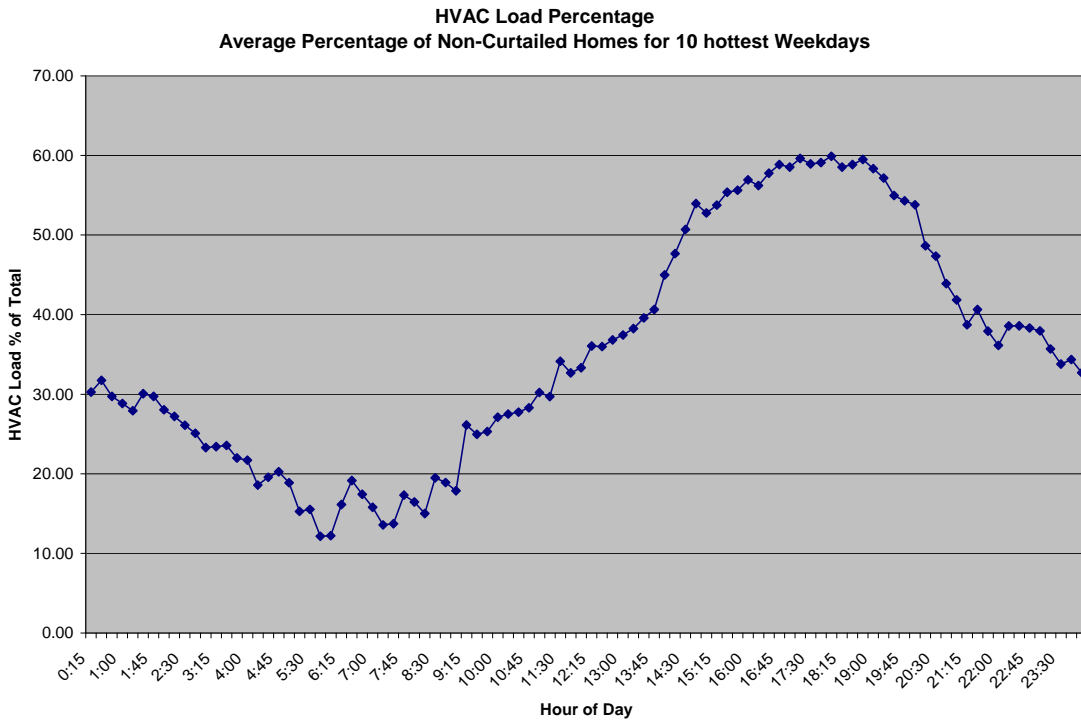


Figure 16 Demand Response and Market Analysis Studies of Residential Load

5.0 LOAD MONITORING APPLICATIONS

The purpose of load monitoring is to serve the needs for better load characterization and better load management, as stated in Section 2.0 Load Monitoring Needs. Load monitoring can find applications in many aspects, including:

- Load monitoring for top-down load composition
- Load monitoring for load composition validation
- Load monitoring for load model validation
- Load monitoring for uncertainty analysis
- Load monitoring for load control performance evaluation

5.1 Load Monitoring for Top-Down Load Composition

The term “top-down” is used in contrast to the “bottom-up” approach, which describes the previous building-simulation-based load composition model. The top-down load composition serves the purpose of estimating load mix and weighting factors that are needed in the bottom-up load composition model. As shown in Figure 17, assuming typical load profiles for individual building types are known, the top-down approach solves for the weighting factors from the total feeder load profile obtained from SCADA data.

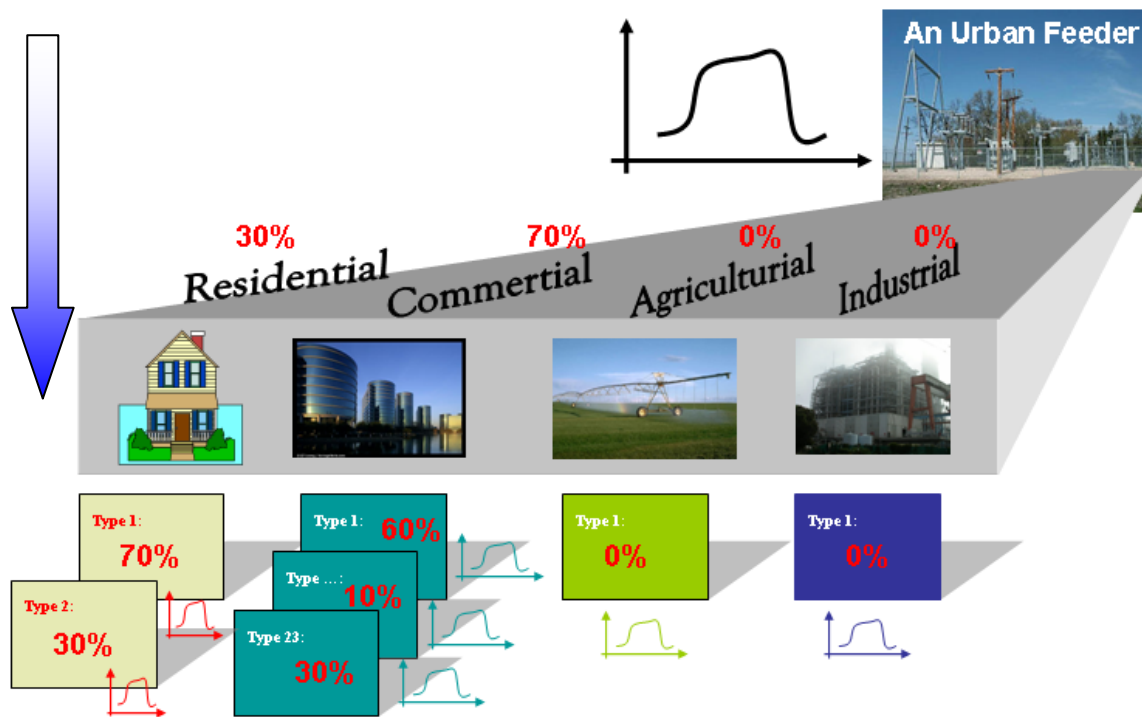


Figure 17 Illustration of the Top-Down Approach for Load Composition Analysis

Technically, the top-down approach employs curve decomposition techniques to separate the measured total load profile (LP_{total}) to the summation of weighted individual load profiles, as illustrated in Figure 18.

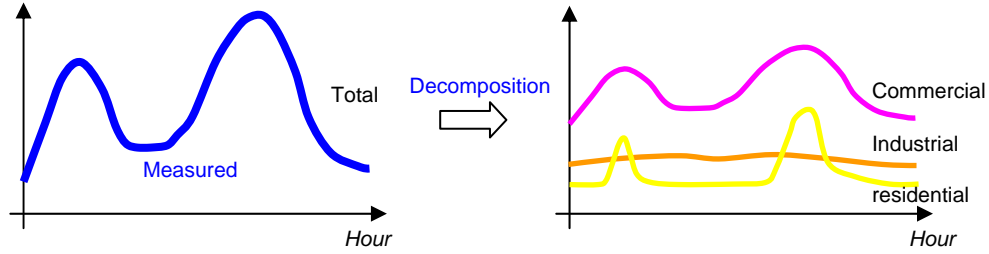


Figure 18 Curve Decomposition for Top-Down Load Composition Analysis

This decomposition can be performed at different levels, and the resulting weight factors represent different levels of load composition information.

$$\text{At the load mix level: } LP_{total} = W_{comm} LP_{comm} + W_{res} LP_{res} + W_{ind} LP_{ind}$$

where LP_{comm} , LP_{res} , LP_{ind} are load profiles of commercial loads, residential loads, and industrial loads, and W_{comm} , W_{res} , W_{ind} are the percentages (load mix) of commercial loads, residential loads, and industrial loads.

$$\text{At the building level: } LP_{total} = W_{School} LP_{School} + W_{Mall} LP_{Mall} + W_{Warehouse} LP_{Warehouse} + \dots$$

where LP_{School} , LP_{Mall} , $LP_{Warehouse}$ are load profiles of schools, shopping malls, and warehouses, and W_{School} , W_{Mall} , $W_{Warehouse}$ are the percentages of schools, shopping malls, and warehouses.

Load monitoring data for this purpose need to capture the basic load shapes for a time period of interest. For 24-hour load profile decomposition, hourly data from SCADA systems would be sufficient.

Preliminary research has been carried out at Pacific Northwest National Laboratory to demonstrate the effectiveness of the approach. Two algorithms have been tested: constrained least square and constrained optimization. Stochastic simulation technique is also employed to provide an estimation of the weighting factors on a statistical basis. To evaluate the top-down approach, virtual feeders are built upon simulation data, as shown in Figure 19. In a virtual feeder, loads are synthesized with known individual load profiles. Given a set of weighting factors, the total feeder load profile can be calculated. Then the top-down decomposition approach is applied to the total load profile with the known individual load profiles to derive the weighting factors. The effectiveness of the top-down is determined by comparing the derived weighting factors and the given weighting factors. Example results on the decomposition of the virtual feeder load profile are given in Figure 20. The constrained least square algorithm can estimate load composition pretty well for cooling load (“cool”), equipment load (“equip”), auxiliary load (“aux”), and lighting load (“light”), as can the constrained optimization. The constrained optimization algorithm can also reasonably estimate the load composition of other load types.

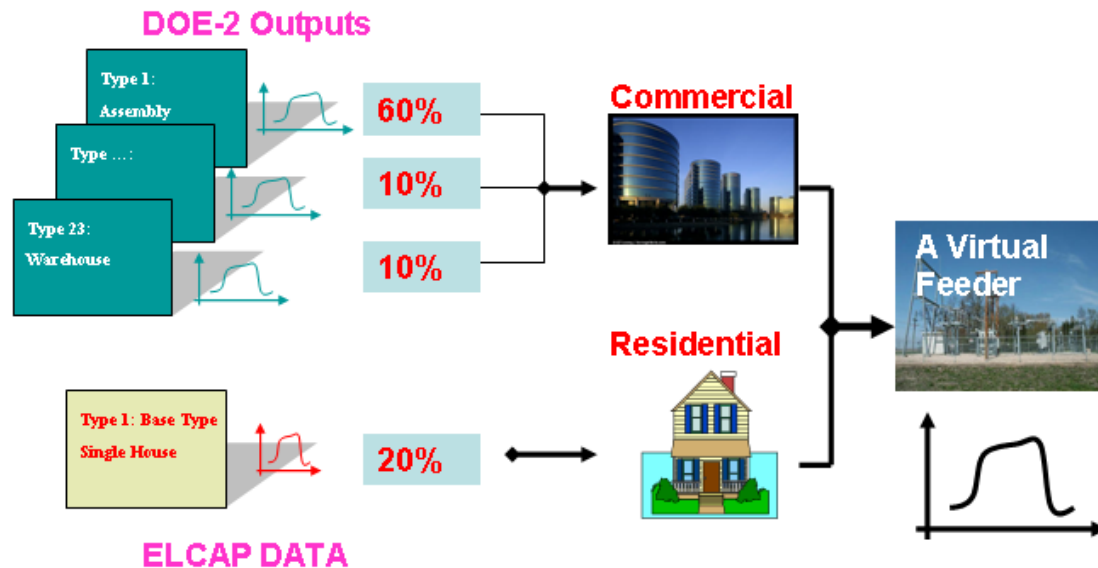


Figure 19 The Setup of a Virtual Feeder

5.2 Load Monitoring for Load Composition Validation

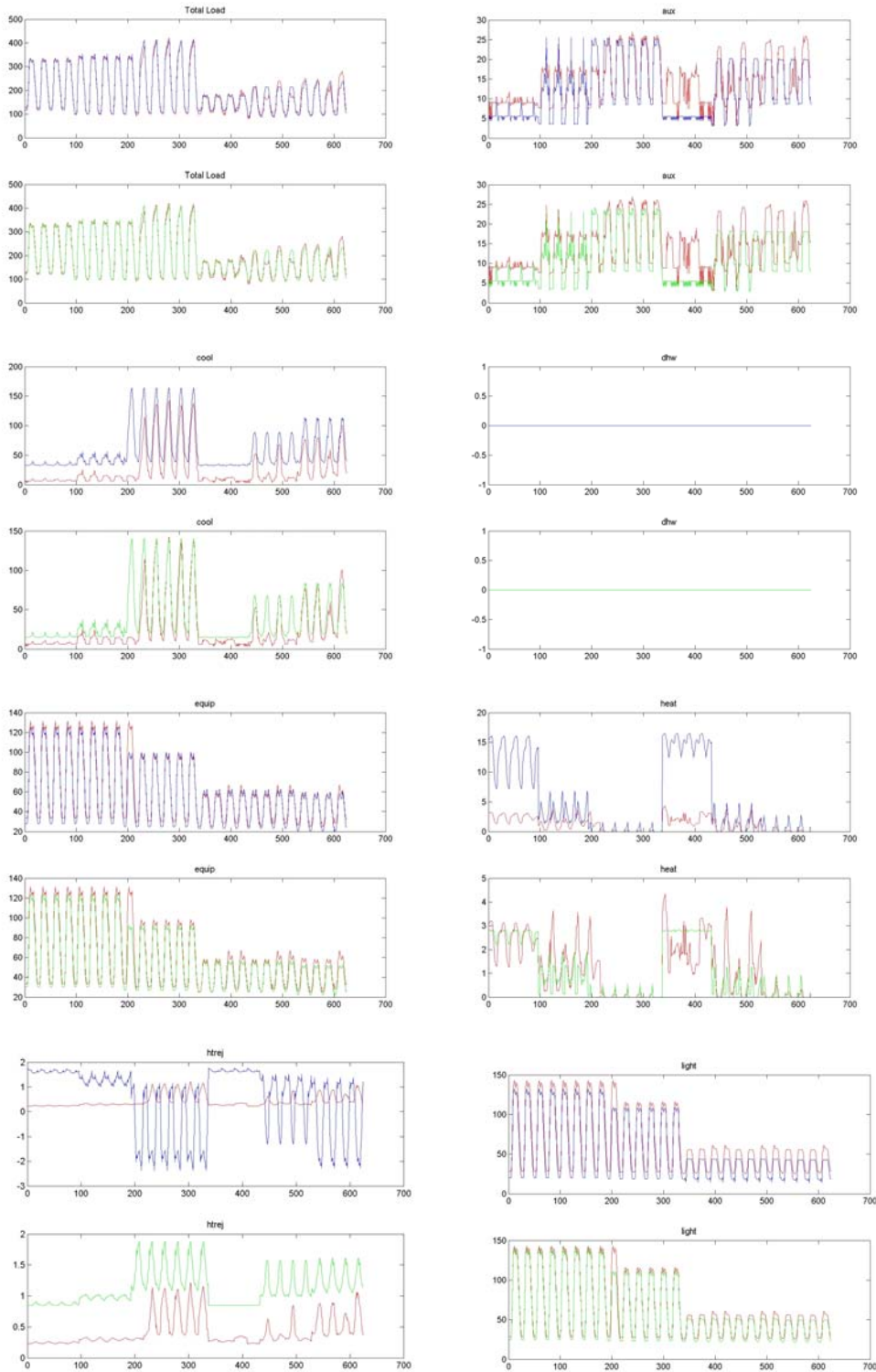
Load profiles generated by the load composition model can be compared with load profiles derived from load monitoring data, e.g., historical SCADA data or building monitoring data. If the load composition model captures the right load characteristics, the load profiles should match SCADA data. Otherwise any mismatch can be used to calibrate the load composition model, e.g., tune load mix and adjust weights. The calibration methodology has yet to be developed.

Load monitoring data for load composition can be of low resolution (e.g., hourly) but of long record, e.g., SCADA.

As an example, Portland feeder data have been used to validate the implementation of the top-down approach. Because the measurement data for typical commercial buildings are not available at this stage, DOE-2 simulation data are used to generate the typical load profiles for 23 building types. Assumptions include:

- The building weighting factors are time invariant.
- Typical load profiles are TYPICAL.
- No agricultural load in the feeder.
- No industrial load in the feeder.

DOE-2 is an industry standard tool for commercial building energy use and cost analysis. With input of building layout, construction types, space usage, conditioning systems (lighting; heating, ventilation and air conditioning (HVAC), etc.), and weather data, DOE-2 performs hourly simulation of building energy use and produces yearly building load profiles. From the yearly profile, daily load profiles were derived for three seasons: summer, winter, and spring, which are considered typical. Figure 21 gives the three-season typical load profiles for sit-down restaurants.



(The red curves are the true load profiles. The blue ones are results obtained using constrained least square. The green ones are results obtained using constrained optimization. The X-axis is time by hour; the Y axis is power consumption by kWh.)

Figure 20 Example Results of the Top-Down Approach for Load Composition Analysis

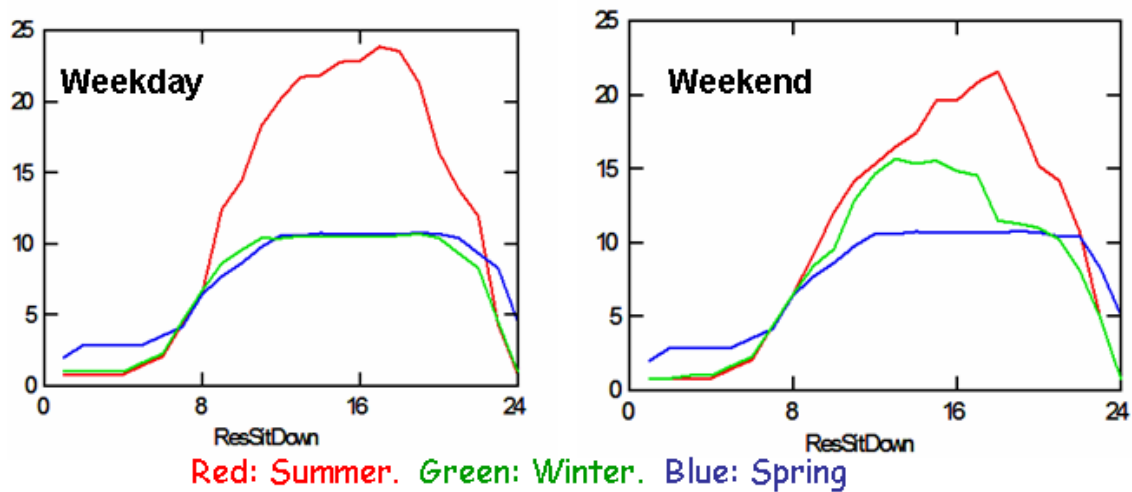


Figure 21 Example Typical Load Profiles for Sit-Down Restaurants.

For residential load, data collected by Bonneville Power Administration (BPA) and PNNL in End-use Load and Customer Assessment Program (ELCAP) are used to generate typical daily residential load profiles for two seasons: summer and winter, as shown in Figure 22.

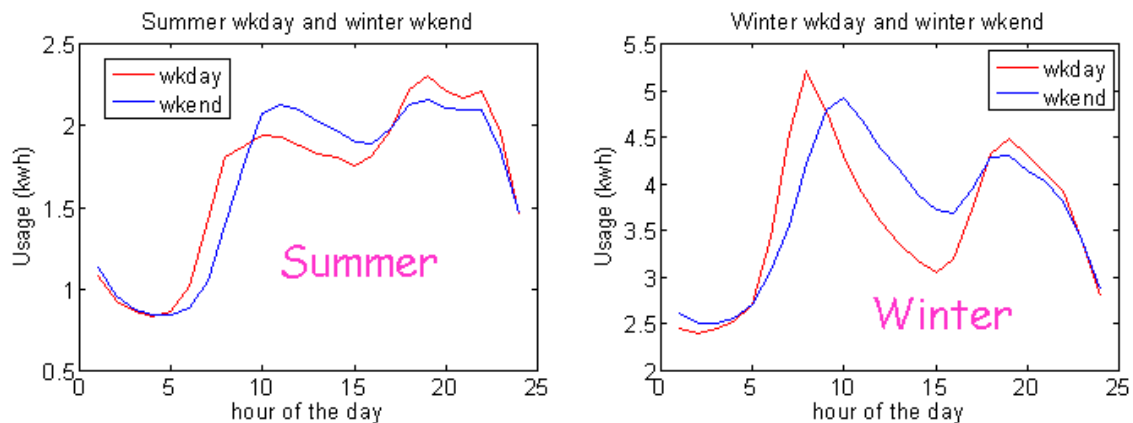
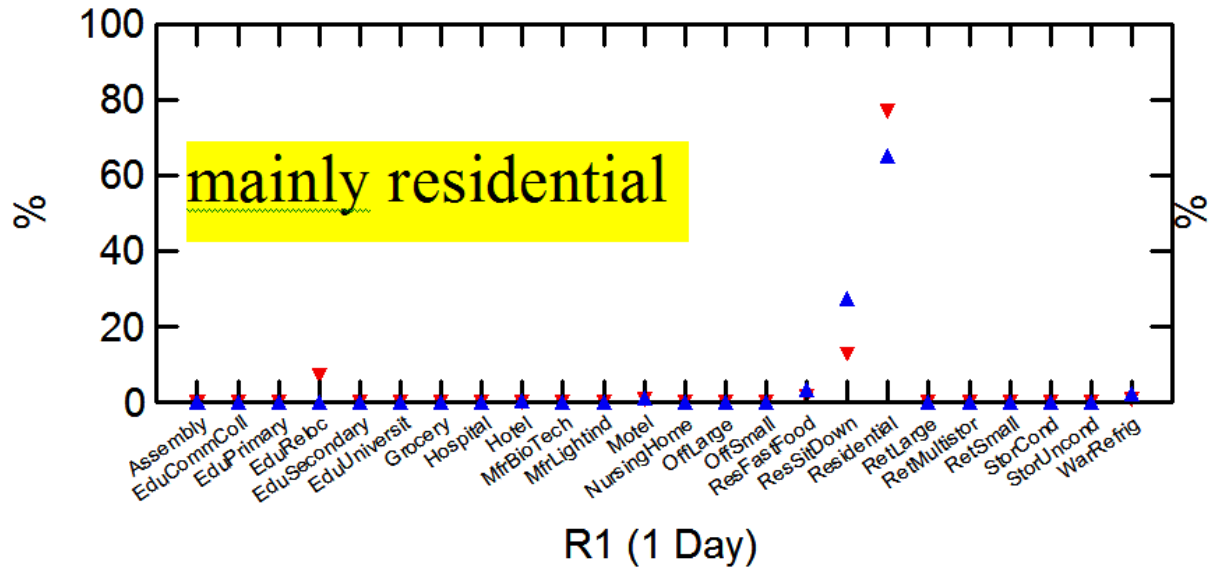


Figure 22 Summer and Winter Typical Load Profiles for Residential Loads.

The developed decomposition algorithm was applied to SCADA data collected for several feeders in Portland area provided by BPA. These feeders are known to supply mixed commercial and residential loads, however the exact mix percentages are unknown. Therefore, the results are not rigorously comparable. It is hoped that by carrying out this preliminary research on the top-down method, a technique that combines the bottom-up and top-down approaches will eventually provide a convenient way to estimate the load composition of distribution feeders. For that purpose, the results are satisfactory. As shown in Figure 23, estimated load composition results are close to that obtained based on the billing information. This example also indicates the validity of the use of load monitoring data for load composition validation purposes.



(Blue and red symbols show load composition percentage obtained by two different decomposition methods as aforementioned. The yellow symbols show the known load composition.)

Figure 23 Example Result of Load Composition Validation for a Portland Feeder Supplying Mainly Residential Loads and Some Small Commercial Loads.

Because measurement data are not available to remove the bias of the DOE-2 modeling results, there exists mismatch between simulation and actual energy consumption. The results are expected to be more accurate once some survey data or field measurement data is obtained to tune the simulation results.

5.3 Load Monitoring for Load Model Validation

General approach of model validation is to compare model simulation against measurements, as having been applied to WECC generator model validation. Load monitoring provides the basis for load model validation.

However, load model validation is far more challenging than generator model validation because of extensive uncertainties and variations of loads. Load models shown in Figure 2 are the aggregated behavior of hundreds of thousands individual load components. It does not make much sense to perfectly match the aggregate model behavior to a specific recording. It is almost certain that the variations and uncertainties would make the load model not match the next recording.

Therefore, load model validation should not focus on how close the curves would match, but should focus on principal load behaviors to match the impact of loads on system studies. If the load model would produce the right high-level system behaviors, it could be concluded that the load model matches the actual load characteristics in principle.

This “in principle” load model validation can be done in two ways: time-domain load model validation and frequency-domain load model validation. Time-domain load model validation compares the time

series curves of simulated system level behavior and recorded monitoring data, while frequency-domain validation compares the frequency/damping contents of the simulation results and actual measurements.

Load monitoring data for this model validation purpose should have enough resolution and time length for capturing system dynamic behaviors. Examples of data sources include phasor measurements (WAMS), PPSM data, and potentially, measurements from the low-cost monitor device DMWG is developing.

5.4 Load Monitoring for Uncertainty Analysis

Statistical analysis can be performed on load monitoring data to quantify load variations over selected time periods. Load monitoring data needed for uncertainty analysis can be low resolution data like SCADA measurements or high resolution data like phasor measurements. Load uncertainty analysis is an ongoing effort under the CEC/LMTF Load Research Program. Further results will be reported once the work is done.

5.5 Load Monitoring for Load Control Performance Evaluation

It is the trend that loads will play a more and more active role in managing the power system. At the individual end-use level, SCE is developing solutions for prolonged voltage recovery as a result of a/c stalling. At a larger scale, active load control has been studied for the purposes of spinning reserves, damping improvement, frequency and power flow regulation, etc. Similar to generator performance monitoring, there is a need to ensure the load behaves as designed for correct credits and control enforcement.

Load monitoring data for load control performance evaluation range in a wide spectrum, depending on the control objective. High resolution data like phasor measurements are needed for evaluating load performance for damping improvement. Lower resolution data of long records are needed for evaluating load performance for spinning reserves, frequency and power flow regulation.

To demonstrate load monitoring applications for load control, the following examples are extracted from the results of the Grid Friendly™ Appliance Project (Hammerstrom *et al.* 2007).

The Grid Friendly Appliance Project was undertaken to demonstrate the performance of the Grid Friendly appliance controller developed at PNNL. The controller was applied to 150 Sears Kenmore residential clothes dryers manufactured by Whirlpool Corporation and 50 water heaters. It was configured to perform autonomous under-frequency load shedding. The under-frequency threshold was set quite high to observe many such events during the project. Consistent with PNNL's Grid-Friendly approach for load control, the permitted load curtailments were performed in ways that did not appreciably inconvenience the appliance owners. Indeed, 358 such events were recorded during the project year, and few appliance owners reported observing or being inconvenienced by the reactions of their appliances.

In this case, the appliance controllers and appliances were observed by communication modules placed at each appliance. There remains lively debate concerning how much, if any, communication is needed to and from such autonomous grid-responsive controllers. There will be inherent costs associated with such communications. Regardless, the communications were useful for the experimental observation of these controllers after they had been positioned in residences in three regions in Washington and Oregon. Examples of a single dryer response and the aggregate appliance response to an under-frequency event

are presented below. The sample size was not large enough, of course, to observe its effect on correcting grid frequency or deferring the actuation of spinning reserve.

Figure 24 shows the response of a single project dryer during an under-frequency event. The dryer was shown to cycle its heating element on and off with a regular pattern as it maintained its constant drum temperature prior to the event. At the onset of the under-frequency event, the dryer heating element load was shed and remained off throughout the event's 3-minute duration. Thereafter, the heating element turned on until the drum returned to its prescribed temperature and resumed its normal operations and duty cycle.

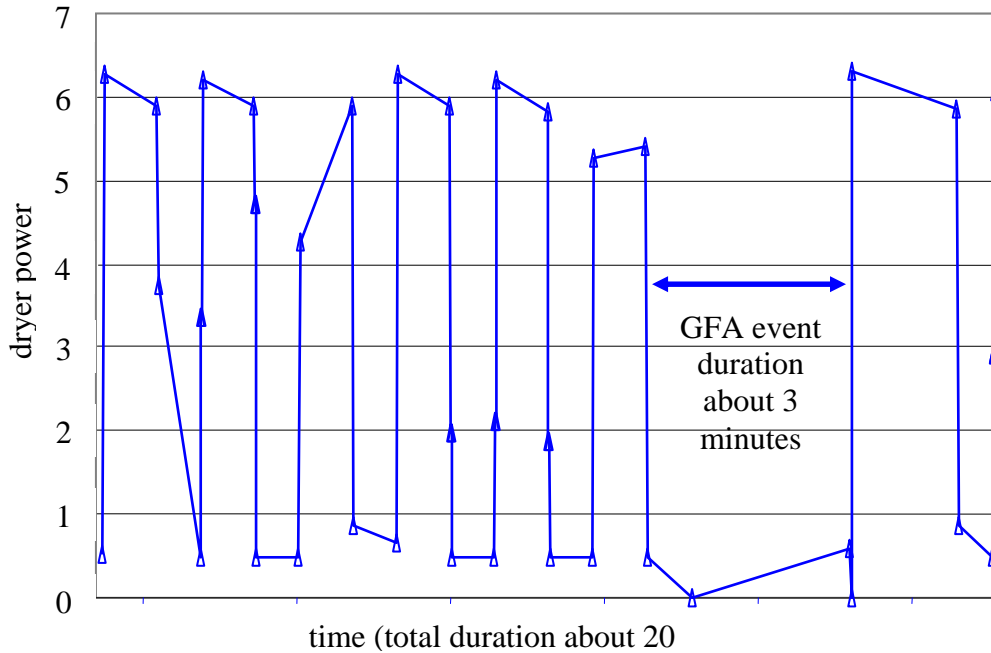


Figure 24 Example Data Logged from Active Project Dryer during an Under-Frequency Event

Figure 25 demonstrates the aggregate response of the controllers at almost 200 appliances. Each appliance replied with an acknowledgement for any under-frequency event that it observed. Each shown point represents one of the 358 events, minimum frequency observed during the event, and the percent fraction of available appliances that recognized the event. Virtually all controllers responded to any under-frequency event that was more than 0.003 Hz below the frequency threshold as measured at PNNL.

6.0 LOAD MONITORING RECOMMENDATIONS

Load monitoring site selection and equipment selection are highly dependent on application purposes. Section 5.0 Load Monitoring Applications summarized five applications of load monitoring:

- Load monitoring for top-down load composition
- Load monitoring for load composition validation
- Load monitoring for load model validation
- Load monitoring for uncertainty analysis
- Load monitoring for load control performance evaluation

The first four of them are focused on load characterization and model development, which is well aligned with current WECC/CEC efforts in the load research area. The last one on load control is case-specific, i.e., load monitoring will reside where the load control is implemented. Its site selection and monitoring requirements are relatively straightforward to determine. Therefore, the following recommendations will mainly focus on the first four applications. Future WECC load monitoring plans should leverage existing load monitoring facilities as much as possible.

6.1 Site Selection

Given the diversity and variety of loads in the WECC, load monitoring needs to cover major load centers and also consider different climate zones and load types. 11 WECC load monitoring locations are identified as:

- Boise, ID
- Boulder, CO
- Calgary, AB
- Cheyenne, WY
- Los Angeles, CA
- Phoenix, AZ
- Portland, OR
- Sacramento, CA
- Salt Lake, UT
- San Francisco, CA
- Vancouver, BC

Large industrial loads have been well studied, and they usually have separate models from the rest of the load. When selecting the sites, primarily consider commercial and residential loads.

6.2 Load Monitoring Levels

For load composition analysis and validation, SCADA measurements at substation levels, where load models are aggregated, would be adequate. The load monitoring efforts would be on working out data collection and sharing issues.

For load model validation, dynamic measurements are needed. Areas that aggregate loads to the 230-kV level may be able to meet their validation needs using WAMS and DFR data. Likewise, even if an area models the lower voltage system, sufficient validation for WECC-wide stability analysis may be obtained from higher voltage monitoring. Monitoring commercially dominated circuits should provide validation

for most WECC commercial load. Validation of residential load models, if desired, will require regional low voltage (<35-kV) monitoring. To sufficiently validate and calibrate load component models, load monitoring at feeder level or even building level is necessary. The challenge with low-voltage level is that one has to wait for events that would have enough impact at the monitoring level so meaningful data could be captured. It is also important to point out that the objective of load model validation is to validate load modeling principles and not to validate each load model in the WECC database. Although it may include lower voltage levels, load monitoring for load model validation doesn't have to cover all the 11 load locations for load composition analysis, and many of the existing load monitoring facilities presented in Section 4.0 Existing Load Monitoring Examples can be leveraged.

For load uncertainty analysis, the studies can be performed for different load levels as well. Substation SCADA measurements, WAMS data, or monitoring data at lower voltage levels can all be useful for characterizing load uncertainties. The load monitoring specified above would be adequate for uncertainty analysis.

6.3 Load Monitoring Equipment

Load monitoring equipment selection depends on what characteristics need to be captured. For load composition analysis and validation, steady-state measurements are needed. Existing SCADA facility can be used. For load model validation, PMUs, PPSMs, DFRs, or the low-cost DMWG monitor should be used to record load dynamics. Existing facilities at BPA, PNM, IPC, PSE, and PG&E are examples and should be further explored in terms of their benefits to load research. For load uncertainty analysis, both types of measurements can be used.

Figure 26 summarizes the overall roadmap for load monitoring. It is important to point out that load monitoring efforts should be consistent with and driven by the load research needs. A three-stage load monitoring effort is suggested in Figure 26.

The first stage is to explore the use of SCADA measurements from the identified 11 WECC locations for load composition studies and load uncertainty analysis. This is relatively easy to implement because existing SCADA infrastructure can be leveraged.

With load monitoring experience gained in the first stage, stage 2 on load monitoring for load model validation as well as load uncertainty analysis can be implemented. Again, to be cost-effective, it starts with existing measurement facilities at several power companies as identified in Section 4.0 Existing Load Monitoring Examples. Feedback on the use of load monitoring data can be used to improve existing monitoring facilities or to identify needs for new monitoring capabilities.

The last stage is to implement load control monitoring along with load control. Load control monitoring may well overlap with the facilities put in place for the first two stages. But any new load monitoring capabilities can be built on experience from the first two stages.

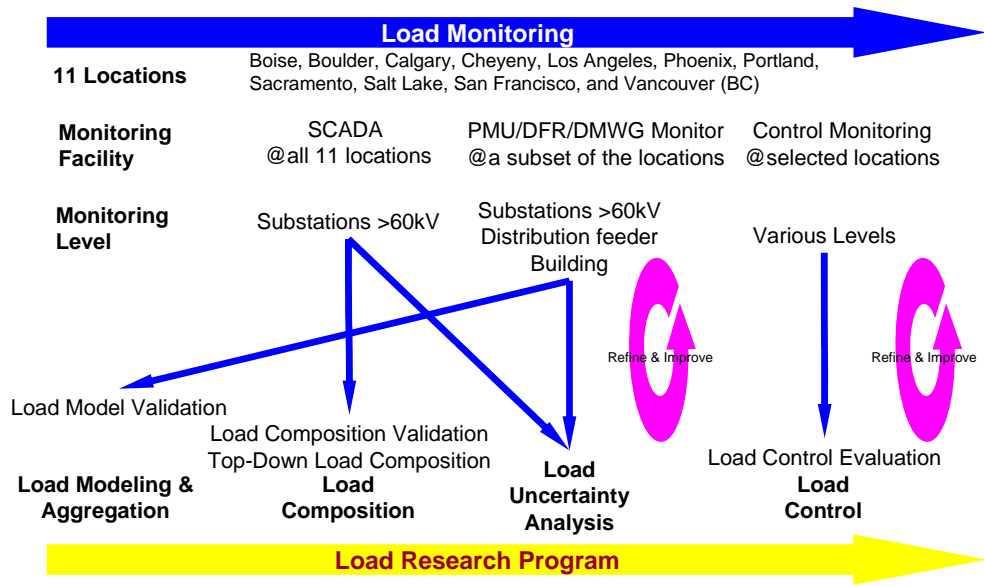


Figure 26. Load Monitoring Roadmap

7.0 REFERENCES

- Centeno, V., Z. Huang, K. Martin, and L. Beard. 2006. "Responses Summary to Questionnaire on PMU Installation and Maintenance." Technical report for the Eastern interconnection Phasor Project of the Consortium for Electric Reliability Technology solutions (CERTS), Available at: http://phasors.pnl.gov/resources_performance.html
- Hammerstrom et al. 2007. Grid Friendly™ Appliances. Available at: http://gridwise.pnl.gov/technologies/transactive_controls.stm
- Huang, Z., D. Kosterev, R. Guttromson, and T. Nguyen. 2006. "Model Validation with Hybrid Dynamic Simulation." In Proceedings of PES-GM2006-The IEEE Power Engineering society General Meeting 2006, Montreal, Canada, June 18-22.
- Kosterev, D. 2004. "Hydro Turbine-Governor Model Validation in Pacific northwest." IEEE Transactions on Power Systems. 19(2):1144-1149.
- Pereira, L., D. Kosterev, P. Mackin, D. Davies, J. Undrill, and Z. Wenchun. 2002. "An Interim Dynamic Induction Motor Model for Stability Studies in the WSCC. IEEE Transactions on Power Systems. 17(4):1108-1115.
- Phadke, A.G., J.S. Thorp, and M.G. Adamiak. 1983. "A New Measurement Technique for Tracking voltage Phasors, Local System Frequency, and Rate of Change of Frequency. IEEE Transactions on Power Apparatus and Systems. PAS-102(5):1025-1038.

APPENDIX A – PMU Specifications and Technical Data

Table A- 1 PMU Specifications and Technical Data

PMU Model	Number of Voltage Inputs	Number of Current Inputs	Number of Digital (on/off) Inputs	Output Data Rate (sps*)	Output Data Format (e.g. IEEE 1344)	Integrate Relay Function?	Time Synchronization Mechanism (e.g. GPS or IRIG-B)	A/D Conversion Numerical Resolution (e.g. 16 bits)	Continuous Data Storage Capability (e.g. stores data for 10 days)	Data Link Protocol (e.g. TCP/IP)	Event Trigger Level (e.g. 2 levels for undervoltage)	Physical Dimension and Weight (WxHxD inch, lbs)	List Price (US\$)
ABB RES 521***	6	12	8	60/30/15	IEEE 1344, PC37.118	No	Built-in GPS clock module	16 bits	No local storage, streaming PMU	TCP/IP UDP selectable from HMI	2 f; 2df/dt; 2 uv; 4 oc plus output contacts	19x10.6x10	\$10,000 ~ \$13,000
Arbiter 1133A***	3	3	4	20	IEEE-1344	Some	Built-in GPS module or IRIG-B		Configurable	Serial Ethernet	32 channels, configurable	1RU 17x1.72x10 5 lbs	\$4,500
Macrodyne 1690***	15 V+I 15 V+I (optional)		16 16 (optional)			No	Built-in GPS receiver. Time signal output (IRIG-B, 1 pps).	16 bits	4 MB 1GB (optional)	RS-232	Flexible software triggers	10.5x14.75x19 45 lbs	
Metha Tech Transcan 2000 IED	8 V+I		16	60	TranScan; Comtrade (optional)		IRIG-B	16 bits	30 min	Ethernet; RS-232; V.34 modem	oc; ov; uv; of; uf; digital triggers		
SEL-734***	3	3	6	20	NA	No	IRIG-B	12 bits	NA	TCP/IP EIA-232	Programmable Logic	7.56x5.67x6.64 5 lbs	\$1,500
SEL-421***	3	3	7	20	NA	Yes	IRIG-B and 1 kpps	16 bits	NA	EIA-232	Programmable Logic	19x5.22x9.5 2 17.5 lbs	\$11,000

(data as of 2003)

*sps: Sample per Second

**pps: Pulse per Second

***Confirmed with vendors

IRIG-B: InterRange Instrumentation Group Time Code Format B.

APPENDIX B – PPSM Cost Breakdown

FINAL PROJECT REPORT

LOAD MODELING TRANSMISSION RESEARCH

APPENDIX I

UNCERTAINTY IN POWER SYSTEM MODELS

Prepared for CIEE By:

Lawrence Berkeley National Laboratory



A CIEE Report

Table of Contents

1.0 INTRODUCTION	4
2.0 SOURCES OF UNCERTAINTY	4
3.0 INFLUENCE OF PARAMETERS ON SYSTEM RESPONSE	5
3.1 <i>Background</i>	5
3.2 <i>Trajectory sensitivities</i>	5
3.3 <i>Quantifying parameter effects</i>	6
3.4 <i>Examples</i>	7
4.0 REDUCING UNCERTAINTY	9
4.1 <i>Model structure</i>	9
4.2 <i>Parameter estimation</i>	10
4.3 <i>Parameter conditioning</i>	10
5.0 IMPACT OF LOAD MODEL UNCERTAINTY	11
5.1 <i>Overview</i>	11
5.2 <i>Load-induced variations in qualitative behavior</i>	11
5.3 <i>Protection operation</i>	12
6.0 APPROACHES TO REDUCING THE IMPACT OF UNCERTAINTY	13
6.1 <i>Trajectory approximation using sensitivities</i>	13
6.2 <i>Probabilistic collocation method</i>	15
6.3 <i>Grazing analysis</i>	15
7.0 CONCLUSIONS	17
REFERENCES	18

1.0 Introduction

Analysis of power system dynamic behavior requires models that capture the phenomena of interest, together with parameter values that ensure those models adequately replicate reality. It is important to distinguish between model fidelity and parameter accuracy. Models are always an approximation. In many cases, the level of approximation is determined by the nature of the study. For example, phasor-based models that are used for dynamic security assessment ignore electromagnetic transient phenomena. In other cases, however, model approximation is a matter of convenience, with the outcome not necessarily providing a good reflection of reality. Load modeling provides an example. It is common for the aggregate behavior of loads to be represented by a voltage dependent model, such as the ZIP model. This is a gross approximation, given the complex composition of loads on most distribution feeders. This deficiency is particularly evident in distribution systems that supply a significant motor load, as the ZIP model cannot capture the delayed voltage recovery associated with induction motors re-accelerating or stalling.

The choice of models is a decision that should be made based on knowledge of the actual system composition and the phenomena that are being studied. Determining parameters for those models, on the other hand, usually relies on comparison of model response with actual measured behavior. Parameter estimation processes seek to minimize the difference between measured and simulated behavior. An overview is provided in Section 4. Different choices for model structure will usually result in different parameter values. This is a consequence of the estimation process trying to compensate for unmodeled, or poorly modeled, effects. In all cases, the models and associated parameter sets are approximations, though the goal should always be to obtain the best possible approximations.

Load models are further complicated by the fact that load composition is continually changing. Even if it were possible to obtain a load model that was perfectly accurate at a particular time, it would be inaccurate a short while later. Developing load models is not a futile exercise though, as overall load composition tends to behave fairly predictably. For example, the composition of a residential feeder will (approximately) follow a 24 hour cycle. But, while composition from one day to the next may be roughly equivalent, morning load conditions may well differ greatly from those in the evening. Seasonal variations may be even more pronounced.

As mentioned previously, all models are approximate to some extent. Model structures for large dominant components, such as synchronous generators, are well established, as are procedures for determining the associated parameter values. Furthermore, parameter values for such devices remain fairly constant over their lifetime. Models that represent an aggregation of many distributed components are much more contentious though, given the inherent uncertainty in the overall composition of the model. This white paper focuses on uncertainty associated with load modeling. Similar issues arise in the modeling of other power system components though, with wind generation being a particularly topical example.

The white paper is organized as follows. Section 2 provides a discussion of the sources of uncertainty in load modeling. The influence of parameter variations on system response is discussed in Section 3. Reduction of uncertainty is considered in Section 4. Parameter estimation is reviewed, and parameter conditioning (identifiability) is discussed. The impact of load model uncertainty is considered in Section 5, while Section 6 reviews various techniques for assessing that impact.

2.0 Sources of Uncertainty

Loads form the major source of uncertainty in power system modeling. Loads are highly distributed, and quite variable, so detailed modeling is impossible. Aggregation provides the only practical approach to incorporating loads into power system studies. For static (power flow) analysis, the approximations inherent in aggregate load models are largely unimportant, as the composition of the load has little impact on results. On the other hand, load composition is very important in the analysis of system dynamic behavior. Different types of loads exhibit quite diverse responses to disturbances. For example, lighting loads vary statically (almost) with voltage, whereas motor loads exhibit dynamic behavior, perhaps even stalling. In fact, each different load type displays unique characteristics. Aggregate load models attempt to blend all those differing responses.

In many cases aggregate load models are required to represent loads that are widely distributed, physically and electrically. Because of this electrical separation, the voltages seen by loads may differ greatly. Such voltage differences may critically affect the response of loads to large disturbances, resulting in diverse load behavior. It is difficult for aggregate load models to capture such diversity. At best, those topological influences can only be crudely approximated.

Accounting for switching-type behavior in aggregate load models is also challenging. When residential air-conditioning compressor motors experience a voltage dip to around 0.6 pu, they almost instantaneously stall. This can be modeled as a mode switch, from running to stalled. As mentioned previously, voltage is usually not uniform across a distribution system. Therefore voltage dips may result in some compressor motors stalling and others not. As motors stall, the resulting high currents will further depress voltages, possibly inducing further stalling. The proportion of stalled motors will depend nonlinearly and temporally on many factors, including the severity of the initiating voltage dip, and the strength and topology of the distribution system. These attributes are difficult to capture, with any degree of certainty, in aggregate load models.

Other devices may also switch under disturbed voltage conditions. Contactors provide an example. They use an electromechanical solenoid to hold a switch in the closed position. When a disturbance depresses the voltage, the solenoid may not be able to hold the switch closed, resulting in unintended tripping of the associated load. The voltage threshold at which such action occurs varies widely. Precise modeling is not possible.

Looking to the future, a number of trends are likely to increase the level of uncertainty associated with aggregate load models. Distribution systems will see a greater penetration of distributed generation as fuel cells and solar cells, for example, become commercially viable. Plug-hybrid electric vehicles (PHEVs) will certainly gain in popularity, and may well become a significant feature of distribution systems. Not only do PHEVs present a load that moves from one location to another, but their vehicle-to-grid capability offers the possibility of highly dispersed generation. All these trends suggest that methods for assessing the impact of uncertainty are set to become increasingly important.

3.0 Influence of Parameters on System Response

3.1 Background

The time evolution of system quantities following a disturbance is referred to as a trajectory. For power systems, trajectories are driven by a system of switched differential-algebraic equations, with the switching required to capture events such as protection operation or limits being encountered. The details of this underlying model structure are not relevant to this report, and so are not included. A thorough discussion can be found in [1]. The concept of trajectories is important though, so a brief overview is provided.

The trajectory of a dynamical system depends on the initial conditions and the choice of parameter values. This dependence is expressed mathematically as the system *flow*, which can be written

$$x(t) = \phi(t, x_0, \theta)$$

where the initial conditions are given by $x_0 = x(0)$, and θ denotes the parameters. For a particular choice of x_0 and θ , the point on the trajectory at time t , denoted $x(t)$ is given by evaluating the flow ϕ at that time. Generally ϕ cannot be written explicitly, but instead is generated numerically by simulation.

The report focuses on the impact of parameter uncertainty on the trajectory. It will be assumed that the initial conditions remain constant¹. For notational convenience, the dependence of ϕ on x_0 will therefore be ignored. Accordingly, trajectories will be given by

$$x(t) = \phi(t, \theta). \tag{1}$$

3.2 Trajectory sensitivities

Sensitivity concepts are generally associated with the linearization of an input-output relationship. Small changes in inputs map through the linearized relationship to small output changes. Trajectory sensitivities fit this framework by describing the changes in the trajectory (the output) resulting from perturbations in the underlying parameters and/or initial conditions (the inputs). They provide a linearization around the trajectory, as against small disturbance analysis

¹All subsequent analysis and techniques can be extended to incorporate variations in the initial conditions.

which builds on linearization around the equilibrium point. Trajectory sensitivity concepts are not new [2], though until recently progress on practical applications was impeded by:

- Computational inefficiency. Sensitivity to each parameter or initial condition required an additional full simulation.
- Non-smooth behavior. Sensitivities were not well defined for situations where events influenced behavior.

However both these limitations have recently been overcome, with efficient computation of trajectory sensitivities now possible for large-scale, non-smooth systems [3].

Trajectory sensitivities provide an insightful way of quantifying the effect that individual parameters have on overall system behavior [4]. A trajectory sensitivity is simply the partial derivative of the trajectory, or equivalently the flow, with respect to the p parameters of interest,

$$\begin{aligned} \Phi_i(t, \theta) &= \frac{\partial \phi_i}{\partial \theta}(t, \theta) \\ &= \begin{bmatrix} \frac{\partial \phi_i}{\partial \theta_1}(t, \theta) & \frac{\partial \phi_i}{\partial \theta_2}(t, \theta) & \dots & \frac{\partial \phi_i}{\partial \theta_p}(t, \theta) \end{bmatrix} \end{aligned} \quad (2)$$

where ϕ_i refers to the i -th element of the vector function ϕ , or equivalently the i -th state, and θ_j is the j -th parameter.

Trajectories are obtained by numerical integration, which generates a sequence of points at discrete time steps t_0, t_1, \dots, t_N along the actual trajectory. The discretized trajectory will be described using the notation

$$\mathbf{x} = [x(t_0) \ x(t_1) \ \dots \ x(t_N)]. \quad (3)$$

Trajectory sensitivities can be calculated efficiently as a byproduct of numerical integration [3, 5, 6]. The corresponding discretized sensitivities can be written,

$$\underline{\Phi}_i(\theta) = \begin{bmatrix} \Phi_i(t_0, \theta) \\ \Phi_i(t_1, \theta) \\ \vdots \\ \Phi_i(t_N, \theta) \end{bmatrix}. \quad (4)$$

Unfortunately, few commercial simulation packages currently provide trajectory sensitivity information. Approximate sensitivities must be generated by varying each parameter in turn by a very small amount, re-simulating, determining the difference in trajectories, and thus finding the sensitivity. The disadvantage of this method is that it is computationally expensive, and requires an additional simulation for each parameter.

3.3 Quantifying parameter effects

Trajectory sensitivities can be used directly to identify significant parameters in a model. Parameters that have a large associated trajectory sensitivity (for part or all of the simulation time) have a larger effect on the trajectory than parameters with smaller sensitivities. A 2-norm can be used to quantify this relative significance. Considering the sensitivity of the i -th system state (trajectory) to the j -th parameter, given by $\Phi_{ij}(t, \theta)$, the 2-norm (squared) is given by

$$\|\Phi_{ij}(t, \theta)\|_2^2 = \int_{t_0}^{t_N} \Phi_{ij}(t, \theta)^2 dt \quad (5)$$

where the period of interest is $t_0 \leq t \leq t_N$. In terms of the discrete-time approximation provided by simulation, the equivalent 2-norm can be written

$$\|\underline{\Phi}_{ij}(\theta)\|_2^2 = \sum_{k=0}^N \Phi_{ij}(t_k, \theta)^2. \quad (6)$$

Parameters that have a relatively large (small) effect on the trajectory result in relatively large (small) values for these norms.

It should be kept in mind that the sensitivities $\Phi(t, \theta)$ are computed for a single disturbance, and thus are applicable only for similar disturbances. Different forms of disturbances may excite the system in ways that accentuate the impact of other parameters. As a general rule, more severe disturbances yield higher sensitivities.

3.4 Examples

The examples throughout the report utilize the IEEE 39 bus system of Figure 1. All generators in this system were represented by a fourth order machine model [7], and were regulated by the IEEE standard AVR/PSS models AC4A and PSS1A [8]. All generator and network data were obtained from [9].

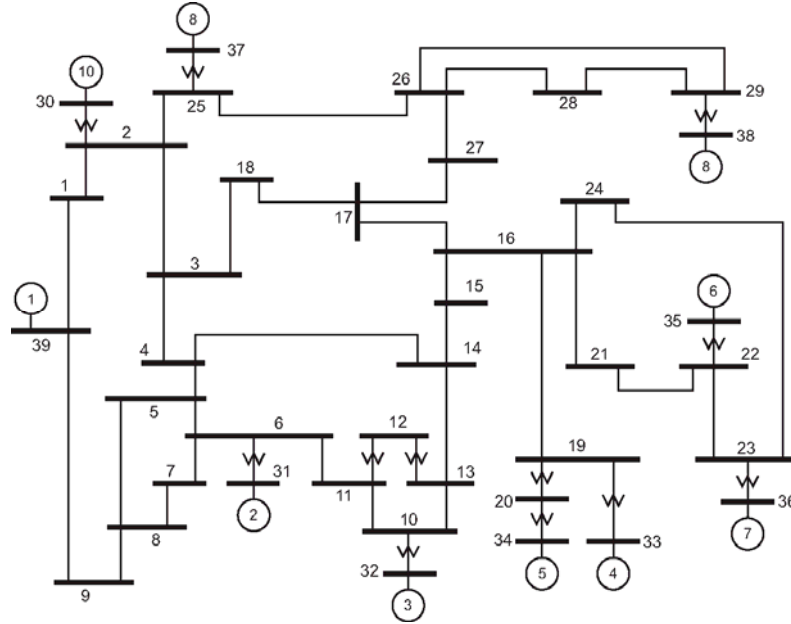


Figure 1: IEEE 39 bus system.

3.4.1 Parameter ranking

As mentioned previously, trajectory sensitivities provide a basis for ranking the relative influence of parameters. Large sensitivities imply that parameter variations have a large effect on behavior, whereas small sensitivities suggest behavior changes very little with parameter variation. In this example, trajectory sensitivities are used to rank the importance of voltage indices at all loads throughout the IEEE 39 bus system. A three-phase fault was applied at bus 16 at 0.1 sec, and cleared (without any line tripping) 0.2 sec later. A static voltage-dependent load model

$$S_v(V) = P_0 V^{\eta_p} + jQ_0 V^{\eta_q} \quad (7)$$

was used for all loads, with $\eta_p = \eta_q = 2$ (constant admittance) in all cases.

The sensitivities of bus 16 voltage V_{16} to load indices η_p and η_q at all buses were computed in conjunction with the nominal trajectory. These trajectory sensitivities are provided in Figure 2, where the vertical axis gives the change in the pu voltage for a unity change in load index values. It is immediately clear that the real power index η_p for bus 20 has a much greater influence on behavior than all other indices. (The reason is that generator 5 is marginally stable for this disturbance scenario, and bus 20 lies on the corridor linking that generator to the rest of the system.) The loads at buses 4, 8 and 23 also display a reasonable, though certainly less pronounced, level of influence. Loads 4 and 8 are influential due to their large size. Load 23 has an important impact on the dynamics of generator 7. The influence of all other loads, for this disturbance scenario, is negligible. Of course a different disturbance could possibly highlight some other set of loads.

Field testing loads to determine their (approximate) voltage dependence is an expensive exercise. However, by utilizing trajectory sensitivities, the most important loads can be immediately identified, and attention focused accordingly. This use of trajectory sensitivities relates to parameter identifiability, and will be discussed further in Section 4.3.

3.4.2 Indicator of stressed conditions

It is shown in [4] that as systems become more heavily stressed, sensitivity to parameter variation increases significantly. This can be illustrated by continuing the previous example. The upper plot of Figure 3 shows the behavior of generator 5 angle (relative to generator 10) for a range of fault clearing times. (The fault clearing time used in the previous example was 0.2 sec.) The critical clearing time is 0.213 sec; slower clearing results in generator 5 losing synchronism. Notice that the angular deviations do not show a great increase, even though instability is imminent.

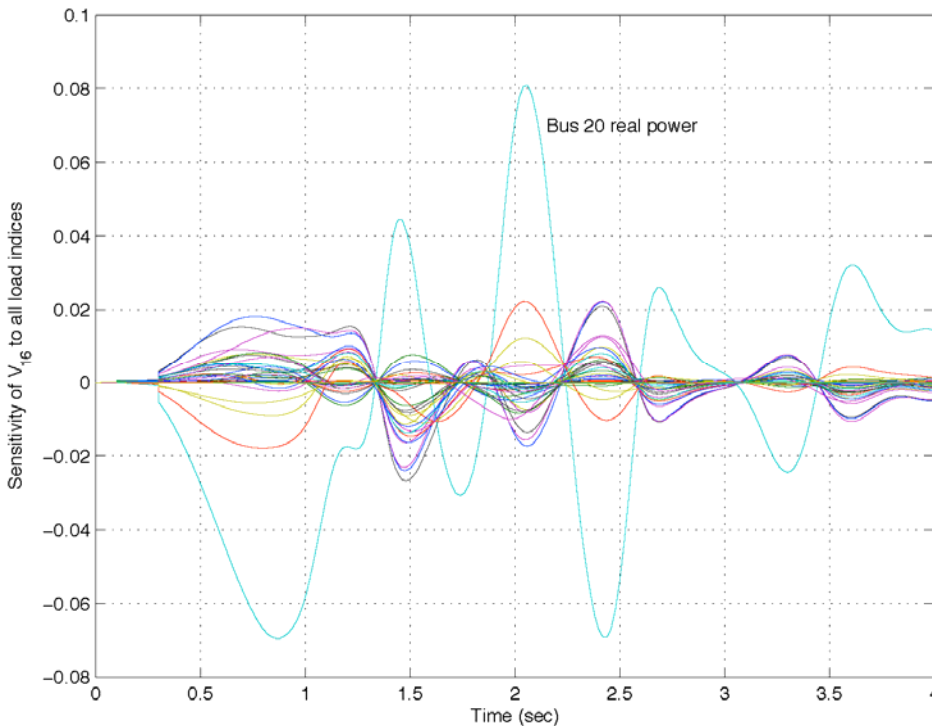


Figure 2: Trajectory sensitivities for all load indices.

The sensitivity of V_{16} to the bus 20 load index η_p , for the same range of fault clearing times, is shown in the lower plot of Figure 3. The deviations exhibited by these trajectory sensitivities grow dramatically as critical conditions are approached. This behavior motivated the sensitivity related measures developed in [10,11] to predict conditions that induce marginal stability. Further work is required though to fully understand and exploit this phenomenon.

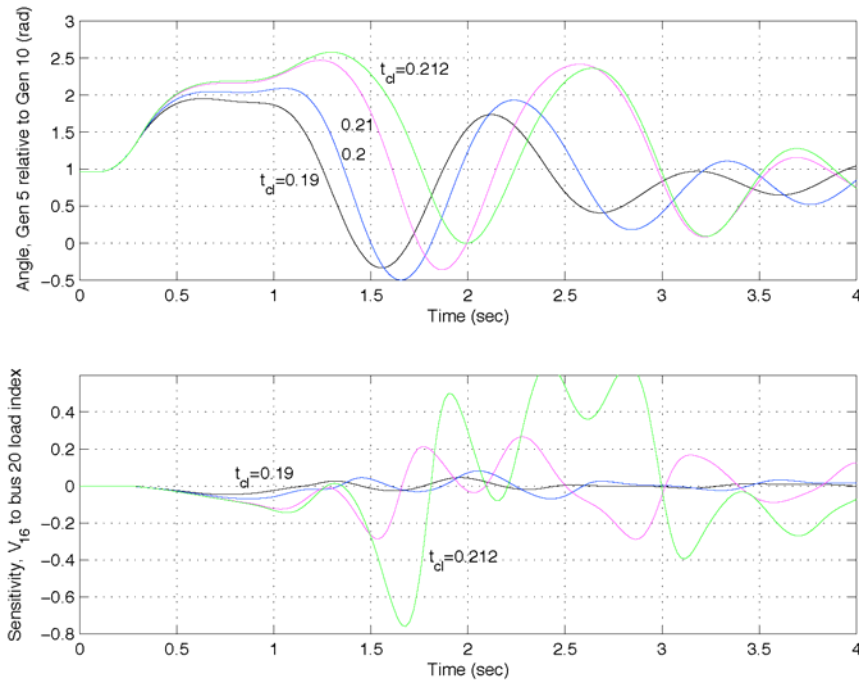


Figure 3: Trajectory and sensitivity variation for increasing system stress.

4.0 Reducing Uncertainty

4.1 Model structure

Load parameter uncertainty can be reduced by structuring models so that they adequately capture the physical characteristics of the actual loads. A ZIP model, for example, provides a poor representation of loads that include a significant proportion of air-conditioner motors. Attempting to replicate motor-induced delayed voltage recovery using such a model is futile. Tuning the ZIP parameters to best match one disturbance would provide no guarantee that the parameters were appropriate for another event. The WECC model of Figure 4, on the other hand, provides a versatile structure that is capable of representing various different load types. The issue with this latter model is one of identifying the multitude of parameters associated with the more complete model structure.

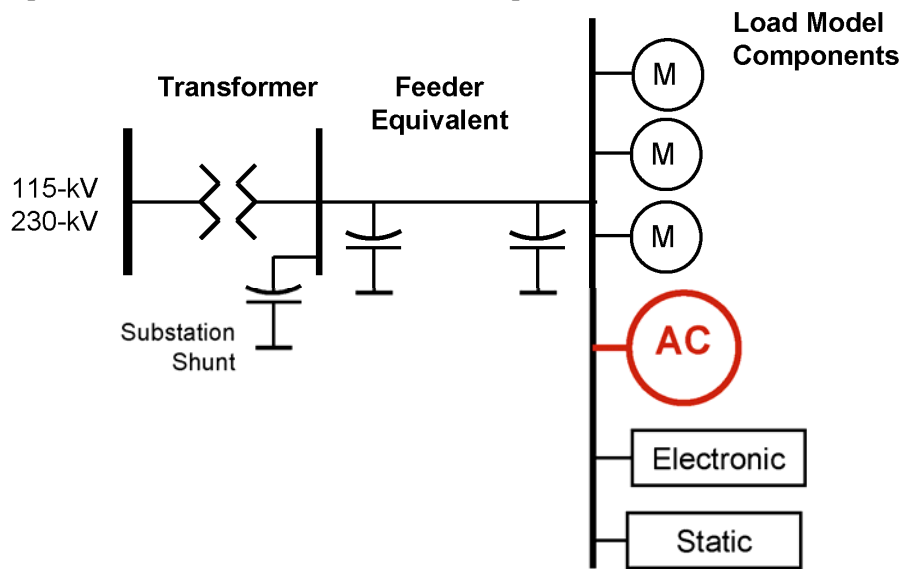


Figure 4: WECC load model structure.

4.2 Parameter estimation

It is often possible to estimate parameter values from disturbance measurements. For example, simply measuring the active and reactive power consumed by a load during a disturbance may yield sufficient information to accurately estimate several model parameters. The aim of parameter estimation is to determine parameter values that achieve the closest match between the measured samples and the model trajectory.

Disturbance measurements are obtained from data acquisition systems that record sampled system quantities. Let a measurement of interest be given by the sequence of samples

$$m = [m_0 \ m_1 \ \dots \ m_N] \quad (8)$$

with the corresponding simulated trajectory being given by

$$\mathbf{x}_i = [x_i(t_0) \ x_i(t_1) \ \dots \ x_i(t_N)], \quad (9)$$

which is the i -th row of \mathbf{x} defined in (3). The mismatch between the measurement and its corresponding (discretized) model trajectory can be written in vector form as

$$e(\theta) = \mathbf{x}_i(\theta) - m \quad (10)$$

where a slight abuse of notation has been used to show the dependence of the trajectory on the parameters θ .

The best match between model and measurement is obtained by varying the parameters so as to minimize the error vector $e(\theta)$ given by (10). It is common for the size of the error vector to be expressed in terms of the 2-norm cost,

$$C(\theta) = \|e(\theta)\|_2^2 = \sum_{k=0}^N e_k(\theta)^2. \quad (11)$$

The desired parameter estimate $\tilde{\theta}$ is then given by

$$\tilde{\theta} = \underset{\theta}{\operatorname{argmin}} C(\theta). \quad (12)$$

This nonlinear least squares problem can be solved using a Gauss-Newton iterative procedure [12]. At each iteration j of this procedure, the parameter values are updated according to

$$\underline{\Phi}_i(\theta^j)^T \underline{\Phi}_i(\theta^j) \Delta\theta^{j+1} = -\underline{\Phi}_i(\theta^j)^T e(\theta^j)^T \quad (13)$$

$$\theta^{j+1} = \theta^j + \alpha^{j+1} \Delta\theta^{j+1} \quad (14)$$

where $\underline{\Phi}_i$ is the trajectory sensitivity matrix defined in (4), and α^{j+1} is a suitable scalar step size².

An estimate of θ which (locally) minimizes the cost function $C(\theta)$ is obtained when $\Delta\theta^{j+1}$ is close to zero. Note that this procedure will only locate local minima though, as it is based on a first-order approximation of $e(\theta)$. However if the initial guess for θ is good, which is generally possible using engineering judgement, then a local minimum is usually sufficient.

4.3 Parameter conditioning

The information content of a measured trajectory determines which parameters may be estimated. Parameters that have a significant effect on the trajectory are generally identifiable. Conversely, parameters that have little effect on trajectory shape are usually not identifiable.

When developing a parameter estimation algorithm, it is necessary to separate identifiable parameters from those that are not, in order to avoid spurious results. This can be achieved using a *subset selection* algorithm [14,15]. This algorithm considers the conditioning of the matrix $\underline{\Phi}_i^T \underline{\Phi}_i$ that appears in (13). If it is well conditioned, then its inverse will be well defined, allowing (13) to be reliably solved for $\Delta\theta^{j+1}$. On the other hand, ill-conditioning of $\underline{\Phi}_i^T \underline{\Phi}_i$ introduces numerical difficulties in solving for $\Delta\theta^{j+1}$, with the Gauss-Newton process becoming unreliable.

The subset selection algorithm considers the eigenvalues of $\underline{\Phi}_i^T \underline{\Phi}_i$ (which are the square of the singular values of $\underline{\Phi}_i$.) Small eigenvalues are indicative of ill-conditioning. The subset selection algorithm separates parameters into those associated with large eigenvalues (identifiable parameters) and the rest which cannot be identified. The latter parameters are subsequently fixed at their original values.

²Numerous line search strategies for determining α are available in [13] and many other references.

Interestingly, the diagonal elements of $\Phi_i^T \Phi_i$ are exactly the values given by the 2-norm (6). If the trajectory sensitivities corresponding to parameters were orthogonal, then $\Phi_i^T \Phi_i$ would be diagonal, and separating the influences of parameters would be straightforward. This is not generally the case though, with the impacts of parameters often being partially correlated. For that reason, large values of (6) are not sufficient to guarantee parameter identifiability.

In summary, two situations lead to parameter ill-conditioning (non-identifiability). The first is where the trajectory sensitivities, corresponding to available disturbance measurements, are small relative to other sensitivities. This group of parameters cannot be estimated from available measurements. That may not be particularly troublesome though, if this is the only disturbance of interest, as their influence on behavior is negligible anyway. However, they may be influential for other disturbances. This should be assessed by considering a variety of viable disturbance scenarios. The second case arises when the trajectory sensitivities are highly correlated. Consequently, the influence of various parameters cannot be separated. This would be the situation, for example, when varying two parameters in unison gave no overall change in behavior. Both parameters are influential, but neither can be estimated without fixing the other. This dilemma may be resolvable by considering various disturbances, in the hope of finding cases where the parameters exert differing influences.

5.0 Impact of load model uncertainty

5.1 Overview

In terms of quantitative analysis, for example matching simulations with measurements, it is absolutely clear that accurate load modeling is vitally important. But for qualitative investigations, where the aim of dynamic simulation is to assess the likelihood of a certain disturbance scenario being stable or unstable, then the need for accurate load modeling is much reduced. In other words, if a system is stable (unstable) for a certain set of load model parameters, then it will most likely also be stable (unstable) for perturbed load models. Insights provided by trajectory sensitivities help explain this conjecture. In fact, for such qualitative assessment, it is more important to know the sensitivity of behavior to load parameters, than to precisely know the parameter values.

A caveat is required though. Most power system failures are not initiated by instability [16], though instability is frequently a consequence. Rather, it is more common for an initiating (relatively minor) disturbance to escalate through reactionary protection operation. Examples of such reactionary effects include zone 3 distance protection unnecessarily tripping feeders, and volts/hz relays tripping generators. The subsequent weakening of the system may induce further protection operation, leading to cascading system failure. It has been found from disturbance analysis that load modeling can be very important in predicting such reactionary protection behavior [17].

Protection is binary; either the system encounters the operating characteristic initiating a trip, or it does not encounter the characteristic and the component remains in service. The bounding case, separating protection operation from non-operation, corresponds to the trajectory *grazing* (just touching) the operation characteristic [18]. Parameter sets that induce grazing are pivotal, in that they divide parameter space into regions that exhibit vastly different behavior [19]. It follows that in potential grazing situations, where reactionary protection operation may or may not occur, special care should be given to understanding the influence of load parameter variations.

5.2 Load-induced variations in qualitative behavior

Previous analysis and examples have suggested that load models have negligible qualitative influence on the behavior of systems that are robustly stable [4]. This will be further illustrated using the IEEE 39 bus system of Figure 1, though in this case the disturbance scenario involves a solid three-phase fault on line 16-21, at the bus 21 end. The fault was cleared after 0.15 sec by tripping the faulted line. That left buses 21 and 23, and generators 6 and 7, radially fed over line 23-24.

The load composition at buses 23 and 24 was modeled parameterically by

$$S_{tot} = \nu S_v + (1 - \nu) S_{ind} \quad (15)$$

where S_{tot} is the total complex power of the load, S_v is the static voltage dependent part of the load given by (7), and S_{ind} is the complex power demanded by the induction motor component. The dynamics underlying S_{ind} are typically described by a third order differential equation model [20]. For this example, both ν_{23} and ν_{24} were nominally set to

0.5. In other words, both loads were composed of 50% static voltage dependent load and 50% induction motor load. The static load component was modeled as constant admittance, while the induction motor component used parameter values from [20, p. 305], with appropriate per unit scaling.

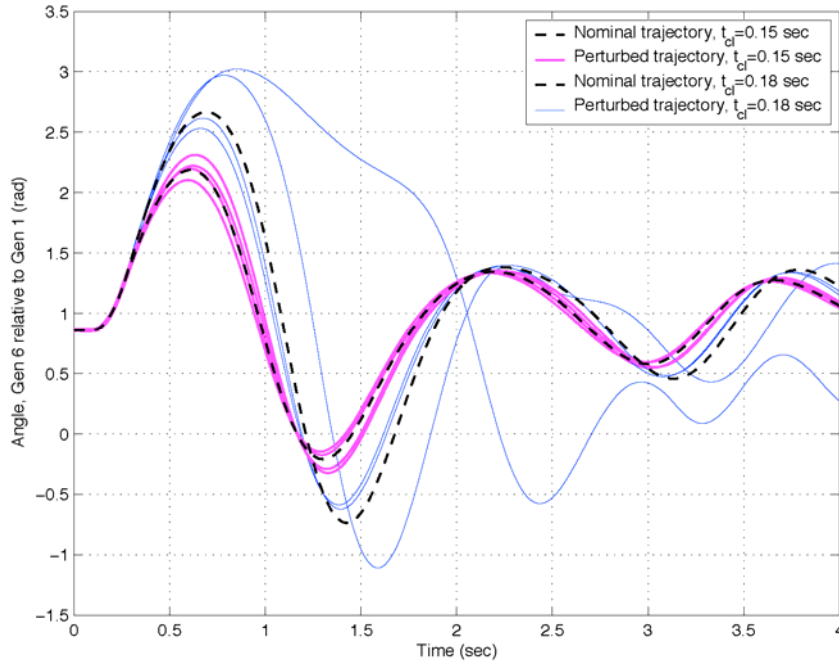


Figure 5: Influence of load parameter perturbations with increased system stress.

The response of generator 6 angle (relative to generator 1), under the nominal load conditions, is shown as a dashed line in Figure 5. The load composition parameters v_{23} and v_{24} were then varied between extremes of 0 and 1. The corresponding behavior is shown as thick solid lines in Figure 5. Notice that this large variation in load composition has negligible effect on the qualitative form of the response.

The fault clearing time was then increased to 0.18 sec, quite close to the critical clearing time of 0.18375 sec. Nominal behavior is again shown as a dashed line, with behavior corresponding to extremes in v_{23} and v_{24} shown as thinner solid lines. In this case, it turns out that reduction of v_{24} to 0 has a marked effect on the qualitative form of the response; the system is only just stable.

This example supports the hypotheses that load modeling only becomes important qualitatively when the system is close to instability, and that proximity to instability can be detected by high sensitivity.

5.3 Protection operation

The previous example showed that for unstressed systems, load composition has negligible effect on the qualitative form of behavior. However that example did not take account of protection. In this example, zone 3 protection at the bus 23 end of line 23-24 is considered. Figure 6 shows the separation³ between the zone 3 mho characteristic [21] and the apparent impedance seen from bus 23. The dashed line was obtained for a fault clearing time of 0.15 sec, and used the nominal set of load parameters. It remains above zero, suggesting the zone 3 characteristic is not entered.

³This distance goes negative when the apparent impedance enters the mho characteristic.

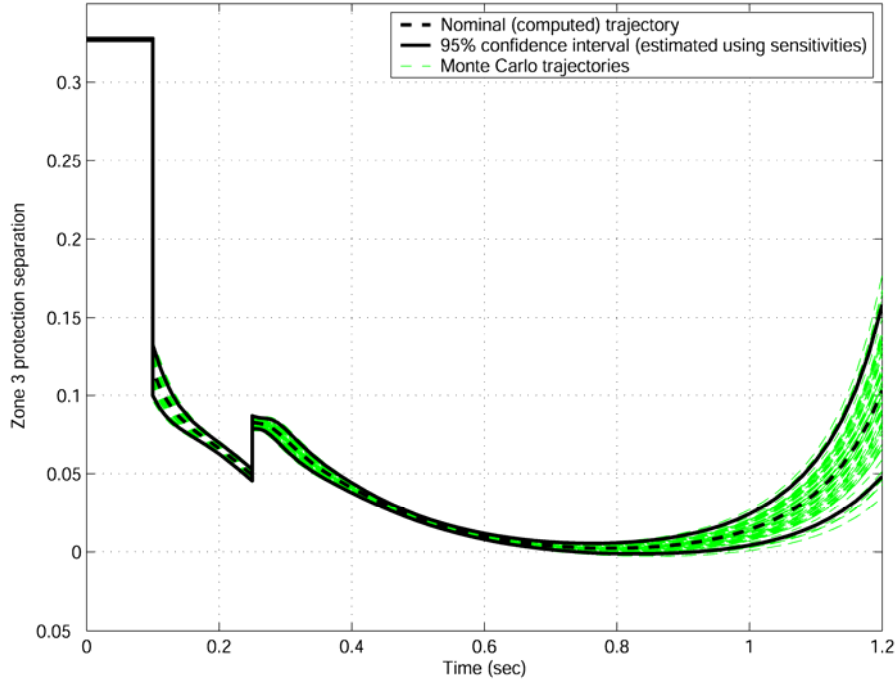


Figure 6: Zone 3 protection on line 23-24, 95% confidence interval bounds.

Uncertainty was introduced into the load composition parameters v_{23} and v_{24} . They were assumed normally distributed, with mean of 0.5 and standard deviation 0.1. A Monte-Carlo process was used to generate thirty random parameter sets, with the resulting trajectories shown in Figure 6. The figure also shows the 95% confidence interval⁴. Notice that it is quite probable for trajectories to pass below zero, suggesting the possibility of a zone 3 trip. Knowledge of the load composition is therefore very important in this case.

6.0 Approaches to reducing the impact of uncertainty

6.1 Trajectory approximation using sensitivities

By expanding the flow (1) as a Taylor series, and neglecting the higher order terms, trajectories arising from perturbing parameters by $\Delta\theta$ can be approximated as

$$\phi(t, \theta + \Delta\theta) \approx \phi(t, \theta) + \Phi(t, \theta)\Delta\theta \quad (16)$$

where $\phi(t, \theta)$ is the trajectory obtained using the nominal set of parameters θ , and the corresponding trajectory sensitivities are given by $\Phi(t, \theta)$. If the perturbations $\Delta\theta$ are relatively small, then the approximation (16) is quite accurate. This accuracy is difficult to quantify though. It is shown in [4] that the higher order terms neglected in (16) become increasingly significant as the system becomes less stable. Nevertheless, the approximations generated by (16) are generally quite accurate.

The affine nature of (16) can be exploited to establish two straightforward approaches to mapping parameter uncertainty through to bounds around the nominal trajectory [4]. The first approach assumes that each uncertain parameter is uniformly distributed over a specified range. Multiple uncertain parameters are therefore uniformly distributed over a multidimensional hyperbox. As time progresses, the affine transformation (16) distorts that hyperbox into a multidimensional parallelotope. A simple algorithm is proposed in [4] for determining the vertices of the time-varying parallelotope that correspond to worst-case behavior.

The example of Section 5.3 can be used to illustrate this process. An uncertainty of ± 0.2 was assumed in both load composition parameters, so that

$$0.3 \leq v_{23}, v_{24} \leq 0.7. \quad (17)$$

⁴It can be expected that 95% of trajectories lie within that bound.

Worst-case analysis was used to explore bounds on behaviour, and in particular to determine whether this uncertainty could affect conclusions regarding protection operation.

The example again focuses on zone 3 protection at the bus 23 end of line 23-24. The dashed line in Figure 7 was obtained using the nominal set of load parameters. As mentioned before, it suggests the zone 3 characteristic is not entered. Based on this nominal trajectory, sensitivities indicated that over the time frame of interest, where the trip signal approached zero, worst behaviour (lowest dip) occurred for load indices $v_{23} = 0.7$ and $v_{24} = 0.3$. Best behaviour (least dip) occurred for $v_{23} = 0.3$ and $v_{24} = 0.7$. The corresponding approximate (sensitivity derived) bounds on behaviour are shown as solid lines in Figure 7. The true (simulated) bounds are shown as dash-dot lines. The sensitivity-based predictions are very accurate over this crucial time period. Every selection of v_{23} and v_{24} from the range (17) results in a trajectory that lies within the bounds shown in Figure 7. Notice that the lower bound passes below zero, indicating the possibility of a zone 3 trip.

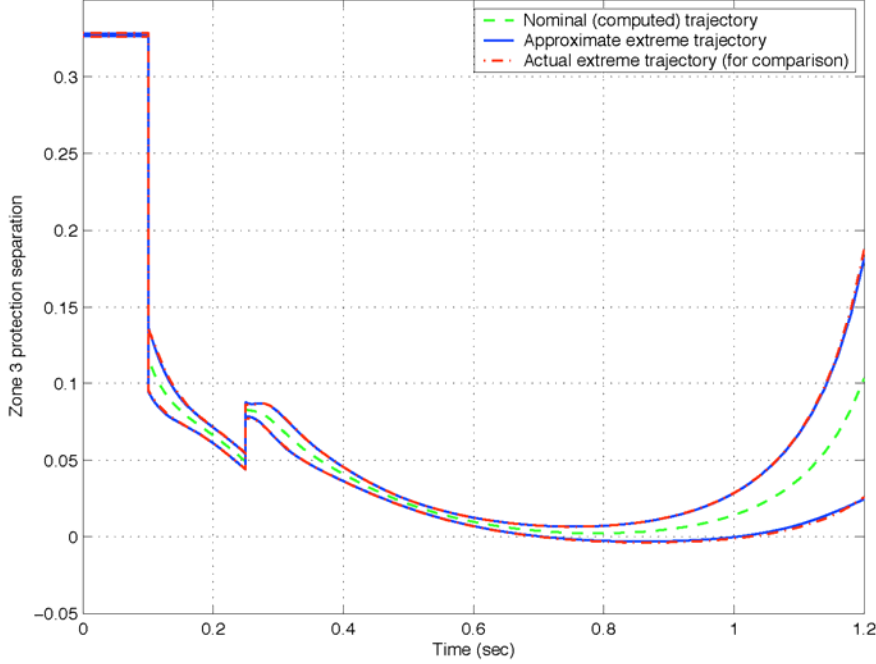


Figure 7: Zone 3 protection on line 23-24, worst-case bounds for $0.3 \leq v_{23}, v_{24} \leq 0.7$.

Often parameter values are not uniformly distributed over the range of uncertainty, but are better described by a normal distribution. Under those conditions, worst-case analysis gives a conservative view of parametric influences. Less conservatism is achieved with probabilistic assessment.

A probabilistic approach to assessing the influence of uncertainty assumes θ is a random vector with mean μ and covariance matrix Σ . It follows that deviations

$$\Delta\theta = \theta - \mu \quad (18)$$

have zero mean and covariance Σ . The nominal flow and corresponding trajectory sensitivities are generated with parameters set to μ . Perturbations in the trajectory at time t are given (approximately) by

$$\Delta x(t) = \Phi(t, \theta) \Delta\theta. \quad (19)$$

It follows from basic statistical properties [22] that perturbations in state i will have mean

$$E[\Delta x_i(t)] = \Phi_i(t, \theta) E[\Delta\theta] = 0 \quad (20)$$

and variance

$$\text{Var}[\Delta x_i(t)] = \Phi_i(t, \theta) \Sigma \Phi_i(t, \theta)^T. \quad (21)$$

Furthermore, if the elements of random vector $\Delta\theta$ are statistically independent, then Σ will be diagonal with elements $\sigma_1^2 \dots \sigma_n^2$. In this case, (21) reduces to

$$\text{Var}[\Delta x_i(t)] = \sum_{j=1}^n \Phi_{ij}(t, \theta)^2 \sigma_j^2. \quad (22)$$

Referring back to the example of Section 5.3, the two load composition parameters v_{23} and v_{24} each had mean $\mu = 0.5$ and variance $\sigma^2 = 0.01$. Equation (22) was used to determine the variance of the zone 3 protection signal at each time step along the trajectory. The bounds shown by solid lines in Figure 6 are constructed from points that are plus/minus 1.96 times the standard deviation away from the nominal trajectory. The choice of 1.96 corresponds to the 95% confidence interval.

6.2 Probabilistic collocation method

The probabilistic collocation method (PCM) provides a computationally efficient approach to building an approximate relationship between random variables and outputs that depend upon those variables. In assessing the impact of parameter uncertainty, it is assumed that the parameters of interest satisfy given probability density functions $f(\lambda)$. The desired outputs are obtained by running a simulation for each randomly chosen set of parameters. Any feature of the trajectory could be chosen as an output, for example the values of states at certain times, and/or the maximum voltage dip.

This section provides an overview of PCM. More complete details are presented in [23]. In order to simplify notation, the discussion will assume a single uncertain parameter. The ideas extend to larger numbers of parameters, though with increased computations.

For a given probability density function $f(\lambda)$, a set of orthonormal polynomials $h_i(\lambda)$ can be determined. The subscript i refers to the order of the polynomial, and orthogonality is defined in terms of the inner product

$$\langle h_i(\lambda), h_j(\lambda) \rangle = \int f(\lambda) h_i(\lambda) h_j(\lambda) d\lambda.$$

Underlying PCM is the assumption that the uncertain parameter λ and the output of interest are related by a polynomial $g(\lambda)$ of order $2n-1$. This is generally not strictly true, though such polynomial approximation is not unusual. Given this "true" relationship $g(\lambda)$ between parameter and output, PCM determines a lower order polynomial $\hat{g}(\lambda)$ such that the mean value for $\hat{g}(\lambda)$ coincides with that of $g(\lambda)$,

$$E[\hat{g}(\lambda)] = E[g(\lambda)].$$

If $g(\lambda)$ is of order $2n-1$, then $\hat{g}(\lambda)$ has order $n-1$, and can be written in terms of the orthonormal polynomials $h_i(\lambda)$ as

$$\hat{g}(\lambda) = g_0 h_0(\lambda) + g_1 h_1(\lambda) + \dots + g_{n-1} h_{n-1}(\lambda). \quad (23)$$

The coefficients g_0, \dots, g_{n-1} are obtained by solving

$$\begin{bmatrix} g(\lambda_1) \\ \vdots \\ g(\lambda_n) \end{bmatrix} = \begin{bmatrix} h_{n-1}(\lambda_1) & \dots & h_0(\lambda_1) \\ \vdots & \ddots & \vdots \\ h_{n-1}(\lambda_n) & \dots & h_0(\lambda_n) \end{bmatrix} \begin{bmatrix} g_{n-1} \\ \vdots \\ g_0 \end{bmatrix} \quad (24)$$

where the λ_i are the roots of $h_n(\lambda)$.

In summary, for a given probability density function $f(\lambda)$ for the uncertain parameter, PCM requires the following computations. The set of orthonormal polynomials h_0, \dots, h_n , corresponding to the given $f(\lambda)$, can be obtained using a straightforward recursive algorithm [24]. The roots of $h_n(\lambda)$ provide the values $\lambda_1, \dots, \lambda_n$ which are used in simulations to obtain the output values $g(\lambda_1), \dots, g(\lambda_n)$. Also, h_0, \dots, h_{n-1} are evaluated at $\lambda_1, \dots, \lambda_n$ to establish the matrix in (24), which is subsequently inverted to obtain the coefficients g_0, \dots, g_{n-1} . These coefficients are used in (23) to give the desired lower-order approximation $\hat{g}(\lambda)$.

6.3 Grazing analysis

As discussed in Section 5, most power system disturbances escalate through events such as operation of protection devices. In order to assess vulnerability to events, triggering conditions such as protection operating characteristics can be conceptualized as hypersurfaces in state space. A trajectory that passes close by a hypersurface, but does not encounter it, will not initiate an event. On the other hand, if the trajectory does encounter the hypersurface, an event will occur, possibly with detrimental consequences.

Trajectories $\phi(t, \theta)$ are parameter dependent. For a certain set of parameters, the trajectory may miss the event triggering hypersurface. The hypersurface may be encountered for a different set of parameters though. These two situations are separated by trajectories that only just touch the hypersurface. This is illustrated in Figure 8. The critical condition, which separates two different forms of behavior, is referred to as *grazing* [18].

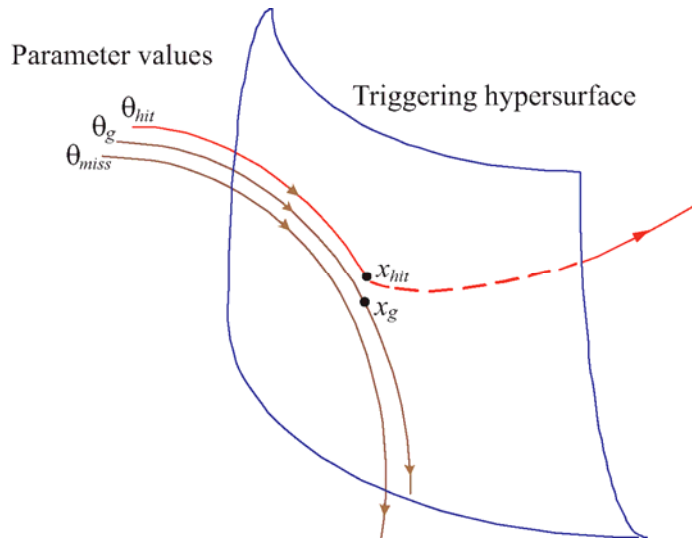


Figure 8: Illustration of grazing.

It is shown in [18] that grazing conditions establish a set of algebraic equations that can be solved using a Newton process. Each iteration of the Newton algorithm requires simulation to obtain the trajectory and associated sensitivities. Such solution processes are known as shooting methods [25]. Full details for grazing applications can be found in [18,19].

Referring to the example illustrated in Figures 6 and 7, grazing analysis can be used to determine the smallest changes in parameters v_{23} and v_{24} that cause the apparent impedance trajectory to just touch the mho characteristic. Such information provides another mechanism for assessing whether system behavior is robust to uncertainty in these parameters.

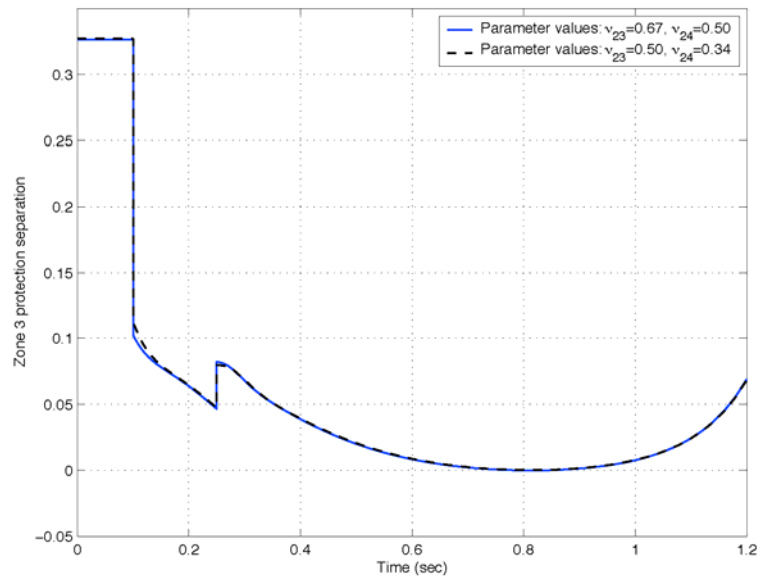


Figure 9: Grazing resulting from two different sets of parameters.

This situation is illustrated in Figure 9. Setting $v_{23} = 0.67$ while holding $v_{24} = 0.5$ results in grazing. Alternatively, grazing also occurs when $v_{23} = 0.5$ and $v_{24} = 0.34$. Other combinations of perturbations in v_{23} and v_{24} also result in grazing. Figure 10 provides a parameter-space view of grazing conditions. The two previous cases have been augmented with a third grazing scenario, where $v_{23} = 0.596$ and $v_{24} = 0.404$. Further grazing points could be

found, using a continuation process, to establish a line in parameter space. Proximity to that line would suggest vulnerability to grazing, and hence to event triggering. This is illustrated in Figure 10. The point corresponding to the nominal parameter values $v_{23} = v_{24} = 0.5$ is shown, along with a dashed line that indicates uncertainty of ± 0.15 in v_{23} and v_{24} . The region describing parameter uncertainty overlaps the line of grazing points. This suggests a finite probability that the mho characteristic will be encountered, and hence that protection will operate.

This grazing-based approach to assessing robustness to uncertainty can be extended to an arbitrary number of parameters. The information derived from such analysis is useful for exploring the relative impact of uncertainty in the different parameters. For example, it may show that a small variation in one of the parameters may induce grazing, whereas a much larger variation could be tolerated in a different parameter. These concepts are explored in [19] in the context of power electronic circuits. Adaptation to power system applications is conceptually straightforward, though has not yet been undertaken.

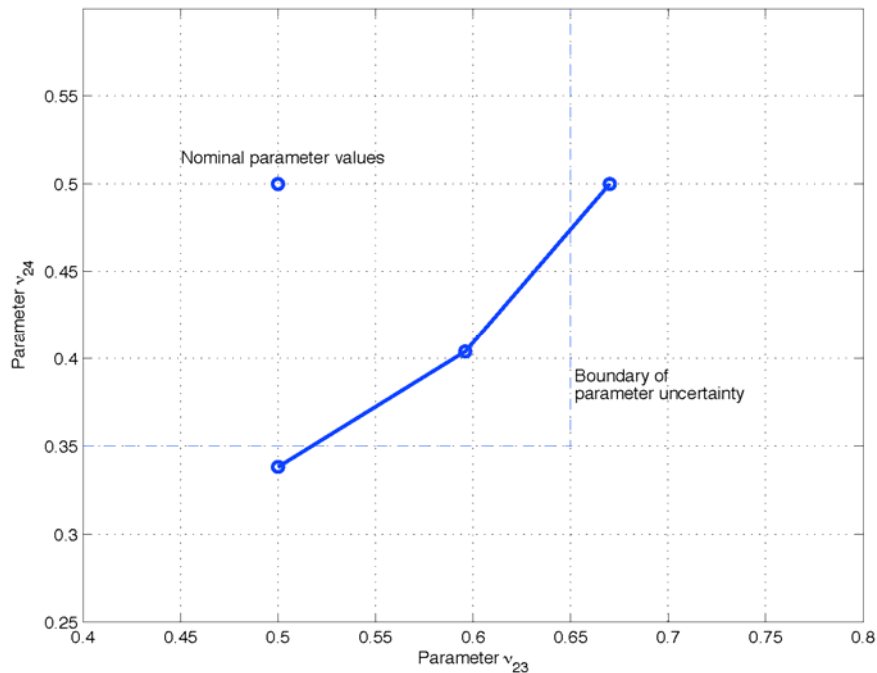


Figure 10: Parameter-space view of vulnerability to grazing conditions.

7.0 Conclusions

All models are an approximation, to some extent. Uncertainty in model-based analysis is therefore unavoidable. Model design should take into account the nature of the phenomena under investigation, with well designed models minimizing the impact of unmodeled effects and of uncertainty. In power systems, the major source of uncertainty arises from the modeling of loads. Accurate modeling is particularly challenging due to the continual variation in load composition.

Trajectory sensitivities provide a numerically tractable approach to assessing the impact of uncertainty in parameters. Such sensitivities describe the variation in the trajectory resulting from perturbations in parameters. Small sensitivities indicate that uncertainty in the respective parameters has negligible impact on behavior. Large sensitivities, on the other hand, suggest that the respective parameters exert a measurable influence on behavior. It is important to minimize the uncertainty in the latter group of parameters. This can be achieved by estimating parameter values from measurements of system disturbances. The parameter estimation process seeks to minimize the difference between measured behavior and simulated response. This difference can be formulated as a nonlinear least squares problem, with the solution obtained via a Gauss-Newton process. Trajectory sensitivities provide the gradient information that underlies that process.

The impact of uncertain parameters is generally not significant for systems that are unstressed. As the stability margin reduces, however, system behavior becomes much more sensitive to parameter perturbations. It is particularly important to consider cases that are on the verge of protection operation. In such cases, uncertainty may make the difference between protection operating or remaining inactive, with the consequences being vastly different.

Various numerical techniques are available for assessing the impact of parameter uncertainty. Trajectory sensitivities can be used to generate approximate trajectories, which in turn allow parameter uncertainty to be mapped to a bound around the nominal trajectory. The probabilistic collocation method can be used to determine (approximately) the statistical distribution associated with important features of a trajectory. This method can also be used to establish an uncertainty bound around the nominal trajectory. The likelihood that uncertain parameters may induce undesirable events, such as reactionary protection operation, can be assessed using techniques that build on grazing concepts.

References

- [1] I.A. Hiskens, "Power system modeling for inverse problems," *IEEE Transactions on Circuits and Systems I: Regular Papers*, vol. 51, no. 3, pp. 539–551, March 2004.
- [2] P.M. Frank, *Introduction to System Sensitivity Theory*, Academic Press, New York, 1978.
- [3] I.A. Hiskens and M.A. Pai, "Trajectory sensitivity analysis of hybrid systems," *IEEE Transactions on Circuits and Systems I: Fundamental Theory and Applications*, vol. 47, no. 2, pp. 204–220, February 2000.
- [4] I.A. Hiskens and J. Alseddiqui, "Sensitivity, approximation and uncertainty in power system dynamic simulation," *IEEE Transactions on Power Systems*, vol. 21, no. 4, November 2006.
- [5] W.F. Feehery, J.E. Tolsma, and P.I. Barton, "Efficient sensitivity analysis of large-scale differential-algebraic systems," *Applied Numerical Mathematics*, vol. 25, pp. 41–54, 1997.
- [6] S. Li, L. Petzold, and W. Zhu, "Sensitivity analysis of differential-algebraic equations: A comparison of methods on a special problem," *Applied Numerical Mathematics*, vol. 32, no. 8, pp. 161–174, 2000.
- [7] P.W. Sauer and M.A. Pai, *Power System Dynamics and Stability*, Prentice Hall, Upper Saddle River, NJ, 1998.
- [8] IEEE Std 421.5-1992, *IEEE Recommended Practice for Excitation System Models for Power System Stability Studies*, Institute of Electrical and Electronics Engineers, Inc., New York, 1992.
- [9] M.A. Pai, *Energy Function Analysis for Power System Stability*, Kluwer Academic Publishers, Boston, MA, 1989.
- [10] I.A. Hiskens, M.A. Pai, and T.B. Nguyen, "Dynamic contingency analysis studies for inter-area transfers," in *Proceedings of 13th Power Systems Computation Conference*, Trondheim, Norway, June 1999.
- [11] T.B. Nguyen, M.A. Pai, and I.A. Hiskens, "Sensitivity approaches for direct computation of critical parameters in a power system," *International Journal of Electrical Power and Energy Systems*, vol. 24, pp. 337–343, 2002.
- [12] I.A. Hiskens, "Nonlinear dynamic model evaluation from disturbance measurements," *IEEE Transactions on Power Systems*, vol. 16, no. 4, pp. 702–710, November 2001.
- [13] J. Nocedal and S.J. Wright, *Numerical Optimization*, Springer-Verlag, New York, 1999.
- [14] M. Burth, G.C. Verghese, and M. Velez-Reyes, "Subset selection for improved parameter estimation in on-line identification of a synchronous generator," *IEEE Transactions on Power Systems*, vol. 14, no. 1, pp. 218–225, February 1999.
- [15] G.H. Golub and C.F. Van Loan, *Matrix Computations*, Johns Hopkins University Press, Baltimore, MD, 3rd edition, 1996.
- [16] G. Andersson, P. Donalek, R. Farmer, N. Hatziaargyriou, I. Kamwa, P. Kundur, N. Martins, J. Paserba, P. Pourbeik, J. Sanchez-Gasca, R. Schulz, A. Stankovic, C. Taylor, and V. Vittal, "Causes of the 2003 major grid blackouts in

- North America and Europe, and recommended means to improve system dynamic performance,” *IEEE Transactions on Power Systems*, vol. 20, no. 4, pp. 1922–1928, November 2005.
- [17] R.H. Craven, T. George, G.B. Price, P.O. Wright, and I.A. Hiskens, “Validation of dynamic modelling methods against power system response to small and large disturbances,” in *Proceedings of CIGRE General Session*, Paris, August 1994.
- [18] V. Donde and I.A. Hiskens, “Dynamic performance assessment: Grazing and related phenomena,” *IEEE Transactions on Power Systems*, vol. 20, no. 4, pp. 1967–1975, November 2005.
- [19] V. Donde and I.A. Hiskens, “Shooting methods for locating grazing phenomena in hybrid systems,” *International Journal of Bifurcation and Chaos*, vol. 16, no. 3, pp. 671–692, March 2006.
- [20] P. Kundur, *Power System Stability and Control*, EPRI Power System Engineering Series, McGraw Hill, 1994.
- [21] J.L. Blackburn, *Protective Relaying Principles and Applications*, Marcel Dekker, New York, 2nd edition, 1998.
- [22] E. Kreyszig, *Introductory Mathematical Statistics*, Wiley, New York, 1970.
- [23] J.R. Hockenberry and B.C. Lesieutre, “Evaluation of uncertainty in dynamic simulation of power system models: The probabilistic collocation method,” *IEEE Transactions on Power Systems*, vol. 19, no. 3, pp. 1483–1491, August 2004.
- [24] P.J. Davis and P. Rabinowitz, *Methods of Numerical Integration*, Academic, New York, 1975.
- [25] T.S. Parker and L.O. Chua, *Practical Numerical Algorithms for Chaotic Systems*, Springer-Verlag, New York, NY, 1989.

FINAL PROJECT REPORT

LOAD MODELING TRANSMISSION RESEARCH

APPENDIX J

**SCOPING STUDY TO ASSESS SOLAR GENERATION
CHARACTERISTICS AND ITS IMPACTS ON LOAD MODELING**

Prepared for CIEE By:

Lawrence Berkeley National Laboratory



University of California
ciee

A CIEE Report

Table of Contents

Preface	i
Table of Contents	ii
1.0 Introduction	1
2.0 PV System Models	3
3.0 System Modeling Issues	5
3.1 Steady-State Concerns	5
3.2 Transient Concerns.....	6
4.0 Candidate System Model	9
5.0 Conclusion	11
6.0 References	11

1.0 INTRODUCTION

As concerns of climate change intensify, renewable energy technologies such as photovoltaic (PV) generation are being deployed in large scale within the electrical grid dominated by conventional electricity sources such as coal, natural gas, and nuclear generation. Solar power generation has been expanding rapidly year after year as illustrated in Fig. 1, which shows the cumulative growth in PV capacity since 1992 within selected countries that are members of International Energy Agency Photovoltaic Power Systems Programme (IEA PVPS). This reported installed capacity represents an annual rate of growth of cumulative installed capacity in the IEA PVPS countries was 40 %, up from the 34 % recorded in 2006, [1].

Annual PV installations in the United States increased 42 % from 145 MW in 2006 to 206.5 MW in 2007. Most of the growth occurred in the grid-connected sector – to over 150 MW during 2007. At the State Government level, renewable portfolio standards (RPS) requiring electricity utilities or electricity providers to supply a certain quantity of their delivered energy from renewable energy sources such as PV have been adopted in 25 states and the District of Columbia. These requirements call for as much as 20 % to 30 % of electricity to come from renewable energy sources in the next 15 to 20 years [1].

In according to a utility solar assessment study, the solar contribution could be quite considerable, realistically reaching 10 percent of total U.S. electricity generation by 2025 by deploying a combination of solar photovoltaic (PV) and concentrating solar power (CSP), as shown in Table I [2].

More than 90% of the installed PV capacity is connected to national electric grids [3]. The increasing connection of distributed generation at distribution levels from a certain penetration level may not only influence the operation and design of distribution systems, but also affect to the operation and stability of transmission system as well. In impact studies for installing these generation systems, the transmission system is generally modeled as a strong – sometimes even as an infinite – voltage source. Thus, the weakening effect that comes with high penetrations of DG therefore has been neglected. Transmission systems in the future however will become weaker and the DG systems may affect significantly the behavior of underlying distribution systems and consequently transmission systems. While there have been some studies of the potential impacts of PV systems on the distribution systems [4], there are no significant works analyzing the impacts of those on transmission systems [5]. Investigation impacts of PV systems on power systems become more important as the penetration level increases.

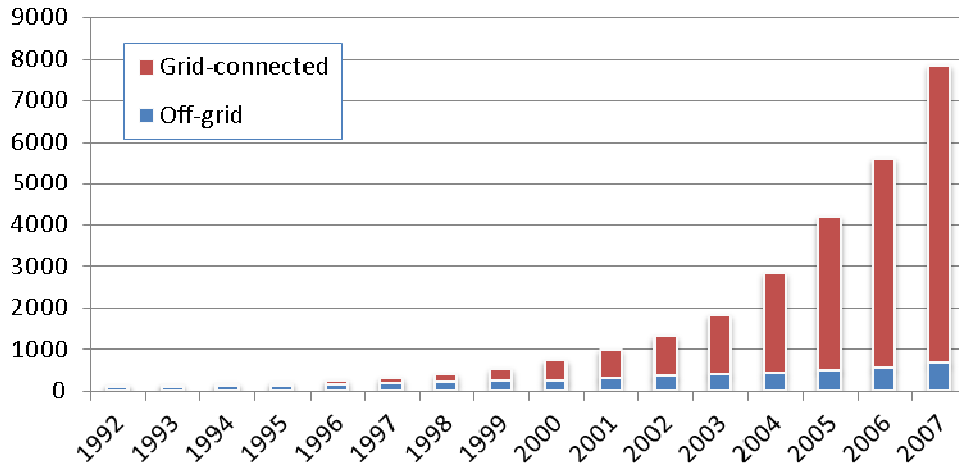


Fig.1. Cumulative installed grid-connected and off-grid PV power in the reporting countries [1].

TABLE I
U.S. Solar Installed Capacity (CSP and PV)

Year	Cumulative Capacity CSP+PV (MW)	Total Annual Generation Combined PV and CSP (MWh)	Total Projected Annual U.S. Elec. Generation/Demand All Sources (MWh)	CSP and PV Share of Total U.S.Elec. Generation
2007	1,284	2,513,665	4,119,235,320	0.06%
2010	3,027	5,849,916	4,219,402,150	0.14%
2015	15,184	29,385,504	4,397,239,160	0.67%
2020	69,260	133,345,983	4,608,068,490	2.89%
2025	255,646	485,723,159	4,858,105,640	10.00%

In this report, a state of the art literature survey is conducted, with a goal to establish a simple and accurate empiric modeling of PV systems to complement load representations that are commonly in use for power system load flow and power system stability analysis studies.

Such a PV model may be used to analyze the impact of PV systems on the transmission systems and distribution systems. The desirable model will permit the representation of all PV systems installed in a distribution area as an equivalent active load by using the source aggregation techniques. To be sure, the model intended will depend on parameters such as installed power, penetration level, location of system, weather condition, rated electrical values etc.

A brief review of the current state of the art of PV system models is presented in Section II, followed by a discussion of issues and concerns related to PV modeling in Section III. Section IV presents the features of a candidate model, followed by a concluding summary in Section V.

2.0 PV System Models

A block diagram of a grid connected PV system is shown in Fig. 2. As may be observed from the block diagram, the properties and behavior of the system will be affected on the output I-V characteristics of photovoltaic array, a maximum power point tracking (MPPT) function generally incorporated in the DC-DC converters, and the DC-AC inverter, besides variations in the solar insolation.

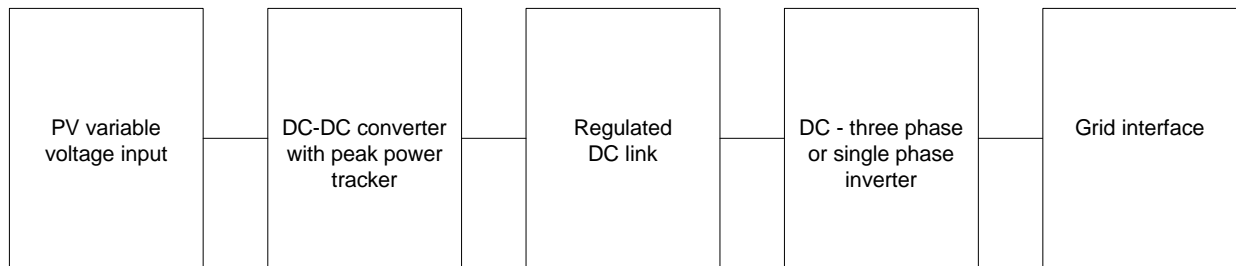


Fig.2. Block diagram of typical grid-connected PV system

There have been parallel efforts to develop models suitable to study their individual impact within the PV generation system and at the grid interface. These models may be classified into three groups: (a) model based on characteristics of PV array, (b) model based on characteristics of specific inverter structure and (c) overall PV system model. The last model is much convenient for interacting with the traditional power flow analysis to obtain steady-state operating status of power grid and PV system. The overall system models use the principle of instantaneous power balance and the principle of power electronic transformation [6,7]. Model development for study of single PV based generation devices have generally focused on developing tools that enable time-domain simulation using tools such as PSCAD, Matlab-Simulink, EMTP, etc. Reference [8] provides an excellent overview of the state of the art from this perspective.

On the other hand, among the models that are aimed at studying their collective behavior and investigate the effects of PVs on power systems, most of them are related to impacts on the distribution systems [9-10]. The few works related studying impacts on transmission systems [11-12], consider general DG technologies beyond PV systems, with machines such as synchronous and induction generators.

Most of the modeling studies of PV systems have generally been based on analytical methods. Although these models exhibit the behavior of PV systems with certain accuracy, they do not reflect the response of PV systems to variable conditions in irradiance, grid voltage, etc. While there are some studies which present experimental test results in grid-connected PV systems in order to show interaction between PV systems and power systems [4], they have not been considered in the model development, with the exception of [13]. In that paper, a model of PV generator capable of simulating its response to changes in irradiance and grid voltage is

established. However, the effect of variations in grid frequency has not been taken into consideration in the model.

3.0 PV System Modeling Issues

When modeling the PV systems in the electric power systems, major issues to be accounted may be grouped into two categories; steady state concerns and transient concerns, as discussed further in the following sub-sections.

3.1. Steady State Concerns

The main steady state issue concerning PV generation is the variation of power generation, which is affected by environmental factors such as location, weather, and climate. The single major parameter that affects the output power of PV generator is the irradiance. Since the irradiance is related to latitude, geographical location of PV systems is used to estimate the irradiance consequently output power.

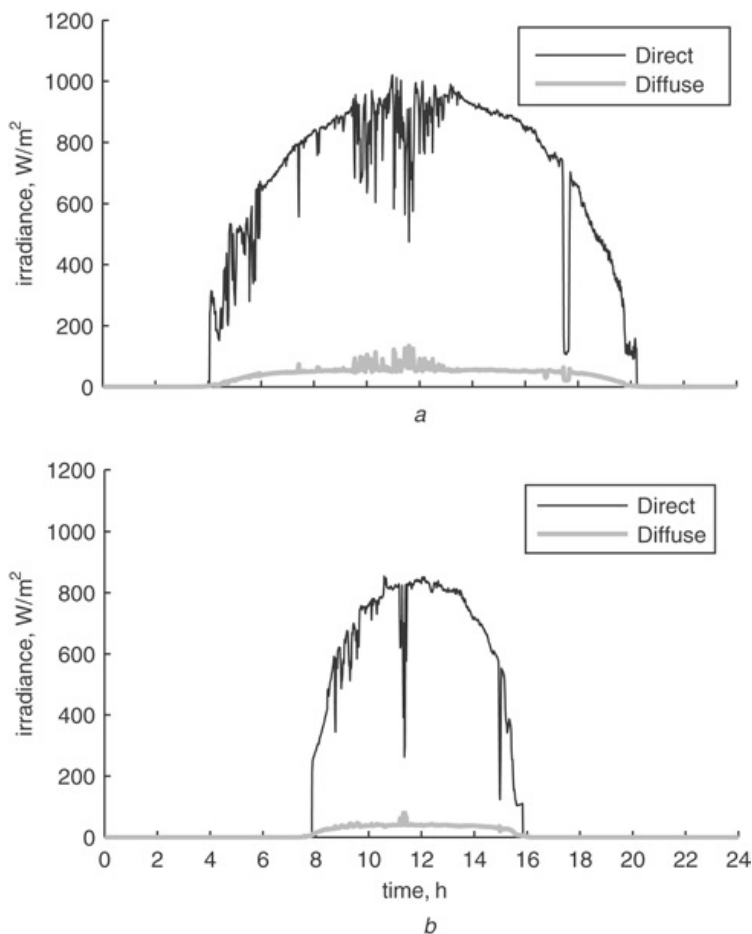


Fig. 3. A graph of measured direct and diffuse irradiance on (a) a summer day, and (b) a winter day (From [4])

For instance, it has been observed daily average irradiance values ranged from 5.0 to 7.5 $kWh/m^2/day$ from a measurement study in which the nineteen monitored systems are located at

geographically diverse sites from San Diego County in the South to Willits in the North [14]. Besides the location, the irradiance changes from hour to hour, day to day, or month to month, output of the PV system may vary with time. For selected summer and winter days, direct and diffuse irradiance measured in study is shown in Fig. 3, [4]. As shown from figure, irradiance changes not only during daytime, but also with season.

PV array power output varies depending on module temperature besides irradiance level. It means that PV array output consequently depends on the weather conditions such as ambient temperature and wind speed. Thus, alternative approaches based on weather rather than cell temperatures may be used to develop system capacity estimates [14].

The steady state irradiance at the location may be more readily integrated with the power system modeling tools. There are some data sources open to public related to PV generation. European Commission Photovoltaic Geographical Information System (PVGIS) has interactive maps for Europe and Africa [14]. National Renewable Energy Laboratory (NREL) has solar maps for USA [15]. These organizations have dynamic solar maps that calculate daily and monthly irradiance throughout the year. Using these data, it may be found the solar insolation for a given location and a specific time.

On the other hand, the properties of the PV generation system itself are more difficult to aggregate. The immediate variability conditions of the generation system will depend on the type of solar array, orientation of the solar array, aging of the solar array, dust, dirt, and snow build up on the solar array, microclimate conditions such as local cloud-cover, etc.

3.2. Transient Concerns

The properties of the components that comprise the PV generation system contribute to the transient issues that affect the behavior of the generation system in the electric grid. The transient concerns that would to be considered in developing the model may be conveniently represented by the voltage and frequency sensitivity PV array properties, MPPT dynamics, DC-DC converter dynamics, overall power conversion efficiency, anti-islanding protection and decoupling protection which inverters for PV systems should comply with, etc.

3.2.1. Frequency and Voltage Sensitivity

Determining the real power and reactive power sensitivity with respect to grid voltage and frequency is required to model PV system accurately. The response of a commercial PV generator to grid voltage change has been studied in laboratory conditions as reported in [13]. Fig.4 illustrates the variation of system output real power to voltage variations at the grid connections. In this study, the effect of frequency change has not been considered. While the power factor (PF) of the PV system is typically 1.0 in residential applications, central power stations can be produced reactive power to realize local voltage regulation. The need and impact of such operational variations have not been definitively established and hence a study of the system with respect to voltage and frequency is in order.

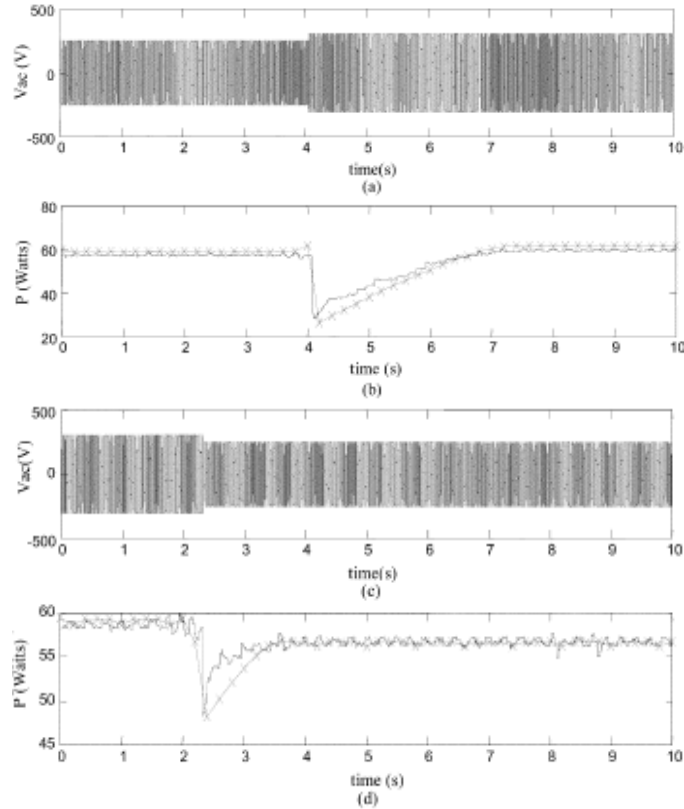


Fig. 4. Response of the PV generator to increase and decrease in grid voltage (From [13])

3.2.2. MPPT Dynamics

A field survey of 387 different models of PV generation systems below 10 kW reported in [17], found that all the units contain a MPPT module. Furthermore, the results of experiments carried out with three different inverters have indicated that the response time of PV generating units is significantly affected by MPPT module dynamics and efficiency [13]. Therefore MPPT dynamics of inverters that form the aggregate representation should be accounted appropriately in the system level models.

3.2.3. Efficiency and derating

While a typical PV system may be rated at a particular power level, equipment dynamics can have drastic impact on output of the system. Power conversion efficiency of the PV system and the de-rating factor of the design together may affect the output power of the system when grid voltage and frequency have variations. The de-rating factors and conversion efficiency may be in 0.1-0.96 ranges, while efficiency may be in the 0.7-0.98 ranges depending on the operating conditions and design cases. Therefore incorporating the collective behavior among these factors are also important in developing an appropriate system level model

3.2.4. Array properties

The solar array of the PV system may vary depending on the crystal used in solar cells; monocrystalline, polycrystalline and amorphous. Since solar cells produced from these

materials have different levels of efficiency and aging behavior, consequently efficiencies and behaviors of PV arrays composed various solar cells also show variety.

3.2.5. Protection set points

Islanding is a condition that occurs when a portion of the utility system is disconnected from the remainder of the utility system but remains energized by the distributed resource (DR). Due to concerns associated with islanded system such as safety issues for service personnel and asynchronous reclose which can cause equipments to damage, the islanding is not usually desired [18, 19]. Thus behavior of the anti-island function of the PV inverter should be considered in terms of its behavior during utility disconnection and disturbances.

Furthermore, compliance settings related to standards for distributed energy resources such as IEEE-1547, UL-1741 require decoupling protection requirements besides other regulations. For instance, a survey of the voltage tolerance curves presented in [19] which investigate 9 commercial PV inverters in the range of about 0.2 to 4 kW reports that all inverters except one are highly sensitive to voltage sags. None of them are capable of withstanding any voltage sag deeper than %50, lasting longer than 40 ms, as illustrated in Fig. 5. Furthermore, voltage rise may also occur at the point of interconnection to the grid. Since interconnection requirements require disconnection during abnormal voltages, PV systems would disconnect themselves from the power systems under such conditions subject to their protection settings, and variable dynamics in response time. Therefore, it is important to consider and include these aspects in the PV system model representation to ensure faithful predictions from the studies.

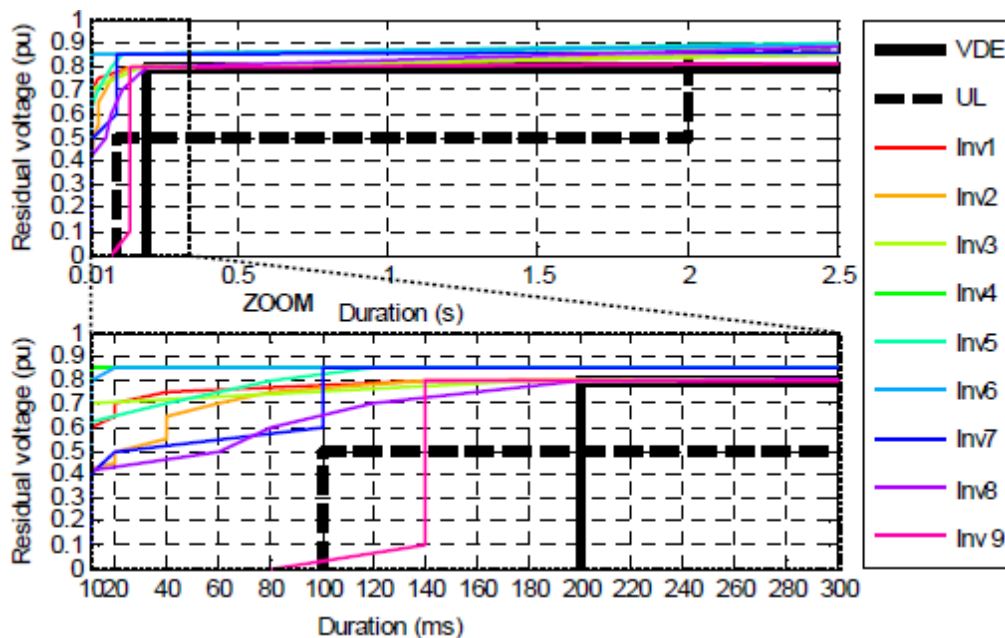


Fig. 5. Voltage tolerance curves of 9 commercial PV inverters (From [19])

3.2.6. Penetration and census

Because the effects on the power systems vary with levels of PV penetration and type of PV generation system from among different commercial manufacturers and vendors, these aspects will have to be accounted appropriately in developing the system model.

4.0 Candidate System Model

Within the context of power system studies, system components such as power sources, loads, transformers and interconnections are widely modeled in an aggregate manner. In this mix, considering the PV system as an active load that injects energy into power system may provide more convenience, since they have not internal inertia. However, establishing the representative analytical model that presents accurately the characteristic of grid-connected PV systems is particularly challenging in light of the discussions presented above. Alternatively, empirical model may be a more practical solution, based on laboratory scale experimental results and data from the real field measurements [13,14,17,20]. Such load modeling approach in power systems is among the preferred approaches in developing and validating modeling tools [21].

It should be mentioned that detailed component-level models (such as those including models of PV array, MPPT part, power electronic converter, etc.) are suitable for analysis of specific PV unit or grid-independent PV system. But the precision of such modeling is generally lost in grid-level studies, where wide aggregations are made of large number PV units (such as residential area installed PV units). Therefore grid-level models that reasonably represent of PV units on the power systems should be main motivation of this study. Towards this aim, an appropriate aggregation method similar to that applied in the load aggregation may be used in order to represent the combined effect of the PV systems installed in a distribution area [22-23].

With such an approach, a simple, practical and faithful PV system model for electrical power systems may be established. The approach should also use an aggregated representation of distribution systems with dynamic and static loads as well as PV systems that is adequate enough for system level studies. Fig. 6 illustrates a candidate representation for PV installations within the distribution system by including a 'PV load model' to exist the load model structure.

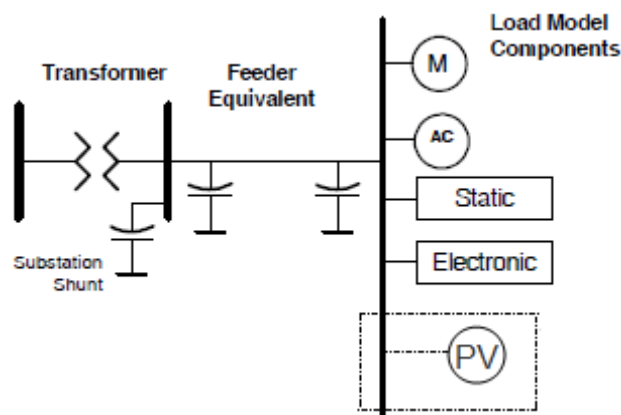


Fig. 6. Structure of a candidate PV system model to be incorporated within the framework of load modeling

The heart of the candidate model is the behavioral representation of the inverter component including the various dynamics such as efficiency, MPPT and protection functions. In order to

develop this, detailed tests may be carried out using several commercial PV inverters found in the market. The objective of these tests is to investigate the inverter dynamics performance during some events typically found in the grid such as voltage, and frequency fluctuations and oscillations. Additionally, transient response tests may also be carried out. For instance, a switching transient test may be used to determine the time delay when suddenly the inverter is connected to grid. Inverter anti-island test, short circuit test, rapid power fluctuation test, etc, will provide complementary data to develop a faithful system representation. Based on test data from an array of tests on a variety of inverters, an aggregate representation that provides a weighted average of model parameters depending on the distribution of different devices among the population within the distribution system.

The development of a practical model with a user-friendly interface will be a challenging task, even given all the representative test data. The results from the test data would be classified and correlated for similarities, and differentiated for variations and an appropriate model representation to accurately represent the bulk behavior will need to be developed. On the other hand, based on the model it would be very easy to obtain results needed by entering some parameters, such as installed power, penetration level, population distribution among different manufacturers' inverters as appropriate, location of system, weather conditions, rated electrical values, into the appropriate program interface.

5.0 Conclusions

In this report, various issues related to PV generation system representation in power system studies have been discussed. A survey of the state of the art has been presented, highlighting the particular limitations and useful approaches in the literature. A summary conclusion may be stated as, "Though there are several PV modeling studies, none of them are suitable for power flow analysis at the grid-level studies in which wide aggregations are made of large number PV generation sources". Various parametric and sensitivity aspects of PV generation sources have been identified and discussed on the basis of the literature in the field, and a candidate modeling approach has been presented. The immediate step in developing the approach further is initiating, conducting and completing comprehensive tests on commercial PV generation inverters in laboratories capable of providing grid emulation. It is learned that Southern California Edison is initiating such tests in concert with the National Renewable Energy Labs [25].

On the basis of the results from the tests, an aggregation and representation method may be developed as a follow on activity. Such an approach will lead to useful and practical tools for studying and preparing for high penetration of PV in the electric grid.

6.0 References

- [1] Trends in Photovoltaic Applications Survey report of selected IEA countries between 1992 and 2007, International Energy Agency Report, 2008
- [2] Utility Solar Assessment (USA) Study Reaching Ten Percent Solar by 2025, Clean-Edge, Co-op Americ
- [3] Picault, D.; Raison, B.; Bacha, S., "Guidelines for evaluating grid connected PV system topologies," Industrial Technology, 2009. ICIT 2009. IEEE International Conference on , vol., no., pp.1-5, 10-13 Feb. 2009
- [4] Thomson, M.; Infield, D.G., "Impact of widespread photovoltaics generation on distribution systems" Renewable Power Generation, IET, vol.1, no.1, pp.33-40, March 2007
- [5] Boemer, J.C.; Gibescu, M.; Kling, W.L., "Dynamic models for transient stability analysis of transmission and distribution systems with distributed generation: An overview" PowerTech, 2009 IEEE Bucharest, vol., no., pp.1-8, June 28 2009-July 2 2009
- [6] Wang Yi-Bo; Wu Chun-Sheng; Liao Hua; Xu Hong-Hua, "Steady-state model and power flow analysis of grid-connected photovoltaic power system" Industrial Technology, 2008. ICIT 2008. IEEE International Conference on, vol., no., pp.1-6, 21-24 April 2008
- [7] Papanikolaou, N.P.; Tatakis, E.C.; Kyritsis, A.C., "Analytical model for PV – Distributed generators, suitable for power systems studies" Power Electronics and Applications, 2009. EPE'09. 13th European Conference on, vol., no., pp.1-10, 8-10 Sept. 2009.
- [8] Amirnaser Yazdani, Anarita Difazio, Hamidreza Ghoddami, Mario Russo, Mehrdad Kazerani, and Kai Strunz, "A General Discussion on Modeling and Simulation of Three-Phase Single-Stage Grid-Connected PhotoVoltaic (PV) Systems", Paper presented at IEEE PES General Meeting, July 2009.
- [9] Azmy, A.M.; Erlich, I., "Identification of dynamic equivalents for distribution power networks using recurrent ANNs" Power Systems Conference and Exposition, 2004. IEEE PES, vol., no., pp. 348-353 vol.1, 10-13 Oct. 2004
- [10] Canova, A.; Giaccone, L.; Spertino, F.; Tartaglia, M., "Electrical Impact of Photovoltaic Plant in Distributed Network," Industry Applications, IEEE Transactions on , vol.45, no.1, pp.341-347, Jan.-feb. 2009
- [11] Thong, V.V.; Driesen, J.; Belmans, R., "Transmission system operation concerns with high penetration level of distributed generation," Universities Power Engineering Conference, 2007. UPEC 2007. 42nd International , vol., no., pp.867-871, 4-6 Sept. 2007
- [12] Reza, M.; Sloomweg, J.G.; Schavemaker, P.H.; Kling, W.L.; van der Sluis, L., "Investigating impacts of distributed generation on transmission system stability," Power Tech Conference Proceedings, 2003 IEEE Bologna , vol.2, no., pp. 7 pp. Vol.2-, 23-26 June 2003

- [13] Yun Tiam Tan; Kirschen, D.S.; Jenkins, N., "A model of PV generation suitable for stability analysis," Energy Conversion, IEEE Transactions on , vol.19, no.4, pp. 748-755, Dec. 2004
- [14] "Measured Performance of California Buydown Program Residential PV Systems", California Energy Commission, Consultant Report, 2004
- [15] <http://re.jrc.ec.europa.eu/pvgis>, European Commission, Joint Research Centre, Photovoltaic Geographical Information System.
- [16] <http://www.nrel.gov/gis/solar.html>, U.S. Department of energy, National Renewable Energy Laboratory
- [17] Salas, V.; Debora, P.J.; Olias, E., "Field analysis of commercial PV inverters in the 5 kW power range with respect to MPPT effectively," Power Electronics and Applications, 2009. EPE '09. 13th European Conference on , vol., no., pp.1-7, 8-10 Sept. 2009
- [18] Fei Wang; Chengcheng Zhang; Zengqiang Mi, "Anti-islanding Detection and Protection for Grid Connected PV System Using Instantaneous Power Theory," Industrial and Information Systems, 2009. IIS '09. International Conference on , vol., no., pp.413-416, 24-25 April 2009
- [19] Kunte, R.S.; Wenzhong Gao, "Comparison and review of islanding detection techniques for distributed energy resources," Power Symposium, 2008. NAPS '08. 40th North American , vol., no., pp.1-8, 28-30 Sept. 2008
- [20] B. Bletterie, R. Brundlinger, and H. Fechner, "Sensitivity of photovoltaic inverters to voltage sags-test results for a set of commercial products" , IEE Conf. Pub. 2005, v2-67 (2005)
- [21] Kosterev, D.; Meklin, A.; Undrill, J.; Lesieutre, B.; Price, W.; Chassin, D.; Bravo, R.; Yang, S., "Load modeling in power system studies: WECC progress update," Power and Energy Society General Meeting - Conversion and Delivery of Electrical Energy in the 21st Century, 2008 IEEE , vol., no., pp.1-8, 20-24 July 2008
- [22] Price, W.W.; Wirgau, K.A.; Murdoch, A.; Mitsche, J.V.; Vaahedi, E.; El-Kady, M., "Load modeling for power flow and transient stability computer studies," Power Systems, IEEE Transactions on , vol.3, no.1, pp.180-187, Feb 1988
- [23] Nozari, Farhad; Kankam, M. David; Price, William W., "Aggregation of Induction Motors for Transient Stability Load Modeling," Power Systems, IEEE Transactions on , vol.2, no.4, pp.1096-1103, Nov. 1987
- [24] Conti, S.; Raiti, S., "Probabilistic Load Flow for Distribution Networks with Photovoltaic Generators Part 1: Theoretical Concepts and Models" Clean Electrical Power, 2007. ICCEP'07. International Conference on, vol., no., pp.132-136, 21-23 May 2007.
- [25] Richard Bravo, Inverter Test Procedures Solar Generation Impact Study Private e-mail communication, 22 Dec 2009.

FINAL PROJECT REPORT

LOAD MODELING TRANSMISSION RESEARCH

APPENDIX K

FAULT-INDUCED DELAYED VOLTAGE RECOVERY

Prepared for CIEE By:

Lawrence Berkeley National Laboratory



University of California
ciee

A CIEE Report

Acknowledgments

The author would like to thank Larry Miller, Llyod Cibulka, and Merwin Brown of the California Institute for Energy and Environment, Richard Bravo of Southern California Edison, and Dmitry Kosterev of the Bonneville Power Administration.

Table of Contents

Acknowledgments	i
Table of Contents	iii
1.0 Introduction	1
2.0 FIDVR Phenomenon	4
3.0 Solutions	8
3.1 Customer Solutions	8
3.2 System Solutions	9
4.0 Conclusions and Recommendations	11

1.0 Introduction

Fault Induced Delayed Voltage Recovery (FIDVR) is a phenomenon observed in the electric power grid in which, as the phrase suggests, is a sustained voltage depression after a fault, eventually rising after some time. A descriptive plot is shown below in Figures 1. In this plot the depressed voltage is observed just after the fault is cleared. The voltage recovery time varies depending on the event, but typical durations range in seconds to tens of seconds. The voltage slowly recovers as the A/C load trips off by its internal protection; once then entire stalled A/C trip off the system, the voltage is higher than the pre-fault level. Reacting to the high voltage, the capacitors switch off to reduce this overvoltage. This is observed in Figure 1 as the voltage tends back down to a nominal level. Finally at the far right of the plot, we note that the voltage subsequently lowers to a level that is again below the pre-fault level. Eventually, on a timescale beyond that shown in Figure 1, system controls will again normalize the voltage.

The initial depressed voltage is troubling because it represents a relatively long period in which the voltage is not controlled. It persists for seconds, instead of cycles. There is justifiable concern that this behavior could directly lead to a widespread outage or leave the system vulnerable to a significant outage as the results of another disturbance. For the same reason, the lower voltage at the end of the trajectory is potentially vulnerable to a second disturbance, especially if key network voltage support is temporarily lacking. Many small outages and several larger outages are attributed to the FIDVR phenomenon.

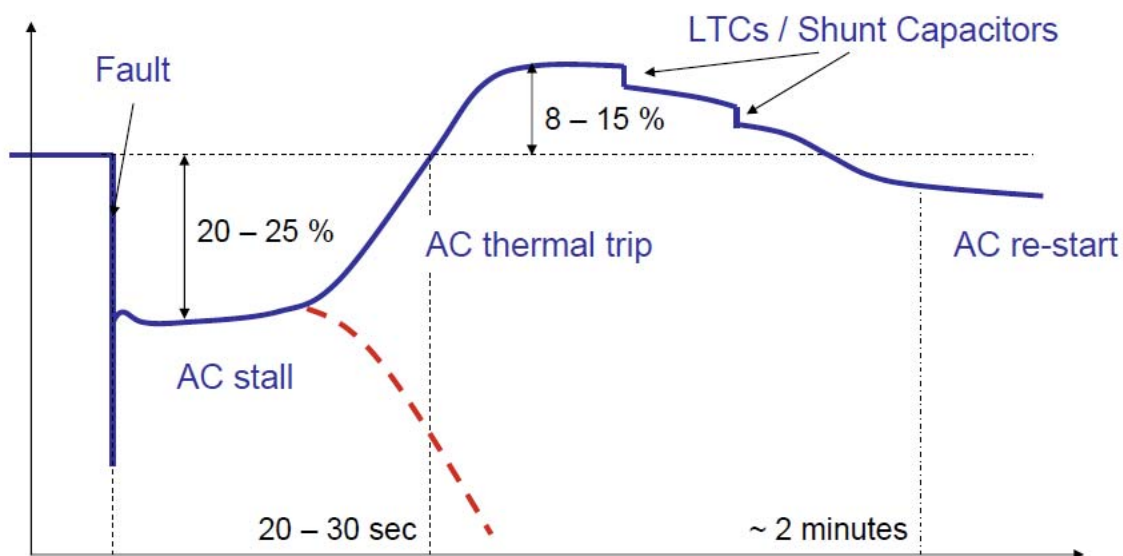


Figure 1. Voltage during a FIDVR event (courtesy of D. Kosterev, BPA).

Fault-induced delayed voltage recovery is not a new phenomenon. While most reports of events are anecdotal, there are a few published papers describing certain events and studying the causes. In regions with a high percentage of air conditioner loads, the problem persists.

In their 1992 paper¹, engineers from Southern California Edison discuss voltage recovery problems they had encountered in the desert regions that they serve. The largest event involved a 1000 square mile region. They also mention other similar incidents at other utilities, including a major blackout in Memphis in 1987.

In his 1997 paper², Florida Power and Light Engineering John Shaffer reports eight incidents of delayed voltage recovery over the preceding decade. These resulted in 200-825 MW of lost load. He mentions a 1988 event with a 10-second voltage recovery. He also points out that most of the load loss was actuated by device protection (in contrast to system controlled protection).

More recent events are not described in journal articles, but have been presented at conferences and workshops. Southern California Edison continues to observe FIDVR events and they are leading research to study causes and propose solutions. One paper presents an undervoltage protection scheme and also shows a plot of a recent disturbance with a 30 second voltage recovery time.³

The state of the art in FIDVR reporting and research has been presented at two recent DOE workshops, in 2008 and 2009. The presentations from these workshops and the related NERC whitepaper summarize present activity in this area.⁴ Events mentioned in presentations at the 2008 workshop include

- More than 50 events observed in Southern California Edison (Devers, Antelope, Vally, Lugo, Rector, Villa Park). The Lugo plane crash resulted in 3500 MW lost load.⁵
- Several incidences in the Arizona Public Service:⁶
 - 2 Pinnacle Peak Capacitor Faults. The second resulted in 1000 MW load loss.

¹ Williams, B.R., W.R. Schmus, and D.C. Dawson, "Transmission Voltage Recovery Delayed by Stalled Air Conditioner Compressors," IEEE Transactions on Power Systems, Vol. 7, No. 3, August 1992.

² Shaffer, J.W., "Air Conditioner Response to Transmission Faults," IEEE Transactions on Power Systems, Vol. 12, No 2, May 1997.

³ Lu, N., B. Yang, Z Huang, and R. Bravo, "The System Impact of Air Conditioner Under-voltage Protection Schemes," Power System Conference and Exposition, 15-18 March, 2009.

⁴ 2008 workshop presentations are available at <http://sites.energetics.com/acstallingworkshop/agenda.html>

The 2009 workshop presentations are not yet posted. The NERC white paper is available at www.nerc.com/docs/pc/tis/FIDV_R_Tech_Ref_V1-1_PC_Approved.pdf.

⁵ Bob Yinger, "A/C/ Stalling at SCE," DOE Workshop, April 22, 2008.

⁶ Baj Agrawal, "APS Experience," DOE Workshop, April 22, 2008.

- Hassayampa 500 kV Fault. Loss of 440 MW load and 2600 MW generation.
- Southern Company⁷ reported on the Union City event in which 1900 MW of load was lost. Almost all the load was tripped by induction motor protection.

At the 2009 FIDVR workshop emphasized the following items:

- Studies suggest that SVCs help alleviate the problem but does not prevent A/C from stalling therefore the FIDVR events may still occur
- Studies also suggest that undervoltage protection devices in A/C units prevents the FIDVR events but creates another problem that is instantaneous overvoltages at high penetrations for these devices.
- The proper solutions is to have the A/C units ride thru the voltage transient or trip only the A/C units that stalled
- NERC TIS will be creating a site under their website to incorporate FIDVR so that other utilities in the country learn from the California experience.

It is clear that FIDVR events can be consequential, they persist, and they pose a challenge to the reliable operation of the power grid.

In this report we summarize some of the research on this topic and discuss potential solutions. In the next section of this report we present the underlying causes that drive FIDVR events, predominately the stalling of compressor-driven induction motors. In the following section we discuss potential solutions. These include the changes that could be made to units, and system controls that could mitigate FIDVR. We also discuss the challenges with implementing the solutions.

⁷ Taylor, "Recent Experience with Fault Induced Delayed Voltage Recovery," DOE Workshop, April 22, 2008.

2.0 FIDVR Phenomenon

To consider solutions to avoid or mitigate FIDVR, it is necessary to study the cause. The physical mechanism to explain the phenomenon is related to the end-use load characteristics of air conditioners and other motor-driven compressor loads. To understand how these end-use devices react to faults, and how they can effect a slow-to-recover depressed voltage, it is necessary to consider their operation in detail.

For a compressor, the average mechanical load faced by an induction motor increases as it literally drives pistons (reciprocating compressor) or turns a “scroll” (scroll type compressor) to compress a gas. The more it is compressed, the greater the operational motor torque is needed. The electrical torque capability for an induction motor is nonlinear and depends on its operating speed. In Figure 2 we show a typical “torque-speed” curve for an induction motor.

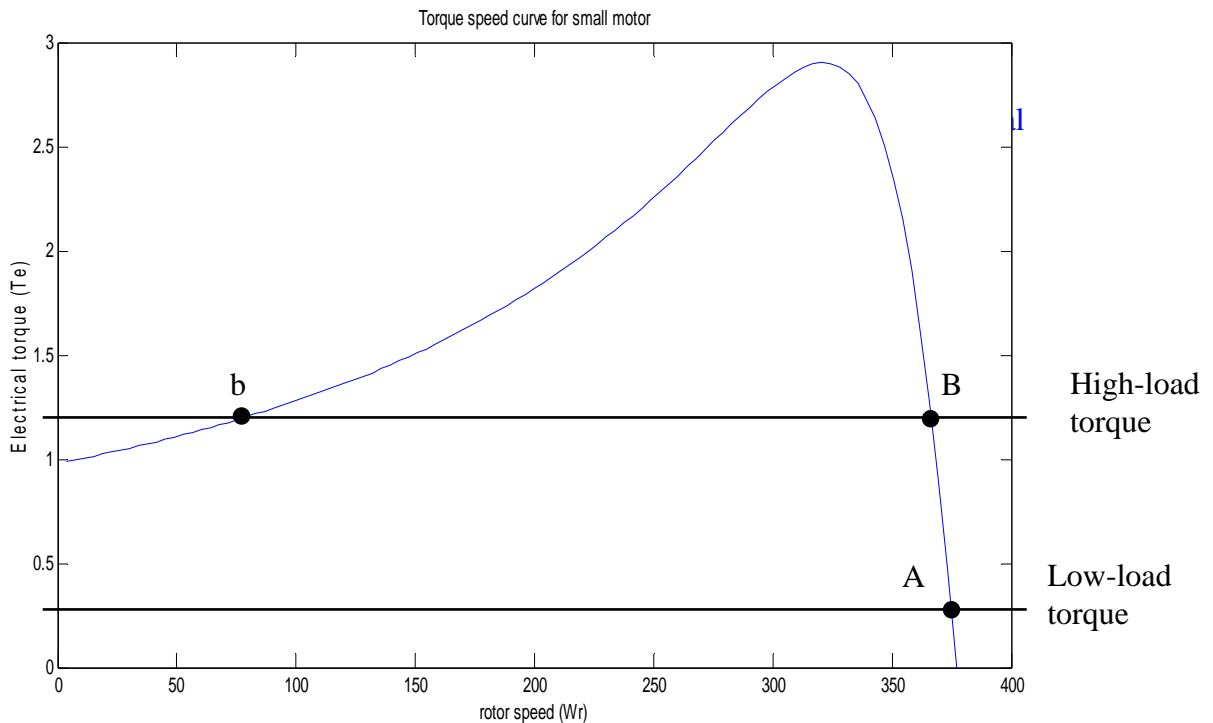


Figure 2. Torque Speed Curve for Motor.

The horizontal axis in Figure 2 is the motor speed expressed in electrical radians/second, and ranges from zero (blocked rotor or stalled) to synchronous speed: $2\pi 60$ (60 Hz). The vertical axis is torque. Superimposed on this plot are two straight-line mechanical load torque curves; one is a low load line meant to represent the compressor when it has been inactive for several minutes. The high load line represents the normal operating load under compression. Important for our discussion is note that the zero-speed electrical torque is less than mechanical torque load. (We discuss this more below.)

When a compressor initially turns on after a few minutes of inactivity the load torque is low, and the motor quickly accelerates to normal high-speed operation. This is denoted by point “A” in Figure 2. With increased compression the mechanical load torque increases and operation tends to point “B” on the plot. This is the normal operating condition for the compressor, and this torque represents the equality of average load torque and electrical torque. For this level of mechanical load we note a second equilibrium denoted as “b” in the plot. Dynamically this other point is unstable.

For purposes of using Figure 2 to describe the phenomenon of FIDVR, we note that this high load torque line intersects the zero-speed axis at a point higher than the electrical load torque. That is, the load torque exceeds the zero-speed torque capability of the motor; if the motor were to stall, it would not be able to restart. And that is exactly what happens: a temporary fault drops the voltage low enough for air conditioner motors to stop, and they are unable to restart when the fault is cleared. The stalled motors draw significant current which causes the observed depressed voltages. Protection equipment eventually remedies this situation.

Motors have two types of protection that are relevant: Contactors that disconnect when the voltage drops below 40%, and an inverse-time characteristic current relay (thermal protection). In practice the stalled voltage is typically larger than the 40% threshold, so the stalled motors stay connected to the grid. The thermal protection does actuate, removing the stalled motors from the grid. As the motors trip off-line, the voltage recovers. The motors don’t trip off simultaneously (3-15 seconds according to one manufacturer⁸), so the recovery appears gradual. The “delay” in “delayed voltage recovery” is due to the delay in motor thermal protection operation.

Once the motors are offline, they will remain offline for some time, until the compressor pressure equilibrates and the motor can restart. (Readers with newer air conditioners, dehumidifiers and other compressor-driven loads may be familiar with this characteristic: these appliances will delay a few minutes to restart after they have been turned off.) The grid response to the accumulated loss of load is to increase the voltage above pre-fault level. As previously noted, network controls will react to then lower the voltage.

⁸ Jayanth, J., and H Pham, “Residential AC Compressor: Low Line Voltage Behavior,” DOE Workshop, April 22, 2008.

The second vulnerable region occurs when air conditioners turn back on. This increased load draws the down the voltage, and without reactive power support the system is potentially susceptible to subsequent events.

The phenomenon as described in the preceding paragraphs is generally accepted as the fundamental mechanism, and it is the mechanism described in the early papers.⁹ More recent testing and model development conducted in the WECC supports this description of the FIDVR mechanism.

There are a few recent additions to the knowledge in this area that are worth mentioning. The models that are examined in the early papers represented an induction motor driving an assumed constant load torque. There are two deficiencies related to the mechanical load in that model: the inertia of the compressor is over-estimated, and the mechanical load torque is not constant. Both of these points help explain the very fast stalling time observed in laboratory tests and in the field. The air conditioner load appears to stall during the fault - measured in cycles. In the models used in the early papers the stalling of the motors is simulated by assertion – when there is voltage drop below a certain threshold, the motor is declared to be in a stalled state. Whereas simulation of the motors using parameters given in the papers do not necessarily capture such a quick stall. In Shaffer's paper¹⁰, critical clearing times are given for three motor models subject to faults of varying severity. For those severe faults with a fault voltage of 0 volts, the critical clearing time to avoid a stall ranges from 2 to 6 cycles. For fault voltages in the range of 50-55% nominal, the critical clearing time ranged from 5 to 21 cycles, depending on the initial load torque (with the range of 19-21 cycles for 1.0 pu torque). The tests in Williamson paper¹¹ demonstrated that the air conditioners stalled within 5 cycles (their fastest test) for fault voltages below 60%. Recent laboratory tests note this quick stall - within 3 cycles (their fastest test).¹²

The models and measurements can be reconciled. First the assumed inertia in the early simulations is too large ($H = 0.28$ seconds). After recent testing, a compressor was disassembled, the rotor pulled, and its inertia was estimated to be $H = 0.03$ seconds. Laboratory tests suggest an inertia of $H=0.03$ to 0.05 seconds. This suggests a much greater propensity to stall.

Second, the load torque is not constant. One of the comments on the Shaffer paper suggested that the compressor torque may not be constant.¹³ At the time, design engineers had informed

⁹ Williams et al; and Shaffer.

¹⁰ Shaffer.

¹¹ Williamson et al.

¹² Gaikwad, A.M., R.J. Bravo, D. Kosterev, S. Yang, A. Maitra, P. Pourbeik, B. Agrawal, R. Ying, and D. Brooks, "Results of Residential Air Conditioner Testing in WECC," IEEE Power Engineering Society General Meeting, 20-24 July, 2008.

¹³ Pal, M.K, Discussion of "Air Conditioner Response to Transmission Faults."

him that the torque could be considered constant for a few seconds after a fault. Recent conversations with air conditioner manufacturers indicate that the load torque is position dependent as the motor drives pistons (reciprocating) or turns the off-center scroll. The compressor load torque resembles a strong triangle wave, and the peak mechanical load torque may exceed peak electrical torque during operation. The compressor relies on the motor inertia to carry through this peak.

The WECC Load Model Task Force has been active in developing improved load models to simulate FIDVR phenomenon. This work has been carried out in large part with support from the California Energy Commission.¹⁴ This work has resulted in the development of two models for simulating compressor-driven motors. The static performance model captures the running and stalled voltage-dependent load characteristics of the motors, with a voltage-specified transition point.¹⁵ A dynamic phasor model suitable for use in positive sequence simulations was developed from a traditional single phase motor model.¹⁶ Both are being incorporated in the standard simulation packages used to study power system behavior in the WECC.

With this understanding of the FIDVR we turn to potential solutions.

¹⁴ WECC Load Modeling Transmission Research Project, CEC Contract 500-02-004.

¹⁵ N. Lu, Y. Xie and Z. Huang, "Air Conditioner Compressor Performance Model," PNNL-177796, Pacific Northwest National Laboratory, 2008.

¹⁶ Lesieutre, B.C., "Recommended Model for Single Phase Compressor," CEC PIER Interim Project Report, Contract 500-02-004, September 2008.

3.0 Solutions

Eliminating FIDVR events will be challenging. The NERC whitepaper emphasizes this point in its executive summary: **“FIDVR events can – and have – occurred following faults cleared in as little as 3 cycles! The number and impact of FIDVR events can be decreased, but their elimination in the near term is unlikely.”** (their emphasis.) To eliminate these events, it would be needed to prevent the air conditioner motors from stalling. Even if new air conditioners were manufactured to avoid stalling, wide-spread use of new units to replace the existing installed base would take many years to change.

In this section we discuss these issues and summarize strategies for mitigating FIDVR problems. We consider customer-level solutions and system level solutions.

3.1. Customer-Level Solutions

The most effective controls may be implemented at the source of the problem: the air conditioning units. There are at least two changes that could reduce FIDVR event or severity of events:

1. Low voltage ride through. Units could be designed to withstand low voltage conditions for a short time to prevent stalling during the fault.
2. Low voltage disconnect. Units could be quickly tripped when the voltage drops to a point at which they would stall. Then, the units would return to operation after random delays, to stagger the return of load.

The first item is ideal in that it would eliminate the problem for normally cleared faults. The application of this solution would require not insignificant changes to the present design of units. One could consider over-sizing motors such that the no-load electrical torque exceeds the normal mechanical torque, with the idea that the motors would be able to restart upon re-excitation after the fault clearing. However, it is not clear that this would be successful – if motors did stall during the fault but attempted to restart simultaneously after the fault, it is likely the voltage would remain low initially. This approach would likely lessen the duration of the event, as some motors trip off-line others may succeed in restarting. Alternatively, one could increase the inertia of the motor/compressor to provide stored mechanical energy with which to ride through the event. Finally, local electrical energy storage coupled through power electronics (also driving the motor), could be implemented to achieve a low voltage ride-through capability. These latter two solutions are technologically feasible, but would increase the cost of such units. It should be expected that manufacturers would be reluctant to implement these without further and equal motivation. Any such changes would likely required modification of standards so that all manufacturers are provided the same objective.

The second item – low voltage disconnect – is practical, and offers the opportunity for effective retrofitting. This type of protection could be implemented on new units, and while it would increase costs, it is not likely be large compared to the solutions mentioned above. Also, this solution could be implemented by under-voltage relays or digital thermostatic control. The low voltage disconnect and delayed reconnect could be programmed into a modern thermostat.¹⁷ A program to retrofit digital thermostats could reduce the FIDVR

¹⁷ To use thermostatic control, the thermostat would need some detection of low line voltage. Otherwise, an under-voltage relay can perform a similar function.

problem when coordinated with system controls, and it should be considered. (See Lu et al for an analysis of under-voltage protection schemes in this context.¹⁸) More generally, new communication and control technologies that enable a customer to actively participate in grid function (i.e., the “smart grid”) could be applied to FIDVR problems.

Unfortunately, the low voltage disconnect solution does not address all of the problem. It should effectively eliminate the delayed voltage recovery portion of the behavior at the expense of immediate loss of load. This will likely result in immediate overvoltages in the system. System level controls would need to be designed to handle this situation.

3.2. System Solutions

System solutions are covered in detail in the NERC whitepaper. Here we draw on the discussion in that document. These solutions include

1. Reduced fault clearing time. This may reduce the occurrence of events. Given the experience with the very short time to stall for compressor-driven motors, this solution will not eliminate all events.
2. Controlled reactive power support. Generators and SVCs can provide controlled reactive power support to lessen the duration and severity of a delayed voltage recovery event.
3. Limit Impacted Load. Specifically design the system to section the load to limit its size in areas particularly vulnerable to FIDVR events. This should help contain the events.
4. Special Protection Schemes (Remedial Action Schemes). A transmission level protection scheme could be designed to contain the effect of a FIDVR event.
5. Under voltage load shedding
6. Energy Savings devices. Reducing the load could lower the risk of a FIDVR event.

In practice, generators and SVCs have been installed to mitigate these events. APS has installed generation in Phoenix, and plan to install SVCs. Southern Company has installed SVCs.

Further studies are needed to analyze the impact of these solutions. Experience and simulations suggest that reduced clearing times will not eliminate all events – the motors stall during faults. At the grid level, controlled reactive power support seem to be the most promising solution. Appropriate devices are expensive, however, and they may not be able to prevent the events, though significant reduction in impact should be expected. (See the Pourbeik presentation that includes a simulation with and without SVC or synchronous condenser support.¹⁹)

¹⁸ Lu, N. B. Yang, Z. Huang, and R. Bravo, “The System Impact of Air Conditioner Under-voltage Protection Schemes,” Power System Conference and Exposition, 15-18 March 2009.

¹⁹ P.Pourbeik, “Experience with A/C Stalling Behavior and Modeling it for Power System Studies,” DOE Workshop, April 22, 2008.

Items 3-5 in the list above are intended to limit the scope of an event once it occurs. Item 3 is local, item 4 is at a higher level, and item 5 is offered as a measure to stop a fast-acting voltage disturbance from transitioning into a slow-acting voltage collapse. The NERC report notes that item 4 may actually be non-compliant with existing rules, and that this needs attention.

The last item, may or may not improve the situation depending the nature of energy savings devices that are used.

In all cases, further study is needed to assess the success of any strategy. Most of the intuition used to consider such options follows balancing power and reactive power under FIDVR scenarios. For those solutions that quickly remove the stalled motors from service, or the feeders that serve them, one needs to be concerned about initiating dynamic instabilities. Detailed studies are needed to ensure there are no unintended consequences.

4.0 Summary and Recommendations

Fault Induced Delayed Voltage Recovery is a serious problem threatening the reliability of the electric power grid. Numerous events have already occurred, some with significant load loss. It is a challenging problem whose fundamental characteristics are driven by load behavior that is largely beyond the control of transmission operators. As Baj Agrawal points out in his presentation,²⁰ “Normally the 12 kV voltage is a slave to the transmission system voltage. However, due to stalled motors, the 12 kV voltage sags heavily and pulls the transmission system voltage lower.”

The most effective solutions are those that can react at the site of the problem. These can also be the hardest to implement. Changes to air conditioner units to provide low voltage ride through would add additional manufacturing expense. Without standards with common requirements for all, manufacturers have a disincentive to implement such changes. Implementing new standards will take time, and even more time will pass before new units dominate the installed base. Digital thermostatic controls are promising; research and perhaps a pilot program should be put in place to determine their effectiveness. One could generalize the use of thermostatic controls to a more distributed use of technology to enable traditional customers to offer valuable grid support. Such efforts fall under the now popular title “smart grid.” As such technologies advance, an eye towards FIDVR mitigation is warranted in those areas susceptible to events.

System level solutions focus on containing and mitigating events. Controlled reactive power sources are essential for this purpose. Studies to assess and quantify their effectiveness are needed. Long term monitoring of events in areas with new generators and SVCs will help determine the value of these resources, and guide additional protection as needed. Research programs for such monitoring and analysis should continue.

It is imperative that California investigate further the way to mitigate the A/C stalling to prevent the FIDVR events that can have a negative impact in the grid, or in a drastic scenario compromise the grid operation like the 2003 northeast blackout event.

²⁰ B. Agrawal, “APS Experience,” DOE Workshop, April 22, 2008.